NOTATION

υ	Poisson's ratio
ρ	Density of material
λ, μ	Lame constants
$\bar{\varepsilon}$	Volumetric strain or dilation
∇^2	Laplacian operator
ε	One-dimensional strain
σ	Stress along any direction
γ	Shear strain deformation
α_b	Acceleration of basement
u, v, w	Displacement along x, y and z directions, respectively
Φ, ψ	Potential function along x and y directions, respectively
ω	Frequency of motion
Ω	Rotation
G	Shear modulus
β	Damping factor
β_R	Resonance criteria
N	Field SPT N-value
C_N	Correction factor for SPT N-value in terms of confining pressure
v_P	P-Wave Velocity
v_S	S-Wave Velocity
v_R	Rayleigh Wave Velocity
v_L	Love Wave Velocity
c_g	Group Velocity
c	Phase Velocity
K_{Rs}	The ratio of the Rayleigh Wave Velocity to the S-Wave Velocity
Kg	Seismic Vulnerability Index
F_g	Predominant Frequency
A_g	H/V Ratio
g	Acceleration due to gravity

f	Natural frequency
W[n]	Windows function
SSMM	Small Scale Microtremor Measurement
SBH	Saidur Borehole
EGL	Existing Ground Level
Vs, SWV	Shear Wave Velocity
H/V	Horizontal to Vertical Spectral ratio
BJ	BUET-JIDPUS
NA	New Academic Building
SCS	Segmental Cross-Spectrum

ABSTRACT

The degree of damage during earthquakes strongly depends on dynamic characteristics of buildings as well as amplification of seismic waves in soils. Among the other approaches, microtremor is, perhaps, the easiest and cheapest way to understand the dynamic characteristics of soil as well as structural element. The purpose of this research is to apply Horizontal to Vertical Spectral ratio **(**H/V) Microtremor Technique for Site Response Analysis within Dhaka city. Non-reference microtremor measurements have been carried out in one hundred and thirty two selected locations within BUET campus and fourty five locations in and around the Dhaka city. The amplitude ratio (H/V) of horizontal to vertical spectra has been used to estimate predominant frequency and amplification.

For spectral analysis three low noise segments of 20.48s each of the recordings have been taken at 100 Hz instrumental sampling. Fast Fourier Transformation (FFT) has been applied on the time domain records. Then, non-reference spectral ratio (H/V) technique has been applied. The resultant of two horizontal components of H/V ratio have been digitally filtered using suitable average smoothing point. After calculating three sets of the H/V ratios at selected location, the mean H/V ratio has been plotted with half standard deviation in order to assess the deviation of microtremor data at different time instants. The stability of microtremor data has been checked in fourteen different locations in various time instants (Morning, Evening and Night) within BUET campus. In this research resultant of H/V ratio data for five different filtering options (Rectangular, Hanning, Hamming, Welch and Blackman) have been carried out to select the most suitable one.

Soil model has been developed in the investigated points using the programme SHAKE. Standard Penetration Test (SPT) has been carried out at twenty seven locations and field Shear Wave Velocity data has been collected in the investigated locations. Existing correlation between Shear Wave Velocity and SPT-N has been used in order to estimate Shear Wave Velocity at twenty eight other locations. These Shear Wave Velocity data has been used as input for the programme SHAKE.

Damage assessment of structures using resonance criteria and damage assessment of soils using Nakamura's Vulnerability Index (Kg) has been executed in the investigated locations.

From the stability of microtremor data, it can be said that non reference Horizontal to Vertical spectral (H/V) ratio provides stable data to estimate predominant frequency and amplification of soil without source effect. Fourier Spectrum along East-West and North-South provides better result to estimate predominant frequency of building. Root multiplication of H/V ratio along East-West and North-South directions shows reliable resultant for the estimation of dynamic properties of soil. The mean peak H/V ratio data

in rectangular window for filtering show similar result to other four windows. The peak of H/V ratio data decreases if higher average smoothing points is applied.

Out of 132 locations within BUET campus the overall mean predominant frequency and mean peak H/V ratio are 1.39 Hz and 2.09. Predominant frequency for most of the locations lie between 1.0 Hz and 1.99 Hz. Out of 45 microtremor observation locations in and around the Dhaka city, the mean predominant frequency varies from 0.48 Hz to 3.65 Hz. On the other hand, the mean Horizontal to Vertical spectral ratio varies from 1.08 to 4.78.

From the comparision of microtremor H/V ratio and Transfer Function obtained from the programme SHAKE, four types of characteristics curves have been observed. Among 42 locations thirty five Transfer function have higher frequency compared to microtremor and one has lower predominant frequency. For six sites two curves have identical frequency. For two sites, no similarity of predominant frequency between microtremor and transfer function have been observed. Microtremor consists of either shear-wave, or surface-wave or a mixture of both waves. Transfer Function obtained from SHAKE is basically shear-wave. Sometimes there will be some similarity between microtremor H/V ratio and Transfer function, but sometimes dissimilarity may also exist.

Out of 45 buildings considered, four buildings have been identified as vulnerable due to resonance criteria within BUET campus. Most of the buildings predominant frequency is not close to the predominant frequency of site soil. The seismic Vulnerability Index (Kg) for 45 sites varies between 0.45 and 31.85. Ten sites have been identified as having moderate vulnerability of soil layers to deform.

ACKNOWLEDGEMENT

The author wishes to express his profound gratitude and sincere appreciation to his supervisor, Dr. Mehedi Ahmed Ansary, Professor, Department of Civil Engineering, Bangladesh University of Engineering & Technology (BUET), Dhaka for his dynamic assistance, constant guidance, invaluable suggestions, enthusiastic encouragement, strong support, generous help, persistent simulation and unfailing enthusiasm at all stages to fulfill this extensive study. It would have been impossible for the author to carry out this study without his guidance and inspiration.

The author wants to express his sincere thanks to Dr. Md. Zoynul Abedin, Professor and Head, Department of Civil Engineering, BUET, for his co-operation.

The author would like to express sincere appreciation to Dr. Abu Siddique, Professor of BUET and Dr. Md. Mahmudur Rahman, Professor, AUST for their interest and suggestions during the present research.

The author conveys special thanks to Bangladesh Network Office for Urban Safety (BNUS) staffs for providing microtremor equipment as well as assistance to fulfill this research. The author is also very grateful to the Civil Engineering Department, BUET for providing all the necessary supports and funds for this whole work.

Finally, the author wishes to express his gratitude to all the members of his family especially his parents for their continuous support and utmost sacrifice without which this thesis work would not come into reality.

APPENDIX-A

SPT-N VALUE AND ESTIMATED SHEAR WAVE VELOCITY

Table A3.1: SPT-N and Shear Wave Velocity at National University

Depth (m)	Soil Description	SPT-N Value	Shear wave velocity (m/s)			
			Ansary et al. (2010)	Ohta and Goto (1978)	Imai and Yoshimura (1970)	Ohba and Toriumi (1970)
1.5	Silty Clay	4	135	123	120	129
3.0	Silty Clay	6	155	152	137	146
4.5	Silty Clay	7	163	169	144	154
6.0	Silty Clay	10	184	190	162	172
7.5	Silty Clay	11	190	202	168	177
9.0	Silty Clay	13	201	215	177	186
10.5	Silty Clay	15	211	227	186	194
12.0	Silty Clay	14	206	231	182	190
13.5	Silty Clay	16	216	242	190	198
15.0	Silty Clay	18	225	252	197	206
16.5	Silty Clay	19	229	259	201	209
18.0	Silty Clay	18	225	261	197	206

Table A3.2: SPT-N and Shear Wave Velocity at Board Bazar, Gazipur

Depth (m)	Soil Description	SPT-N Value	Shear wave velocity (m/s)			
			Ansary et al. (2010)	Ohta and Goto (1978)	Imai and Yoshimura (1970)	Ohba and Toriumi (1970)
1.5	Silty Clay	3	150	117	109	118
3.0	Silty Clay	8	197	159	151	160
4.5	Silty Clay	8	197	173	151	160
6.0	Silty Clay	8	197	183	151	160
7.5	Silty Clay	9	203	195	157	166
9.0	Silty Clay	17	243	225	194	202
10.5	Fine Sand	15	211	191	186	194
12.0	Silty Clay	9	203	214	157	166
13.5	Silty Clay	11	215	227	168	177
15.0	Silty Clay	11	215	232	168	177
16.5	Silty Clay	12	220	240	173	181
18.0	Silty Clay	14	230	250	182	190
19.5	Silty Clay	16	239	260	190	198
20.0	Silty Clay	18	247	267	197	206

Table A3.3: SPT-N and Shear Wave Velocity at Kaunia, Boro Bari

Depth (m)	Soil Description	SPT-N Value	Shear wave velocity (m/s)			
			Ansary et al. (2010)	Ohta and Goto (1978)	Imai and Yoshimura (1970)	Ohba and Toriumi (1970)
1.5	Silty Clay	4	135	103	120	129
3.0	Silty Clay	5	172	147	129	138
4.5	Silty Clay	7	190	169	144	154
6.0	Silty Clay	10	209	190	162	172
7.5	Silty Clay	11	215	202	168	177
9.0	Silty Clay	13	225	215	177	186
10.5	Silty Clay	14	230	225	182	190
12.0	Silty Clay	15	235	234	186	194
13.5	Silty Clay	16	239	242	190	198
15.0	Silty Clay	18	247	252	197	206
16.5	Clayey Silt	20	233	215	204	213
18.0	Clayey Silt	24	248	226	217	225
19.5	Clayey Silt	25	251	231	220	228
20.0	Sandy Silt	28	261	237	228	236

Table A3.4: SPT-N and Shear Wave Velocity at Tongi, Ershadnagar

Depth (m)	Soil Description	SPT-N Value	Shear wave velocity (m/s)			
			Ansary et al. (2010)	Ohta and Goto (1978)	Imai and Yoshimura (1970)	Ohba and Toriumi (1970)
1.5	Silty Clay	6	182	132	137	146
3.0	Silty Clay	11	215	168	168	177
4.5	Clayey Silt	9	178	148	157	166
6.0	Clayey Silt	11	190	162	168	177
7.5	Sandy Silt	13	201	174	177	186
9.0	Sandy Silt	9	178	170	157	166
10.5	Fine Sand	11	190	181	168	177
12.0	Fine Sand	12	196	189	173	181
13.5	Silty Clay	8	197	215	151	160
15.0	Silty Clay	15	235	244	186	194
16.5	Silty Clay	10	209	232	162	172
18.0	Silty Fine Sand	16	216	211	190	198
19.5	Silty Fine Sand	17	221	216	194	202
20.0	Silty Fine Sand	17	221	218	194	202

Table A3.5: SPT-N and Shear Wave Velocity at Tongi BSCIC area

Depth (m)	Soil Description	SPT-N Value	Shear wave velocity (m/s)			
			Ansary et al. (2010)	Ohta and Goto (1978)	Imai and Yoshimura (1970)	Ohba and Toriumi (1970)
1.5	Fine Sand (Filling)	4	135	103	120	129
3.0	Fine Sand (Filling)	5	145	123	129	138
4.5	Silty Clay	3	150	146	109	118
6.0	Silty Clay	4	162	162	120	129
7.5	Silty Clay	5	172	176	129	138
9.0	Silty Clay	11	215	209	168	177
10.5	Silty Fine Sand	11	190	181	168	177
12.0	Silty Fine Sand	13	201	191	177	186
13.5	Silty Fine Sand	16	216	203	190	198
15.0	Silty Fine Sand	20	233	215	204	213
16.5	Silty Fine Sand	25	251	228	220	228
18.0	Silty Fine Sand	30	268	239	233	241
19.5	Silty Fine Sand	37	287	252	250	257
20.0	Silty Fine Sand	37	287	253	250	257

Table A3.6: SPT-N and Shear Wave Velocity at Abdullahpur

Depth (m)	Soil Description	SPT-N Value	Shear wave velocity (m/s)			
			Ansary et al. (2010)	Ohta and Goto (1978)	Imai and Yoshimura (1970)	Ohba and Toriumi (1970)
1.5	Rubbish	3	122	90	109	118
3.0	Silty Clay	11	215	168	168	177
4.5	Silty Clay	12	220	185	173	181
6.0	Silty Clay	10	209	190	162	172
7.5	Silty Clay	10	209	216	162	172
9.0	Silty Fine Sand	11	190	175	168	177
10.5	Silty Fine Sand	16	216	193	190	198
12.0	Silty Fine Sand	18	225	202	197	206
13.5	Silty Fine Sand	21	237	212	208	216
15.0	Silty Fine Sand	25	251	223	220	228
16.5	Silty Fine Sand	28	261	232	228	236
18.0	Silty Fine Sand	49	316	260	275	281
19.5	Silty Fine Sand	50	318	265	276	282
20.0	Silty Fine Sand	50	318	266	276	282

Table A3.7: SPT-N and Shear Wave Velocity at Ijtema field

Depth (m)	Soil Description	SPT-N Value	Shear wave velocity (m/s)			
			Ansary et al. (2010)	Ohta and Goto (1978)	Imai and Yoshimura (1970)	Ohba and Toriumi (1970)
1.5	Silty Clay	5	172	128	129	138
3.0	Silty Clay	10	209	165	162	172
4.5	Silty Clay	11	215	182	168	177
6.0	Clayey Silt	13	201	166	177	186
7.5	Fine Sand	17	221	182	194	202
9.0	Silty Fine Sand	24	248	200	217	225
10.5	Silty Fine Sand	25	251	208	220	228
12.0	Silty Fine Sand	29	264	219	231	239
13.5	Silty Fine Sand	34	279	231	243	251
15.0	Silty Fine Sand	37	287	239	250	257
16.5	Silty Fine Sand	41	297	248	259	266
18.0	Silty Fine Sand	43	302	254	263	270
19.5	Silty Fine Sand	45	307	260	267	273
20.0	Silty Fine Sand	45	307	262	267	273

Table A3.8: SPT-N and Shear wave velocity at Ashulia Toll Plaza

Depth (m)	Soil Description	SPT-N Value	Shear wave velocity (m/s)			
			Ansary et al. (2010)	Ohta and Goto (1978)	Imai and Yoshimura (1970)	Ohba and Toriumi (1970)
1.5	Silty Fine Sand (Filling)	1	84	82	76	84
3.0	Silty Clay	3	150	138	109	118
4.5	Sandy Silt	5	145	134	129	138
6.0	Silty Fine Sand	10	184	159	162	172
7.5	Silty Fine Sand	14	206	176	182	190
9.0	Silty Fine Sand	17	221	189	194	202
10.5	Silty Fine Sand	19	229	199	201	209
12.0	Silty Fine Sand	20	233	206	204	213
13.5	Silty Fine Sand	22	241	214	211	219
15.0	Silty Fine Sand	26	255	225	223	231
16.5	Silty Fine Sand	32	273	237	239	246
18.0	Silty Fine Sand	36	285	247	248	255
19.5	Silty Fine Sand	39	292	254	255	262
20.0	Silty Fine Sand	40	295	256	257	264

Table A3.9: SPT-N and Shear Wave Velocity at Uttara Phase-3

Depth (m)	Soil Description	SPT-N Value	Shear wave velocity (m/s)			
			Ansary et al. (2010)	Ohta and Goto (1978)	Imai and Yoshimura (1970)	Ohba and Toriumi (1970)
1.5	Silty Fine Sand	2	107	96	96	104
3.0	Silty Fine Sand	3	122	109	109	118
4.5	Silty Clay	9	203	157	157	166
6.0	Silty Clay	11	215	168	168	177
7.5	Silty Clay	13	225	177	177	186
9.0	Clayey Silt	13	225	177	177	186
10.5	Sandy Silt	9	178	157	157	166
12.0	Sandy Silt	12	196	173	173	181
13.5	Sandy Silt	13	201	177	177	186
15.0	Sandy Silt	15	211	186	186	194
16.5	Sandy Silt	14	206	182	182	190
18.0	Clayey Silt	16	216	190	190	198
19.5	Clayey Silt	18	225	197	197	206
20.0	Clayey Silt	18	225	197	197	206

Table A3.10: SPT-N and Shear Wave Velocity at Mirpur DOHS

Depth (m)	Soil Description	SPT-N Value	Shear wave velocity (m/s)			
			Ansary et al. (2010)	Ohta and Goto (1978)	Imai and Yoshimura (1970)	Ohba and Toriumi (1970)
1.5	Silty Fine Sand (Filling)	6	155	111	137	146
3.0	Silty Fine Sand (Filling)	5	145	123	129	138
4.5	Silty Fine Sand (Filling)	6	155	138	137	146
6.0	Silty Clay	10	209	190	162	172
7.5	Silty Clay	11	215	202	168	177
9.0	Clayey Silt	8	171	166	151	160
10.5	Clayey Silt	10	184	178	162	172
12.0	Fine Sand	12	196	189	173	181
13.5	Fine Sand	16	216	203	190	198
15.0	Silty Clay	16	239	247	190	198
16.5	Silty Clay	15	235	249	186	194
18.0	Silty Clay	18	247	261	197	206
19.5	Silty Clay	22	261	275	211	219
20.0	Silty Clay	23	264	278	214	222

Table A3.11: SPT-N and Shear Wave Velocity at Ashiyan city, Askona, Dakkhin Khan

Depth (m)	Soil Description	SPT-N Value	Shear wave velocity (m/s)			
			Ansary et al. (2010)	Ohta and Goto (1978)	Imai and Yoshimura (1970)	Ohba and Toriumi (1970)
1.5	Silty Fine Sand (Filling)	4	135	103	120	129
3.0	Silty Fine Sand (Filling)	5	145	123	129	138
4.5	Silty Clay	4	162	153	120	129
6.0	Silty Clay	3	150	155	109	118
7.5	Silty Clay	3	150	162	109	118
9.0	Silty Clay	4	162	176	120	129
10.5	Silty Clay	4	162	182	120	129
12.0	Silty Clay	7	190	205	144	154
13.5	Silty Fine Sand	30	268	226	233	241
15.0	Silty Fine Sand	36	285	238	248	255
16.5	Silty Fine Sand	42	300	249	261	268
18.0	Silty Clay	8	197	228	151	160
19.5	Silty Clay	10	209	240	162	172
20.0	Silty Clay	10	209	242	162	172

Table A3.12: SPT-N and Shear wave velocity at Purbachal-1, Randokpur Hazi Bari, Rupganj

Depth (m)	Soil Description	SPT-N Value	Shear wave velocity (m/s)			
			Ansary et al. (2010)	Ohta and Goto (1978)	Imai and Yoshimura (1970)	Ohba and Toriumi (1970)
1.5	Silty Clay	3	150	117	109	118
3.0	Silty Clay	5	172	147	129	138
4.5	Silty Clay	3	150	146	109	118
6.0	Silty Clay	2	133	144	96	104
7.5	Silty Clay	4	162	170	120	129
9.0	Silty Fine Sand	9	178	170	157	166
10.5	Silty Fine Sand	17	221	195	194	202
12.0	Silty Fine Sand	15	211	196	186	194
13.5	Sandy Silt	16	216	203	190	198
15.0	Sandy Silt	13	201	200	177	186
16.5	Silty Fine Sand	10	184	195	162	172
18.0	Silty Fine Sand	13	201	207	177	186
19.5	Silty Fine Sand	16	216	218	190	198
20.0	Silty Fine Sand	16	216	219	190	198

Table A3.13: SPT-N and Shear Wave Velocity at Purbachal-2, American City

Depth (m)	Soil Description	SPT-N Value	Shear wave velocity (m/s)			
			Ansary et al. (2010)	Ohta and Goto (1978)	Imai and Yoshimura (1970)	Ohba and Toriumi (1970)
1.5	Silty Fine Sand (Filling)	3	122	98	109	118
3.0	Silty Fine Sand (Filling)	2	107	105	96	104
4.5	Silty Fine Sand (Filling)	2	107	114	96	104
6.0	Silty Fine Sand (Filling)	1	84	108	76	84
7.5	Silty Clay	2	133	151	96	104
9.0	Silty Clay	2	133	157	96	104
10.5	Silty Clay	1	110	144	76	84
12.0	Silty Clay	1	110	147	76	84
13.5	Silty Clay	2	133	170	96	104
15.0	Silty Clay	2	133	173	96	104
16.5	Silty Clay	1	110	157	76	84
18.0	Silty Clay	1	110	160	76	84
19.5	Silty Clay	8	197	231	151	160
20.0	Silty Clay	8	197	233	151	160

Table A3.14: SPT-N and Shear wave velocity at Purbachal Park (Picnic Park)

Depth (m)	Soil Description	SPT-N Value	Shear wave velocity (m/s)			
			Ansary et al. (2010)	Ohta and Goto (1978)	Imai and Yoshimura (1970)	Ohba and Toriumi (1970)
2	Silty Fine Sand (Filling)	5	145	107	129	138
3	Silty Fine Sand (Filling)	6	155	127	137	146
5	Silty Fine Sand (Filling)	4	135	129	120	129
6	Silty Clay	2	133	144	96	104
8	Silty Clay	3	150	162	109	118
9	Silty Clay	7	190	194	144	154
11	Silty Clay	10	209	212	162	172
12	Clayey Silt	12	196	189	173	181
14	Clayey Silt	13	201	196	177	186
15	Clayey Silt	14	206	202	182	190
17	Clayey Silt	16	216	211	190	198
18	Clayey Silt	18	225	219	197	206
20	Clayey Silt	20	233	227	204	213
20	Clayey Silt	20	233	228	204	213

Table A3.15: SPT-N and Shear wave velocity at Adjacent to Mirpur Zoo

Depth (m)	Soil Description	SPT-N Value	Shear wave velocity (m/s)			
			Ansary et al. (2010)	Ohta and Goto (1978)	Imai and Yoshimura (1970)	Ohba and Toriumi (1970)
1.5	Silty Fine Sand (Filling)	5	145	107	129	138
3.0	Silty Fine Sand (Filling)	6	155	127	137	146
4.5	Silty Fine Sand (Filling)	5	145	134	129	138
6.0	Silty Clay	6	182	174	137	146
7.5	Silty Clay	6	182	182	137	146
9.0	Silty Clay	7	190	194	144	154
10.5	Silty Clay	9	203	209	157	166
12.0	Silty Clay	11	215	222	168	177
13.5	Clayey Silt	13	201	196	177	186
15.0	Sandy Silt	16	216	207	190	198
16.5	Silty Fine Sand	18	225	215	197	206
18.0	Silty Fine Sand	21	237	225	208	216
19.5	Silty Fine Sand	26	255	237	223	231
20.0	Silty Fine Sand	26	255	238	223	231

Table A3.16: SPT-N and Shear wave velocity at Kuril Flyover

Depth (m)	Soil Description	SPT-N Value	Shear wave velocity (m/s)			
			Ansary et al. (2010)	Ohta and Goto (1978)	Imai and Yoshimura (1970)	Ohba and Toriumi (1970)
1.5	Silty Fine Sand	4	135	103	120	129
3.0	Silty Fine Sand	4	135	119	120	129
4.5	Silty Clay	1	110	121	76	84
6.0	Silty Clay	2	133	144	96	104
7.5	Silty Clay	2	133	151	96	104
9.0	Silty Clay	10	209	206	162	172
10.5	Silty Clay	11	215	216	168	177
12.0	Silty Clay	12	220	225	173	181
13.5	Silty Clay	14	230	236	182	190
15.0	Clayey Silt	20	233	215	204	213
16.5	Clayey Silt	23	244	225	214	222
18.0	Clayey Silt	24	248	230	217	225
19.5	Clayey Silt	27	258	239	226	233
20.0	Clayey Silt	27	258	240	226	233

Table A3.17: SPT-N and Shear Wave Velocity at Purachal, Uttar Badda

Depth (m)	Soil Description	SPT-N Value	Shear wave velocity (m/s)			
			Ansary et al. (2010)	Ohta and Goto (1978)	Imai and Yoshimura (1970)	Ohba and Toriumi (1970)
1.5	Silty Fine Sand (Filling)	7	163	114	144	154
3.0	Silty Fine Sand (Filling)	8	171	133	151	160
4.5	Silty Fine Sand (Filling)	5	145	134	129	138
6.0	Organic Clay	1	110	128	76	84
7.5	Organic Clay	3	150	162	109	118
9.0	Silty Clay	5	172	183	129	138
10.5	Silty Clay	8	197	204	151	160
12.0	Silty Clay	11	215	222	168	177
13.5	Silty Clay	12	220	230	173	181
15.0	Sandy Silt	26	255	225	223	231
16.5	Sandy Silt	30	268	235	233	241
18.0	Sandy Silt	33	276	243	241	248
19.5	Silty Fine Sand	38	290	253	252	259
20.0	Silty Fine Sand	38	290	254	252	259

Table A3.18: SPT-N and Shear Wave Velocity at City Corporation, Gabtoli

Depth (m)	Soil Description	SPT-N Value	Shear wave velocity (m/s)			
			Ansary et al. (2010)	Ohta and Goto (1978)	Imai and Yoshimura (1970)	Ohba and Toriumi (1970)
1.5	Silty Fine Sand (Filling)	6	155	111	137	146
3.0	Silty Fine Sand (Filling)	5	145	123	129	138
4.5	Silty Fine Sand (Filling)	3	122	122	109	118
6.0	Silty Clay	5	172	169	129	138
7.5	Silty Clay	4	162	170	120	129
9.0	Clayey Silt	6	155	158	137	146
10.5	Clayey Silt	7	163	168	144	154
12.0	Sandy Silt	9	178	180	157	166
13.5	Sandy Silt	10	184	187	162	172
15.0	Sandy Silt	10	184	191	162	172
16.5	Sandy Silt	13	201	204	177	186
18.0	Sandy Silt	13	201	207	177	186
19.5	Silty Fine Sand	15	211	216	186	194
20.0	Silty Fine Sand	15	211	217	186	194

Table A3.19: SPT-N and Shear Wave Velocity at Umme Had Nagar, Nadda

Depth (m)	Soil Description	SPT-N Value	Shear wave velocity (m/s)			
			Ansary et al. (2010)	Ohta and Goto (1978)	Imai and Yoshimura (1970)	Ohba and Toriumi (1970)
1.5	Silty Fine Sand (Filling)	1	84	82	76	84
3.0	Silty Fine Sand (Filling)	1	84	94	76	84
4.5	Silty Clay	7	190	169	144	154
6.0	Silty Clay	2	133	144	96	104
7.5	Silty Clay	8	197	191	151	160
9.0	Silty Clay	15	235	221	186	194
10.5	Silty Clay	13	225	222	177	186
12.0	Clayey Silt	13	201	191	177	186
13.5	Sandy Silt	27	258	222	226	233
15.0	Sandy Silt	33	276	234	241	248
16.5	Clayey Silt	36	285	242	248	255
18.0	Clayey Silt	32	273	242	239	246
19.5	Sandy Silt	35	282	249	246	253
20.0	Sandy Silt	35	282	251	246	253

Table A3.20: SPT-N and Shear Wave Velocity at South Banasree

Depth (m)	Soil Description	SPT-N Value	Shear wave velocity (m/s)			
			Ansary et al. (2010)	Ohta and Goto (1978)	Imai and Yoshimura (1970)	Ohba and Toriumi (1970)
1.5	Silty Fine Sand (Filling)	5	145	107	129	138
3.0	Silty Fine Sand (Filling)	6	155	127	137	146
4.5	Silty Clay	4	162	153	120	129
6.0	Silty Clay	5	172	169	129	138
7.5	Silty Clay	1	110	134	76	84
9.0	Silty Clay	1	110	139	76	84
10.5	Silty Clay	3	150	173	109	118
12.0	Silty Clay	2	133	166	96	104
13.5	Silty Clay	4	162	191	120	129
15.0	Silty Clay	9	203	224	157	166
16.5	Silty Clay	26	274	273	223	231
18.0	Silty Fine Sand	33	276	243	241	248
19.5	Silty Fine Sand	40	295	255	257	264
20.0	Silty Fine Sand	40	295	256	257	264

Table A3.21: SPT-N and Shear Wave Velocity at Kalunagar, Hazaribagh

Depth (m)	Soil Description	SPT-N Value	Shear wave velocity (m/s)			
			Ansary et al. (2010)	Ohta and Goto (1978)	Imai and Yoshimura (1970)	Ohba and Toriumi (1970)
1.5	Silty Fine Sand (Filling)	4	135	103	120	129
3.0	Silty Fine Sand (Filling)	5	145	123	129	138
4.5	Silty Fine Sand (Filling)	5	145	134	129	138
6.0	Silty Fine Sand (Filling)	8	171	153	151	160
7.5	Silty Fine Sand (Filling)	9	178	163	157	166
9.0	Silty Fine Sand	12	196	178	173	181
10.5	Silty Fine Sand	12	196	184	173	181
12.0	Silty Fine Sand	14	206	194	182	190
13.5	Silty Fine Sand	12	196	193	173	181
15.0	Silty Fine Sand	13	201	200	177	186
16.5	Silty Fine Sand	15	211	209	186	194
18.0	Silty Fine Sand	17	221	217	194	202
19.5	Silty Fine Sand	19	229	225	201	209
20.0	Silty Fine Sand	19	229	226	201	209

Table A3.22: SPT-N and Shear Wave Velocity at Rab-10, Plot, Kamrangirchar

Depth (m)	Soil Description	SPT-N Value	Shear wave velocity (m/s)			
			Ansary et al. (2010)	Ohta and Goto (1978)	Imai and Yoshimura (1970)	Ohba and Toriumi (1970)
1.5	Silty Fine Sand (Filling)	3	122	98	109	118
3.0	Silty Fine Sand (Filling)	7	163	130	144	154
4.5	Fine Sand	6	155	138	137	146
6.0	Fine Sand	7	163	150	144	154
7.5	Fine Sand	9	178	163	157	166
9.0	Silty Clay	7	190	198	144	154
10.5	Fine Sand	7	163	168	144	154
12.0	Fine Sand	18	225	202	197	206
13.5	Fine Sand	19	229	209	201	209
15.0	Silty Fine Sand	20	233	215	204	213
16.5	Silty Fine Sand	21	237	221	208	216
18.0	Silty Fine Sand	25	251	232	220	228
19.5	Silty Fine Sand	28	261	240	228	236
20.0	Silty Fine Sand	28	261	241	228	236

Table A3.23: SPT-N and Shear Wave Velocity at Basundhara River view

Depth (m)	Soil Description	SPT-N Value	Shear wave velocity (m/s)			
			Ansary et al. (2010)	Ohta and Goto (1978)	Imai and Yoshimura (1970)	Ohba and Toriumi (1970)
1.5	Silty Fine Sand (Filling)	3	122	98	109	118
3.0	Silty Fine Sand (Filling)	5	145	123	129	138
4.5	Clayey Silt	3	122	122	109	118
6.0	Clayey Silt	6	155	146	137	146
7.5	Silty Fine Sand	10	184	166	162	172
9.0	Clayey Silt	4	135	148	120	129
10.5	Clayey Silt	5	145	158	129	138
12.0	Clayey Silt	4	135	156	120	129
13.5	Clayey Silt	5	145	166	129	138
15.0	Silty Clay	2	133	173	96	104
16.5	Silty Clay	3	150	189	109	118
18.0	Silty Clay	4	162	202	120	129
19.5	Clayey Silt	7	163	190	144	154
20.0	Clayey Silt	7	163	191	144	154

Table A3.24: SPT-N and Shear Wave Velocity at Jilmil Project, Equria

Depth (m)	Soil Description	SPT-N Value	Shear wave velocity (m/s)			
			Ansary et al. (2010)	Ohta and Goto (1978)	Imai and Yoshimura (1970)	Ohba and Toriumi (1970)
1.5	Silty Fine Sand (Filling)	2	107	92	96	104
3.0	Silty Clay	4	162	154	120	129
4.5	Silty Clay	3	150	146	109	118
6.0	Silty Clay	7	190	179	144	154
7.5	Silty Clay	8	197	191	151	160
9.0	Silty Fine Sand	24	248	200	217	225
10.5	Silty Fine Sand	27	258	211	226	233
12.0	Silty Fine Sand	28	261	218	228	236
13.5	Silty Fine Sand	30	268	226	233	241
15.0	Silty Fine Sand	23	244	220	214	222
16.5	Silty Fine Sand	27	258	231	226	233
18.0	Silty Fine Sand	29	264	238	231	239
19.5	Silty Fine Sand	31	271	244	236	244
20.0	Silty Fine Sand	31	271	245	236	244

Table A3.25: SPT-N and Shear Wave Velocity at Rajendapur

Depth (m)	Soil Description	SPT-N Value	Shear wave velocity (m/s)			
			Ansary et al. (2010)	Ohta and Goto (1978)	Imai and Yoshimura (1970)	Ohba and Toriumi (1970)
1.5	Silty Fine Sand (Filling)	4	135	103	120	129
3.0	Silty Fine Sand (Filling)	5	145	123	129	138
4.5	Silty Fine Sand (Filling)	5	145	134	129	138
6.0	Silty Clay	10	209	194	162	172
7.5	Silty Clay	9	203	199	157	166
9.0	Clayey Silt	5	145	153	129	138
10.5	Clayey Silt	7	163	168	144	154
12.0	Clayey Silt	8	171	176	151	160
13.5	Clayey Silt	8	171	180	151	160
15.0	Clayey Silt	9	178	188	157	166
16.5	Fine Sand	21	237	221	208	216
18.0	Silty Fine Sand	23	244	228	214	222
19.5	Silty Fine Sand	26	255	237	223	231
20.0	Silty Fine Sand	26	255	238	223	231

Table A3.26: SPT-N and Shear Wave Velocity at Bramangaon

Depth (m)	Soil Description	SPT-N Value	Shear wave velocity (m/s)			
			Ansary et al. (2010)	Ohta and Goto (1978)	Imai and Yoshimura (1970)	Ohba and Toriumi (1970)
1.5	Silty Fine Sand (Filling)	4	135	103	120	129
3.0	Silty Fine Sand (Filling)	5	145	123	129	138
4.5	Silty Fine Sand (Filling)	5	145	134	129	138
6.0	Clayey Silt	7	163	150	144	154
7.5	Sandy Silt	8	171	160	151	160
9.0	Clayey Silt	5	145	153	129	138
10.5	Clayey Silt	5	145	158	129	138
12.0	Clayey Silt	5	145	163	129	138
13.5	Clayey Silt	4	135	160	120	129
15.0	Clayey Silt	5	145	170	129	138
16.5	Clayey Silt	6	155	179	137	146
18.0	Clayey Silt	7	163	187	144	154
19.5	Clayey Silt	8	171	194	151	160
20.0	Clayey Silt	8	171	195	151	160

Table A3.27: SPT-N and Shear Wave Velocity at BJ01

Depth (m)	Soil Description	SPT-N Value	Shear wave velocity (m/s)			
			Ansary et al. (2010)	Ohta and Goto (1978)	Imai and Yoshimura (1970)	Ohba and Toriumi (1970)
1.5	Silty Clay	1	110	92	76	84
3.0	Silty Clay	2	133	159	96	104
4.5	Silty Clay	15	235	202	186	194
6.0	Silty Clay	12	220	190	173	181
7.5	Clayey Silt	18	225	182	197	206
9.0	Silty Fine Sand	24	248	193	217	225
10.5	Silty Fine Sand	28	261	200	228	236
12.0	Silty Fine Sand	30	268	214	233	241
13.5	Silty Fine Sand	35	282	220	246	253
15.0	Silty Fine Sand	41	297	234	259	266

Table A3.28: SPT-N and Shear Wave Velocity at BJ02

Depth (m)	Soil Description	SPT-N Value	Shear wave velocity (m/s)			
			Ansary et al. (2010)	Ohta and Goto (1978)	Imai and Yoshimura (1970)	Ohba and Toriumi (1970)
1.5	Silty Clay	2	133	109	96	104
3.0	Silty Clay	10	209	165	162	172
4.5	Silty Clay	17	243	196	194	202
6.0	Silty Clay	14	230	201	182	190
7.5	Clayey Silt	8	171	160	151	160
9.0	Silty Fine Sand	20	233	194	204	213
10.5	Silty Fine Sand	25	251	208	220	228
12.0	Silty Fine Sand	29	264	219	231	239
13.5	Silty Fine Sand	33	276	229	241	248
15.0	Silty Fine Sand	35	282	237	246	253

Table A3.29: SPT-N and Shear Wave Velocity at BJ03

Depth (m)	Soil Description	SPT-N Value	Shear wave velocity (m/s)			
			Ansary et al. (2010)	Ohta and Goto (1978)	Imai and Yoshimura (1970)	Ohba and Toriumi (1970)
1.5	Silty Clay	3	150	117	109	118
3.0	Silty Clay	14	230	175	182	190
4.5	Silty Clay	12	220	185	173	181
6.0	Clayey Silt	10	184	159	162	172
7.5	Clayey Silt	15	211	178	186	194
9.0	Silty Fine Sand	20	233	194	204	213
10.5	Silty Fine Sand	23	244	205	214	222
12.0	Silty Fine Sand	26	255	215	223	231
13.5	Silty Fine Sand	30	268	226	233	241
15.0	Silty Fine Sand	36	285	238	248	255

Table A3.30: SPT-N and Shear Wave Velocity at BJ04

Depth (m)	Soil Description	SPT-N Value	Shear wave velocity (m/s)			
			Ansary et al. (2010)	Ohta and Goto (1978)	Imai and Yoshimura (1970)	Ohba and Toriumi (1970)
1.5	Silty Clay	8	197	139	151	160
3.0	Silty Clay	13	225	173	177	186
4.5	Silty Clay	11	215	182	168	177
6.0	Silty Clay	9	203	186	157	166
7.5	Clayey Silt	10	184	166	162	172
9.0	Silty Fine Sand	16	216	187	190	198
10.5	Silty Fine Sand	21	237	202	208	216
12.0	Silty Fine Sand	27	258	216	226	233
13.5	Silty Fine Sand	33	276	229	241	248
15.0	Silty Fine Sand	39	292	241	255	262

Table A3.31: SPT-N and Shear Wave Velocity at BJ05

Depth (m)	Soil Description	SPT-N Value	Shear wave velocity (m/s)			
			Ansary et al. (2010)	Ohta and Goto (1978)	Imai and Yoshimura (1970)	Ohba and Toriumi (1970)
1.5	Silty Clay	6	182	132	137	146
3.0	Silty Clay	12	220	170	173	181
4.5	Silty Clay	13	225	187	177	186
6.0	Clayey Silt	10	184	159	162	172
7.5	Clayey Silt	13	201	174	177	186
9.0	Silty Fine Sand	20	233	194	204	213
10.5	Silty Fine Sand	25	251	208	220	228
12.0	Silty Fine Sand	30	268	220	233	241
13.5	Silty Fine Sand	35	282	232	246	253
15.0	Silty Fine Sand	40	295	242	257	264

Table A3.32: SPT-N and Shear Wave Velocity at NA01

Depth (m)	Soil Description	SPT-N Value	Shear wave velocity (m/s)			
			Ansary et al. (2010)	Ohta and Goto (1978)	Imai and Yoshimura (1970)	Ohba and Toriumi (1970)
1.5	Clayey Silt	2	107	92	96	104
3.0	Silty Clay	17	243	181	194	202
4.5	Silty Clay	18	247	198	197	206
6.0	Silty Clay	10	209	190	162	172
7.5	Fine Sandy Silty	16	216	180	190	198
9.0	Silty Fine Sand	18	225	191	197	206
10.5	Silty Fine Sand	23	244	205	214	222
12.0	Silty Fine Sand	23	244	211	214	222
13.5	Silty Fine Sand	26	255	220	223	231
15.0	Silty Fine Sand	33	276	234	241	248

Table A3.33: SPT-N and Shear Wave Velocity at NA02

Depth (m)	Soil Description	SPT-N Value	Shear wave velocity (m/s)			
			Ansary et al. (2010)	Ohta and Goto (1978)	Imai and Yoshimura (1970)	Ohba and Toriumi (1970)
1.5	Clayey Silt	2	107	92	96	104
3.0	Silty Clay	8	197	185	151	160
4.5	Silty Clay	20	254	203	204	213
6.0	Silty Clay	10	209	194	162	172
7.5	Sandy Silt	17	221	180	194	202
9.0	Silty Fine Sand	19	229	191	201	209
10.5	Silty Fine Sand	20	233	205	204	213
12.0	Silty Fine Sand	25	251	211	220	228
13.5	Silty Fine Sand	26	255	220	223	231
15.0	Silty Fine Sand	33	276	234	241	248

Table A3.34: SPT-N and Shear Wave Velocity at NA03

Depth (m)	Soil Description	SPT-N Value	Shear wave velocity (m/s)			
			Ansary et al. (2010)	Ohta and Goto (1978)	Imai and Yoshimura (1970)	Ohba and Toriumi (1970)
1.5	Clayey Silt	1	84	82	76	84
3.0	Silty Clay	11	215	168	168	177
4.5	Silty Clay	16	239	194	190	198
6.0	Silty Clay	19	251	212	201	209
7.5	Fine Sandy Silty	20	233	187	204	213
9.0	Silty Fine Sand	21	237	196	208	216
10.5	Silty Fine Sand	22	241	204	211	219
12.0	Silty Fine Sand	25	251	214	220	228
13.5	Silty Fine Sand	28	261	223	228	236
15.0	Silty Fine Sand	32	273	233	239	246

Table A3.35: SPT-N and Shear Wave Velocity at NA04

Depth (m)	Soil Description	SPT-N Value	Shear wave velocity (m/s)			
			Ansary et al. (2010)	Ohta and Goto (1978)	Imai and Yoshimura (1970)	Ohba and Toriumi (1970)
1.5	Silty Clay	5	172	128	129	138
3.0	Silty Clay	15	235	177	186	194
4.5	Silty Clay	19	251	200	201	209
6.0	Silty Clay	13	225	199	177	186
7.5	Fine Sandy Silty	13	201	174	177	186
9.0	Fine Sandy Silty	18	225	191	197	206
10.5	Silty Fine Sand	22	241	204	211	219
12.0	Silty Fine Sand	21	237	207	208	216
13.5	Silty Fine Sand	29	264	224	231	239
15.0	Silty Fine Sand	36	285	238	248	255

Table A3.36: SPT-N and Shear Wave Velocity at NA05

Depth (m)	Soil Description	SPT-N Value	Shear wave velocity (m/s)			
			Ansary et al. (2010)	Ohta and Goto (1978)	Imai and Yoshimura (1970)	Ohba and Toriumi (1970)
1.5	Clayey Silt	8	197	139	151	160
3.0	Silty Clay	13	225	173	177	186
4.5	Silty Clay	14	230	190	182	190
6.0	Silty Clay	10	209	190	162	172
7.5	Fine Sandy Silty	12	220	205	173	181
9.0	Silty Fine Sand	18	225	191	197	206
10.5	Silty Fine Sand	20	233	200	204	213
12.0	Silty Fine Sand	33	276	224	241	248
13.5	Silty Fine Sand	30	268	226	233	241
15.0	Silty Fine Sand	25	251	223	220	228
16.5	Silty Fine Sand	26	255	229	223	231
18.0	Silty Fine Sand	31	271	240	236	244
19.5	Silty Fine Sand	33	276	247	241	248

Table A3.37: SPT-N and Shear Wave Velocity at NA06

Depth (m)	Soil Description	SPT-N Value	Shear wave velocity (m/s)			
			Ansary et al. (2010)	Ohta and Goto (1978)	Imai and Yoshimura (1970)	Ohba and Toriumi (1970)
1.5	Silty Clay	9	203	141	157	166
3.0	Silty Clay	17	243	181	194	202
4.5	Silty Clay	25	271	209	220	228
6.0	Silty Clay	14	230	201	182	190
7.5	Fine Sandy Silty	10	184	153	162	172
9.0	Fine Sandy Silty	18	225	191	197	206
10.5	Silty Fine Sand	24	248	207	217	225
12.0	Silty Fine Sand	37	287	228	250	257
13.5	Silty Fine Sand	35	282	232	246	253
15.0	Silty Fine Sand	36	285	238	248	255

Table A3.38: SPT-N and Shear Wave Velocity at NA07

Depth (m)	Soil Description	SPT-N Value	Shear wave velocity (m/s)			
			Ansary et al. (2010)	Ohta and Goto (1978)	Imai and Yoshimura (1970)	Ohba and Toriumi (1970)
1.5	Silty Clay	2	107	107	96	104
3.0	Silty Clay	5	145	173	129	138
4.5	Silty Clay	22	261	196	211	219
6.0	Silty Clay	22	261	201	211	219
7.5	Fine Sandy Silty	10	184	174	162	172
9.0	Fine Sandy Silty	7	163	196	144	154
10.5	Silty Fine Sand	20	233	204	204	213
12.0	Silty Fine Sand	24	248	211	217	225
13.5	Silty Fine Sand	34	279	237	243	251
15.0	Silty Fine Sand	41	297	248	259	266

Table A3.39: SPT-N and Shear Wave Velocity at NA09

Depth (m)	Soil Description	SPT-N Value	Shear wave velocity (m/s)			
			Ansary et al. (2010)	Ohta and Goto (1978)	Imai and Yoshimura (1970)	Ohba and Toriumi (1970)
1.5	Clayey Silt	4	135	103	120	129
3.0	Silty Clay	18	247	183	197	206
4.5	Silty Clay	15	235	192	186	194
6.0	Silty Clay	10	209	190	162	172
7.5	Silty Clay	7	190	187	144	154
9.0	Fine Sandy Silty	15	211	185	186	194
10.5	Silty Fine Sand	21	237	202	208	216
12.0	Silty Fine Sand	21	237	207	208	216
13.5	Silty Fine Sand	32	273	228	239	246
15.0	Silty Fine Sand	33	276	234	241	248
16.5	Silty Fine Sand	40	295	247	257	264
18.0	Silty Fine Sand	42	300	253	261	268
19.5	Silty Fine Sand	44	305	259	265	271

Table A3.40: SPT-N and Shear Wave Velocity at NA10

Depth (m)	Soil Description	SPT-N Value	Shear wave velocity (m/s)			
			Ansary et al. (2010)	Ohta and Goto (1978)	Imai and Yoshimura (1970)	Ohba and Toriumi (1970)
1.5	Clayey Silt	5	145	107	129	138
3.0	Silty Clay	13	225	177	177	186
4.5	Silty Clay	17	243	201	194	202
6.0	Silty Clay	14	230	206	182	190
7.5	Silty Fine Sand	13	201	174	177	186
9.0	Silty Fine Sand	21	237	196	208	216
10.5	Silty Fine Sand	22	241	204	211	219
12.0	Silty Fine Sand	23	244	211	214	222
13.5	Silty Fine Sand	40	295	237	257	264
15.0	Silty Fine Sand	46	309	248	269	275

APPENDIX-B

MICROTREMOR H/V RATIO AT 45 LOCATIONS IN DHAKA CITY

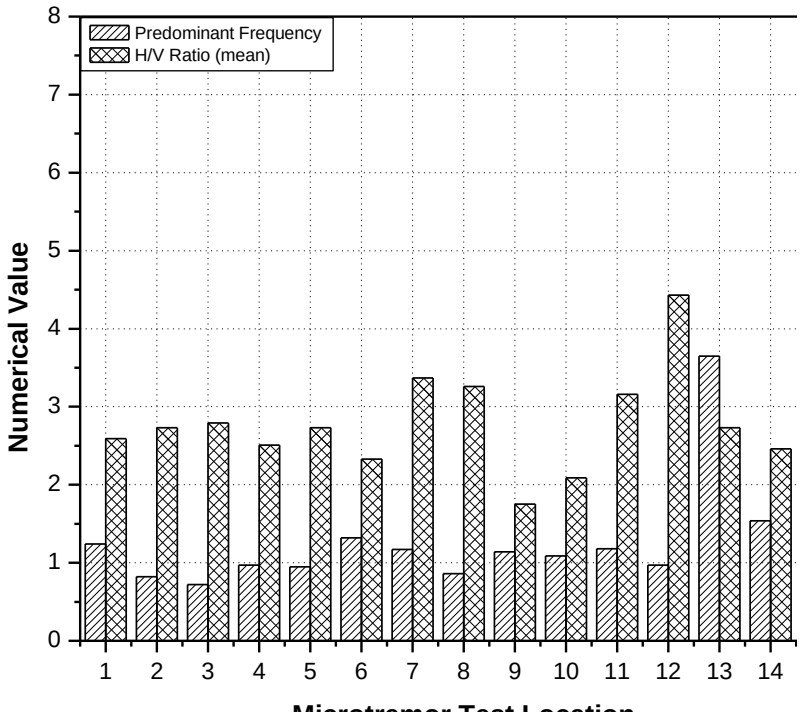

(a) Microtremor Test Location from 1 to 15

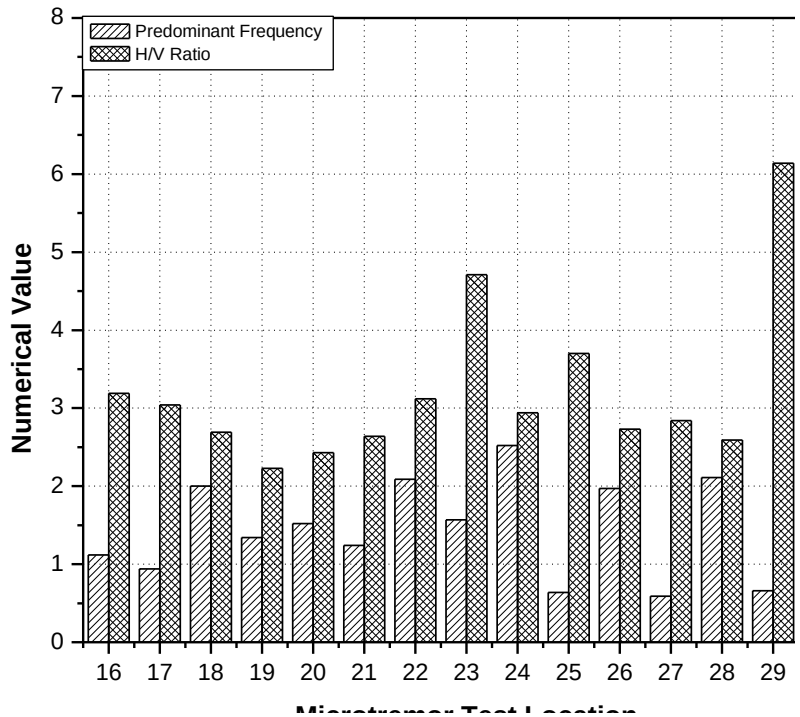

(b) Microtremor Test Location from 16 to 30

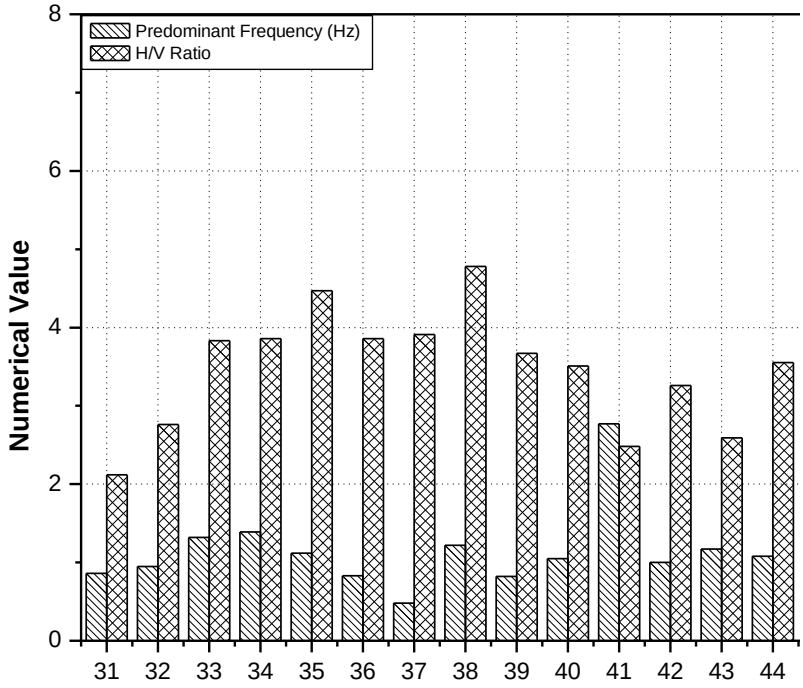

Figure B3.30 [(a), (b) and (c)]: Predominant Frequency and H/V ratio at 45 sites in and around Dhaka city.

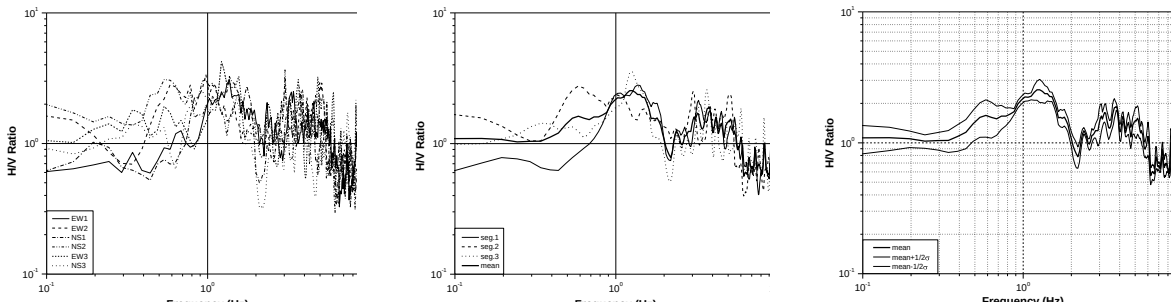

Figure B3.31: Predominant frequency and H/V ratio at National University.

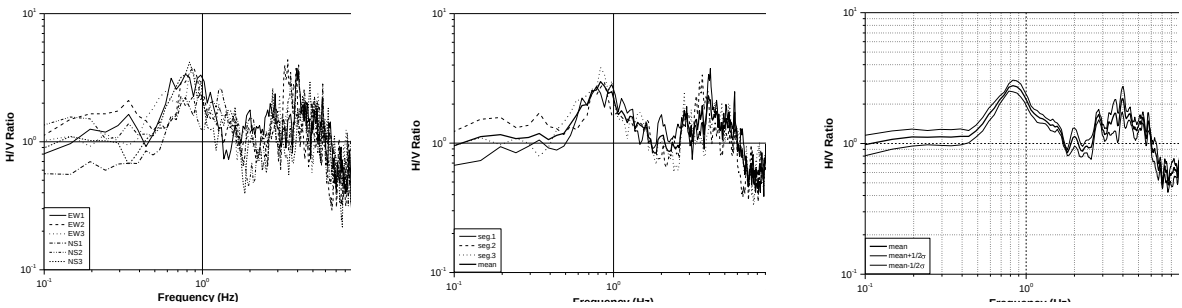

Figure B3.32: Predominant frequency and H/V ratio at Board Bazar Gazipur.

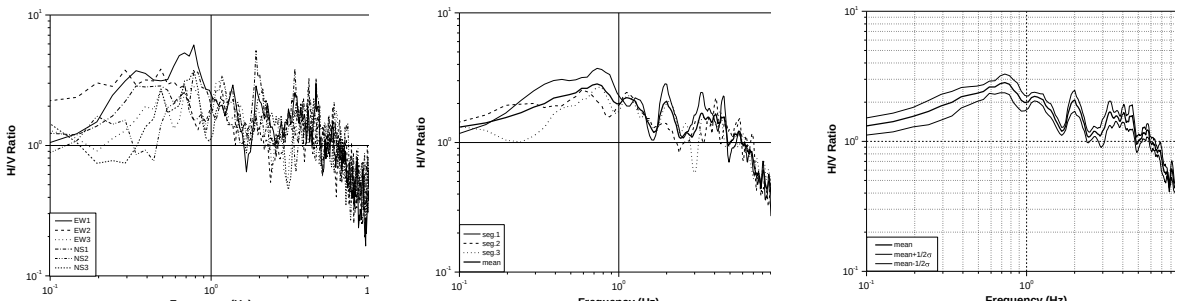

Figure B3.33: Predominant frequency and H/V ratio at Kaunia, Boro Bari.

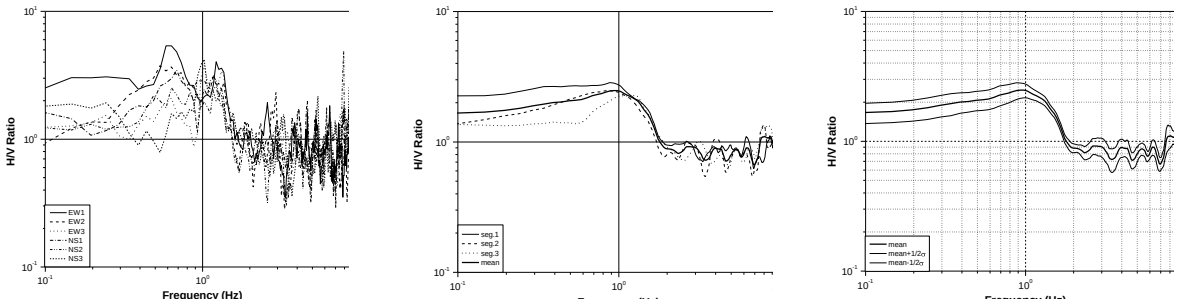

Figure B3.34: Predominant frequency and H/V ratio at Tongi, Ershadnagar.

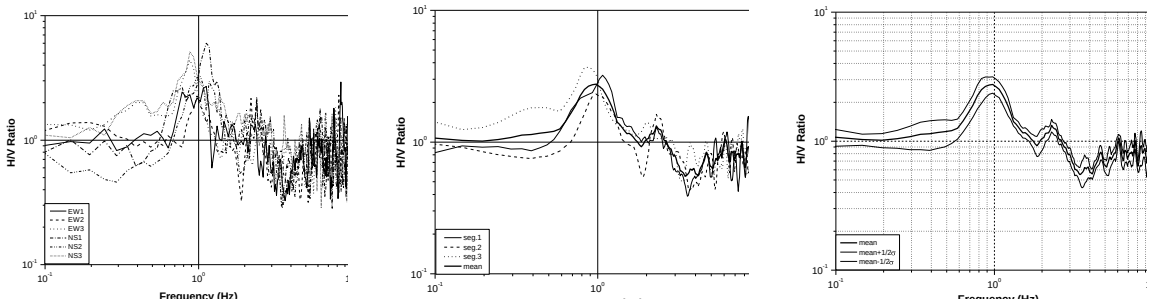

Figure B3.35: Predominant frequency and H/V ratio at Tongi BSCIC area.

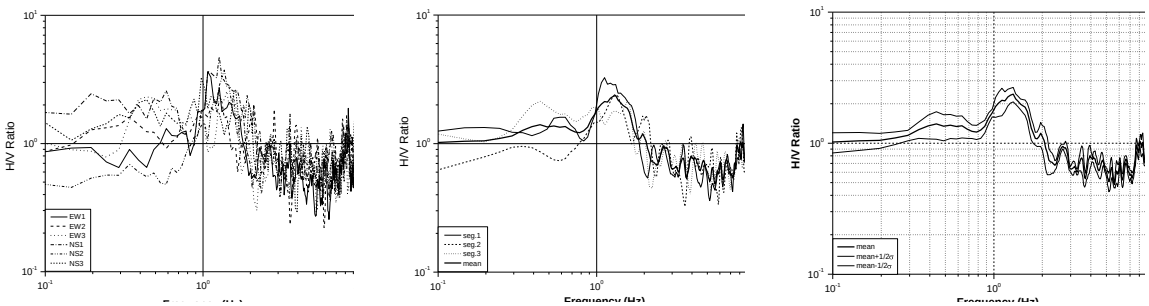

Figure B3.36: Predominant frequency and H/V Ratio at Abdullahpur.

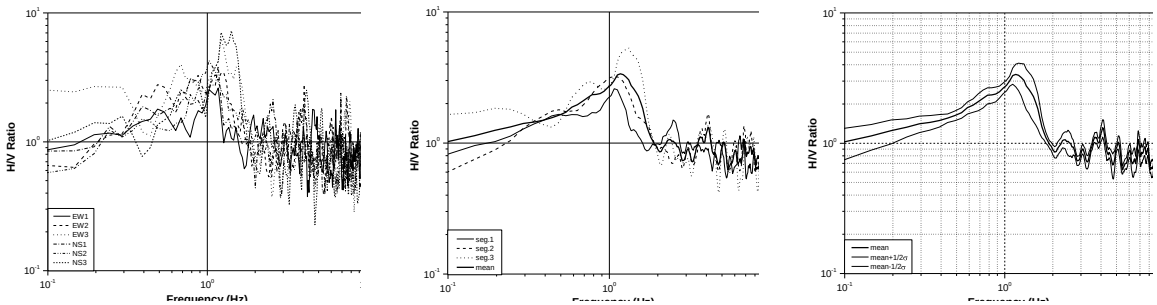

Figure B3.37: Predominant frequency and H/V ratio at Ijtema Field (North and East side).

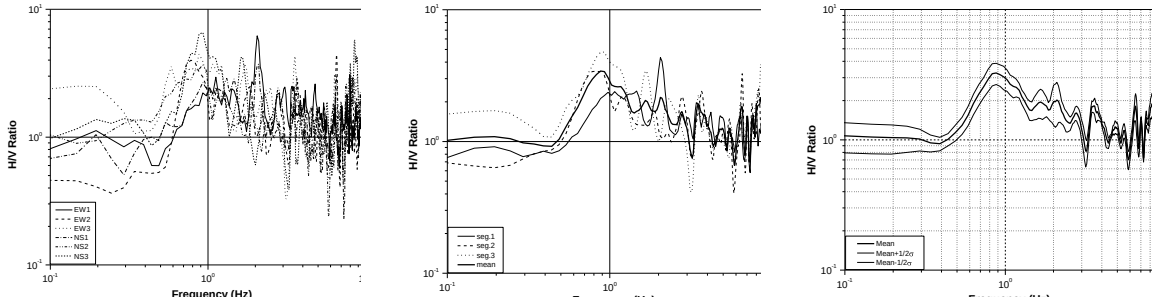

Figure B3.38: Predominant frequency and H/V ratio at Ijtema Field (South and West side).

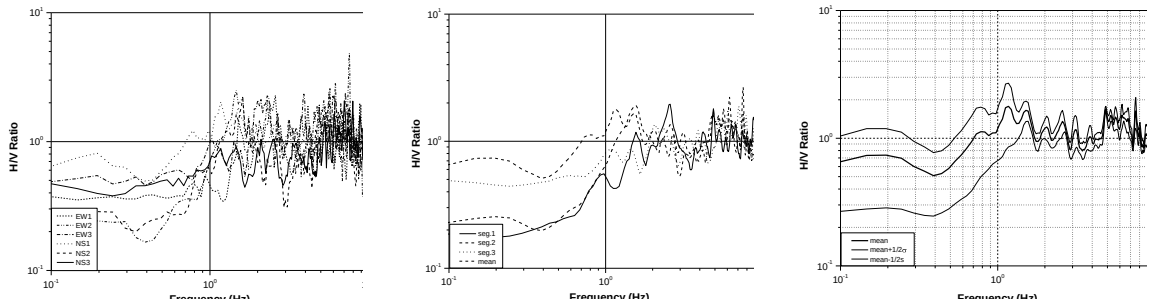

Figure B3.39: Predominant frequency and H/V Ratio at Ashulia Toll Plaza.

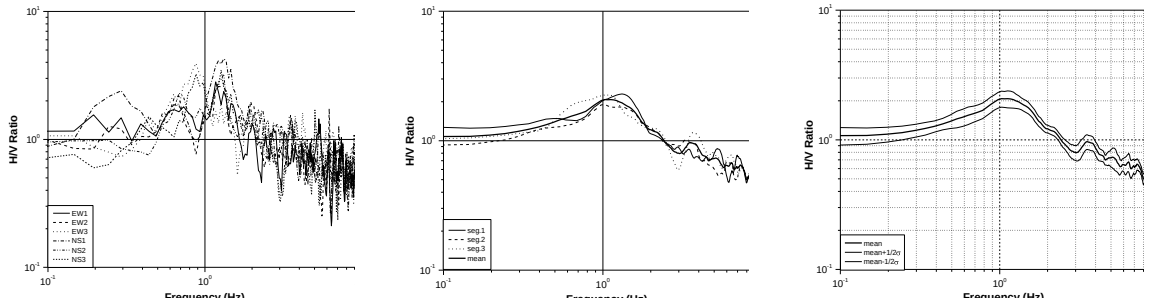

Figure B3.40: Predominant frequency and H/V ratio at Uttar Khan.

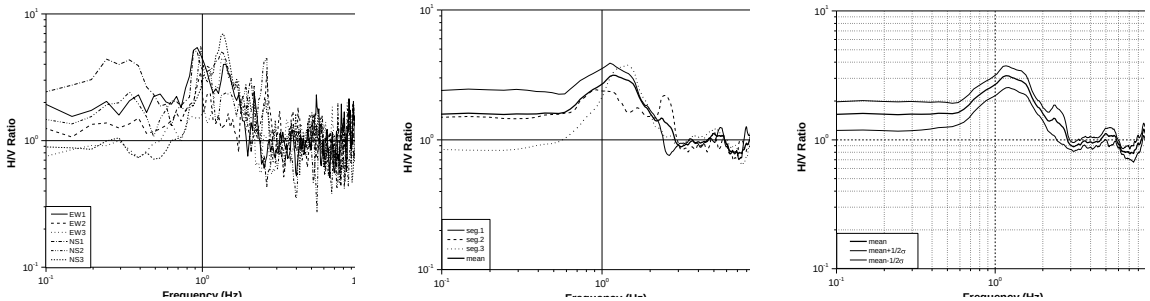

Figure B3.41: Predominant frequency and H/V ratio at Uttara Phase-3 (North Side).

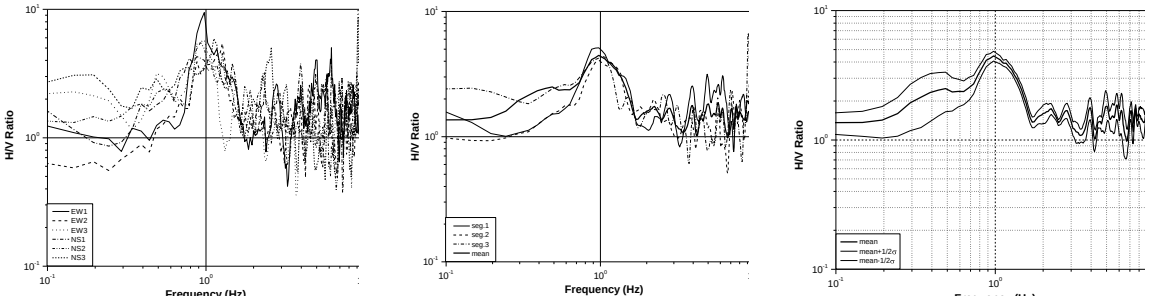

Figure B3.42: Predominant frequency and H/V ratio at Uttara Phase-3 (South Side).

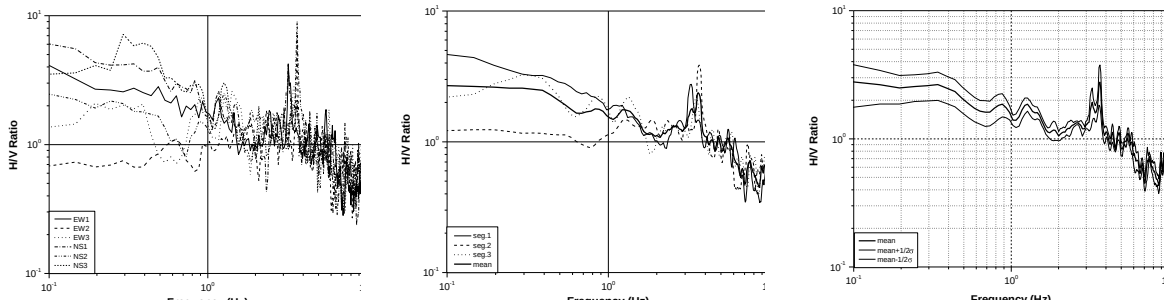

Figure B3.43: Predominant frequency and H/V ratio at Uttara Azampur.

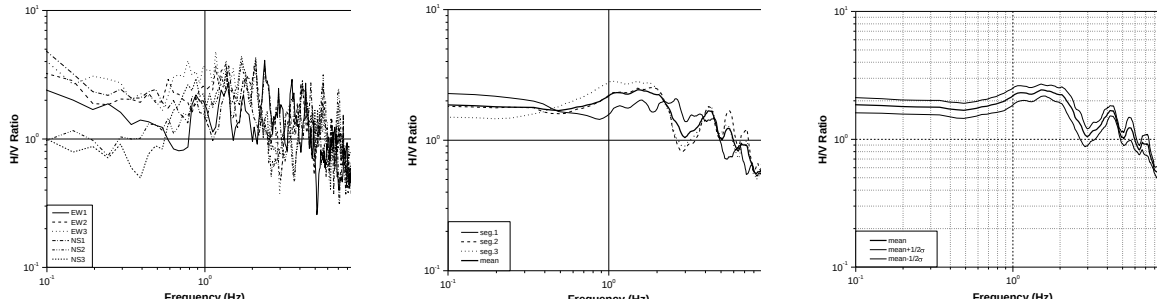

Figure B3.44: Predominant frequency and H/V ratio at Mirpur DOHS (South side).

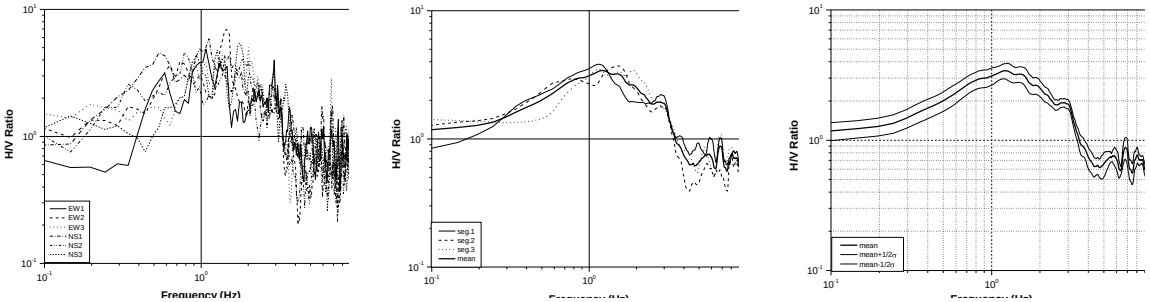

Figure B3.45: Predominant frequency and H/V ratio at Mirpur DOHS (North side).

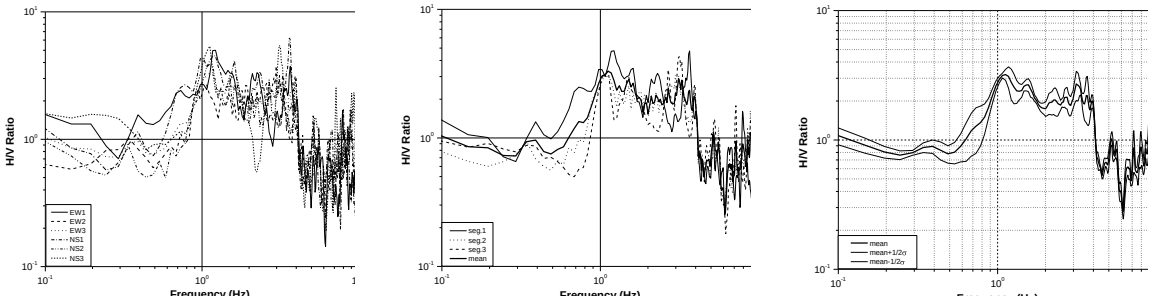

Figure B3.46: Predominant frequency and H/V Ratio at Ashiyan City.

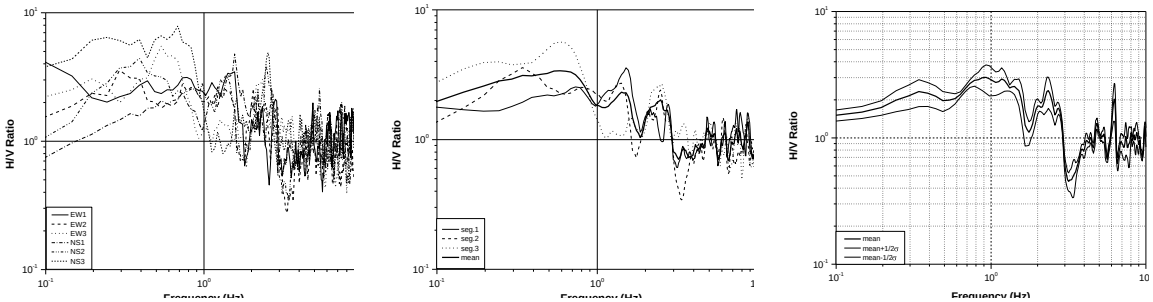

Figure B3.47: Predominant frequency and H/V ratio at Randokpur, RupGanj.

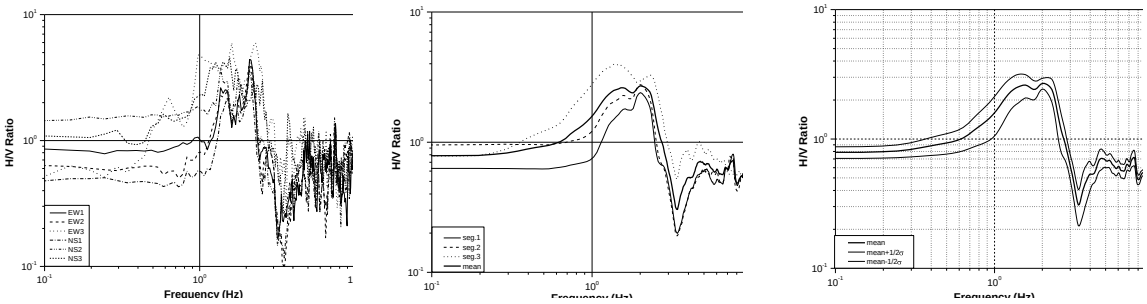

Figure B3.48: Predominant frequency and H/V ratio at American City, Purbachal.

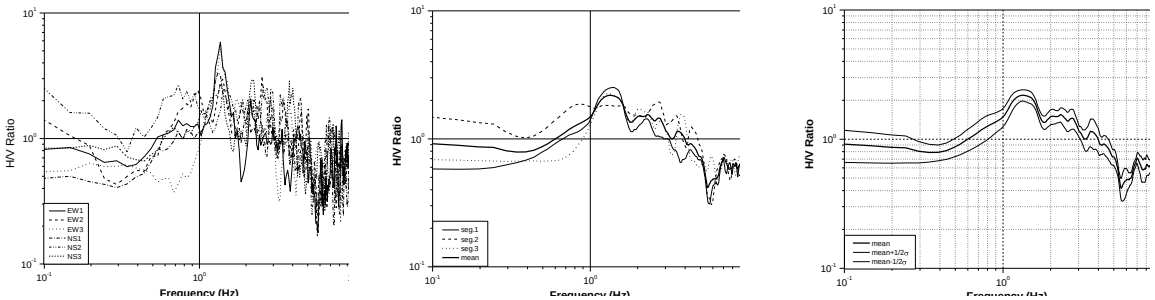

Figure B3.49: Predominant frequency and H/V ratio at Picnic Park, Gazipur.

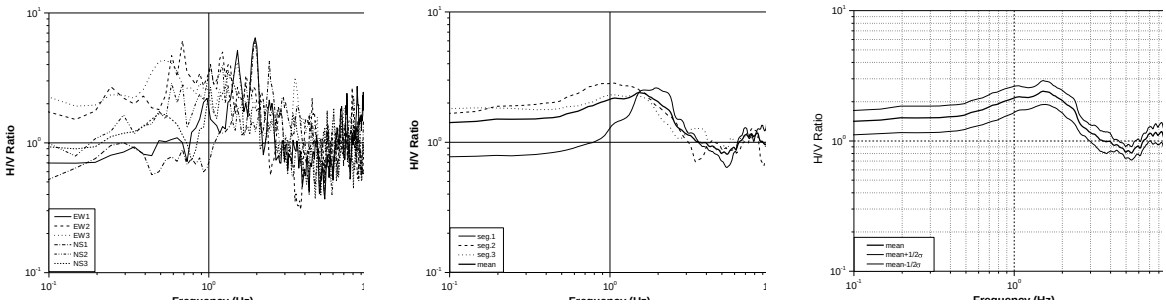

Figure B3.50: Predominant frequency and H/V Ratio at Mirpur Zoo.

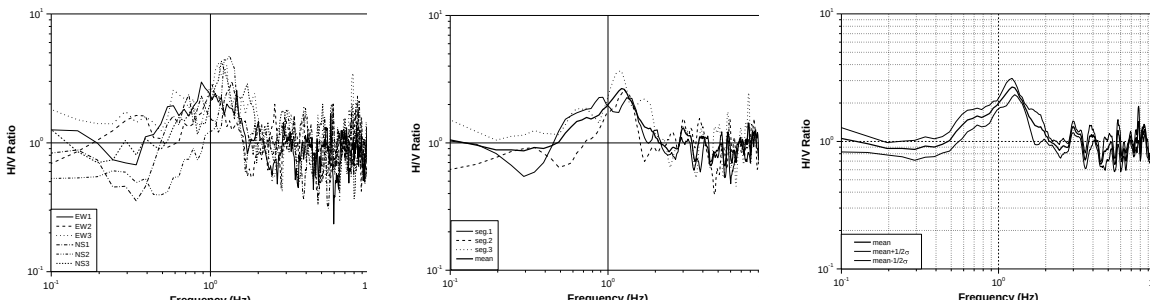

Figure B3.51: Predominant frequency and H/V ratio at Pallabi.

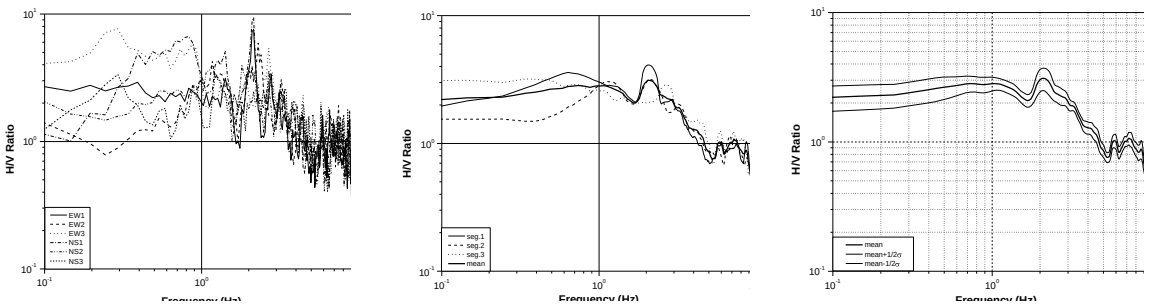

Figure B3.52: Predominant frequency and H/V ratio at Block-B, Bashundhara.

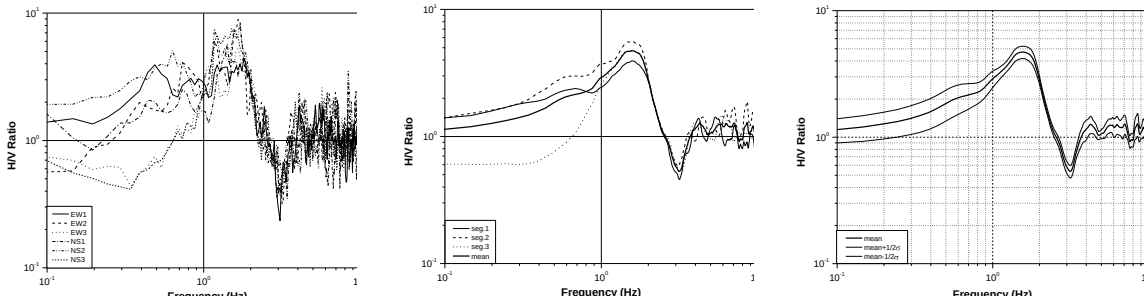

Figure B3.53: Predominant frequency and H/V ratio at Block-D, Bashundhara.

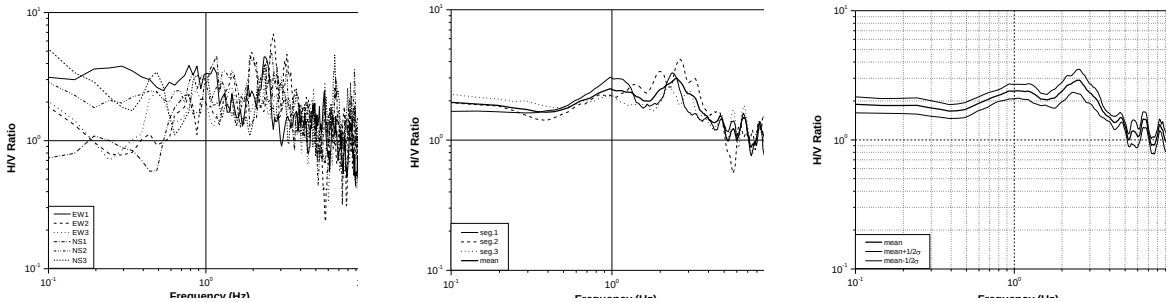

Figure B3.54: Predominant frequency and H/V ratio at Block-H, Bashundhara.

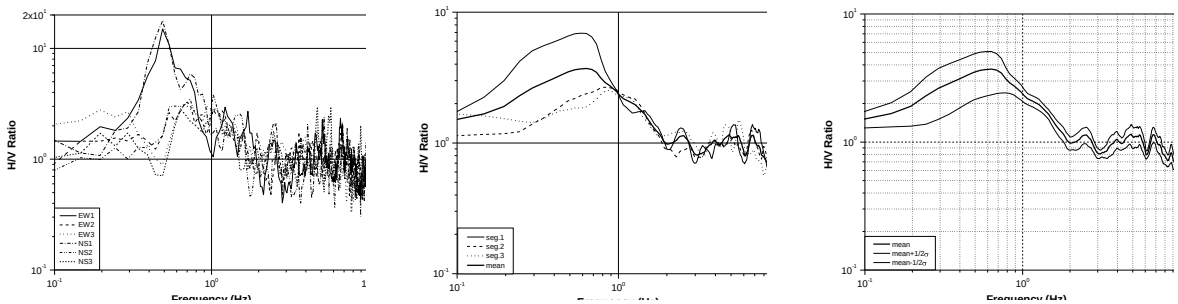

Figure B3.55: Predominant frequency and H/V ratio at Civil Aviation Field.

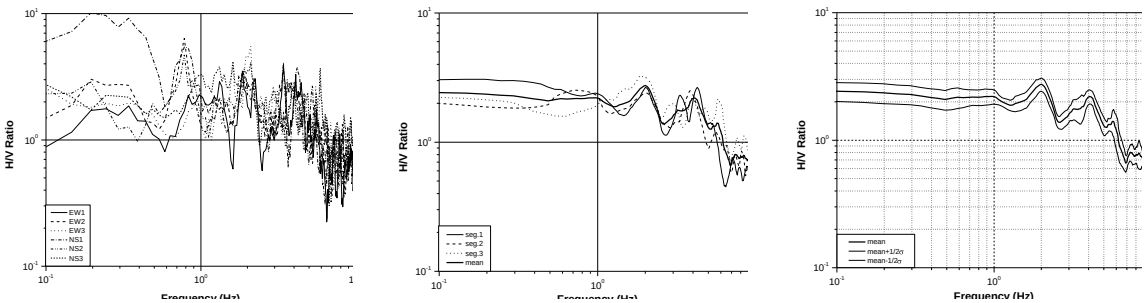

Figure B3.56: Predominant frequency and H/V ratio at Kuril, Flyover.

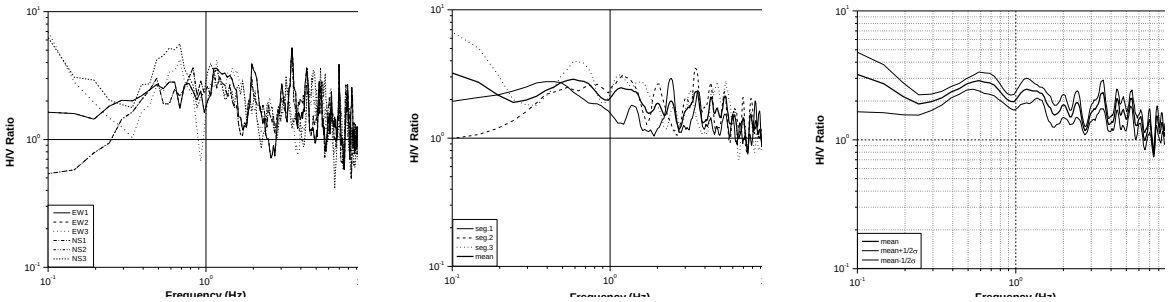

Figure B3.57: Predominant frequency and H/V ratio at Sarengbari.

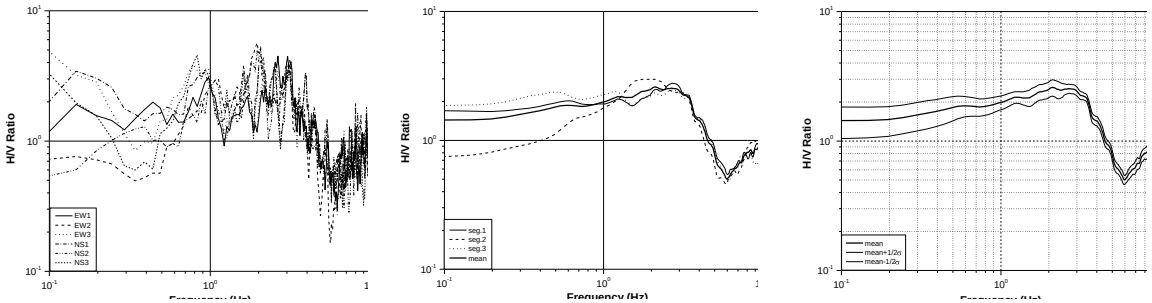

Figure B3.58: Predominant frequency and H/V ratio at Purachal, Uttar Badda.

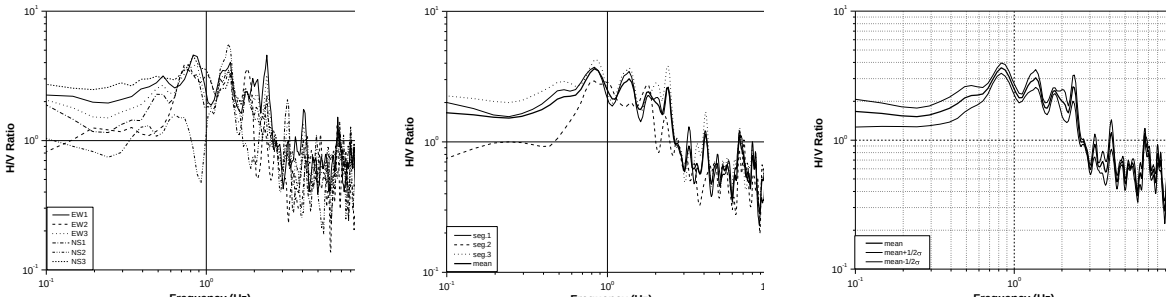

Figure B3.59: Predominant frequency and H/V ratio at Gabtoli City Corporation.

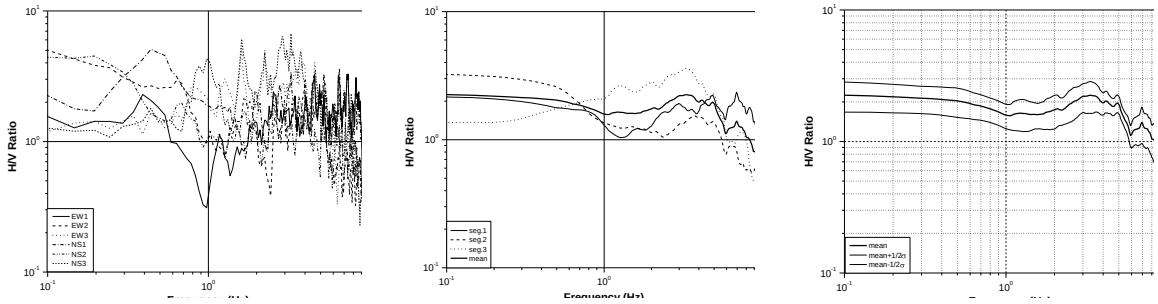

Figure B3.60: Predominant frequency and H/V Ratio at Adabor.

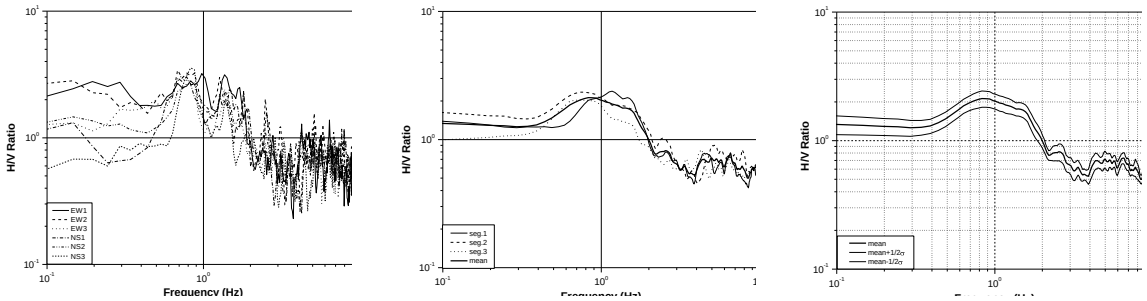

Figure B3.61: Predominant frequency and H/V Ratio at Agargaon Trade Fair.

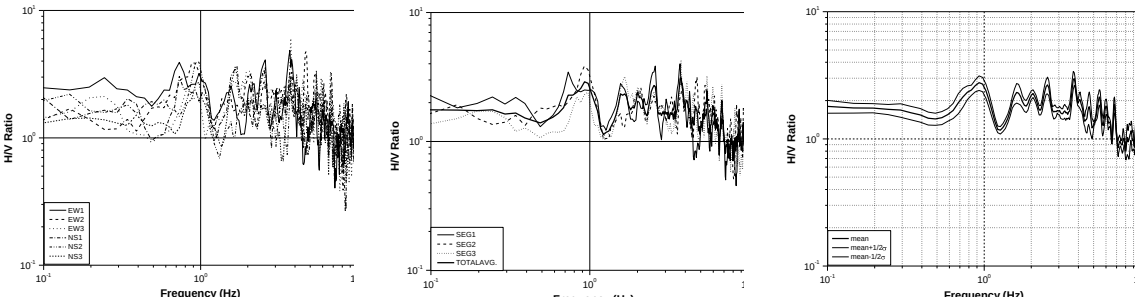

Figure B3.62: Predominant frequency and H/V Ratio at Aftab Nagar Housing Project.

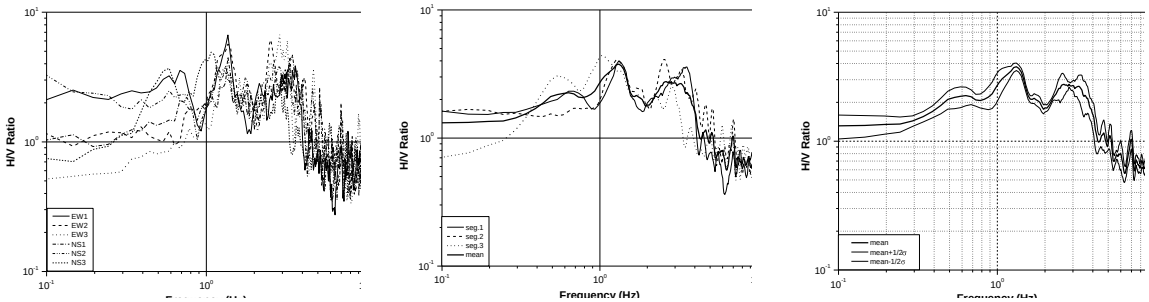

Figure B3.63: Predominant frequency and H/V Ratio at Nadda.

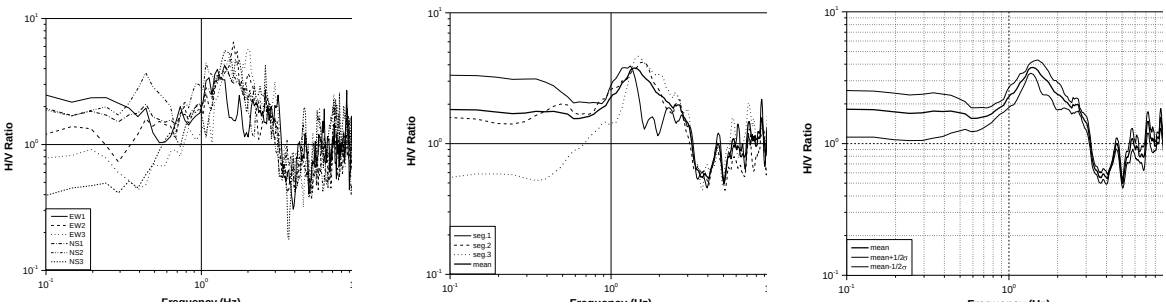

Figure B3.64: Predominant frequency and H/V ratio at South Banasree.

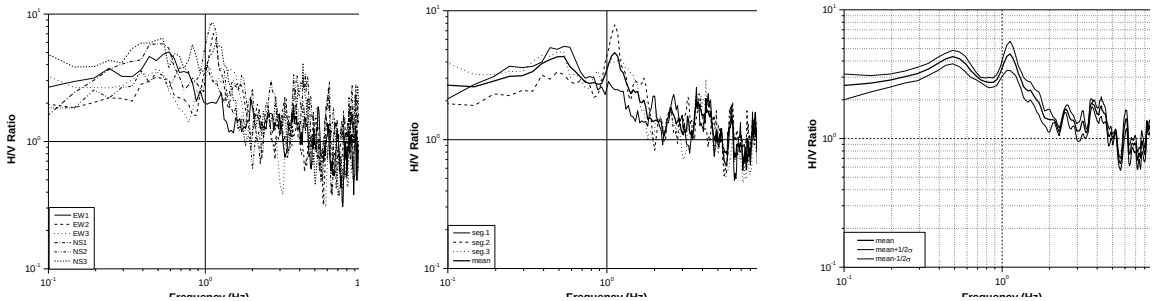

Figure B3.65: Predominant frequency and H/V ratio at Basila Garden City.

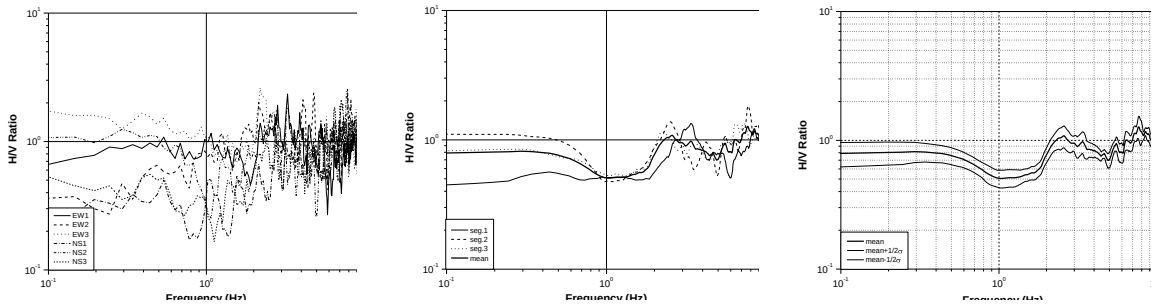

Figure B3.66: Predominant frequency and H/V ratio at Royer Bazar.

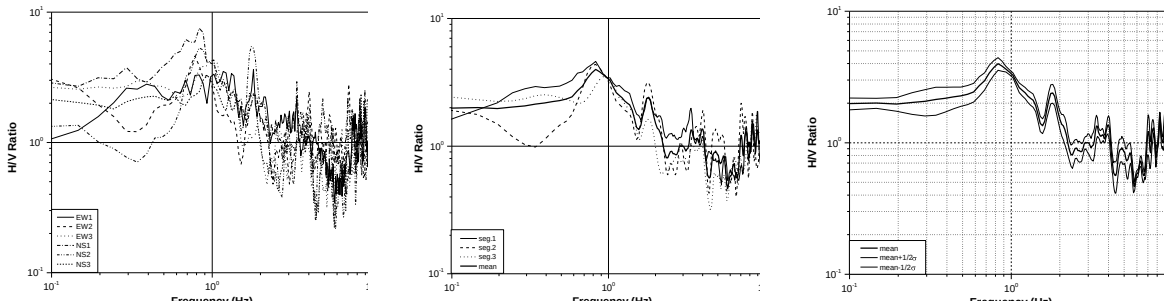

Figure B3.67: Predominant frequency and H/V ratio at Hazaribagh.

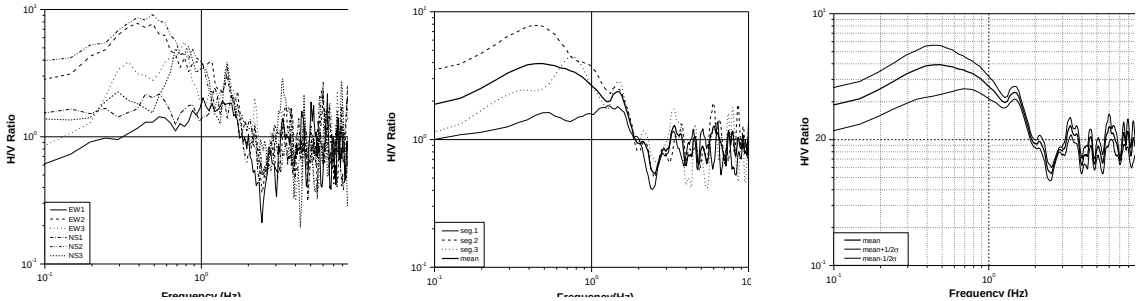

Figure B3.68: Predominant frequency and H/V ratio at Rab-10 Plot, Kamrangirchar.

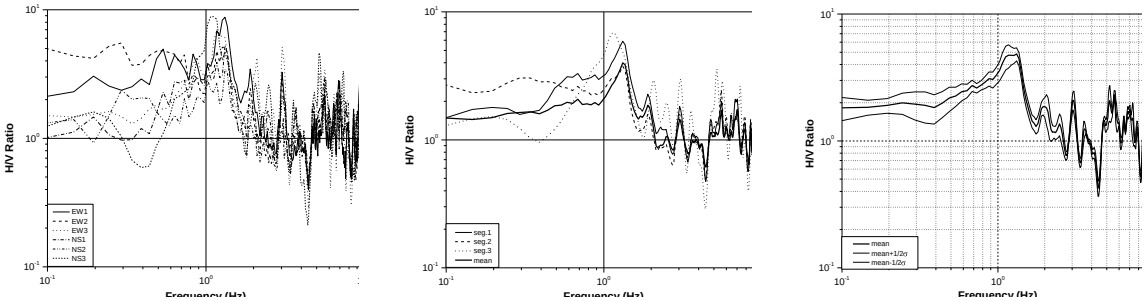

Figure B3.69: Predominant frequency and H/V ratio at Sosan Ghat, Kamrangirchar.

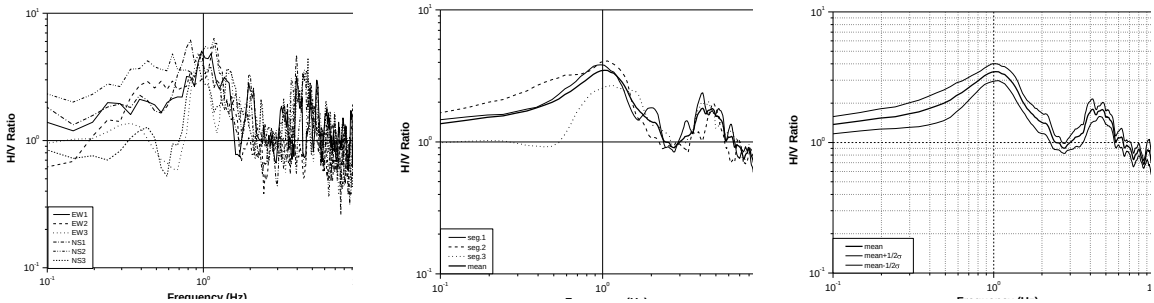

Figure B3.70: Predominant frequency and H/V ratio at Bashundhara Riverview Project.

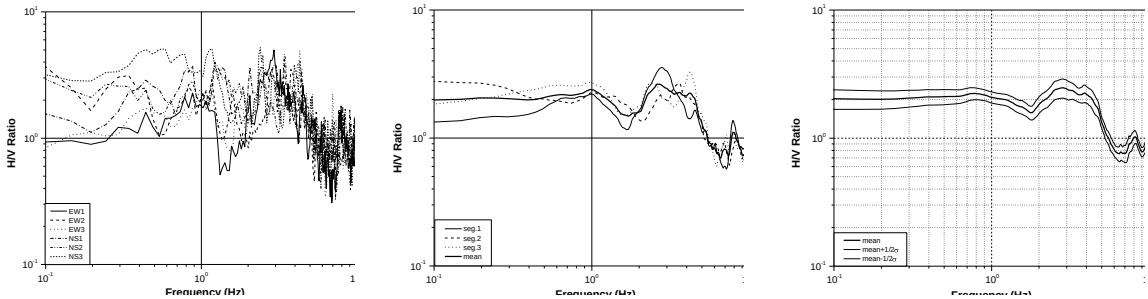

Figure B3.71: Predominant frequency and H/V ratio at Matuail, Demra.

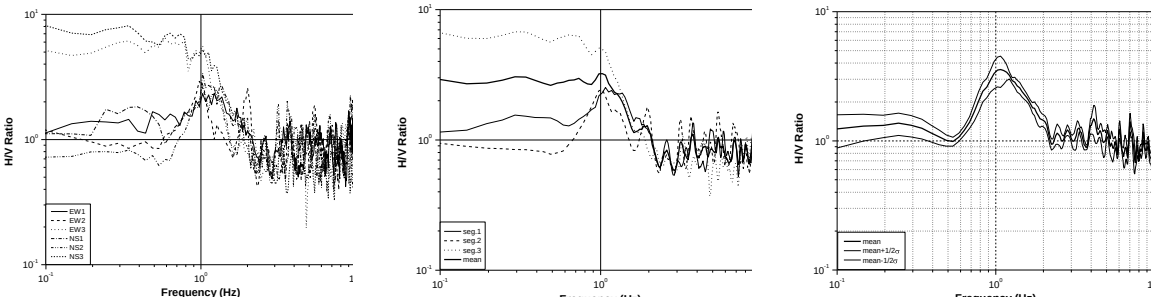

Figure B3.72: Predominant frequency and H/V ratio at Jilmil Project.

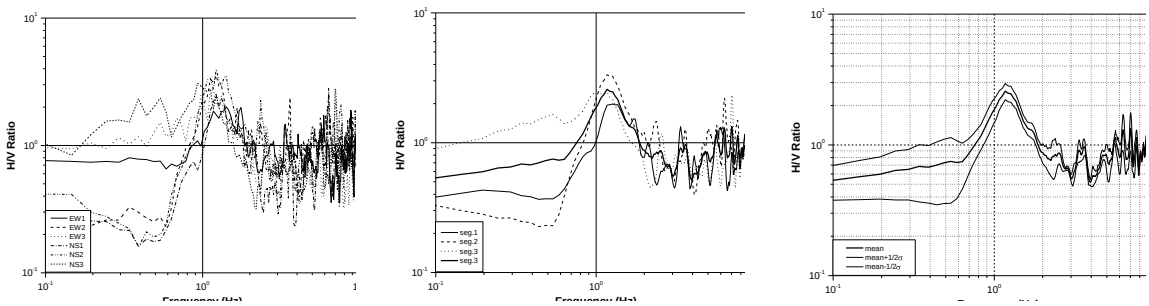

Figure B3.73: Predominant frequency and H/V ratio at Rajendapur.

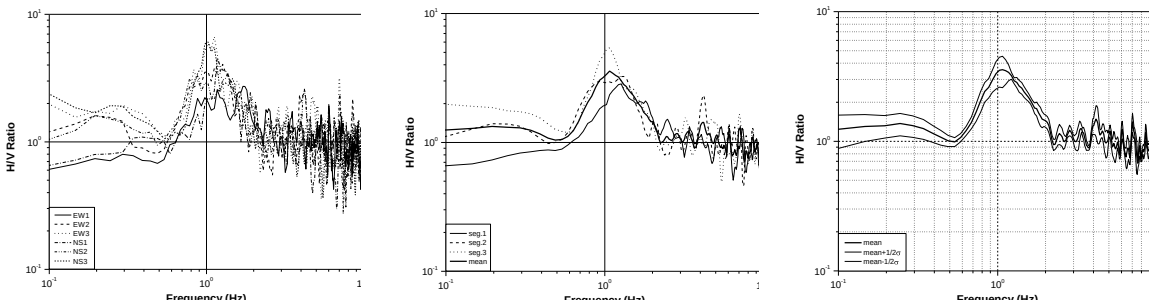

Figure B3.74: Predominant frequency and H/V ratio at Bramangaon.

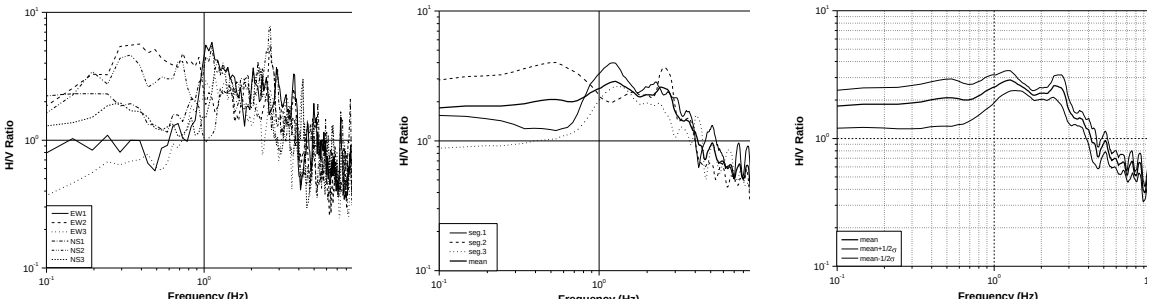

Figure B3.75: Predominant frequency and H/V ratio at Meradia, Dhaka.

APPENDIX-C

MICROTREMOR H/V RATIO AT 132 LOCATIONS WITHIN BUET CAMPUS

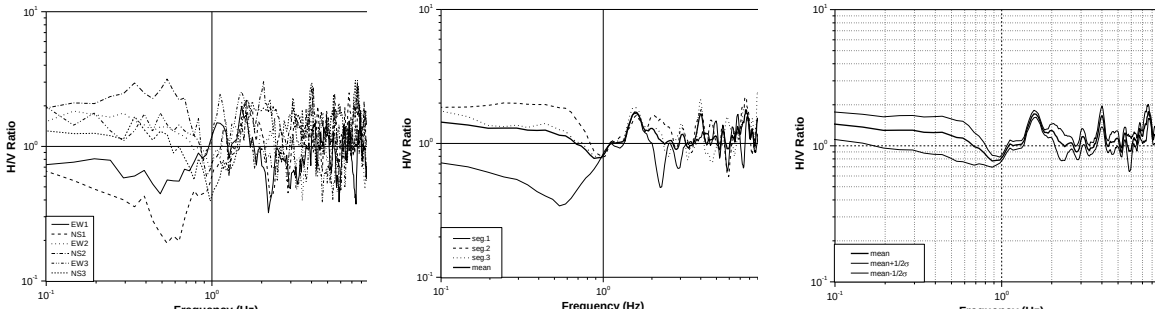

Figure C3.76: Predominant Frequency and H/V Ratio at MT01.

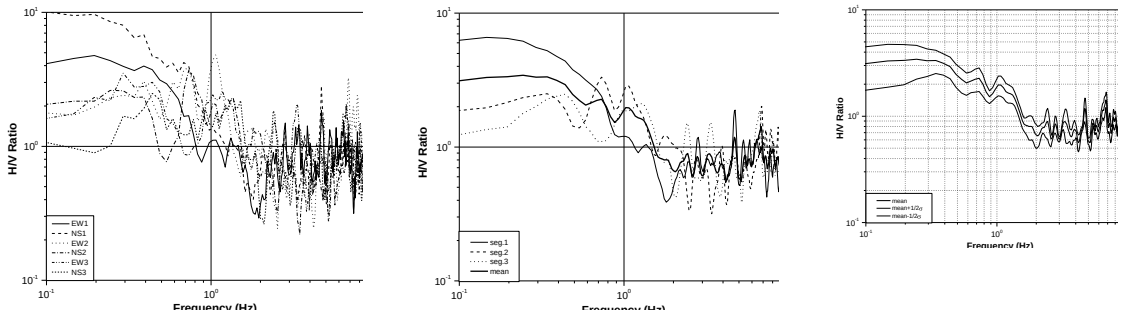

Figure C3.77: Predominant Frequency and H/V Ratio at MT02.

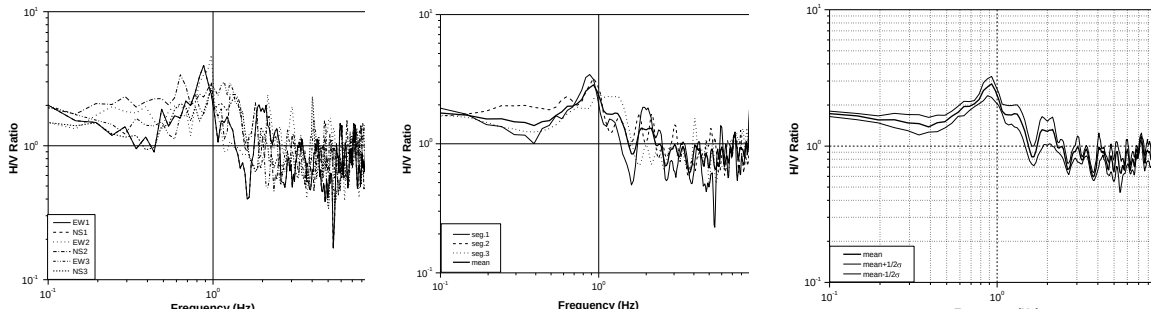

Figure C3.78: Predominant Frequency and H/V Ratio at MT03.

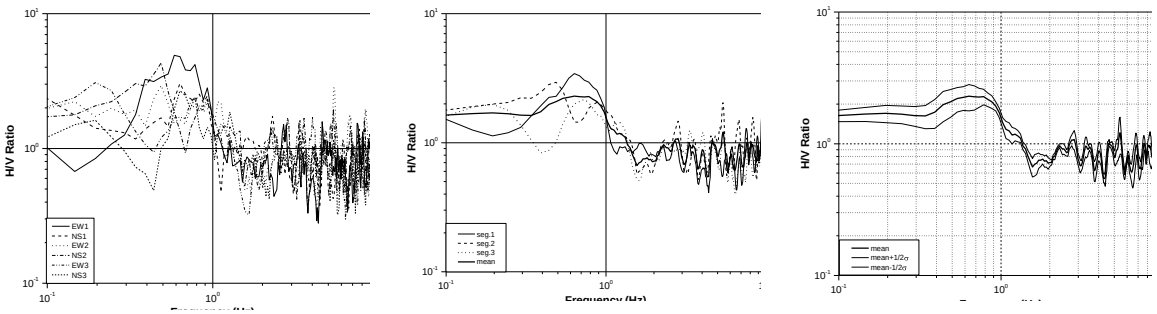

Figure C3.79: Predominant Frequency and H/V Ratio at MT04.

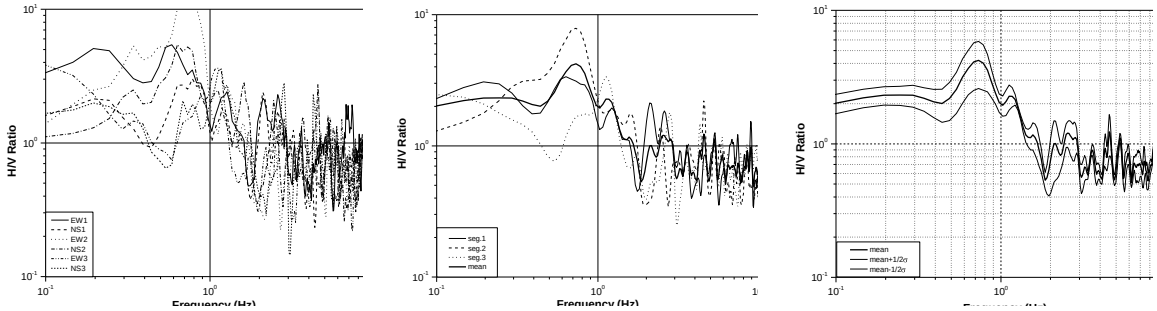

Figure C3.80: Predominant Frequency and H/V Ratio at MT05.

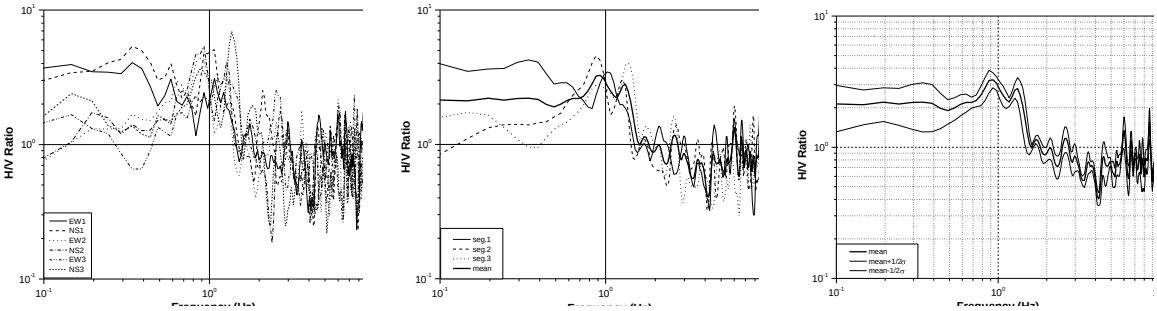

Figure C3.81: Predominant Frequency and H/V Ratio at MT06.

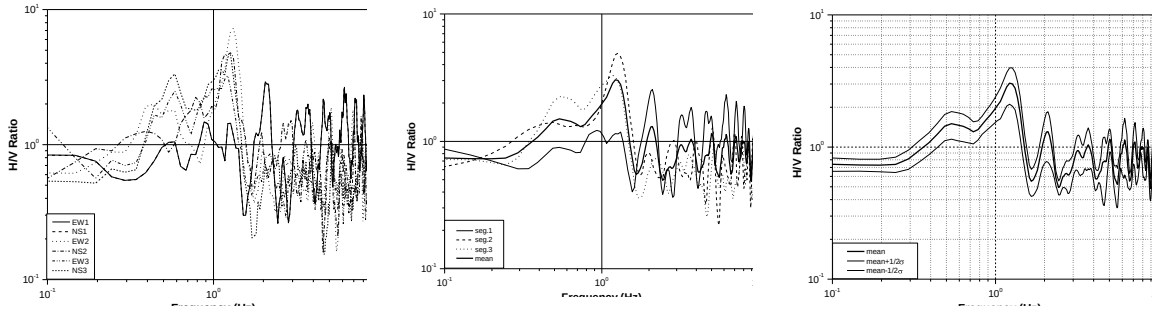

Figure C3.82: Predominant Frequency and H/V Ratio at MT07.

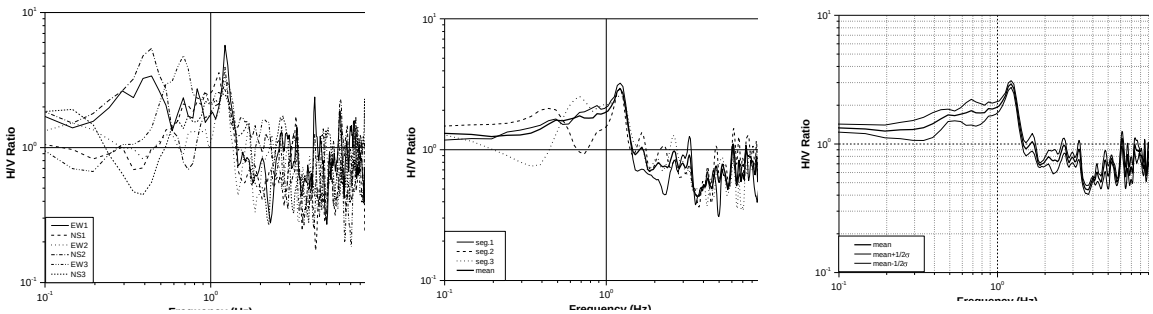

Figure C3.83: Predominant Frequency and H/V Ratio at MT08.

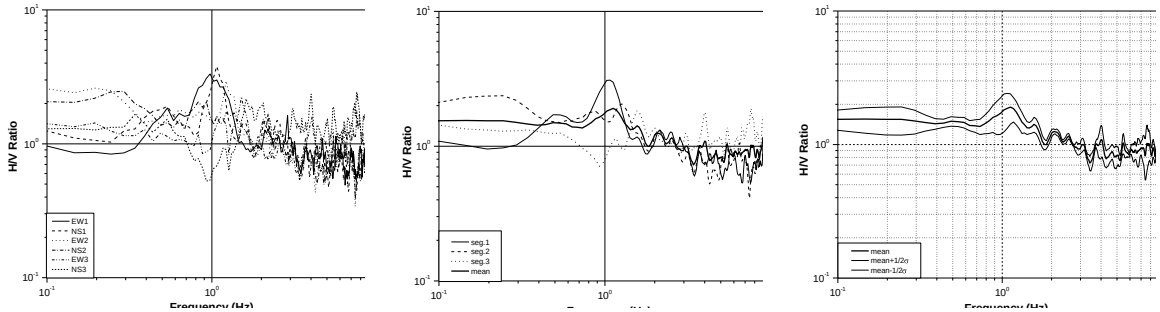

Figure C3.84: Predominant Frequency and H/V Ratio at MT09.

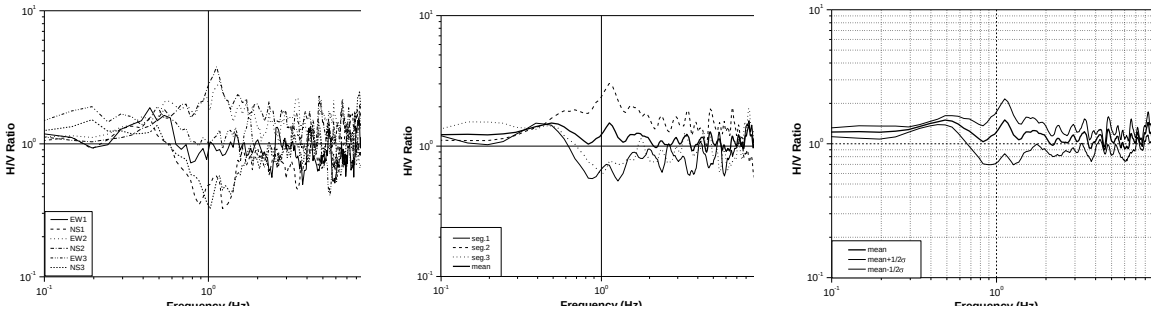

Figure C3.85: Predominant Frequency and H/V Ratio at MT10.

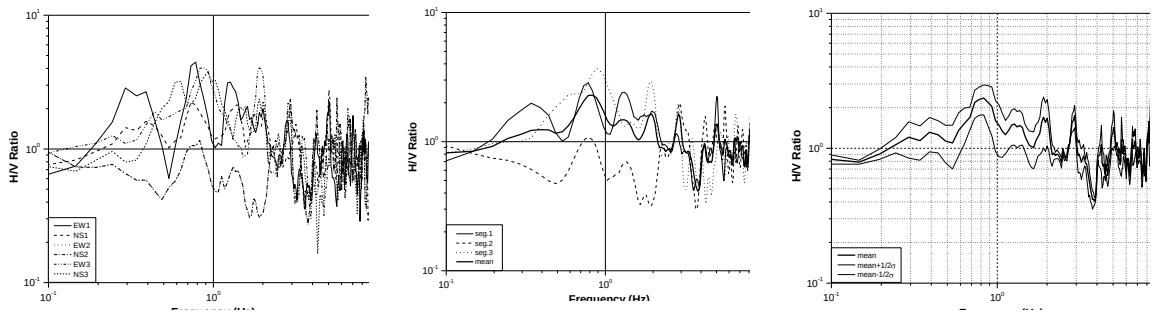

Figure C3.86: Predominant Frequency and H/V Ratio at MT11.

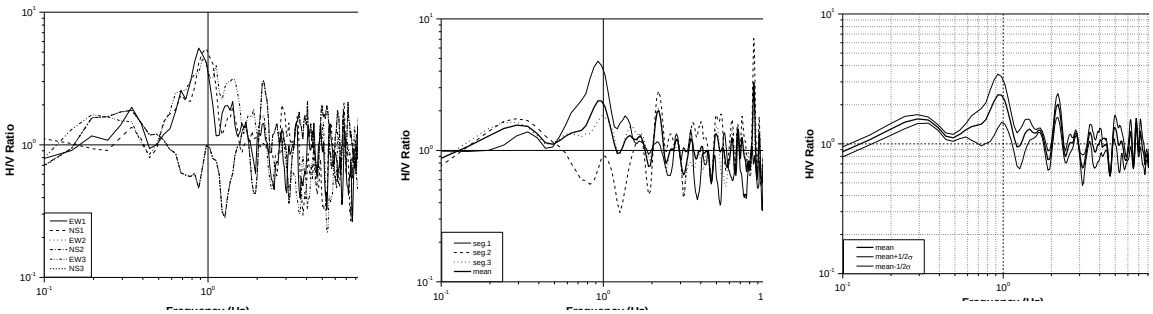

Figure C3.87: Predominant Frequency and H/V Ratio at MT12.

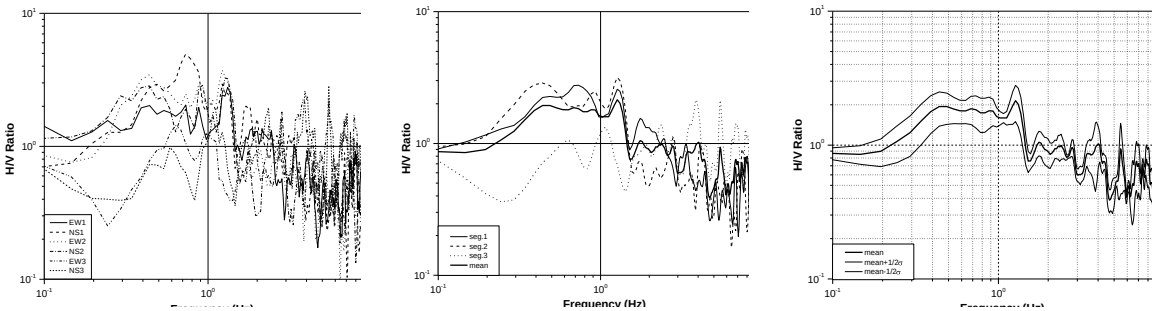

Figure C3.88: Predominant Frequency and H/V Ratio at MT13.

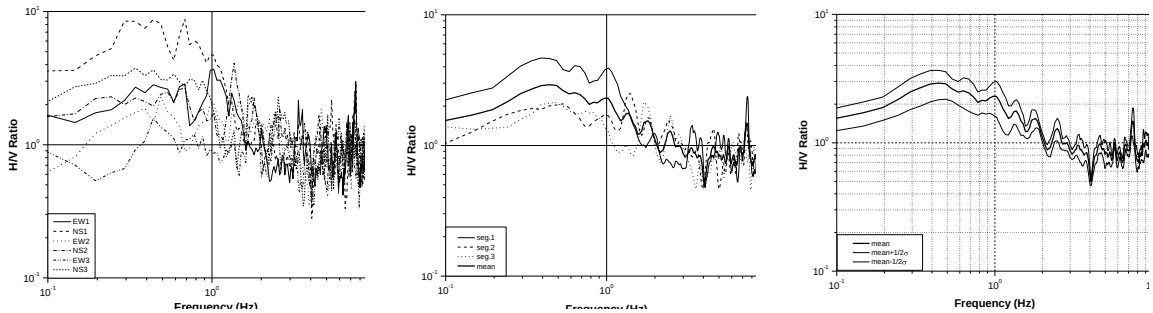

Figure C3.89: Predominant Frequency and H/V Ratio at MT14.

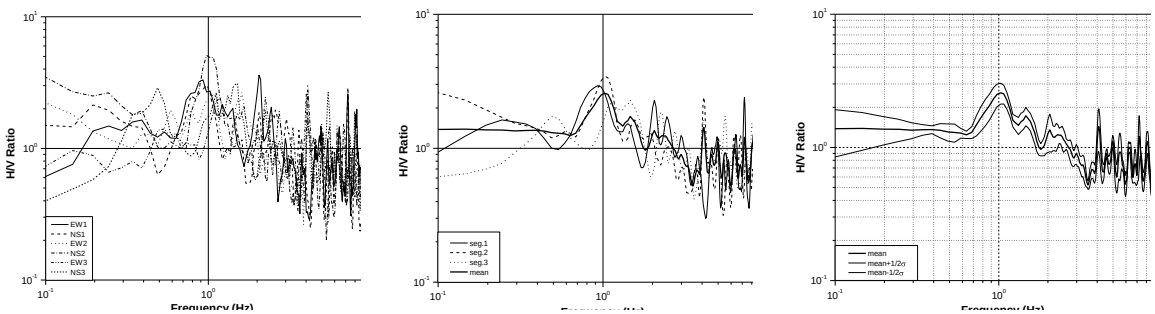

Figure C3.90: Predominant Frequency and H/V Ratio at MT15.

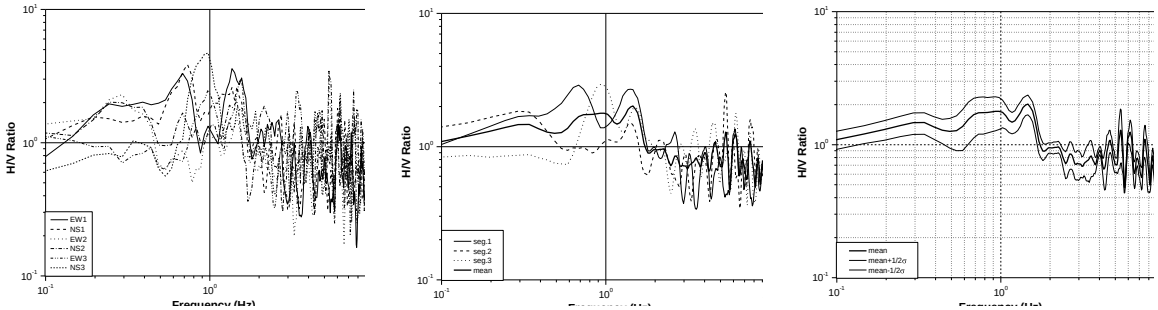

Figure C3.91: Predominant Frequency and H/V Ratio at MT16.

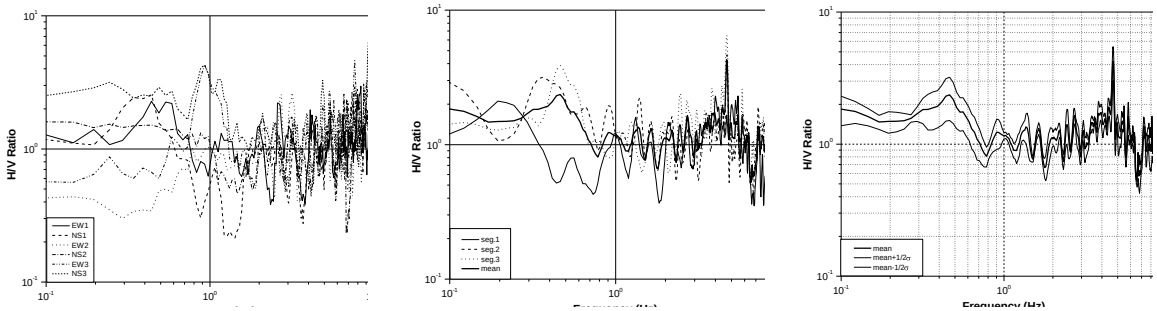

Figure C3.92: Predominant Frequency and H/V Ratio at MT17.

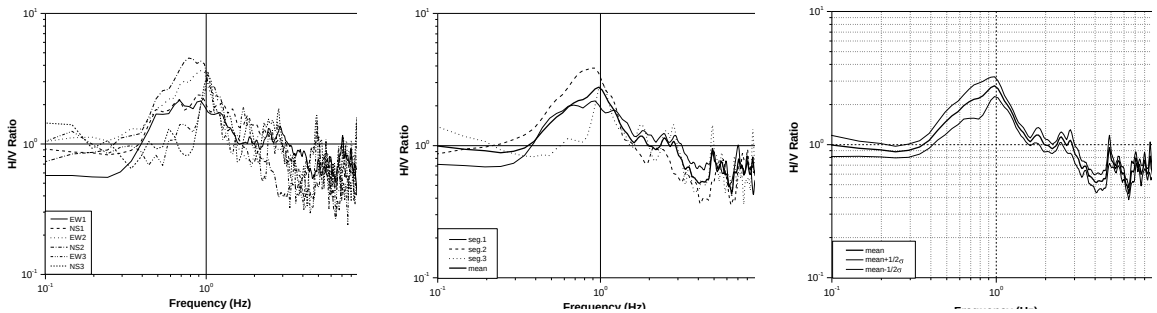

Figure C3.93: Predominant Frequency and H/V Ratio at MT18.

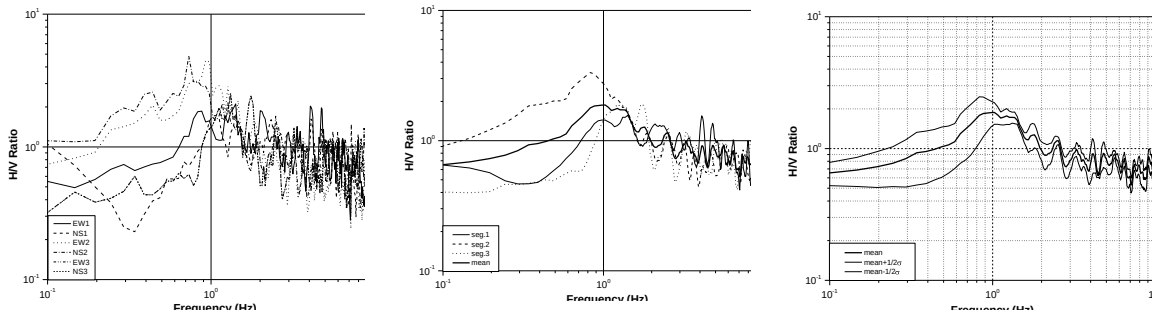

Figure C3.94: Predominant Frequency and H/V Ratio at MT19.

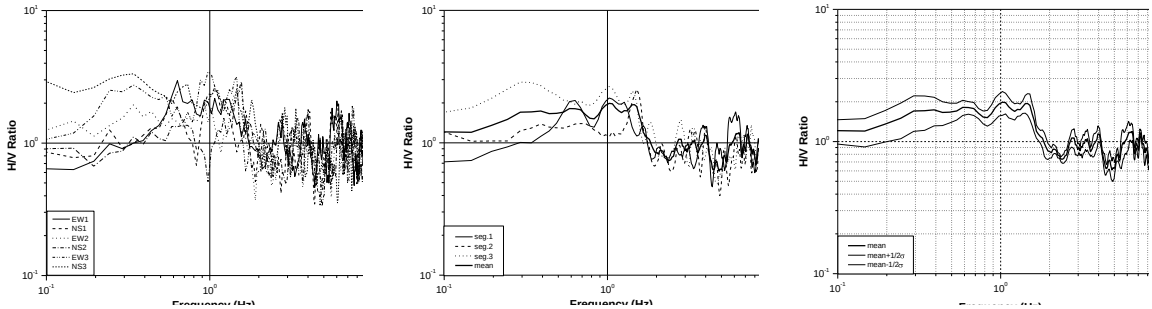

Figure C3.95: Predominant Frequency and H/V Ratio at MT20.

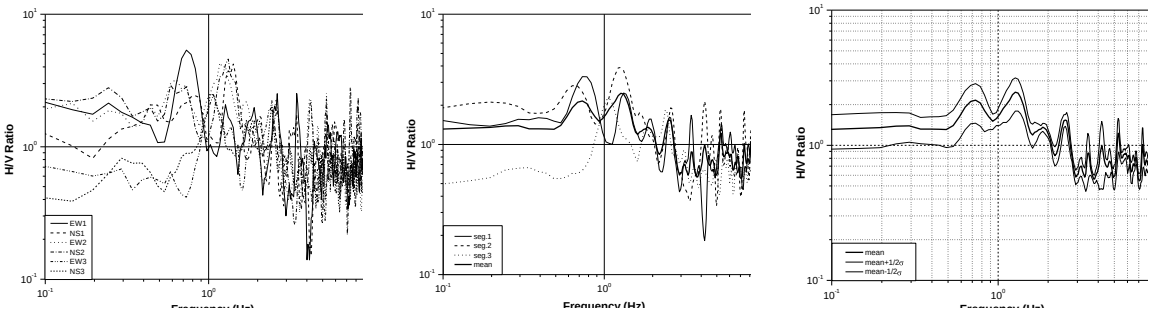

Figure C3.96: Predominant Frequency and H/V Ratio at MT21.

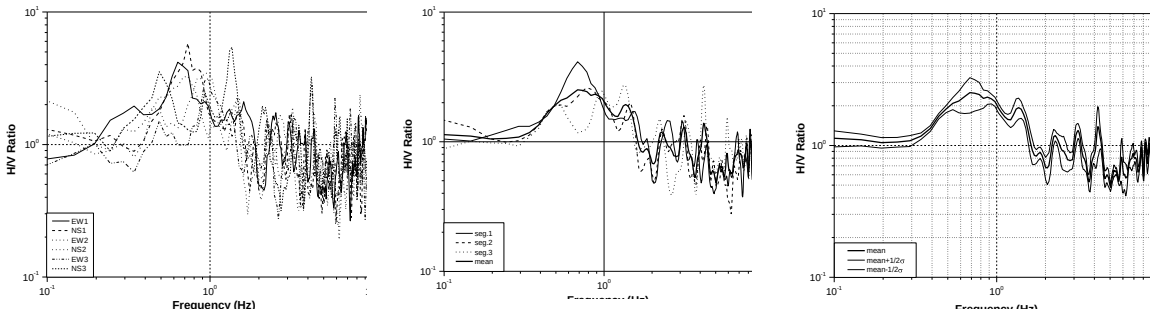

Figure C3.97: Predominant Frequency and H/V Ratio at MT22.

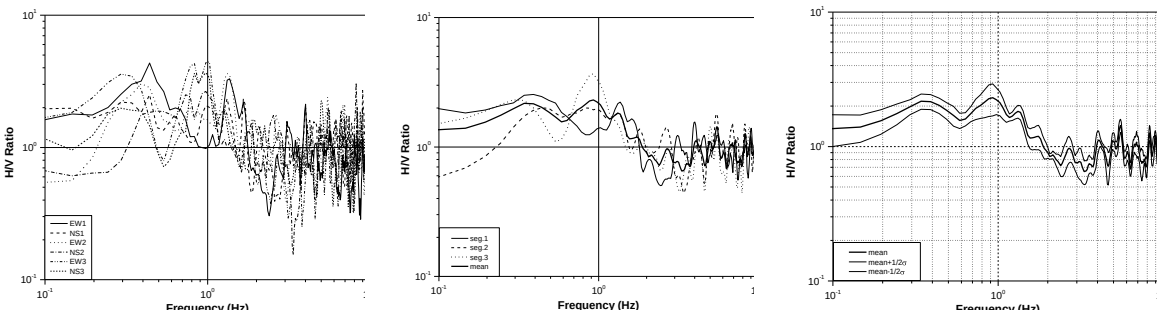

Figure C3.98: Predominant Frequency and H/V Ratio at MT23.

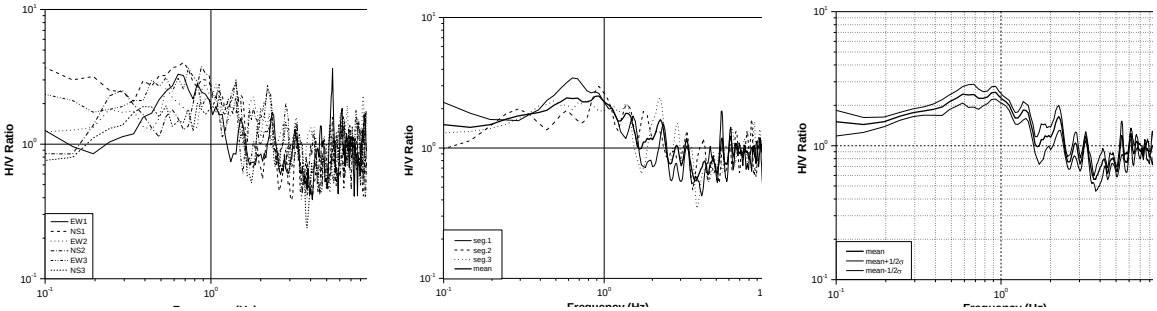

Figure C3.99: Predominant Frequency and H/V Ratio at MT24.

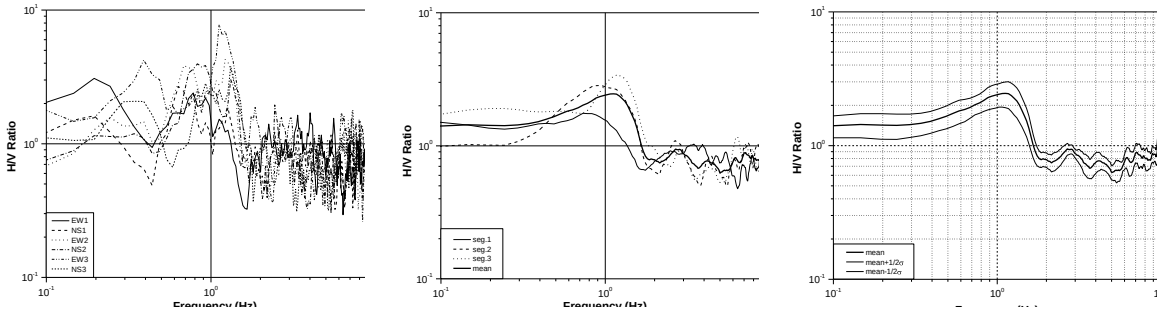

Figure C3.100: Predominant Frequency and H/V Ratio at MT25.

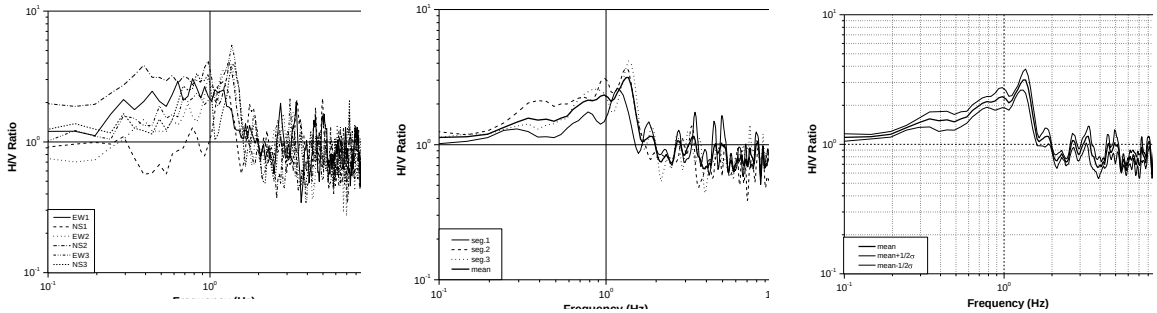

Figure C3.101: Predominant Frequency and H/V Ratio at MT26.

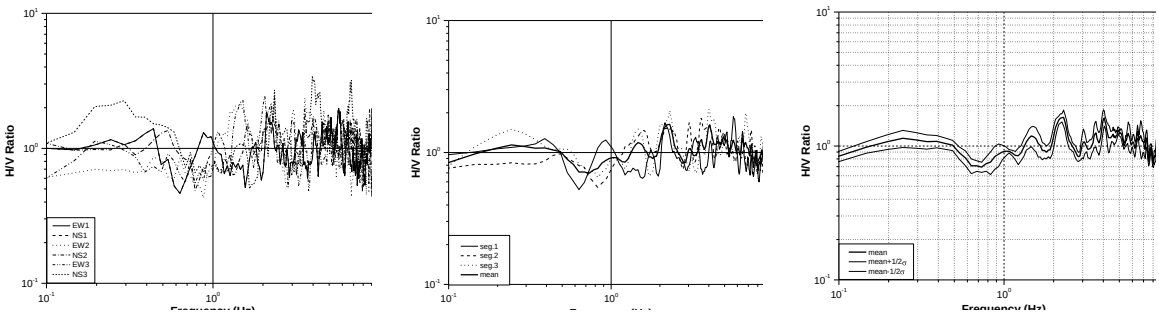

Figure C3.102: Predominant Frequency and H/V Ratio at MT27.

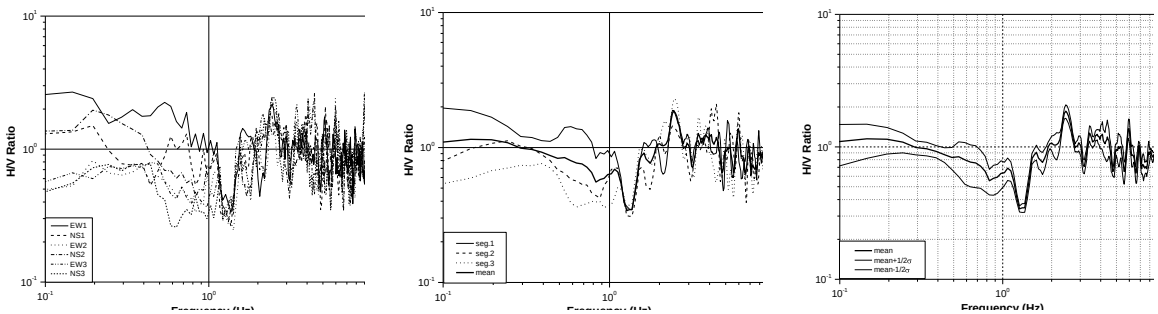

Figure C3.103: Predominant Frequency and H/V Ratio at MT28.

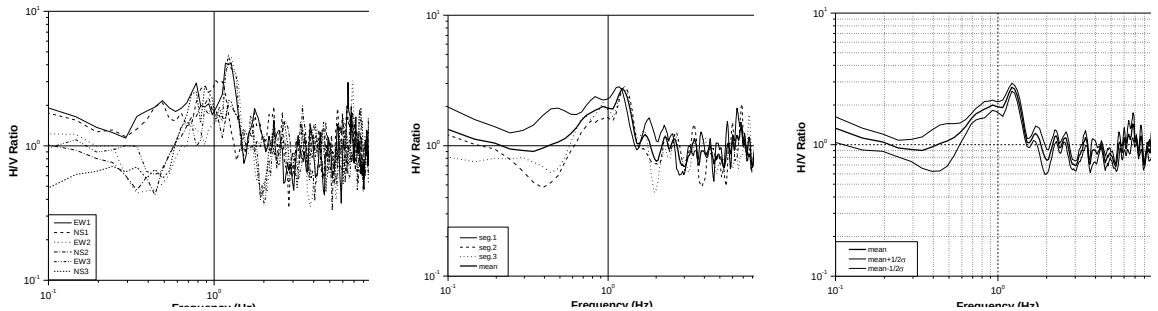

Figure C3.104: Predominant Frequency and H/V Ratio at MT29.

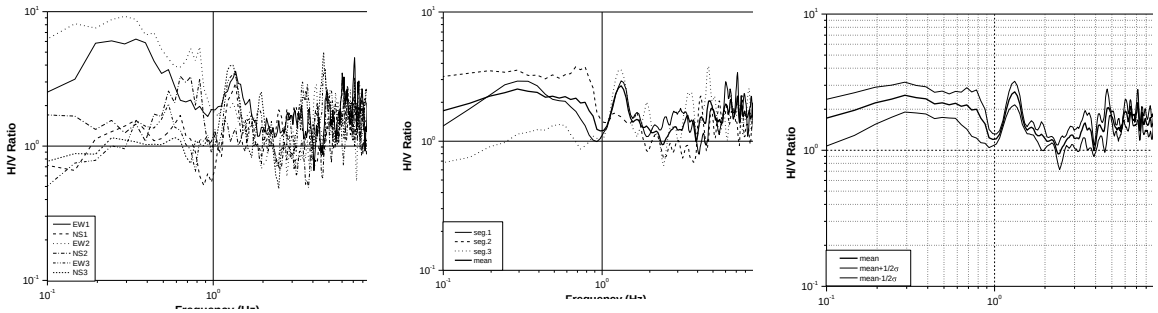

Figure C3.105: Predominant Frequency and H/V Ratio at MT30.

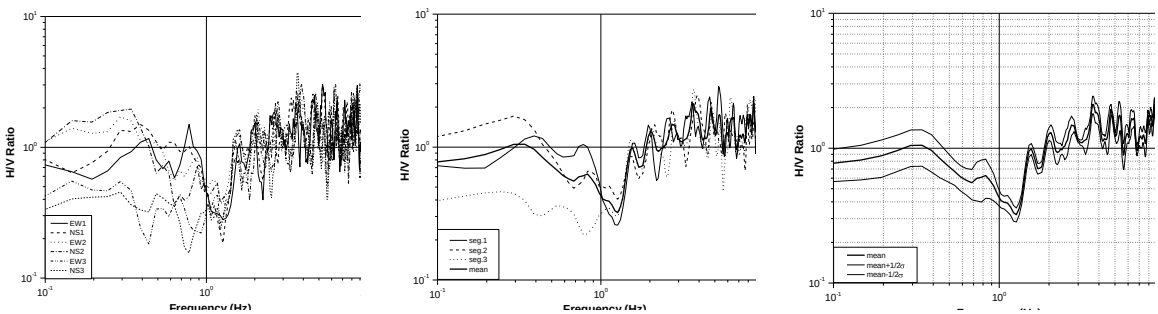

Figure C3.106: Predominant Frequency and H/V Ratio at MT31.

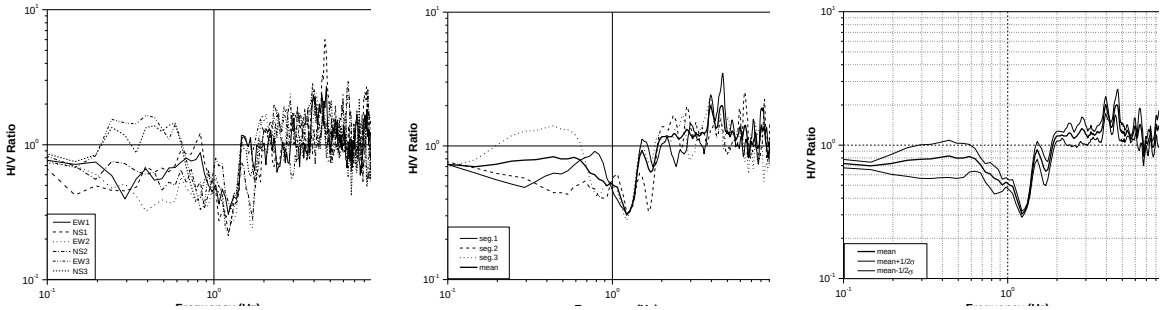

Figure C3.107: Predominant Frequency and H/V Ratio at MT32.

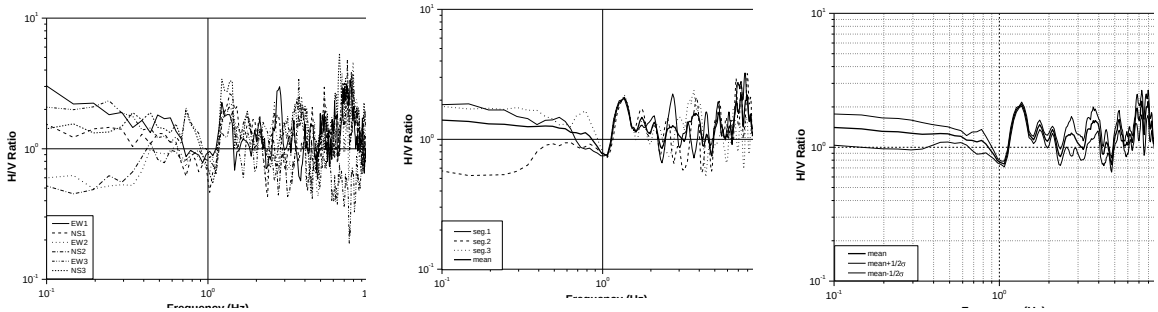

Figure C3.108: Predominant Frequency and H/V Ratio at MT33.

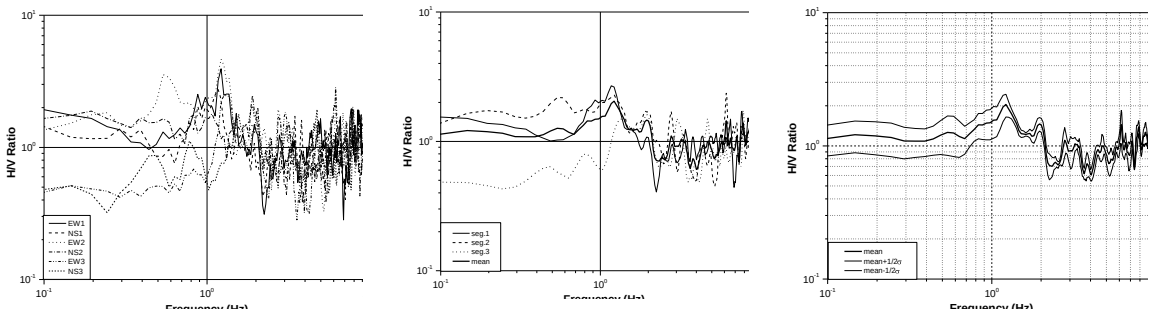

Figure C3.109: Predominant Frequency and H/V Ratio at MT34.

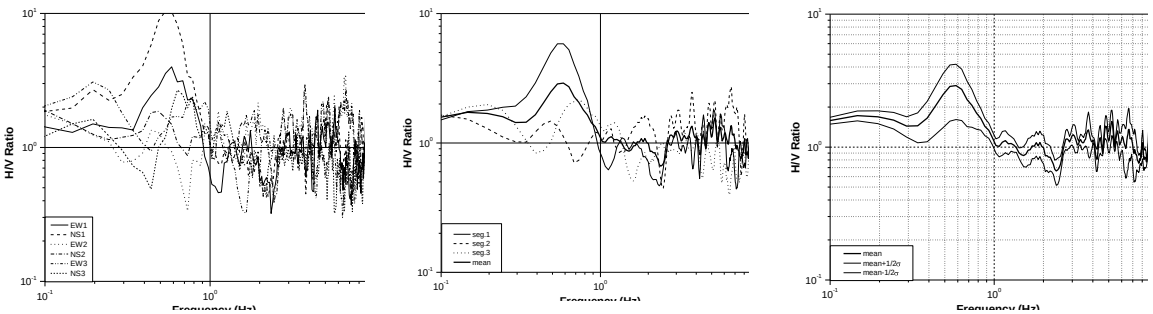

Figure C3.110: Predominant Frequency and H/V Ratio at MT35.

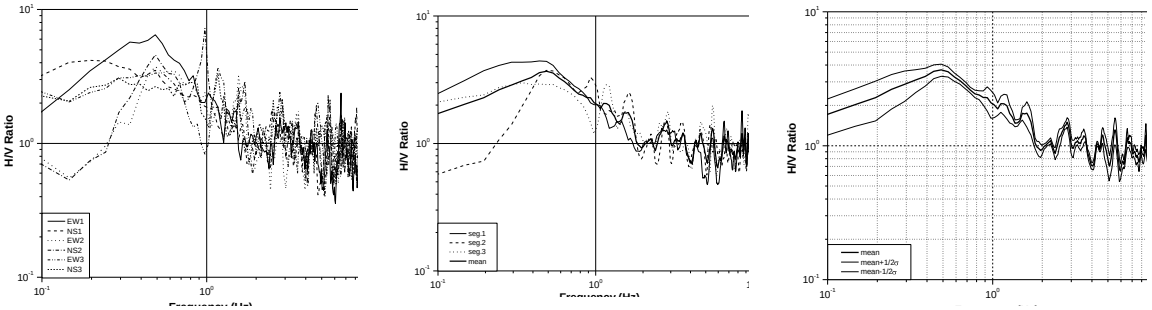

Figure C3.111: Predominant Frequency and H/V Ratio at MT36.

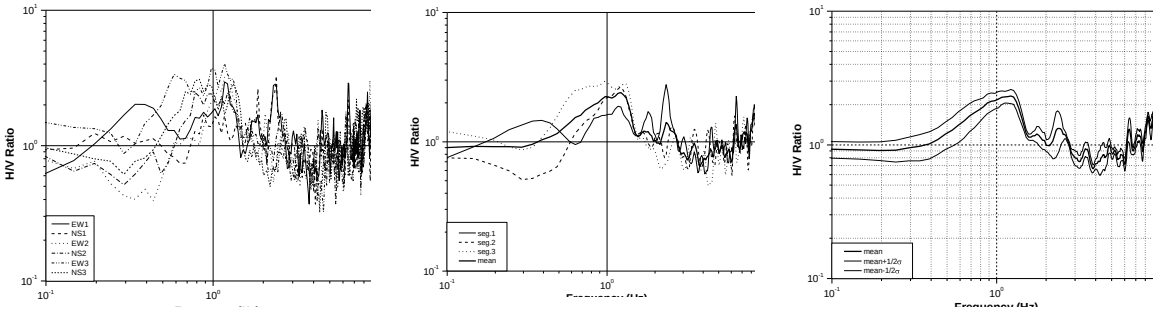

Figure C3.112: Predominant Frequency and H/V Ratio at MT37.

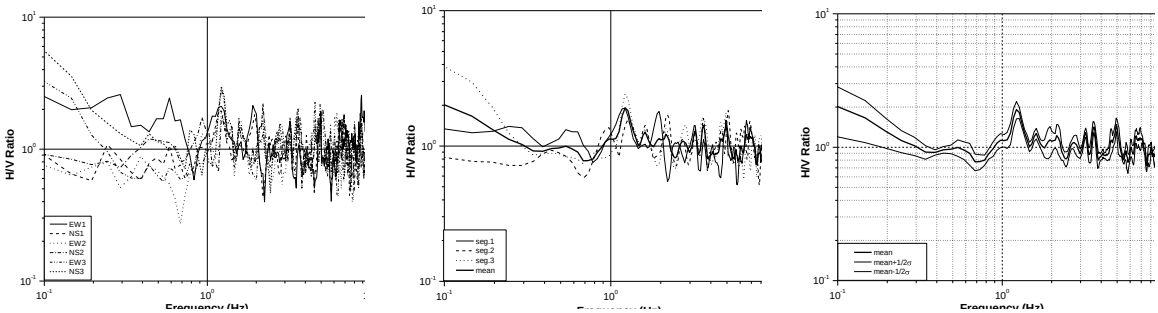

Figure C3.113: Predominant Frequency and H/V Ratio at MT38.

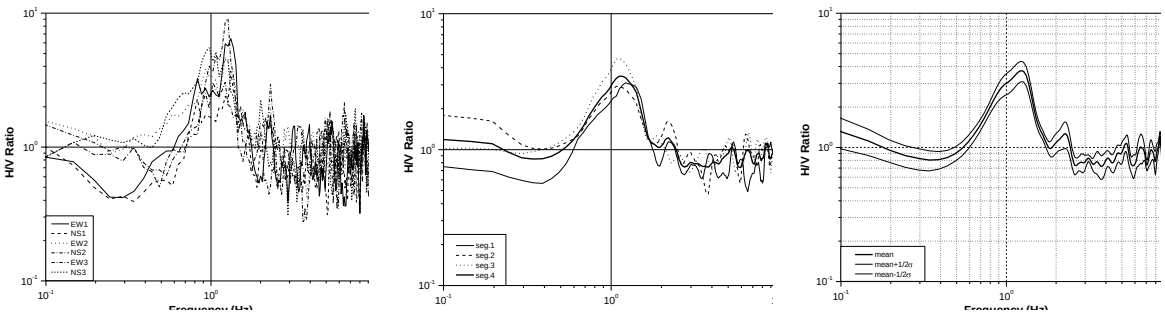

Figure C3.114: Predominant Frequency and H/V Ratio at MT39.

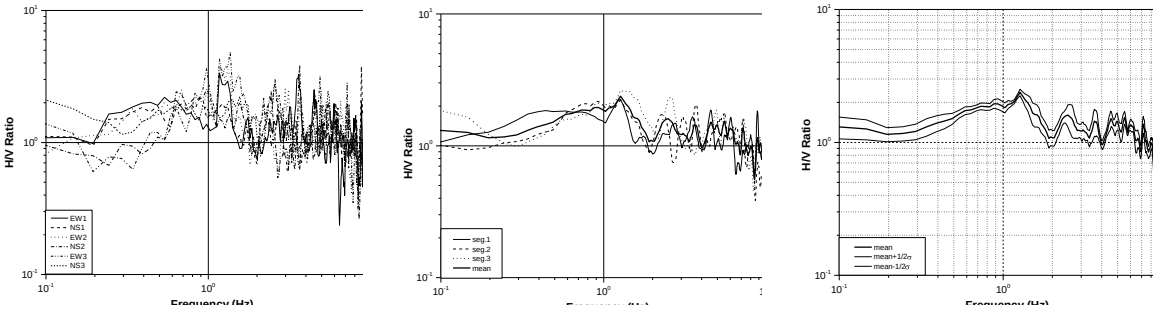

Figure C3.115: Predominant Frequency and H/V Ratio at MT40.

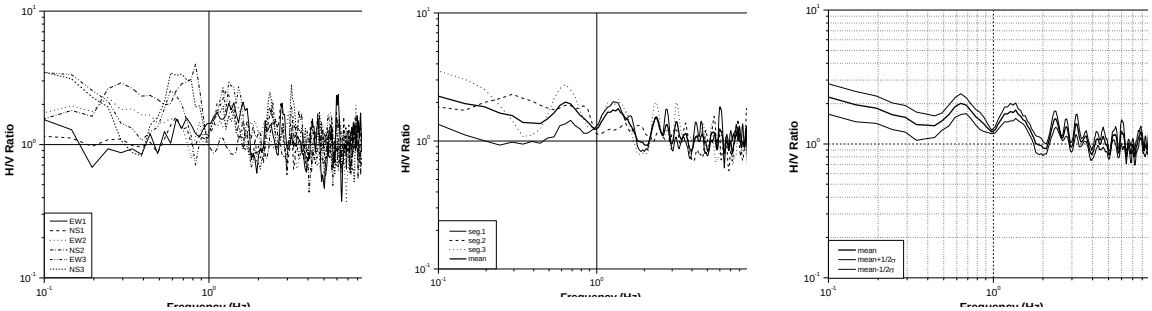

Figure C3.116: Predominant Frequency and H/V Ratio at MT41.

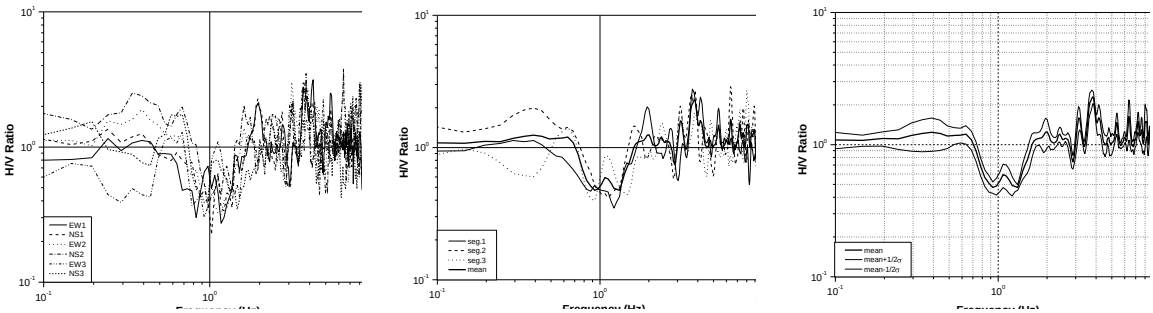

Figure C3.117: Predominant Frequency and H/V Ratio at MT42.

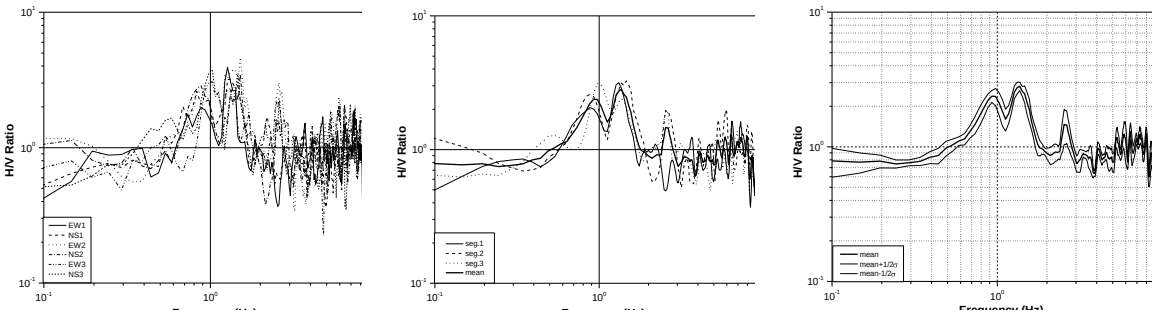

Figure C3.118: Predominant Frequency and H/V Ratio at MT43.

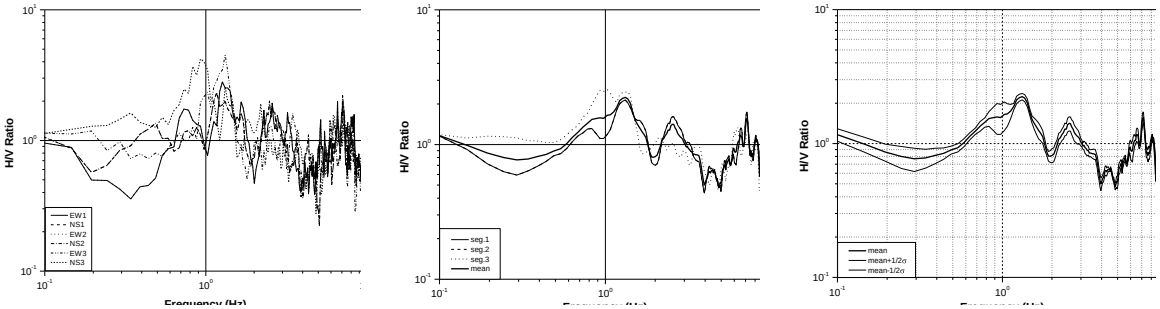

Figure C3.119: Predominant Frequency and H/V Ratio at MT44.

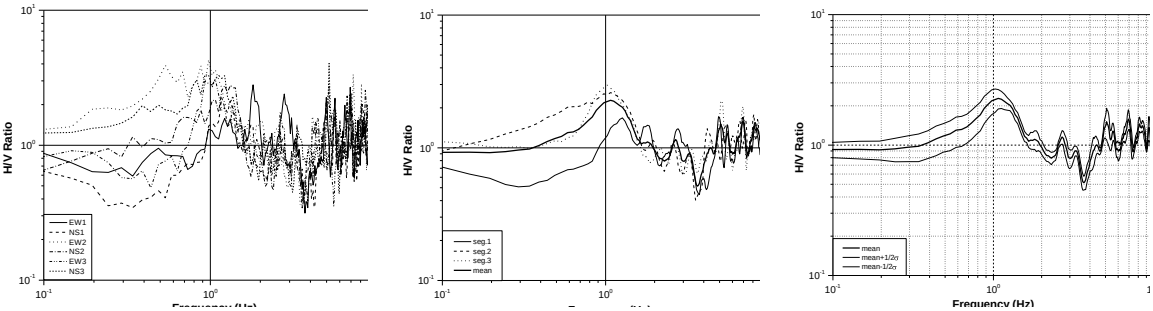

Figure C3.120: Predominant Frequency and H/V Ratio at MT45.

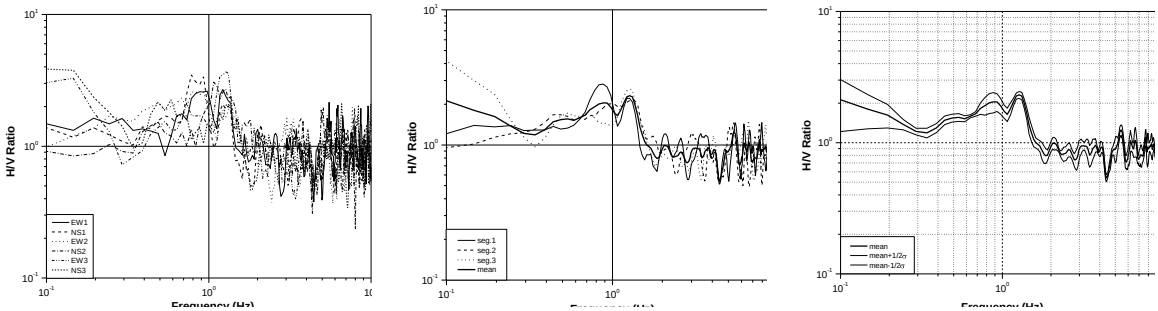

Figure C3.121: Predominant Frequency and H/V Ratio at MT46.

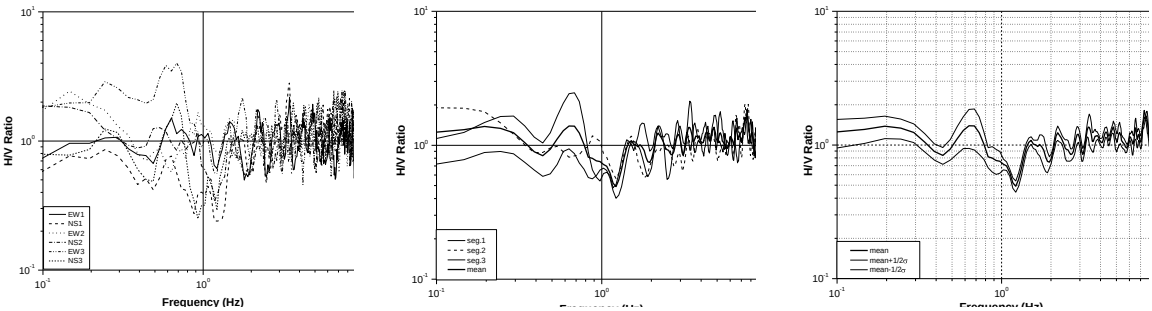

Figure C3.122: Predominant Frequency and H/V Ratio at MT47.

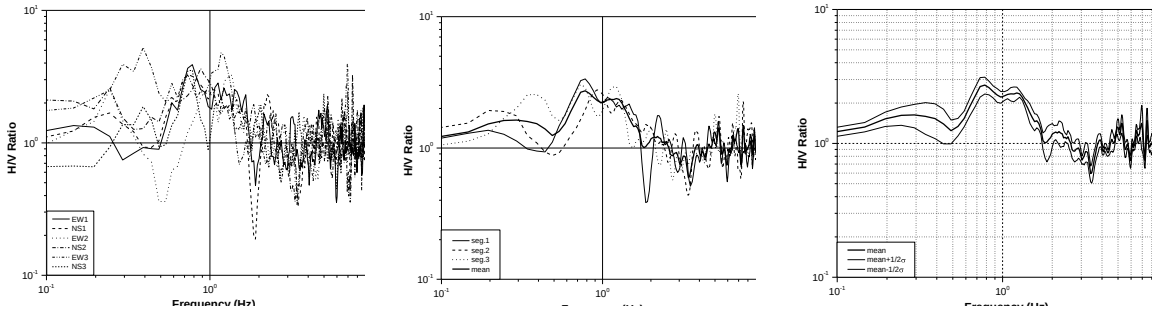

Figure C3.123: Predominant Frequency and H/V Ratio at MT48.

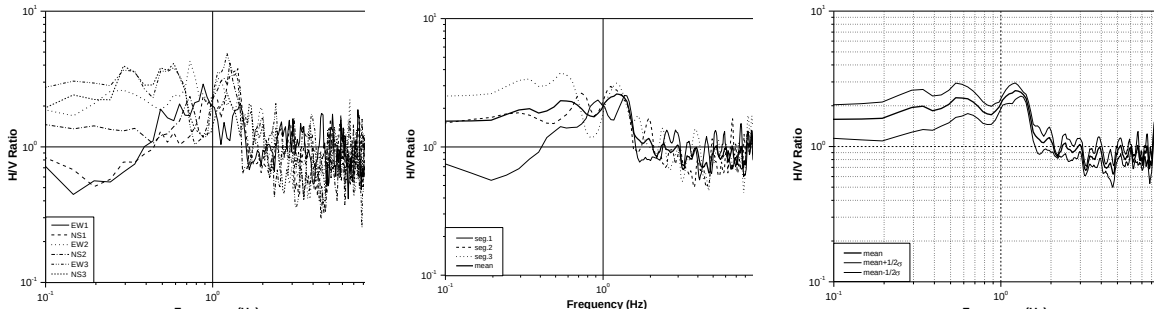

Figure C3.124: Predominant Frequency and H/V Ratio at MT49.

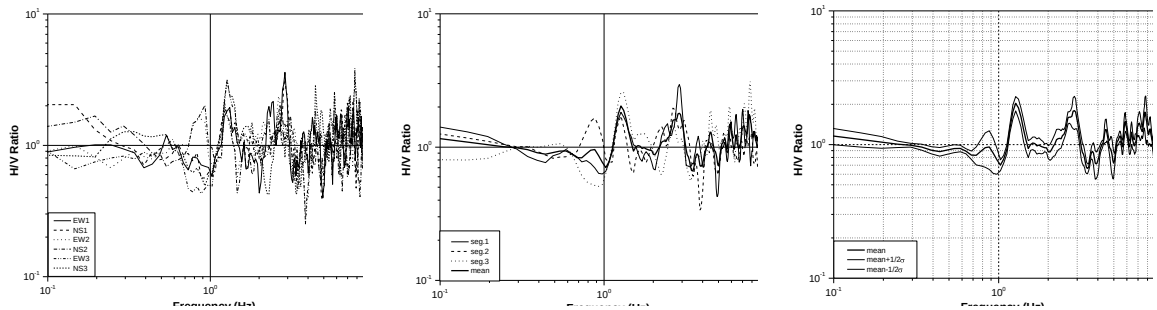

Figure C3.125: Predominant Frequency and H/V Ratio at MT50.

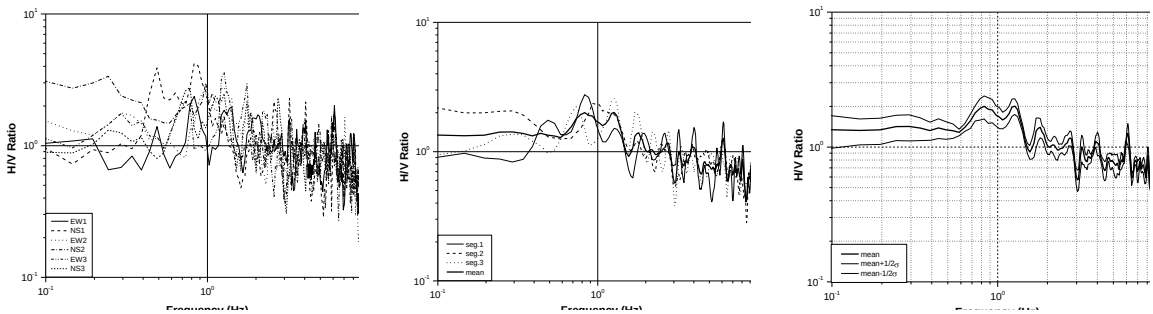

Figure C3.126: Predominant Frequency and H/V Ratio at MT51.

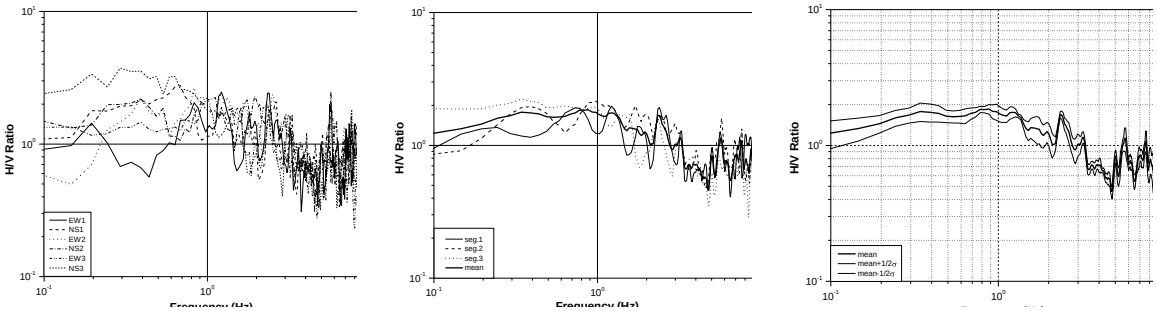

Figure C3.127: Predominant Frequency and H/V Ratio at MT52.

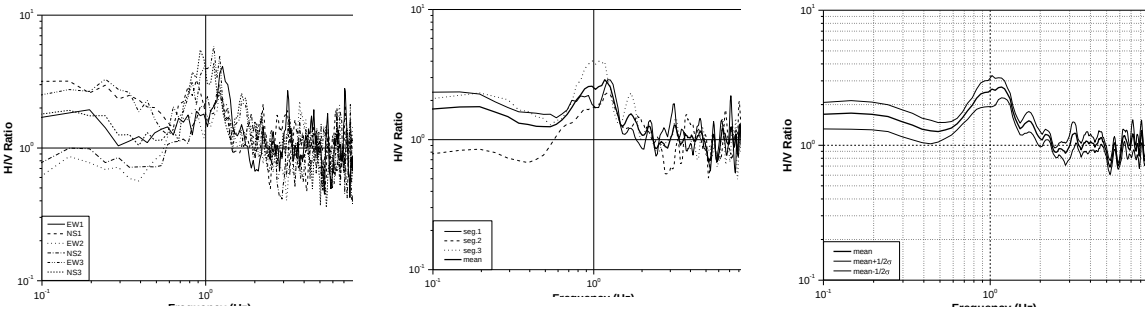

Figure C3.128: Predominant Frequency and H/V Ratio at MT53.

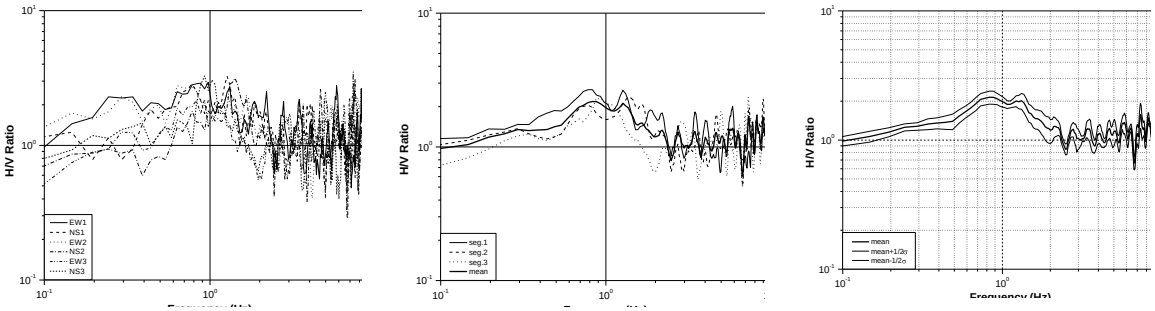

Figure C3.129: Predominant Frequency and H/V Ratio at MT54.

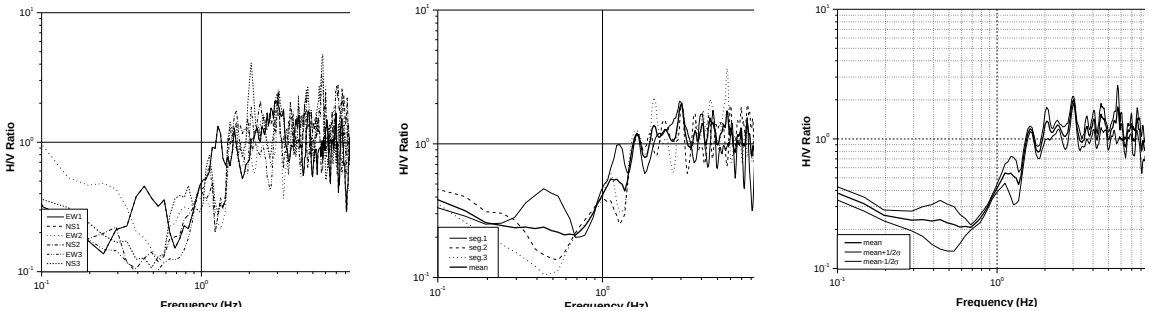

Figure C3.130: Predominant Frequency and H/V Ratio at MT55.

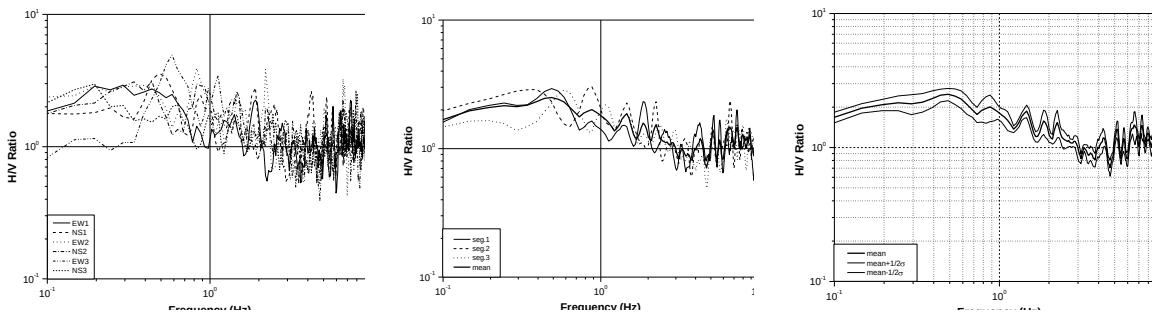

Figure C3.131: Predominant Frequency and H/V Ratio at MT56.

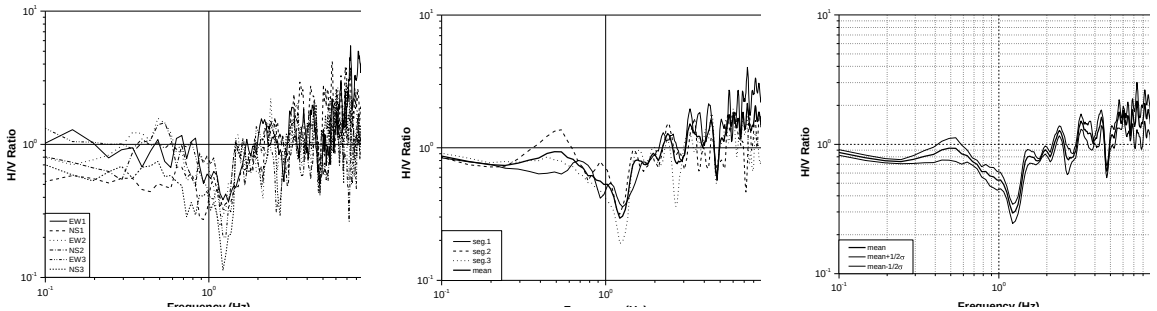

Figure C3.132: Predominant Frequency and H/V Ratio at MT57.

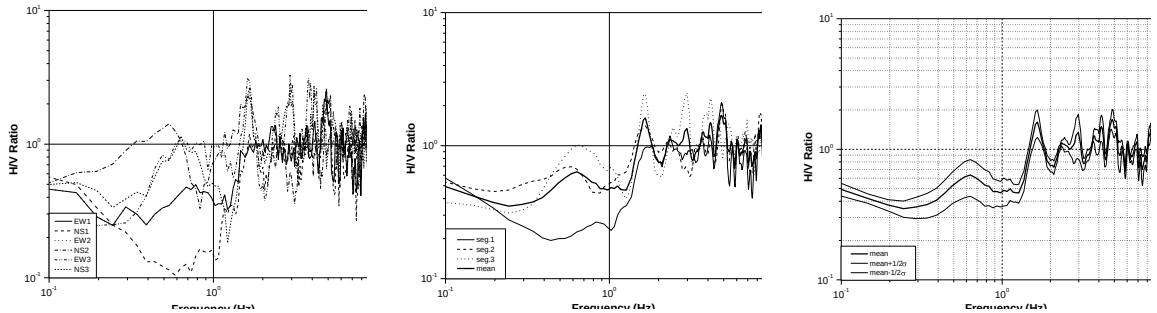

Figure C3.133: Predominant Frequency and H/V Ratio at MT58.

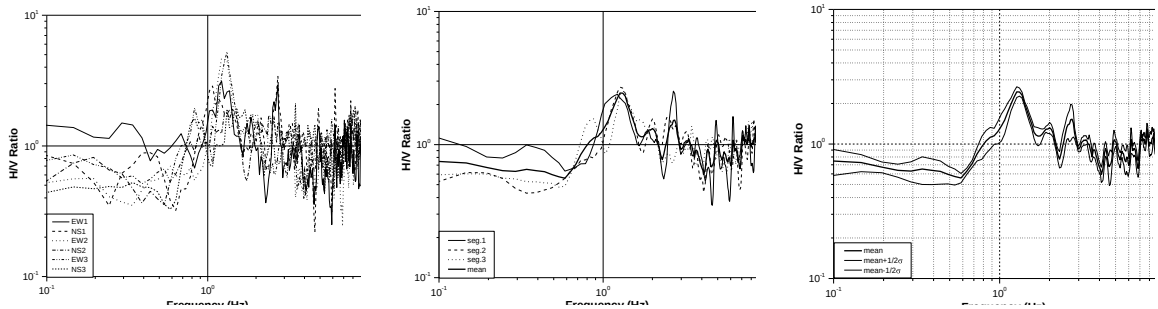

Figure C3.134: Predominant Frequency and H/V Ratio at MT59.

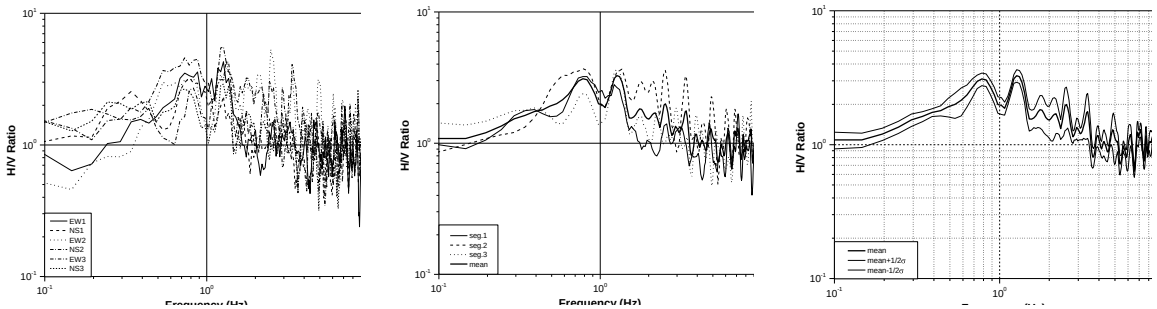

Figure C3.135: Predominant Frequency and H/V Ratio at MT60.

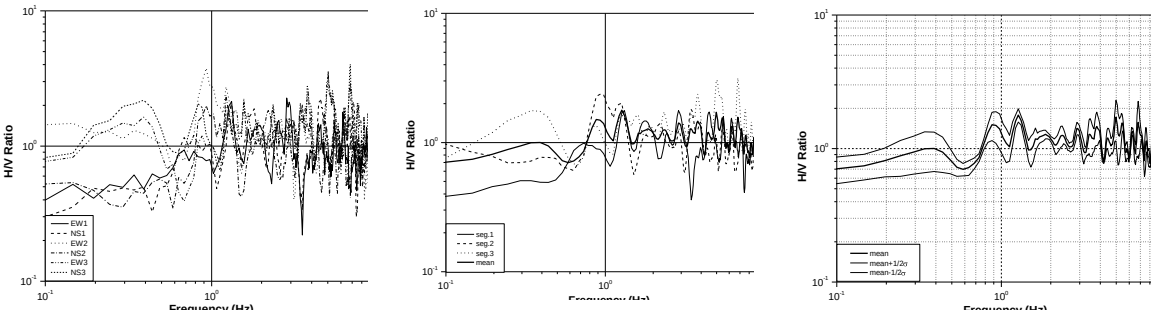

Figure C3.136: Predominant Frequency and H/V Ratio at MT61.

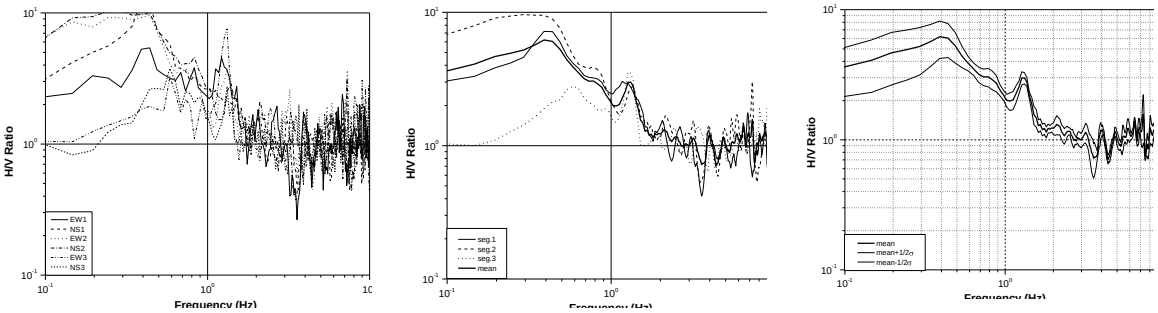

Figure C3.137: Predominant Frequency and H/V Ratio at MT62.

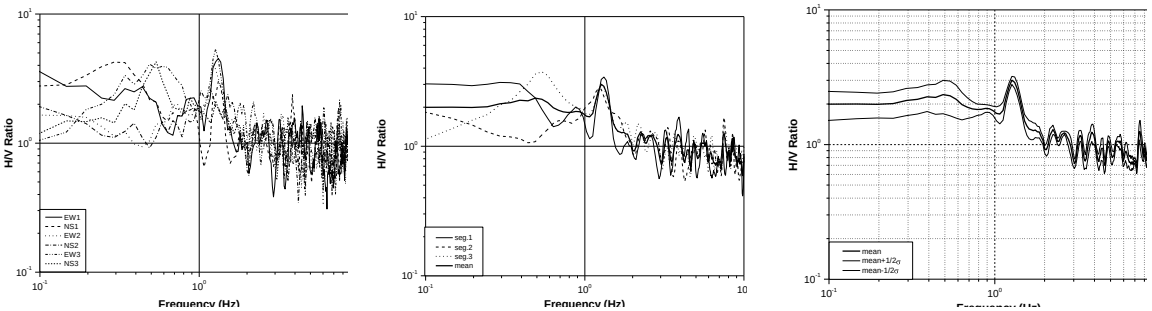

Figure C3.138: Predominant Frequency and H/V Ratio at MT63.

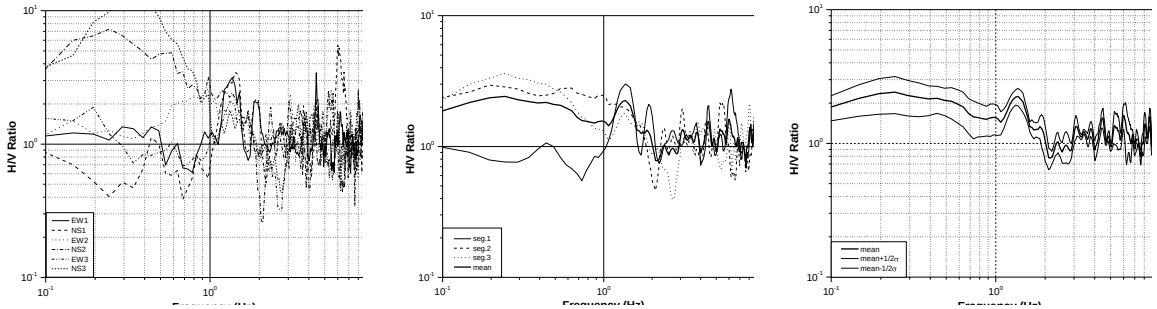

Figure C3.139: Predominant Frequency and H/V Ratio at MT64.

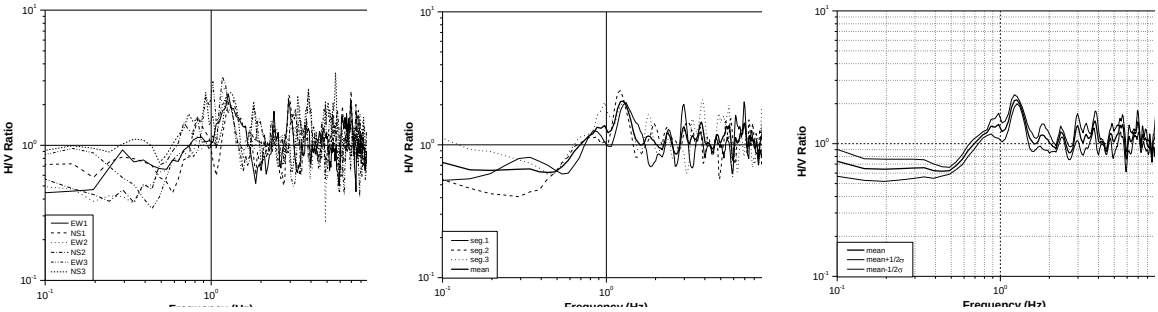

Figure C3.140: Predominant Frequency and H/V Ratio at MT65.

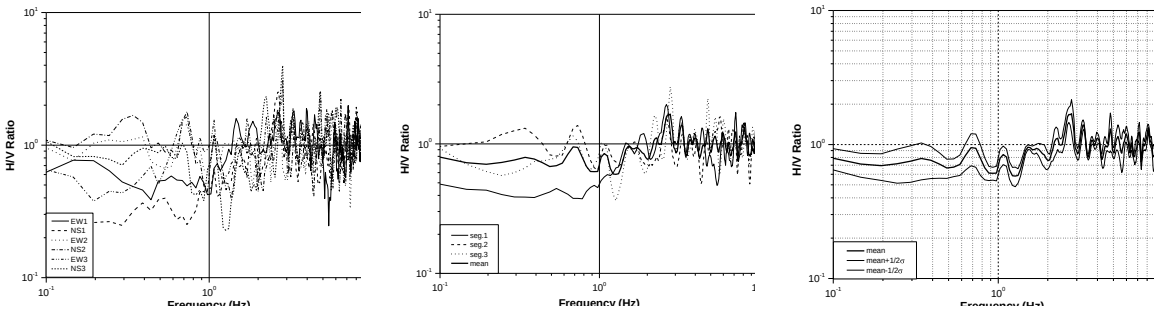

Figure C3.141: Predominant Frequency and H/V Ratio at MT66.

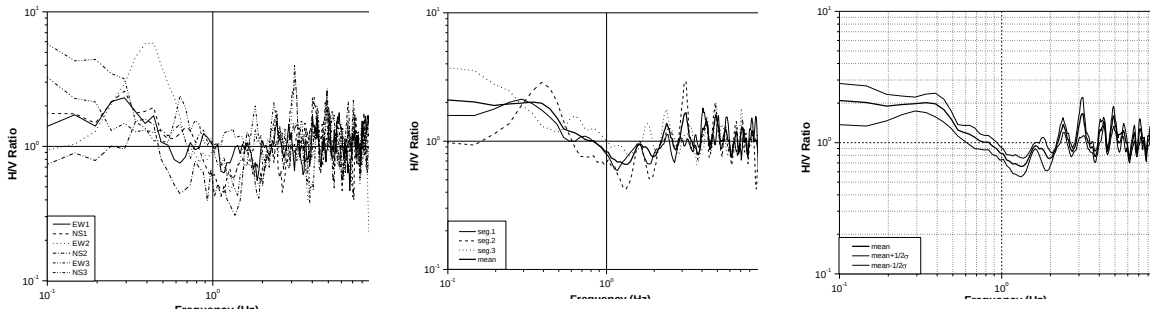

Figure C3.142: Predominant Frequency and H/V Ratio at MT67.

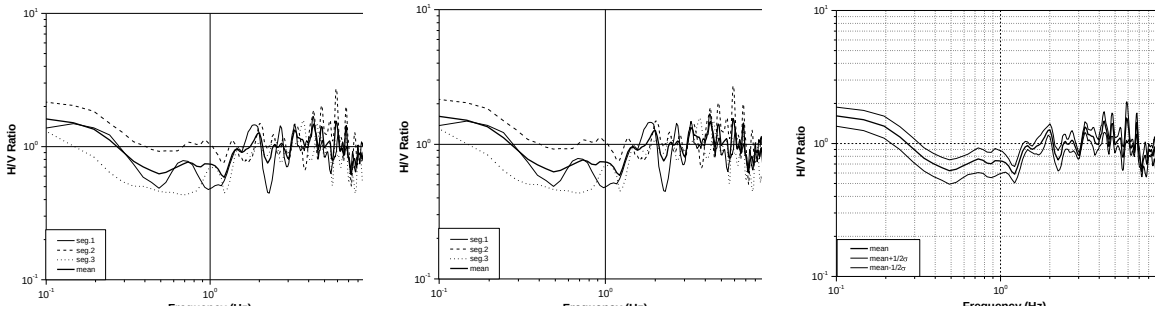

Figure C3.143: Predominant Frequency and H/V Ratio at MT68.

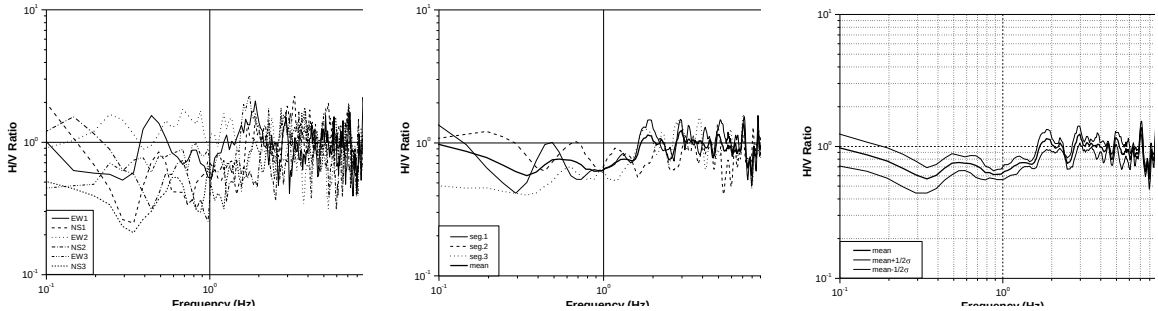

Figure C3.144: Predominant Frequency and H/V Ratio at MT69.

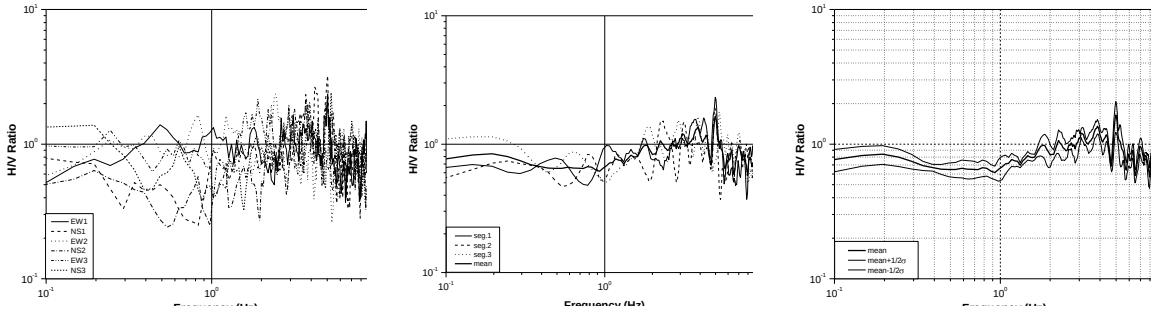

Figure C3.145: Predominant Frequency and H/V Ratio at MT70.

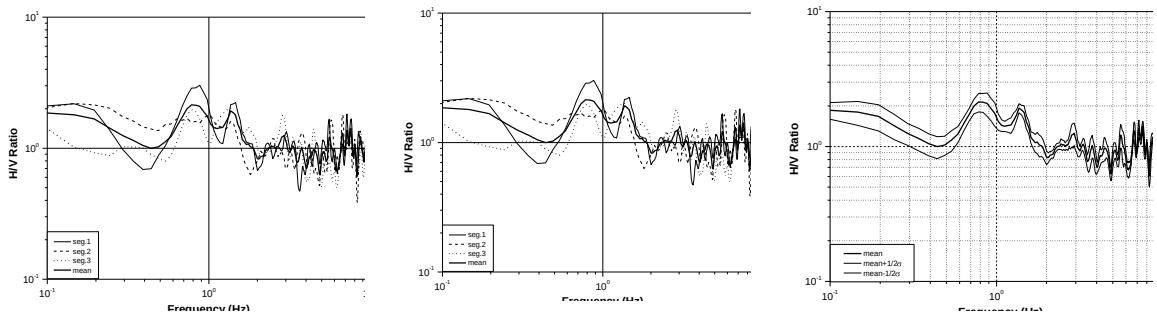

Figure C3.146: Predominant Frequency and H/V Ratio at MT71.

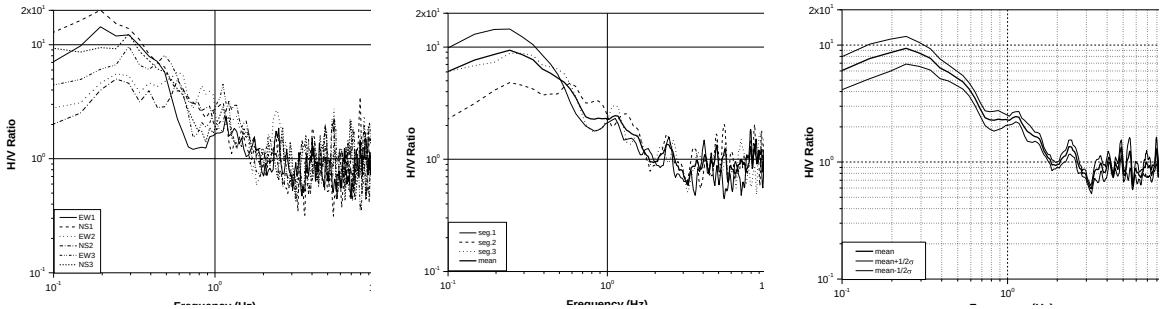

Figure C3.147: Predominant Frequency and H/V Ratio at MT72.

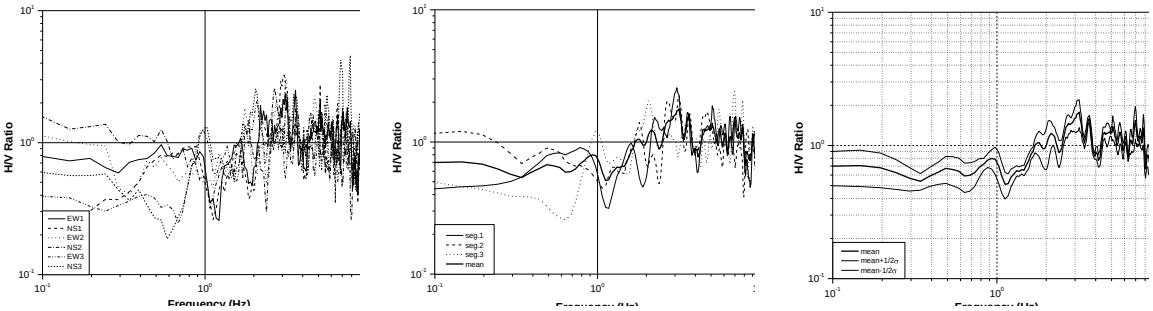

Figure C3.148: Predominant Frequency and H/V Ratio at MT73.

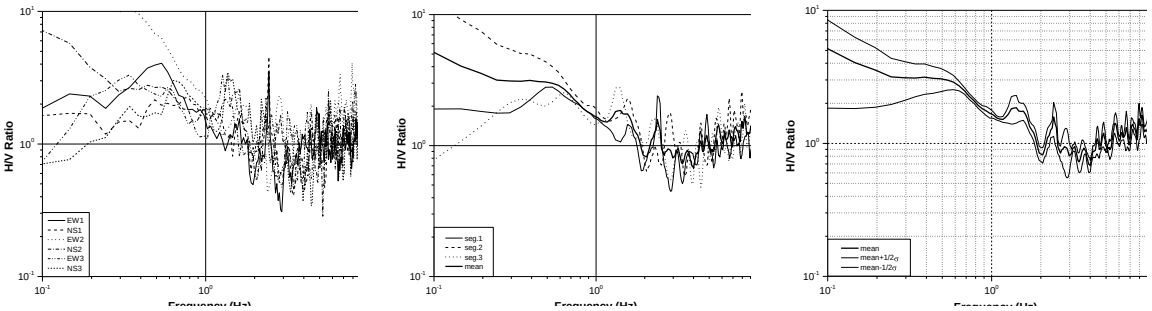

Figure C3.149: Predominant Frequency and H/V Ratio at MT74.

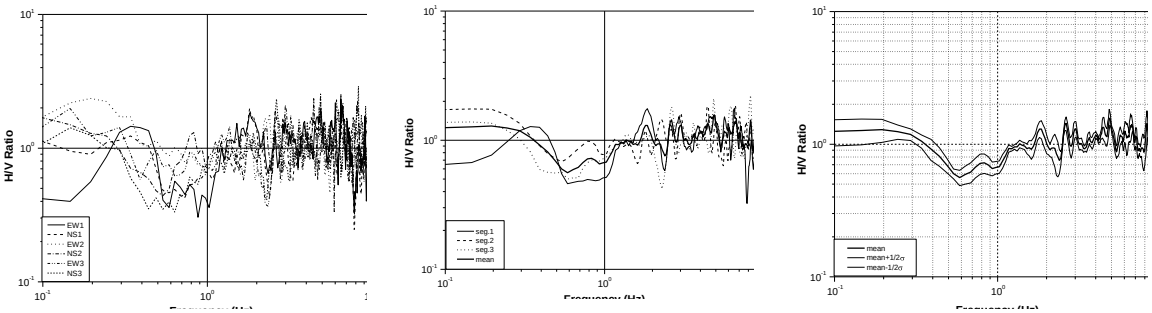

Figure C3.150: Predominant Frequency and H/V Ratio at MT75.

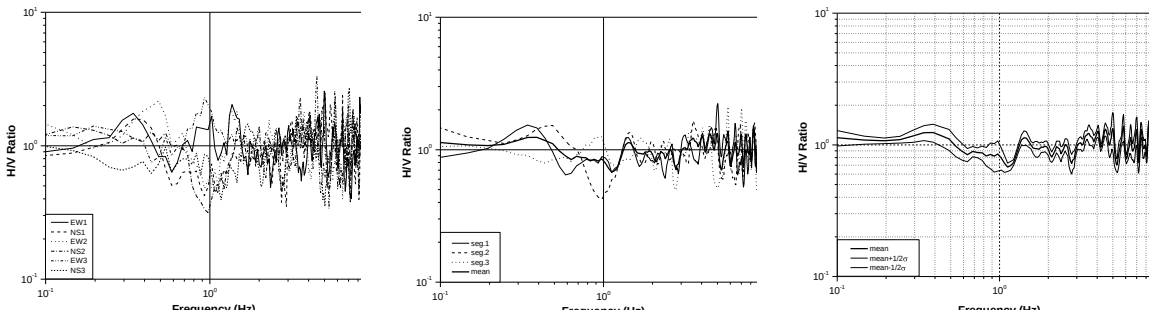

Figure C3.151: Predominant Frequency and H/V Ratio at MT76.

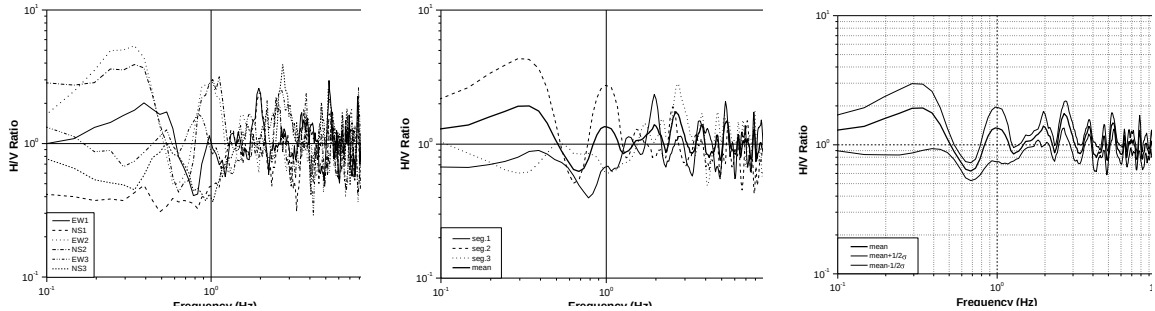

Figure C3.152: Predominant Frequency and H/V Ratio at MT77.

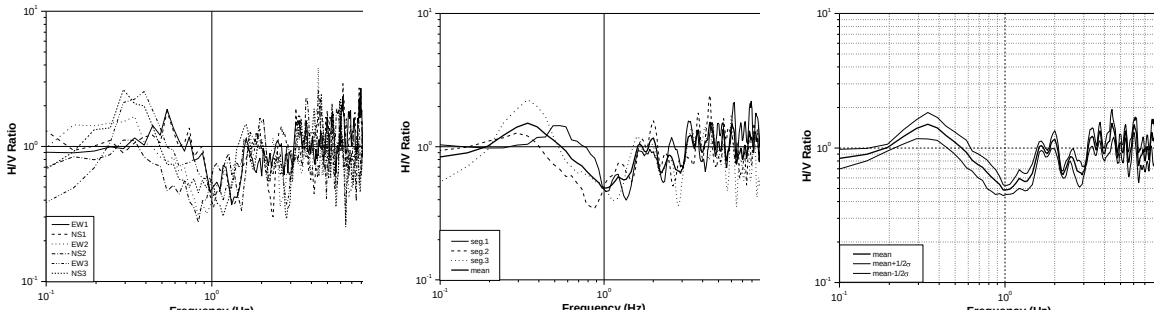

Figure C3.153: Predominant Frequency and H/V Ratio at MT78.

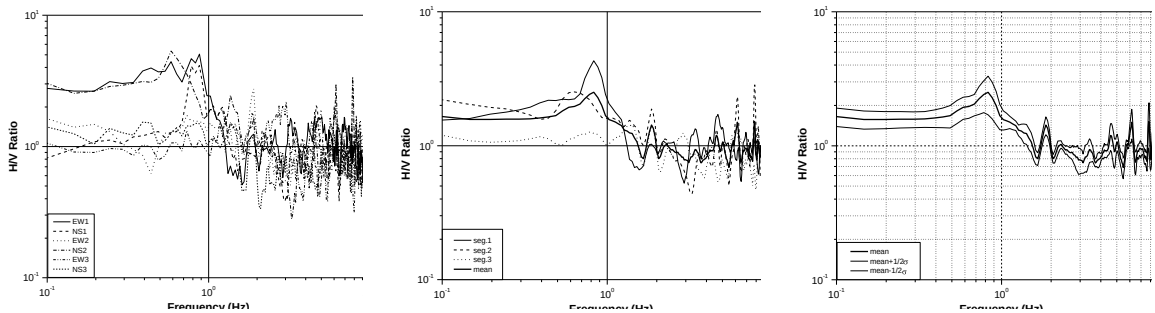

Figure C3.154: Predominant Frequency and H/V Ratio at MT79.

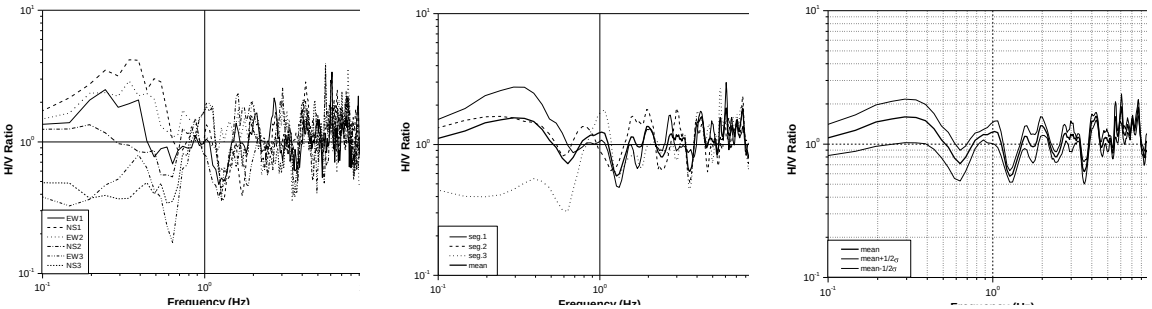

Figure C3.155: Predominant Frequency and H/V Ratio at MT80.

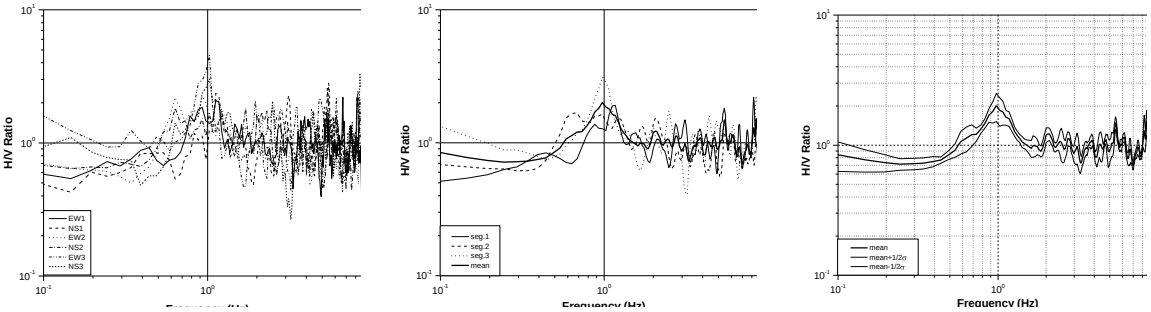

Figure C3.156: Predominant Frequency and H/V Ratio at MT81.

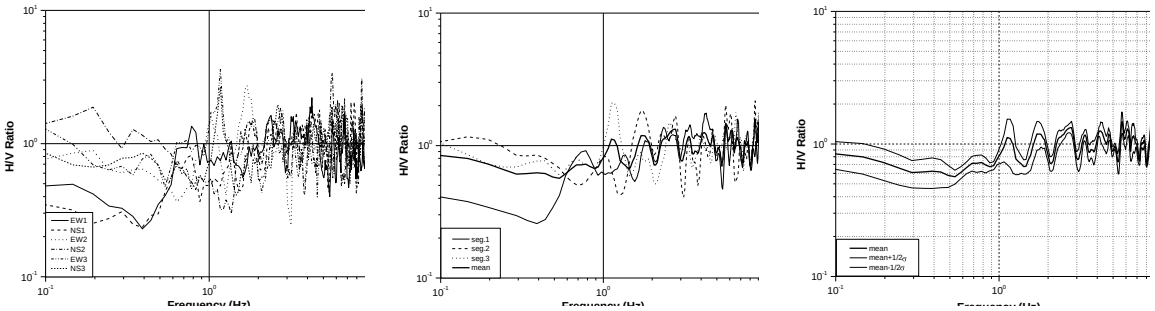

Figure C3.157: Predominant Frequency and H/V Ratio at MT82.

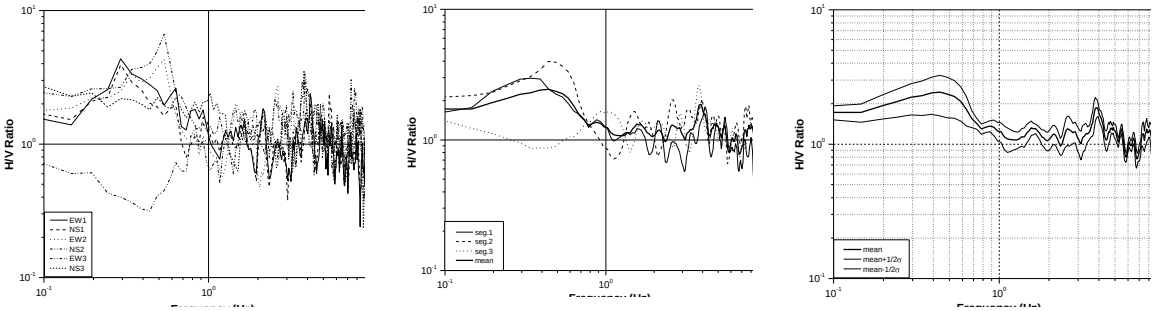

Figure C3.158: Predominant Frequency and H/V Ratio at MT83.

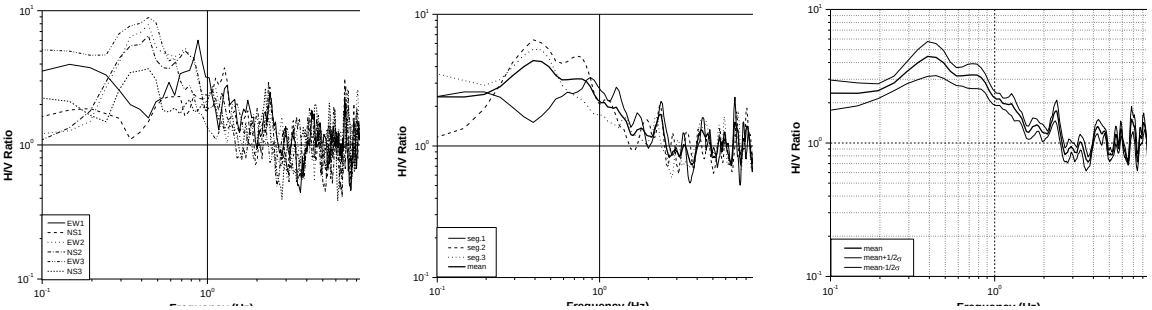

Figure C3.159: Predominant Frequency and H/V Ratio at MT84.

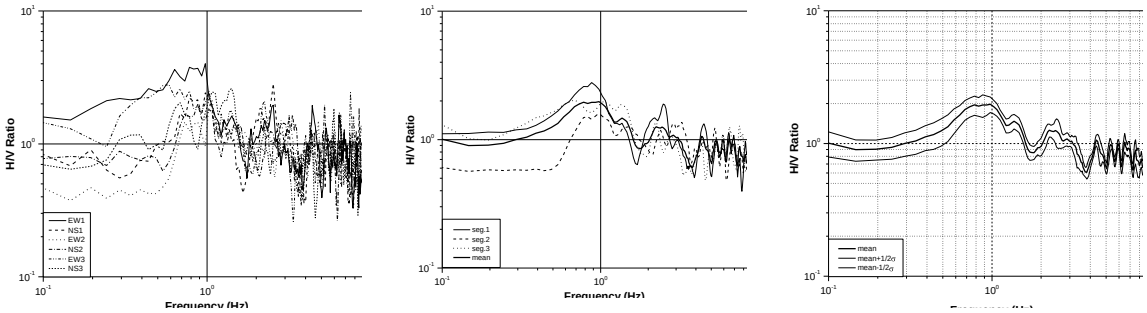

Figure C3.160: Predominant Frequency and H/V Ratio at MT85.

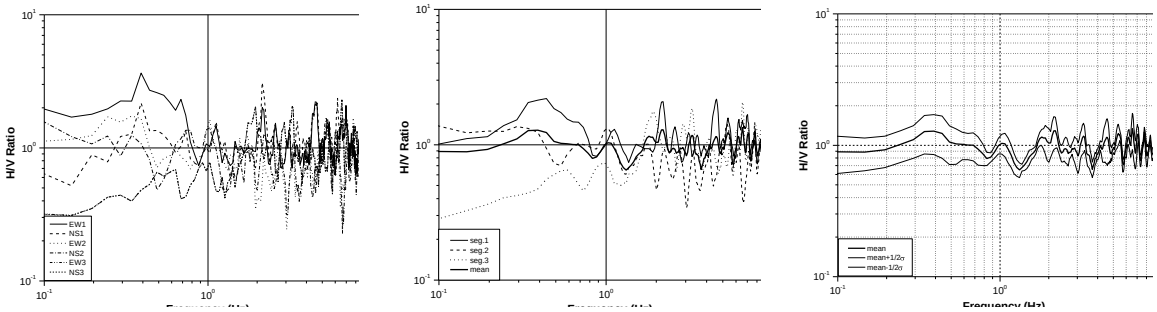

Figure C3.161: Predominant Frequency and H/V Ratio at MT86.

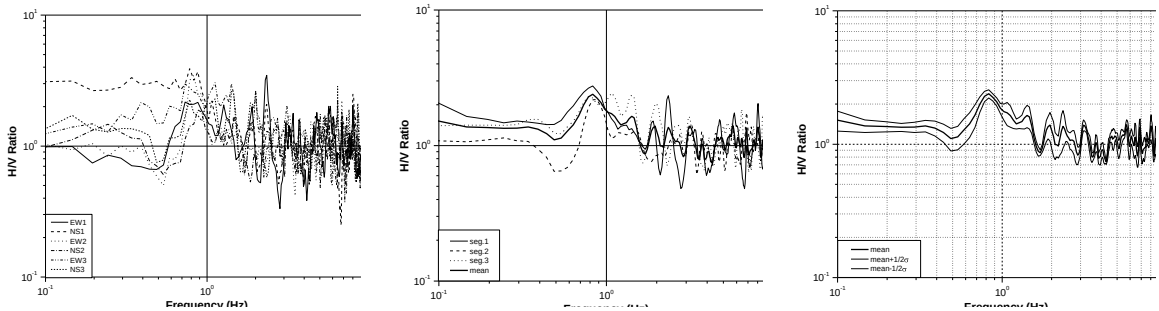

Figure C3.162: Predominant Frequency and H/V Ratio at MT87.

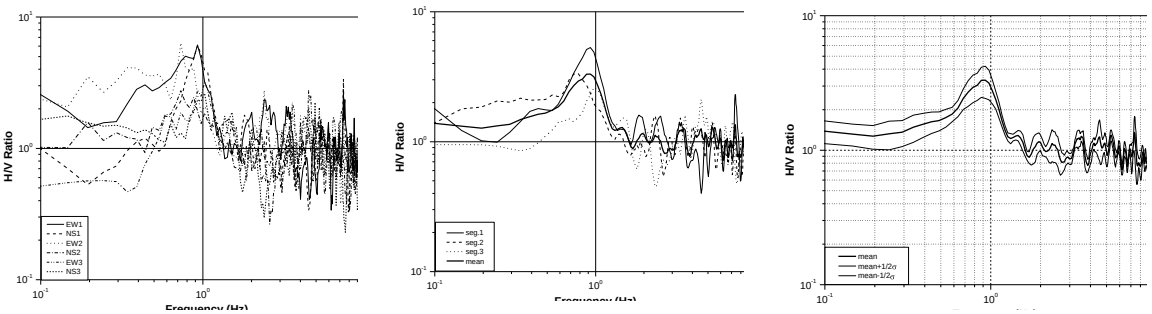

Figure C3.163: Predominant Frequency and H/V Ratio at MT88.

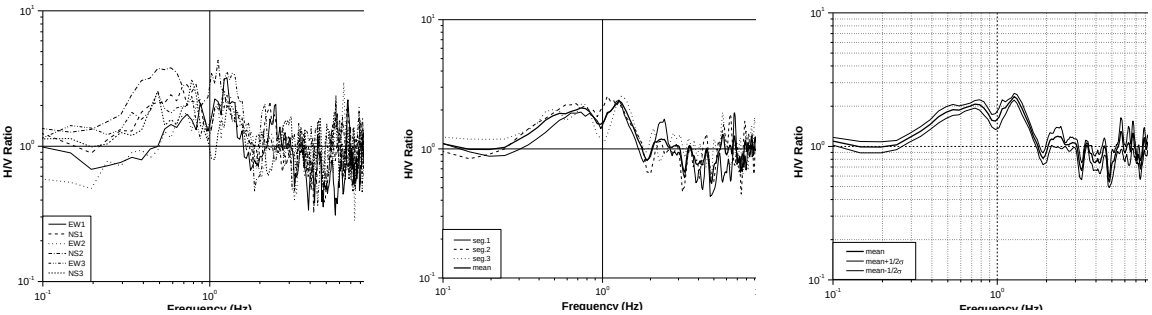

Figure C3.164: Predominant Frequency and H/V Ratio at MT89.

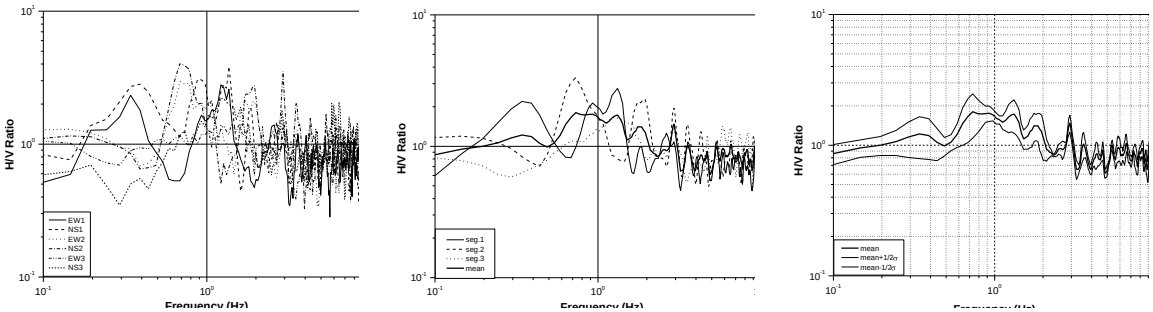

Figure C3.165: Predominant Frequency and H/V Ratio at MT90.

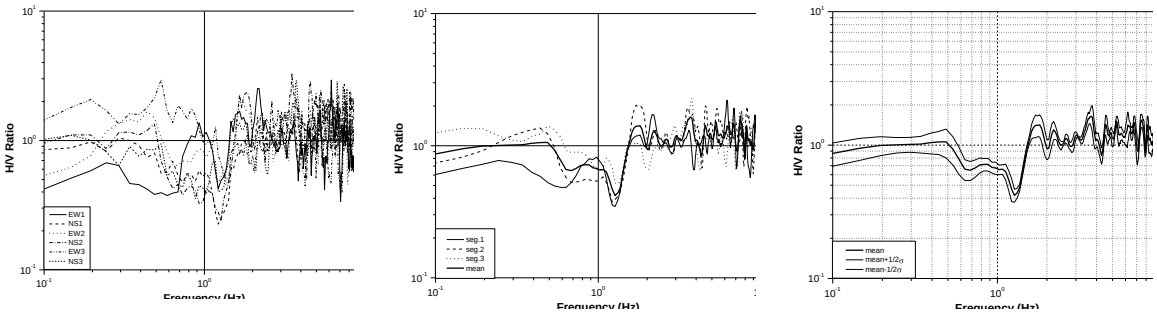

Figure C3.166: Predominant Frequency and H/V Ratio at MT91

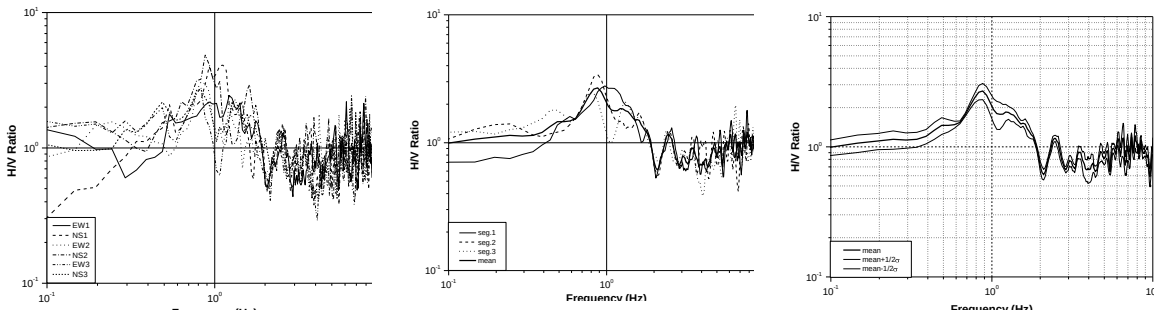

Figure C3.167: Predominant Frequency and H/V Ratio at MT92.

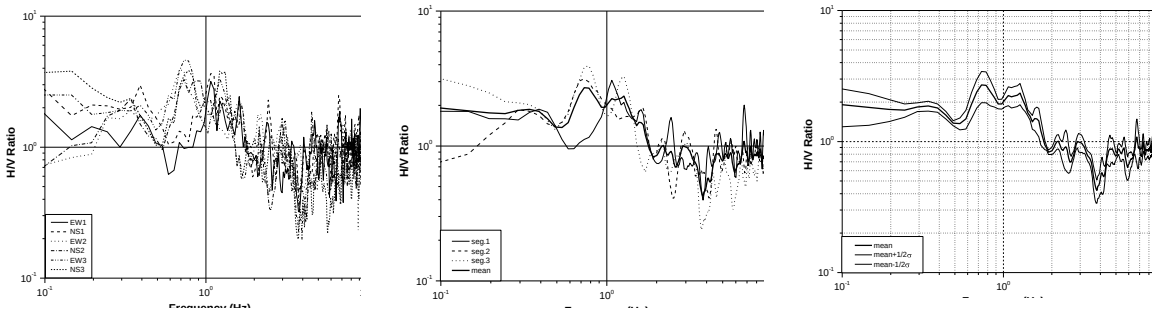

Figure C3.168: Predominant Frequency and H/V Ratio at MT93.

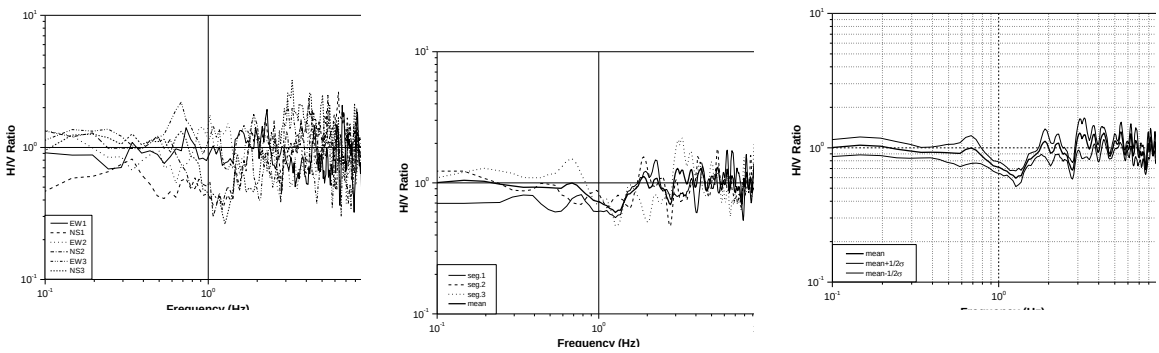

Figure C3.169: Predominant Frequency and H/V Ratio at MT94.

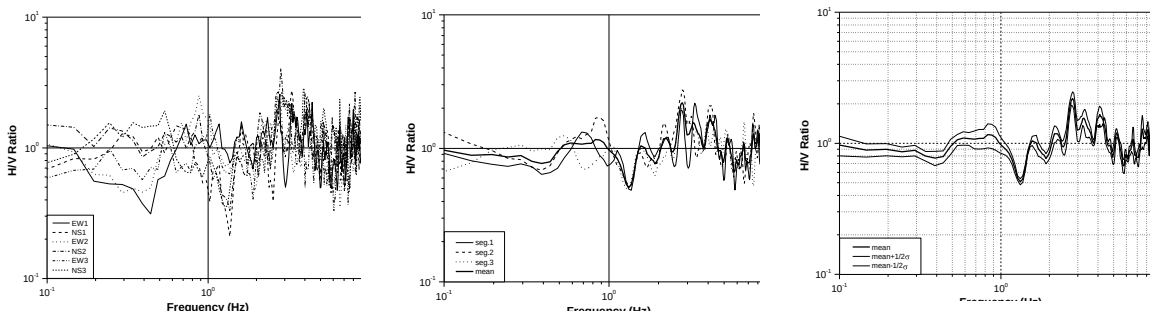

Figure C3.170: Predominant Frequency and H/V Ratio at MT95.

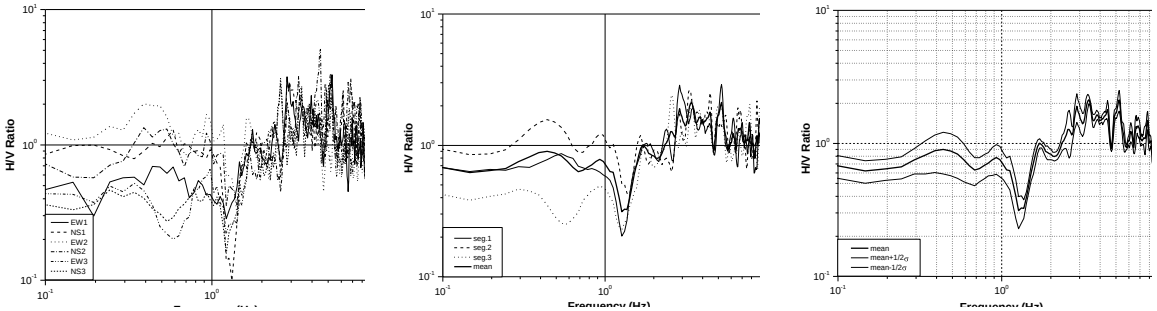

Figure C3.171: Predominant Frequency and H/V Ratio at MT96.

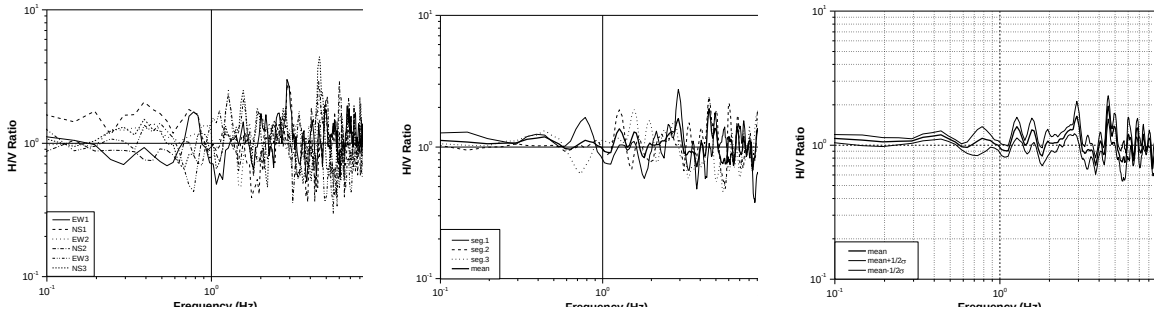

Figure C3.172: Predominant Frequency and H/V Ratio at MT97.

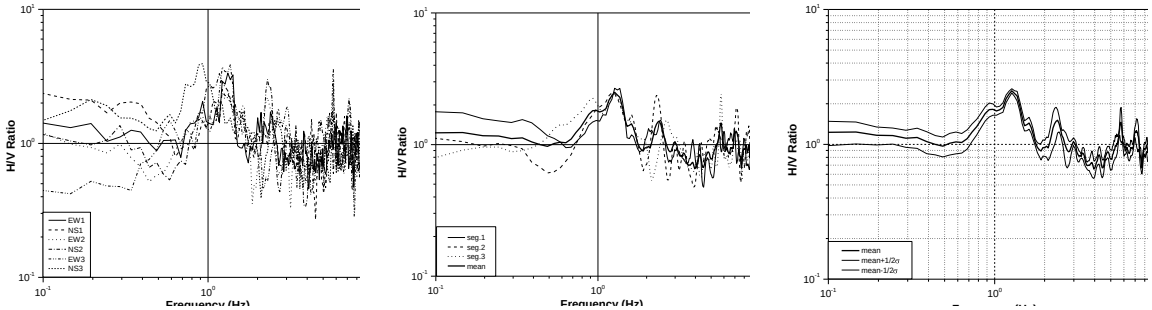

Figure C3.173: Predominant Frequency and H/V Ratio at MT98.

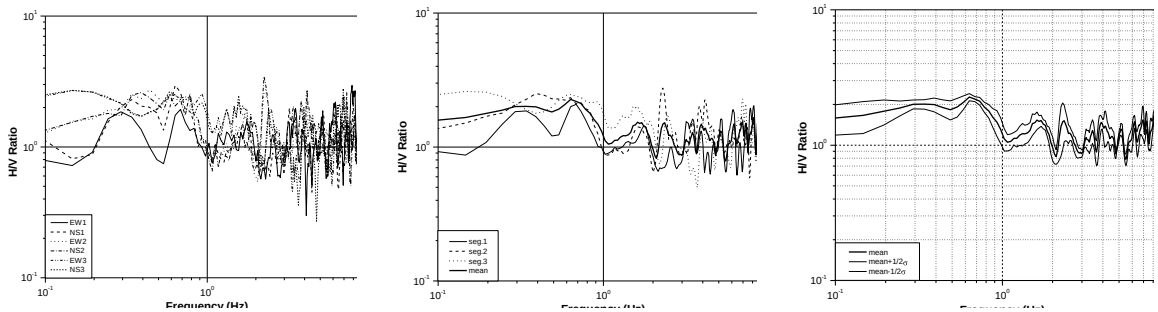

Figure C3.174: Predominant Frequency and H/V Ratio at MT99.

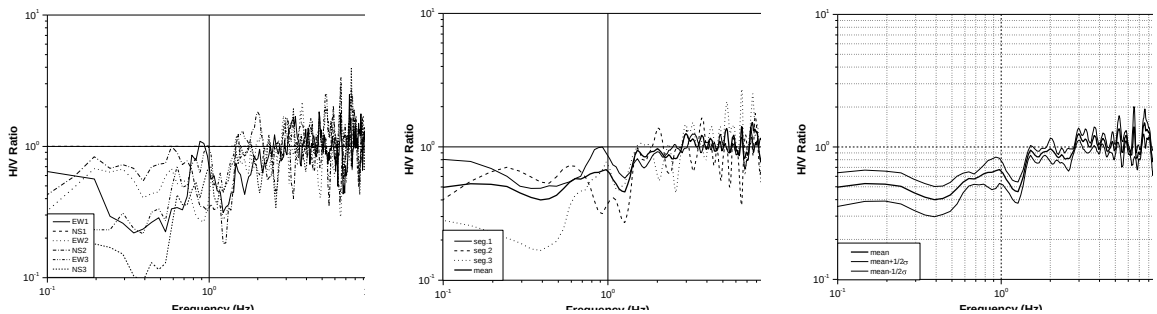

Figure C3.175: Predominant Frequency and H/V Ratio at MT100.

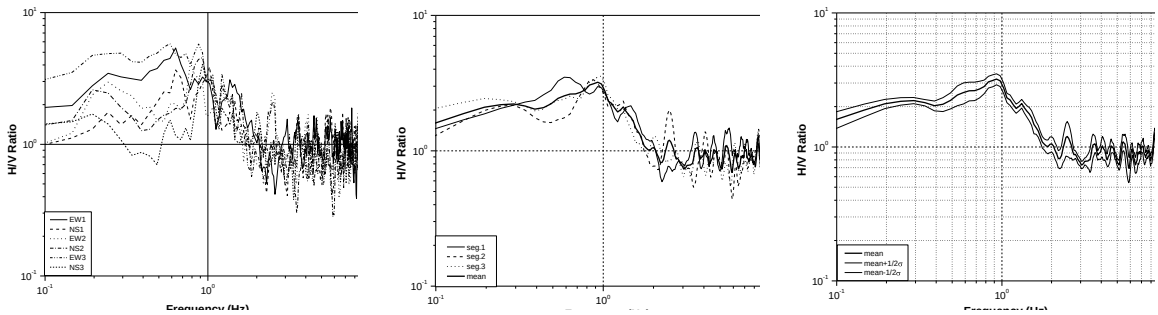

Figure C3.176: Predominant Frequency and H/V Ratio at MT101.

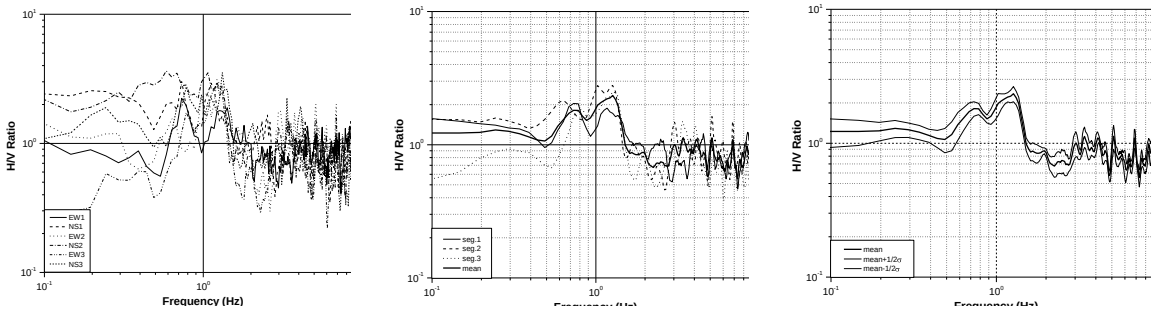

Figure C3.177: Predominant Frequency and H/V Ratio at MT102.

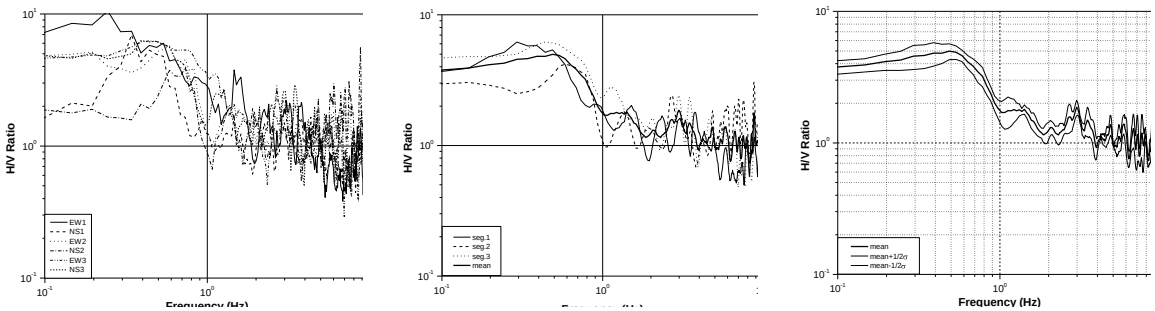

Figure C3.178: Predominant Frequency and H/V Ratio at MT103.

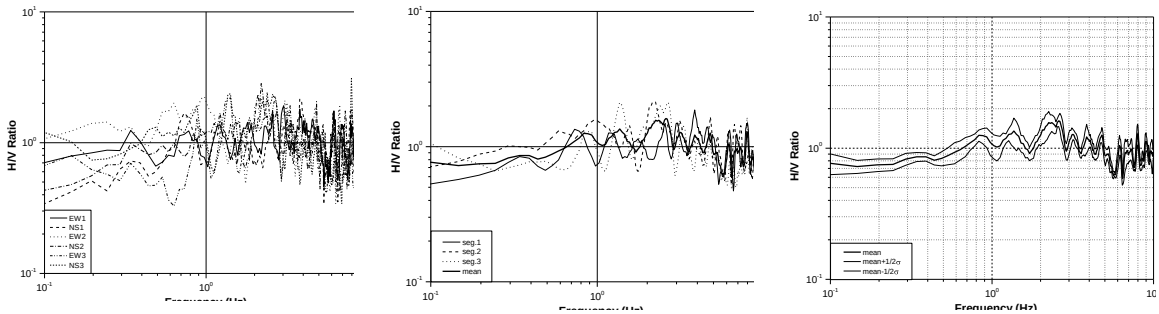

Figure C3.179: Predominant Frequency and H/V Ratio at MT104.

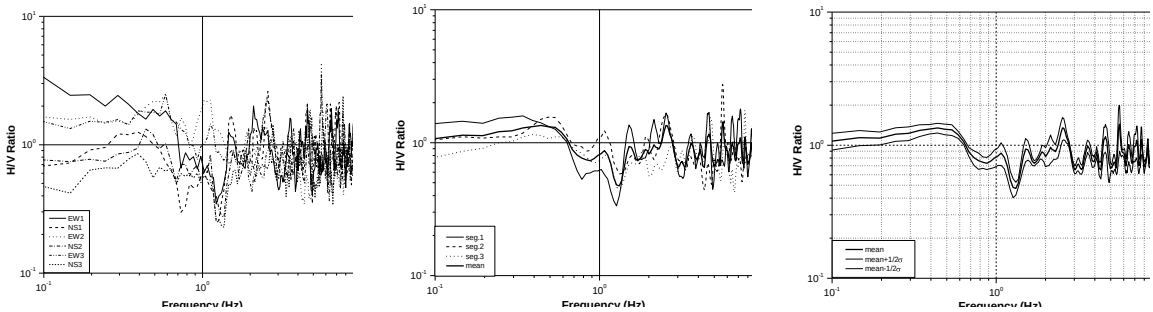

Figure C3.180: Predominant Frequency and H/V Ratio at MT105.

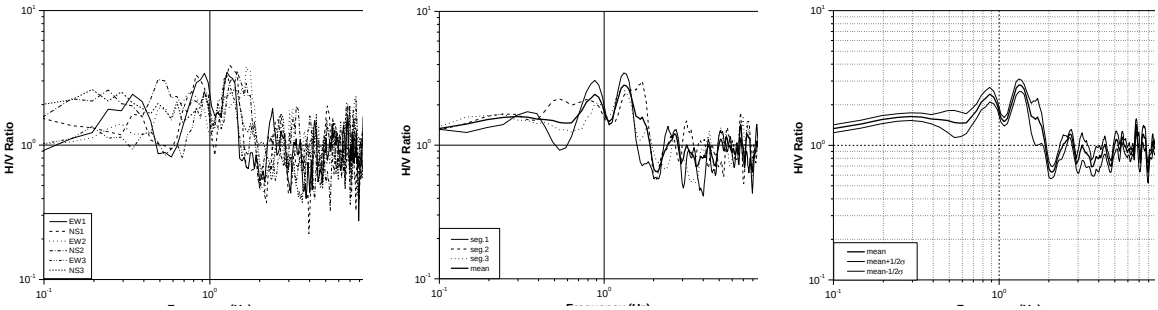

Figure C3.181: Predominant Frequency and H/V Ratio at MT106.

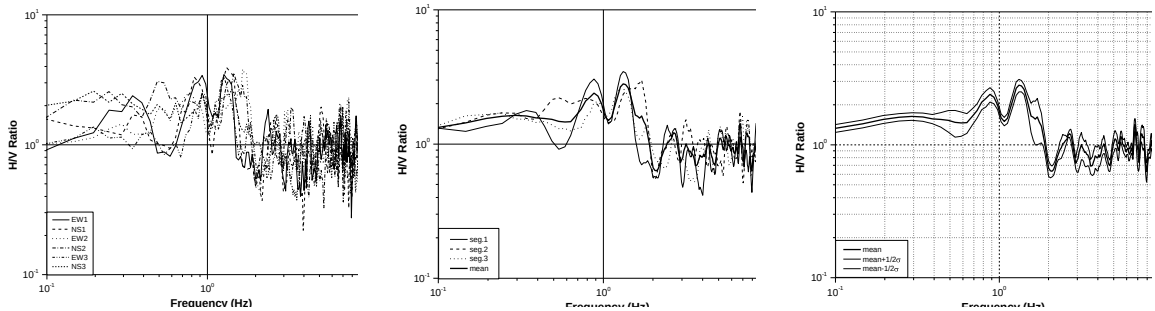

Figure C3.182: Predominant Frequency and H/V Ratio at MT107.

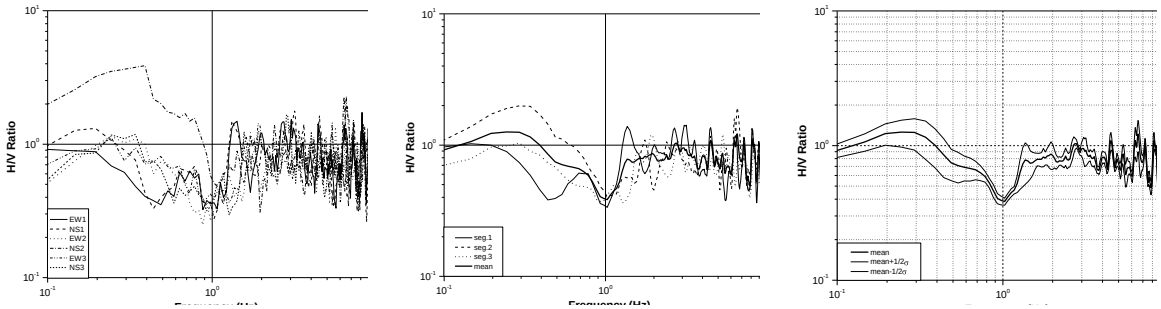

Figure C3.183: Predominant Frequency and H/V Ratio at MT108.

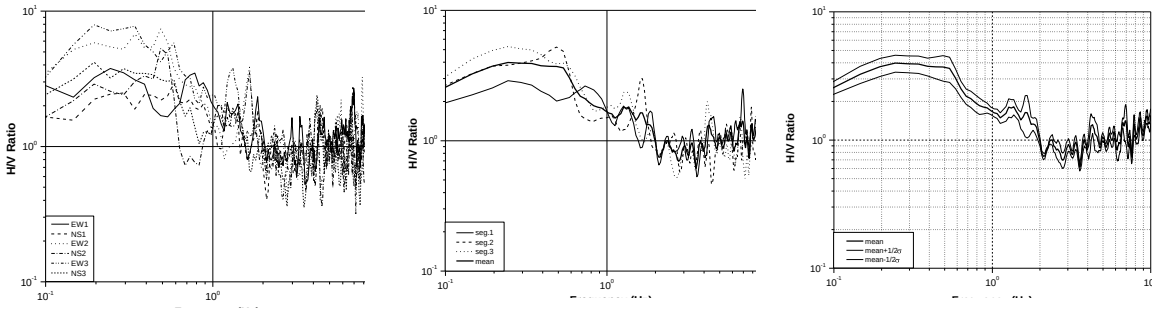

Figure C3.184: Predominant Frequency and H/V Ratio at MT109.

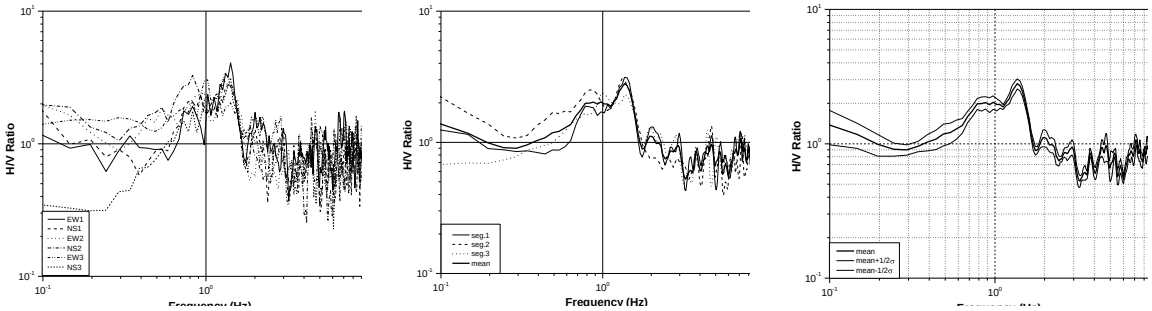

Figure C3.185: Predominant Frequency and H/V Ratio at MT110.

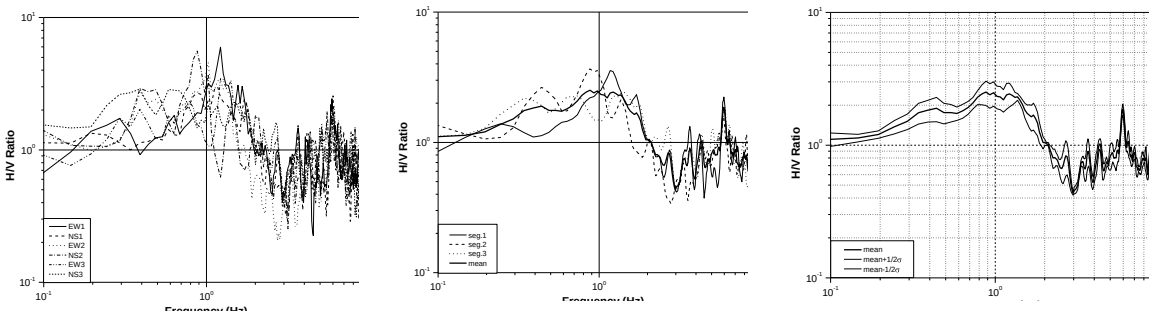

Figure C3.186: Predominant Frequency and H/V Ratio at MT111.

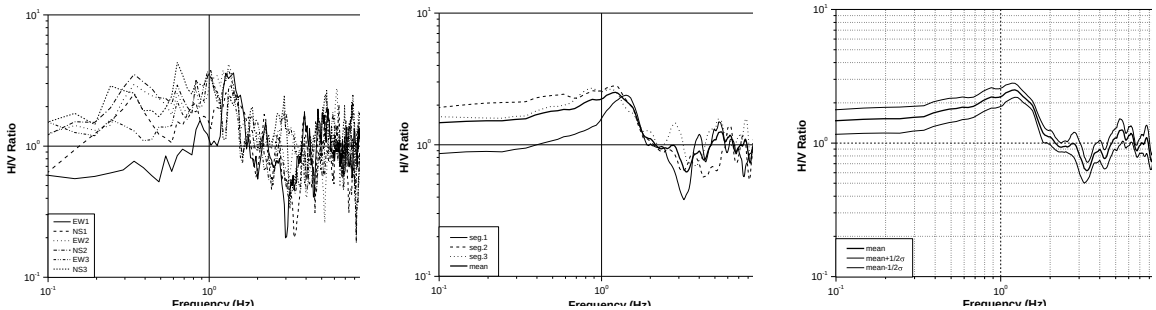

Figure C3.187: Predominant Frequency and H/V Ratio at MT112.

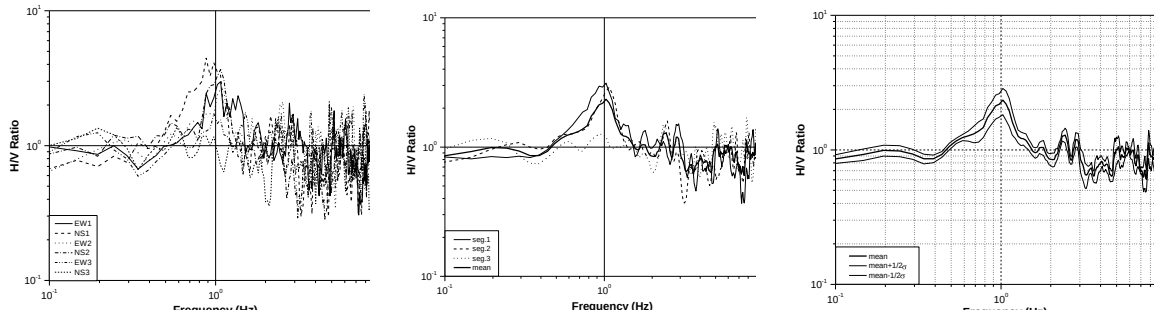

Figure C3.188: Predominant Frequency and H/V Ratio at MT113.

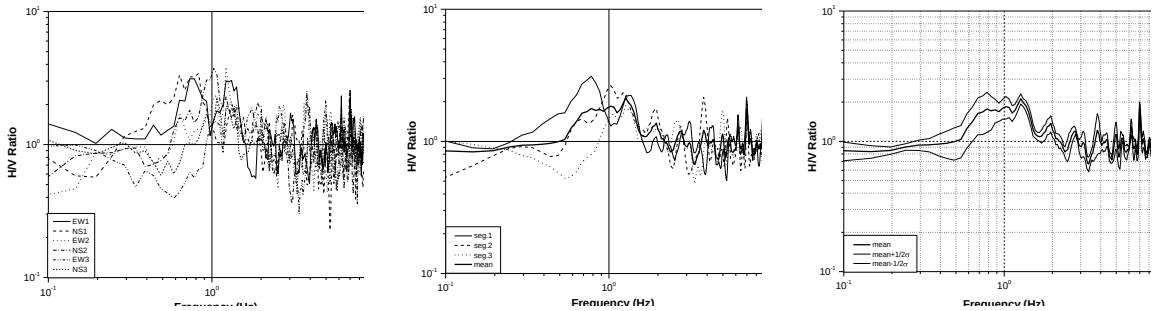

Figure C3.189: Predominant Frequency and H/V Ratio at MT114.

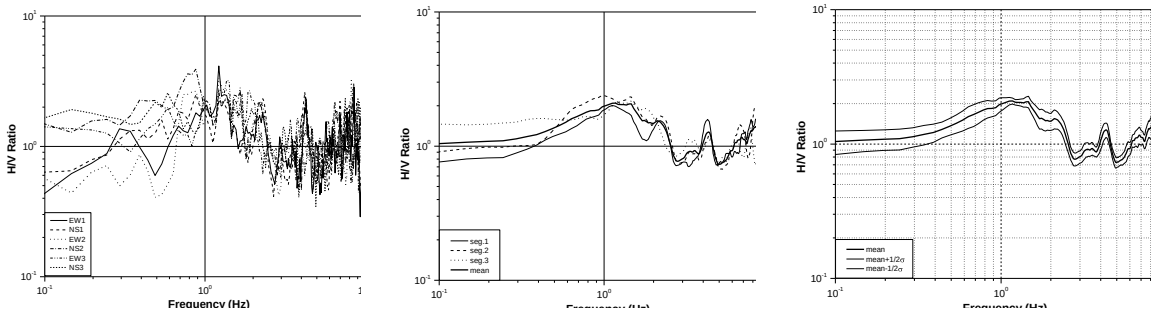

Figure C3.190: Predominant Frequency and H/V Ratio at MT115.

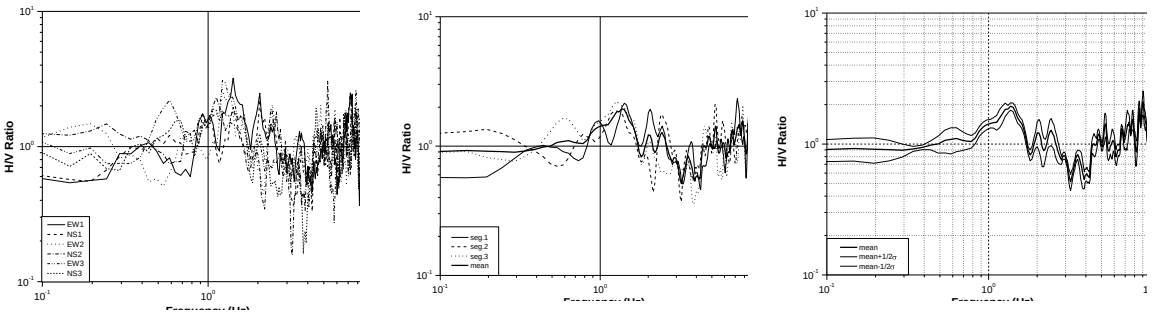

Figure C3.191: Predominant Frequency and H/V Ratio at MT116.

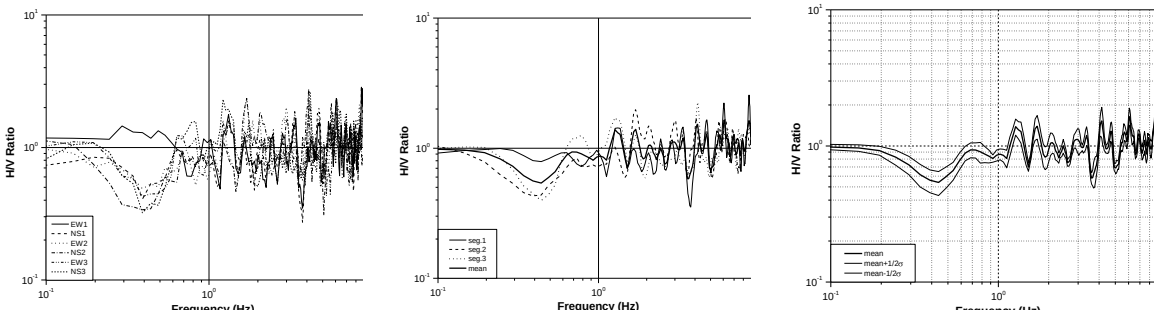

Figure C3.192: Predominant Frequency and H/V Ratio at MT117.

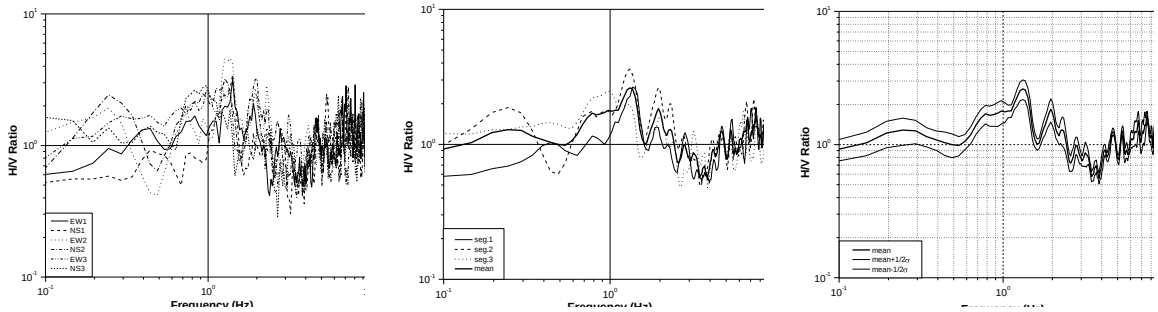

Figure C3.193: Predominant Frequency and H/V Ratio at MT118

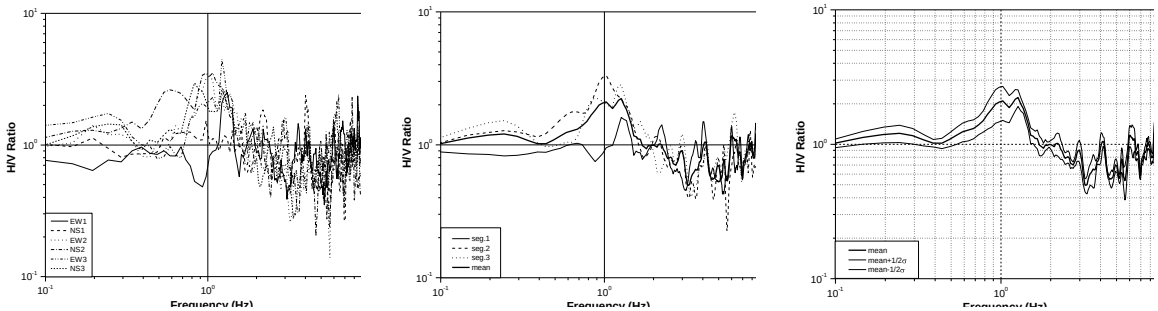

Figure C3.194: Predominant Frequenc19y and H/V Ratio at MT119.

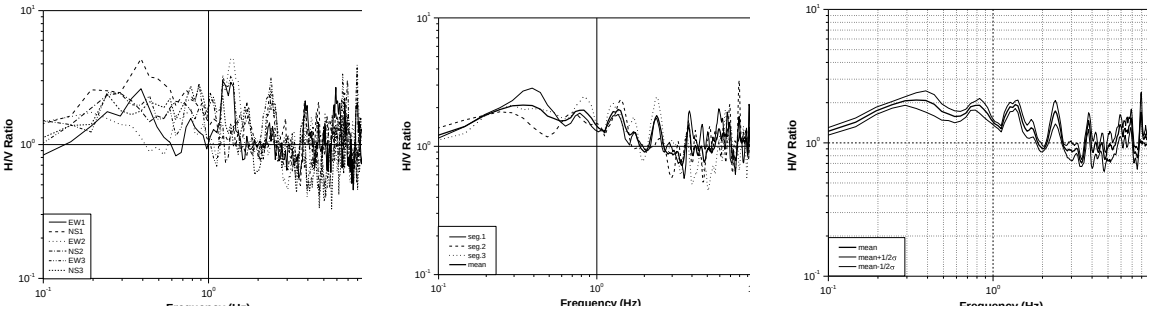

Figure C3.195: Predominant Frequency and H/V Ratio at MT120.

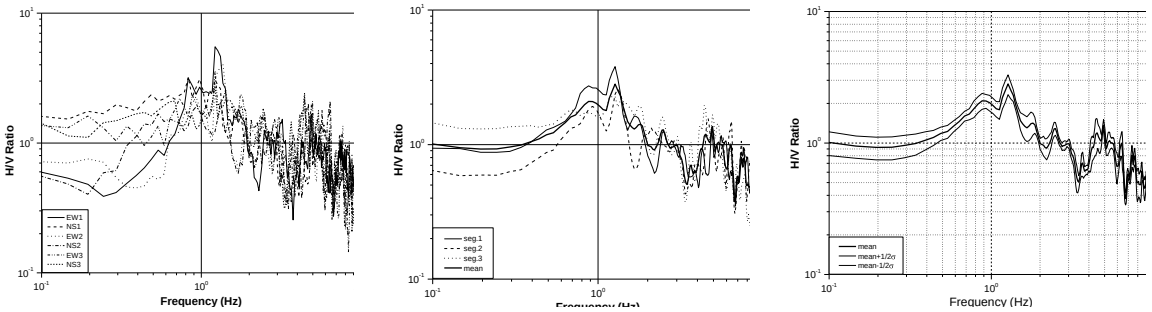

Figure C3.196: Predominant Frequency and H/V Ratio at MT121.

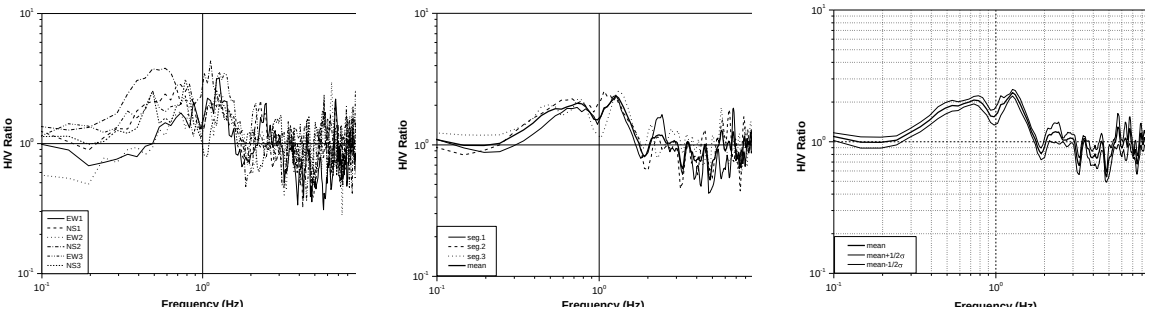

Figure C3.197: Predominant Frequency and H/V Ratio at MT122.

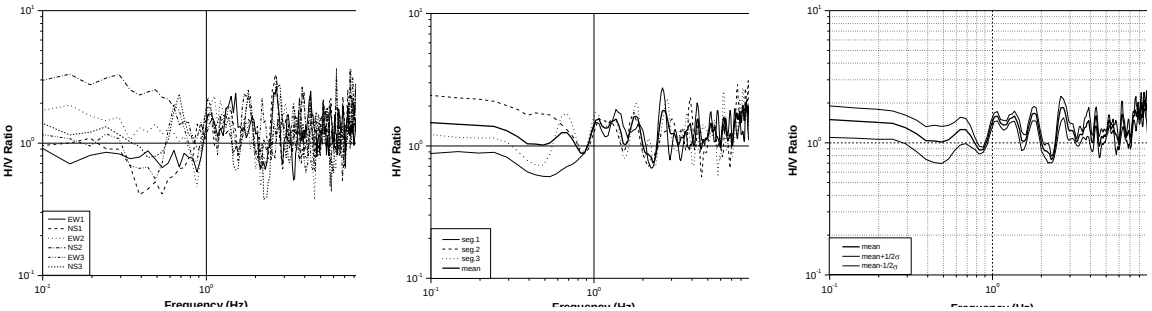

Figure C3.198: Predominant Frequency and H/V Ratio at MT123.

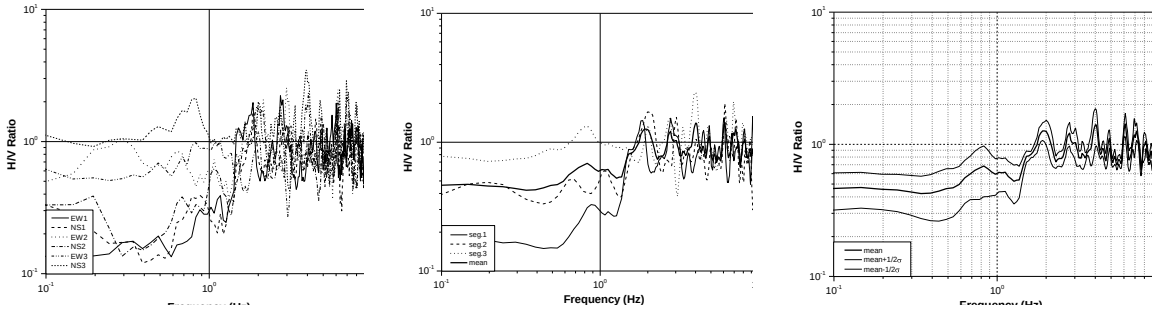

Figure C3.199: Predominant Frequency and H/V Ratio at MT124.

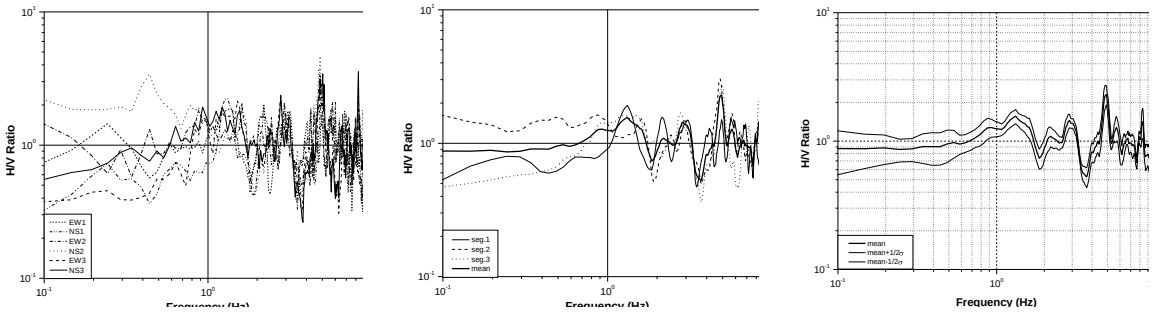

Figure C3.200: Predominant Frequency and H/V Ratio at MT125.

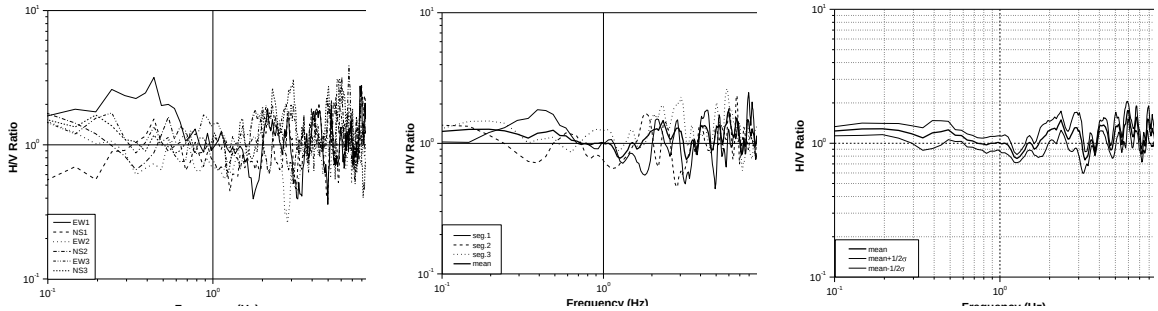

Figure C3.201: Predominant Frequency and H/V Ratio at MT126.

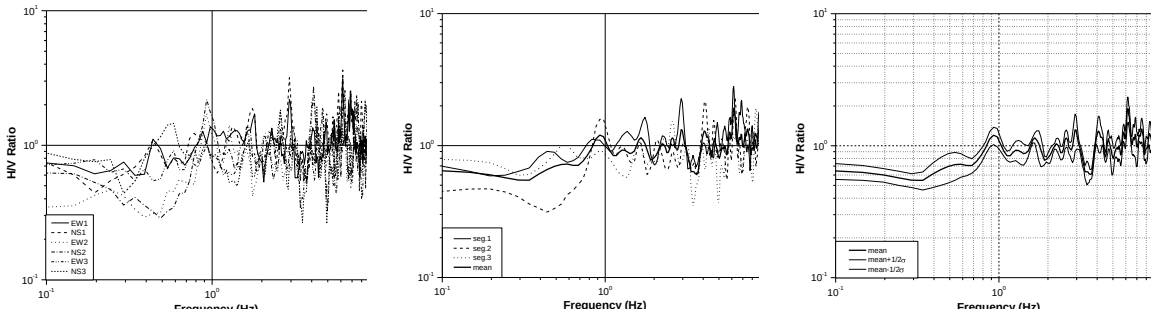

Figure C3.202: Predominant Frequency and H/V Ratio at MT127.

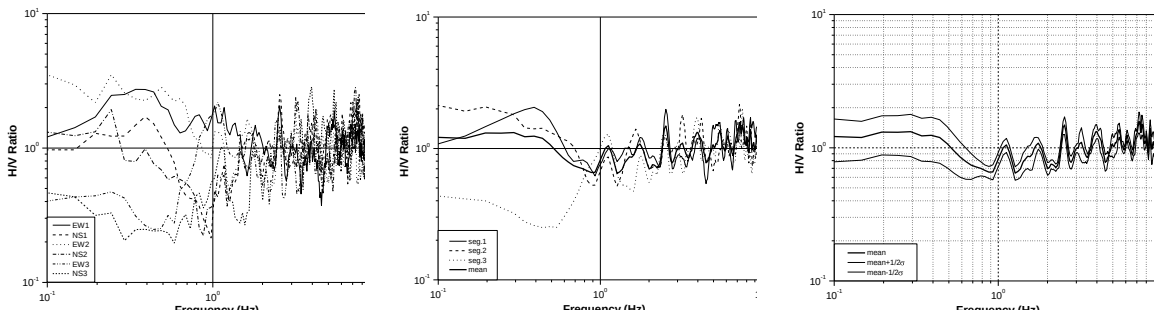

Figure C3.203: Predominant Frequency and H/V Ratio at MT128.

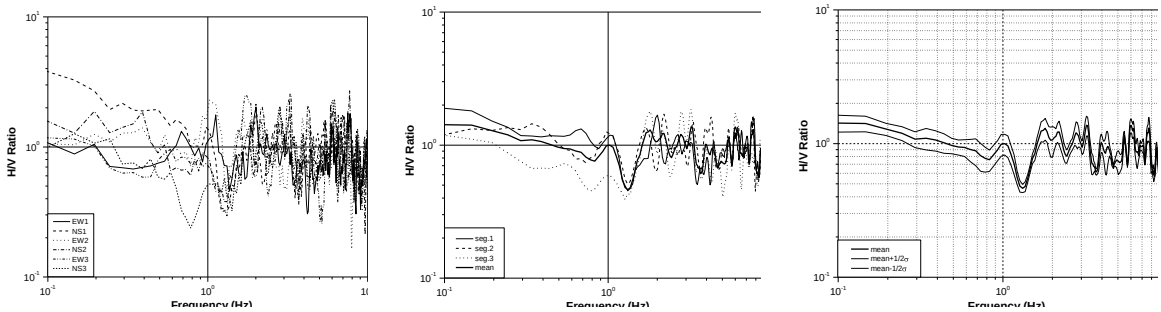

Figure C3.204: Predominant Frequency and H/V Ratio at MT129.

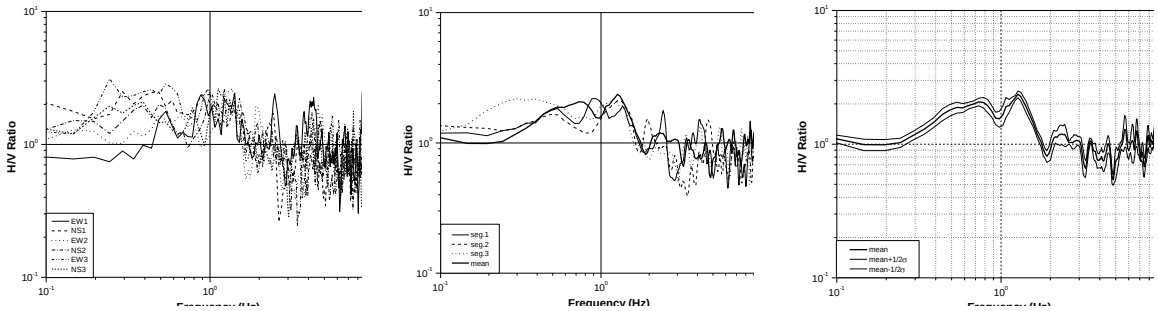

Figure C3.205: Predominant Frequency and H/V Ratio at MT130.

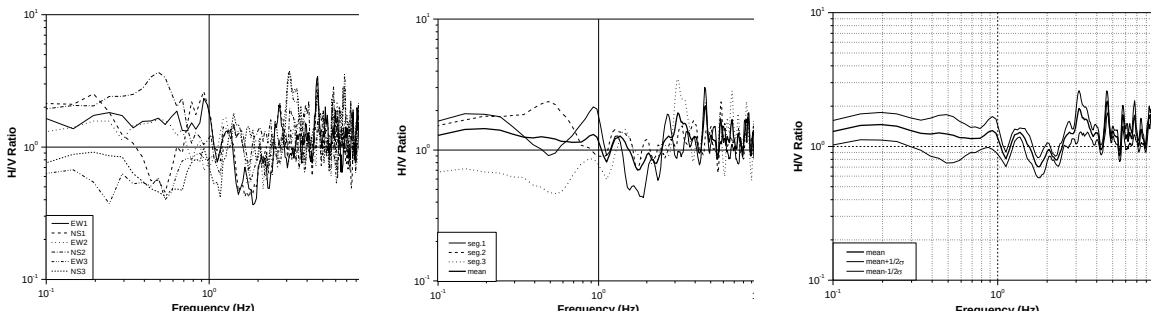

Figure C3.206: Predominant Frequency and H/V Ratio at MT131.

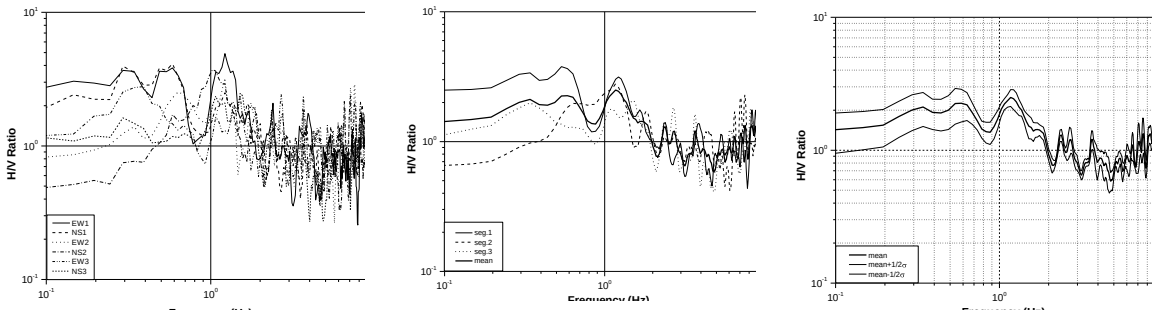

Figure C3.207: Predominant Frequency and H/V Ratio at MT132.

APPENDIX-D

MICROTREMOR FOURIER SPECTRUM OF SELECTED BUET BUILDINGS

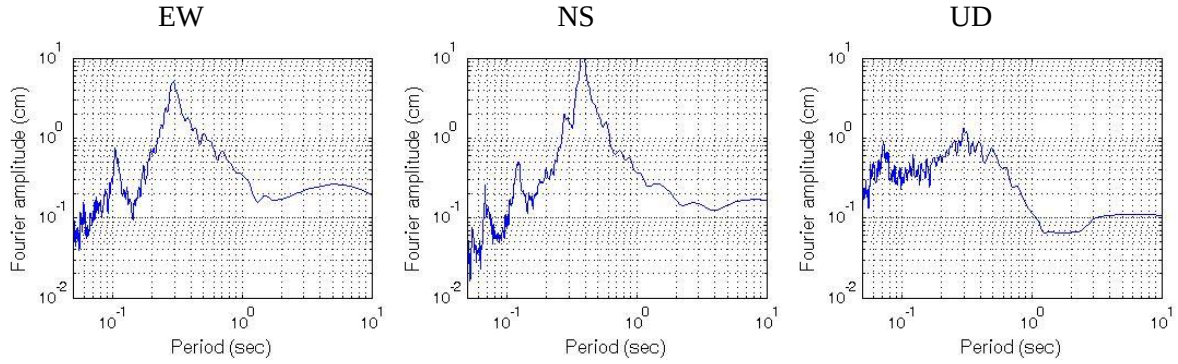

(a) top floor

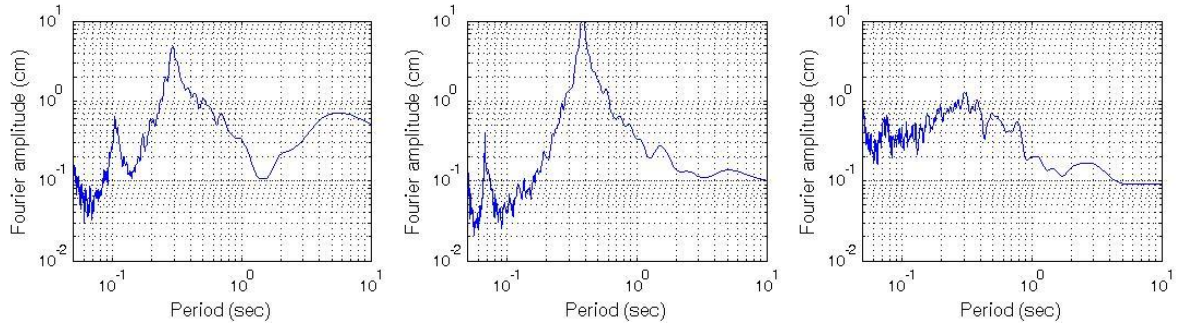

(b) 3rd floor

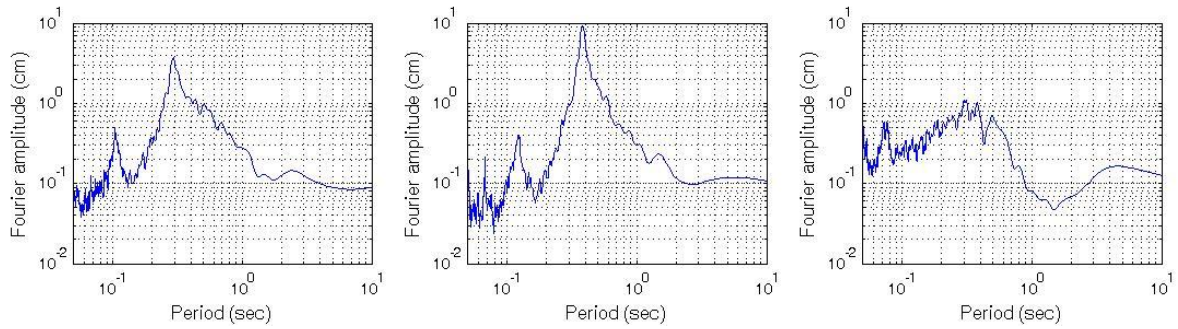

(c) 2nd floor

Figure D3.208: Predominant Period and Fourier spectrum of IFCDR Building.

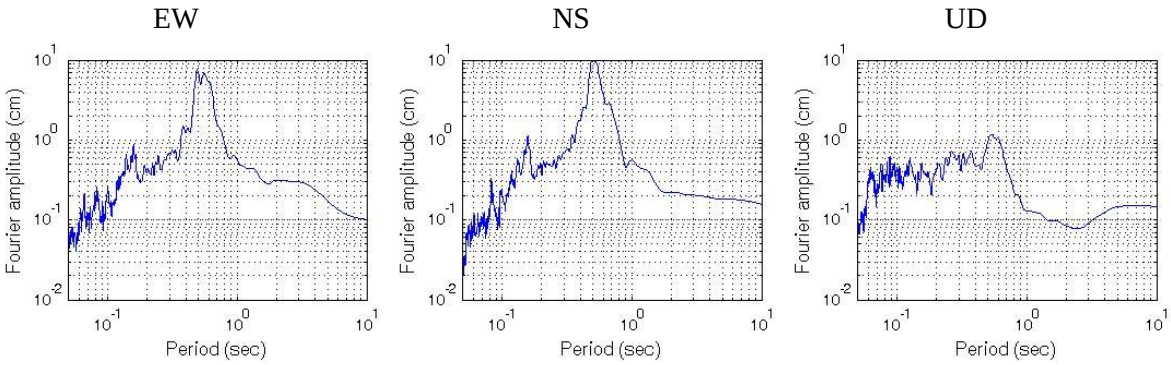

(a) top floor

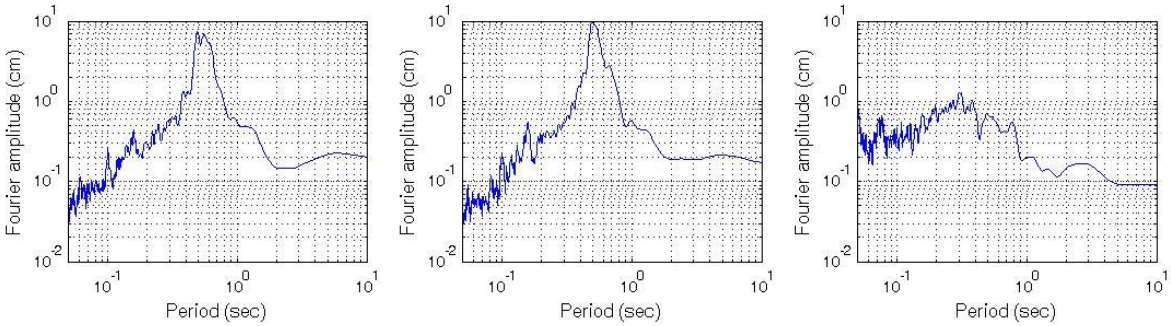

(b) 9th floor

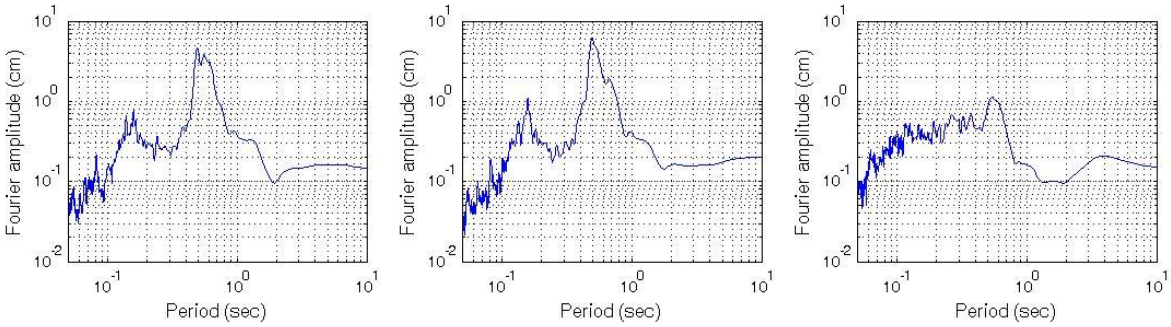

(c) 4th floor

Figure D3.209: Predominant Period and Fourier spectrum of 11 Storey Tower Building.

EW NS UD

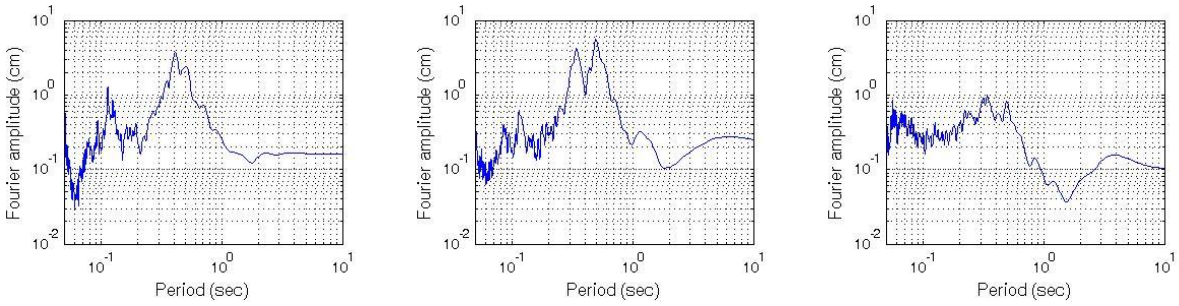

(a) top floor (center)

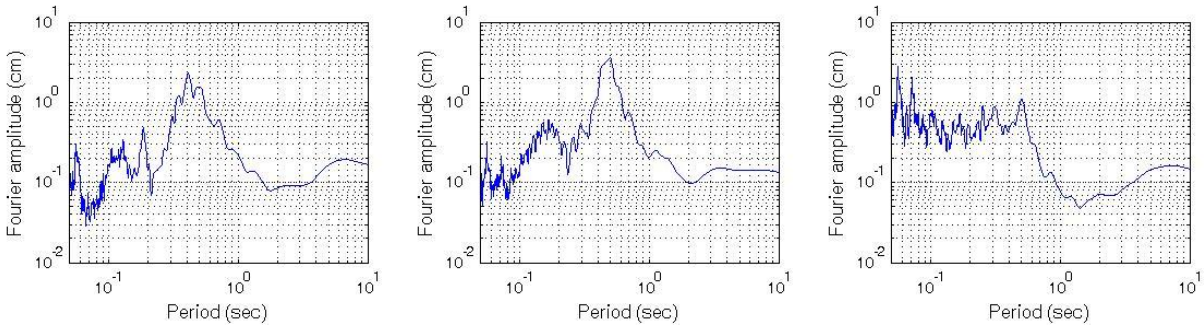

(b) 3rd floor (left)

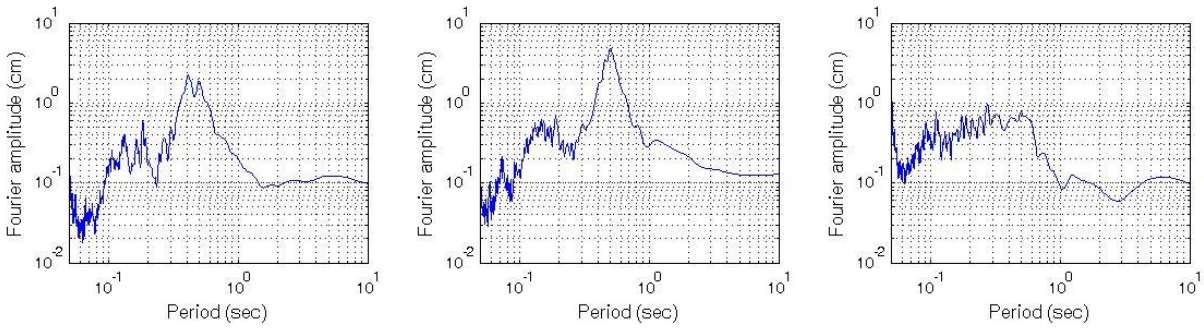

(d) 3rd floor (right)

Figure D3.210: Predominant Period and Fourier spectrum of Civil Engineering Building.

EW NS UD

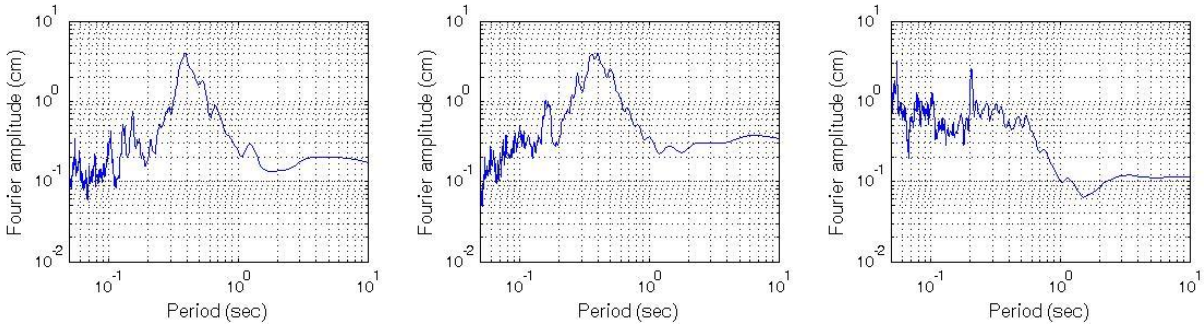

(a) top floor (right)

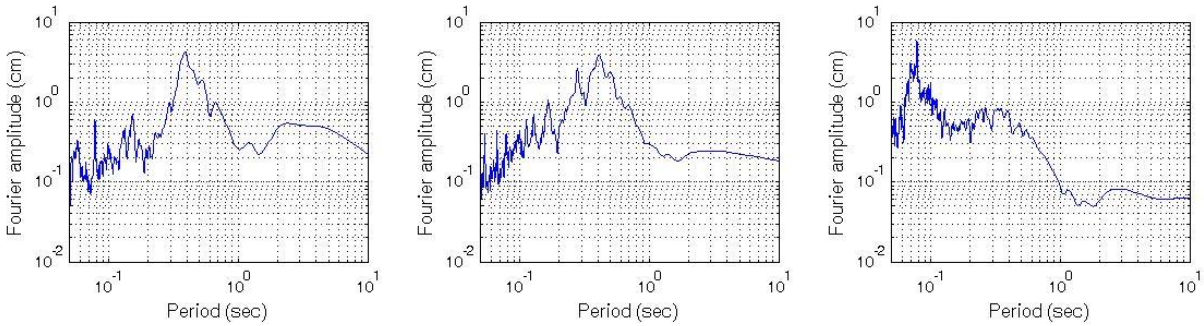

(b) top floor (left)

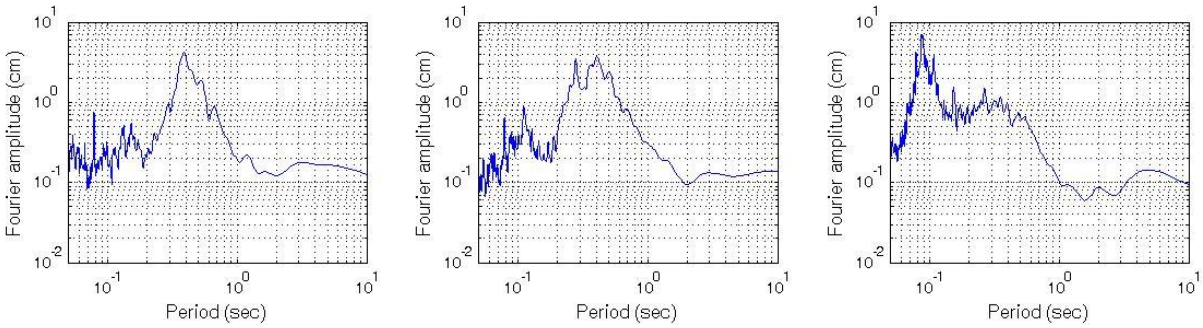

(b) top floor (center)

Figure D3.211: Predominant Period and Fourier spectrum of EME Building.

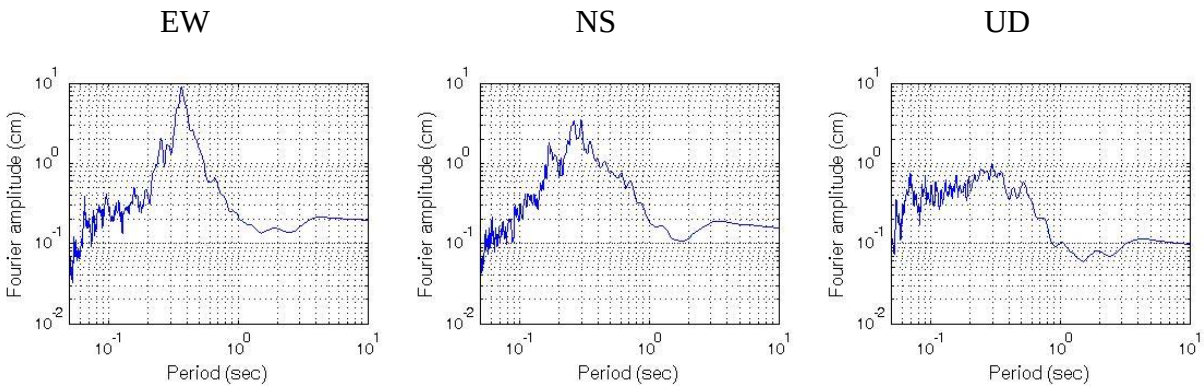

(c) top floor

Figure D3.212: Predominant Period and Fourier spectrum of Library Building.

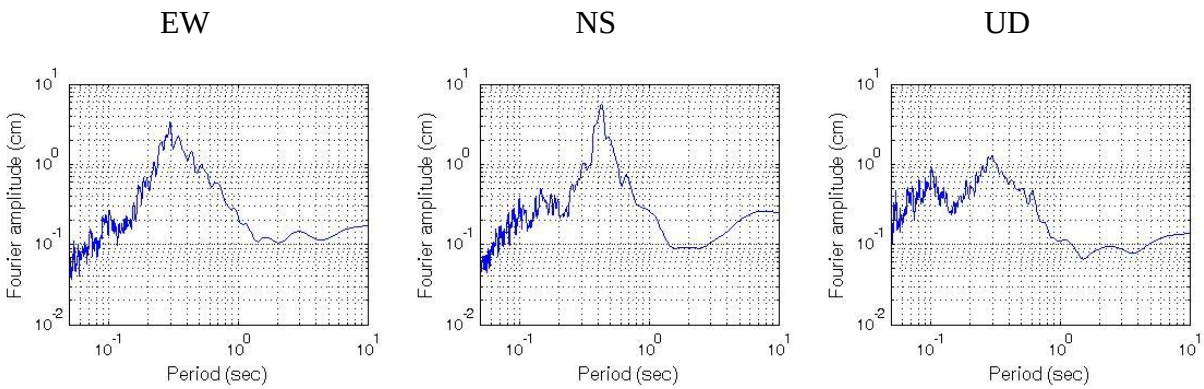

(a) 3rd floor (right)

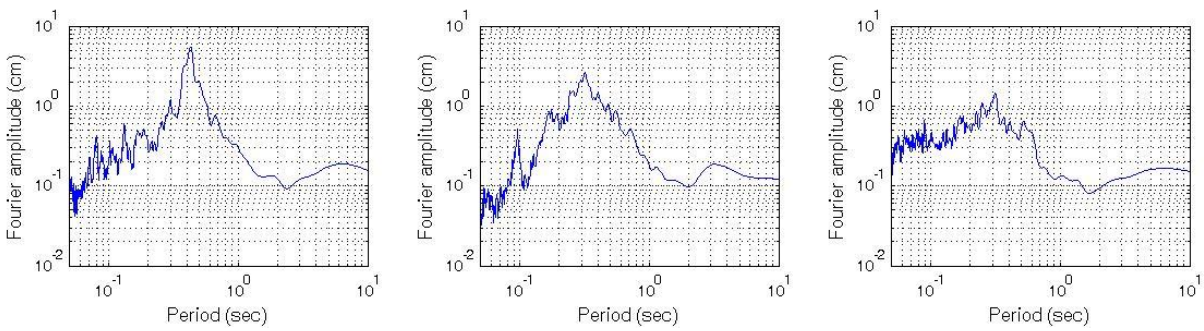

(b) 3rd floor (left)

Figure D3.213: Predominant Period and Fourier spectrum of Architecture Building.

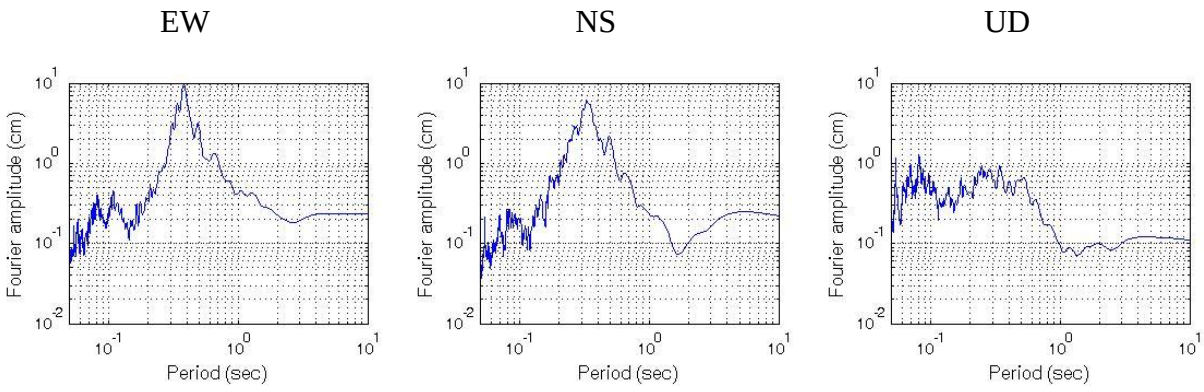

(a) top floor

Figure D3.214: Predominant Period and Fourier spectrum of URP Building.

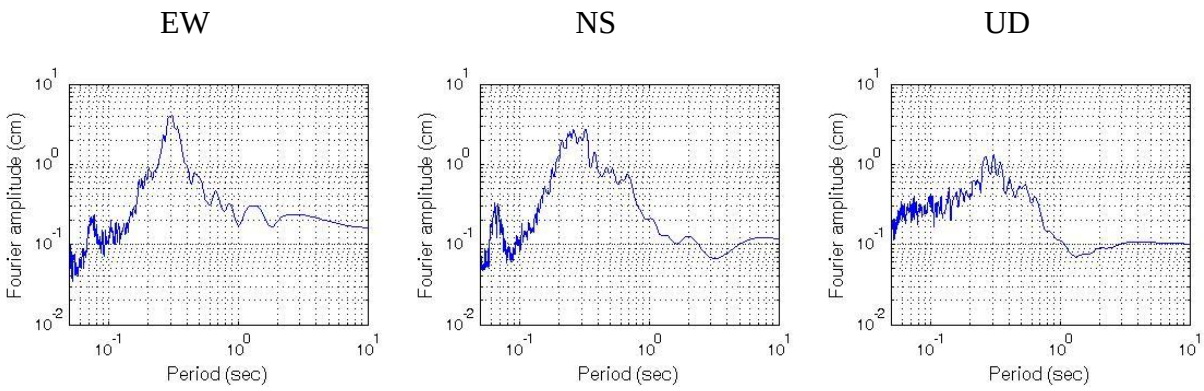

(a) top floor

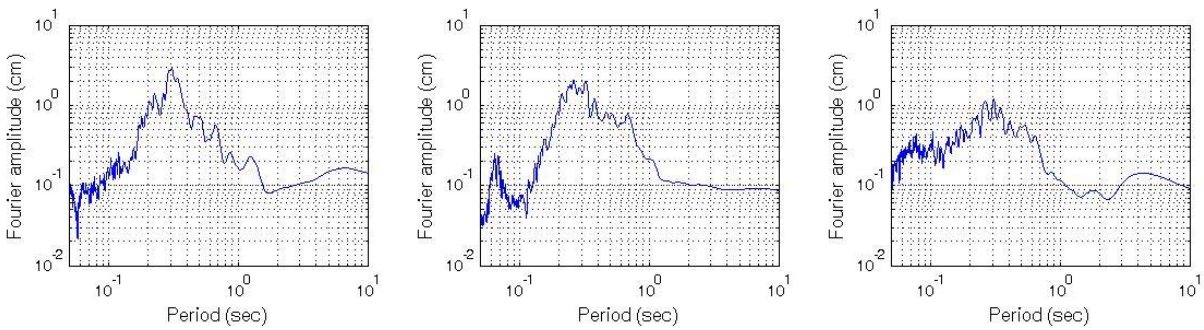

(b) 2nd floor

Figure D3.215: Predominant Period and Fourier spectrum of ARC Building.

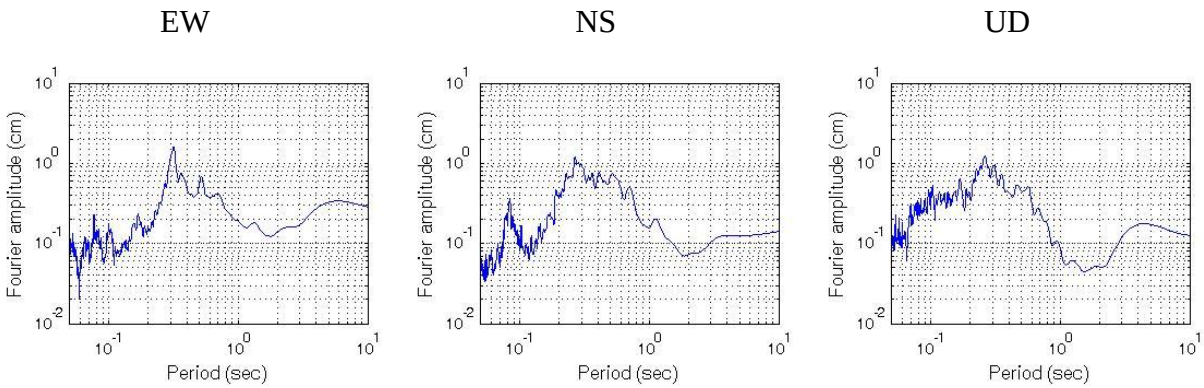

(a) 3rd floor

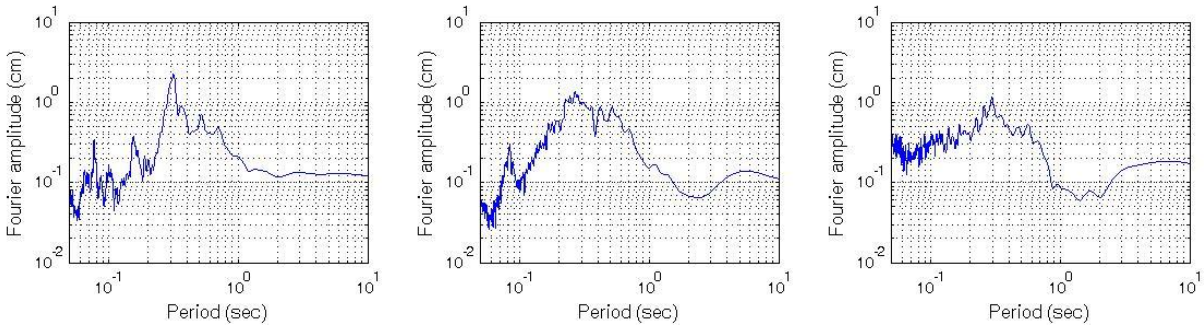

(c) 2nd floor

Figure D3.216: Predominant Period and Fourier spectrum of New Academic Building.

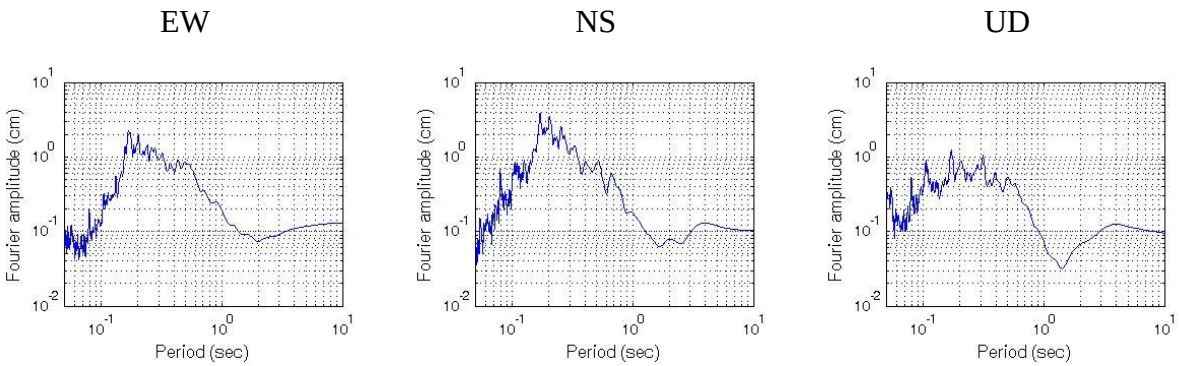

(a) top floor

Figure D3.217: Predominant Period and Fourier spectrum of Controller of Examination Building.

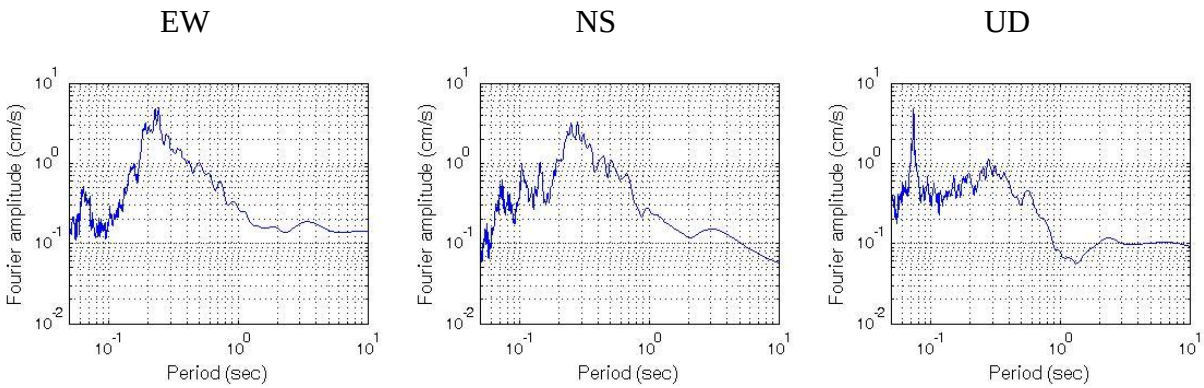

(a) top floor (left)

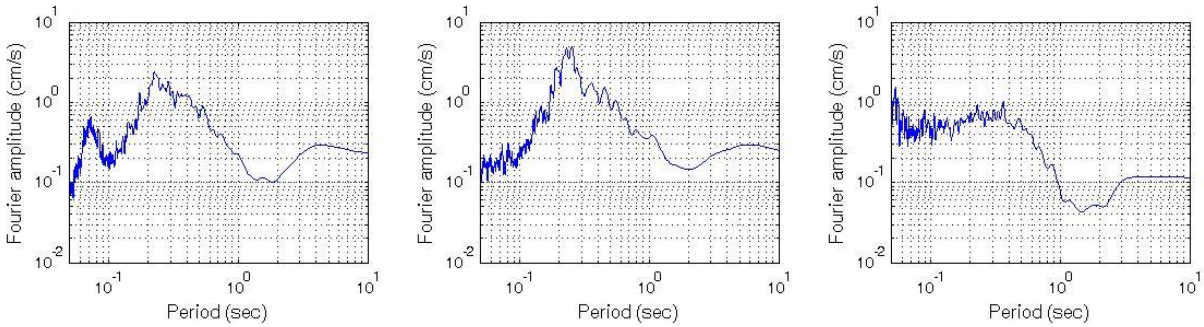

(b) top floor (right)

Figure D3.218: Predominant Period and Fourier spectrum of Engineering University School Building.

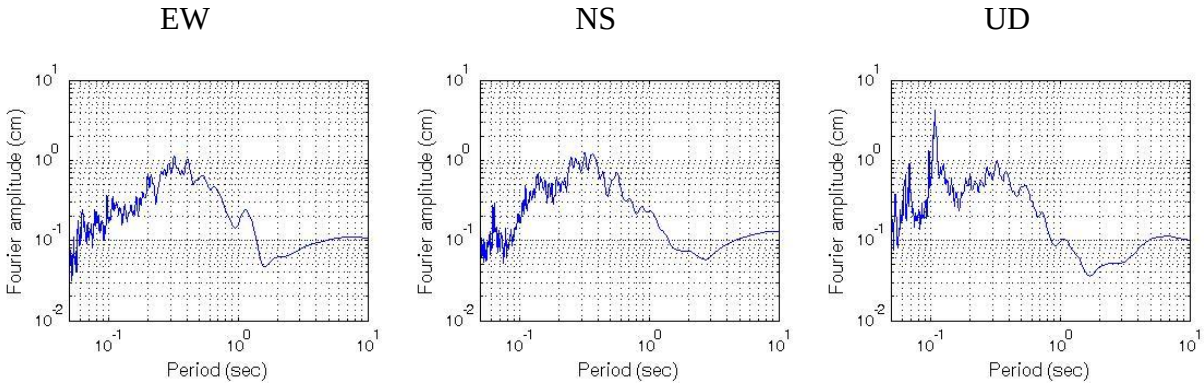

(a) 3rd floor (North Block)

Figure D3.219: Predominant Period and Fourier spectrum of Titumir Hall.

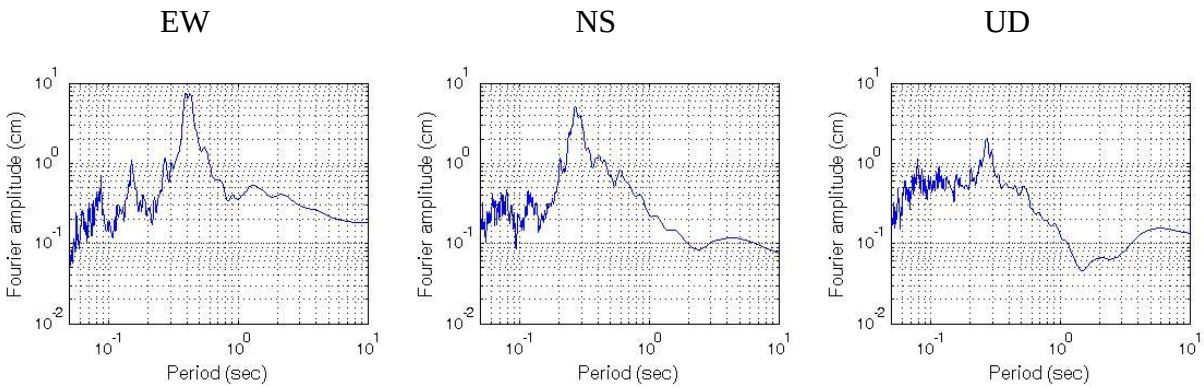

(a) 4th floor

Figure B3.220: Predominant Period and Fourier spectrum of Sher-e-Bangla Hall.

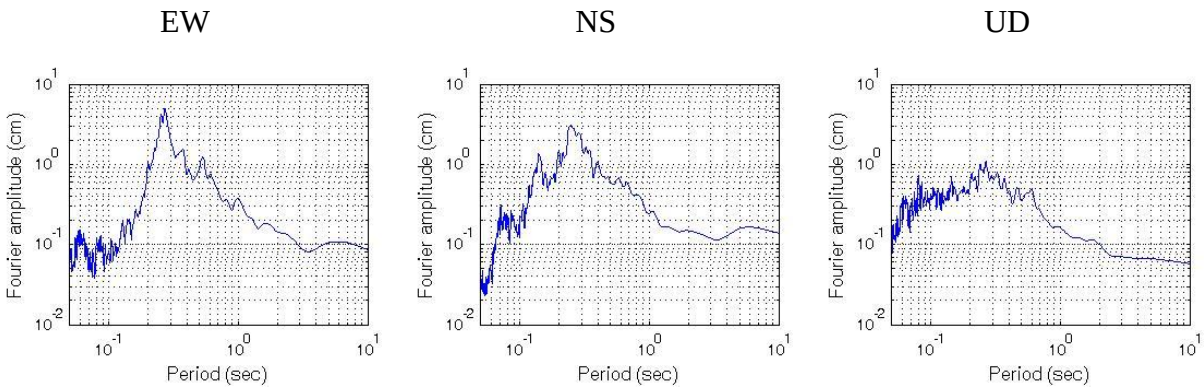

(a) 4th floor

Figure D3.221: Predominant Period and Fourier spectrum of Dr. MA Rashid Hall.

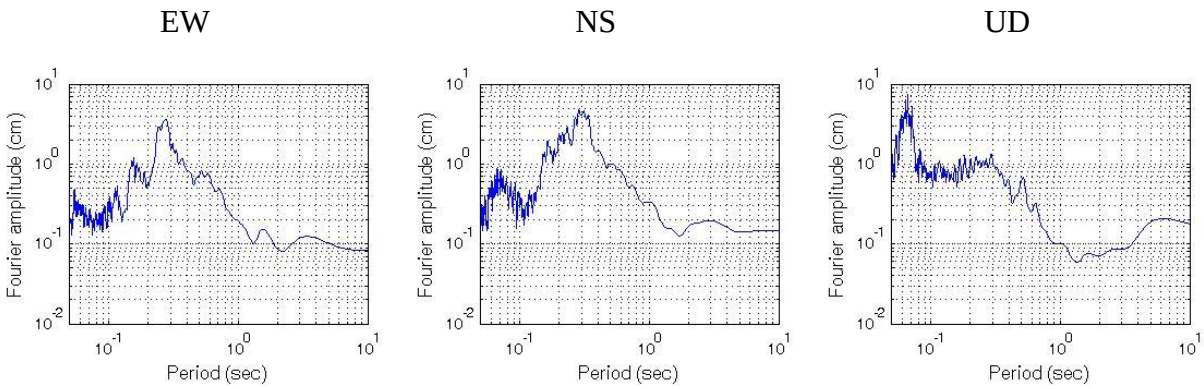

(a) 4th floor (middle)

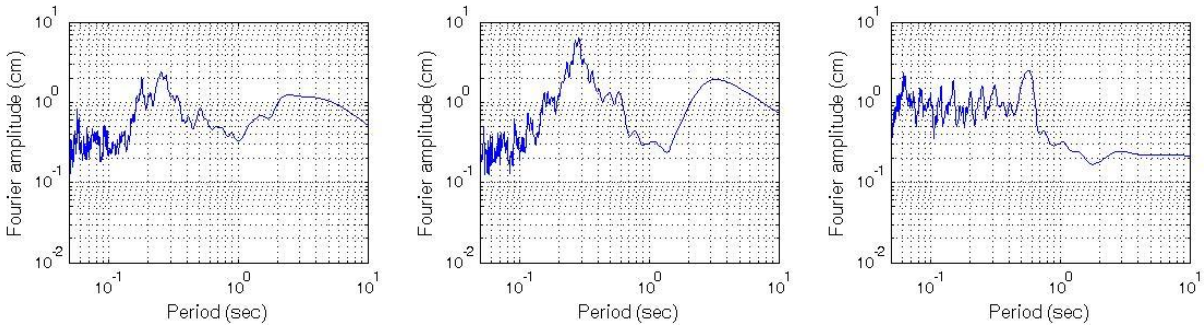

(b) 4th floor (right)

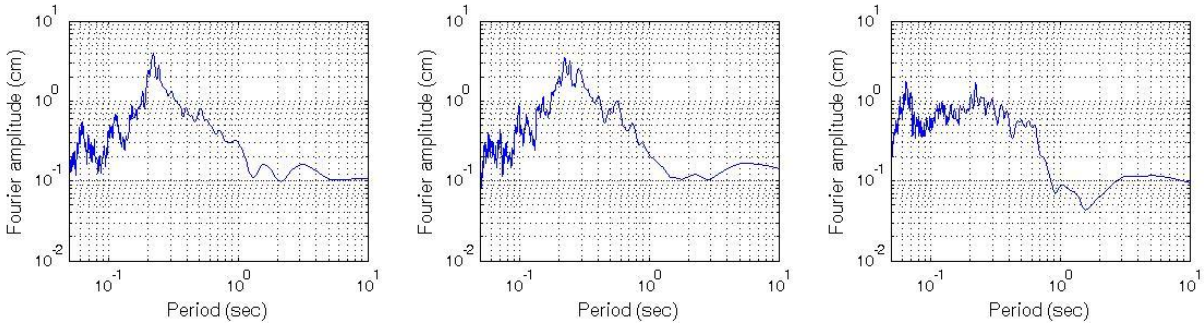

(c) 3rd floor (left)

Figure D3.222: Predominant Period and Fourier spectrum of Ahsan-Ullah Hall.

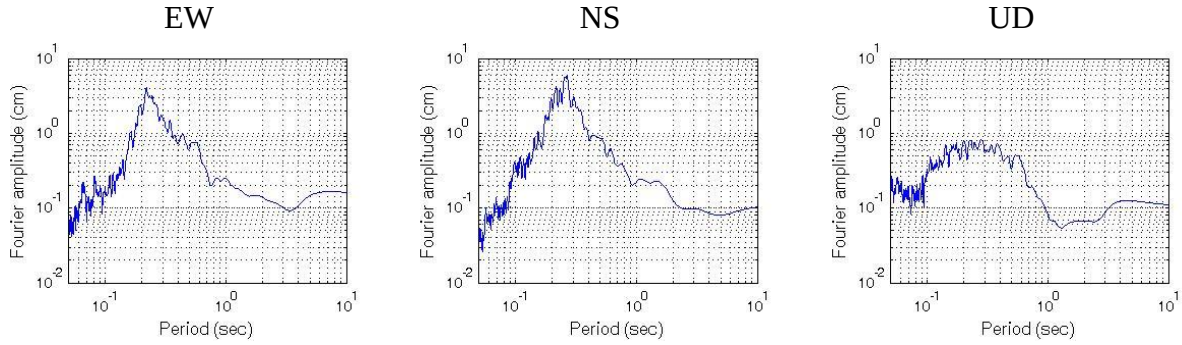

(a) top floor (right)

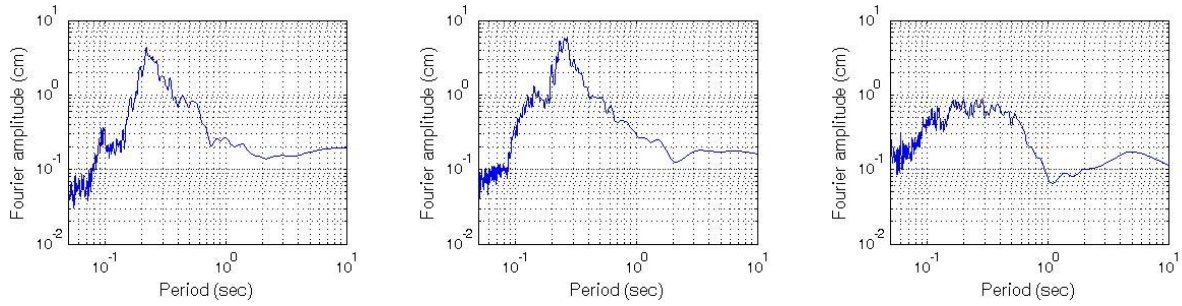

(d) top floor (left)

Figure D3.223: Predominant Period and Fourier spectrum of Shahid Smrity Hall (Middle Building).

EW NS UD

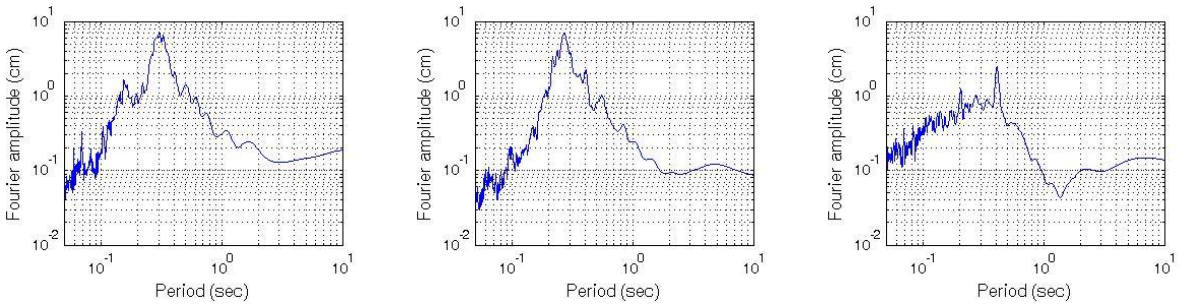

(a) top floor (center)

Figure D3.224: Predominant Period and Fourier spectrum of Shahid Smrity Hall (North Building).

EW NS UD

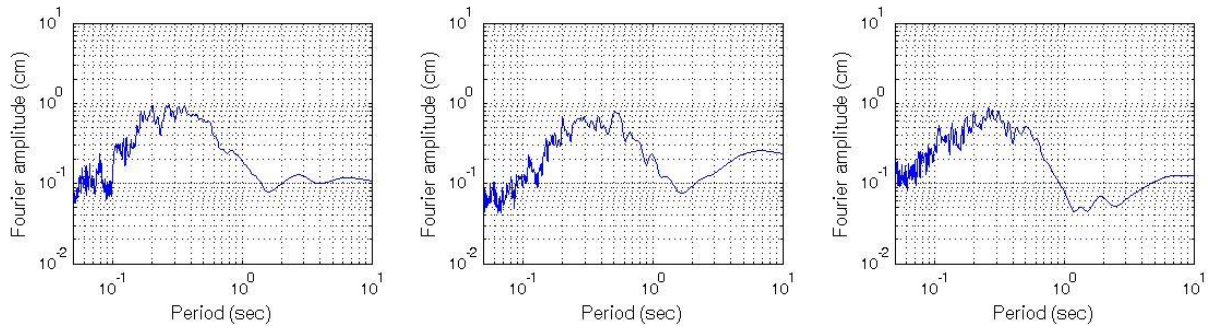

(a) 1st floor

Figure D3.225: Predominant Period and Fourier spectrum of Register Building.

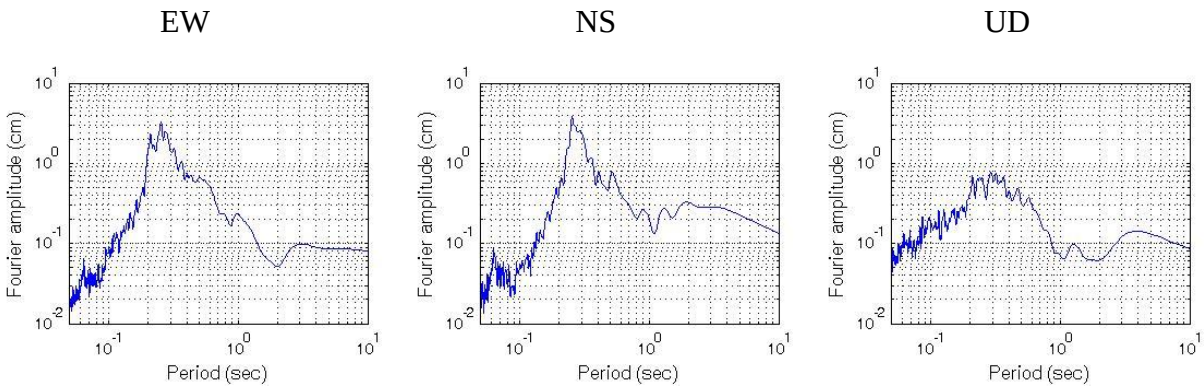

(a) 3rd floor

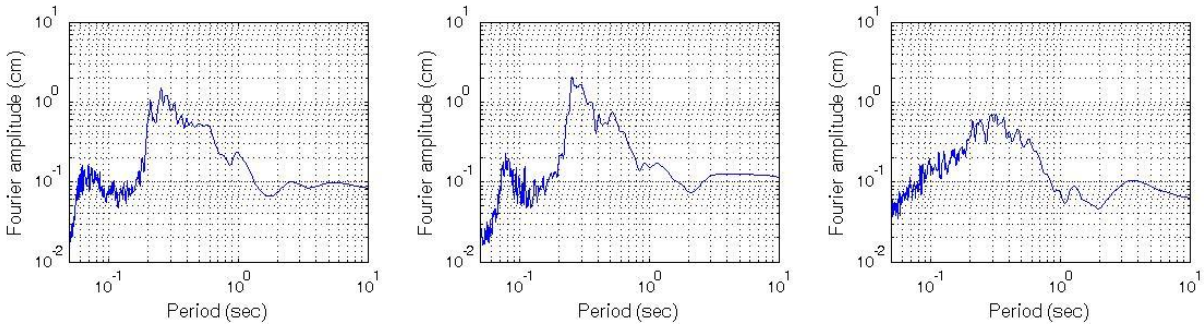

(b) 1st floor

Figure D3.226: Predominant Period and Fourier spectrum of Building # 1.

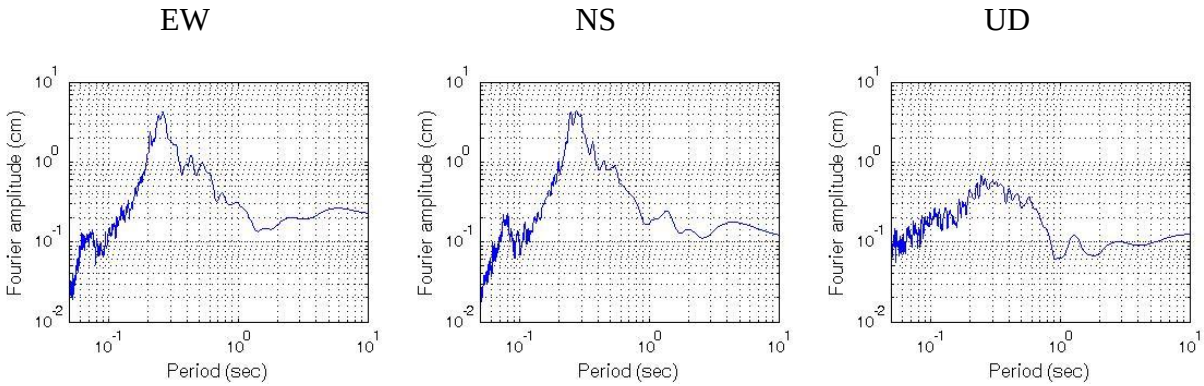

(a) top floor

Figure D3.227: Predominant Period and Fourier spectrum of Building # 2.

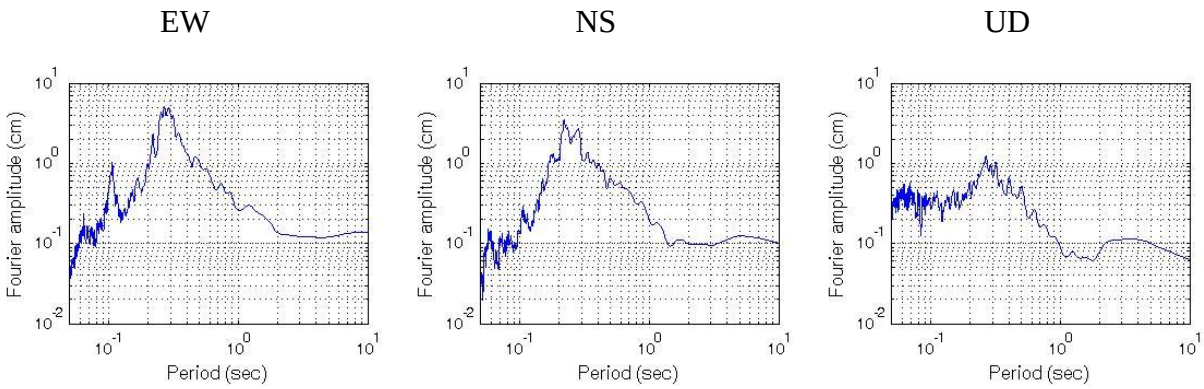

(a) top floor

Figure D3.228: Predominant Period and Fourier spectrum of Building # 3.

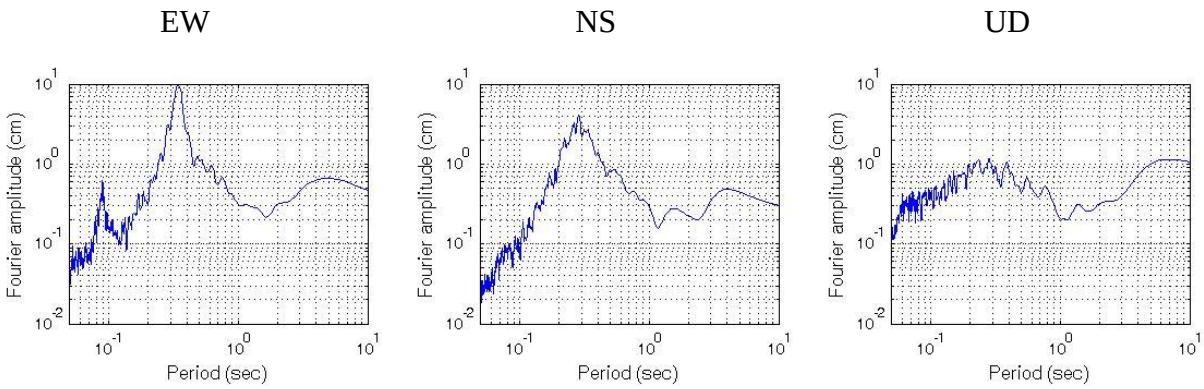

(a) 4th floor

Figure D3.229: Predominant Period and Fourier spectrum of Building # 4.

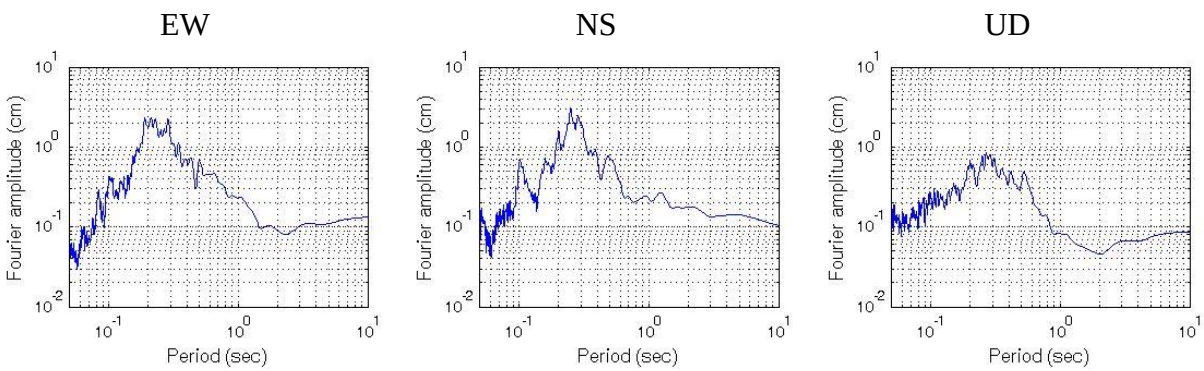

(a) top floor (left)

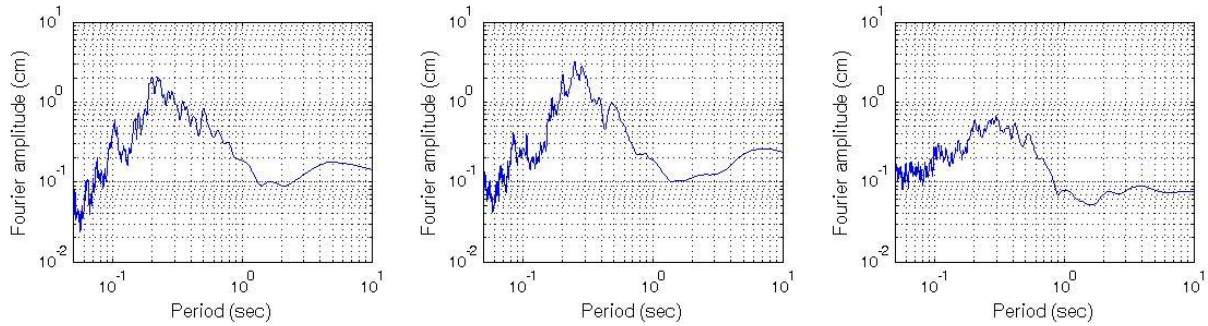

(b) top floor (right)

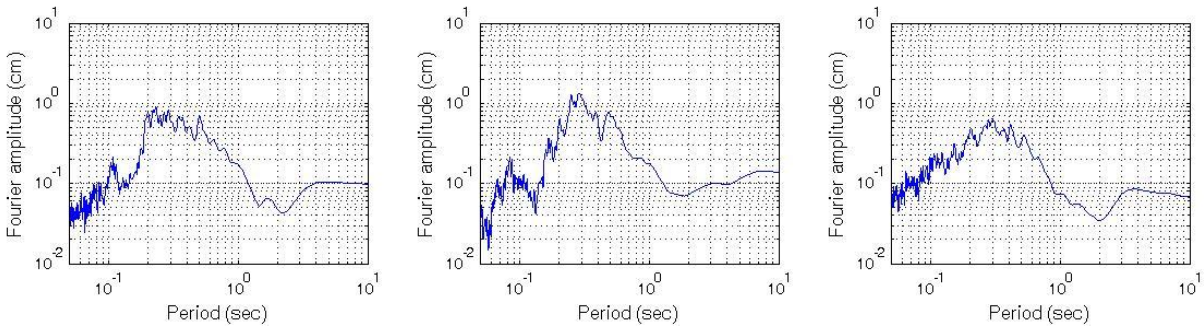

(c) 1st floor (right)

Figure D3.230: Predominant Period and Fourier spectrum of Building # 5.

EW NS UD

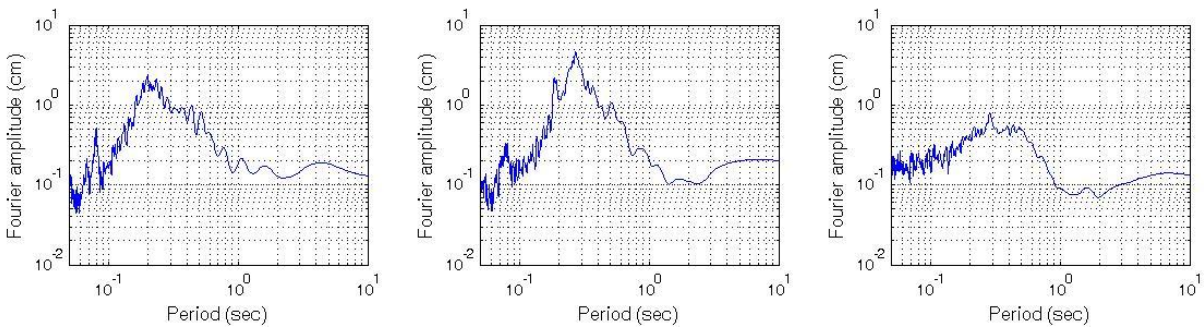

(a) top floor

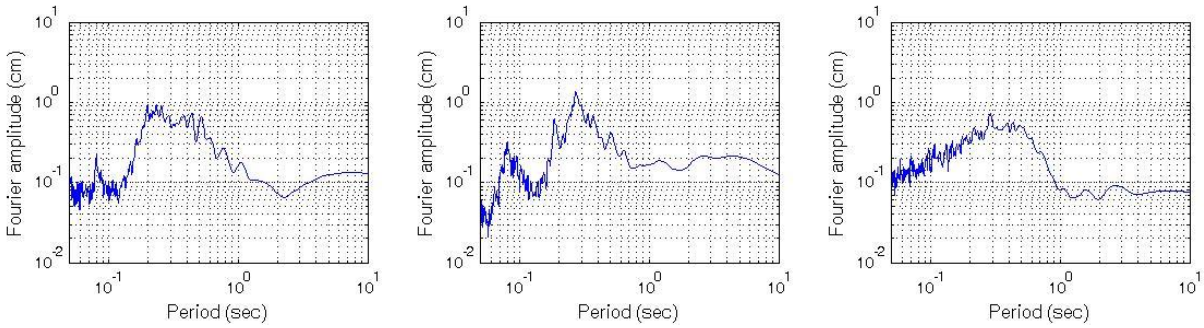

(b) 1st floor

Figure D3.231: Predominant Period and Fourier spectrum of Building # 6.

EW NS UD

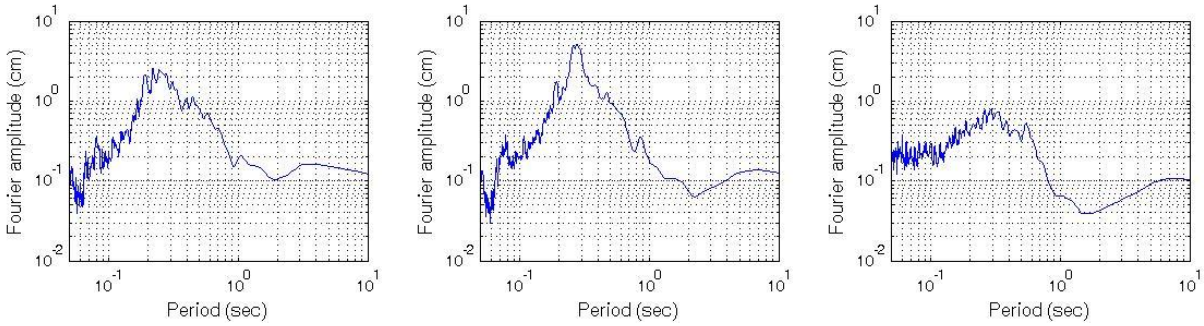

(a) top floor

Figure D3.232: Predominant Period and Fourier spectrum of Building # 7.

EW NS UD

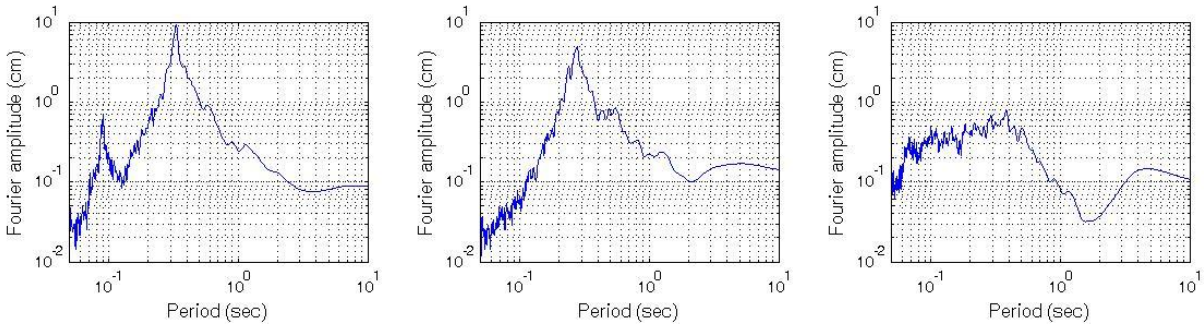

(a) 4th floor

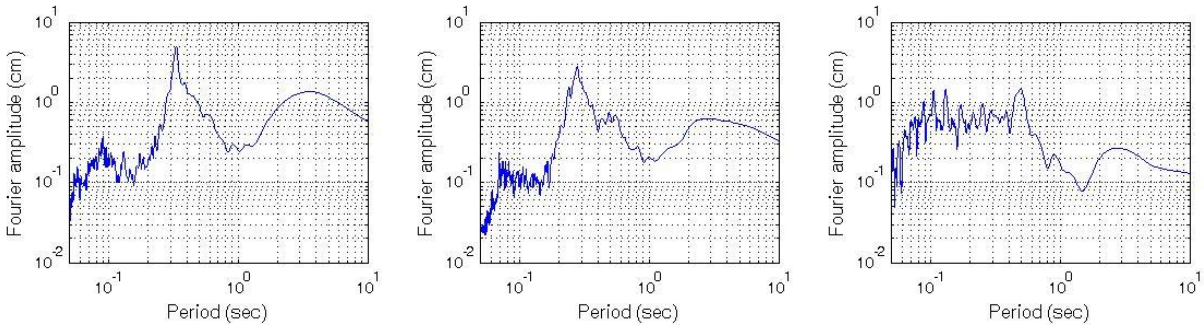

(b) 2nd floor

Figure D3.233: Predominant Period and Fourier spectrum of Building # 8.

EW NS UD

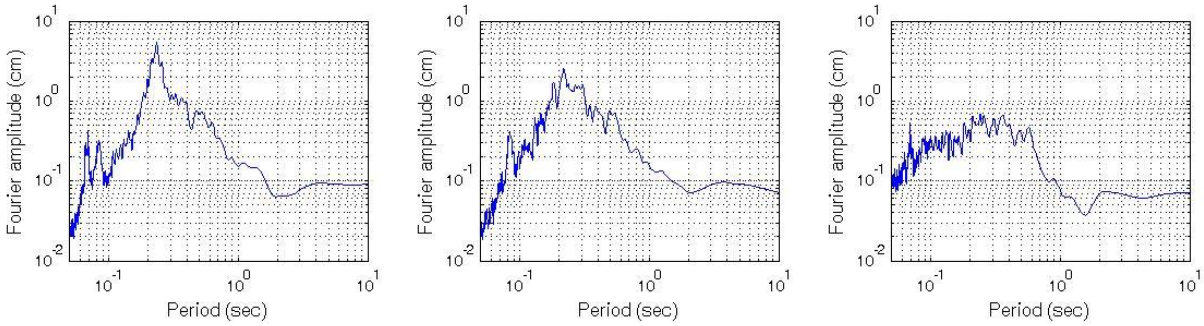

(a) 4th floor

Figure D3.234: Predominant Period and Fourier spectrum of Building # 9.

EW NS UD

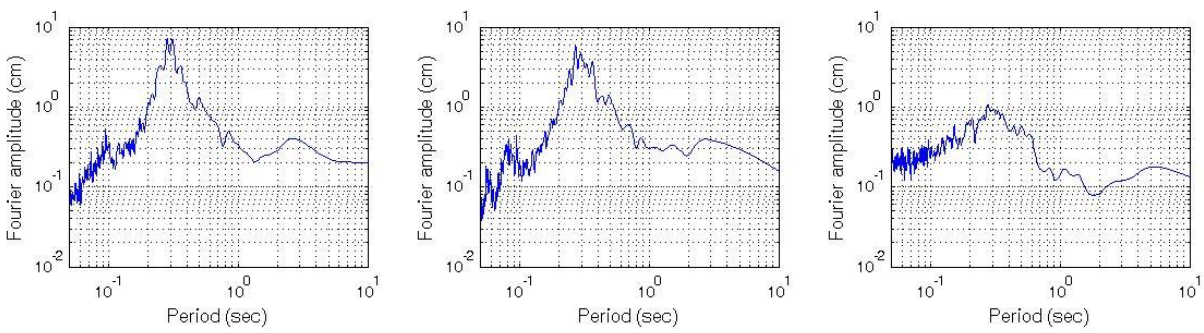

(a) top floor

Figure D3.235: Predominant Period and Fourier spectrum of Building # 12.

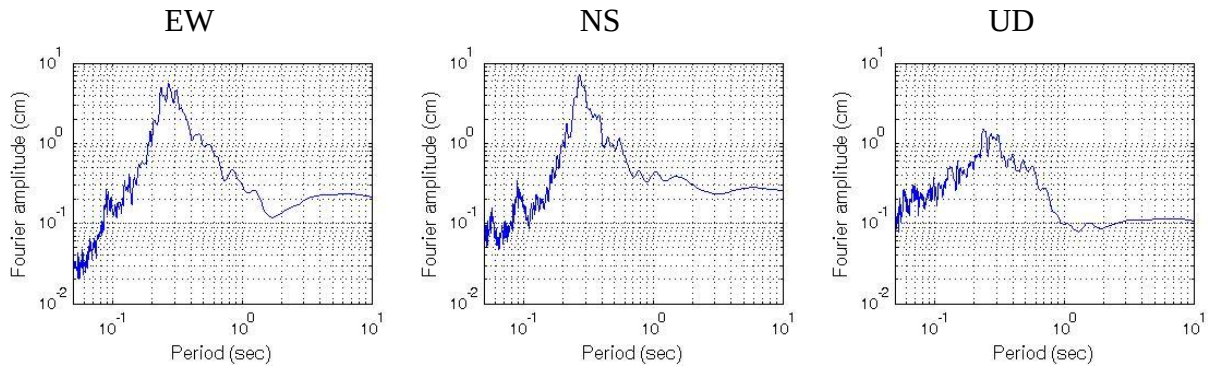

(a) top floor

Figure D3.236: Predominant Period and Fourier spectrum of Building # 13.

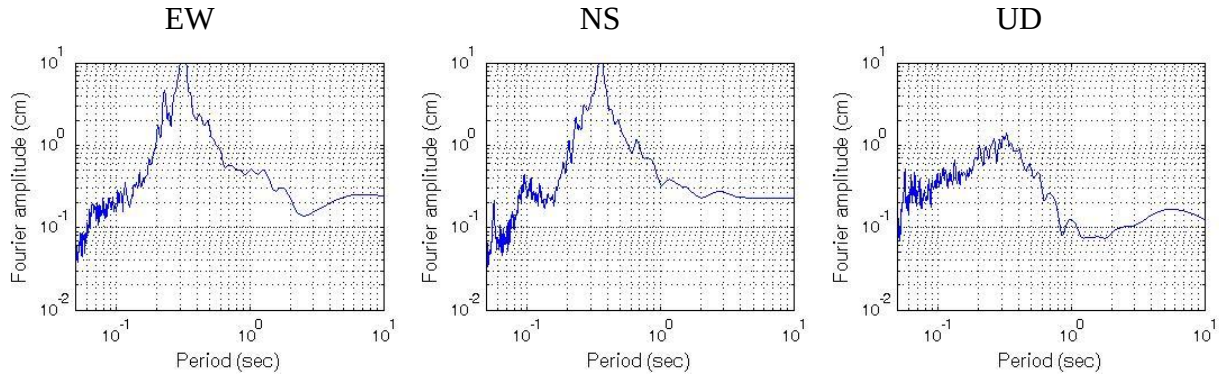

(a) top floor

Figure D3.237: Predominant Period and Fourier spectrum of Building # 14.

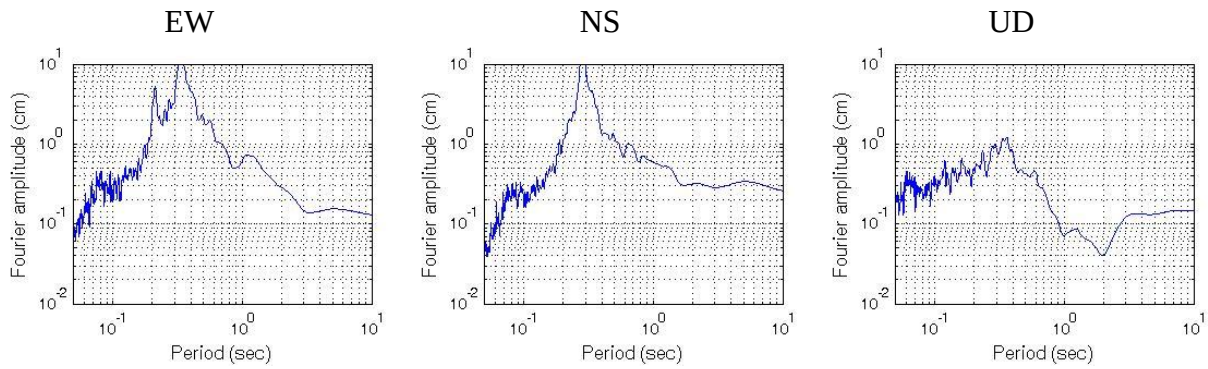

(a) top floor

Figure D3.238: Predominant Period and Fourier spectrum of Building # 1.

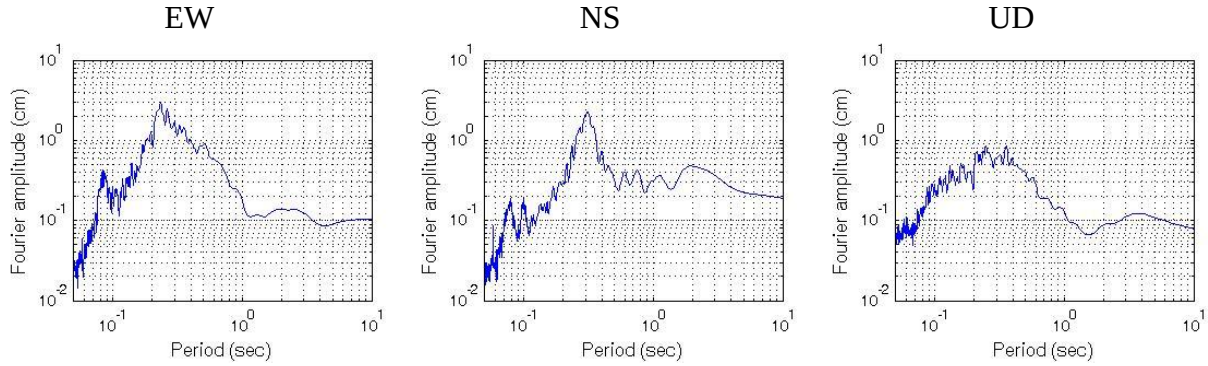

(a) top floor

Figure D3.239: Predominant Period and Fourier spectrum of Building # 21.

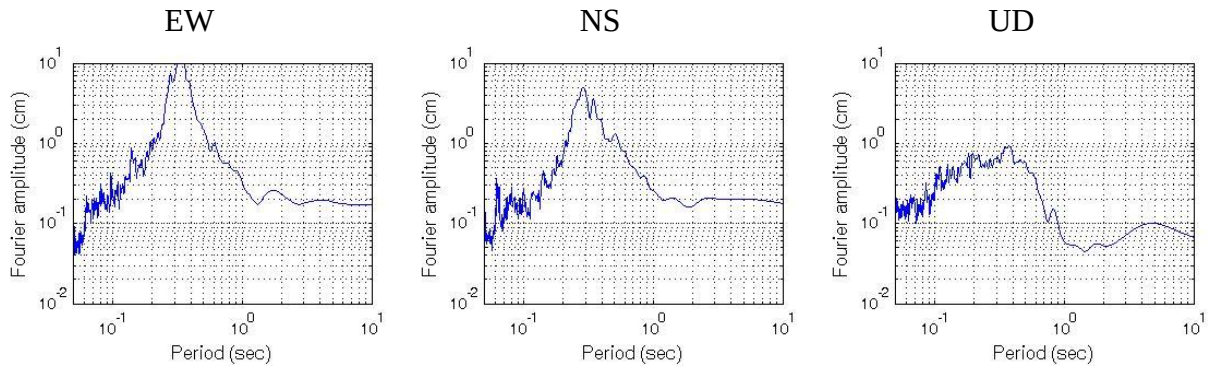

(a) top floor

Figure D3.240: Predominant Period and Fourier spectrum of Building # 22.

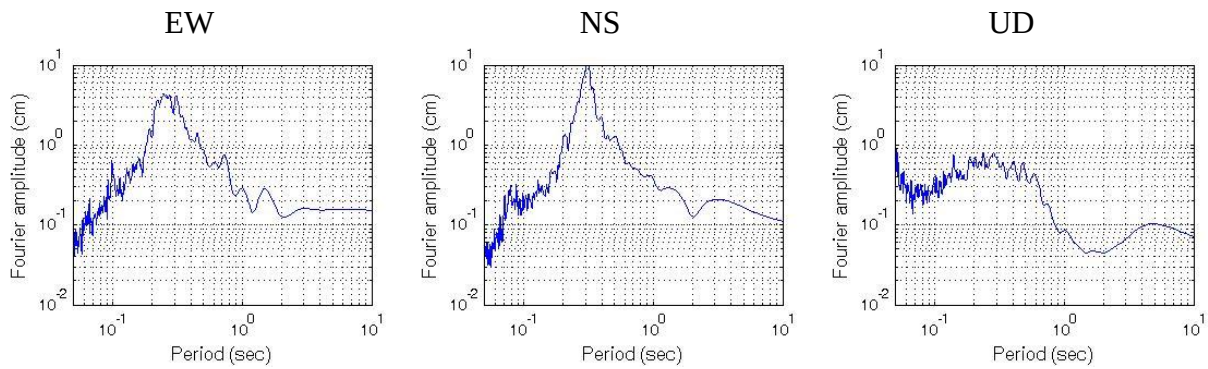

(a) top floor

Figure D3.241: Predominant Period and Fourier spectrum of Building # 23.

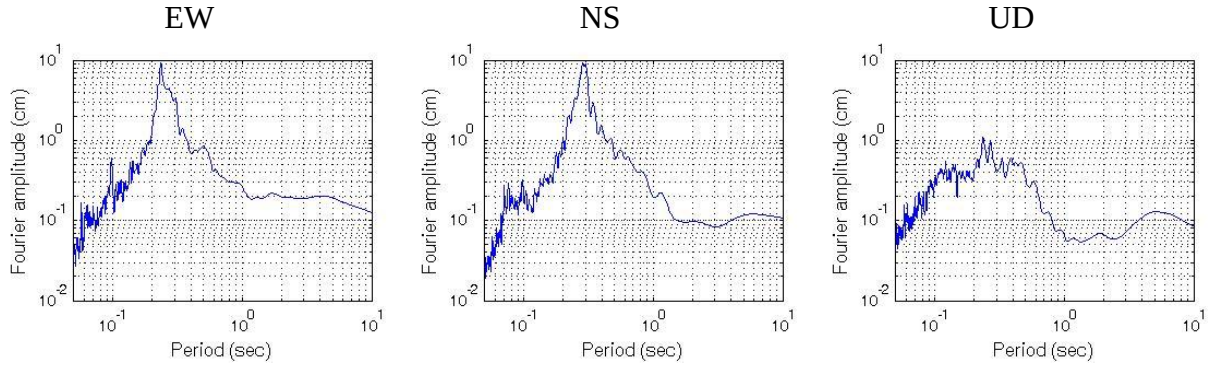

(a) 3rd floor

Figure D3.242: Predominant Period and Fourier spectrum of Building # 24.

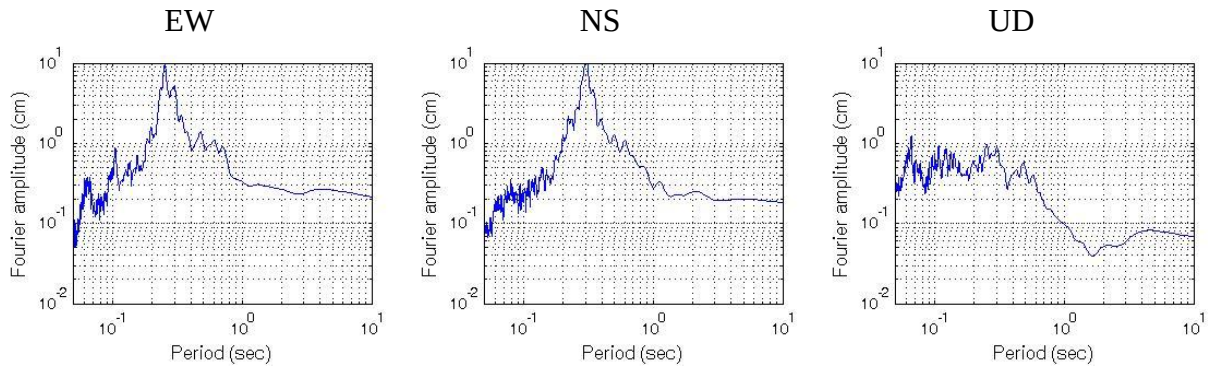

(a) 3rd floor

Figure D3.243: Predominant Period and Fourier spectrum of Building # 25.

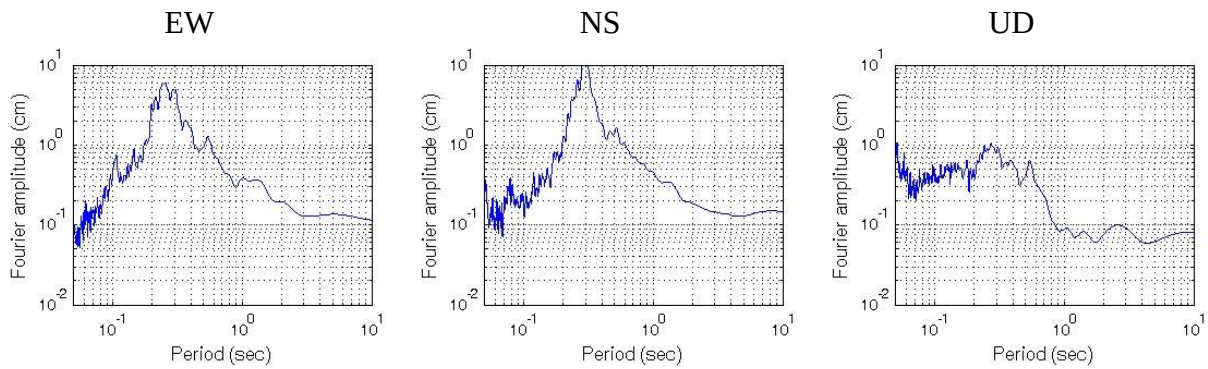

(a) top floor

Figure D3.244: Predominant Period and Fourier spectrum of Building # 26.

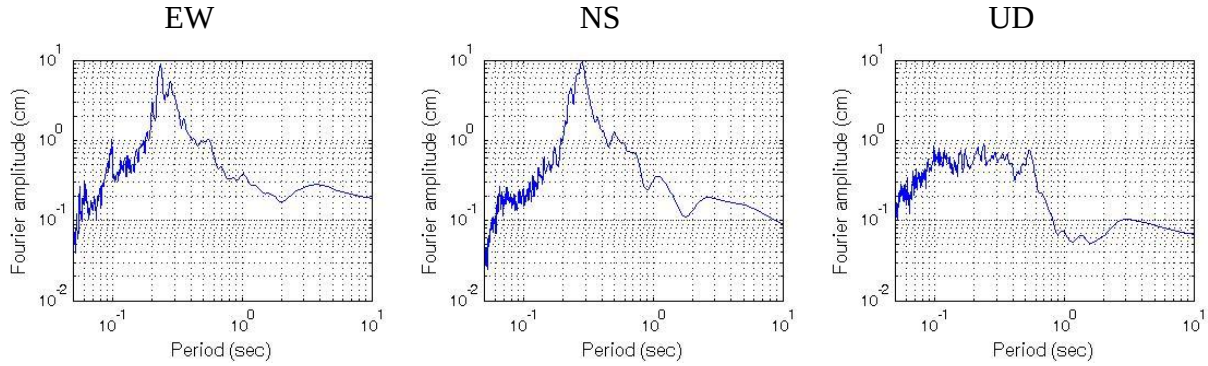

(a) top floor

Figure D3.245: Predominant Period and Fourier spectrum of Building # 27.

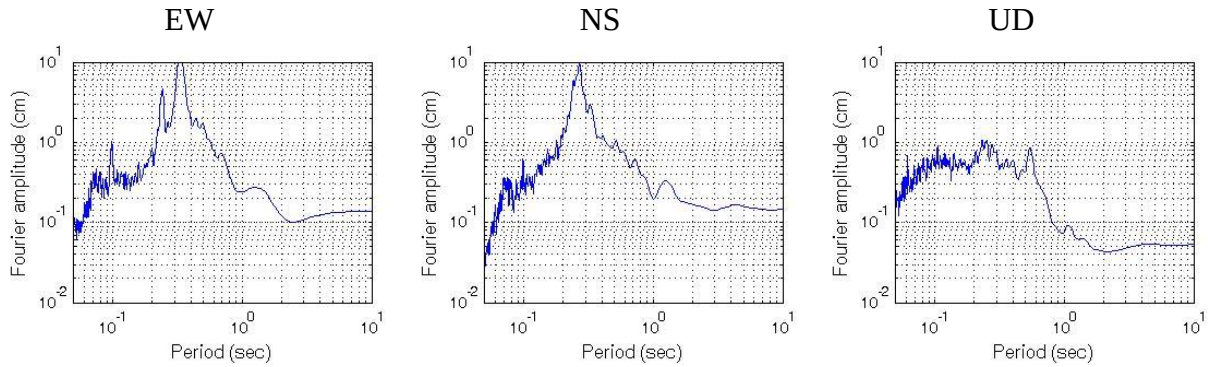

(a) top floor

Figure D3.246: Predominant Period and Fourier spectrum of Building # 28.

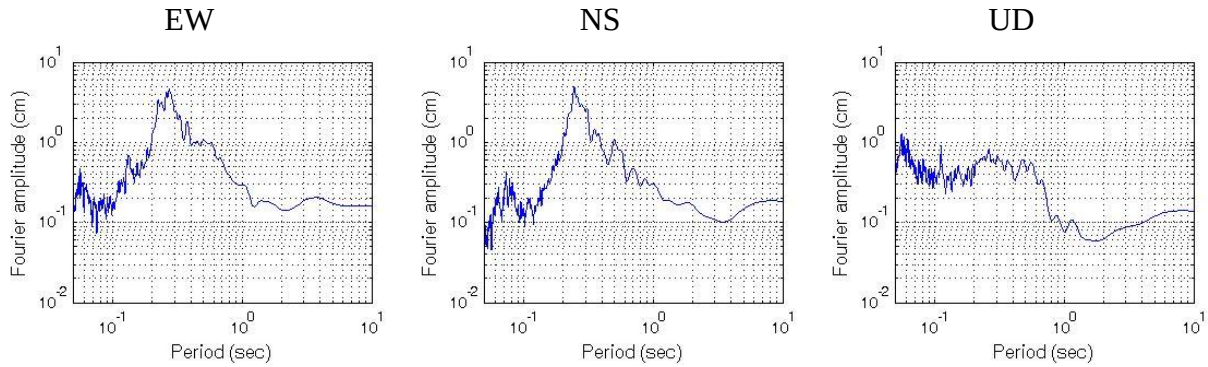

(a) top floor (left)

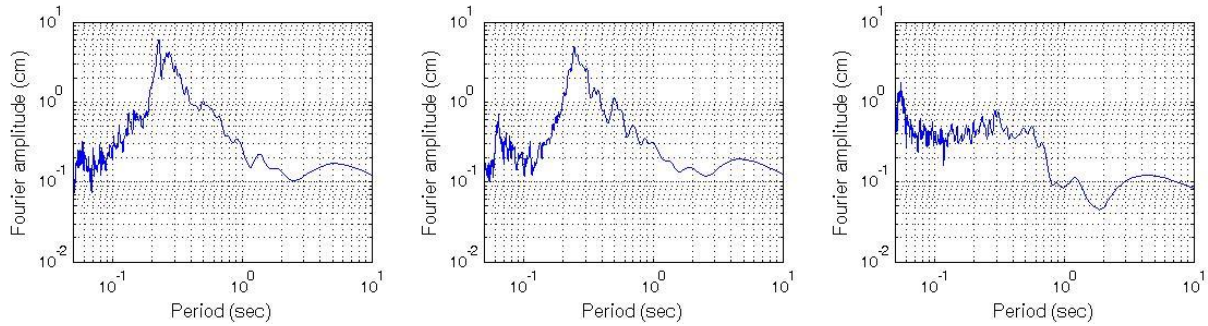

(b) top floor (right)

Figure D3.247: Predominant Period and Fourier spectrum of Building # 30.

EW NS UD

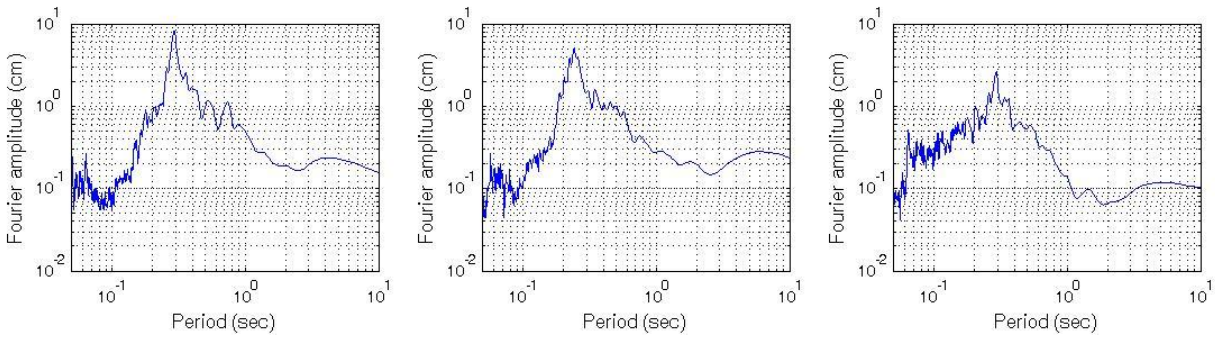

(a) 4th floor

Figure D3.248: Predominant Period and Fourier spectrum of Building # 43.

EW NS UD

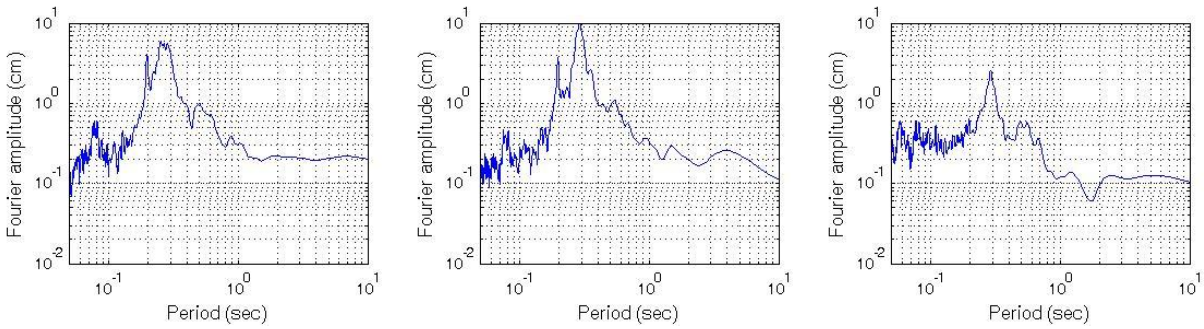

(a) top floor

Figure D3.249: Predominant Period and Fourier spectrum of Building # 45.

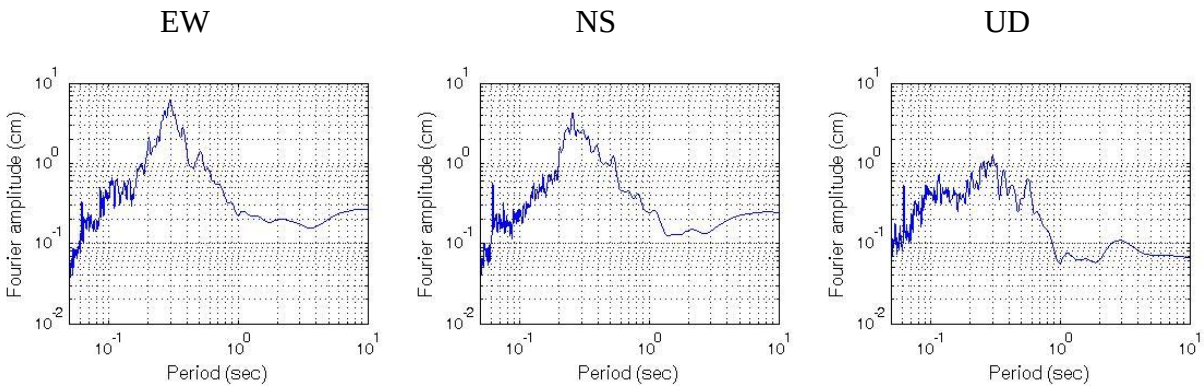

(a) top floor

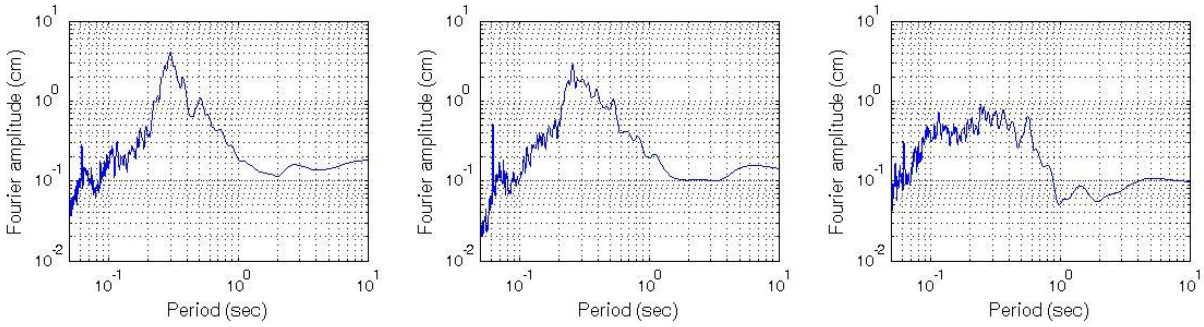

(b) 2nd floor

Figure D3.250: Predominant Period and Fourier spectrum of Building # 46.

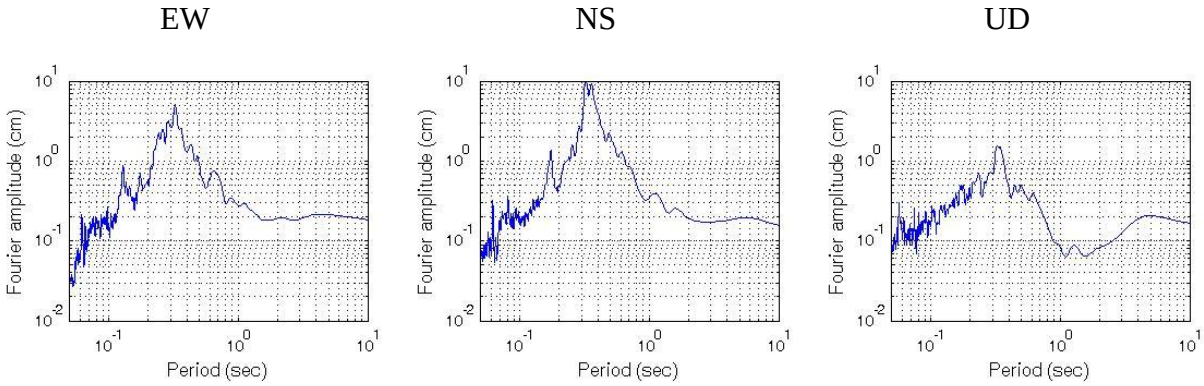

(a) top floor (right)

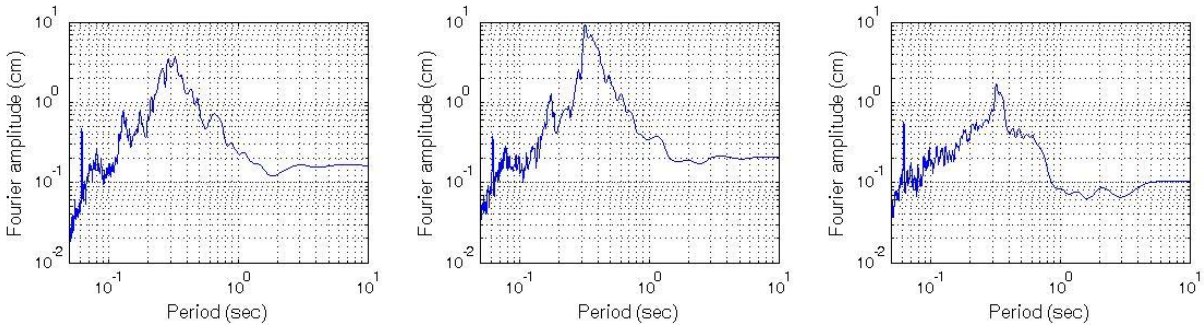

(b) top floor (left)

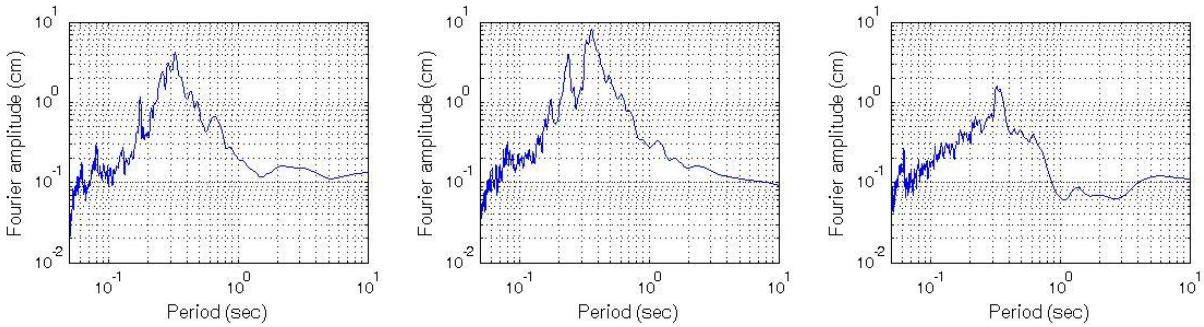

(c) top floor (middle)

Figure D3.251: Predominant Period and Fourier spectrum of Building # 47.

EW NS UD

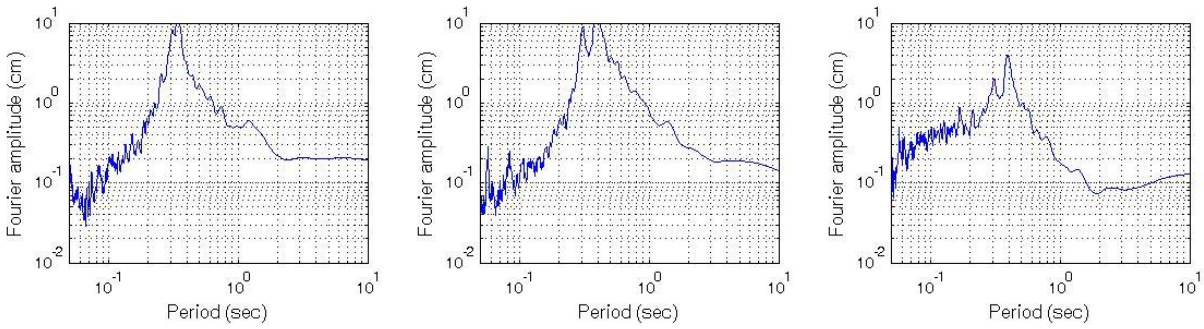

(a) 5th floor

Figure D3.252: Predominant Period and Fourier spectrum of Building # 62.

APPENDIX-E

COMPARISON OF MICROTREMOR WITH TRANSFER FUNCTION USING THE PROGRAMME SHAKE

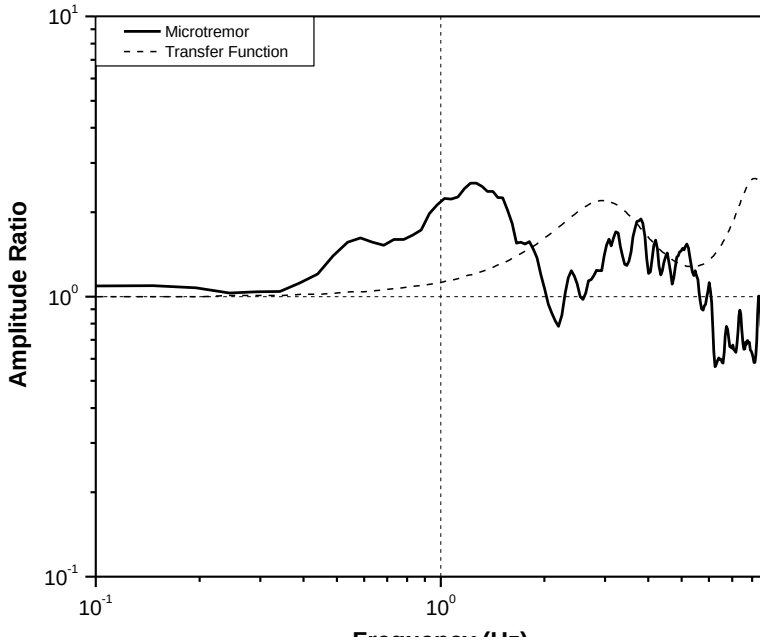

Figure E4.1: Amplitude ratios of microtremor and theoretical transfer function of shear wave at National University.

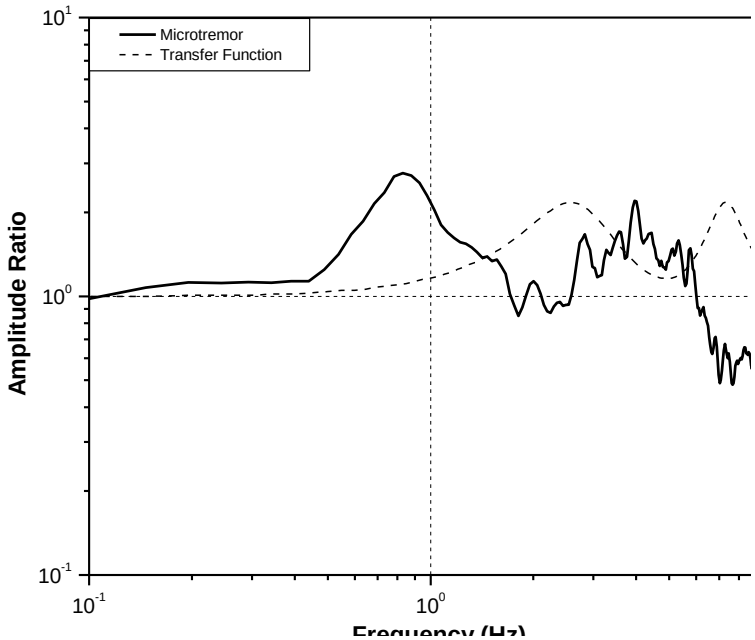

Figure E4.2: Amplitude ratios of microtremor and theoretical transfer function of shear wave at Board Bazar Gazipur.

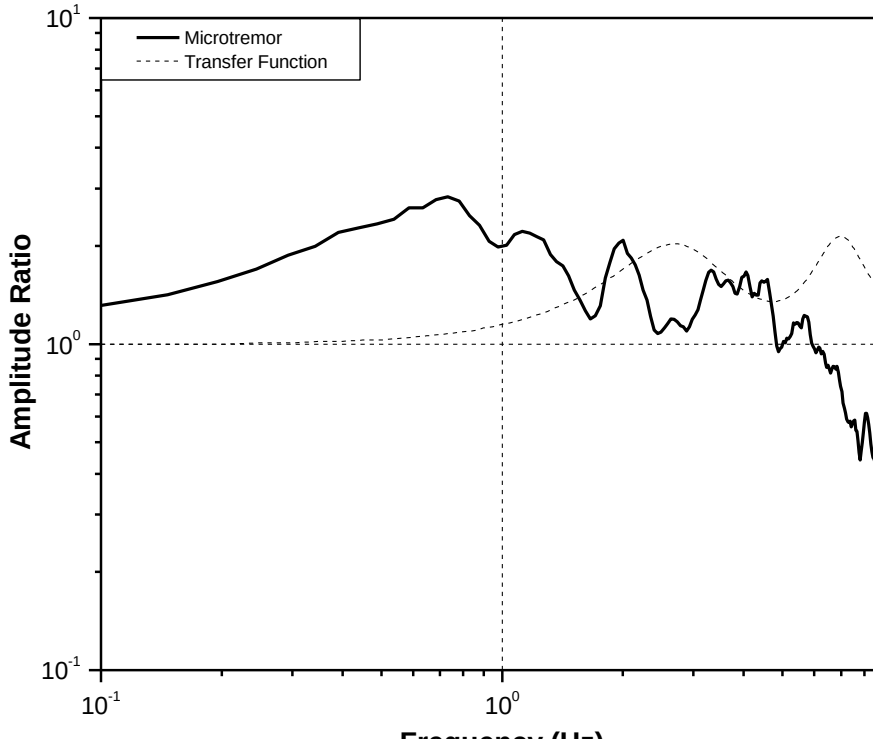

Figure E4.3: Amplitude ratios of microtremor and theoretical transfer function of shear wave at Kaunia, Boro Bari.

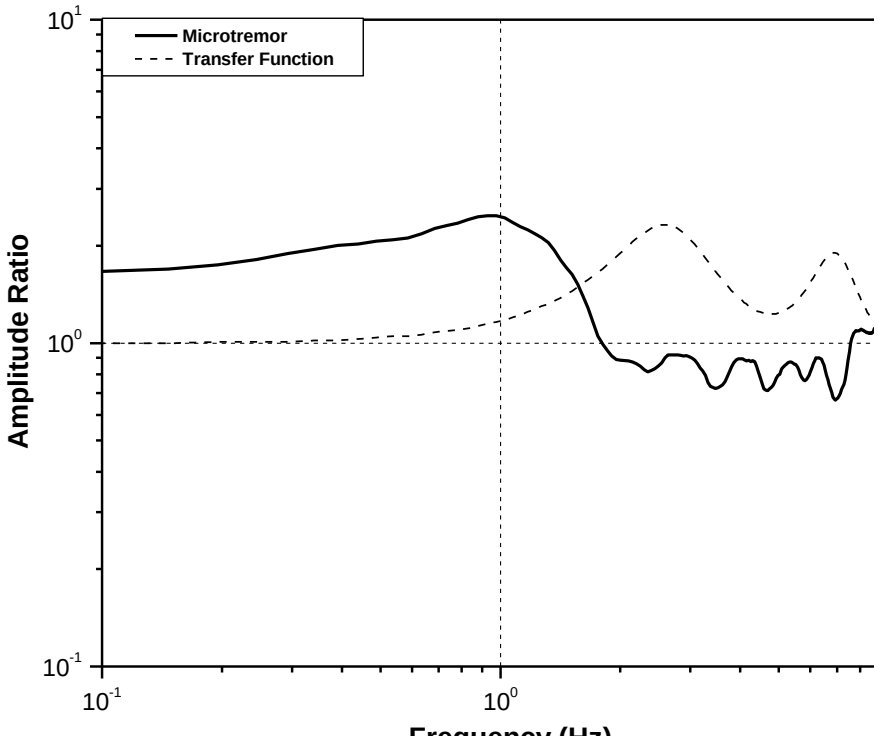

Figure E4.4: Amplitude ratios of microtremor and theoretical transfer function of shear wave at Tongi, Ershadnagar.

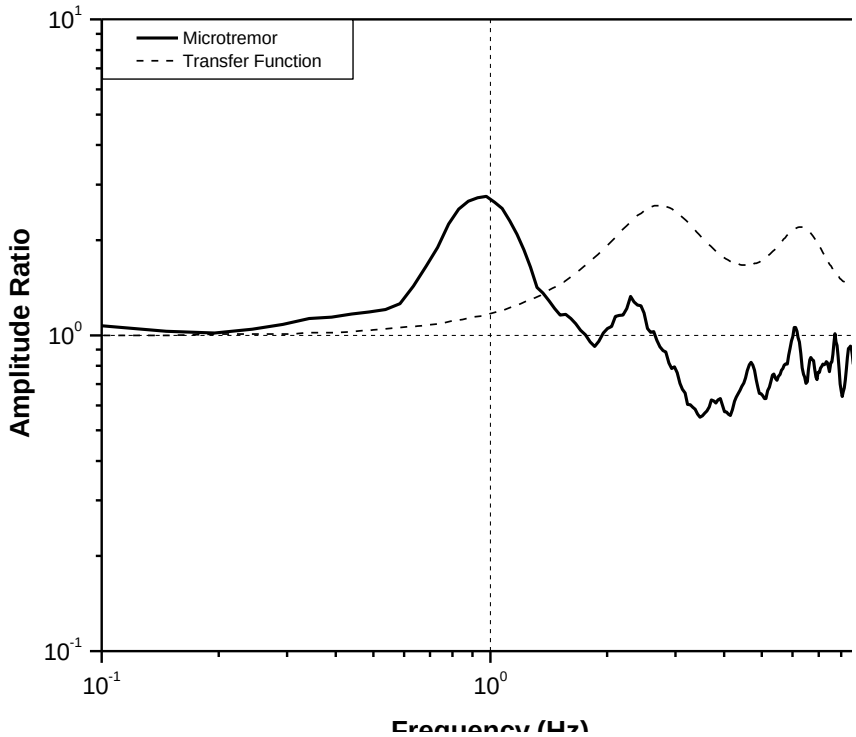

Figure E4.5: Amplitude ratios of microtremor and theoretical transfer function of shear wave at Tongi BSCIC area.

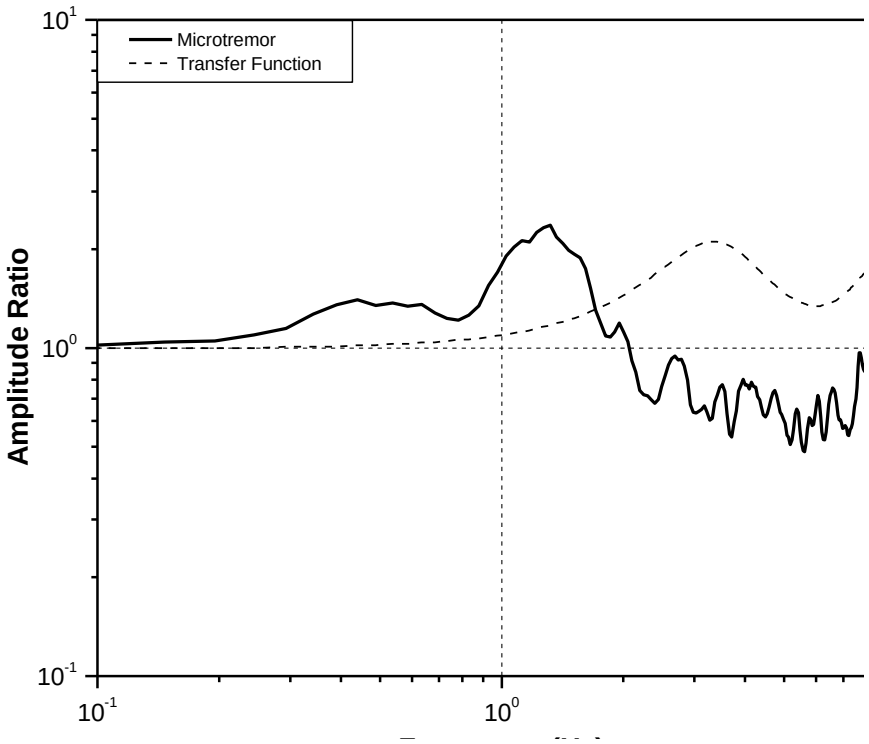

Figure E4.6: Amplitude ratios of microtremor and theoretical transfer function of shear wave at Abdullahpur.

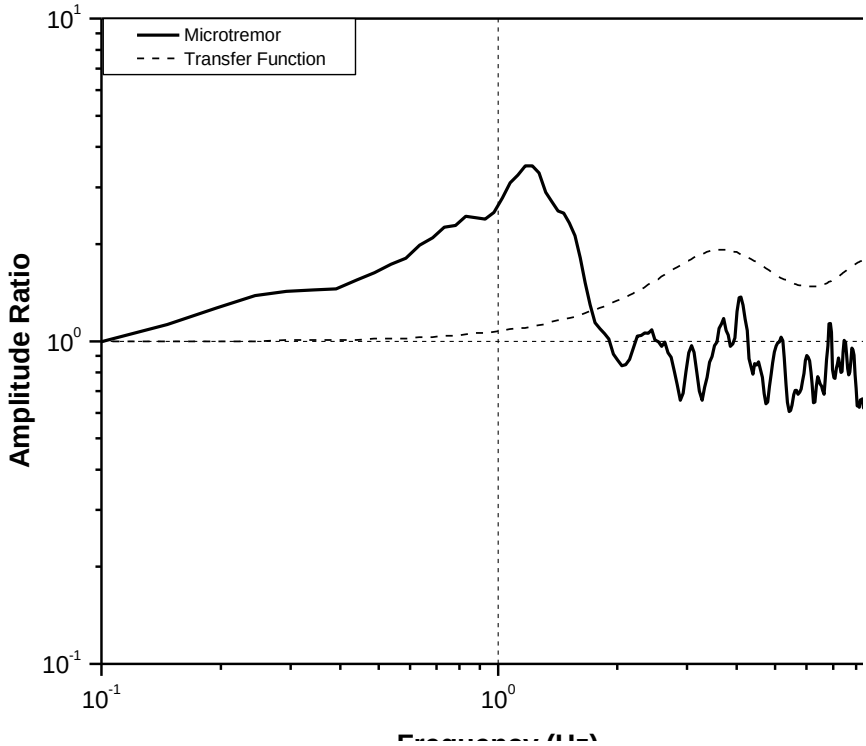

Figure E4.7: Amplitude ratios of microtremor and theoretical transfer function of shear wave at Ijtema Field (North and East side).

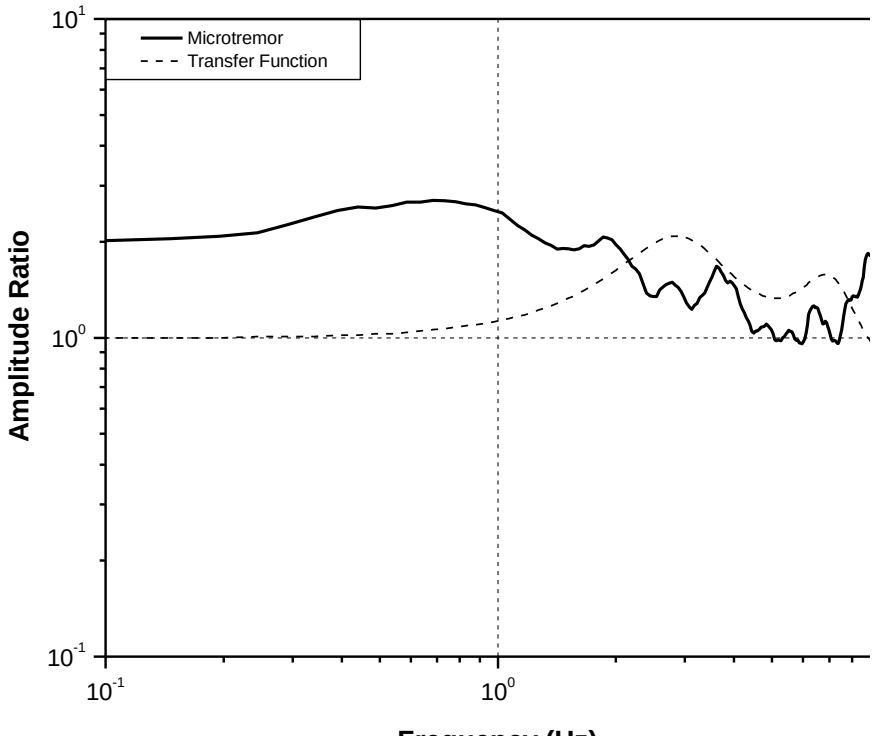

Figure E4.8: Amplitude ratios of microtremor and theoretical transfer function of shear wave at Ijtema Field (South and West side).

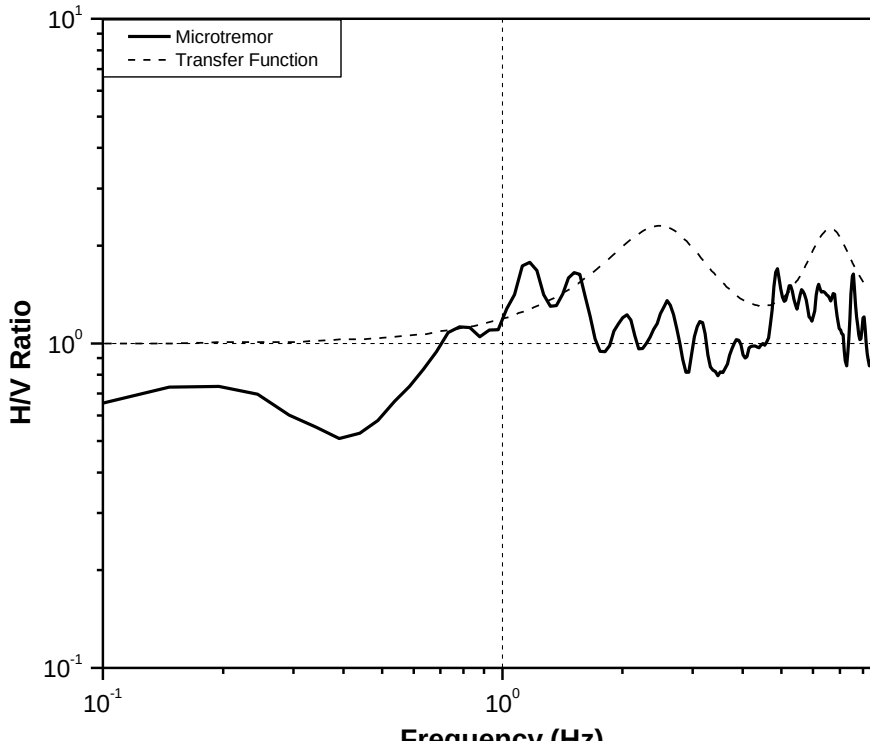

Figure E4.9: Amplitude ratios of microtremor and theoretical transfer function of shear wave at Ashulia Toll Plaza.

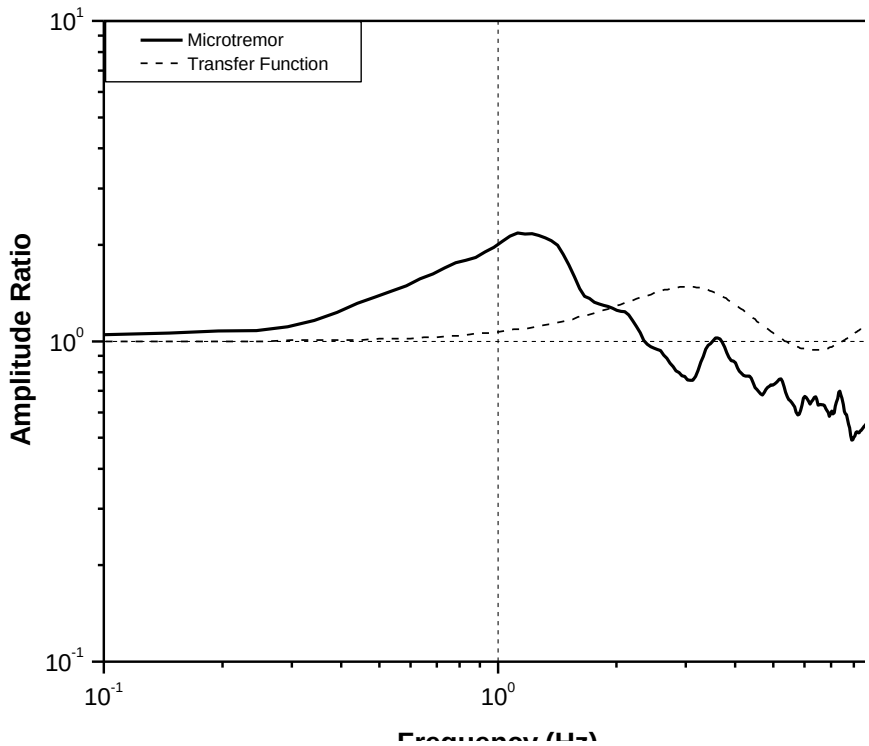

Figure E4.10: Amplitude ratios of microtremor and theoretical transfer function of shear wave at Uttar Khan.

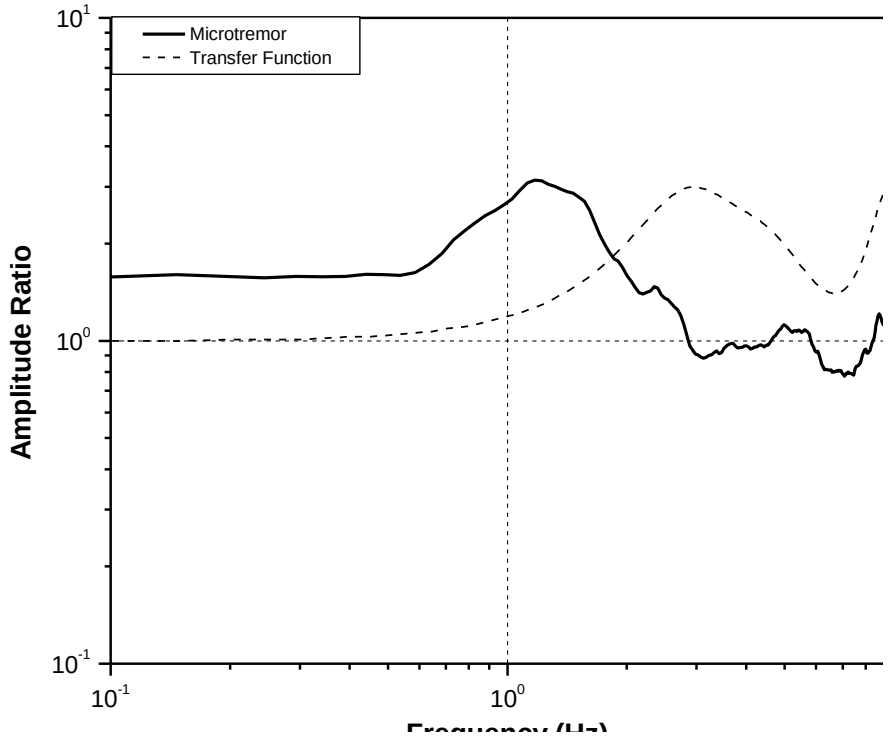

Figure E4.11: Amplitude ratios of microtremor and theoretical transfer function of shear wave at Uttara Phase-3 (North Side).

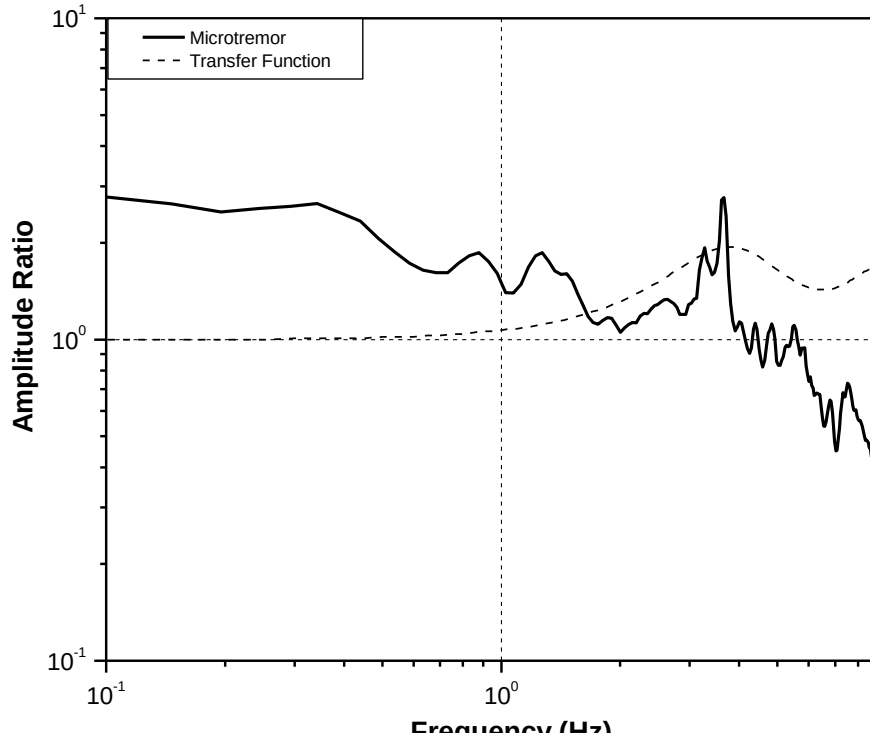

Figure E4.12: Amplitude ratios of microtremor and theoretical transfer function of shear wave at Uttara Azampur.

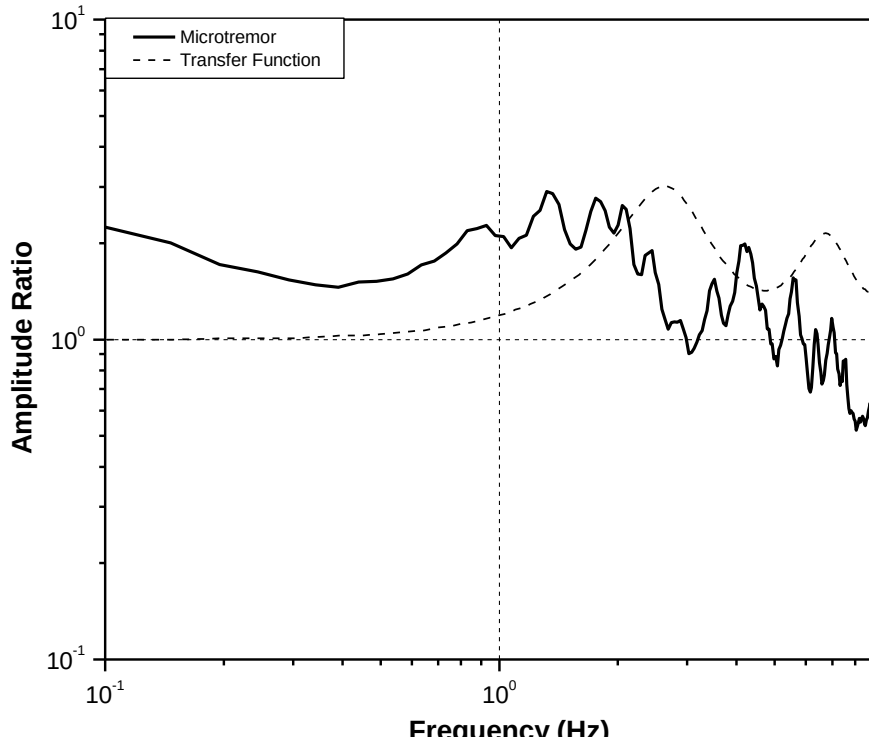

Figure E4.13: Amplitude ratios of microtremor and theoretical transfer function of shear wave at Mirpur DOHS (South side).

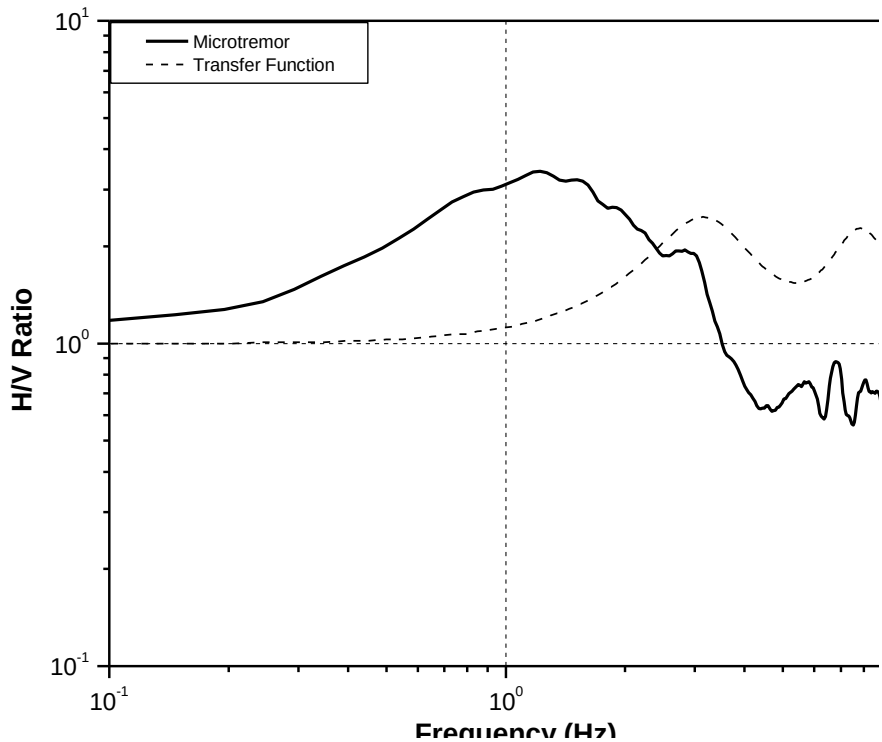

Figure E4.14: Amplitude ratios of microtremor and theoretical transfer function of shear wave at Mirpur DOHS (North Side).

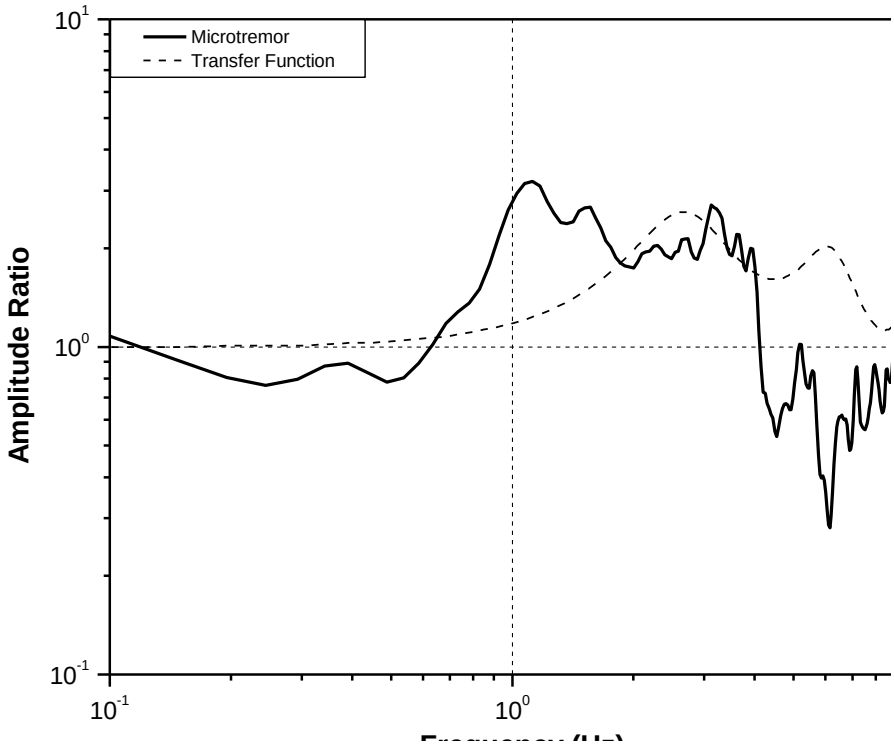

Figure E4.15: Amplitude ratios of microtremor and theoretical transfer function of shear wave at Ashiyan City.

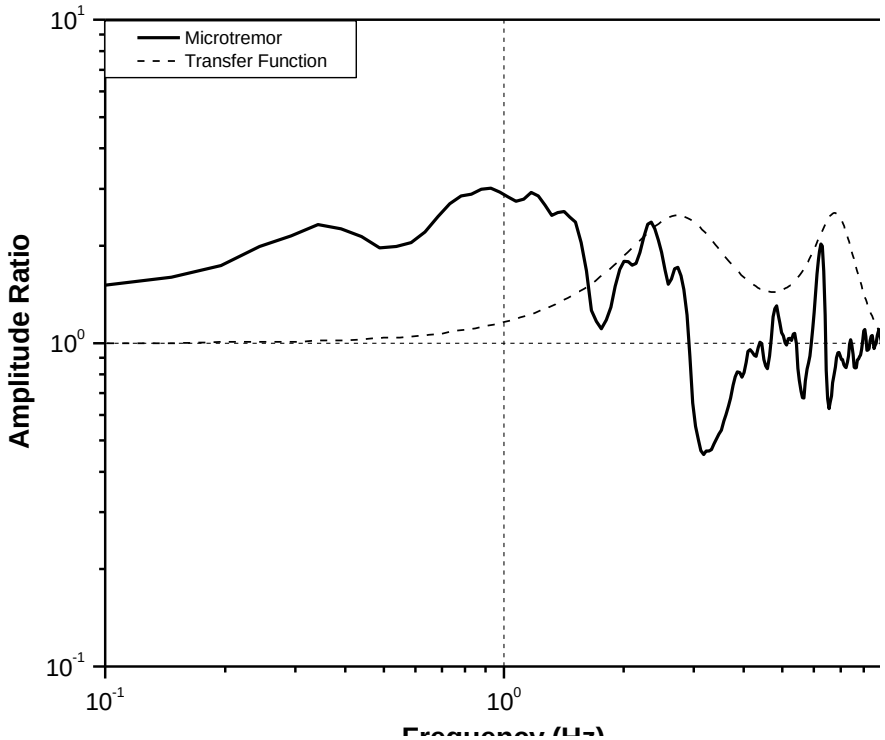

Figure E4.16: Amplitude ratios of microtremor and theoretical transfer function of shear wave at Randokpur, RupGanj.

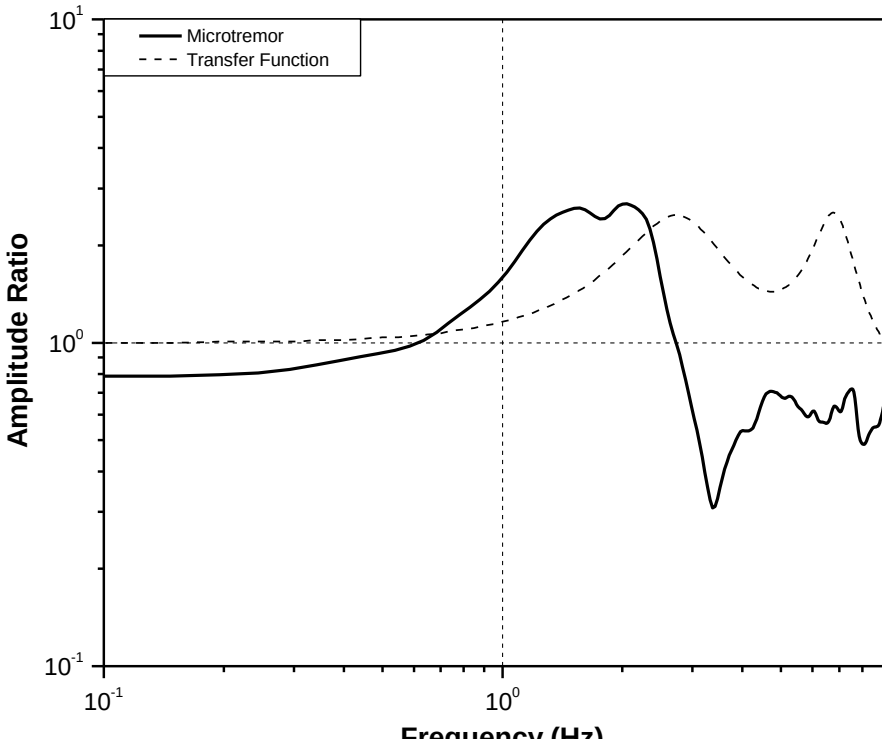

Figure E4.17: Amplitude ratios of microtremor and theoretical transfer function of shear wave at American City, Purbachal.

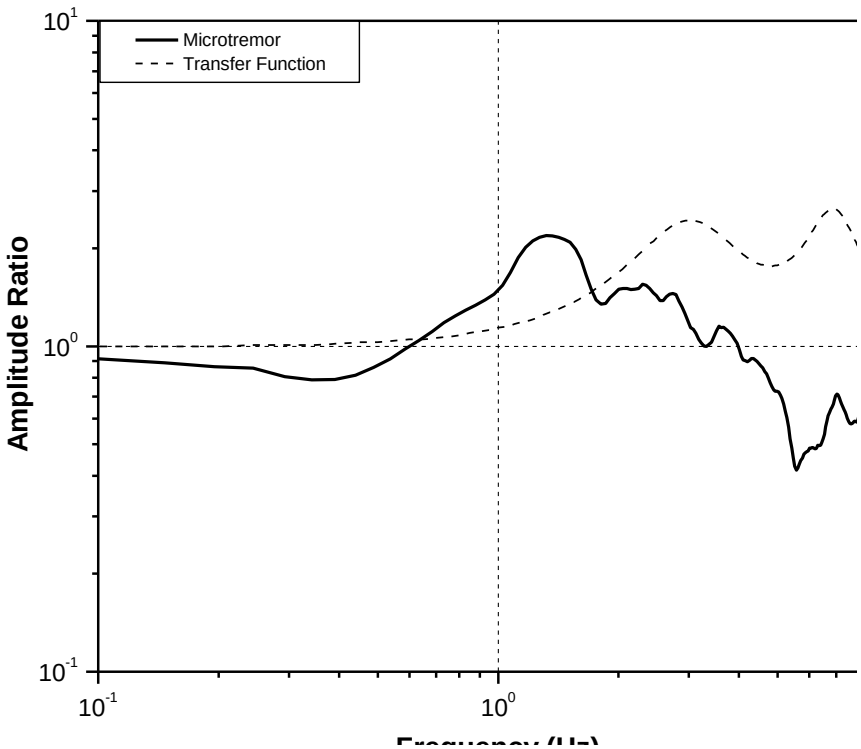

Figure E4.18: Amplitude ratios of microtremor and theoretical transfer function of shear wave at Picnic Park, Gazipur.

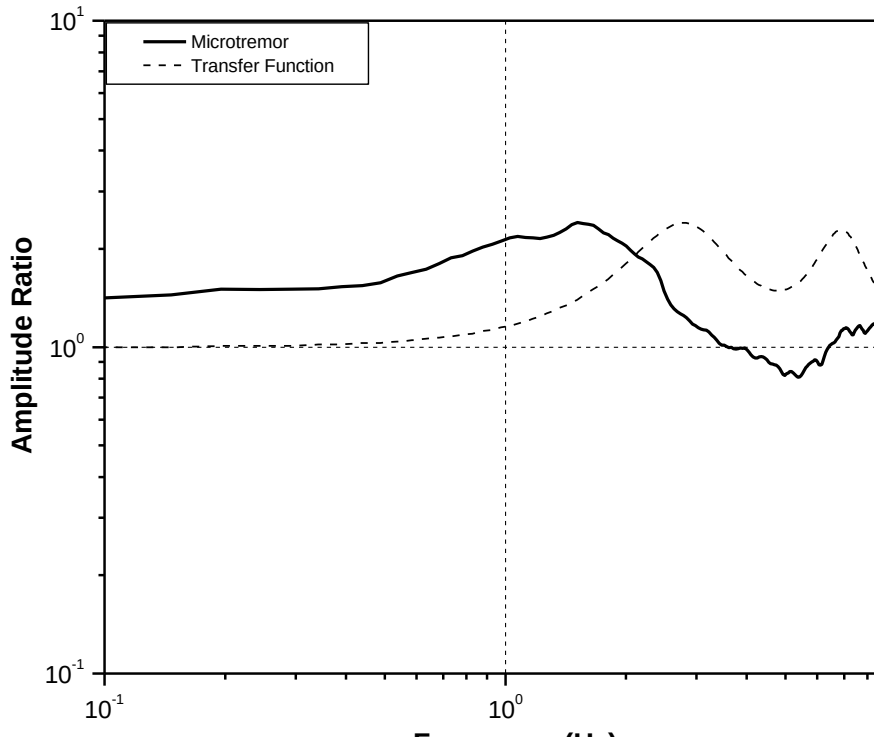

Figure E4.19: Amplitude ratios of microtremor and theoretical transfer function of shear wave at Mirpur Zoo.

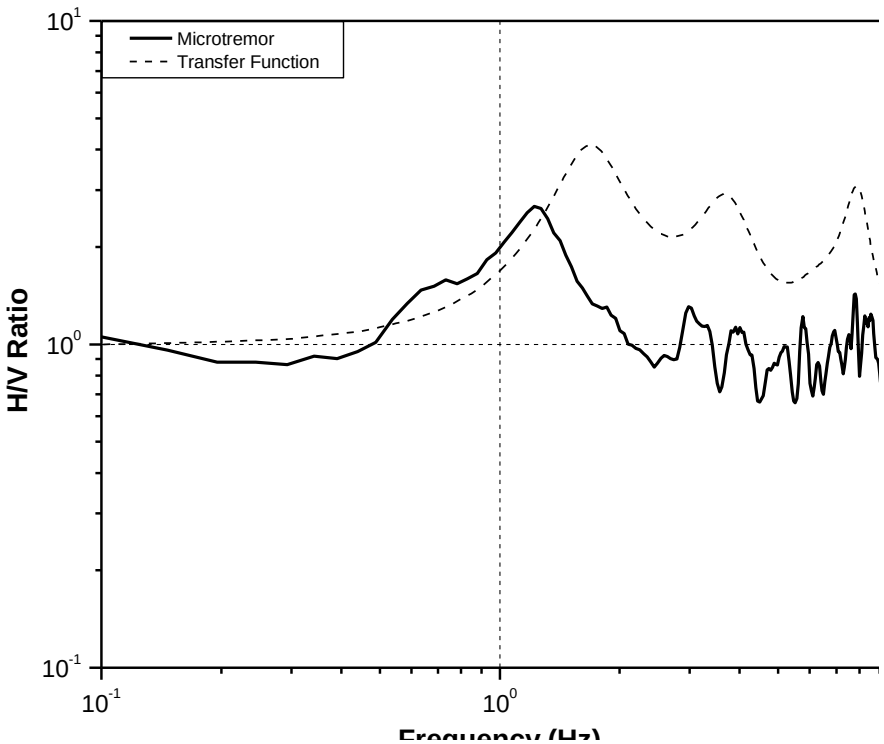

Figure E4.20: Amplitude ratios of microtremor and theoretical transfer function of shear wave at Pallabi.

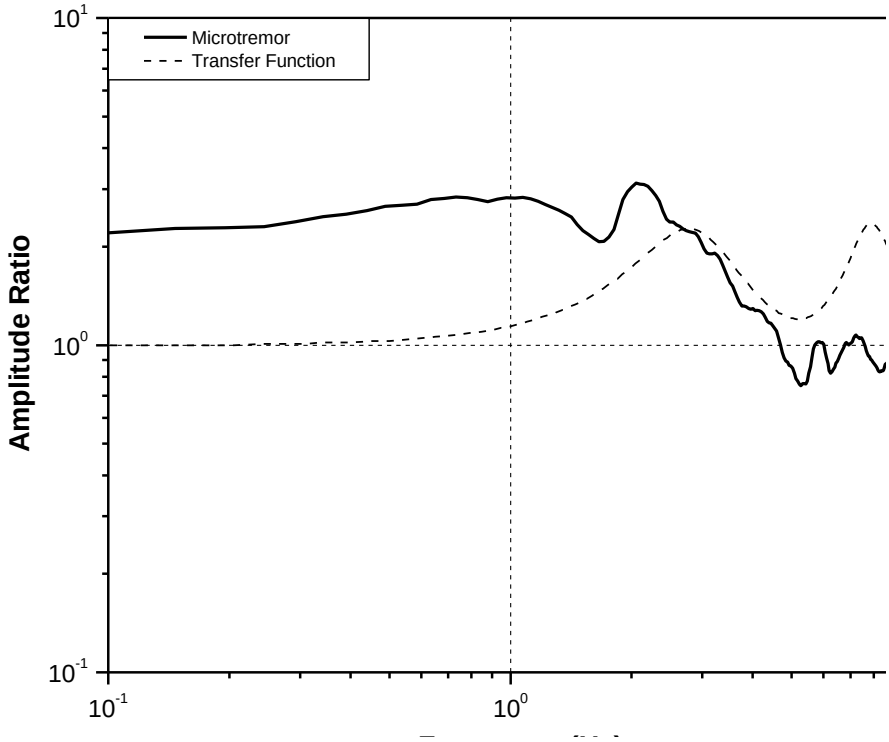

Figure E4.21: Amplitude ratios of microtremor and theoretical transfer function of shear wave at Block-B, Bashundhara.

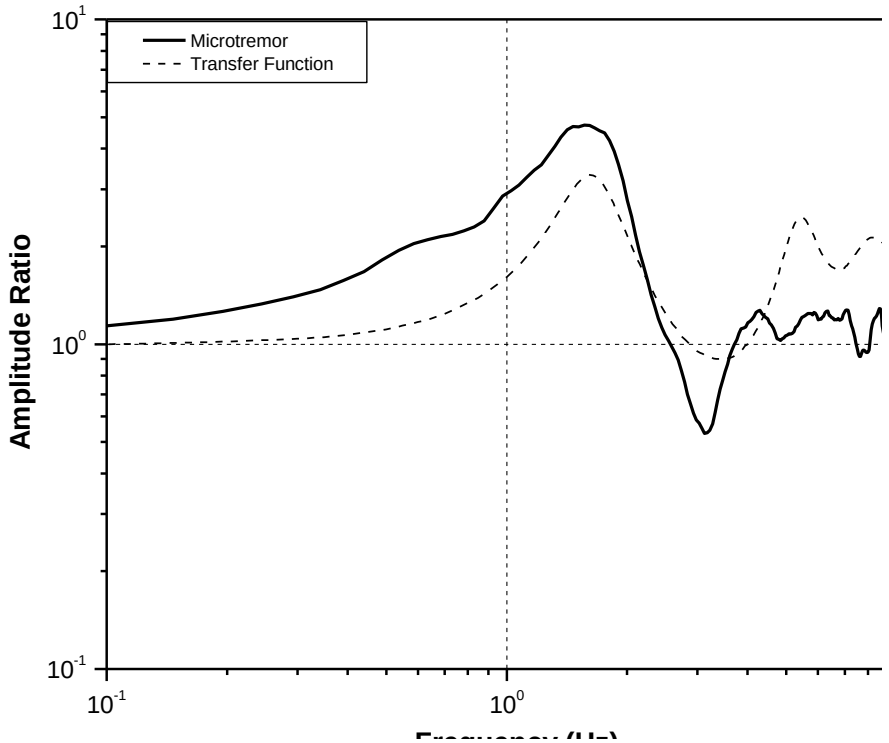

Figure E4.22: Amplitude ratios of microtremor and theoretical transfer function of shear wave at Block-D, Bashundhara.

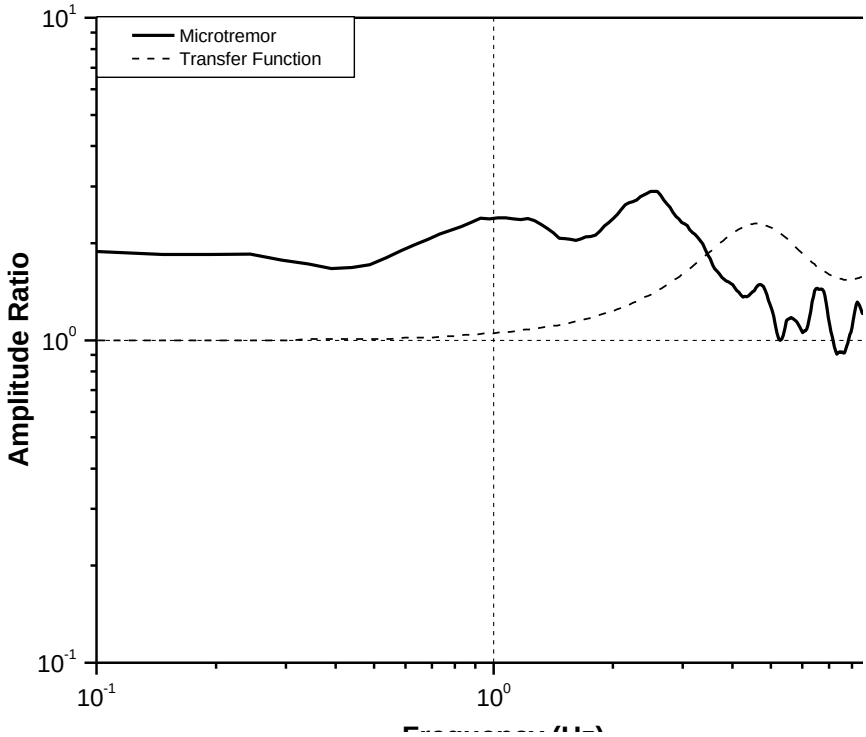

Figure E4.23: Amplitude ratios of microtremor and theoretical transfer function of shear wave at Block-H, Bashundhara.

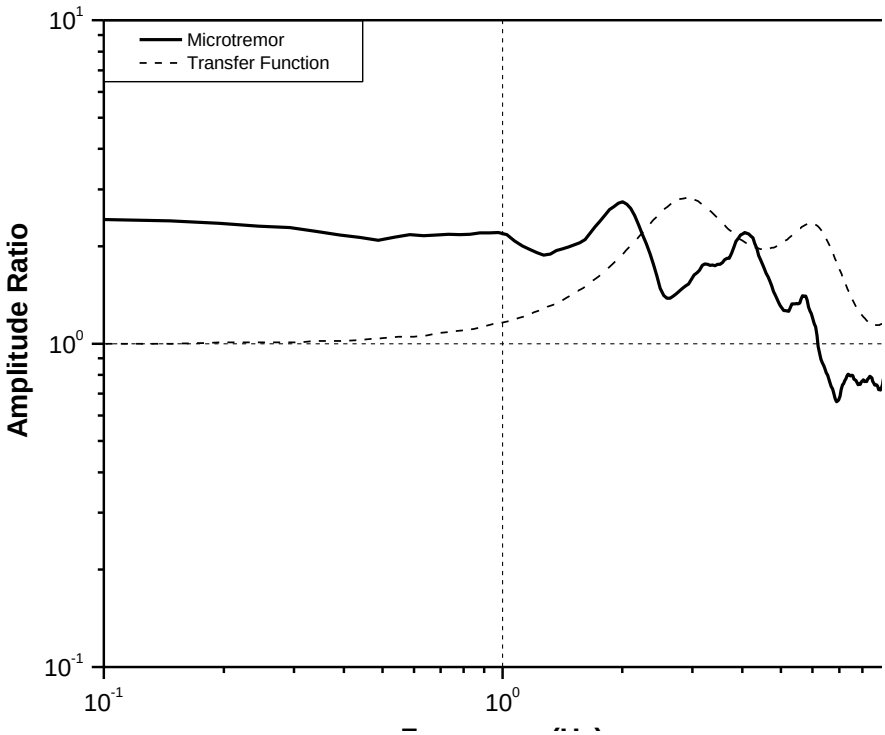

Figure E4.24: Amplitude ratios of microtremor and theoretical transfer function of shear wave at Kuril, Flyover.

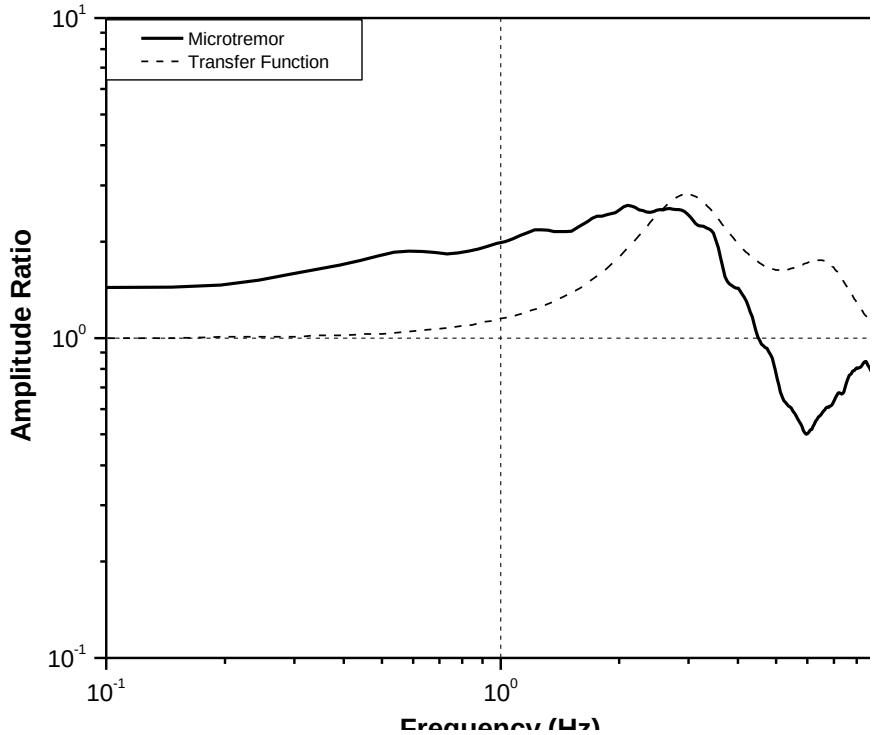

Figure E4.25: Amplitude ratios of microtremor and theoretical transfer function of shear wave at Purachal, Uttar Badda.

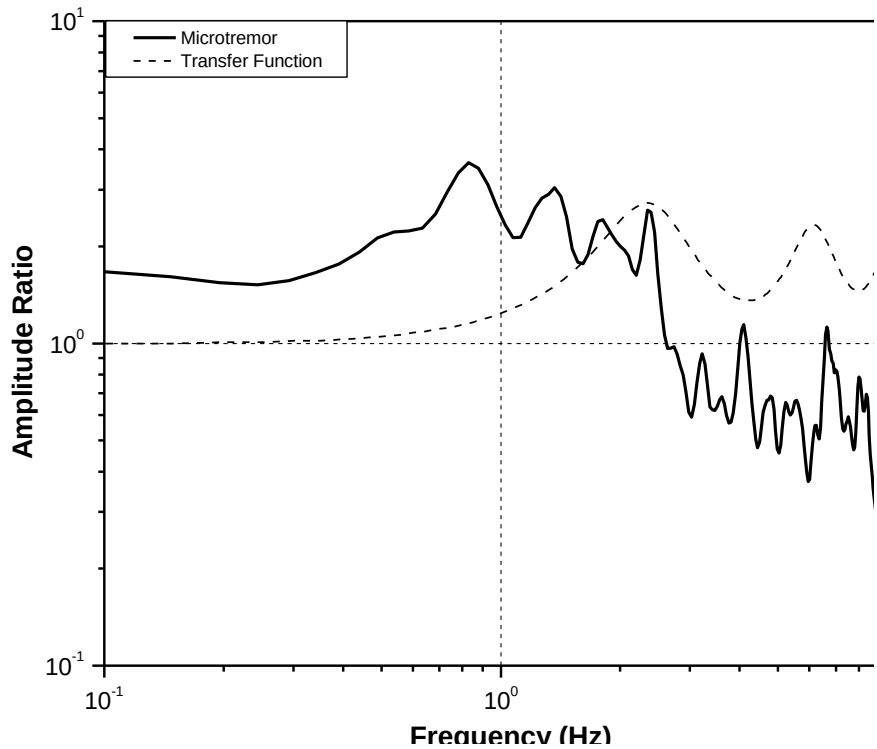

Figure E4.26: Amplitude ratios of microtremor and theoretical transfer function of shear wave at Gabtoli City Corporation.

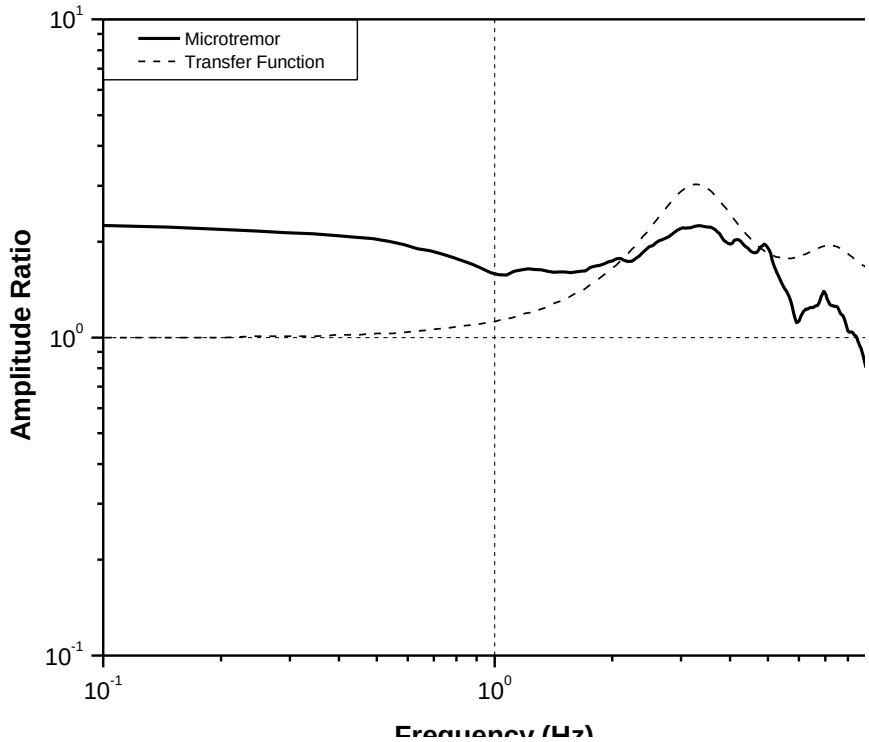

Figure E4.27: Amplitude ratios of microtremor and theoretical transfer function of shear wave at Adabor.

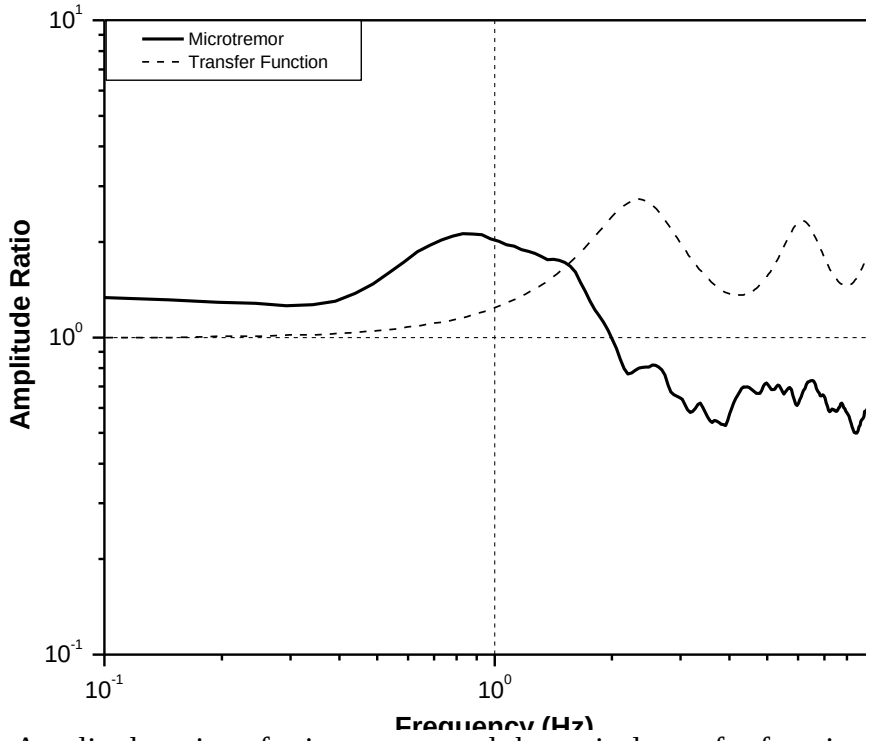

Figure E4.28: Amplitude ratios of microtremor and theoretical transfer function of shear wave at Agargaon Trade Fair.

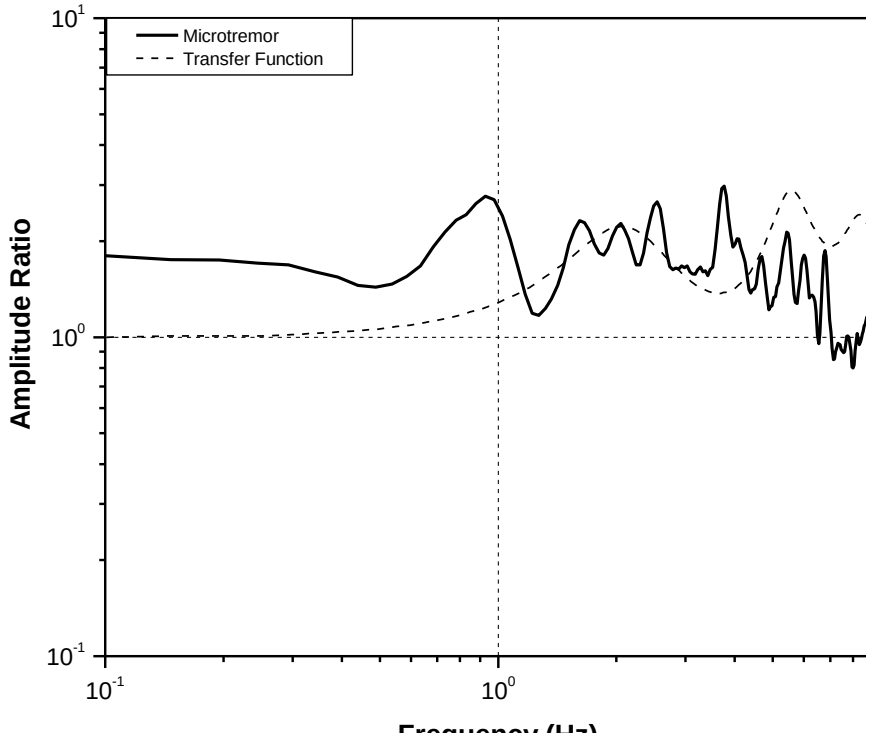

Figure E4.29: Amplitude ratios of microtremor and theoretical transfer function of shear wave at Aftab Nagar Housing Project.

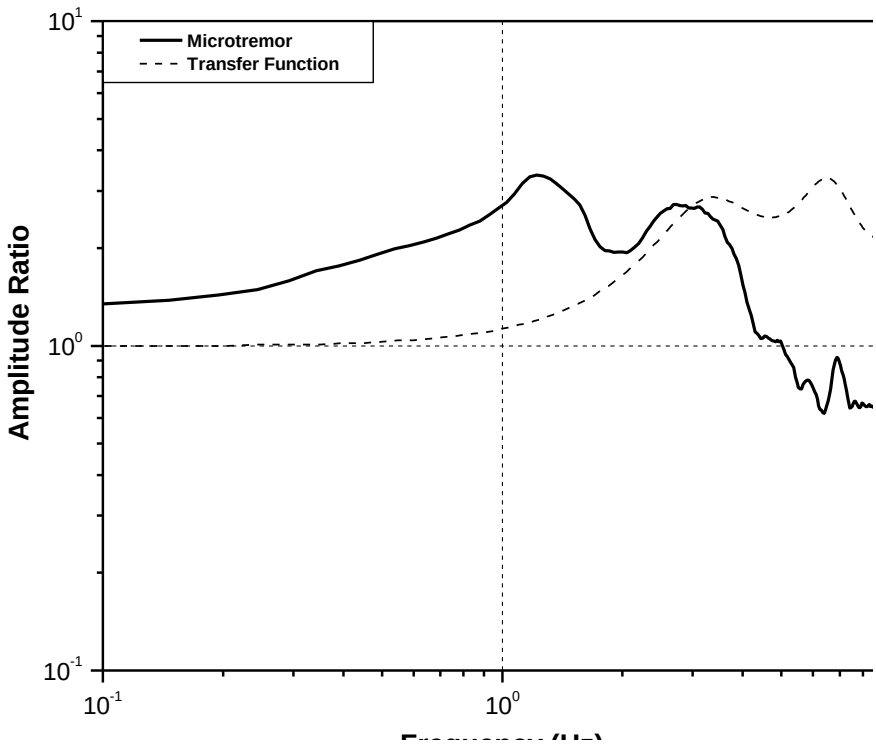

Figure E4.30: Amplitude ratios of microtremor and theoretical transfer function of shear wave at Nadda.

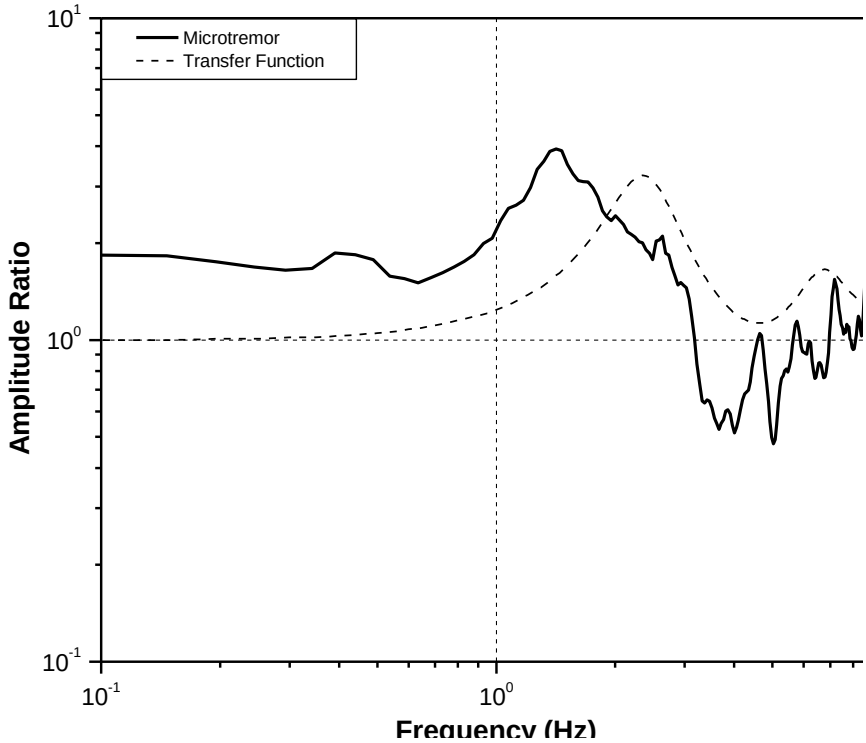

Figure E4.31: Amplitude ratios of microtremor and theoretical transfer function of shear wave at South Banasree.

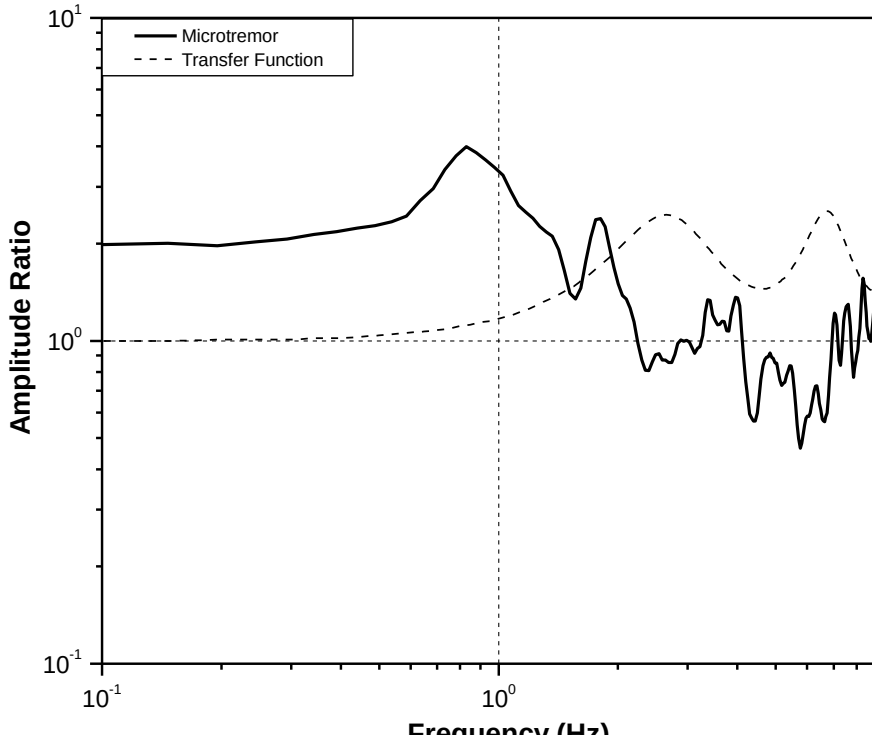

Figure E4.32: Amplitude ratios of microtremor and theoretical transfer function of shear wave at Hazaribagh.

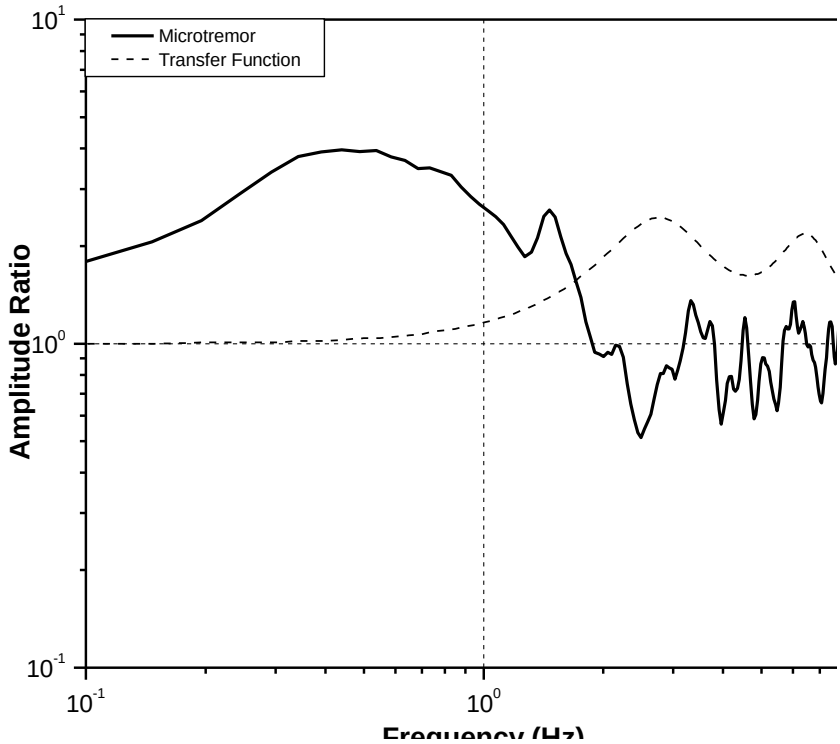

Figure E4.33: Amplitude ratios of microtremor and theoretical transfer function of shear wave at Rab-10 Plot, Kamrangirchar.

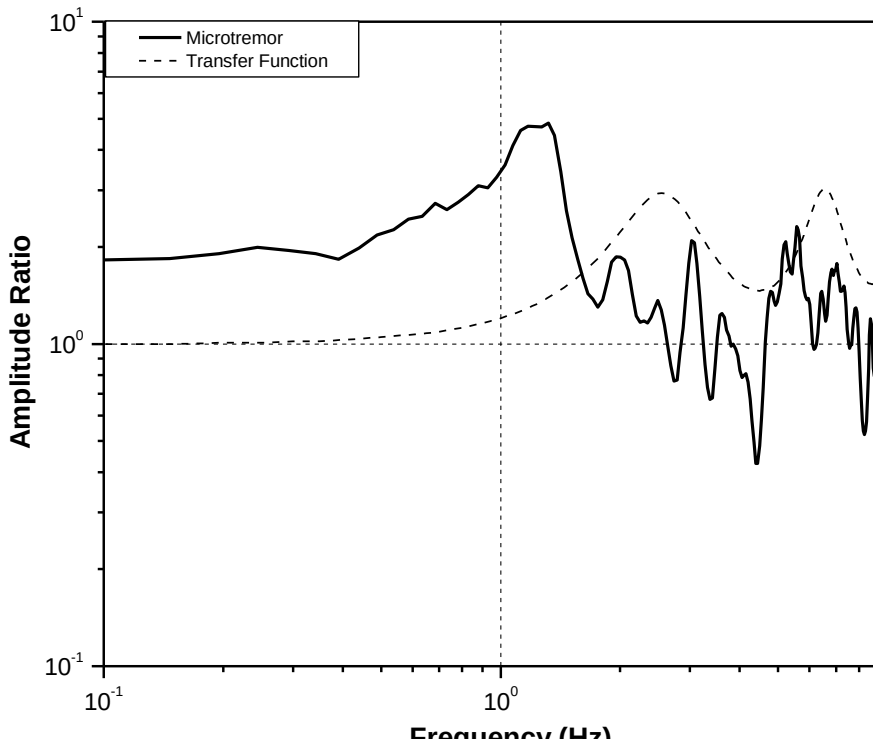

Figure E4.34: Amplitude ratios of microtremor and theoretical transfer function of shear wave at Sosan Ghat, Kamrangirchar.

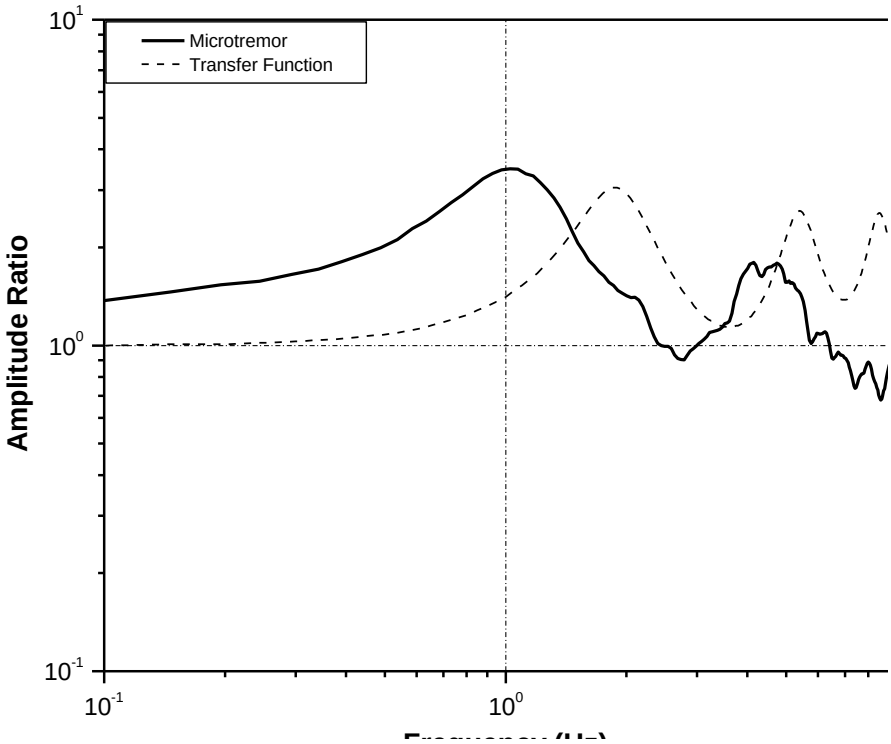

Figure E4.35: Amplitude ratios of microtremor and theoretical transfer function of shear wave at Bashundhara Riverview Project.

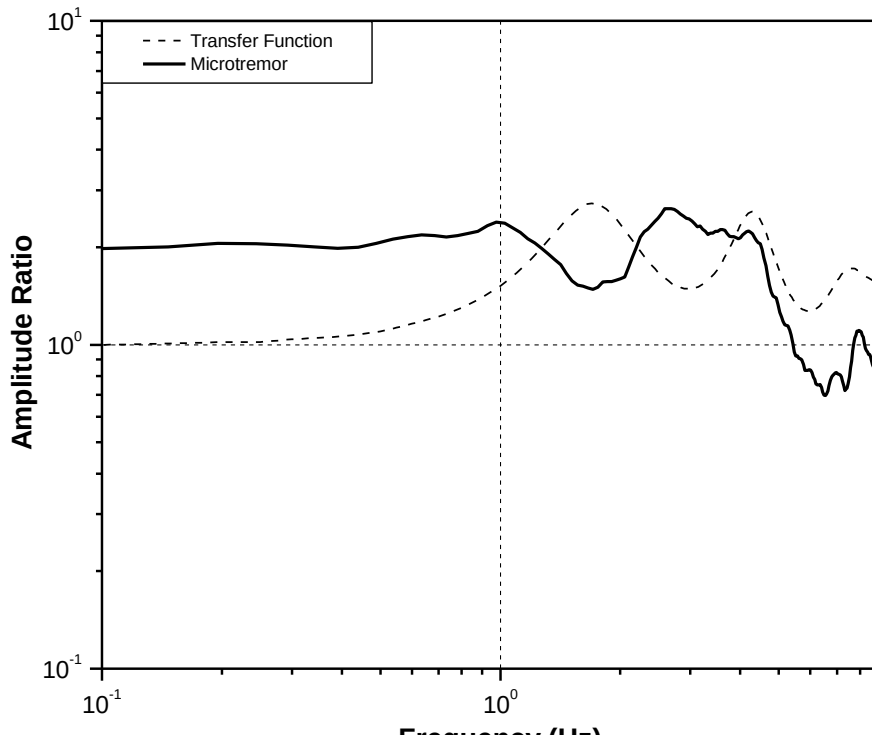

Figure E4.36: Amplitude ratios of microtremor and theoretical transfer function of shear wave at Matuail, Demra.

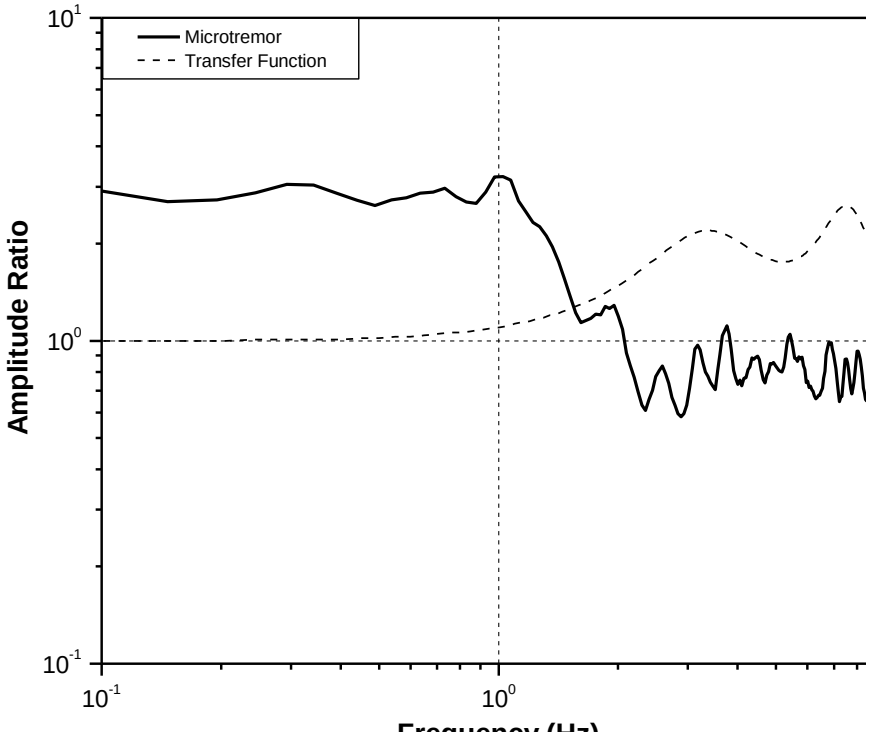

Figure E4.37: Amplitude ratios of microtremor and theoretical transfer function of shear wave at Jilmil Project.

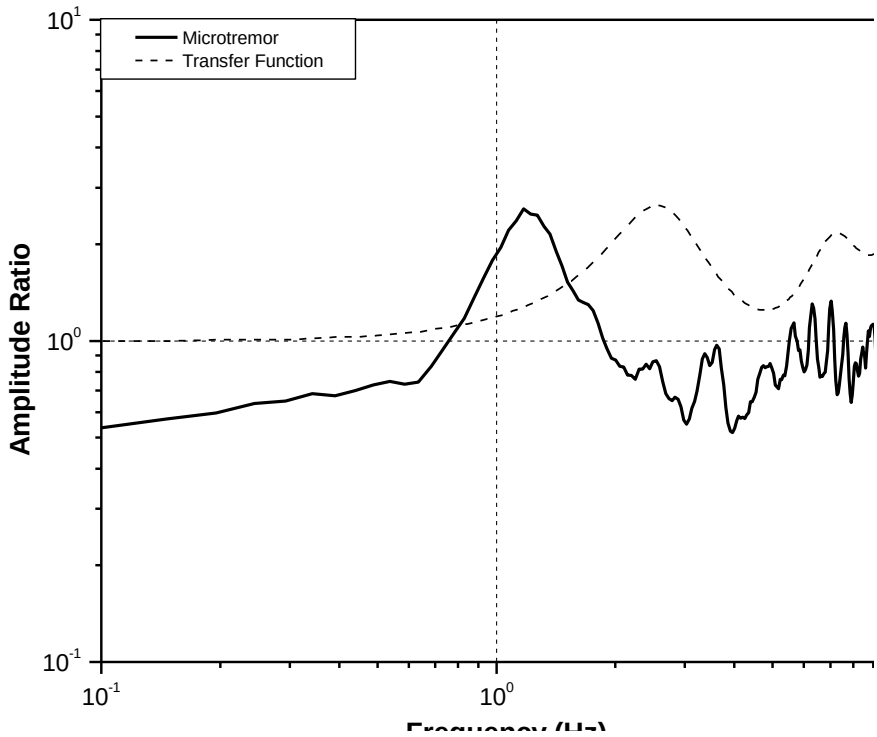

Figure E4.38: Amplitude ratios of microtremor and theoretical transfer function of shear wave at Rajendapur.

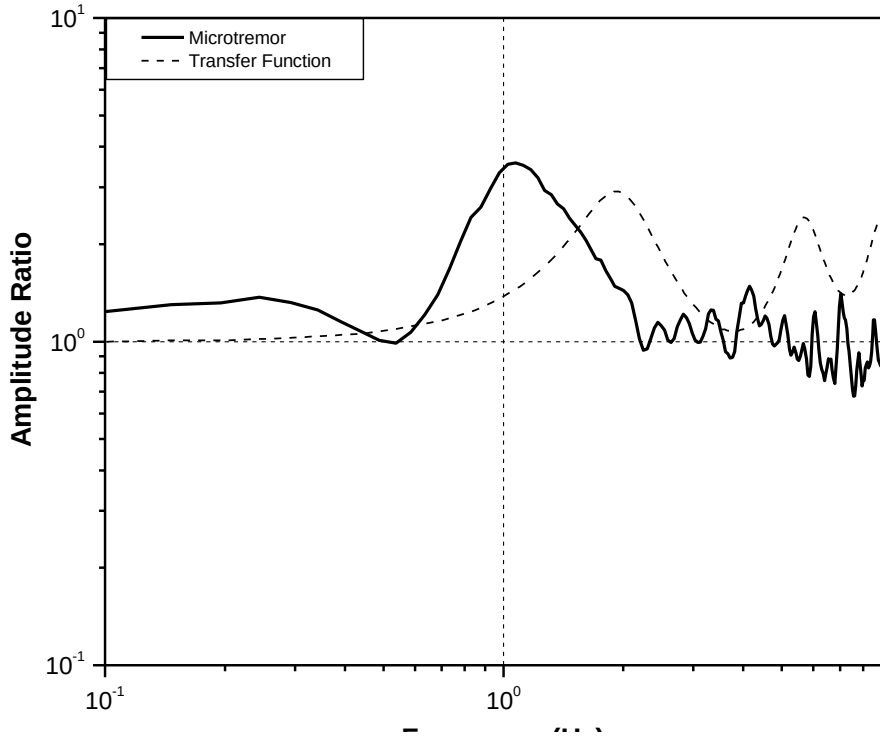

Figure E4.39: Amplitude ratios of microtremor and theoretical transfer function of shear wave at Bramangaon.

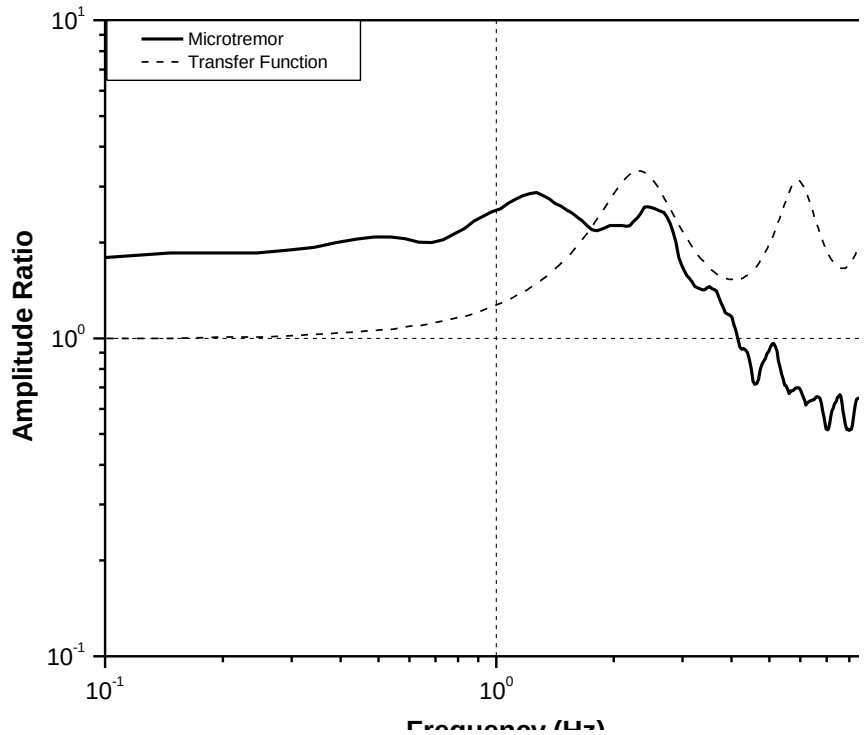

Figure E4.40: Amplitude ratios of microtremor and theoretical transfer function of shear wave at Meradia, Dhaka.

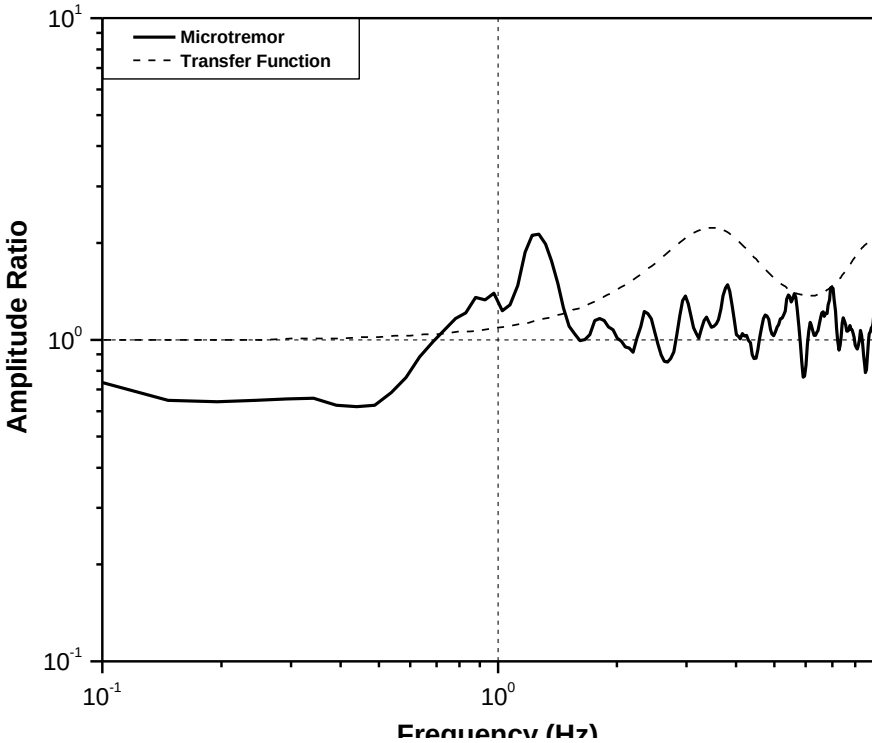

Figure E4.41: Amplitude ratios of microtremor and theoretical transfer function of shear wave at BUET filed ground.

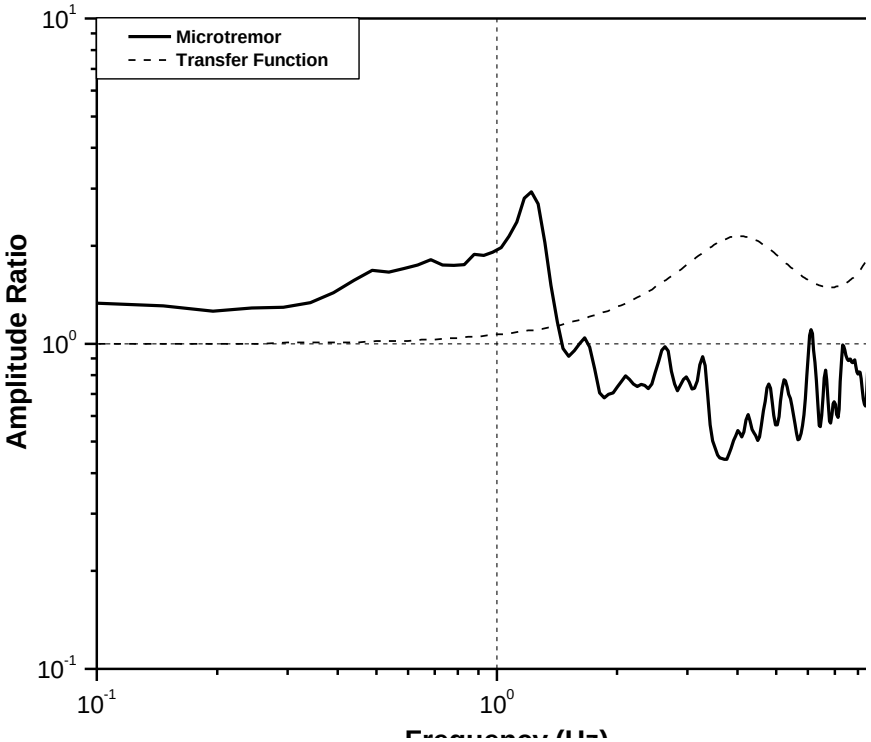

Figure E4.42: Amplitude ratios of microtremor and theoretical transfer function of shear wave at West Palashi (Microtremor test location-MT08 and Borehole-NA03).

CHAPTER 1

INTRODUCTION

1.1 GENERAL

In the recent past, Bangladesh has not suffered any damaging large earthquakes, but in the past few hundred years, several large catastrophic earthquakes struck this area. So far, all the major recent earthquakes have occurred away from major cities, and have affected relatively sparsely populated areas. In 1897, an earthquake of magnitude 8.7 caused serious damages to buildings in the northeastern part of India (including Bangladesh) and 1542 people were killed. Recently, Bilham et al. (2001) pointed out that there is high possibility that a huge earthquake will occur around the Himalayan region based on the difference between energy accumulation in this region and historical earthquake occurrence. The population increase around this region is at least 50 times than the population of 1897 and city like Dhaka has population exceeding several millions. It is a cause for great concern that the next great earthquake may occur in this region at any time.

The use of microtremor, an idea pioneered by Kanai et al. (1954) turns into one of the most appealing approaches in the site effects studies, due to its relatively low economic cost and the possibility of recordings without strict spatial or time restrictions (Rodriguez and Midorikawa, 2002). The H/V spectral ratio technique of microtremors gained popularity in the early nineties, after the publication of several papers (Nakamura, 1989; Field and Jacob, 1993; Lermo and Chávez-García, 1994) claiming the ability of this technique to estimate the site response of soft sedimentary deposits satisfactorily. This method is rather attractive in developing countries characterized by a moderate seismicity, where only very limited resources are available for seismic hazard studies. The H/V spectral ratio determined from microtremors has shown a clear peak that is well correlated with the fundamental resonance frequency at “soft” soil sites (Bard, 2004;

Horike et al., 2001; Field et al., 1995; Lachet and Bard, 1994; Lermo and Chávez-García, 1993). Comparison of microtremor and earthquake spectral ratios at strong-motion instrument sites across SW British Columbia showed similar fundamental periods and in greater Victoria remarkably similar amplitudes, validating the use of the method for linear earthquake site response Molnar et al. (2007).

Ohmachi et al. (1991) and Lermo and Chávez-García (1994) applied the H/V ratio method to analyze microtremor measurements. Lermo and Chávez-García (1993) used it to assess the empirical function of the S-wave, part of an earthquake record, obtained from three cities in Mexico. Their results clearly indicated that the H/V ratio could provide a robust estimate of frequency and amplitude of the first resonant mode, albeit not of the higher modes. In the meantime, Field and Jacob (1993) and Field et al. (1995) considered the response of sedimentary layers to ambient seismic noise and claimed that the H/V ratio method has been an effective and reliable tool to identify the fundamental resonance frequencies of all layered sedimentary basin. Further evidence has been given by Suzuki et al. (1995) who used both microtremor and strong-motion data in Hokkaido, Japan and ascertained that the peak frequency determined by the H/V ratio seemed to correspond with the predominant frequency estimated from the thickness of an alluvial layer. Based on numerical calculations, many other researchers (Lermo and Chávez-García, 1993, 1994; Lachet and Bard, 1994; Dravinski et al., 1996) have shown that the H/V ratio method is obviously able to predict fundamental resonant frequency well. Huang et al. (2002) found that the ground vulnerability index (Kg) values in the liquefied areas have been higher than those in the neighboring areas without liquefaction at 42 points in central Taiwan. This study shows supporting evidence for the first time that the H/V ratios of microtremor can be a good alternative indicator for an area's potential for liquefaction. Site amplification characteristics can be evaluated by one-point two-component surface recordings of earthquake ground motion, in a similar manner as proposed by Nakamura for microtremor (Ansary et al., 1996).

For seismic microzonation of Dhaka city, microtremor observation has been carried out at fourty five reclaimed and Non-reclaimed area in and around the Dhaka city. Standard

Penetration Test (SPT) has been executed at twenty seven locations of these points. Shear Wave velocity has been used to develop soil model. Six PS logging as well as SPT data, which are executed within the study area (CDMP, 2009) and eight Shear Wave Velocity as well as SPT data has been collected (Hossain, 2009). The SPT boring data of BUET campus has also been collected. Empirical SPT correlation developed by Ansary et al. (2010) has been used in this study to convert Field SPT N-value to Shear Wave Velocity. Finally, Soil model has been developed using 1D Response Analysis using the programme SHAKE. Comparison between microtremor and theoretical Transfer Function by the programme SHAKE has been carried out.

For Resonance analysis microtremor observation has been carried out at one hundred and thirty two selected locations within BUET campus and fourty five buildings in BUET campus. Finally, seismic damage has been assessed using Nakamura (2000)'s Vulnerability Index.

Although it is not possible to prevent such calamities, it is however, possible to mitigate the impacts of earthquake. Specific roles and responsibilities relating to earthquake hazard should be emphasized in our disaster mitigation plan. Bangladesh is a country characterized by a moderate seismicity with almost no resources available for large scale seismic hazard studies. The objective of this thesis is to analyze seismic hazard in and around Dhaka city in terms of dynamic charactersistics of soil (Predominant frequency and Amplification).

1.2 OBJECTIVE OF THE RESEARCH

The main purpose of this research is to estimate the dynamic response of soil using microtremor H/V technique. Dynamic response of soil is very important for the seismic hazard assessment of densely populated urban city like Dhaka. In order to carry out this research specific locations have been selected.

The followings are the specific objectives of the research:

(i) To examine the effectiveness of using Horizontal to Vertical Spectral Ratio (H/V) of microtremor to estimate predominant frequency and amplification.

(ii) To develop soil models to obtain transfer function using the computer programme SHAKE.

(iii) To compare microtremor results with ID response analysis of SHAKE.

(iv) To justify resonance criterion between soil and structure in the study area.

(v) To estimate damage of soils using Nakamura's (2000) Vulnerability Index (Kg).

1.3 STUDY AREA AND SITE SELECTION

To check the stability of microtremor observation fourteen locations of West Palashi within BUET campus has been selected. For this purpose, observation has been made at different time instants within a day from morning to midnight. After checking the stability of microtremor data, microtremor observation has been carried out at one hundred and eighteen additional locations within the BUET campus, where latitude varies from 23°43'16.58" N to 23°43'59.44" N and longitude varies from 90°23'13.31"E to 90°23'43.56" E (see Figure 1.1).

To assess the characteristics of soils in the reclaimed and non-reclaimed area in and around the Dhaka city fourty five locations have been selected to obtain microtremor observation (See Figure 1.2). These microtremor observation sites are situated at latitude from 23˚38´15.10″ N to 23˚56´46.54″ N and longitude from 90˚20´24.92″ E to 90˚33´50″ E. Among these fourty five locations, at twenty seven locations sub-soil investigation has been carried out. The geology and geomorphology of the study area has been illustrated in section 1.5 of this chapter.

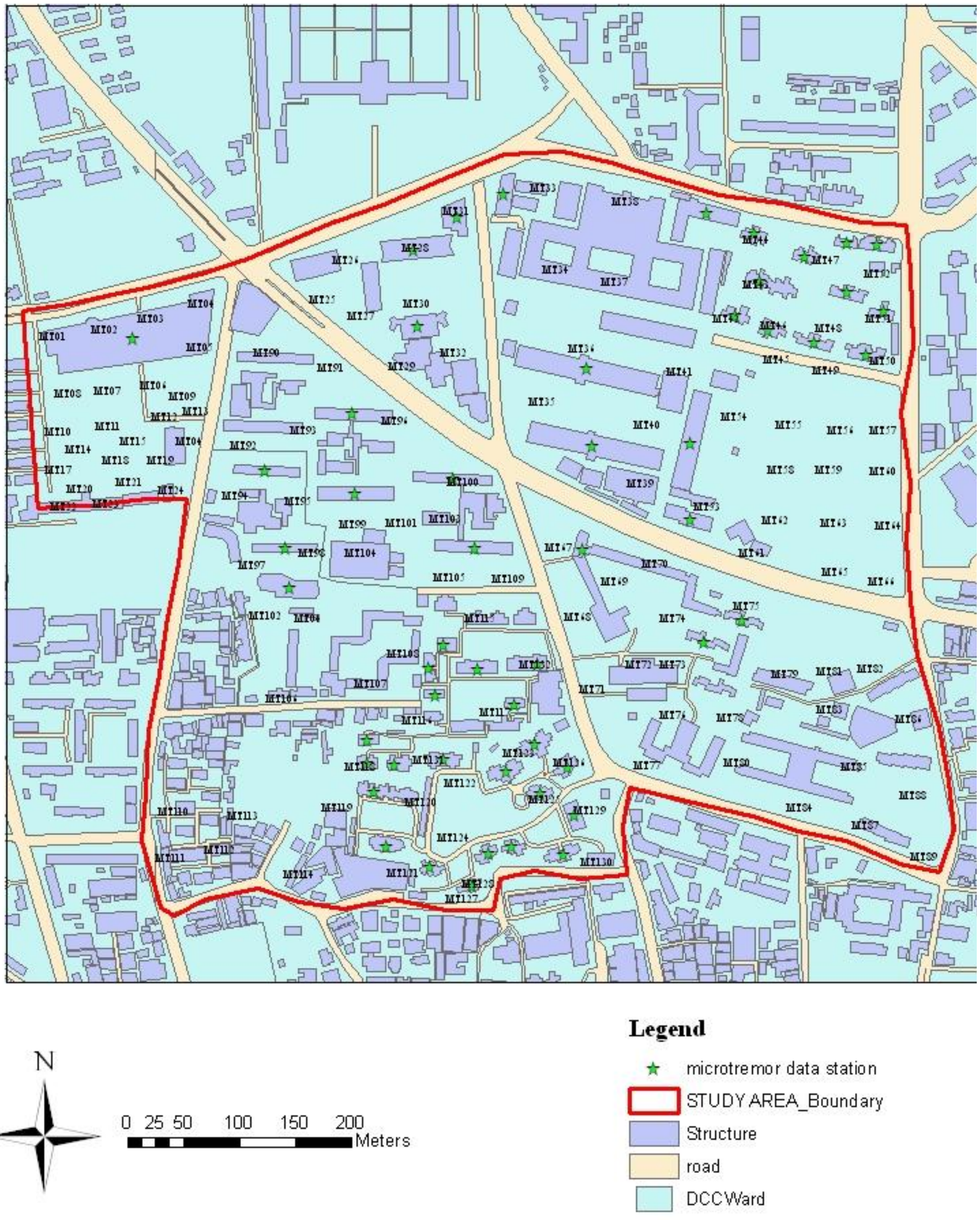

Figure 1.1: One hundred and thirty two microtremor observation in the free field locations of BUET campus.

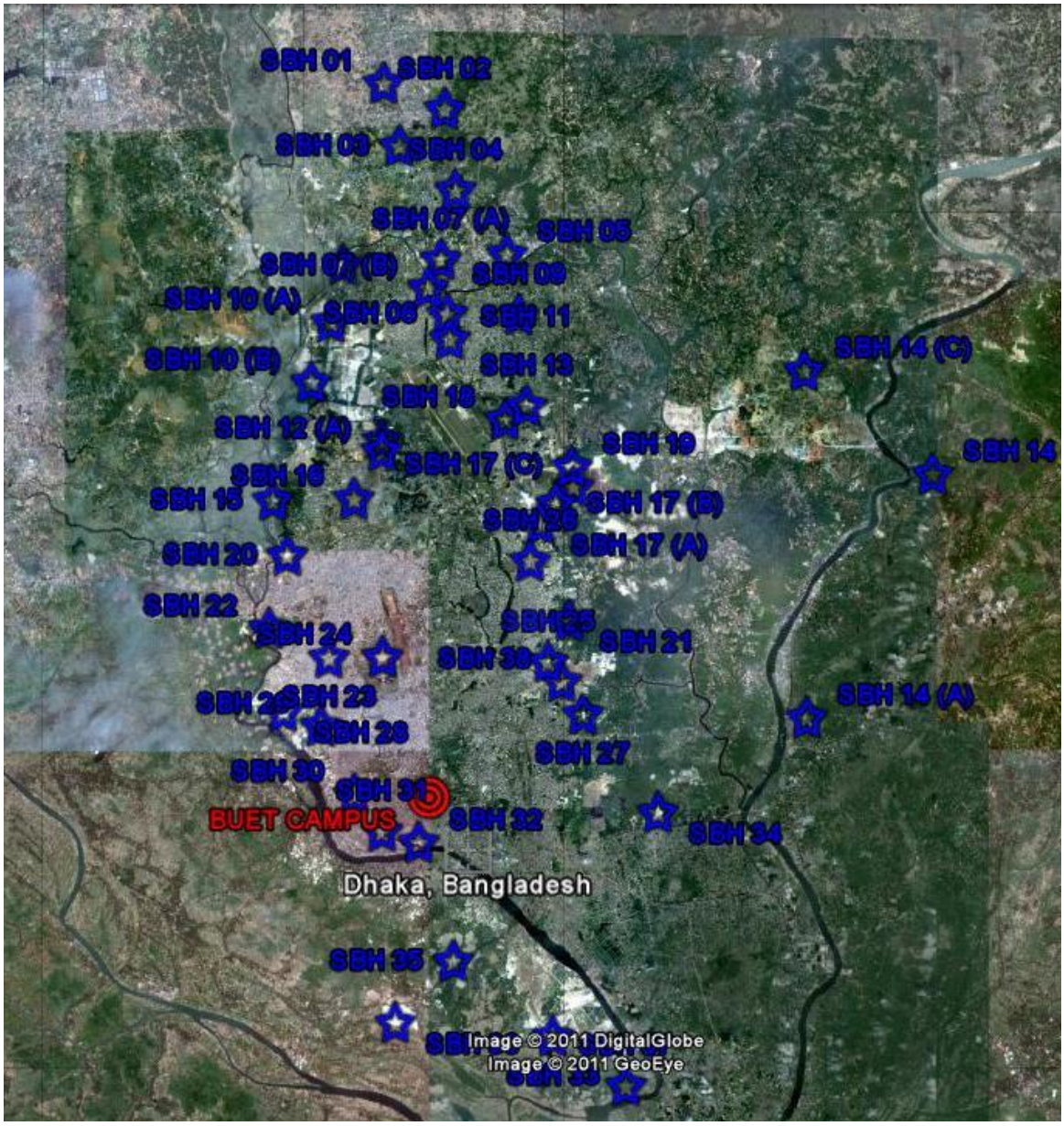

Figure 1.2: Fourty five selected locations for microtremor observation in and around the Dhaka city. (Source: Google map)

1.4 OUTLINE OF METHODOLOGY

The amplitude ratio (H/V) of horizontal to vertical spectra of microtremor has become popular to determine predominant period and amplification of a site. It is well known that, degree of damage during earthquakes strongly depends on dynamic characteristics of buildings as well as amplification of seismic waves. Among the other time consuming and expensive approaches, microtremor is the easiest and cheapest way to understand the dynamic characteristics of soil as well as structural element. In a short period of time it provides several information including natural frequency, amplification and vibration characteristics of soil and structure at different frequencies.

Following steps have been followed in this research:

A. Microtremor Analysis

Microtremor observation has been carried out in selected locations of Dhaka city. Each record comprises of three components, viz., EW, NS and UD. For spectral analysis three noise-free segments of 20.48s of the recordings have been taken at 100 Hz instrumental sampling. At each point of sensor location microtremor data recording have been carried out at different time of the day.

Time domain data is not suitable for the clear identification of soil response due to ambient noise. This is why First Fourier Transformation (FFT) has been applied on the time domain records. After smoothing the corresponding spectra, spectral ratio (H/V) technique have been applied to derive transfer functions. The applied sequences are given below:

I. FFT Transformation:

At first, Fourier spectra of the two horizontal directions (East-West and North-South) and the vertical component (Up-Down) have been calculated.

II. Smoothing of the Spectra

After Fast Fourier transformation (FFT), the combined horizontal and vertical spectra have been digitally filtered applying a logarithmic window with a suitable bandwidth coefficient. These filtering techniques have been applied to reduce the distortion of peak

amplitudes.

III. **Calculation of the Soil Response functions:**

The smoothed combined horizontal spectrum have been divided with the smoothed vertical component to plot Horizontal to vertical spectral ratio (H/V) which will provide the desired predominant frequency and corresponding amplification factor of the investigated portions (20.48 s) of records.

IV. **Estimation of Predominant Frequency and Amplification:**

After calculating three sets of the H/V ratios at selected grid, they have been normalized to obtain a relatively non-biased site specific H/V ratio. Then, Normalized H/V ratios at different time of the day have been plotted in Logarithmic window. From this normalized H/V ratio the predominant frequency and corresponding amplification factor of this site have been taken.

B. Soil Investigation

Twenty seven Standard Penetration Test (SPT) have been carried out for subsoil investigations at study locations. Empirical soil correlation has been used to convert SPT N-value to Shear Wave Velocity.

C. Develop Soil Model for Site Response Analysis

Soil model of investigated locations have been developed using the program SHAKE.

D. Comparison between Theoretical Transfer Function with Microtremor H/V ratio

Theoretical transfer function obtained from one dimensional soil response analysis using the programme SHAKE has been compared with microtremor H/V ratio. This output data have been used for estimation of predominant frequency and site amplification.

The brief methodology of this research has been shown through a flowchart in Figure 1.3.

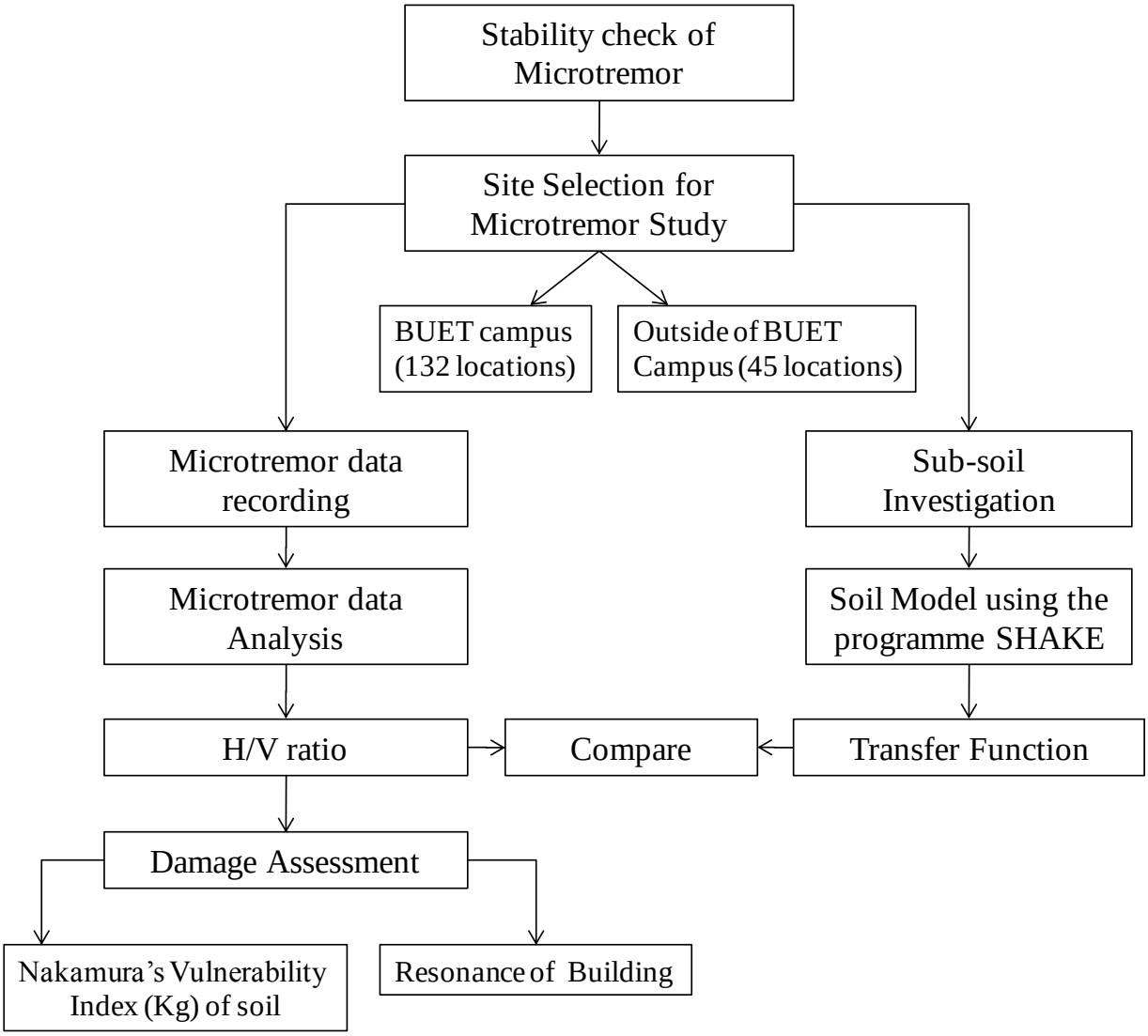

Figure 1.3: Flow chart for Microtremor Research in the Dhaka city.

The whole research has been carried out in the following phases according to Figure 1.3.:

a. Stability of microtremor data has been carried out at fourteen different locations in different time instants from morning to midnight within a day. Time domain data has been converted to frequency domain data because time domain data do not show dynamic properties of soil. So, Fourier transformation of three segments of 20.48 s long time history data along EW, NS and UD of these locations has been carried out. Then, the stability of Fourier spectra data has been checked at different time instants. Fourier spectra data do not show the amplification and stable data for site response. Therefore, Horizontal to Vertical spectral ratio data has been calculated from these Fourier spectra data. The mean H/V spectra data with half standard deviation with mean have been calculated and shown in logarithmic window. Stability of H/V ratio data at fourteen locations has been compared. H/V ratios are more stable than Fourier spectra data. From this conclusion, the analysis of Horizontal to Vertical spectra ratio (H/V) has been applied for microtremor data analysis.

b. For details study of microtremor observations, one hundred and thirty two points have been selected within BUET campus from morning to midnight. These data are located in the same geological units. However, from the analysis of these data, most of the locations did not show significant amplification due to the presence of stiff soil within BUET campus. For this reason, fourty five locations outside BUET have been selected. These locations include both reclaimed and non-reclaimed areas of Dhaka city.

c. For the assessment of soil response of reclaimed and non-reclaimed sites outside the BUET campus microtremor observation has been conducted at fourty five locations in and around the Dhaka city in consideration of different geological units. Microtremor observation has been carried out about ten geomorphic units (According to Figure 3.2) and nine geomorphic units (According to Figure 3.3).

d. Field investigations include 27 (Twenty seven) boreholes up to a depth of 20 m out of 45 locations outside BUET. For another 15 locations SPT-N value data have been collected from other sources. PS-loggings at 6 locations and SSMM data at 8 locations for Shear Wave Velocity exist among these locations.

e. Soil model has been developed at 42 locations out of 45. Among these locations, for 14 locations, shear-wave data have been directly obtained from the field. For rest 28 locations, empirical soil correlations developed by Ansary et al. (2010) and other empirical correlations (After TC4, ISSMFE, 1993) have been used to convert SPT-N value to shear-wave velocity.

f. Microtremor H/V ratio has been compared with the transfer function obtained from 1D soil response analysis at 42 locations.

g. Microtremor observation at fourty five buildings in the BUET campus have already been carried out. The predominant frequency of these observed building and adjacent soil obtained in this study has been compared to establish the resonance criteria.

h. For the damage assessment of soils at the observed locations Nakamura's (2000) Vulnerability Index (Kg) has been used.

1.5 GEOLOGY AND GEOMORPHOLOGY OF THE STUDY AREA

Dhaka city is the most densely populated metropolitan cities in the world, which is extending from in all directions day by day due to rapid urbanization. All the observation points of this research are located in and around the Dhaka city. The study areas are situated latitude from 23˚38´15.10″ N to 23˚56´46.54″ N and longitude from 90˚20´24.92″ E to 90˚33´50″ E. The BUET campus is located at latitudes from 23°43'16.58" N to 23°43'59.44" N and longitude from 90°23'13.31" E to 90°23'43.56" E. In total the city has 90 wards and 725 mohallas. Dhaka district has an area of 1463.60 km^2; and is bounded by

the districts of Gazipur, Tangail, Munshiganj, Rajbari, Narayanganj, Manikganj (Banglapedia, 2006). Dhaka is situated at the southern tip of a Pleistocene terrace, the Madhupur Tract. The major geomorphic units of the city are: the high land or the Dhaka terrace, the low lands or Floodplains, Depressions and abandoned Channels. Low lying swamps and marshes located in and around the city are other major topographic features. The elevation of the greater Dhaka city varies from 2 m to 13 m above the Mean sea Level (MSL).

1.5.1 Geological Subdivisions of Dhaka City

The geology of various locations Bangladesh is shown in Figure 1.4. The sediments of Bangladesh Geology has been classified into five major groups, which are Coastal deposits, Deltaic deposits, Paludal deposits, Alluvial deposits and Residual deposits. These five major groups are sub-divided into sixteen different geological units. The geology of our study area is located in three major groups, which are paludal deposits, Residual deposits and Alluvial deposits. The geological units are ppc (Marshy clay and peat, asd (Alluvial sand), asl (Alluvial silt), asc (Alluvial silt and clay) and rm (Modhupur clay residium). The brief descriptions of these five geological units are given below:

(a) ppc (Marshly clay and peat): ppc is generally Marsh clay and peat-gray or bluish gray clay, black herbaceous peat and yellowish-gray silt. Alternating beds of peat and peat clay common in bills and large structurally controlled depression; peat is thickest in different parts.

(b) **asd (Alluvial sand):** The common asd is Alluvial Sand-Light to brownish grey, coarse sand to fine silty sand. Sand is generally subrounded; constitutes channel, bar and levee deposits along rivers and larger tributaries; small and medium-scale crossbeds and laminations are common Brahmaputra river sand is medium to fine. Grain size decreases generally from North to South and away from channels. Brahmaputra sand contains mostly quartz, feldspar, mica, and significant amount of heavy minerals, indicating that

the sand is first cycle sediments from the Himalayan Mountains and the Indian shield. Meghna sand contains quartz-rich, reworked sediments from sandy tertiary rocks in the Fold Belt embedded with sediment derived from igneous rocks of the Shillong Plateaus.

(c) **asl (Alluvial Silt):** The asl is alluvial silt- Light to medium grey, fine sandy to clayey silt. Commonly poorly stratified; average grain size decreases away from main channels, chiefly deposited in flood basins and interstream areas. Unit includes small block swamp deposits during episodic or unusually large floods. Illite is the most abundant clay flooded annually, included in this unit are thin western of sand spread by episodic large floods over flood plain silts.

(d) **asc (Alluvial silt and clay):** The asl is generally Medium dark gray to clay; colour is darker as amount of organic material increases. Map unit is a combination of alluvial and paludal deposits; includes flood-basin silt, back swamp silty clay and organic rich clay is sag ponds and large depressions. Some depressions contain peat. Large area underlain by this unit is dry only a few months of the year; the deeper part of depressions and bils (bhils) contain water throughout the year.

(e) **rm (Madhupur clay residuum):** Madhupur Clay is the oldest sediment exposed in and around the city area having characteristic topography and drainage. Madhupur Clay characterized by Light yellowish-grey, orange, light to brick-red, and grayish white, micaceous silty clay to sandy clay; plastic and abundantly motted in upper 8 m; contains dominantly quartz, minor feldspar (orthoclase greater than plagioclase) and mica; sand content increases with depth, Dominantly clay minerals are kaolinite and illite. Iron manganese oxide nodules concentrated in zones; calcium carbonate nodules rare. Locally, a cohesive, 35 cm thick iron oxide zone is preserved near the surface of residuum.

Figure 1.4: Geology Map of Bangladesh. (Source: Geological Survey of Bangladesh, GSB)

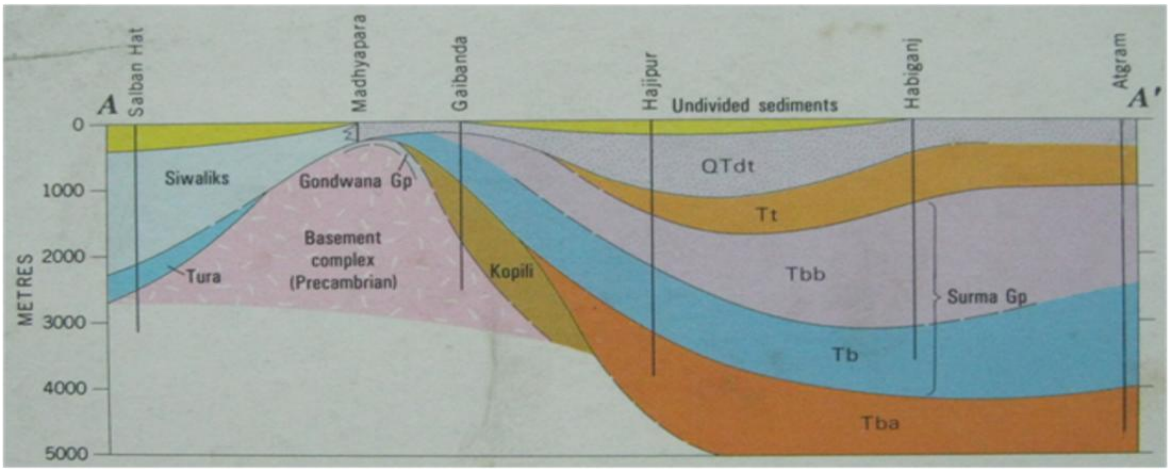

(a) Section along A-A'

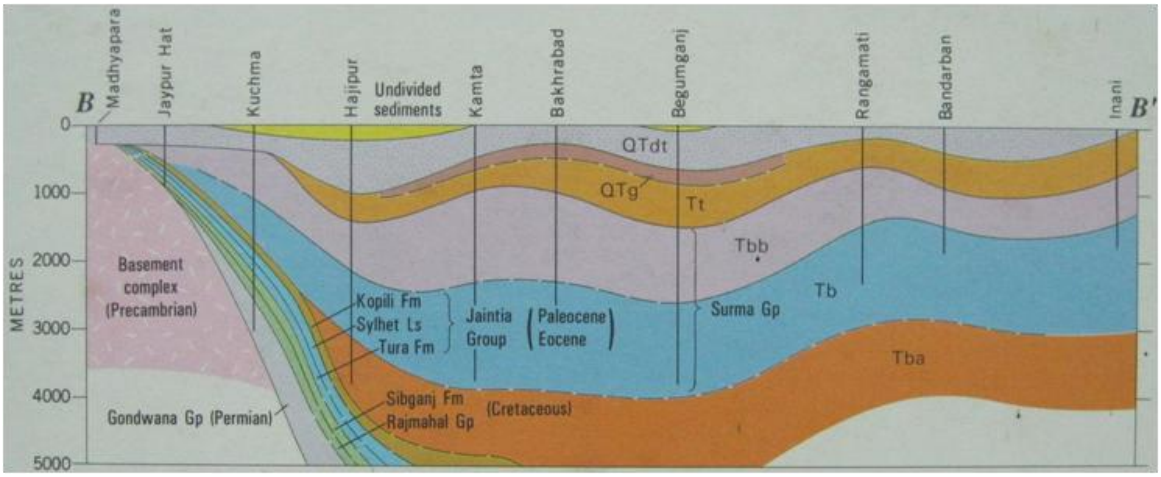

(b) Section along B-B'

Figure 1.5: Correlation of stratigraphic Sections from the Himalayan Foredeep across the Bengal Basin. (Source: Geological Survey of Bangladesh, GSB)

Geotechnical Characteristics of the Madhupur Clay in Dhaka city and its surroundings vary significantly both aerially and vertically. The evaluated parameters, particularly its low strength and high compressibility values indicate that the Clay, to some extent, is problematic for engineering construction. The moisture content and plastic limit results show that Madhupur Clay is normally consolidated to over-consolidated. The clay is

normal to active and has intermediate to high plasticity. The compressibility values suggest that the clay is very low to highly compressible at different locations.

Bed Rock:

Figure 1.5 shows the correlation of two stratigraphic sections along A-A' and B-B' from the Himalayan Foredeep across the Bengal Basin. The bed rock formation can be divided into five groups, which are St. Martin limestone, Dihing and Dupi Tila Formation undivided, Tipam Group, Surma Group and Jaintia Group. Figure 1.6 demonstrates the classification of bed rock according to stratigrahical section.

The negative rock units represent sediments derived from Himalayan mountains and Shillong plateau of Indian and from the Arakan Yoma mountain of Myanmar. Then eogene formations are probably time transgressive to the south and to the west; their lithological varies vertically and horizontally with distance from the source. All Neogene rock units except the Dupi Tila Formation and identified and mapped on the basis of the original type section in Asam (Khan and Munimullah, 1988). Age assignments are based on fossils on correlation with rock units in India.

The paleogene rock units represent sediments deposited on the edge of the Indian shield; they are exposed only along the eastern part of the northern border. Type sections are in Assam, India and correlation is made on the basis of marine fossils and lithology.

In northwestern Bangladesh, subsurface equivalent of the Neogene and Paleogene rocks have been given different names (Khan and Munimullah, 1988) is correlated with the Tipam and Surma Groups and the Bogra Formation (Oligocene) with the Barail Formation.

The classification of bed rocks are follows:

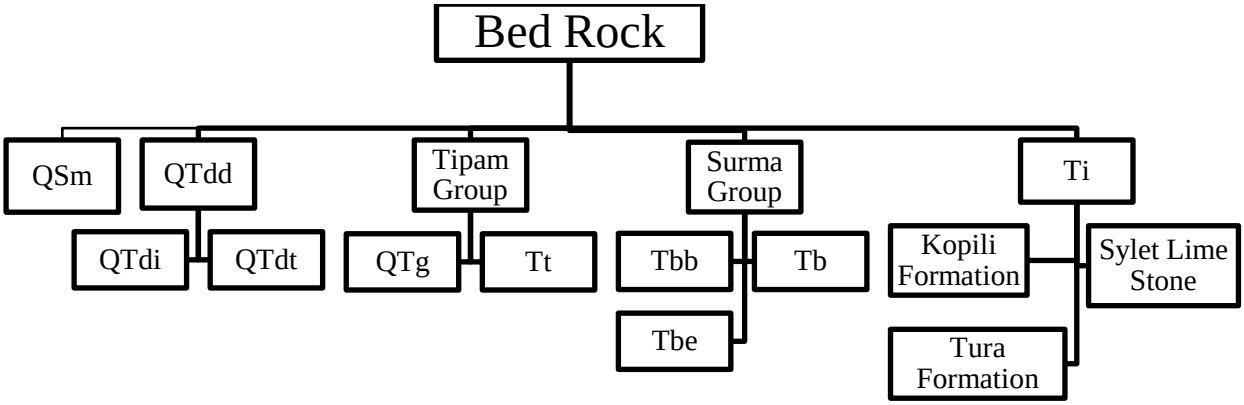

Where,

QSm: St. Martin Limestone (Pleistocene)
QTdd: Dihing and Dupi Tila Formation undivided
QTdi: Dihing Formation (Pleistocene and Pliocene)
QTdt: Dupi Tila Formation (Pleistocene and Pliocene)
QTg: Girujan clay (Pleistocene and Neogene)
Tt: Tipam Sandstone (Neogene)
Tbb: Boka Bill Formation (Neogene)
Tb: Bhuban Formation (Miocene)
Tbe: Barail Formation (Oliogocene)

Figure 1.6: Geological classification of Bed Rock.

1.5.2 Geomorphological subdivisions of Dhaka city

Various geomorphological maps with suitable geomorphic unit have been developed for Dhaka city. Figure 1.7 demonstrates the geomorphological map of Dhaka city with eighteen geomorphic units. These geomorphic units are classified into two major sub-division units, which are Denundational landform and Fluvial landform. The geology of the subsoil of eighteen geomorphic units has also been illustrated in Figure 1.7.

In addition to these, Geomorphological subdivision of Dhaka city as well as superimposed study points is also shown in Figure 3.2 and Figure 3.3. Figure 3.3 shows the geomorphological map of Dhaka city with fifteen different geomorphic units. These geomorphic units represent the soil conditions or surface geology of Dhaka city. Figure 3.2 illustrates the fourty five microtremor observation locations in eighteen geomorphic

units. On the other hand, the geomorphological map of Dhaka city area with eighteen geomorphic units and four categories of landfills have been demonstrated in Figure 3.3.

Some important geomorphic units from the geomorphological maps are discussed in below:

a) Active Channel deposits

The greater Dhaka city is drained by four major perennial rivers: the Buriganga, the Shitalakhay, the Turag and the Balu. These perennial rivers carry a huge quantity of suspended and bed load sediments, like sand, silt and clay. Sometimes, the river bed sediments are used for filling materials of lowland areas.

b) Abandoned Channel deposits

Late Quaternary climatic episodes had created numerous deeply incised channels on the Madhupur reddish-brown surfaces. These are now the abandoned channels. Gulshan, Bonani and Dhanmandi Lakes were such kind of palaeochannels. The palaeochannels had north-south flow in the central zone of Dhaka city and discharged its water into the Buriganga. The channels had a lot of tributaries and distributaries. Mid Holocene sea level rise changed the hydrodynamic condition of the river systems. As a result these incised palaeochannels have been filled up with Holocene sediments. The sediments are mostly cross bedded sand and clay with some involutions of post depositional sedimentary structures, containing humic materials and concretions. Those concretions are the reworked materials, can be found in the Madhupur Formation.

c) Alluvial Gullies

The surface and subsurface water flow of Early Holocene amplified monsoon had created innumerous gullies in the margin of the central zone (north-south elongated) of Dhaka city. These gullies have been deeply incised (when sea level was low compared to the present MSL) whereby middle and lower part of Madhupur Formation have been exposed. These gullies are now filled up with Holocene sediments.

d) Lateral and point bars

These are the Holocene deposits exposed at the left (north) bank of the river Buriganga at Kamrangi char area and Mitford locality. It covers a small area along the river side of the Balu. The sediments are represented by grayish to yellowish brown silty sand with humic contents.

e) Swamps

There are swamps or marshy land in Dhaka city. Swamp of Khilgaon, Ashulia, DND area and the areas inside the western barrage (Beribadh) represent such marshy land. These are the man made water logged areas where recent unconsolidated alluvium sediments are depositing.

f) Flood plains

The Dhaka city is surrounded by recent floodplain (except a small portion of northern side). These are the flood plains of the rivers Buriganga, Balu, Turag and Shitalakhay. The floodplains are annually flooded having some increments of alluvial sediments. Initial Madhupur surface was eroded away during the Late Pleistocene and Early Holocene time and had created some erosional depressions. During Mid-Holocene, these erosional depressions were filled up with brackish water sediments as sea level was high compared to present sea level. Sea level started to drop after mid Holocene and the tidal or brackish water sediments aerially exposed. During the present time, these tidal flood deposits are overlying by annual increments of flood plain deposits.

g) Tidal flat deposits

The Mid Holocene sea level rise changed the hydrodynamic condition of the river system. Incised valleys have been filled up with Holocene sediments. The Buriganga, Turag, Balu and Shitalakhay rivers are acting just like the tidal rivers. Low land areas, in particular areas near the banks of these tidal rivers have been inundated with brackish water and tidal sediments have been deposited and Rasulbag, a locality on the right bank of the river Shitalakhay are the area of a tidal. Thickness of tidal deposits more than 30 meters.

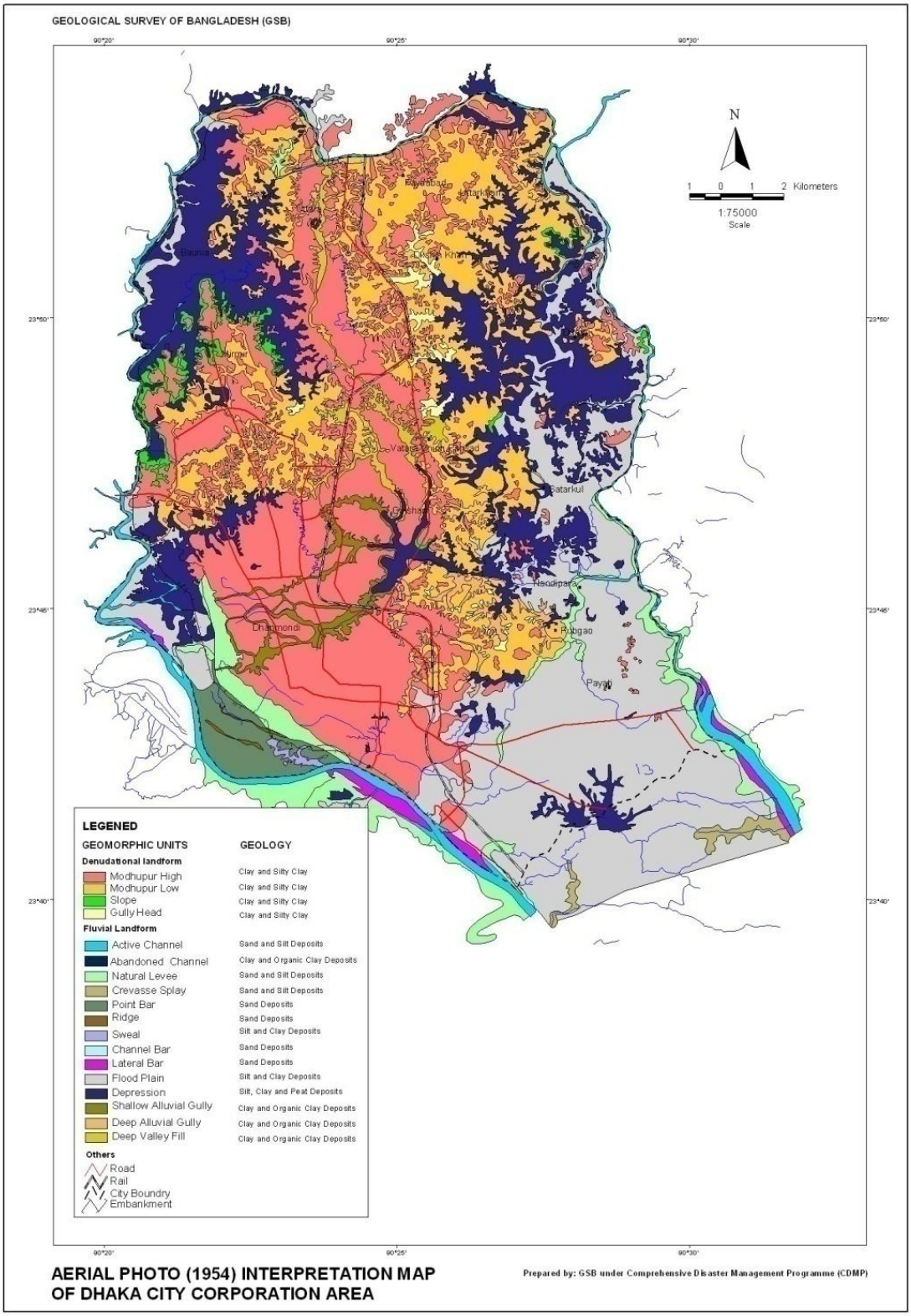

Figure 1.7: Geomorphological Map of Dhaka City. (Source: Geological Survey of Bangladesh, 2008)

1.5.3 Seismicity and Tectonics

Tectonics and geology of Bangladesh and adjoining areas have been discussed in details by Matin et al. (1983), Sesoren (1984) and Khan (1991). It is revealed in the above literature that stratigraphy, structure and surface geology of Bangladesh are related to its tectonic evolution.

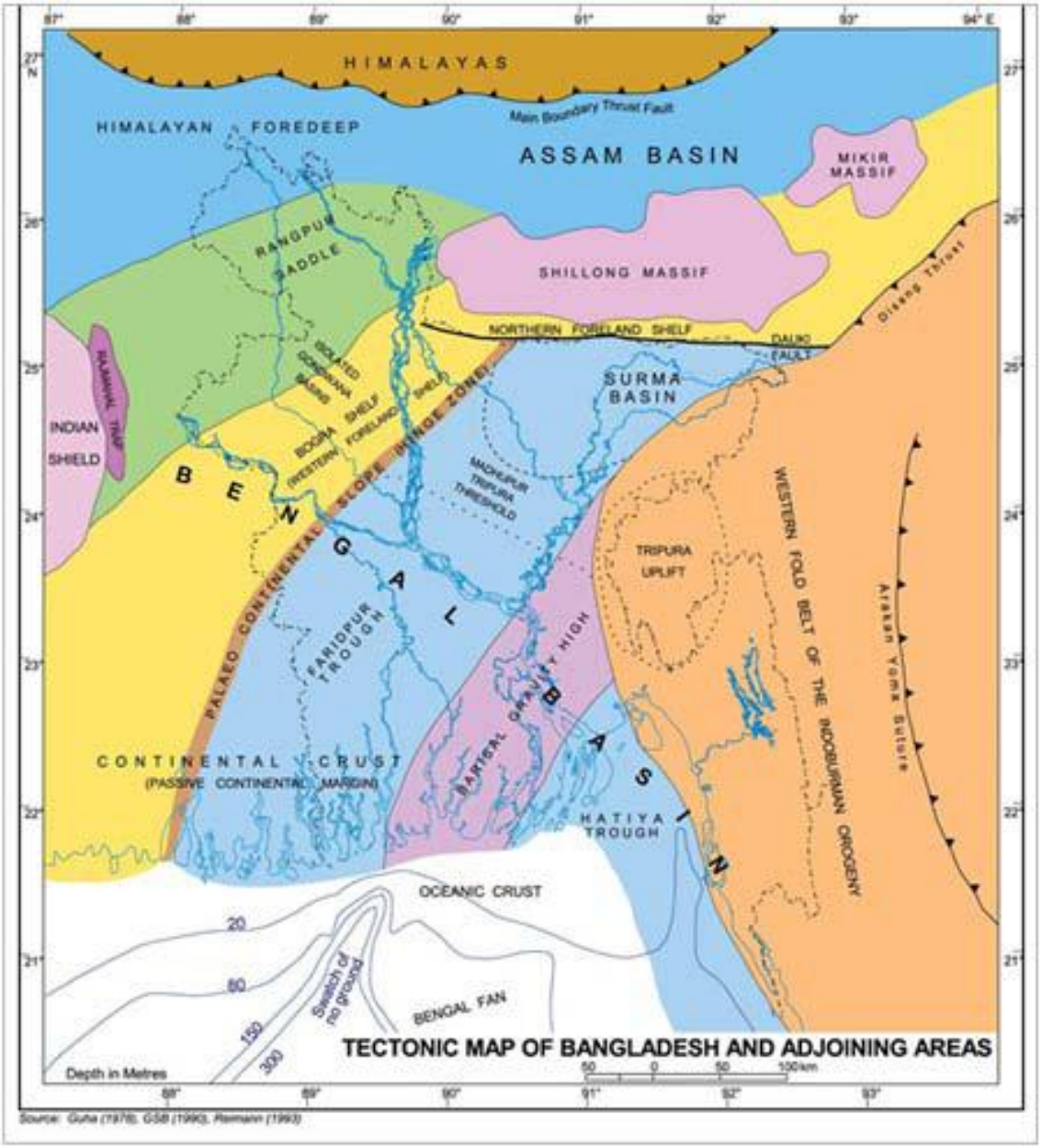

Figure 1.8: Tectonic Map of Bangladesh. (Source: Banglapedia)

Basically Bangladesh is bounded by the Indian Shield on the west, by the Cenozoic Indo Burma ranges on east, by the Precambrian shilling massif on the north east (Curry and Moore, 1974). The Ganges, Brahmaputra and Meghna rivers have formed this large delta (Figure 1.8). The evolution of the Bengal Basin is interlinked with that of the Himalayas and the Indo-Burma-ranges, resulting from the collision of the Indian and Eurasian plates during Tertiary period. The initial separation on India from Antarctica in Early Cretaceous occurred along the north east continental margin of India (Curry and Moore, 1974). There after the gradual thinning and subsidence caused inundation of the coastal region in late Cretaceous. India drifted north during late Cretaceous to late Eocene and a miogeosynclinal wedge with thickness in excess of 10 km (Curry and Moore, 1974) built up on the basin floor. Dhaka is a part of this basin.

The Precambrian rocks form the basement of all geological formations of Bengal Basin and Shield areas. Seismic profiles indicate that the sediments are approximately 10 km thick in both west of Chittagong and South East of Faridpur district. The sediments are deeper than 10 km towards the Surma Basin area and decreases to 8 km in region beneath the confluence of the Ganges and the Jamuna River.

1.6 OVERVIEW OF THE THESIS

The main purpose of this research is to estimate dynamic response of soils at different locations of Predominant frequency and Horizontal to Vertical spectral (H/V) ratio.

Chapter one describes Ground idea of the current research, its scopes and objectives, methodology, geology and geomorphology of the study area.

Chapter 2 presents the literature review that includes Past research of microtremor, Microtremor Horizontal to Vertical spectral (H/V) ratio technique, relationship between microtremor and strong motion, Correlation between Field SPT N-value and Shear Wave Velocity, Theory of 1D Response Analysis using programme SHAKE, Various microtremor and seismic waves, Resonance between site soil and building. In addition to this, the past research for the application of microtremor H/V ratio for damage assessment of any site soil and building has been included.

Chapter 3 is the main part of this research which represents data collection and analysis for this research. This chapter includes geomorphological classification of selected sites, sub-soil charactersistics of investigated locations using Standard Penetration Test (SPT), estimation of Shear Wave Velocity for input in Programme SHAKE, Microtremor Data collection, Stability of microtremor data, various effects on the result of microtremor data. The comparision of microtremor analysis result at different locations of study area has been demonstrated as well. The remains of analysis result have been included in APPENDIX-A, APPENDIX-B, APPENDIX-C and APPENDIX-D.

Chapter 4 represents the comparison of microtremor data with theoretical analysis. The main part of this chapter is the analysis result and comparison between microtremor and 1D response analysis using Programme SHAKE. Finally, the damage assessment of site soil and building of observed locations has been included. The comparison of amplitude ratio between microtremor and transfer function of the fourty two locations have been included in APPENDIX-E.

The final chapter, chapter 5 is a summary of the microtremor H/V technique, comparison of amplification at various locations, comparision of microtremor data and theoretical result, and damage assessment of the study locations. The specific conclusions and recommendations have been discussed in this chapter. Finally, the scope of future researches using microtremor has been included.

CHAPTER 3

DATA COLLECTION AND ANALYSIS

3.1 GENERAL

Damage in recent earthquakes showed that local site conditions have a significant effect on ground motion. Site response studies play an important role in seismic microzonation studies. The application of microtremor is to determine dynamic characteristics (predominant frequency and amplification factor). Nowadays microtremor measurements are generalized in site characterization due to their simplicity, low cost and minimal disturbance to other activities.

In the traditional spectral ratio method, H_S/H_r, site and source effects are estimated from observation at a reference site. In practice, adequate reference site are not always available especially in flat areas where exposed rock is not available. Therefore, methods have been developed that do not need reference sites (Bard 1994). Several recent applications of this technique have proved to be effective in estimating predominant frequency (Field and Jacob 1973; Ohmachi et al. 1994) and amplification factors (Lermo and Chavez-Garcia 1994; Konno and Ohmachi 1995). The reality of microtremor H/V technique for site response analysis has been discussed in Chapter 2.

Several methods have been proposed for spectral calculation of ground motions including microtremor. Fourier spectrum is the most convenient one that is used widely. Some investigations showed that different methods give similar results (Dimitriu et al. 1998). However some researchers declare that a suitable spectral method gives more reliable results (Ghayamghamian and Kawakami 1997). That's why three segments of spectra have been selected to compute the mean segmental cross spectra. Standard deviation of mean has also been calculated to show the deviation of mean value from six spectra in East-West and North-South direction. Subsoil investigation has also been executed in the test location to compute the Shear Wave Velocity which has been used in 1D response analysis using the programme SHAKE.

3.2 LOCATION OF INVESTIGATED SITES WITHIN THE STUDY AREA

3.2.1 Geological and Geomorphological classification

Local site conditions substantially affect the characteristics of seismic waves during earthquakes. Soft alluvial deposits tend to amplify certain frequencies of ground motion and extend the duration of motion which may cause further earthquake damage. The expected variation in the ground motion, according to the geological site conditions, make it necessary to perform a more detailed seismic hazard assessment for a metropolitan area. To accurately identify the variation of seismic hazards at different locations within the metropolis, one may conduct seismic microzonation that requires subdividing an area into zones with respect to the geological characteristics of the sites.

Therefore, microtremor measurement at 45 selected locations in and around Dhaka city as well as 132 locations within BUET campus has been executed in consideration of diversified geological and geomorphological units. Most of the locations in and around Dhaka city are situated in various geomorphological units. But, all of the selected points in BUET campus are located in the same geological and geomorphological unit. 45 selected locations have been shown in Figure 3.1.

Two geomorphological maps of Dhaka city from different source are shown in Figure 3.2 and Figure 3.3. Microtremor measurements points have been superimposed in these two geomorphological maps. Some locations are situated out of the geomorphological map in Figure 3.2 and Figure 3.3. The geomorphological classifications of these locations have been presented in Table 3.1. Table 3.1 represents 45 test locations, their ID, latitude, longitude and geomorphological classification according to Figure 3.2 and Figure 3.3. The test locations have been classified in different geomorphological unit. Figure 3.2 has been divided by 15 geomorphological units. On the other hand, Figure 3.3 has been divided by 22 geomorphological units. 132 selected locations of BUET campus in Figure 3.55 has been classified as Upper Modhupur Terrace according to Figure 3.2 and Higher Pleistocene Terrace according to Figure 3.3.

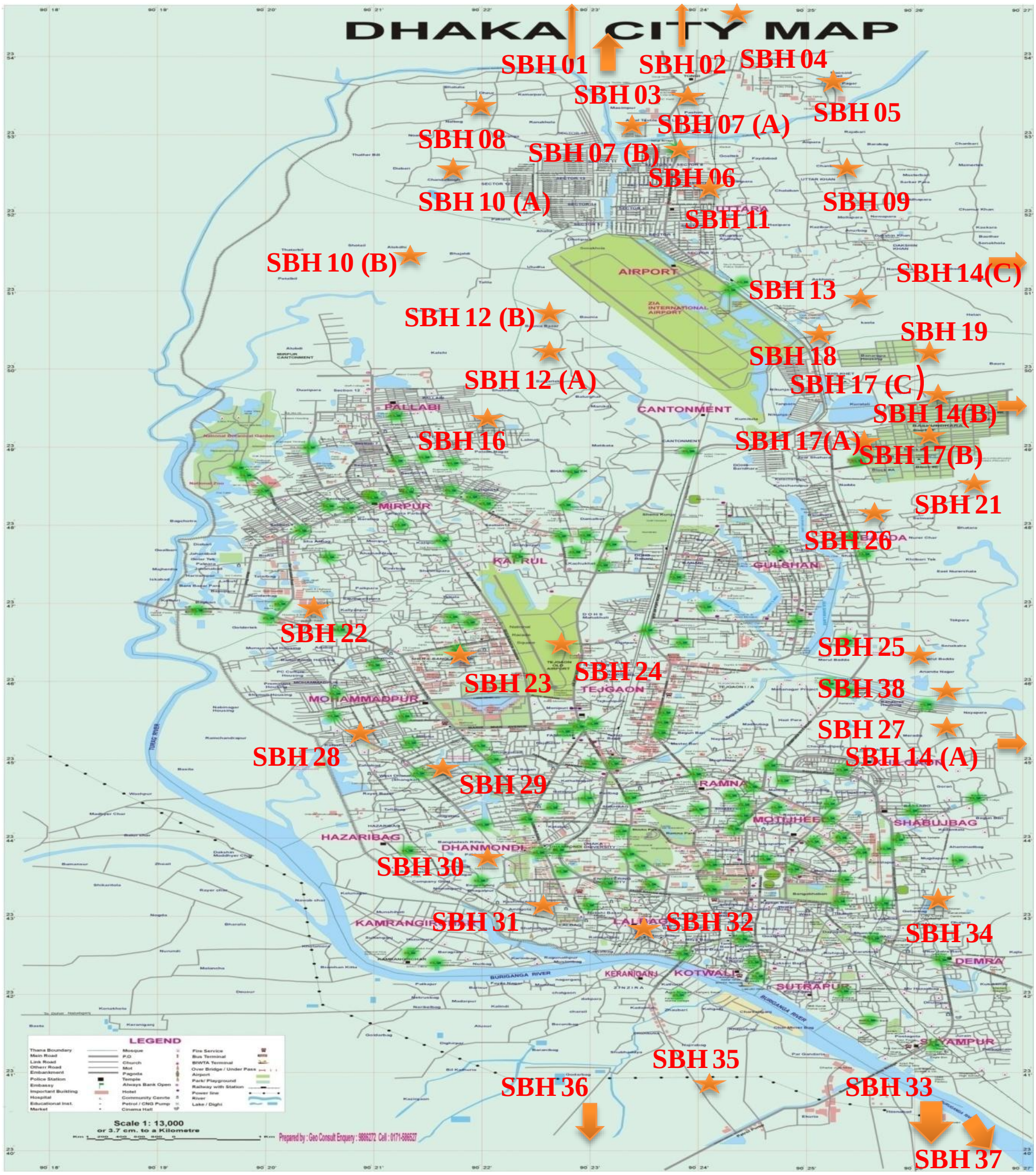

Figure 3.1: Microtremor observation at fourty five selected locations in and around Dhaka City.

From Table 3.1, 45 selected locations are situated in 10 different geomorphic units according to Figure 3.2. On the other hand, same 45 locations are located in 9 different geomorphic units according to Figure 3.3. Most of the points in Table 3.1 have been selected on the basis of recent filling. But, there is no specific classification of geomorphological unit of filling area in Figure 3.2. However, Figure 3.3 shows specific geomorphic unit of recent filling. So, both Figure 3.2 and Figure 3.3 have been justified to classify 45 sites in different geomorphic units.

Table 3.1: Geological and Geomorphological classification of the study area

SL. No.	ID	Location	Latitude	Longitude	Geomorphological Classification	
					After Figure 3.2	After Figure 3.3
1	SBH-01	National University	23˚56′46.54″	90˚22′43.93″	Upper Modhupur Terrace	High Pleistocene terrace
2	SBH-02	Board Bazaar, Gazipur	23˚56′18″	90˚23′58″	Upper Modhupur Terrace	Moderately High Pleistocene terrace
3	SBH-03	Kaunia, Boro Bari, Moddopara	23˚55′37″	90˚23′03″	Shallow Alluvium Gully	Moderately High Pleistocene terrace
4	SBH-04	Tongi, Ershadnagar	23°54'48"	90°24'11"	Lower Modhupur Terrace	Moderately High Pleistocene terrace
5	SBH-05	Tongi BSCIC area	23°53'37.18"	90°25'13.35"	Lower Modhupur Terrace	Thick fill
6	SBH-06	Abdullahpur	23˚52′31″	90˚24′01″	Deep Alluvium Gully	Highly Erosional Lower Pleistocene terrace
7	SBH-07(A)	Ijtema field (North and East side)	23˚53′31.13″	90˚23′53.39″	Shallow Alluvium Gully	Deep alluvial valley
8	SBH-07 (B)	Ijtema Field (South and West side)	23˚52′59.96″	90˚23′37.91″	Shallow Alluvium Gully	Deep alluvial valley
9	SBH-08	Ashulia Toll Plaza	23°53'25.40"	90°21'54.61"	Deep Marshly Land	Deep marshly land
10	SBH-9	Uttar Khan	23′52′30″	90˚25′28″	Lower Modhupur Terrace	Highly Erosional Lower Pleistocene terrace
11	SBH-10(A)	Uttara Phase 3 (North side)	23˚52′22″	90˚21′40″	Deep Marshly Land	Moderately thick fill
12	SBH-10(B)	Uttara Phase 3 (South side)	23˚51′15″	90˚21′16″	Deep Marshly Land	Moderately thick fill

SL. No.	ID	Location	Latitude	Longitude	Geomorphological Classification	
					After Figure 3.2	After Figure 3.3
13	SBH-11	Azampur School, Uttara	23˚52′03″	90˚24′04″	Upper Modhupur terrace	Moderately High Pleistocene terrace
14	SBH-12 (A)	Mirpur DOHS (South side)	23˚49′59″	90˚22′42″	Upper Modhupur terrace	High Pleistocene terrace
15	SBH-12 (B)	Mirpur DOHS (North side)	23˚50′11″	90˚22′42″	Upper Modhupur terrace	High Pleistocene terrace
16	SBH-13	Ashiyan city, Askona, Dakkhin Khan	23˚50′49″	90˚25′37″	Swamp/Depression	Moderately Thick fill
17	SBH-14(A)	Purbachal-1, Randokpur Hazi bari, Rupganj	23˚45′03″	90˚31′17″	Lower Modhupur Terrace	Thick fill
18	SBH-14(B)	Purbachal-2, American City	23˚49′33″	90˚33′50″	Lower Modhupur Terrace	Thick fill
19	SBH-14(C)	Purbachal Picnic Park, Gazipur	23˚51′28″	90˚31′14″	Lower Modhupur Terrace	Thick fill
20	SBH-15	Adjacent to Mirpur Zoo	23˚49′04.14″	90˚20′29.63″	Natural levee	Thick fill
21	SBH-16	Field Ground, Pallabi	23˚49′06″	90˚22′08″	Upper Modhupur terrace	Thick fill
22	SBH-17 (A)	Block-B, Basundhara	23˚48′38″	90˚25′54″	Lower Modhupur Terrace	Moderately High Pleistocene terrace
23	SBH-17 (B)	Block-D, Basundhara	23˚49′00.49″	90˚26′12.95″	Back swamp	Moderately High Pleistocene terrace
24	SBH-17 (C)	Block-H, Basundhara	23˚49′19″	90˚26′34″	Back swamp	Moderately High Pleistocene terrace
25	SBH-18	Civil Aviation Quarter	$23^0$50′33.61″	$90^0$25′11.22″	Upper Modhupur terrace	Higher Pleistocene terrace
26	SBH-19	Kuril Flyover	23˚49′41.51″	90˚26′32.06″	Swamp/Depression	Thick fill
27	SBH-20	Sarengbari, Mipur-2	23˚48′03.24″	90˚20′47.10″	Swamp/Depression	Deep marshly land
28	SBH - 21	Purachal, Uttar Badda	23˚46′51″	90˚26′29″	Back swamp	Deep marshly land
29	SBH-22	City Corporation, Gabtoli	23˚46′41.99″	90˚20′24.92″	Flood plain	Moderately thick fill
30	SBH-23	Adabor	23˚46′09.75″	90˚21′37.62″	Shallow alluvium Gully	Moderately thick fill
31	SBH-24	Agargoan Trade Fair area	23˚46′10.56″	90˚22′42.73″	Upper Modhupur Terrace	Higher Pleistocene terrace

SL. No.	ID	Location	Latitude	Longitude	Geomorphological Classification	
					After Figure 3.2	After Figure 3.3
32	SBH-25	Aftab Nagar Housing Project	23˚46′04.98″	90˚26′03.22″	Flood plain	Thick fill
33	SBH-26	Umme Had Nagar, Nadda	23˚47′57.17″	90˚25′41.61″	Swamp/Depression	Moderately thick fill
34	SBH-27	South Banasree	23˚45′07.17″	90˚26′45.36″	Flood plain	Thick fill
35	SBH-28	Basila Garden City	23˚45′10.29″	90˚20′42.36″	Back Swamp	Thick fill
36	SBH-29	Royer Bazar Boddhobumi	23˚44′54″	90˚21′28″	River Bar	Gently sloping Erosional terrace edge
37	SBH-30	Kalunagar, Hazaribagh	23˚43′38.50″	90˚22′08.62″	River Bar	Thick fill
38	SBH-31	Rab-10, Plot, Kamrangirchar	23˚42′57.58″	90˚22′42.11″	River Bar	Moderately thick fill
39	SBH-32	Sosan Ghat, Kamrangirchar	23˚42′44.81"	90˚23′26.51″	Natural levee	Deep Marshly land
40	SBH-33	Basundhara River view	23˚39′10″	90˚26′09″	Flood plain	Moderately Thick fill
41	SBH-34	Matuail, Demra	23˚43′18.24″	90˚28′16.48″	Swamp/Depression	Younger active floodplain
42	SBH-35	Jilmil Project, Equria	23˚40′33.40″	90˚24′08.42″	Shallow alluvium Gully	Thick fill
43	SBH-36	Rajendapur	23˚39′25″	90˚22′58″	Deep alluvium Gully	Thick fill
44	SBH-37	Bramangaon	23˚38′15.10″	90˚27′37.35″	Flood plain	Deep alluvial valley
45	SBH-38	Meradia, Uttar Banasree	23˚45′43.57″	90˚26′19.67″	Flood plain	Thick fill

According to Figure 3.2, 45 selected locations have been classified into following groups:

8-Upper Modhupur Terrace [SBH 01; SBH 02; SBH 11; SBH 12(A); SBH 12(B); SBH 16; SBH 18 ; SBH 24], 5-Shallow Alluvium Gully [SBH 03; SBH 07(A); SBH 07(B); SBH 23; SBH 35], 7-Lower Modhupur Terrace [SBH 04; SBH 05; SBH 09; SBH 14(A); SBH 14(B); SBH 14(C); 17(A)], 2-Deep Alluvium Gully (SBH 06; SBH 3), 3-Deep Marshly Land [SBH 08; SBH 10(A); SBH 10(B)], 5-Swamp/Depression (SBH 13; SBH 19; SBH 20; SBH 26; SBH 34), 2-Natural Levee (SBH 15; SBH 32), 4-Back Swamp [SBH (B); SBH 17(C); SBH 21; SBH 28], 6-Flood Plain (SBH 22; SBH 25; SBH 27; SBH 33; SBH 37; SBH 8) and 3- River Bar (SBH 29; SBH 30; SBH 31).

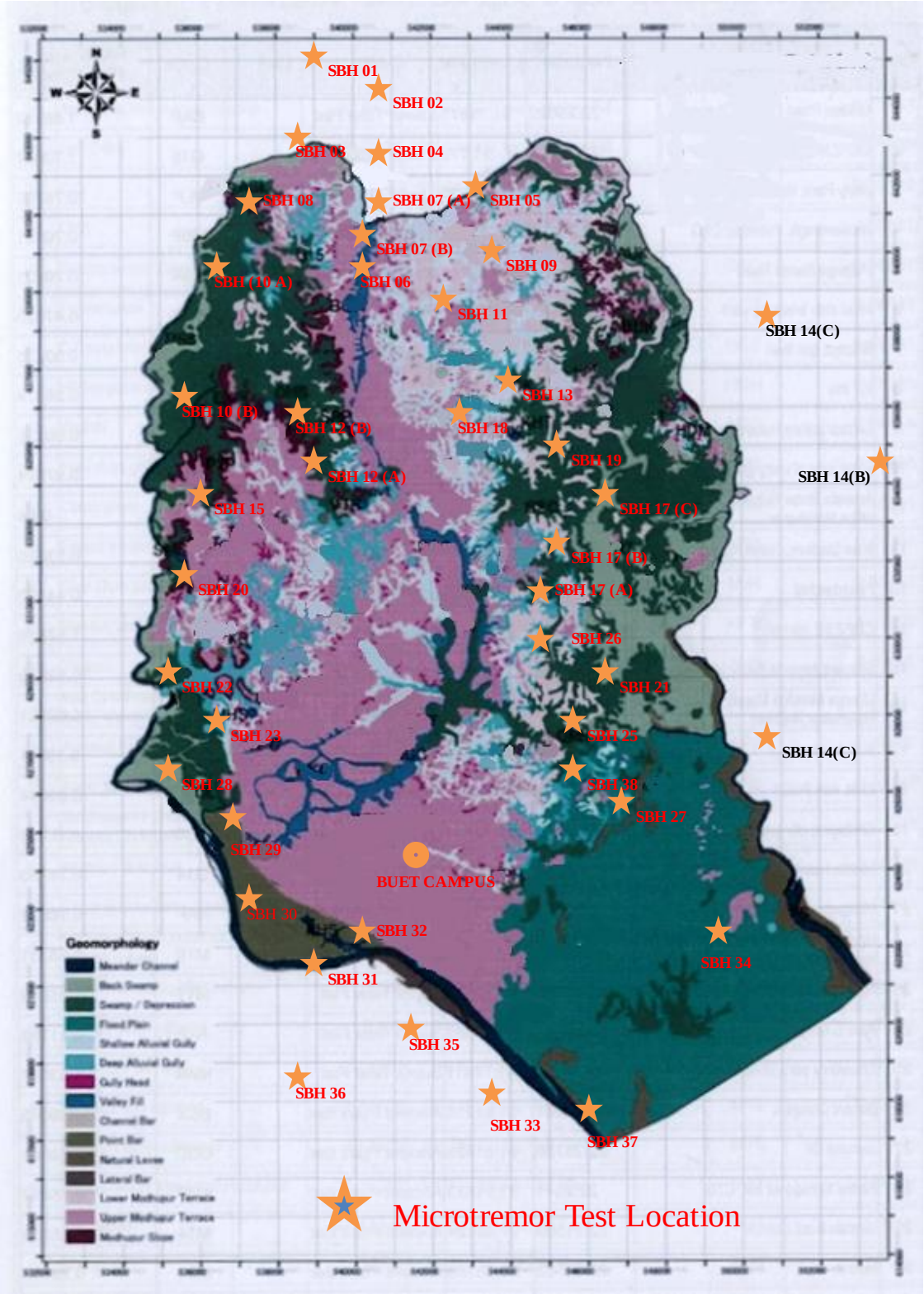

Figure 3.2: Superimposed study points on geomorphological map of Dhaka city. (Source: Geological Survey of Bangladesh, GSB)

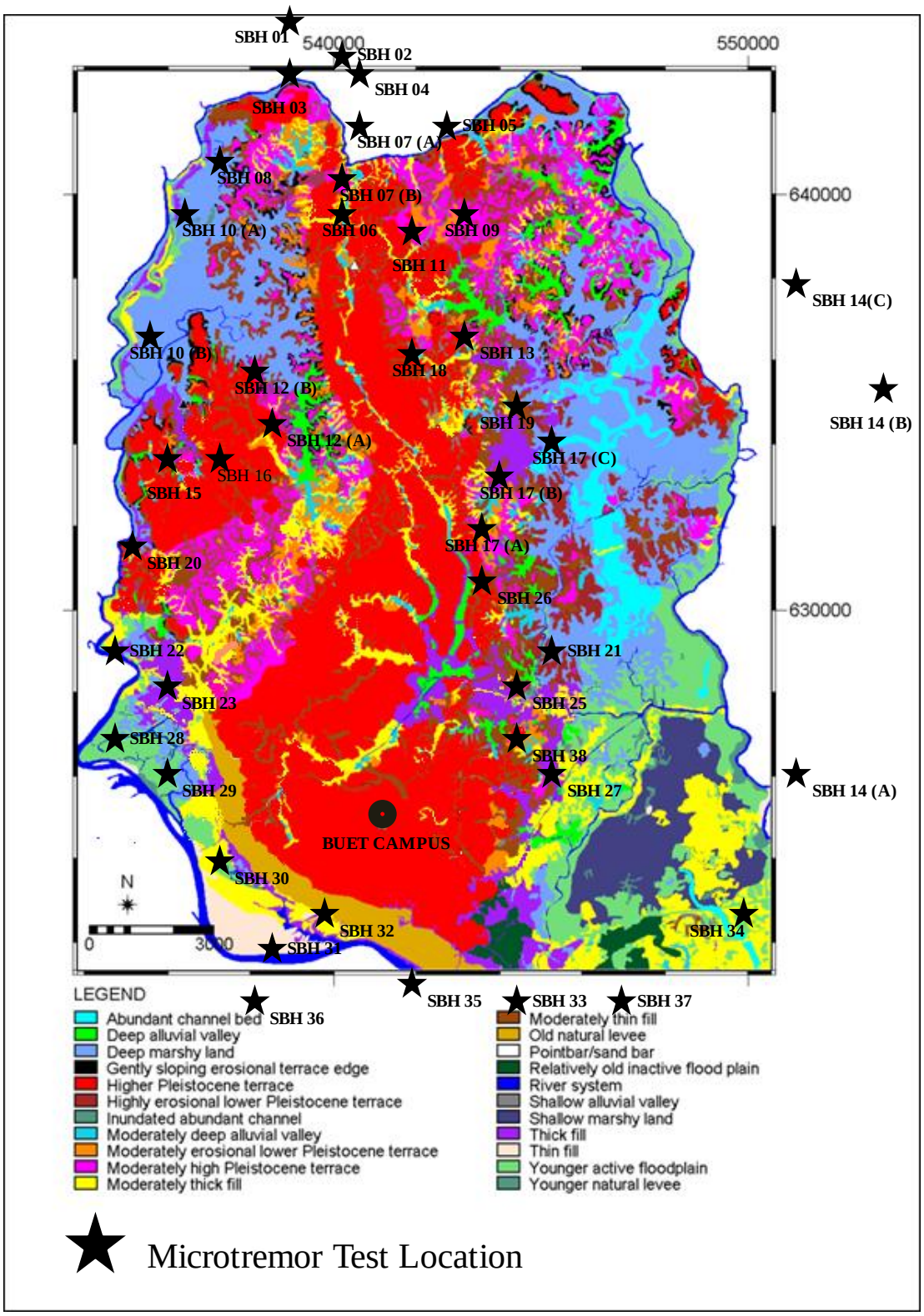

Figure 3.3: Superimposed study points on Geomorphological Map of Dhaka City.

(Source: A. S. M. Maksud Kamal)

The common geomorphic unit is Deeply Marshly Land, which is found at SBH 8 (Ashulia Toll Plaza, Latitude-23°53'25.40" and Longitude- 90°21'54.61") in both Figure 3.2 and Figure 3.3. Out of 45 selected locations, 8 selected locations have been classified into Upper Modhupur Terrace geomorphological unit, which is the most predominant geomorphological unit in Figure 3.2. The second most common geomorphological unit is Lower Modhupur Terrace. However, it is not possible to classify filling area because of not having any geomorphological unit in Figure 3.2. Therefore, Figure 3.3 is required to justify these locations in actual geomorphic unit.

According to Figure 3.3, 45 selected locations are classified into following groups:

14-Thick fill [SBH 05; SBH 14(A); SBH 14(B); SBH 14(C); SBH 15; SBH 16; SBH 19; SBH 25; SBH 27; SBH 28; SBH 30; SBH 35; SBH 36; SBH 38], 8-Moderately Thick fill [SBH 10(A); SBH 10 (B); SBH 13; SBH 22; SBH 23; SBH 26; SBH 31; SBH 33], 5-Higher Pleistocene Terrace [SBH 01; SBH 12(A); SBH 12(B); SBH 18; SBH 24], 7-Moderately Higher Pleistocence terrace [SBH 02; SBH 03; SBH 04; SBH 11; SBH 17(A); SBH 17(B); SBH 17(C)], 3-deep alluvium valley [07(A); 07(B); SBH 37], 4-Deep Marshly Land (SBH 08; SBH 20; SBH 21; SBH 32), 2-Highly Erosional Lower Pleistocene Terrace (SBH 06; SBH 09), 1-Younger active flood plain (SBH 34) and 1-Gently Sloping Erosional Terrace (SBH 29).

Out of 45 sites, the most predominant geomorphological unit is Thick fill, which is found in 14 locations in Figure 3.3. The second most common geomorphological unit is moderately thick fill. The geomorphological unit of Moderately Higher Pleistocene Terrace, which is 7, is higher than Higher Pleistocene Terrace.

Therefore, it can be said that the majority of the microtremor test locations are situated in recent fill area.

3.2.2 Sub-Soil Characteristics

Sub-soil investigation is necessary for the analysis of dynamic characteristics of soil. Shear wave velocity (SWV) is used to develop soil model. For this study Standard Penetration Test (SPT) has been carried out at 27 locations in and around the Dhaka city. SPT data has been collected from other sources as well. SPT is conducted in the area following procedure described in ASTM D1586. Shear wave velocity from 6 PS loggings as well as SPT data has been collected (CDMP, 2009). SWV from Small Scale Microtremor Measurement (SSMM) as well as SPT data has been collected at the microtremor Test location (Hossain, 2009). Finally, SWV has been estimated using SPT and SWV correlation (Ansary et al., 2010) where there is no SWV test result. The other three soil correlations (Ohta and Goto 1978; Imai and Yoshimura 1970; Ohba and Toriumi 1970) have been used to compare SWV. Various sub-soil investigation results have been presented in this section and Appendix-A.

(1) Sub-Soil Characteristics of National University, Tongi (SBH 01)

SPT Results

The soil profiles of the borehole are shown in Table A3.1. From the disturbed soil sample, the borehole consists of two soil layers. The silty clay layer, which is light brown medium stiff and high plastic, varies from 0 to 5.0 m from EGL. On the other hand, the silty clay layer, which is light brown to brown stiff to very stiff, exists from 5 to 18.5 m from EGL. The uncorrected SPT N-value of this site varies from 4 to 19. The SPT-N value of medium stiff light brown silty clay varies from 4 to 7. The SPT N-value of stiff to very stiff light brown to brown silty clay layer varies between 7 and 19.

Shear Wave Velocity Results

There is no PS logging and SSMM test result in National University, Tongi. Therefore, shear wave velocity has been estimated using correlation. Table A3.1 shows estimated SWV using different soil correlation. According to soil correlation proposed by Ansary et al. (2010), the shear wave velocity varies from 135 to 229 m/sec. From soil correlation developed by Ohta and Goto (1978), SWV exists from 123 to 261 m/sec. On the other hand, SWV of Ohba and Toriumi (1970), which varies from 129 to 206 m/sec, shows

slightly higher value than Imai and Yoshimura (1970), which shows ranging between 120 and 201 m/sec.

(2) Sub-Soil Characteristics of Board Bazaar, Gazipur (SBH 02)

SPT Results

The soil profiles of the borehole are shown in Table A3.2. The borehole consists of four soil layer. The silty clay layer, which is soft light brown and high plastic, varies from 0 to 2.50 m from EGL. The silty clay of stiff light brown with high plastic exists from 2.5 to 8.5 m from EGL. The medium dense brown silty fine sand varies from 8.5 to 10.0 m. The stiff to very stiff light brown silty clay varies between 10 and 20 m. The uncorrected SPT N-value of this site varies from 3 to 18. The SPT-N value of stiff light brown silty clay varies from 5 to 9. The SPT N-value of stiff to very stiff light brown to brown silty clay varies from 15 to 18.

Shear Wave Velocity Results

There is no PS logging and SSMM test result in Board Bazaar, Gazipur. Therefore, shear wave velocity has been estimated using soil correlation. Table A3.2 presents SWV using different methods. From soil correlation proposed by Ansary et al (2010), SWV varies from 150 to 247 m/sec. From SPT correlation developed by Ohta and Goto (1978), SWV exists from 117 to 267 m/sec.

(3) Sub-Soil Characteristics of Kaunia, Boro Bari, Moddopara (SBH 03)

SPT Results

The soil profiles of the borehole are shown in Table A3.3. The borehole consists of five soil layers. The grey loose silty fine sand varies from 0 to 2.0 m from EGL. The stiff to very stiff light brown Silty Clay with trace fine sand high plastic exists from 5.5 to 15.5 m from EGL. The medium dense brown silty fine sand varies from 8.5 to 10.0 m. The very stiff brown clayey silt with fine sand med. compress varies between 15.5 to 18.5 m. The uncorrected SPT N-value of this site varies from 4 to 28. The SPT-N value of stiff to very stiff light brown silty clay with trace fine sand high plastic varies between 8 and 18. The

SPT N-value of very stiff brown clayey silt with fine sand medium compress layer exists between 18 and 24.

Shear Wave Velocity Results

There is no PS logging and SSMM test result in Kaunia, Boro Bari. So, the value of shear wave velocity has been estimated using soil correlation. Table A3.3 presents SWV using different methods. From soil correlation proposed by Ansary et al. (2010), the shear wave velocity varies from 135 to 261 m/sec. From SPT correlation developed by Ohta and Goto (1978), SWV exists between 103 and 237 m/sec.

(4) Sub-soil Characteristics of Tongi, Ershadnagar (SBH 04)

SPT Results

The soil profile of the borehole has been demonstrated in Table A3.4. The borehole consists of six soil layers. The medium stiff to stiff light brown silty Clay with trace grits and fine sand high plastic varies from 0 to 3.5 m from EGL. The medium dense to loose brown sandy silt with trace mica exists from 6.5 to 9.5 m from EGL. The medium dense brown silty fine sand with trace mica varies from 8.5 to 10.0 m. The stiff grey to light brown silty clay with fine sand high plastic varies between 12.5 to 17.0 m. The uncorrected SPT N-value of this site varies from 6 to 17. The SPT N-value of stiff to medium stiff light brown silty clay varies between 2 and 11. The SPT N-value of medium dense brown silty fine sand layer exists from 9 to 12. The SPT N-value of stiff grey to light brown silty clay varies between 10 and 12.

Shear Wave Velocity Results

Table A3.4 represents shear wave velocity using four different methods. From soil correlation proposed by Ansary et al. (2010), SWV varies from 182 to 221 m/sec. From SPT correlation developed by Ohta and Goto (1978), SWV exists from 132 to 244 m/sec. On the other hand, SWV of Ohba and Toriumi (1970), which varies from 146 to 202 m/sec, shows slightly higher value than Imai and Yoshimura (1970), which shows ranging between 137 to 194 m/sec.

(5) Sub-Soil Characteristics of Tongi BSCIC area (SBH 05)

SPT Results

The soil profile of the borehole has been shown in Table A3.5. The borehole consists of six soil layers. The grey loose silty Fine Sand with trace mica varies from 0 to 3.5 m from EGL. The soft dark grey silty clay with trace organic matter exists from 3.5 to 6.5 m from EGL. The medium stiff to stiff light brown to grey silty clay trace fine sand varies from 6.5 to 9.5 m. The medium dense brown silty fine sand with trace clay varies between 12.5 to 15.5 m. The uncorrected SPT N-value of this site varies from 4 to 37. The SPT N-value of soft dark grey silty clay varies from 4 to 5. The SPT N-value of medium dense brown silty fine sand varies from 13 to 20. The SPT N-value of medium dense to dense grey silty fine sand varies between 20 and 37.

Shear Wave Velocity Results

Table A3.5 represents shear wave velocity using four different methods. From soil correlation proposed by Ansary et al. (2010), SWV varies from 135 to 287 m/sec. From SPT correlation developed by Ohta and Goto (1978), SWV exists from 103 to 253 m/sec. On the other hand, SWV of Ohba and Toriumi (1970), which varies from 129 to 257 m/sec, shows slightly higher value than Imai and Yoshimura (1970), which shows ranging between 120 to 250 m/sec.

(6) Sub-Soil Characteristics of Abdullahpur (SBH 06)

SPT Results

The soil profile of the borehole is presented in Table A3.6. The borehole consists of four soil layers. The top layer of soil exist rubbish which varies from 0 to 2 m. The stiff reddish brown silty clay trace grits and fine sand high plastic exists from 2 to 5 m from EGL. The stiff brown silty clay trace fine sand high plastic varies from 5 to 8 m. The medium dense to very dense brown silty clay trace mica varies between 8 and 20 m. The uncorrected SPT N-value of this site varies from 11 to 50. The SPT-N value of stiff reddish brown silty clay varies from 5 to 12. The SPT N-value of medium dense to very dense brown silty clay varies between 10 and 50.

Shear Wave Velocity Results

Table A3.6 represents shear wave velocity using four soil correlations. SWV varies from 122 to 318 m/sec (Ansary et al., 2010). SWV exists between 90 and 266 m/sec (Ohta and Goto, 1978). On the other hand, SWV of Ohba and Toriumi (1970), which varies from 118 to 282 m/sec, shows slightly higher value than Imai and Yoshimura (1970), which shows ranging between 109 to 276 m/sec.

(7) Sub-Soil Characteristics of Ijtema Field (SBH 07 (A))

SPT Results

The soil profile of the borehole is shown in Table A3.7. The borehole consists of four soil layers. The top layer of soil exist medium stiff to stiff light brown silty clay which varies from 0 to 5 m. The medium dense to dense brown silty fine sand trace clay varies between 8 and 20 m. The uncorrected SPT N-value of this site varies from 5 to 45. The SPT-N value of medium stiff to stiff light brown silty clay varies from 5 to 11. The SPT N-value of medium dense to dense brown silty fine sand varies from 17 to 45.

Shear Wave Velocity Results

Table A3.7 represents shear wave velocity using four different methods. SWV varies from 172 to 307 m/sec (Ansary et al., 2010). SWV exists between 128 and 262 m/sec (Ohta and Goto, 1978). On the other hand, SWV of Ohba and Toriumi (1970), which varies from 138 to 273 m/sec, shows slightly higher value than Imai and Yoshimura (1970), which shows ranging between 129 to 267 m/sec.

(8) Sub-Soil Characteristics of Ashulia Toll Plaza (SBH 08)

SPT Results

The soil profile of the borehole is shown in Table A3.8. The borehole consists of four soil layers. The top layer of soil exists filling grey very loose silty fine sand which varies from 0 to 2 m. The medium dense to dense reddish brown to brown silty fine sand varies between 5 and 20 m. The uncorrected SPT N-value of this site varies from 1 to 40. The

SPT-N value of medium dense to dense reddish brown to brown silty fine sand varies between 5 and 39.

Shear Wave Velocity Results

Table A3.8 represents shear wave velocity using four different methods. SWV varies from 84 to 295 m/sec (Ansary et al., 2010). SWV exists between 82 and 256 m/sec (Ohta and Goto, 1978). On the other hand, SWV of Ohba and Toriumi (1970), which varies from 84 to 264 m/sec, shows slightly higher value than Imai and Yoshimura (1970), which shows ranging between 76 and 257 m/sec.

(9) Sub-Soil Characteristics of Uttar Khan (SBH 9)

SPT Results

The soil profiles of the borehole are shown in Table 3.2. The only thick clay layer exists in this borehole. The thick clay layer exists from 0 to 24 m. The SPT N-value of clay layer varies between 14 and 74.

Table 3.2: SPT-N and Shear Wave Velocity at Uttar Khan

Depth (m)	Soil Description	SPT-N Value	Shear wave velocity (m/s) from PS-logging				
			CDMP (2009)	Ansary et al. (2010)	Ohta and Goto (1978)	Imai and Yoshimura (1970)	Ohba and Toriumi (1970)
1.5	Clay	20	412	254	162	204	213
3.0	Clay	45	412	319	213	267	273
4.5	Clay	50	412	329	236	276	282
6.0	Clay	40	412	309	240	257	264
7.5	Clay	62	292	349	271	297	302
9.0	Clay	30	292	285	248	233	241
10.5	Clay	14	292	230	225	182	190
12.0	Clay	22	292	261	249	211	219
13.5	Clay	22	292	261	255	211	219
15.0	Clay	24	292	268	265	217	225
16.5	Clay	28	292	279	277	228	236
18.0	Clay	24	292	268	274	217	225
19.5	Clay	24	292	268	279	217	225
21.0	Clay	38	292	304	306	252	259
22.5	Clay	74	292	367	348	315	319
24.0	Clay	44	292	317	322	265	271

Shear Wave Velocity Results

Table 3.2 represents shear wave velocity by direct PS logging (CDMP, 2009) and four soil correlations. According to PS logging, SWV varies from 292 to 412. From soil correlation proposed by Ansary et al (2010), SWV varies between 254 and 349 m/sec. SWV exists from 162 to 348 m/sec (Ohta and Goto, 1978). On the other hand, SWV of Ohba and Toriumi (1970), which varies from 190 to 319 m/sec, shows slightly higher value than Imai and Yoshimura (1970), which shows ranging between 182 to 315 m/sec.

(10) Sub-Soil Characteristics of Uttara Phase-3 (SBH 10 (A))

SPT Results

The soil profile of the borehole is represented in Table A3.9. The borehole consists of five soil layers. The top layer of soil exists filling grey very loose silty fine sand which varies from 0 to 3.5 m. The stiff grey silty clay trace fine sand varies between 3.5 to 8 m. The loose to medium dense grey sandy silt with clay varies between 9.5 and 17 m. The uncorrected SPT N-value of this site varies from 2 to 18. The SPT N-value of the stiff grey silty clay varies from 3 to 13. The SPT N-value of loose to medium dense grey sandy silt varies between 9 and 15.

Shear Wave Velocity Results

Table A3.9 represents shear wave velocity using four different methods. SWV varies from 107 to 225 m/sec (Ansary et al, 2010). From SPT correlation developed by Ohta and Goto (1978), SWV exists between 96 and 197 m/sec. On the other hand, SWV of Ohba and Toriumi (1970), which varies from 104 to 206 m/sec, shows slightly higher value than Imai and Yoshimura (1970), which shows ranging between 96 and 197 m/sec.

(11) Sub-Soil Characteristics of Azampur School, Uttara (SBH 11)

SPT Results

The soil profile of the borehole is shown in Table 3.3. This borehole exist three soil layers. The top layer exists clay from 0 to 6 m. The sandy silt layer varies between 6 and 13.5 m. The lower clay layer varies between 13.5 and 20. The uncorrected SPT N-value of this site varies from 12 to 20. The SPT N-value of the uppermost clay layer varies from

12 to 20. The SPT N-value of silty clay layer varies from 12 to 18. The SPT N-value of the bottom clay layer varies between 13 and 20.

Table 3.3: SPT-N and Shear Wave Velocity at Azampur School, Uttara

Depth (m)	Soil Description	SPT-N Value	Shear wave velocity (m/s) from SSMM				
			SSMM Hossain (2009)	Ansary et al. (2010)	Ohta and Goto (1978)	Imai and Yoshimura (1970)	Ohba and Toriumi (1970)
1.5	Clay	15	210	235	154	186	194
3.0	Clay	20	208	254	186	204	213
4.5	Clay	17	208	243	196	194	202
6.0	Clay	12	212	220	196	173	181
7.5	Sandy Silt	12	230	196	172	173	181
9.0	Sandy Silt	14	230	206	183	182	190
10.5	Sandy Silt	17	245	221	195	194	202
12.0	Sandy Silt	18	265	225	202	197	206
13.5	Sandy Silt	17	265	221	205	194	202
15.0	Clay	20	285	254	257	204	213
16.5	Clay	13	285	225	243	177	186
18.0	Clay	14	305	230	250	182	190
19.5	Clay	17	325	243	263	194	202
20.0	Clay	18	325	247	267	197	206

Shear Wave Velocity Results

Table 3.3 represents shear wave velocity using SSMM method (Hossain, 2009) and four soil correlations. According to SSMM, SWV varies from 208 to 325. SWV varies between 221 and 247 m/sec (Ansary et al., 2010). SWV exists between 154 and 267 m/sec (Ohta and Goto, 1978). On the other hand, SWV of Ohba and Toriumi (1970), which varies from 181 to 213 m/sec, shows slightly higher value than Imai and Yoshimura (1970), which shows ranging between 173 to 204 m/sec.

(12) Sub-Soil Characteristics of Mirpur DOHS (South side) (SBH-12(A))

SPT Results

The soil profile of the borehole is shown in Table 3.4 (Tanvir, 2009). The borehole exists three soil layers. The top layer exists filling sand layer from 0 to 3 m. The organic clay layer varies from 3 to 9 m. The bottom sand layer varies between 9 and 18 m. The

uncorrected SPT N-value of this site varies from 2 to 19. The SPT N-value of the uppermost clayey silt layer varies from 6 to 8. The SPT N-value of sand layer varies from 4.5 to 18.

Table 3.4: SPT-N and Shear Wave Velocity at Mirpur DOHS (South side)

Depth (m)	Soil Description	SPT-N Value	Shear wave velocity (m/s) from SSMM				
			SSMM Hossain (2009)	Ansary et al. (2010)	Ohta and Goto (1978)	Imai and Yoshimura (1970)	Ohba and Toriumi (1970)
1.50	Filling Sand	3	78	122	98	109	118
3.00	Filling Sand	4	92	135	119	120	129
4.50	Organic Clay	1	102	110	121	76	84
6.00	Organic Clay	2	105	133	144	96	104
7.50	Organic Clay	3	115	150	162	109	118
9.00	Organic Clay	5	115	145	153	129	138
10.50	Sand	7	125	163	168	144	154
12.00	Sand	9	135	178	180	157	166
13.50	Sand	10	135	184	187	162	172
15.00	Sand	17	142	221	209	194	202
16.50	Sand	18	142	225	215	197	206
18.00	Sand	20	150	233	223	204	213

Shear Wave Velocity Results

Table 3.4 represents shear wave velocity by direct SSMM method (Hossain, 2009) and four correlated methods. According to SSMM, SWV varies from 78 to 150. SWV varies from 110 to 233 m/sec (Ansary et al., 2010). From SPT correlation developed by Ohta and Goto (1978), SWV exists from 98 to 223 m/sec. On the other hand, SWV of Ohba and Toriumi (1970), which varies from 84 to 213 m/sec, shows slightly higher value than Imai and Yoshimura (1970), which shows ranging between 76 and 204 m/sec.

(13) Sub-Soil Characteristics of Mirpur DOHS (North Side) (SBH 12 (B))

SPT Results

The soil profile of the borehole is shown in Table A3.10. The borehole consists of five soil layers. The top layer of soil exists filling grey very loose silty fine sand which varies from 0 to 5.5 m. The stiff to very stiff light brown silty clay with trace fine sand high plastic varies between 16 and 22 m. The uncorrected SPT N-value of this site varies from

6 to 22. The SPT N-value of the grey very loose silty fine sand varies from 5 to 6. The SPT N-value of stiff brown clayey silt with fine sand medium compress varies from 8 to 10. The SPT N-value of stiff to very stiff light brown silty clay varies between 16 and 22.

Shear Wave Velocity Results

Table A3.10 represents shear wave velocity using four different methods. SWV varies from 155 to 264 m/sec (Ansary et al., 2010). SWV exists from 111 to 278 m/sec (Ohta and Goto, 1978). On the other hand, SWV of Ohba and Toriumi (1970), which varies from 146 to 222 m/sec, shows slightly higher value than Imai and Yoshimura (1970), which shows ranging between 137 and 214 m/sec.

(14) Sub-Soil Characteristics of Ashiyan city, Askona, Dakkhin Khan (SBH 13)

SPT Results

The soil profile of the borehole is shown in Table A3.11. The borehole consists of six soil layers. The top layer of soil exists filling grey loose silty fine sand which varies from 0 to 3.5 m. The soft to medium stiff grey silty clay trace fine sand medium plastic varies between 7 and 12.5 m. The dense brown silty fine sand trace mica varies between 12.5 and 17 m. The uncorrected SPT N-value of this site varies from 4 to 42. The SPT N-value of soft to medium stiff grey silty clay varies from 3 to 7. The SPT N-value of stiff grey silty clay varies from 17 to 20.

Shear Wave Velocity Results

Table A3.11 represents shear wave velocity at four different methods. SWV varies from 135 to 300 m/sec (Ansary et al., 2010). SWV exists between 103 and 249 m/sec (Ohta and Goto, 1978). On the other hand, SWV of Ohba and Toriumi (1970), which varies from 129 to 268 m/sec, shows slightly higher value than Imai and Yoshimura (1970), which shows ranging between 120 to 261 m/sec.

(15) Sub-Soil Characteristics of Purbachal-1, Randokpur Hazi Bari, Rupganj (SBH 14(A))

SPT Results

The soil profile of the borehole is shown in Table A3.12. This borehole consists of six soil layers. The soft grey silty clay trace fine sand medium plastic varies from 2 to 8 m. The medium dense grey silty fine sand trace mica varies between 15.5 and 20 m. The uncorrected SPT N-value of this site varies from 2 to 17. The SPT N-value of soft grey silty clay varies from 2 to 4. The SPT N-value of medium dense grey silty fine sand varies from 13 to 16.

Shear Wave Velocity Results

Table A3.12 shows shear wave velocity using four different methods. SWV varies from 133 to 216 m/sec (Ansary et al., 2010). SWV exists between 117 and 219 m/sec (Ohta and Goto, 1978). On the other hand, SWV of Ohba and Toriumi (1970), which varies from 104 to 202 m/sec, shows slightly higher value than Imai and Yoshimura (1970), which shows ranging between 96 and 190 m/sec.

(16) Sub-Soil Characteristics of Purbachal-2, American City (SBH 14(B))

SPT Results

The soil profile of the borehole is represented in Table A3.13. This borehole consists of three soil layers. The top layer exists filling of very loose grey silty fine sand trace mica varies from 0 to 6.5 m. The very soft grey silty clay trace fine sand medium to high plastic varies between 6.5 and 18.5 m. The bottom layer of medium stiff grey silty clay varies from 18.5 to 20. The uncorrected SPT N-value of this site varies from 1 to 8. The SPT N-value of filling is 1. The SPT N-value of very soft grey silty clay varies between 1 and 2.

Shear Wave Velocity Results

Table A3.13 represents shear wave velocity using four different methods. SWV varies from 84 to 197 m/sec (Ansary et al., 2010). SWV exists between 98 and 233 m/sec (Ohta and Goto, 1978). On the other hand, SWV of Ohba and Toriumi (1970), which varies from 84 to 160 m/sec, shows slightly higher value than Imai and Yoshimura (1970), which shows ranging between 76 and 151 m/sec.

(17) Sub-Soil Characteristics of Purbachal Picnic Park, Gazipur (SBH 14(C))

SPT Results

The soil profile of the borehole is shown in Table A3.14. This borehole consists of four soil layers. The top layer exists filling of loose grey silty fine sand trace mica varies from 0 to 5.5 m. The bottom layer of stiff to very stiff light brown clayey silt varies between 11.5 and 20 m. The uncorrected SPT N-value of this site varies from 2 to 20. The SPT N-value of filling loose grey silty fine Sand varies from 4 to 6.

Shear Wave Velocity Results

Table A3.14 represents shear wave velocity using four different methods. SWV varies from 133 to 233 m/sec (Ansary et al., 2010). SWV exists between 107 and 228 m/sec (Ohta and Goto, 1978). On the other hand, SWV of Ohba and Toriumi (1970), which varies from 138 to 213 m/sec, shows slightly higher value than Imai and Yoshimura (1970), which shows ranging between 96 and 204 m/sec.

(18) Sub-Soil Characteristics of Adjacent to Mirpur Zoo (SBH 15)

SPT Results

The soil profile of the borehole is shown in Table A3.15. The borehole consists of six soil layers. The top layer exists filling of loose grey silty fine sand trace mica varies from 0 to 5.5 m. The medium stiff to stiff grey silty clay trace fine sand high plastic varies from 8 to 12.5 m. The bottom layer of medium dense brown silty fine sand trace mica varies between 16 and 26 m. The uncorrected SPT N-value of this site varies from 15.5 to 26. The SPT N-value of medium stiff to stiff grey silty clay varies from 6 to 11. The SPT N-value of the bottom layer varies between 16 and 26 m.

Shear Wave Velocity Results

Table A3.15 demonstrates shear wave velocity using four different methods. SWV varies from 145 to 255 m/sec (Ansary et al., 2010). From SPT correlation developed by Ohta and Goto (1978), SWV exists from 107 to 238 m/sec. On the other hand, SWV of Ohba and Toriumi (1970), which varies from 138 to 231 m/sec, shows slightly higher value than Imai and Yoshimura (1970), which shows ranging between 129 to 223 m/sec.

(19) Sub-Soil Characteristics of Field Ground, Pallabi (SBH 16)

SPT Results

The soil profile of the borehole is shown in Table 3.5. The borehole consists of four soil layers. The top layer exists filling of loose grey silty fine sand trace mica varies from 0 to 1.5 m. The clay layer varies from 3 to 18 m. The bottom layer of clay layer varies between 21 and 24 m. The uncorrected SPT N-value of this site varies from 1 to 22. The SPT N-value of thick clay layer varies from 1 to 12. The SPT N-value of sand layer varies from 8 to 22 m.

Shear Wave Velocity Results

Table 3.5 demonstrates shear wave velocity using four different methods. SWV by PS logging varies from 78 to 230 (CDMP, 2009). From soil correlation proposed by Ansary et al. (2010), SWV varies from 84 to 247 m/sec. From SPT correlation developed by Ohta and Goto (1978), SWV exists from 82 to 277 m/sec. On the other hand, SWV of Ohba and Toriumi (1970), which varies from 84 to 206 m/sec, shows slightly higher value than Imai and Yoshimura (1970), which shows ranging between 76 and 197 m/sec.

Table 3.5: SPT-N and Shear Wave Velocity at Field Ground, Pallabi

Depth (m)	Soil Description	SPT-N Value	Shear wave velocity (m/s) from PS-logging				
			CDMP (2009)	Ansary et al. (2010)	Ohta and Goto (1978)	Imai and Yoshimura (1970)	Ohba and Toriumi (1970)
1.5	Filling Sand	1	78	84	82	76	84
3.0	Clay	1	78	110	112	76	84
4.5	Clay	1	78	110	121	76	84
6.0	Clay	1	78	110	128	76	84
7.5	Clay	1	78	110	134	76	84
9.0	Clay	5	134	172	183	129	138
10.5	Clay	4	134	162	182	120	129
12.0	Clay	3	134	150	178	109	118
13.5	Clay	1	134	110	151	76	84
15.0	Clay	1	134	110	154	76	84
16.5	Clay	7	134	190	219	144	154
18.0	Clay	12	230	220	244	173	181
19.5	Sand	8	230	171	194	151	160
21.0	Sand	22	230	241	234	211	219
22.5	Clay	10	230	209	247	162	172
24.0	Clay	18	230	247	277	197	206

(20) Sub-Soil Characteristics of Block-B, Bashundhara (SBH 17 (A))

SPT Results

The soil profile of the borehole is shown in Table 3.6. This borehole exists three soil layers. The top layer exists filling of sand from 0 to 3 m. The thick clay layer exists between 3 and 13.5 m. The bottom layer of sand varies from 13.5 to 21 m. The uncorrected SPT N-value of this site varies from 5 to 34. The SPT N-value of filling sand varies from 5 to 7. The SPT N-value of thick clay layer varies from 5 to 14. The SPT N-value of bottom sand layer varies from 10 to 34.

Shear Wave Velocity Results

Table 3.6 represents shear wave velocity using SSMM method and four correlated methods. According to SSMM, SWV varies from 120 to 270. SWV varies from 145 to 279 m/sec (Ansary et al., 2010). From SPT correlation developed by Ohta and Goto (1978), SWV exists between 107 and 252 m/sec. On the other hand, SWV of Ohba and Toriumi (1970), which varies from 138 to 251 m/sec, shows slightly higher value than Imai and Yoshimura (1970), which shows ranging between 129 and 243 m/sec.

Table 3.6: SPT-N and Shear Wave Velocity at Block-B, Bashundhara

Depth (m)	Soil Description	SPT-N Value	Shear wave velocity (m/s) from SSMM				
			SSMM Hossain (2009)	Ansary et al. (2010)	Ohta and Goto (1978)	Imai and Yoshimura (1970)	Ohba and Toriumi (1970)
1.5	Filling Sand	5	120	145	107	129	138
3.0	Filling Sand	7	120	163	130	144	154
4.5	Clay	5	140	172	159	129	138
6.0	Clay	11	170	215	193	168	177
7.5	Clay	14	190	230	210	182	190
9.0	Clay	7	190	190	194	144	154
10.5	Clay	8	212	197	204	151	160
12.0	Clay	10	225	209	218	162	172
13.5	Clay	12	225	220	230	173	181
15.0	Sand	10	230	184	191	162	172
16.5	Sand	11	230	190	198	168	177
18.0	Sand	27	245	258	235	226	233
19.5	Sand	30	270	268	243	233	241
21.0	Sand	34	270	279	252	243	251

(21) Sub-Soil Characteristics of Block-D, Bashundhara (SBH 17 (B))

SPT Results

The soil profile of the borehole is shown in Table 3.7. This borehole exists three soil layers. The top layer exists filling of very soft to soft light brown to brown silty clay trace fine sand from 0 to 11 m. The very soft silty dark grey silty clay trace fine sand varies between 11 and 18.5 m. The bottom layer of medium dense grey silty fine sand varies from 18.5 to 21.5 m. The uncorrected SPT N-value of this site varies from 1 to 21. The SPT N-value of filling sand varies from 1 to 4. The SPT N-value of medium dense grey silty fine sand varies from 2 to 21.

Table 3.7: SPT-N and Shear Wave Velocity at Block-D, Bashundhara

Depth (m)	Soil Description	SPT-N Value	Shear wave velocity (m/s) from SSMM				
			SSMM Hossain (2009)	Ansary et al. (2010)	Ohta and Goto (1978)	Imai and Yoshimura (1970)	Ohba and Toriumi (1970)
1.5	Silty Clay	1	101	110	97	76	84
3.0	Silty Clay	2	101	133	126	96	104
4.5	Silty Clay	4	101	162	153	120	129
6.0	Silty Clay	3	101	150	155	109	118
7.5	Silty Clay	3	101	150	162	109	118
9.0	Silty Clay	4	137	162	176	120	129
10.5	Silty Clay	2	137	133	162	96	104
12.0	Silty Clay	1	137	110	147	76	84
13.5	Silty Clay	1	137	110	151	76	84
15.0	Silty Clay	1	137	110	154	76	84
16.5	Silty Clay	1	137	110	157	76	84
18.0	Silty Clay	2	137	133	180	96	104
19.5	Silty Fine Sand	17	137	221	221	194	202
21.0	Silty Fine Sand	21	231	237	232	208	216

Shear Wave Velocity Results

Table 3.7 represents shear wave velocity using SSMM method (Hossain, 2009) and four correlated methods. According to SSMM, SWV varies from 101 to 231. From soil correlation proposed by Ansary et al. (2010), SWV varies from 110 to 237 m/sec. From

SPT correlation developed by Ohta and Goto (1978), SWV exists between 97 and 232 m/sec. On the other hand, SWV of Ohba and Toriumi (1970), which varies from 84 to 216 m/sec, shows slightly higher value than Imai and Yoshimura (1970), which shows ranging between 76 and 208 m/sec.

(22) Sub-Soil Characteristics of Block-H, Bashundhara (SBH 17 (C))

SPT Results

The soil profile of the borehole is shown in Table 3.8 (CDMP, 2009). This borehole exists of two soil layers. The top layer exists filling of fine sand from 0 to 3 m. The thick clay layer varies between 3 and 21 m. The uncorrected SPT N-value of this site varies from 3 to 37. The SPT N-value of clay varies from 1 to 4. The SPT N-value of the bottom layer varies from 17 to 37.

Table 3.8: SPT-N and Shear Wave Velocity at Block-H, Bashundhara

Depth (m)	Soil Description	SPT-N Value	Shear wave velocity (m/s) from PS-logging				
			CDMP (2009)	Ansary et al. (2010)	Ohta and Goto (1978)	Imai and Yoshimura (1970)	Ohba and Toriumi (1970)
1.5	Fill	3	96	122	98	109	118
3.0	Fill	5	259	145	123	129	138
4.5	Clay	17	259	243	196	194	202
6.0	Clay	15	259	235	203	186	194
7.5	Clay	10	259	209	199	162	172
9.0	Clay	12	259	220	212	173	181
10.5	Clay	13	259	225	222	177	186
12.0	Clay	28	364	279	260	228	236
13.5	Clay	21	364	258	253	208	216
15.0	Clay	35	364	297	282	246	253
16.5	Clay	37	364	302	290	250	257
18.0	Clay	20	364	254	266	204	213
19.5	Clay	27	364	277	285	226	233
21.0	Clay	21	364	258	277	208	216

Shear Wave Velocity Results

Table 3.8 represents shear wave velocity using PS logging (CDMP, 2009) and four correlated methods. According to PS logging, SWV varies from 96 to 364. SWV varies from 122 to 302 m/sec (Ansary et al., 2010). SWV exists between 98 and 285 m/sec (Ohta and Goto, 1978). On the other hand, SWV of Ohba and Toriumi (1970), which varies from 118 to 253 m/sec, shows slightly higher value than Imai and Yoshimura (1970), which shows ranging between 109 and 250 m/sec.

(23) Sub-Soil Characteristics of Kuril Flyover (SBH 19)

SPT Results

The soil profile of the borehole is shown in Table A3.16. This borehole consists of four soil layers. The top layer exists filling of loose grey silty fine sand trace mica varies from 0 to 3.5 m. The very soft grey silty clay trace fine sand medium plastic varies between 3.5 and 8 m. The stiff grey to light brown silty clay varies from 8 to 14.0. The bottom layer of very stiff light brown clayey silt with fine sand varies from 14 to 20. The uncorrected SPT N-value of this site varies from 1 to 27. The SPT N-value of filling is 4. The SPT N-value of very soft grey silty clay varies from 1 to 4.

Shear Wave Velocity Results

Table A3.16 represents shear wave velocity using four different methods. SWV varies from 135 to 258 m/sec (Ansary et al., 2010). SWV exists between 103 and 240 m/sec (Ohta and Goto, 1978). On the other hand, SWV of Ohba and Toriumi (1970), which varies from 84 to 233 m/sec, shows slightly higher value than Imai and Yoshimura (1970), which shows ranging between 76 and 226 m/sec.

(24) Sub-Soil Characteristics of Purachal, Uttar Badda (SBH 21)

SPT Results

The soil profile of the borehole is represented in Table A3.17. The borehole consists of five soil layers. The top layer exists filling of loose grey silty fine sand trace mica varies from 0 to 5 m. The medium stiff to stiff light brown silty clay varies between 8 and 14.5

m. The medium dense to dense brown sandy silt varies from 14.5 to 18.5. The bottom layer of dense brown silty fine sand varies from 33 to 38. The uncorrected SPT N-value of this site varies from 1 to 38. The SPT N-value of filling varies from 5 to 8. The SPT N-value of medium stiff to stiff light brown silty clay trace grits varies between 3 and 12.

Shear Wave Velocity Results

Table A3.17 represents shear wave velocity using four different methods. SWV varies from 163 to 290 m/sec (Ansary et al., 2010). SWV exists between 114 and 254 m/sec (Ohta and Goto, 1978). On the other hand, SWV of Ohba and Toriumi (1970), which varies from 84 to 259 m/sec, shows slightly higher value than Imai and Yoshimura (1970), which shows ranging between 76 and 252 m/sec.

(25) Sub-Soil Characteristics of City Corporation, Gabtoli (SBH 22)

SPT Results

The soil profile of the borehole is shown in Table A3.18. This borehole consists of five soil layers. The top layer exists filling of loose grey silty fine sand trace mica varies from 0 to 5 m. The medium stiff dark grey silty clay trace organic matter medium plastic varies between 5 and 8 m. The loose to medium dense grey sandy silt with clay varies from 11 to 18.5 m. The bottom layer of medium dense grey silty fine sand trace mica varies from 13 to 15 m. The uncorrected SPT N-value of this site varies from 3 to 15. The SPT N-value of filling varies from 3 to 6. The SPT N-value of loose to medium dense grey sandy silt varies between 7 and 13.

Shear Wave Velocity Results

Table A3.18 represents shear wave velocity using four different methods. SWV varies from 155 to 211 m/sec (Ansary et al., 2010). From SPT correlation developed by Ohta and Goto (1978), SWV exists from 111 to 216 m/sec. On the other hand, SWV of Ohba and Toriumi (1970), which varies from 138 to 194 m/sec, shows slightly higher value than Imai and Yoshimura (1970), which shows ranging between 109 to 186 m/sec.

(26) Sub-Soil Characteristics of Adabor (SBH 23)

SPT Results

The soil profile of the borehole is shown in Table 3.9 (Tanvir, 2009). The borehole consists of four soil layers. The top layer exists filling of fine sand from 0 to 3 m. The clay layer varies between 3 and 10.5 m. The sand layer varies between 12 and 16.5. The uncorrected SPT N-value of this site varies from 2 to 37. The SPT N-value of clay varies between 2 and 13. The SPT N-value of sand layer varies from 22 to 37.

Shear Wave Velocity Results

Table 3.9 represents shear wave velocity by direct SSMM method (Hossain, 2009) and four correlated methods. According to SSMM, SWV varies from 85 to 230. From soil correlation proposed by Ansary et al. (2010), SWV varies from 107 to 287 m/sec. SWV exists between 92 and 258 m/sec (Ohta and Goto (1978). On the other hand, SWV of Ohba and Toriumi (1970), which varies from 104 to 216 m/sec, shows slightly higher value than Imai and Yoshimura (1970), which shows ranging between 96 and 250 m/sec.

Table 3.9: SPT-N and Shear Wave Velocity at Adabor

Depth (m)	Soil Description	SPT-N Value	Shear wave velocity (m/s) from SSMM				
			SSMM Hossain (2009)	Ansary et al. (2010)	Ohta and Goto (1978)	Imai and Yoshimura (1970)	Ohba and Toriumi (1970)
1.5	Filling Sand	2	85	107	92	96	104
3.0	Filling Sand	3	108	122	113	109	118
4.5	Clay	2	130	133	136	96	104
6.0	Clay	2	150	133	144	96	104
7.5	Clay	2	165	133	151	96	104
9.0	Clay	5	165	172	183	129	138
10.5	Clay	13	180	225	222	177	186
12.0	Sand	30	198	268	220	233	241
13.5	Sand	35	220	282	232	246	253
15.0	Sand	37	220	287	239	250	257
16.5	Sand	22	220	241	223	211	219
18.0	Clay	21	230	258	268	208	216

(27) Sub-Soil Characteristics of Agargoan Trade Fair area (SBH 24)

SPT Results

The soil profile of the borehole is shown in Table 3.10 (CDMP, 2009). This borehole consists of two soil layers. The top layer exists filling of fine sand from 0 to 4.5 m. The bottom thick clay layer varies between 4.5 and 24 m. The uncorrected SPT N-value of this site varies from 5 to 35. The SPT N-value of the uppermost filling sand varies from 5 to 23. The SPT N-value of the bottom clay layer varies between 21 and 35.

Shear Wave Velocity Results

Table 3.10 represents shear wave velocity by direct PS logging method (CDMP, 2009) and four correlated methods. According to PS logging, SWV varies from 150 to 300 m/sec. SWV varies from 145 to 297 m/sec (Ansary et al., 2010). From SPT correlation developed by Ohta and Goto (1978), SWV exists from 107 to 310 m/sec. On the other hand, SWV of Ohba and Toriumi (1970), which varies from 138 to 253 m/sec, shows slightly higher value than Imai and Yoshimura (1970), which shows ranging between 129 and 246 m/sec.

Table 3.10: SPT-N and Shear Wave Velocity at Agargoan Trade Fair area

Depth (m)	Soil Description	SPT-N Value	Shear wave velocity (m/s) from PS-logging				
			CDMP (2009)	Ansary et al. (2010)	Ohta and Goto (1978)	Imai and Yoshimura (1970)	Ohba and Toriumi (1970)
1.5	Filling Sand	5	150	145	107	129	138
3.0	Filling Sand	11	150	190	141	168	177
4.5	Filling Sand	23	200	244	173	214	222
6.0	Clay	21	200	258	215	208	216
7.5	Clay	21	200	258	225	208	216
9.0	Clay	21	239	258	234	208	216
10.5	Clay	22	239	261	243	211	219
12.0	Clay	22	239	261	249	211	219
13.5	Clay	22	239	261	255	211	219
15.0	Clay	27	300	277	270	226	233
16.5	Clay	26	300	274	273	223	231
18.0	Clay	23	300	264	272	214	222
19.5	Clay	28	300	279	286	228	236
21.0	Clay	30	300	285	294	233	241
22.5	Clay	30	300	285	298	233	241
24.0	Clay	35	300	297	310	246	253

(28) Sub-Soil Characteristics of Aftab Nagar Housing Project (SBH 25)

SPT Results

The soil profile of the borehole is shown in Table 3.11 (CDMP, 2009). The borehole consists of six soil layers. The top filling sand layer varies from 0 to 3 m. The thick sand layer exists between 12 and 24 m. The SPT N-value of filling sand varies from 2 to 3. The SPT N-value of the bottom thick sand layer varies between 18 and 29.

Table 3.11: SPT-N and Shear Wave Velocity at Aftab Nagar Housing Project

Depth (m)	Soil Description	SPT-N Value	Shear wave velocity (m/s) from PS-logging				
			CDMP (2009)	Ansary et al. (2010)	Ohta and Goto (1978)	Imai and Yoshimura (1970)	Ohba and Toriumi (1970)
1.5	Filling Sand	3	124	122	98	109	118
3.0	Filling Sand	2	124	107	105	96	104
4.5	Sand	2	124	107	114	96	104
6.0	Clay	8	211	197	183	151	160
7.5	Sand	10	211	184	166	162	172
9.0	Clay	13	211	225	215	177	186
10.5	Clay	18	211	247	235	197	206
12.0	Sand	18	211	225	202	197	206
13.5	Sand	24	211	248	217	217	225
15.0	Sand	20	211	233	215	204	213
16.5	Sand	17	211	221	213	194	202
18.0	Sand	24	211	248	230	217	225
19.5	Sand	27	211	258	239	226	233
21.0	Sand	27	211	258	242	226	233
22.5	Sand	25	211	251	242	220	228
24.0	Sand	29	211	264	252	231	239

Shear Wave Velocity Results

Table 3.11 represents shear wave velocity by direct PS logging method (CDMP, 2009) and four soil correlations. According to PS logging, SWV varies from 124 to 211 m/sec. From soil correlation proposed by Ansary et al. (2010), SWV varies between 107 to 264 m/sec. From SPT correlation developed by Ohta and Goto (1978), SWV exists from 98 to 252 m/sec. On the other hand, SWV of Ohba and Toriumi (1970), which varies from 118

to 239 m/sec, shows slightly higher value than Imai and Yoshimura (1970), which shows ranging between 96 to 231 m/sec.

(29) Sub-Soil Characteristics of Umme Had Nagar, Nadda (SBH 26)

SPT Results

The soil profile of the borehole is shown in Table A3.19. This borehole consists of nine soil layers. The top layer exists filling of very loose grey silty fine sand varies from 0 to 3.5 m. The medium stiff grey silty clay varies between 3.5 and 5 m. The stiff light brown silty clay varies from 8 to 11. The medium dense to dense light brown sandy silt varies from 12.5 to 15.5. The bottom layer of dense brown sandy silt trace clay varies from 18.5 to 20. The uncorrected SPT N-value of this site varies from 1 to 36. The SPT N-value of filling is 1. The SPT N-value of stiff light brown silty clay varies from 8 to 15. The SPT N-value of medium dense to dense light brown sandy silt varies between 13 and 33.

Shear Wave Velocity Results

Table A3.19 represents shear wave velocity using four different methods. SWV varies from 84 to 285 m/sec (Ansary et al., 2010). From SPT correlation developed by Ohta and Goto (1978), SWV exists from 82 to 251 m/sec. On the other hand, SWV of Ohba and Toriumi (1970), which varies from 84 to 253 m/sec, shows slightly higher value than Imai and Yoshimura (1970), which shows ranging between 76 and 246 m/sec.

(30) Sub-Soil Characteristics of South Banasree (SBH 27)

SPT Results

The soil profile of the borehole is shown in Table A3.20. This borehole consists of four soil layers. The top layer exists filling of very loose grey silty fine sand trace mica varies from 0 to 4 m. The medium stiff to very soft dark grey to grey silty clay varies between 4 and 14 m. The bottom layer of medium dense to dense brown silty fine sand varies from 16 to 20 m. The uncorrected SPT N-value of this site varies from 1 to 40. The SPT N-value of medium stiff to very soft dark grey to grey silty clay varies from 1 to 6. The SPT N-value of medium dense to dense brown silty fine sand varies from 9 to 40.

Shear Wave Velocity Results

Table A3.20 represents shear wave velocity using four different methods. From soil correlation proposed by Ansary et al. (2010), SWV varies from 133 to 295 m/sec. SWV exists between 107 and 273 m/sec (Ohta and Goto, 1978). On the other hand, SWV of Ohba and Toriumi (1970), which varies from 84 to 264 m/sec, shows slightly higher value than Imai and Yoshimura (1970), which shows ranging between 76 and 257 m/sec.

(31) Sub-Soil Characteristics of Kalunagar, Hazaribagh (SBH 30)

SPT Results

The soil profile of the borehole is shown in Table A3.21. This borehole consists of two soil layers. The top layer of soil exists filling of loose grey silty fine sand varies from 0 to 8 m. The bottom layer of medium dense grey silty fine sand varies from 8 to 20. The uncorrected SPT N-value of this site varies from 1 to 40. The SPT N-value of filling sand varies from 4 to 9. The SPT N-value of the bottom layer varies between 9 and 19.

Shear Wave Velocity Results

Table A3.21 represents shear wave velocity using four different methods. From soil correlation proposed by Ansary et al. (2010), SWV varies from 135 to 229 m/sec. SWV exists between 103 and 226 m/sec (Ohta and Goto, 1978). On the other hand, SWV of Ohba and Toriumi (1970), which varies from 129 to 209 m/sec, shows slightly higher value than Imai and Yoshimura (1970), which shows ranging between 120 and 201 m/sec.

(32) Sub-Soil Characteristics of Rab-10, Plot, Kamrangirchar (SBH 31)

SPT Results

The soil profile of the borehole is shown in Table A3.22. The borehole consists of five soil layers. The top layer exists filling of very loose to loose light brown silty fine sand varies from 0 to 3.5 m. The loose to medium dense grey fine sand and silt trace mica varies from 9.5 to 14 m. The bottom layer of medium dense grey silty fine sand trace mica varies from 14 to 20. The uncorrected SPT N-value of this site varies from 3 to 28.

The SPT N-value of filling sand varies from 3 to 7. The SPT N-value of loose to medium dense grey fine sand and silt varies from 7 to 19. The SPT N-value of bottom layer varies from 19 to 28.

Shear Wave Velocity Results

Table A3.22 represents shear wave velocity using four different methods. SWV varies from 122 to 261 m/sec (Ansary et al., 2010). From SPT correlation developed by Ohta and Goto (1978), SWV exists from 98 to 261 m/sec. On the other hand, SWV of Ohba and Toriumi (1970), which varies from 118 to 236 m/sec, shows slightly higher value than Imai and Yoshimura (1970), which shows ranging between 109 and 228 m/sec.

(33) Sub-Soil Characteristics of Sosan Ghat, Kamrangirchar (SBH 32)

Table 3.12: SPT-N and Shear Wave Velocity at Sosan Ghat, Kamrangirchar

Depth (m)	Soil Description	SPT-N Value	Shear wave velocity (m/s) from SSMM				
			SSMM Hossain (2009)	Ansary et al. (2010)	Ohta and Goto (1978)	Imai and Yoshimura (1970)	Ohba and Toriumi (1970)
1.5	Filling Sand	7	100	163	114	144	154
3.0	Filling Sand	9	112	178	136	157	166
4.5	Filling Sand	10	134	209	179	162	172
6.0	Organic Clay	1	150	110	128	76	84
7.5	Organic Clay	2	160	133	151	96	104
9.0	Clay	12	160	220	212	173	181
10.5	Clay	13	165	225	222	177	186
12.0	Clay	15	170	235	234	186	194
13.5	Clay	14	170	230	236	182	190
15.0	Clay	15	180	235	244	186	194
16.5	Sand	22	180	241	223	211	219
18.0	Sand	25	200	251	232	220	228

SPT Results

The soil profile of the borehole is demonstrated in Table 3.12 (Tanvir, 2009). The borehole consists of four soil layers. The top layer exists filling of fine sand from 0 to 4.5 m. The organic clay layer varies between 4.5 and 7.5 m. The lower clay layer varies

between 7.5 and 15. The uncorrected SPT N-value of this site varies from 1 to 25. The SPT N-value of filling sand varies from 7 to 10. The SPT N-value of clay layer varies between 12 and 15.

Shear Wave Velocity Results

Table 3.12 represents shear wave velocity by direct SSMM method (Hossain, 2009) and four correlated methods. According to SSMM, SWV varies from 100 to 200. SWV varies from 133 to 251 m/sec (Ansary et al., 2010). SWV exists between 114 and 244 m/sec (Ohta and Goto, 1978). On the other hand, SWV of Ohba and Toriumi (1970), which varies from 84 to 228 m/sec, shows slightly higher value than Imai and Yoshimura (1970), which shows ranging between 96 and 220 m/sec.

(34) Sub-Soil Characteristics of Basundhara River view (SBH 33)

SPT Results

The soil profile of the borehole is shown in Table A3.23. The borehole consists of six soil layers. The top layer exists filling of very loose to loose grey silty fine sand varies from 0 to 3.5 m. The medium stiff grey clayey silt with fine sand medium compress varies from 8 to 14 m. The uncorrected SPT N-value of this site varies from 2 to 10. The SPT N-value of filling sand varies from 3 to 5. The SPT N-value of medium stiff grey clayey silt varies from 4 to 10. The SPT N-value of soft silty grey silty clay trace fine sand varies from 2 to 5.

Shear Wave Velocity Results

Table A3.23 represents shear wave velocity using four different methods. SWV varies from 122 to 184 m/sec (Ansary et al., 2010). SWV exists from 98 to 202 m/sec (Ohta and Goto, 1978). On the other hand, SWV of Ohba and Toriumi (1970), which varies from 104 to 172 m/sec, shows slightly higher value than Imai and Yoshimura (1970), which shows ranging between 96 and 162 m/sec.

(35) Sub-Soil Characteristics of Matuail, Demra (SBH 34)

SPT Results

The soil profile of the borehole is shown in Table 3.13. This borehole exists five soil layers. The filling sand varies from 0 to 3.5 m. The stiff grey silty clay varies from 8.5 to 14 m. The bottom layer of grey clayey silt varies from 14 to 20 m. The uncorrected SPT N-value of this site varies from 2 to 23. The SPT N-value of the uppermost filling sand varies from 3 to 4. The SPT N-value of stiff grey silty clay varies from 7 to 17.

Shear Wave Velocity Results

Table 3.13 represents shear wave velocity using PS loggings method (CDMP, 2009) and four correlated methods. According to PS loggings, SWV varies from 101 to 231. SWV varies from 122 to 244 m/sec (Ansary et al., 2010). From SPT correlation developed by Ohta and Goto (1978), SWV exists from 98 to 244 m/sec. On the other hand, SWV of Ohba and Toriumi (1970), which varies from 118 to 222 m/sec, shows slightly higher value than Imai and Yoshimura (1970), which shows ranging between 96 and 214 m/sec.

Table 3.13: SPT-N and Shear Wave Velocity at Matuail, Demra

Depth (m)	Soil Description	SPT-N Value	Shear wave velocity (m/s) from PS-logging				
			CDMP (2009)	Ansary et al. (2010)	Ohta and Goto (1978)	Imai and Yoshimura (1970)	Ohba and Toriumi (1970)
1.5	Silty Fine Sand (Filling)	3	101	122	98	109	118
3.0	Silty Fine Sand (Filling)	4	101	135	119	120	129
4.5	Silty Clay	2	101	133	136	96	104
6.0	Silty Clay	2	101	133	144	96	104
7.5	Silty Clay	3	137	150	162	109	118
9.0	Silty Clay	8	137	197	198	151	160
10.5	Silty Clay	10	137	209	212	162	172
12.0	Silty Clay	14	137	230	231	182	190
13.5	Silty Clay	17	137	243	244	194	202
15.0	Clayey Silt	18	137	225	211	197	206
16.5	Clayey Silt	20	137	233	219	204	213
18.0	Clayey Silt	22	137	241	227	211	219
19.5	Clayey Silt	23	231	244	232	214	222
20.0	Clayey Silt	23	231	244	233	214	222

(36) Sub-Soil Characteristics of Jilmil Project, Equria (SBH 35)

SPT Results

The soil profile of the borehole is demonstrated in Table A3.24. This borehole consists of three soil layers. The top layer exists filling of very loose grey silty fine sand varies from 0 to 2 m. The soft to medium stiff grey silty clay varies from 2 to 8.5 m. The medium dense to dense grey silty fine sand varies from 8.5 to 20 m. The uncorrected SPT N-value of this site varies from 2 to 31. The SPT N-value of filling sand is 2. The SPT N-value of soft to medium stiff grey silty clay varies between 2 to 15. The SPT N-value of the bottom layer varies from 15 to 31.

Shear Wave Velocity Results

Table A3.24 represents shear wave velocity using four different methods. SWV varies from 107 to 271 m/sec (Ansary et al., 2010). SWV exists between 92 and 245 m/sec (Ohta and Goto, 1978). On the other hand, SWV of Ohba and Toriumi (1970), which varies from 104 to 244 m/sec, shows slightly higher value than Imai and Yoshimura (1970), which shows ranging between 96 and 236 m/sec.

(37) Sub-Soil Characteristics of Rajendapur (SBH 36)

SPT Results

The soil profile of the borehole is shown in Table A3.25. This borehole consists of five soil layers. The top layer exists filling of loose light grey silty fine sand varies from 0 to 5.5 m. The medium stiff to stiff grey clayey silt varies from 8 to 15.5 m. The uncorrected SPT N-value of this site varies from 4 to 26. The SPT N-value of filling sand varies from 4 to 5. The SPT N-value of medium stiff to stiff grey clayey silt varies from 5 to 9. The SPT N-value of the bottom layer varies between 21 and 26.

Shear Wave Velocity Results

Table A3.25 represents shear wave velocity using four different methods. SWV varies from 135 to 255 m/sec (Ansary et al., 2010). SWV exists between 103 and 238 m/sec (Ohta and Goto, 1978). On the other hand, SWV of Ohba and Toriumi (1970), which varies from 129 to 231 m/sec, shows slightly higher value than Imai and Yoshimura (1970), which shows ranging between 120 and 223 m/sec.

(38) Sub-Soil Characteristics of Bramangaon (SBH 37)

SPT Results

The soil profile of the borehole is shown in Table A3.26. This borehole exists four soil layers. The top layer exists filling of loose grey silty fine sand varies from 0 to 5 m. The medium stiff grey clayey silt with fine sand varies from 8 to 20 m. The uncorrected SPT N-value of this site varies from 4 to 8. The SPT N-value of filling sand varies from 4 to 5. The SPT N-value of the bottom layer varies from 5 to 8.

Shear Wave Velocity Results

Table A3.26 represents shear wave velocity using four different methods. SWV varies from 135 to 171 m/sec (Ansary et al., 2010). SWV exists from 103 to 195 m/sec (Ohta and Goto, 1978). On the other hand, SWV of Ohba and Toriumi (1970), which varies from 129 to 160 m/sec, shows slightly higher value than Imai and Yoshimura (1970), which shows ranging between 120 and 151 m/sec.

(39) Sub-Soil Characteristics of Meradia, Uttar Banasree (SBH 38)

SPT Results

The soil profile of the borehole is shown in Table 3.14. This borehole exists three soil layers. The top layer exists filling of fine sand from 0 to 4.5 m. The organic clay layer varies between 4.5 and 12 m. The lower clay layer varies between 12 and 18. The uncorrected SPT N-value of this site varies from 2 to 22. The SPT N-value of filling sand

varies from 2 to 4. The SPT N-value of organic clay layer varies from 2 to 4. The SPT N-value of bottom clay layer varies from 17 to 22.

Shear Wave Velocity Results

Table 3.14 represents shear wave velocity using SSMM method (Hossain, 2009) and four correlated methods. According to SSMM, SWV varies from 90 to 195. From soil correlation proposed by Ansary et al (2010), SWV varies from 107 to 261 m/sec. SWV exists between 111 and 217 m/sec (Ohta and Goto, 1978). On the other hand, SWV of Ohba and Toriumi (1970), which varies from 104 to 209 m/sec, shows slightly higher value than Imai and Yoshimura (1970), which shows ranging between 96 and 201 m/sec.

Table 3.14: SPT-N and Shear Wave Velocity at Meradia, Uttar Banasree

Depth (m)	Soil Description	SPT-N Value	Shear wave velocity (m/s) from SSMM				
			SSMM Hossain (2009)	Ansary et al. (2010)	Ohta and Goto (1978)	Imai and Yoshimura (1970)	Ohba and Toriumi (1970)
1.5	Silty Fine Sand (Filling)	3	90	122	111	137	146
3.0	Silty Fine Sand (Filling)	4	102	135	130	144	154
4.5	Silty Fine Sand (Filling)	2	118	107	133	151	160
6.0	Organic Clay	2	130	133	111	96	104
7.5	Organic Clay	3	130	150	116	96	104
9.0	Organic Clay	8	138	197	120	96	104
10.5	Organic Clay	10	148	209	142	109	118
12.0	Organic Clay	14	157	230	154	120	129
13.5	Clay	17	157	243	184	162	172
15.0	Clay	18	170	247	194	173	181
16.5	Clay	20	170	254	207	190	198
18.0	Clay	22	195	261	217	201	209

(40) Sub-Soil Characteristics of BUET Play ground

SPT Results

The soil profile of the borehole is shown in Table 3.15. This borehole exists two soil layers. The top layer exist clayey silt layer from 0 to 4.5 m. The bottom sand layer exists from 4.5 to 18 m. The uncorrected SPT N-value of this site varies from 2 to 19. The SPT

N-value of the uppermost clayey silt layer varies from 6 to 8. The SPT N-value of sand layer varies from 4.5 to 18.

Shear Wave Velocity Results

Table 3.15 represents shear wave velocity using SSMM method (Hossain, 2009) and four correlated methods. According to SSMM, SWV varies from 178 to 260 m/sec. SWV varies from 107 to 229 m/sec (Ansary et al., 2010). From Ohta and Goto (1978), SWV exists from 121 to 221 m/sec. On the other hand, SWV of Ohba and Toriumi (1970), which varies from 104 to 209 m/sec, shows slightly higher value than Imai and Yoshimura (1970), which shows ranging between 96 and 201 m/sec.

Table 3.15: SPT-N and Shear Wave Velocity at BUET Play ground

Depth (m)	Soil Description	SPT-N Value	Shear wave velocity (m/s) from SSMM				
			SSMM Hossain (2009)	Ansary et al. (2010)	Ohta and Goto (1978)	Imai and Yoshimura (1970)	Ohba and Toriumi (1970)
1.50	Clayey Silt	6	178	182	135	137	146
3.00	Clayey Silt	7	178	190	159	144	154
4.50	Clayey Silt	8	180	197	177	151	160
6.00	Sand	2	190	107	121	96	104
7.50	Sand	2	205	107	127	96	104
9.00	Sand	2	205	107	131	96	104
10.50	Sand	3	220	122	145	109	118
12.00	Sand	4	230	135	156	120	129
13.50	Sand	10	230	184	187	162	172
15.00	Sand	12	245	196	197	173	181
16.50	Sand	16	245	216	211	190	198
18.00	Sand	19	260	229	221	201	209

(41) Sub-Soil Characteristics of West Palashi, BUET campus

The BUET campus is situated in latitude 23°43'16.58" N to 23°43'59.44" N and longitude 90°23'13.31"E to 90°23'43.56" E. Microtremor observation has been executed at 132 selected points in soil. The geology of whole BUET campus is Upper Modhupur Terrace (Figure 3.2) and High Pleistocene terrace (Figure 3.3). There is no filling in this site.

SPT Results

Total 14 SPT boreholes data have been collected from West Palashi, BUET Campus. Table A3.27 to A3.31 shows soil profiles of five boreholes at BUET-JIDPUS building, West Palashi, BUET Campus (Dhaka Soil, 2008). Table 3.32 to 3.40 represent soil profiles of nine boreholes at New Academic building, West Palashi, BUET campus (Unique Boring and Engineering, 2005).

From Table A3.27 to A3.31, the uppermost silty clay varies from 0 to 6.0 m. Clayey silt exists below the silty clay layer between 4.5 to 7.5 m. The bottom layer of silty fine sand varies from 7.5 to 15 m.

From Table A3.32 to A3.40, clay silt exists between 0 to 1.5 m soils in most of the boreholes. The silty clay varies ranging between 1.5 and 7.5 m. In some borehole, fine sandy silt exists between 6 and 9 m. In all the boreholes, the bottom soil layer is silty fine sand.

Shear Wave Velocity Results

Table A3.27 to A3.40 represent shear wave velocity using four correlated methods.

From Table A3.27 to A3.31, SWV varies from 110 to 297 m/sec (Ansary et al., 2010). From SPT correlation developed by Ohta and Goto (1978), SWV exists between 92 and 242 m/sec. On the other hand, SWV of Ohba and Toriumi (1970), which varies from 84 to 266 m/sec, shows slightly higher value than Imai and Yoshimura (1970), which shows ranging between 76 and 259 m/sec.

From Table 3.32 to 3.40, SWV varies from 84 to 309 m/sec (Ansary et al., 2010). From SPT correlation developed by Ohta and Goto (1978), SWV exists from 82 to 259 m/sec. On the other hand, SWV of Ohba and Toriumi (1970), which varies from 84 to 275 m/sec, shows slightly higher value than Imai and Yoshimura (1970), which shows ranging between 76 and 269 m/sec.

3.3 MICROTREMOR DATA COLLECTION

The ground is always vibrating at minute amplitudes. Microtremors are ambient vibrations of the ground caused by natural or artificial disturbances such as wind, sea waves, traffic, human activities and industial machinery. Microtremor data has been collected in consideration of noise in different geological and geomorphological unit (Figure 3.2 and Figure 3.3).

Microtremor measurement has been carried out in 132 selected locations (Figure 3.34) within BUET campus. In BUET campus, 240 second duration were recorded at different times in the specific locations. The measurements were carried out from morning to midnight in order to minimize artificial noises due to traffic and human activities. In BUET campus, most of the selected points were near the busy road. Special care has been taken during data recording. In West Polashi of BUET campus, there was an 8 MW with 1500 rpm Electric Power Plant. Although there is a machine foundation below the generator, this generator produces some noise in adjacent ground. So, microtremor observation has been executed at different times during ON and OFF condition to justify soil response due to this effect.

Microtremor observation at 45 sites has been carried out in and around Dhaka city. Traffic movement, human activities, any power plant and noise from other sources have been considered during data recording as well. Most of the microtremor observation has been executed in consideration of recent filling. However, some non recent filling areas have also been selected for observation. Figure 3.1 shows 45 selected locations in and around Dhaka city. Some location is not demonstrated specifically in Dhaka city map due to not having full area coverage map. These points are shown using arrow mark in Figure 3.1.

Figure 3.4 demonstrates microtremor measurement apparatus for data recording. This includes Geodas 15-HS equipment (Data logger and Laptop), Sensor, Cable, Battery and GPS. Mtobs.exe software is used to record microtremor data. Although there are five sensors in this observation system, two or three sensors have been used for data recording. Sensor has been used in consideration of surface condition, weather, time and

geology of sites. CR4.5-1S velocity type sensor with sensitivity coefficient 0.0882μm/sec/digit has been used in observation system. Sensors comprise three components, which can record the horizontal motion (in Latitude and Longitude directions) and the vertical motions (up and down). Microtremor sensor sensitivity was 295900μm/sec/V. The converting speed was 50 kHz. The sampling frequency was 100 Hz. The amplification factor was used 20 db in observation system. Figure 3.5 shows some pictures of microtremor measurement at BUET campus, Demra and Ashulia Toll Plaza. These pictures are taken at different time during microtremor data recording.

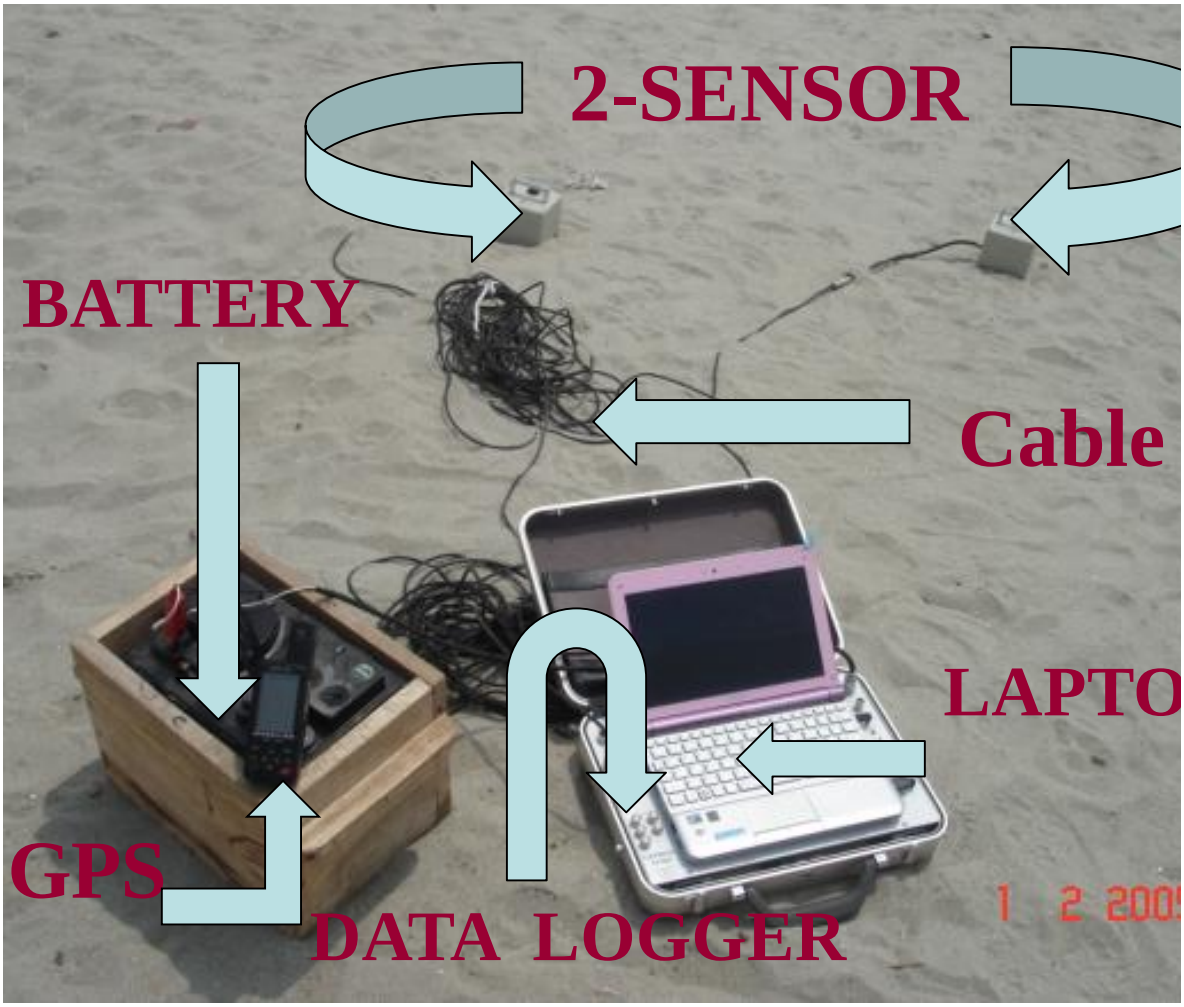

Figure 3.4: Microtremor measurement apparatus.

(a) West Polasi, BUET at 4:00 PM

(b) BUET campus at night

(c) Matuail, Demra (Left) and Ashulia Toll Plaza (Right) at afternoon

Figure 3.5: Microtremor data recording in and around Dhaka city.

3.4 MICROTREMOR DATA ANALYSIS

Velocity time history field microtremor data has been recorded in Mtobs.exe software with suitable number of observation channels, observation length, observation frequency, specific low or high pass filter code, amplification ratio, observation latitude and longitude, observation time and observation channel mode. Figure 3.6 shows a typical time history field data recording of Uttara Phase-3 (North side) at 4:30 PM on 9 April, 2011. The content of all input data are 2 CR4.5-1S velocity type sensors, 24000 observation data length, 100Hz sampling frequency, 0.05 Hz Low-pass filter, 20db amplification ratio, Latitude-23˚52´22″and Longitude-90˚21´40″.

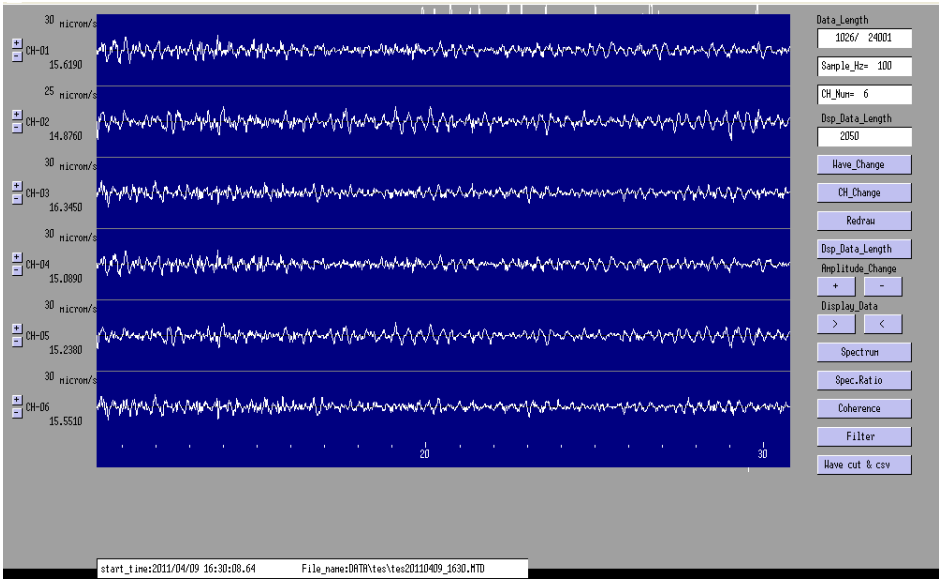

Figure 3.6: Time history field data recording at Uttara Phase-3 (North side).

Figure 3.7 [(a), (c) and (e)] shows time history microtremor data at segment 1, 2 and 3 with 2050 observed data length. Segment 1 illustrates time history data of 20.5 s from 40 s to 60.5 s. Segment 2 demonstrates time history data of 20.5 s from 100 s to 120.5 s. Segment 3 presents time history data of 20.5 s from 60 s to 80.5 s.

Time history data is not suitable to estimate the dynamic properties (predominant frequency and amplification ratio). So, transformation of time domain data to frequency domain data is required with Fourier Transformation. Therefore, Fast Fourier

Transformation (FFT) has been used to transfer time domain data to frequency domain data. Figure 3.7 [(b), (d) and (f)] presents Fast Fourier Transformation data at segment 1, 2 and 3 in EW, NS and UD directions, respectively. This transformation data is shown in logarithmic window in frequency from 0.1 Hz to 10 Hz and in Fourier Spectrum from 0.01 μm to 10 μm.

Only the Fourier Spectrum along three subsequent directions is not appropriate to estimate the predominant frequency and amplification. So, Horizontal to Vertical spectral ratio (H/V) is required to determine the dynamic properties of soil. Horizontal to Vertical Spectral Ratio (H/V) is determined dividing by Fourier Spectrum of UD direction to the Fourier Spectrum of EW or NS direction.

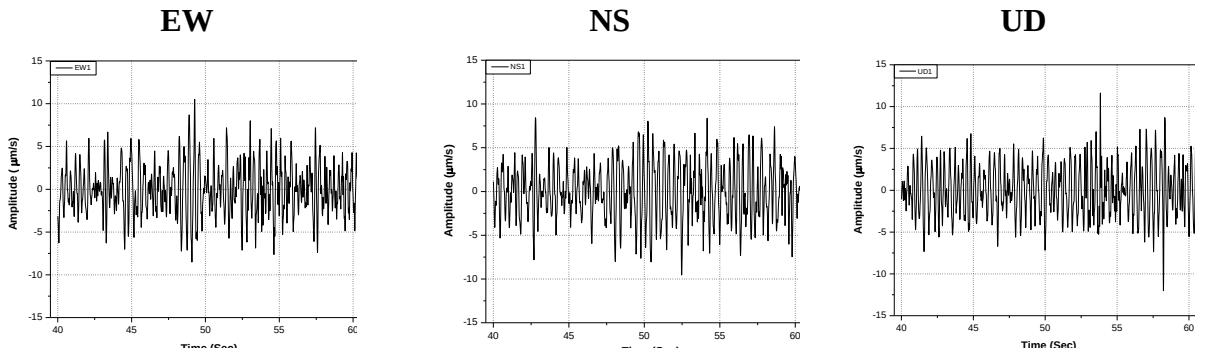

(a) Time History data of segment 1 from 40 sec to 60.5 sec

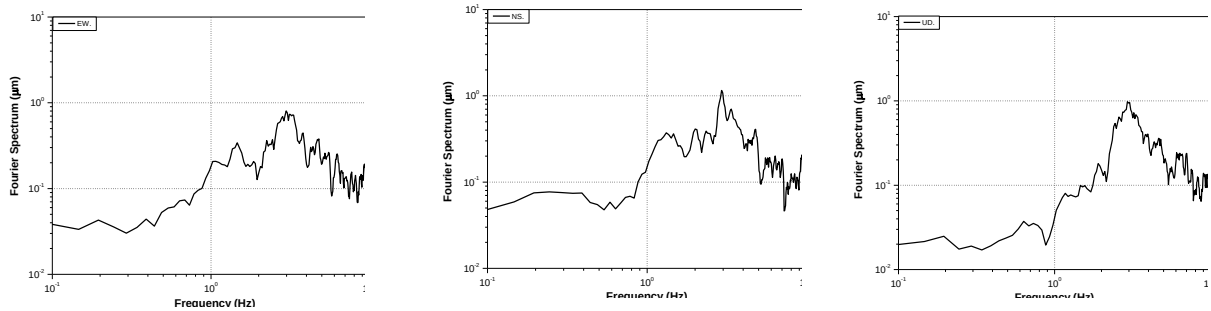

(b) Fourier Transformation of Segment 1 in EW, NS and UD direction

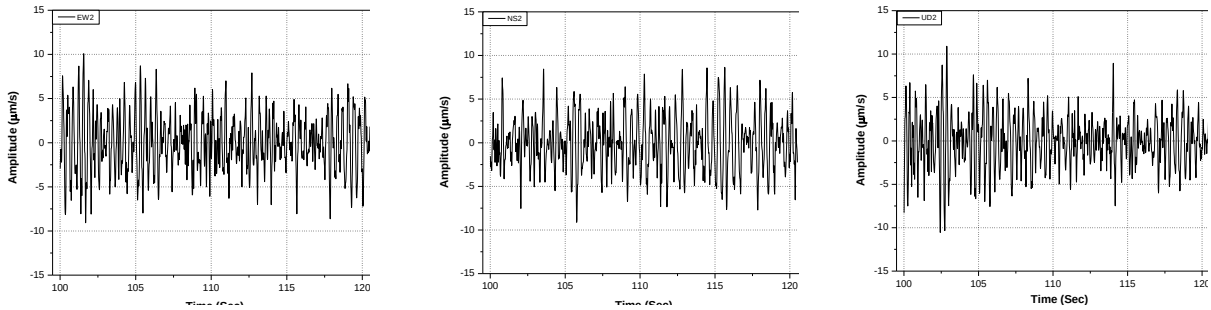

(c) Time History data of segment 2 from 100 sec to 120.5 sec

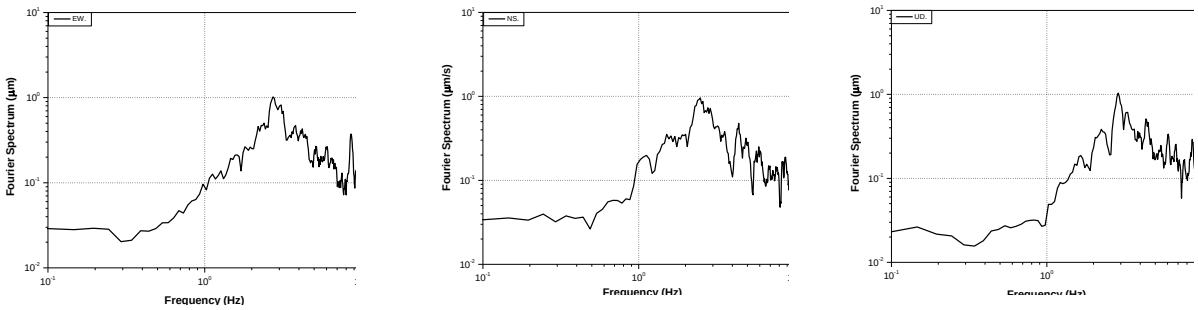

(d) Fourier Transformation of Segment 2 in EW, NS and UD direction

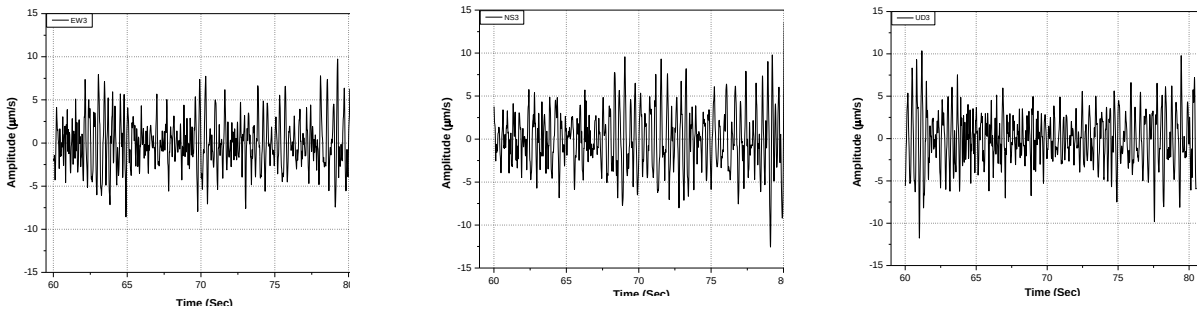

(e) Time History data of segment 1 from 60 sec to 80.5 sec

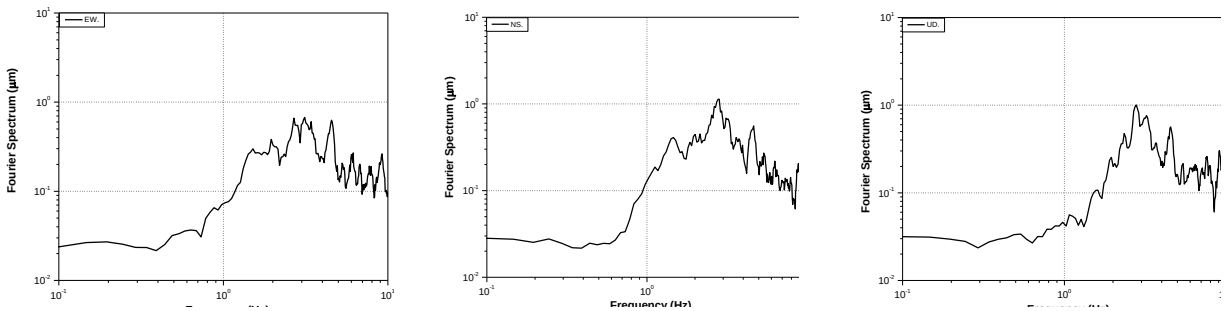

(f) Fourier Transformation of Segment 2 in EW, NS and UD direction

Figure 3.7: Fourier Transformation of three segments at Uttara Phase-3 (North side).

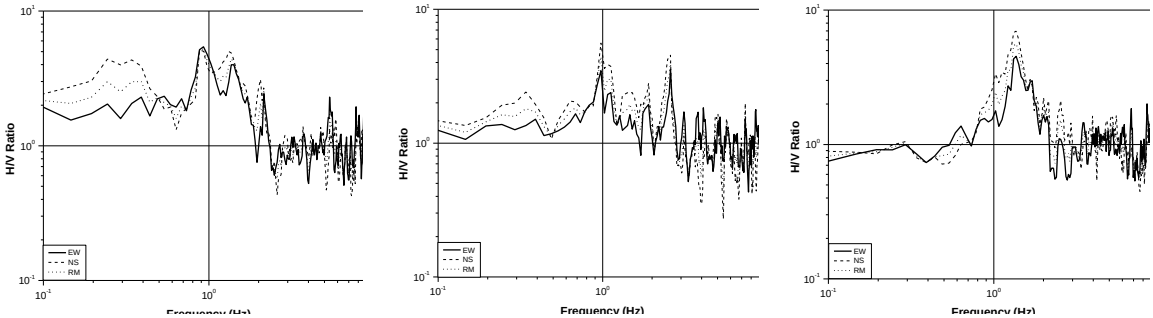

Segment 1 **Segment 2** **Segment 3**

(a) H/V Ratio of EW, NS and their mean at Segment 1, 2 and 3

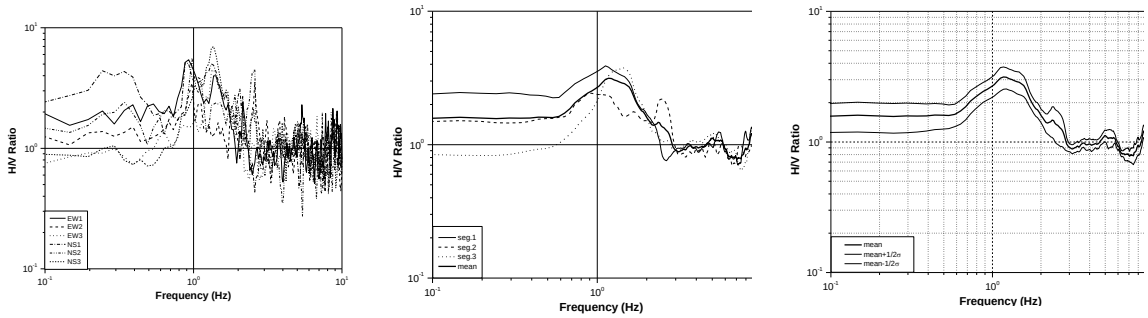

(b) Mean H/V ratio with Standard Deviation

Figure 3.8: Predominant Frequency and H/V ratio at Uttara Phase-3 (North side).

Figure 3.8 (a) shows the Horizontal to Vertical Spectral ratio (H/V) of segment 1, 2 and 3 in EW and NS directions, respectively. The square root of EW and NS direction H/V ratio in segment 1, 2 and 3 is calculated. Then, mean of the square root H/V ratio value is plotted with standard deviation 0.5σ. 0.5σ standard deviation represents the deviation of six H/V ratio data from mean in three segments. Figure 3.8 (b) presents the mean H/V ratio with six segmental H/V ratio in EW and NS direction. In addition to this, three segmental square root H/V ratio and their mean H/V Ratio is shown in Figure 3.8 (b). The plotted data is smoothed with suitable log- window to understand clearly the Predominant frequency (Hz) and Horizontal to vertical spectral ratio (H/V).

3.4.1 Stability of Microtremor Data

Microtremor is the combination of shear wave, Rayleigh wave and Love wave. The effect of different waves on microtremor data is significant. Therefore, stability check of

microtremor data is important to estimate dynamic properties of any site soil. To carry out this research velocity time history data have been recorded time ranging between morning to midnight at 14 locations in West Palashi, BUET. The observation microtremor data recording varies from 5 to 20 minutes. Ten minutes observation time has been taken in most of the observation points. Three segments of 20.48 s time domain data have been used to transform frequency domain spectrum. In order to get low noise data these Fourier spectra have been filtered using rectangular windows. The mean of these three segments of frequency domain data have been calculated using smoothing function with average smoothing point 5. Mean Fourier spectrum along EW, NS and UD directions have been plotted in logarithmic windows from 0.1 Hz to 10 Hz along predominant frequency and from 0.001μm to 1μm along Fourier amplitude spectrum, respectively. From these observations, stability of time variation microtremor data has been compared from Fourier spectrum. The horizontal to vertical spectral ratio has also been calculated in these locations to analyze the stability of H/V ratio with Fourier spectrum. Both Fourier spectrum and H/V ratio of fourteen observation points at different times have been included in this section.

3.4.1.1 Stability of Amplitude of Fourier Spectrum

Frequency domain Fourier spectra of fourteen observation points have been demonstrated from Figure 3.9 to 3.13 along EW, NS and UD, respectively. Instead of using all the observed time records, three to four different times instants are selected from 24 hour observation for fourteen sites, for investigation. Figure 3.9 shows the vertical and horizontal Fourier spectra of microtremors observed at MT05, MT06 and MT07. The mean peak value of Fourier spectra varies from 2.1 Hz to 3.1 Hz for both the horizontal and vertical motions. Figure 3.9 (a) shows three time instants (13:07 PM, 16:20 PM and 01:06 AM) and their mean value. Figure 3.9 (b) shows three time instants (18:29 PM, 00:08 AM and 01:29 AM) where as Figure 3.9 (c) represents three time instants (11:34 AM, 16:55 PM and 19:41 PM). From figure 3.9, it can be concluded that Fourier spectra along EW, NS and UD directions are stable at these observation points. The stable Fourier spectra along vertical directions have been found around 3.0 Hz.

In Figure 3.10 Fourier spectra of microtremor observations at MT08, MT09 and MT10 have been illustrated along EW, NS and UD directions, respectively. The overall peak

value of the Fourier spectra lies between 3.02 Hz and 3.84 Hz for both the horizontal and vertical motions. From Figure 3.10 (a), the horizontal motion of MT08 in the afternoon (11:34 AM and 16:55 PM) has a peak from 3.34 Hz to 4.4 Hz and in night (00:01 AM and 01:21 AM); it varies between 2.75 Hz and 2.95 Hz along EW direction. The peak along NS direction in the afternoon varies between 2.29 Hz and 2.57 Hz whereas it lies from 2.61 Hz to 2.94 Hz in night. The stable peak along vertical direction is 3.59 Hz in afternoon and it varies from 2.42 Hz to 3.02 Hz in night. The stable fourier spectra of MT 09 and MT 10 have been shown in Figure 3.10 (b) and Figure 3.10 (c). From Figure 3.10, it can be concluded that Fourier amplitude spectrum are stable along EW, NS and UD directions, respectively.

The frequency domain Fourier spectra at MT11, MT12 and MT13 are illustrated in Figure 3.11. The mean peak Fourier amplitude spectrum varies between 2.20 Hz and 3.74 Hz for both the horizontal and vertical motions for all three locations. The Fourier spectra at MT 11 and MT 12 are almost stable. The amplitude of these sites is around 3 Hz. But, the Fourier spectra at MT 13 are slightly different from MT 11 and MT 12. The mean peak of Fourier spectra at MT 13 varies from 2.72 Hz to 3.26 Hz. The peak Fourier spectra at MT 13 lies between 0.13 µm and 0.37µm.

Figure 3.12 shows Fourier spectra of microtremor observations at MT15, MT16 and MT19 along EW, NS and UD directions, respectively. The mean peak amplitude of spectra varies from 1.94 Hz to 3.77 Hz for both the horizontal and vertical motions for all three locations. The mean peak Fourier amplitude has been found around 3.5 Hz along the vertical directions. The Fourier spectra at MT16 are more stable than other two locations along EW, NS and UD directions, respectively.

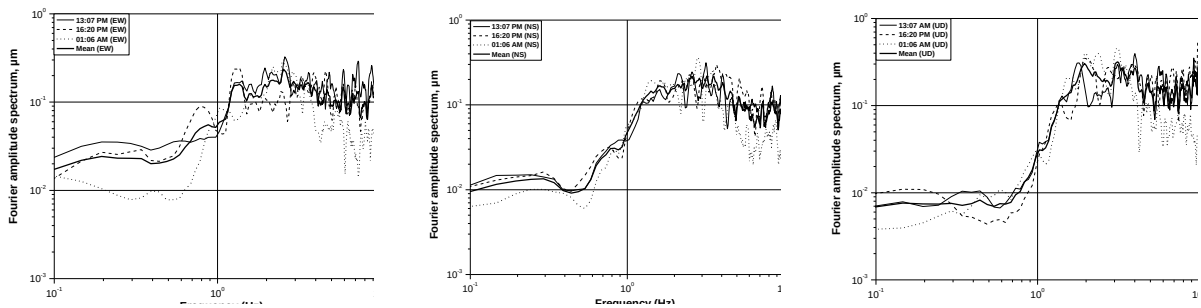

(a) MT05

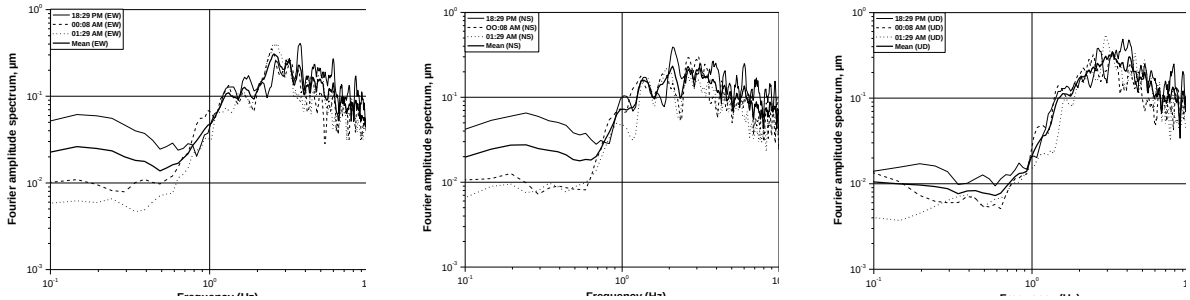

(b) MT06

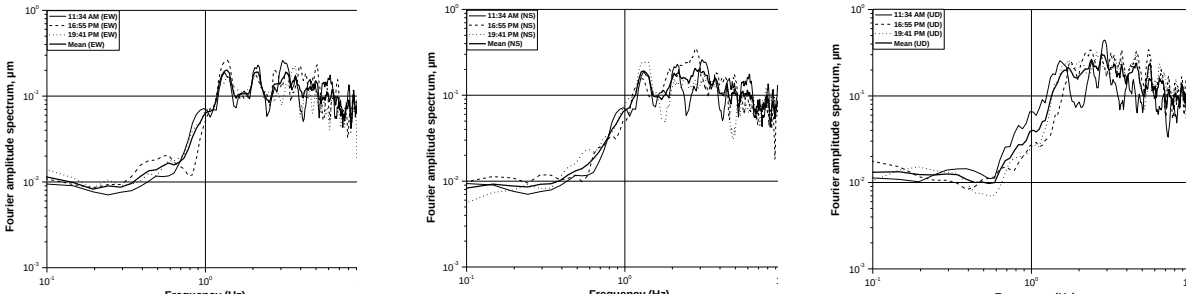

(c) MT07

Figure 3.9 [(a), (b) and (c)]: Stability of Fourier Spectrum at different times along EW, NS and UD directions at MT05, MT06 and MT07.

The Fourier spectra of MT22 and MT23 are shown in Figure 3.13. The peak value of the spectra lies between 2.48 Hz and 4.08 Hz for both the horizontal and vertical motions for all three locations. Figure 3.13(a) shows the variation of Fourier spectra at MT22 at four time instants (12:48 PM, 15:53 PM, 11: 31 and 00:38 PM) along EW, NS and UD directions, respectively. The variation of four time instants (12:48 PM, 15:53 PM, 11:46 PM and 00:46) of MT23 has been demonstrated in Figure 3.13 (b). From Figure 3.13, it can be said that the Fourier spectra in night are stable.

From the Fourier spectra analysis of 14 sites, it can be said that the amplitude level of Fourier spectra vary at different time instants of a day. The Fourier spectra at night are more stable than other time instants within a day. In the most of the sites Fourier spectra vary along EW and NS directions, respectively. It is not possible to estimate the dynamic characteristics (Predominant frequency and Amplification) of these sites on the basis of the amplitude level of Fourier spectra.

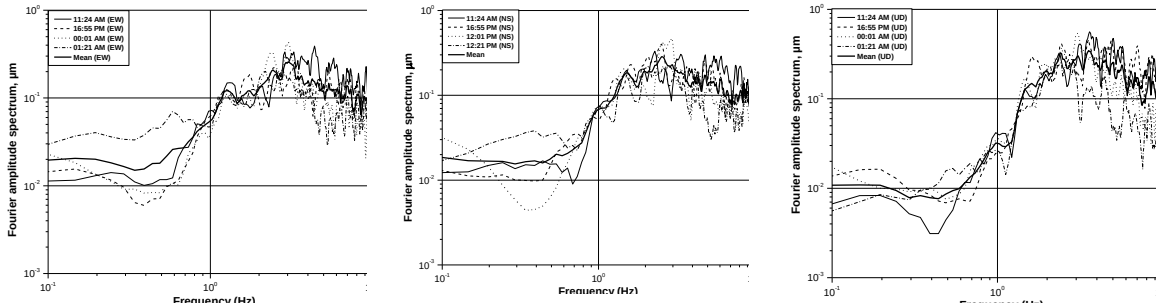

(a) MT08

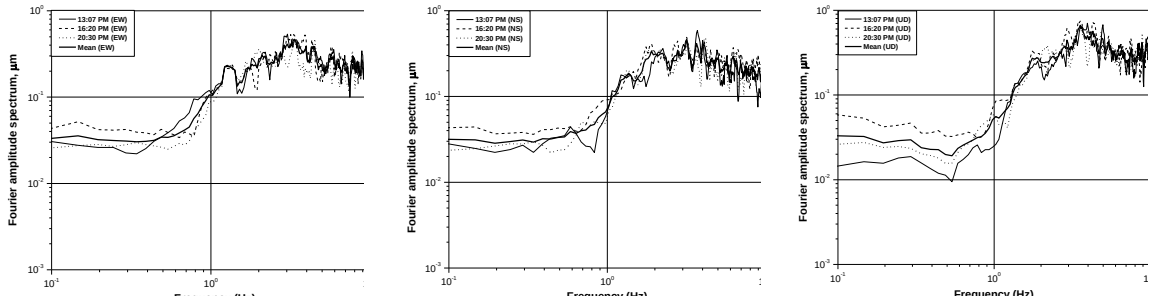

(b) MT09

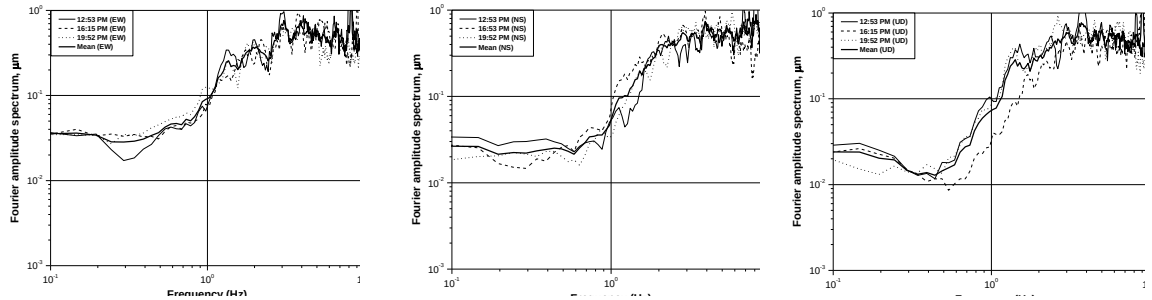

(c) MT10

Figure 3.10 [(a), (b) and (c)]: Stability of Fourier Spectrum at different times along EW, NS and UD directions at MT08, MT09 and MT10.

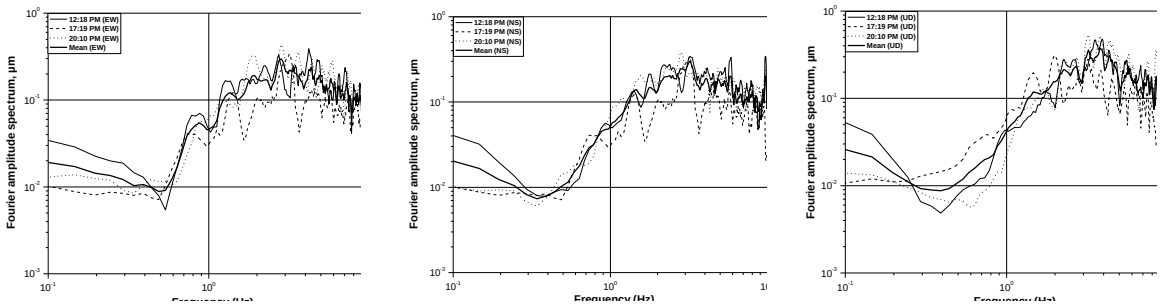

(a) MT11

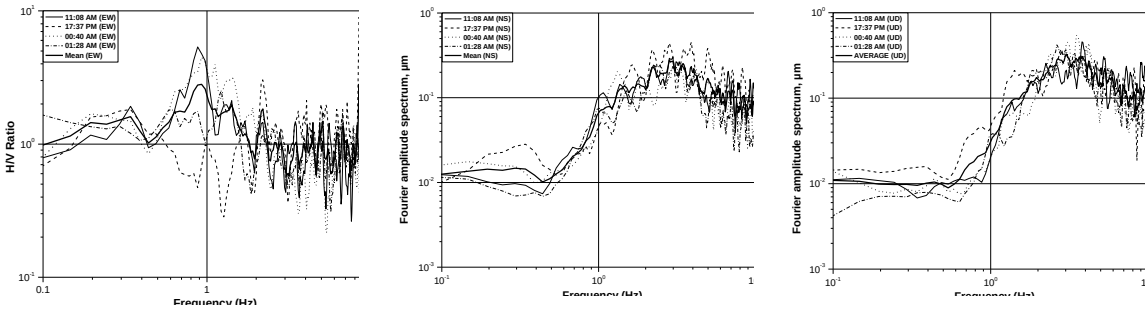

(b) MT12

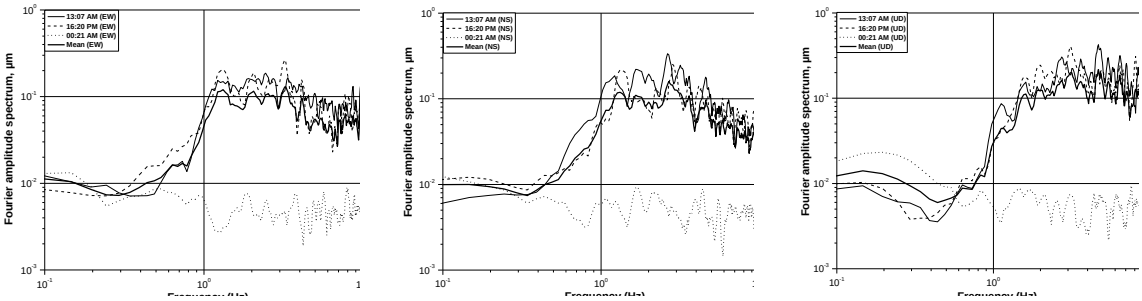

(c) MT13

Figure 3.11 [(a), (b) and (c)]: Stability of Fourier Spectrum at different times along EW, NS and UD directions at MT11, MT12 and MT13.

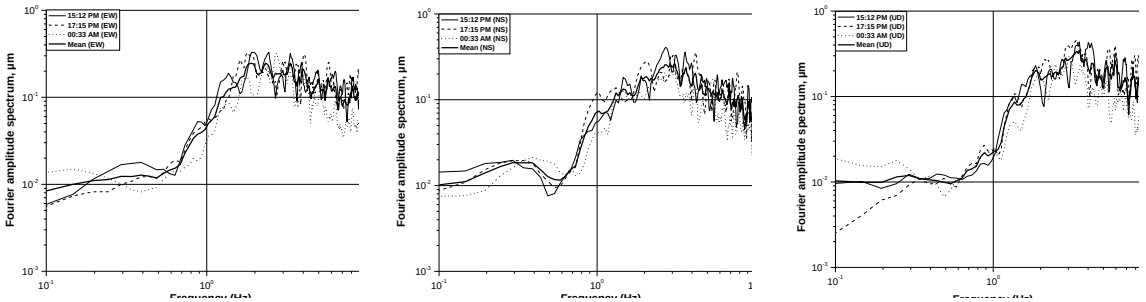

(a) MT15

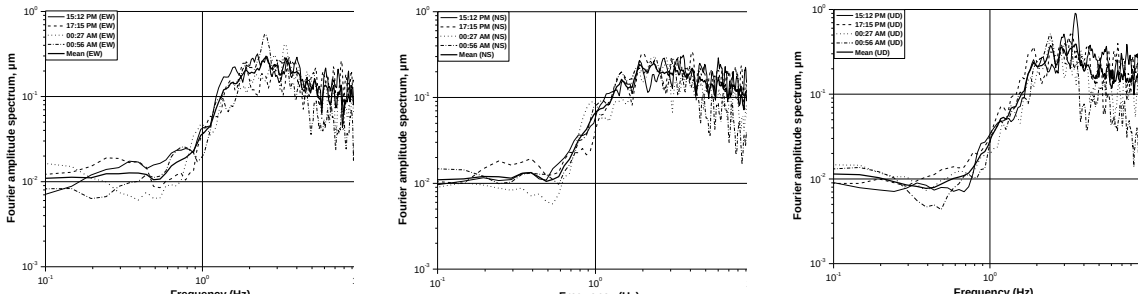

(b) MT16

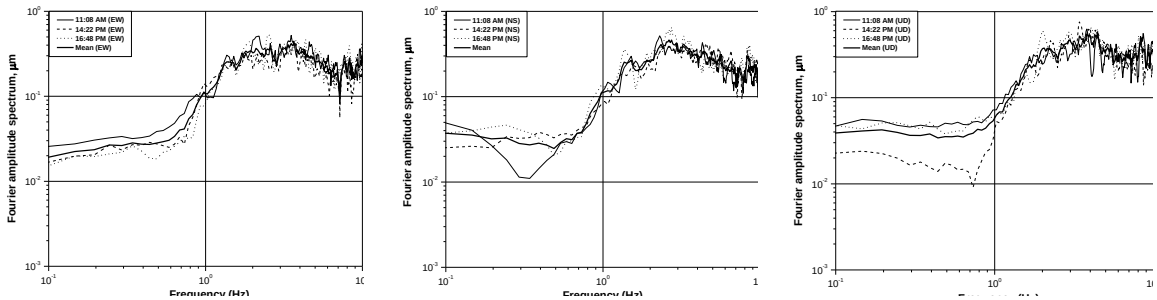

(c) MT19

Figure 3.12 [(a), (b) and (c)]: Stability of Fourier Spectrum at different times along EW, NS and UD directions at MT15, MT16 and MT19.

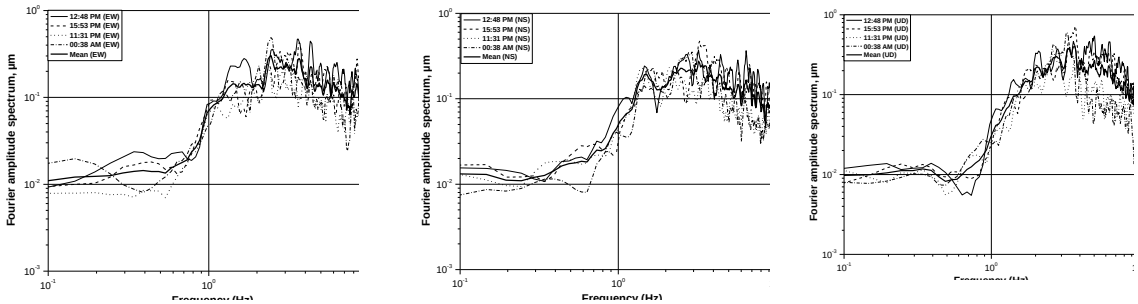

(a) MT22

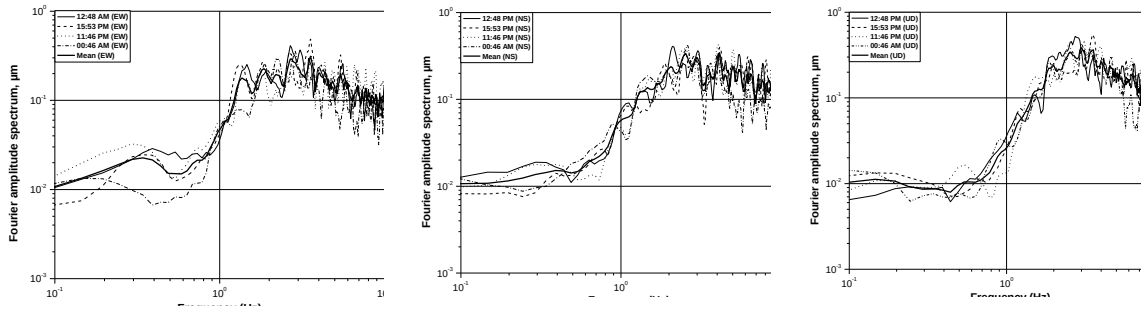

(b) MT23

Figure 3.13 [(a) and (b)]: Stability of Fourier Spectrum at different times along EW, NS and UD directions at MT22 and MT23.

3.4.1.2 Stability of Horizontal to Vertical Spectral Ratio

The amplitude ratio calculated in this study is defined by Nakamura (1989). Amplitude ratios of Fourier amplitude spectra of EW and NS components, respectively, to that of the UD components, AR_{EW} and AR_{NS}, are obtained as follows:

$$AR_{EW} = \frac{F_{EW}}{F_{UD}} \quad AR_{NS} = \frac{F_{NS}}{F_{UD}} \tag{3.1}$$

Where,F_{EW}, F_{NS} and F_{UD} are the Fourier amplitude spectra in the EW, NS and vertical direction, respectively.

The Horizontal to Vertical spectral ratio along EW and NS directions are shown from Figure 3.14 to 3.18. In Figure 3.14, amplitude ratios, AR_{EW} and AR_{NS} of the Fourier spectra of two horizontal components, are shown for three different time instants (13:07 PM, 16:20 PM and 01:06 AM) of MTO5, MT06 and MT07, respectively. The characteristics of the peak frequency of the amplitude ratios are different from those for Fourier spectra (Figure 3.9). The mean predominant frequency of two horizontal directions at MT05 and MT06 are stable. The mean predominant frequency of two horizontal directions at MT05 is around 0.77 whereas this value is around 0.94 at MT05 along EW and NS directions, respectively. The mean peak amplitude ratio is around 1.25 at MT07. Although the Fourier spectra are not stable with time, the amplitude ratios at different time instants along three directions within a day are stable at these sites.

Figure 3.15 shows stability of H/V ratio data at different time instants at MT08, MT09 and MT10 along EW and NS components, respectively. The peak Fourier amplitude ratios of MT08, which are around 1.20 Hz, are similar to the Fourier amplitude ratios at MT10. The peak amplitude ratio of MT09 is around 1.20 Hz along EW component and around 1.06 Hz along NS component, where the change of amplitude ratio of the spectra at different time instants of a day is comparatively small.

Figure 3.16 represents Stability of H/V ratio data at different time instants at MT11, MT12 and MT13 along EW and NS components, respectively. The peak Fourier amplitude ratios of MT10 varies between 0.78 Hz and 0.88 Hz where this value is around 0.93 Hz at MT12. The peak amplitude ratio of MT13 is around 1.22 Hz at MT13 in both Horizontal components.

The pattern of the amplitude spectra ratio at MT15, MT16 and MT19 are illustrated in Figure 3.17. Figure 3.17(a) and Figure 3.17(b) show the of amplitude change of Fourier spectra at three different time instants are comparatively small. The amplitude spectra

ratio of four different time instants (15:12 PM, 17:15 PM, 00:27 AM and 00:56 AM) and their mean value are stable (Figure 3.17 (b)).

Figure 3.18 shows the stability of H/V ratio data at four different time instants at MT22 and MT23 along EW and NS components, respectively. Figure 3.18 (a) represent the amplitude spectra ratio of MT22 is around 0.96 Hz along EW component and around 0.73 Hz along NS component. The peak amplitude ratio of MT23 lies between 0.98 Hz and 1.32 Hz along the two horizontal directions. The change of amplitude spectra ratio at four different time instants (12:48 PM, 15:53 PM, 11:31 PM and 00:38 AM) at MT 22 and four different time instants (12:48 PM, 15:53 PM, 11:46 PM and 00:46 AM) at MT 23 are stable.

From analysis of Fourier spectra ratio from Figure 3.14 to 3.18, it can be concluded that the change of amplitude ratio at different time instants of a day is comparatively small. In addition to this, the amplitude ratio is less influenced by the source of vibration than the Fourier spectrum of any direction and may reflect the particular charactersistics of the site. Therefore, the Horizontal to Vertical spectra ratio has been found more reliable to estimate dynamic properties (Predominant frequency and Amplification) of any particular soil.

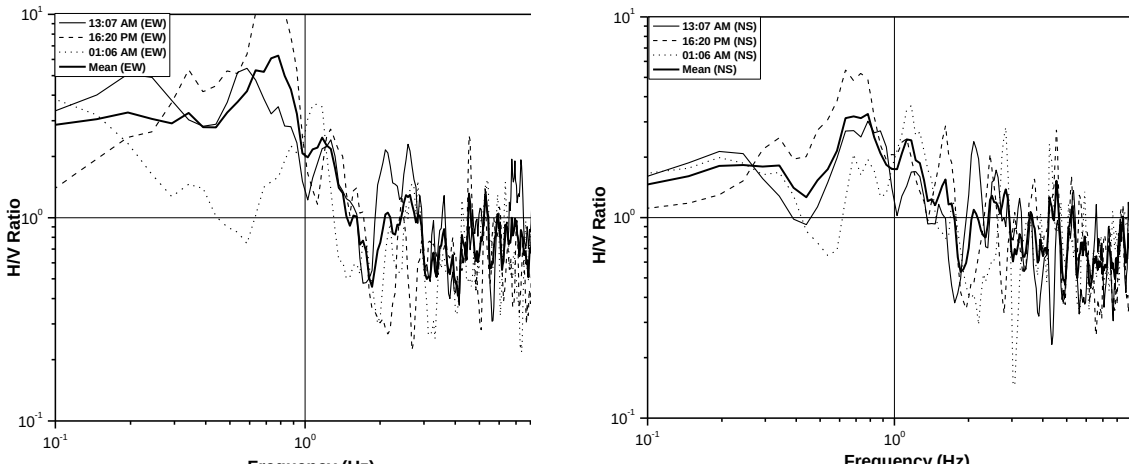

(a) MT05

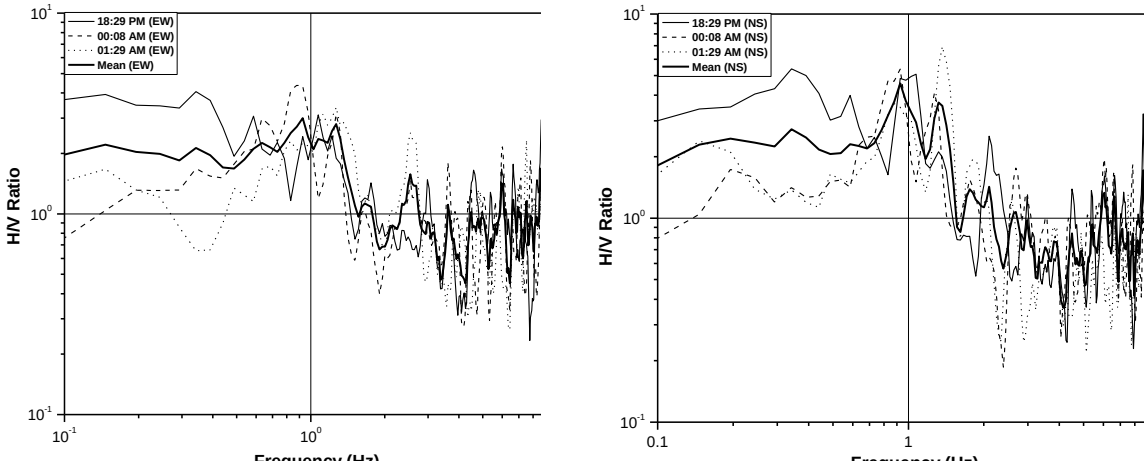

(b) MT06

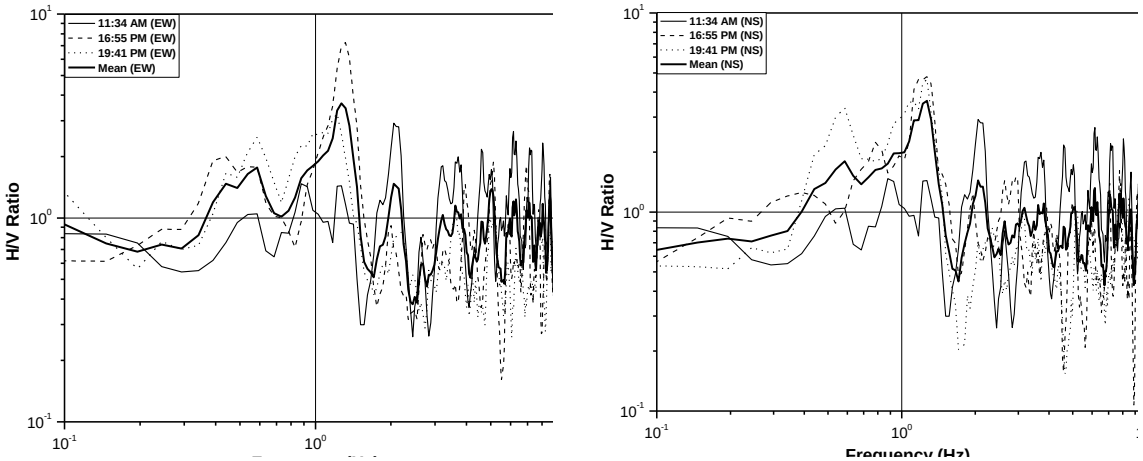

(c) MT07

Figure 3.14 [(a), (b) and (c)]: Stability of H/V ratio data at different times along EW and NS direction at MT05, MT06 and MT07.

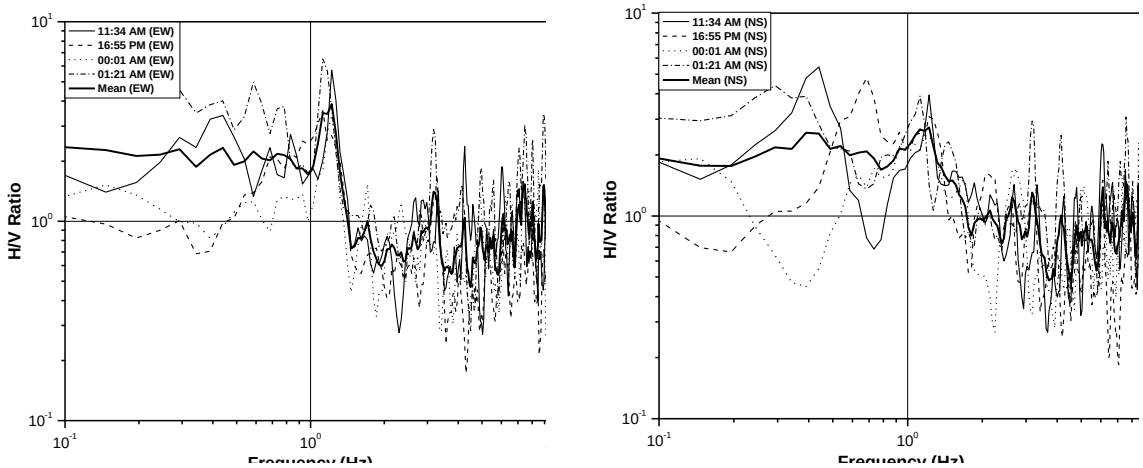

(a) MT08

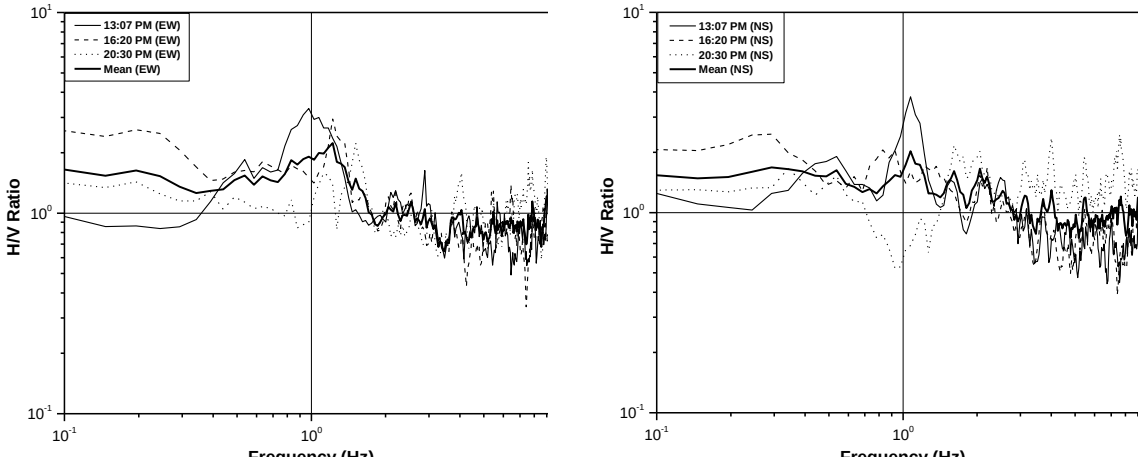

(b) MT09

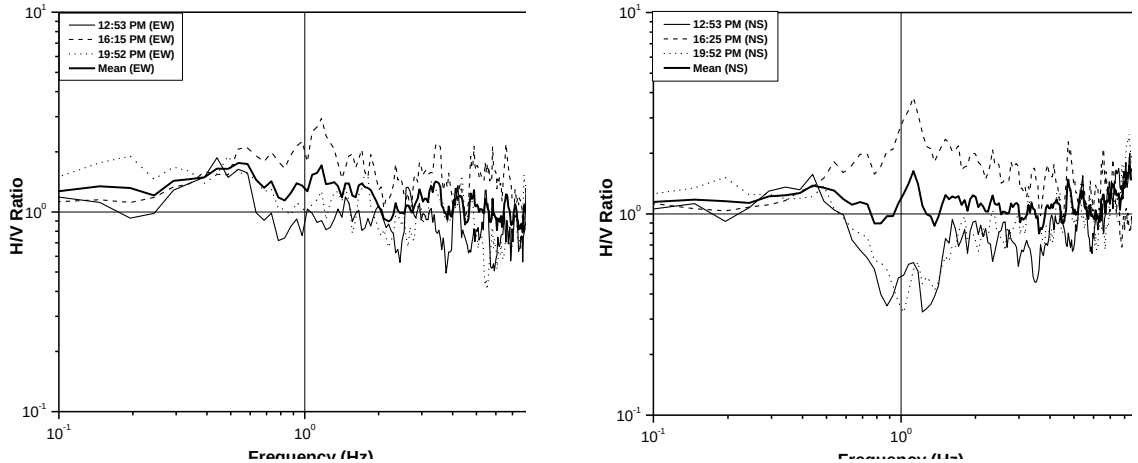

(c) MT10

Figure 3.15 [(a), (b) and (c)]: Stability of H/V ratio data at different times along EW and NS direction at MT08, MT09 and MT10.

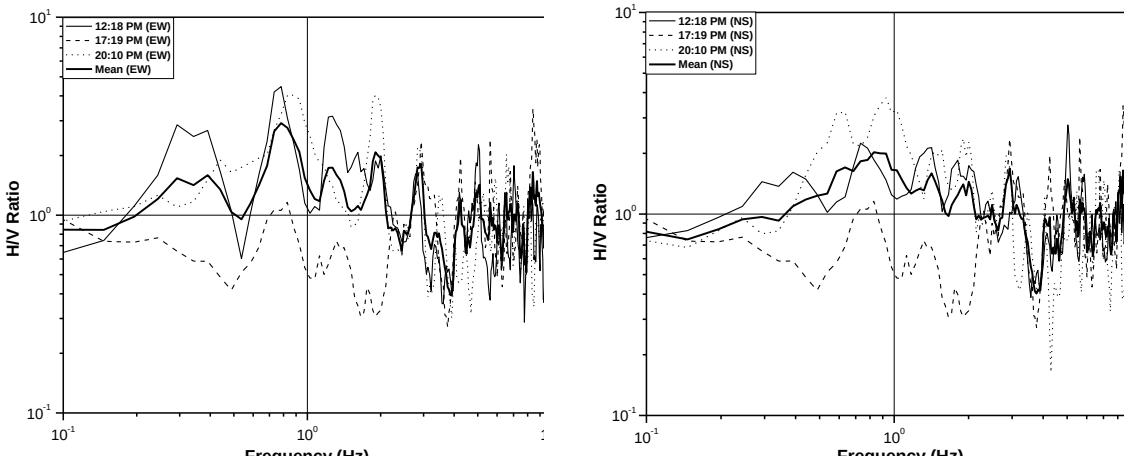

(a) MT11

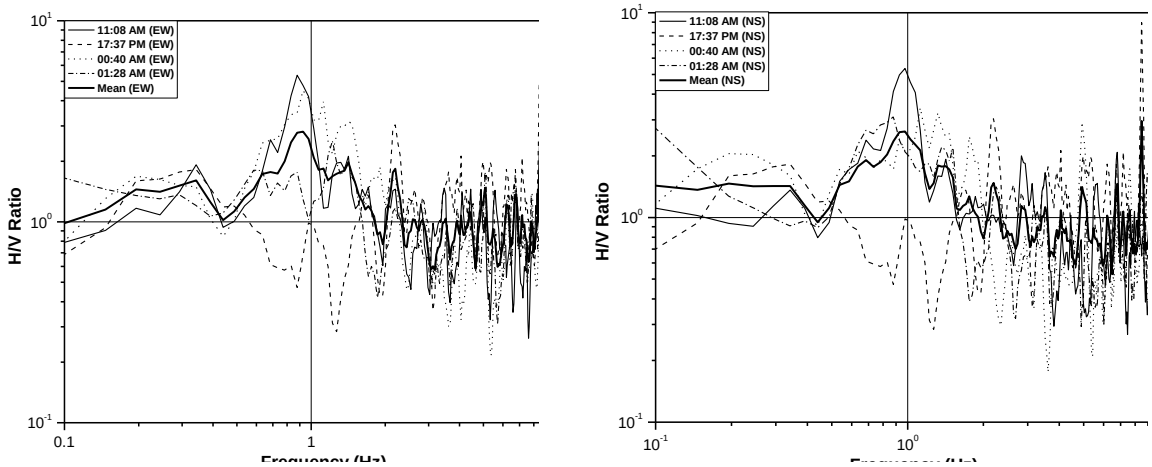

(b) MT12

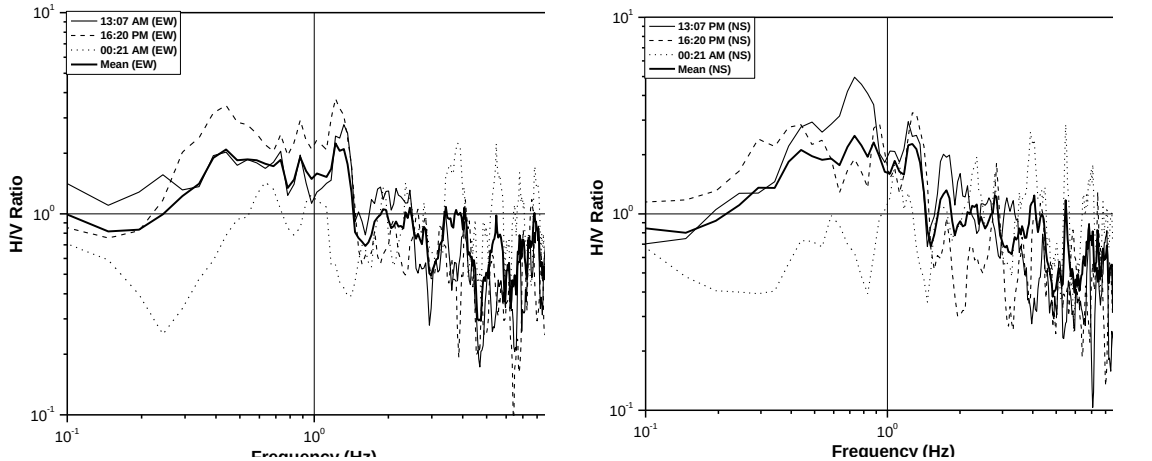

(c) MT13

Figure 3.16 [(a), (b) and (c)]: Stability of H/V ratio data at different times along EW and NS direction at MT11, MT12 and MT13.

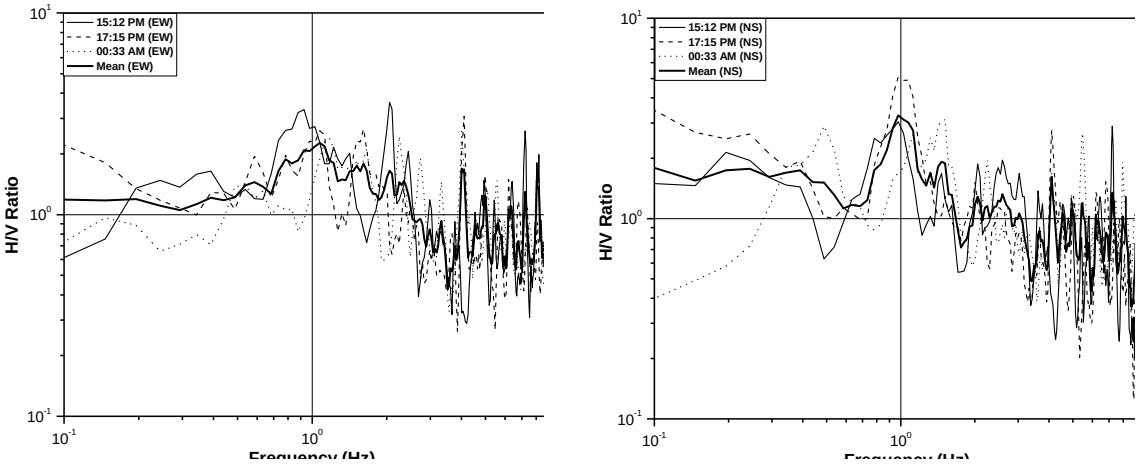

(a) MT15

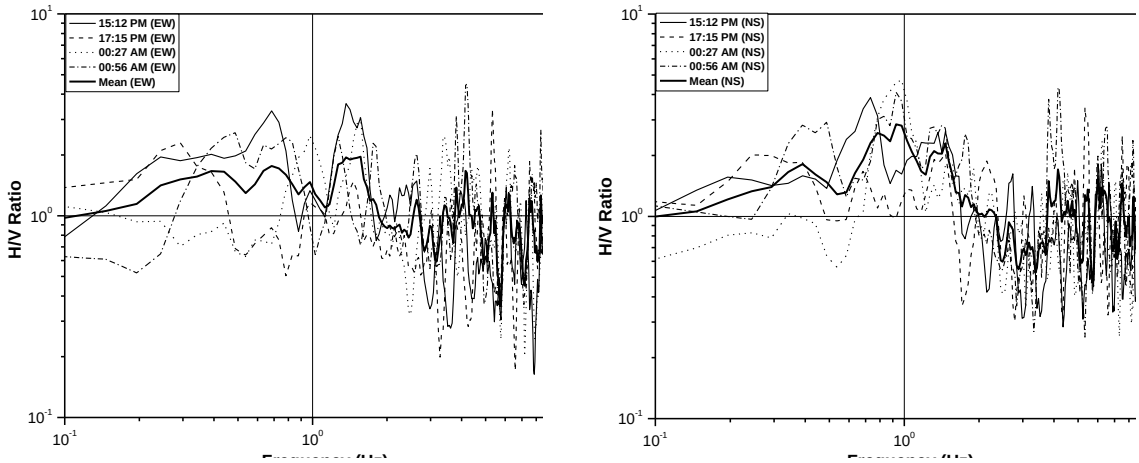

(b) MT16

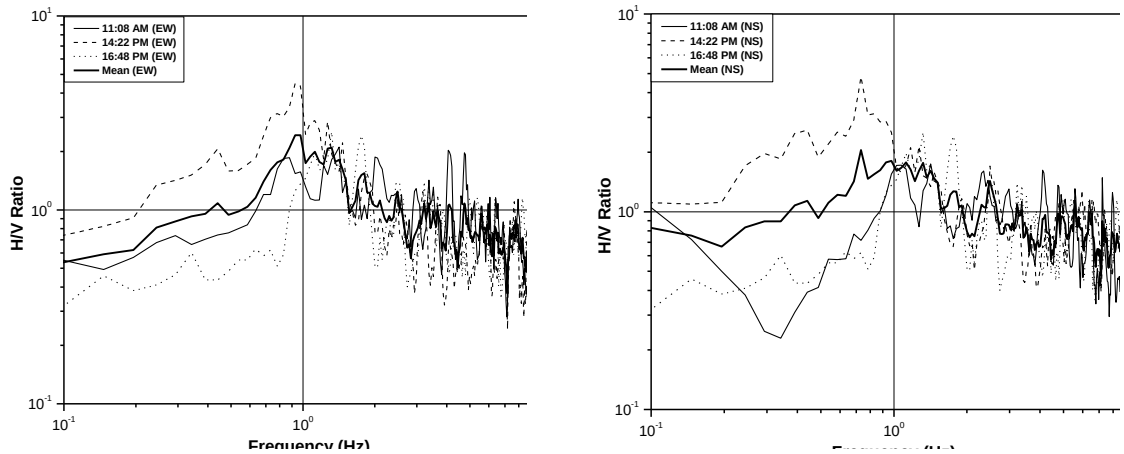

(c) MT19

Figure 3.17 [(a), (b) and (c)]: Stability of H/V ratio data at different times along EW and NS direction at MT15, MT16 and MT19.

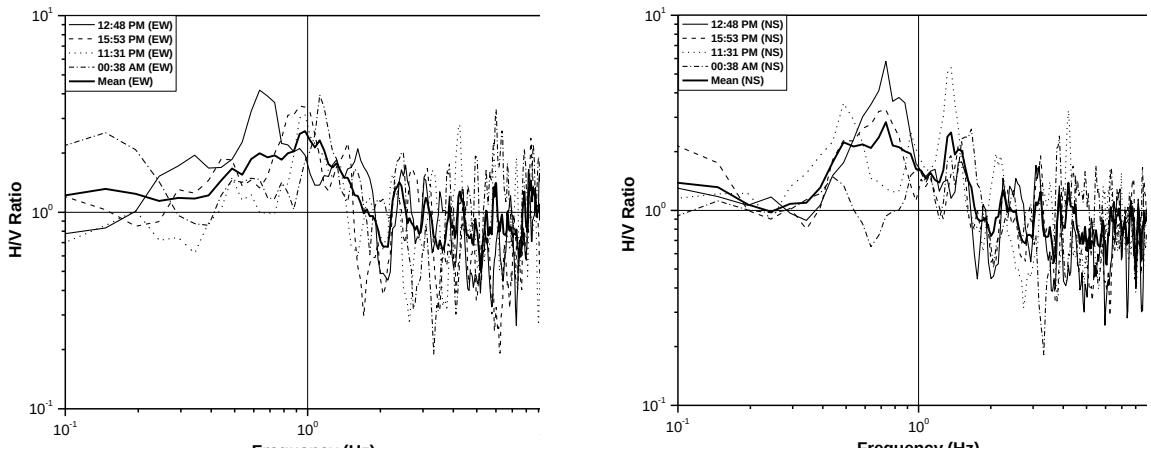

(a) MT22

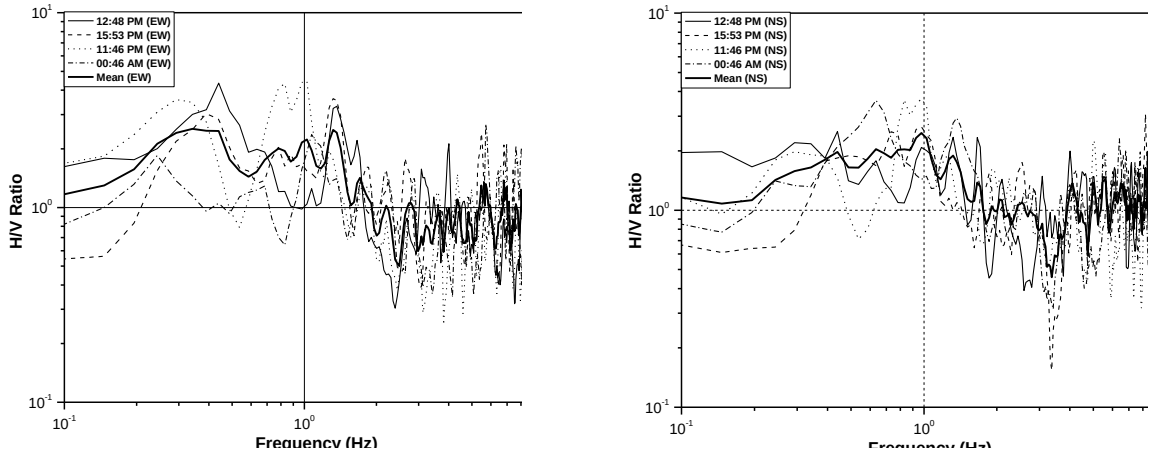

(b) MT23

Figure 3.18 [(a) and (b)]: Stability of H/V ratio data at different times along EW and NS direction at MT22 and MT23.

3.4.2 Resultant of H/V Ratio Curve

Microtremor H/V ratio has been found along East-West and North-South direction, respectively. To estimate Predominant frequency and H/V ratio resultant of two direction spectrum is necessary. Four resultant of two direction H/V ratio curve are RM, RMS, RS and mean. The resultant H/V ratio can be represented in four ways. These are follows:

(a) Root multiplication, RM:

RM = $\sqrt{HV_{EW} * HV_{NS}}$

(b) Root mean square, RMS:

RMS = $\sqrt{\frac{HV_{EW}^2+HV_{NS}^2}{2}}$

(c) Root square, RS:

RS = $\sqrt{HV_{EW}^2 + HV_{NS}^2}$

(d) Mean = $\frac{HV_{EW}+HV_{NS}}{2}$

Where,

HV_{EW} = Horizontal to Vertical Spectral Ratio along East-West direction

HV_{NS} = Horizontal to Vertical Spectral Ratio along North-South direction

The resultant H/V ratio has been shown from Figure 3.19 to Figure 3.21. These three graphs represent the comparison of H/V ratio resultant in four ways.

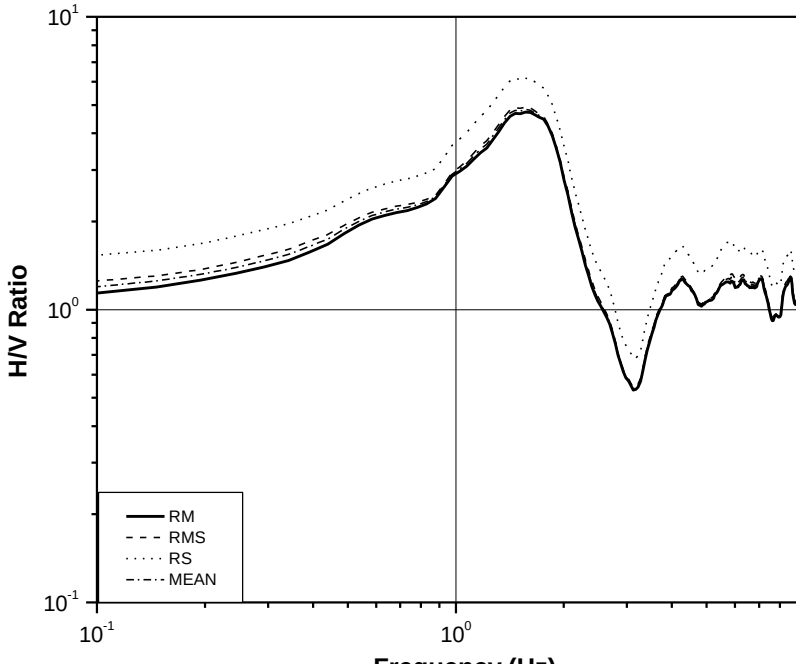

Figure 3.19: Comparision of RM, RMS, RS and MEAN resultant H/V ratio of EW and NS direction at Bashundhara, Block-D.

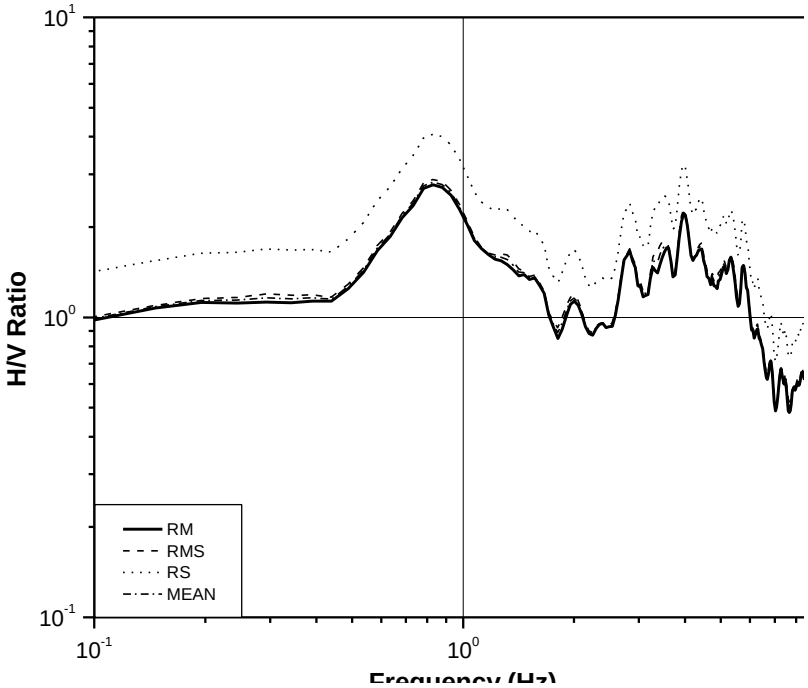

Figure 3.20: Comparision of RM, RMS, RS and MEAN resultant H/V ratio of EW and NS direction at Board Bazar, Gazipur.

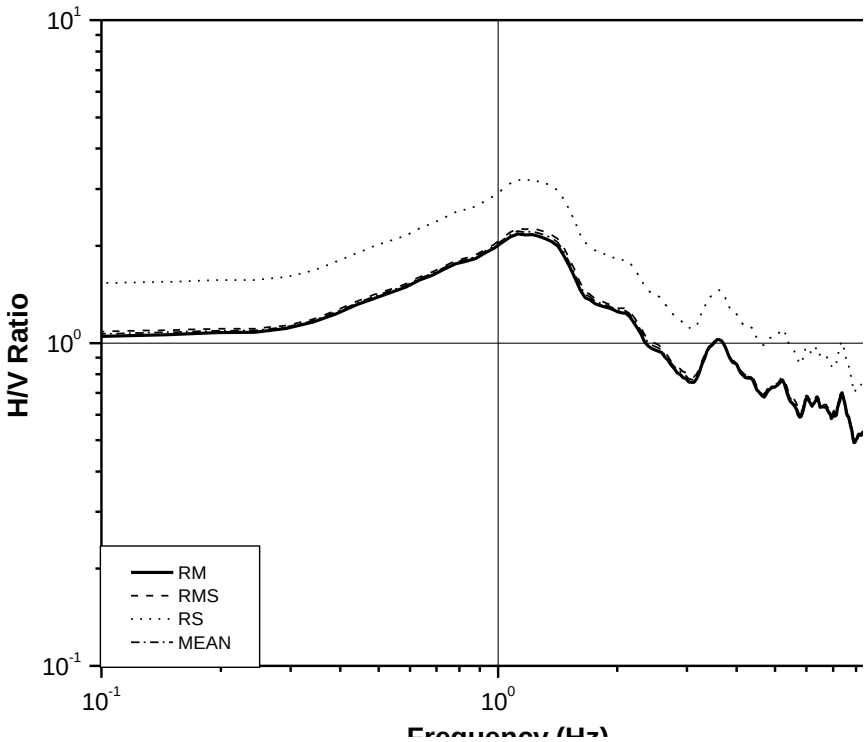

Figure 3.21: Comparision of RM, RMS, RS and MEAN resultant H/V ratio of EW and NS direction at Uttar Khan.

Figure 3.19 shows comparison of RM, RMS, RS and MEAN resultant H/V ratio of EW and NS direction at Bashundhara, Block-D. Figure 3.20 and 3.21 demonstrate comparison of H/V ratio in Board Bazar, Gazipur and Uttar Khan, respectively. From Figure 3.19 to Figure 3.21, it can be said that square root H/V ratio shows higher value than others. The RM, RS and mean H/V ratio show almost similar value. For this study, Root multiplication H/V ratio has been analyzed to estimate predominant frequency and H/V ratio.

3.4.3 Window Effect on Microtremor data

Fourier transformation using various analysis windows has significant effect on Horizontal to Vertical spectral ratio (H/V). The most common five types of analysis windows are Rectangular, Hanning, Hamming, Welch and Blackman windows. Fast Fourier transformation can be done in five time windows. The equations of five windows are shown from Equation 3.2 to Equation 3.6. These equations are follows:

1) Rectangular Window

$$W[n] = 1 \text{ for } 0 \leq n \geq N \text{ and zero otherwise} \tag{3.2}$$

2) Welch Window:

$$W[n] = 1 - \left[\frac{n - \frac{1}{2}(N-1)}{\frac{1}{2}(N+1)}\right]^2 \tag{3.3}$$

3) Hanning Window:

$$W[n] = \frac{1}{2}\left[1 - \cos\left(\frac{2\Pi n}{N-1}\right)\right] \tag{3.4}$$

4) Hamming Window

$$W[n] = 0.54 - 0.46 \cos\left(\frac{2\Pi n}{N-1}\right) \tag{3.5}$$

5) Blackman Window:

$$W[n] = 0.42 - 0.5 \cos\left(\frac{2\Pi n}{N-1}\right) + 0.08 \cos\left(\frac{4\Pi n}{N-1}\right) \tag{3.6}$$

Where,

W[n] = Windows function, n = Index number and N = Total number of data points

Figure 3.22 to 3.25 show the analysis result of microtremor data of three segments at Bramangaon. Microtremor Time history data of three segments has been Fourier transformed using five windows. Figure 3.22 shows the analysis result of segment 1 in five windows at Bramangaon. From Figure 3.22, rectangular window shows different H/V ratio result than other four windows. The other four H/V curve gives almost similar pattern. However, predominant frequency is same in all the five cases. Rectangular window gives lower peak value of H/V ratio than other methods at segment 2 (Figure 3.23). From Figure 3.24, the rectangular window shows similar predominant frequency and H/V ratios to other windows. The mean H/V ratio and predominant frequent of five methods are represented in Figure 3.25. According to Figure 3.25, the pattern of H/V ratio curve in rectangular window is similar to other four windows. From the analysis of mean H/V ratio curve in five windows, it can be said that rectangular window is more suitable than other windows to estimate predominant frequency and H/V ratio. Therefore, rectangular window is selected to analyze the microtremor data in this study. This rectangular windows is suitable than others to assess dynamic properties.

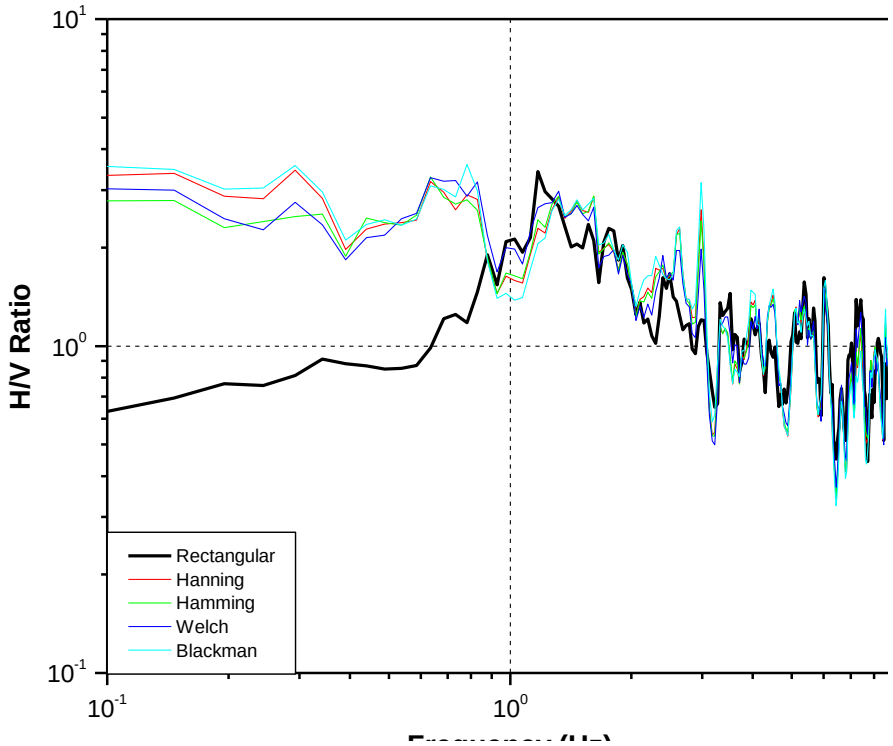

Figure 3.22: Five different windows effect on Microtremor data at segment 1 of Bramangaon.

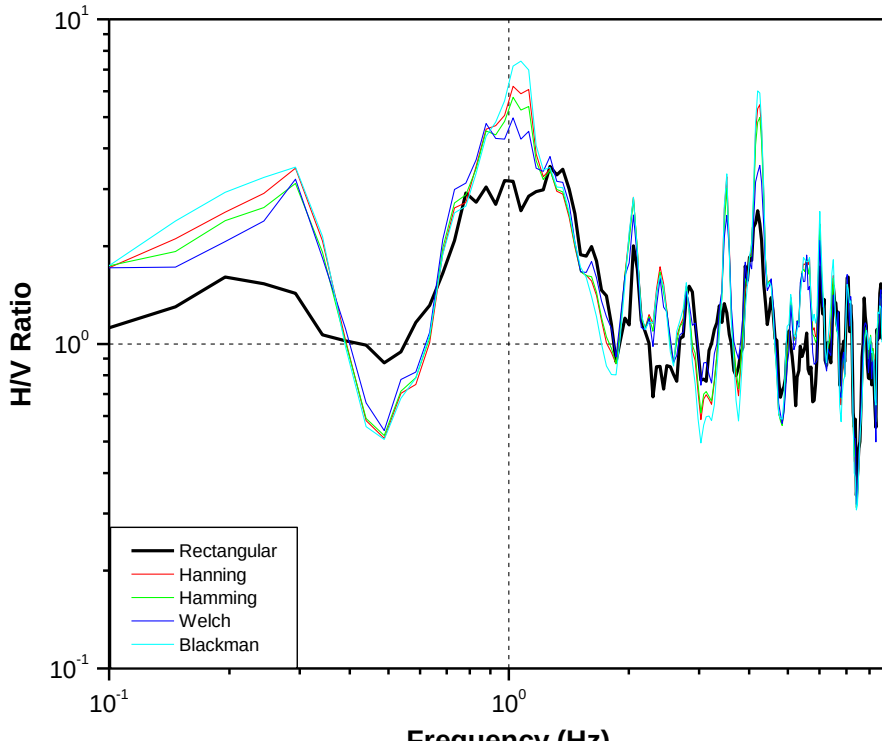

Figure 3.23: Five different windows effect on Microtremor data at segment 2 of Bramangaon.

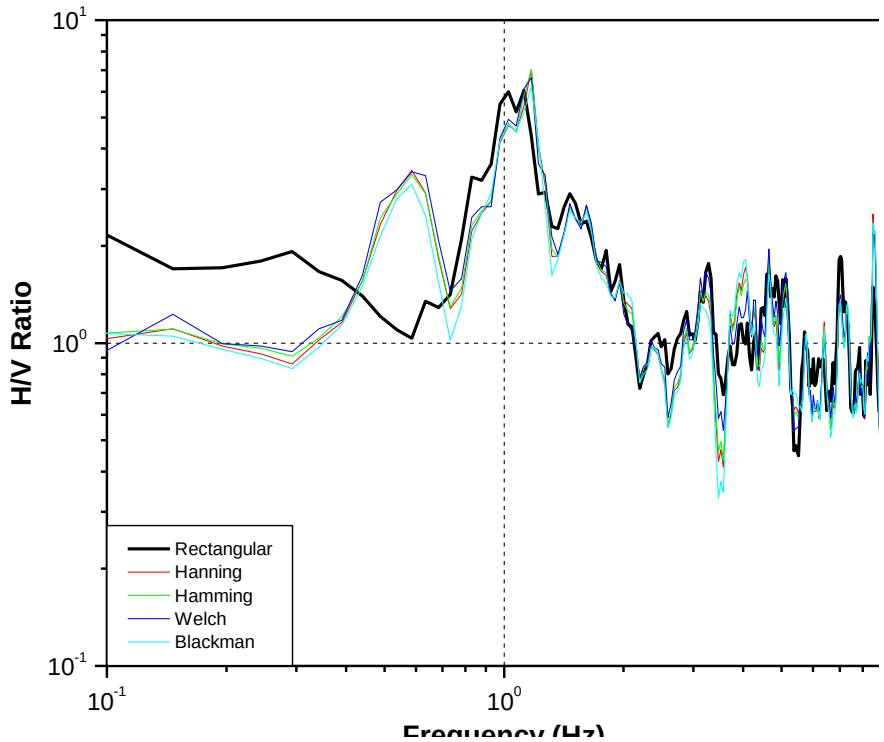

Figure 3.24: Five different windows effect on Microtremor data at segment 3 of Bramangaon.

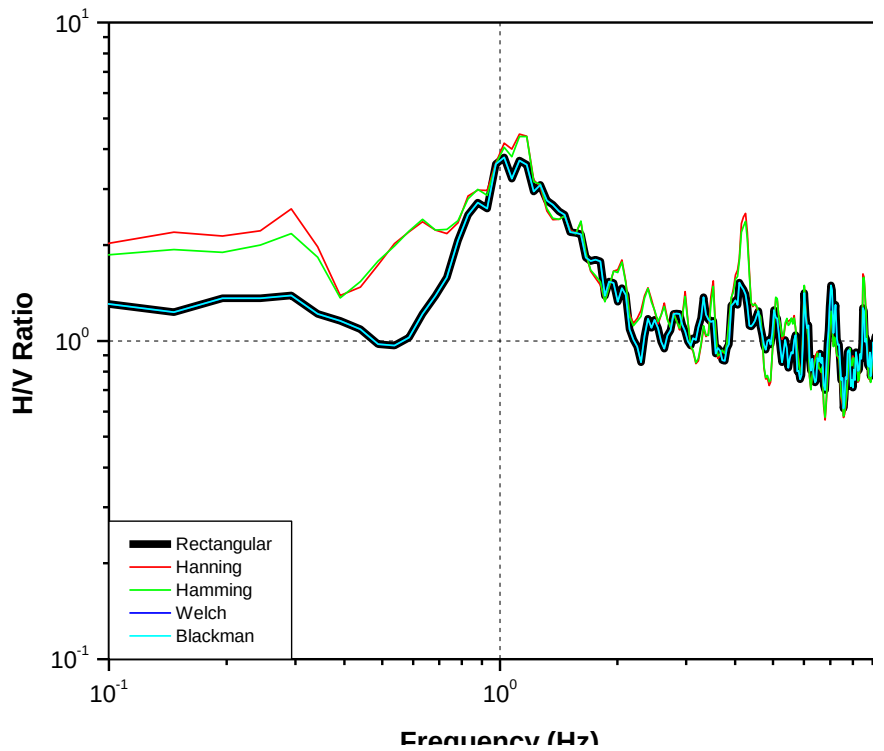

Figure 3.25: Five different windows effect on mean microtremor data at Bramangaon.

3.4.4 Smoothing Effect on Microtremor Data

Smoothing of microtremor data has significant effect to estimate predominant frequency and H/V ratio of any particular site. In some microtremor measurement locations, it is difficult to estimate dynamic properties. In that case, smoothing of data with suitable smoothing point gives accurate data. Therefore, almost all the microtremor locations data has been smoothed with suitable smoothing point. Generally, H/V ratio decreases and predominant frequency changes with the increase of smoothing point. So, proper justification is required before applying smoothing point on microtremor logarithmic window. Figure 3.26 to 3.29 show four mean microtremor data with smoothing effect. Different smoothing points have been applied to determine predominant frequency and H/V ratio. Figure 3.26 shows that the peak H/V becomes decreases due to applying different smoothing point. Figure 3.27, 3.28 and 3.29 illustrate the application of suitable smoothing point to determine Predominant frequency and H/V ratio of soil. It is difficult to determine predominant frequency and H/V ratio.

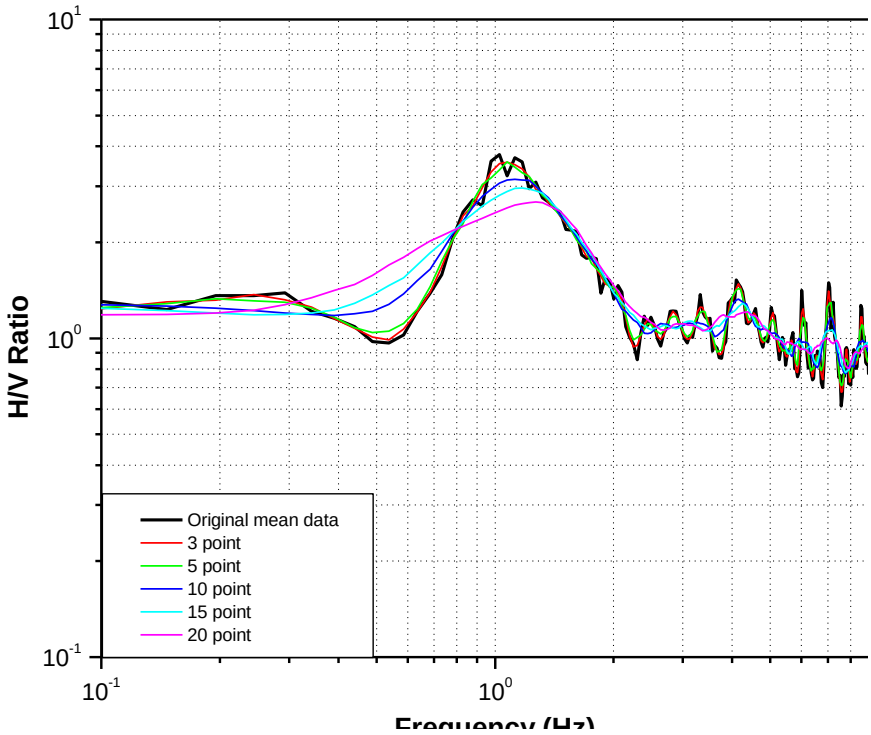

Figure 3.26: Variation of predominant frequency and H/V ratio due to smoothing effect at Bramangaon.

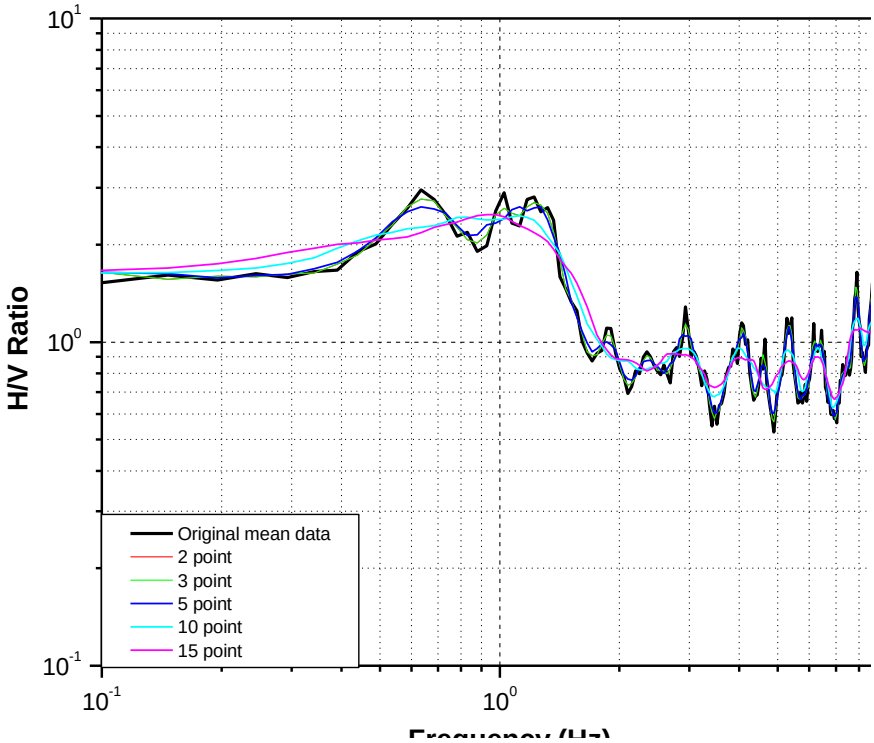

Figure 3.27: Variation of predominant frequency and H/V ratio due to smoothing effect at Tongi, Ershadnagar.

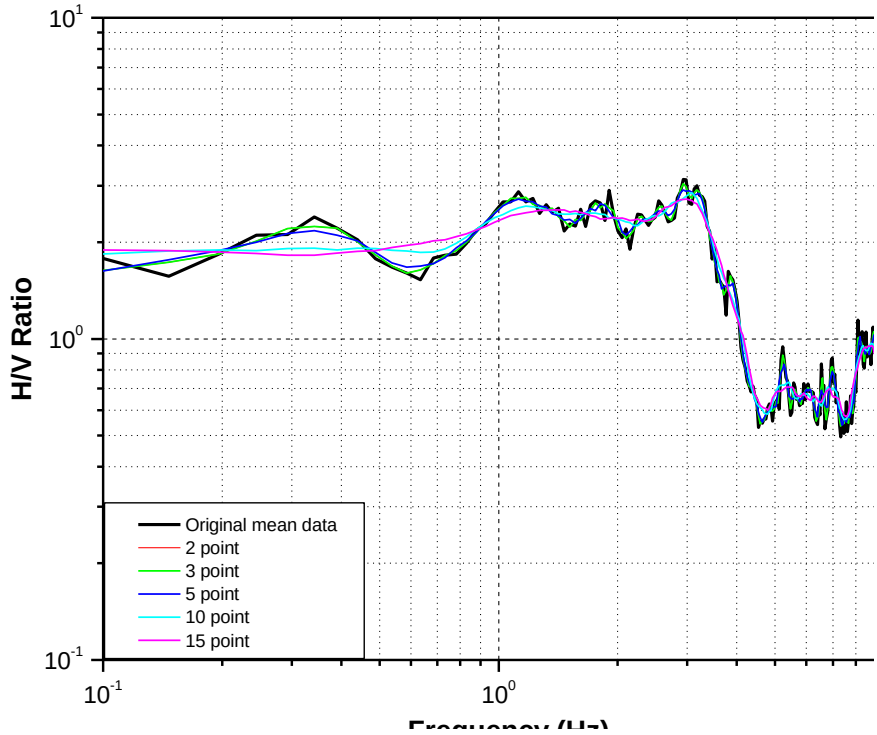

Figure 3.28: Variation of predominant frequency and H/V ratio due to smoothing effect at Ashiyan city.

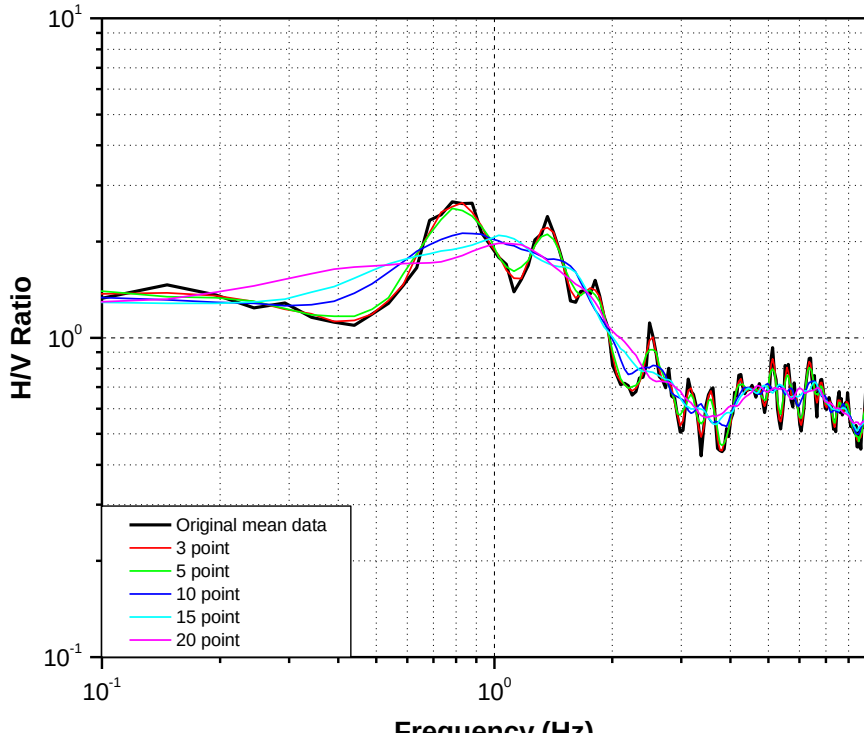

Figure 3.29: Variation of predominant frequency and H/V ratio due to smoothing effect at Agargaon Trade Fair.

3.5 ANALYSIS RESULT

Field time history microtremor data of 132 locations within BUET campus and 45 sites in and around Dhaka city has been analyzed according to section 3.4. The mean H/V ratio and standard deviation at 45 locations has been included in this chapter. The remains of analysis results of these locations are shown in APPENDIX-B. Microtremor analysis results at 132 locations in soil and 45 buildings within BUET campus are presented in this chapter. But, details Figures are illustrated in APPENDIX-C and APPENDIX-D.

3.5.1 Microtremor Analysis Result in and around Dhaka City

Microtremor measurement has been carried out in 45 locations at latitude lies from 23˚38′15.10″ to 23˚56′46.54″ and longitude lies from 90˚20′24.92″ to 90˚33′50″. Obtained velocity records are converted from time domain to frequency domain to get the Fourier Spectrum and it has been smoothed by using rectangular window with average smoothing point 5.

Table 3.16: Microtremor Test Location, Predominant Frequency and H/V ratio in and around the Dhaka city

Serial Number	ID	Location	Latitude	Longitude	Predominant Frequency	H/V Ratio (RM)
1	SBH-01	National University	23˚56´46.54″	90˚22´43.93″	1.24	2.59
2	SBH-02	Board Bazaar, Gazipur	23˚56´18″	90˚23´58″	0.82	2.73
3	SBH-03	Kaunia, Boro Bari, Moddopara	23˚55´37″	90˚23´03″	0.72	2.79
4	SBH-04	Tongi, Ershadnagar	23°54'48"	90°24'11"	0.97	2.51
5	SBH-05	Tongi BSCIC area	23°53'37.18"	90°25'13.35"	0.95	2.73
6	SBH-06	Abdullahpur	23˚52´31″	90˚24´01″	1.32	2.33
7	SBH-07(A)	Ijtema field (North and East side)	23˚53´31.13″	90˚23´53.39″	1.17	3.37
8	SBH-07 (B)	Ijtema Field (South and West side)	23˚52´59.96″	90˚23´37.91″	0.86	3.26
9	SBH-08	Ashulia Toll Plaza	23°53'25.40"	90°21'54.61"	1.14	1.75
10	SBH-9	Uttar Khan	23´52´30″	90˚25´28″	1.09	2.09
11	SBH-10(A)	Uttara Phase 3 (North side)	23˚52´22″	90˚21´40″	1.18	3.16
12	SBH-10(B)	Uttara Phase 3 (South side)	23˚51´15″	90˚21´16″	0.97	4.47
13	SBH-11	Azampur School, Uttara	23˚52´03″	90˚24´04″	3.65	2.73
14	SBH-12 (A)	Mirpur DOHS (South side)	23˚49´59″	90˚22´42″	1.54	2.46
15	SBH-12 (B)	Mirpur DOHS (North side)	23˚50´11″	90˚22´42″	1.21	3.44
16	SBH-13	Ashiyan city, Askona, Dakkhin Khan	23˚50´49″	90˚25´37″	1.12	3.19
17	SBH-14(A)	Purbachal-1, Randokpur Hazi bari, Rupganj	23˚45´03″	90˚31´17″	0.94	3.04
18	SBH-14(B)	Purbachal-2, American City	23˚49´33″	90˚33´50″	2.00	2.69
19	SBH-14(C)	Purbachal Picnic Park, Gazipur	23˚51´28″	90˚31´14″	1.34	2.23
20	SBH-15	Adjacent to Mirpur Zoo	23˚49´04.14″	90˚20´29.63″	1.52	2.43
21	SBH-16	Field Ground, Pallabi	23˚49´06″	90˚22´08″	1.24	2.64
22	SBH-17 (A)	Block-B, Basundhara	23˚48´38″	90˚25´54″	2.09	3.12
23	SBH-17 (B)	Block-D, Basundhara	23˚49´00.49″	90˚26´12.95″	1.57	4.71
24	SBH-17 (C)	Block-H, Basundhara	23˚49´19″	90˚26´34″	2.52	2.94

Serial Number	ID	Location	Latitude	Longitude	Predominant Frequency	H/V Ratio (RM)
25	SBH-18	Civil Aviation Quarter	23^{0}50′33.61″	90^{0}25′11.22″	0.64	3.70
26	SBH-19	Kuril Flyover	23˚49′41.51″	90˚26′32.06″	1.97	2.73
27	SBH-20	Sarengbari, Mipur-2	23˚48′03.24″	90˚20′47.10″	0.59	2.84
28	SBH -21	Purachal, Uttar Badda	23˚46′51″	90˚26′29″	2.11	2.59
29	SBH-22	City Corporation, Gabtoli	23˚46′41.99″	90˚20′24.92″	0.82	3.67
30	SBH-23	Adabor	23˚46′09.75″	90˚21′37.62 ″	3.35	2.26
31	SBH-24	Agargoan Trade Fair area	23˚46′10.56″	90˚22′42.73″	0.86	2.12
32	SBH-25	Aftab Nagar Housing Project	23˚46′04.98″	90˚26′03.22″	0.95	2.76
33	SBH-26	Umme Had Nagar, Nadda	23˚47′57.17″	90˚25′41.61″	1.32	3.83
34	SBH-27	South Banasree	23˚45′07.17″	90˚26′45.36″	1.39	3.86
35	SBH-28	Basila Garden City	23˚45′10.29″	90˚20′42.36″	1.12	4.47
36	SBH-29	Royer Bazar Boddhobumi	23˚44′54″	90˚21′28″	2.57	1.08
37	SBH-30	Kalunagar, Hazaribagh	23˚43′38.50″	90˚22′08.62″	0.83	3.86
38	SBH-31	Rab-10, Plot, Kamrangirchar	23˚42′57.58″	90˚22′42.11″	0.48	3.91
39	SBH-32	Sosan Ghat, Kamrangirchar	23˚42′44.81"	90˚23′26.51″	1.21	4.78
40	SBH-33	Basundhara River view	23˚39′10″	90˚26′09″	1.05	3.51
41	SBH-34	Matuail, Demra	23˚43′18.24″	90˚28′16.48″	2.77	2.48
42	SBH-35	Jilmil Project, Equria	23˚40′33.40″	90˚24′08.42″	1.00	3.26
43	SBH-36	Rajendapur	23˚39′25″	90˚22′58″	1.17	2.59
44	SBH-37	Bramangaon	23˚38′15.10″	90˚27′37.35″	1.08	3.55
45	SBH-38	Meradia, Uttar Banasree	23˚45′43.57″	90˚26′19.67″	1.26	2.84

Table 3.16 shows predominant frequency and square root of Horizontal to Vertical spectral ratio (H/V) at 45 locations in and around the Dhaka city. The locations, latitude and longitude of 45 locations are also demonstrated in Table 3.16. Figure B3.30 represents the comparison of predominant frequency and H/V ratio among these locations. Details of predominant frequency, mean H/V ratio and standard deviation are

illustrated from Figure B3.31 to Figure A3.75. The basic six H/V ratio, square root of H/V ratio in three segments and their mean H/V ratio are also illustrated in APPENDIX-B.

Table 3.16 shows the predominant frequency and H/V ratio at 45 locations. Out of 45 microtremor observation locations, the maximum predominant frequency is 3.65 Hz, where H/V ratio is 2.73, at Azampur School, Uttara (Lat. 23˚52´03″ and Long. 90˚24´04″). The geology of this location is Upper Modhupur terrace (Figure 3.2) and Moderately High Pleistocene terrace (Figure 3.3). Figure 3.30 shows the Horizontal to Vertical spectral ratio (H/V) ranging between 1.81 and 3.74. The basic six H/V ratio in three segments along EW and NS direction, H/V ratio of three segments and their mean value are shown in Figure B3.43. On the other hand, the minimum predominant frequency is 0.48 Hz, where H/V ratio is 3.91, Rab-10, Plot, Kamrangirchar (Lat. 23˚42´57.58″and Long. 90˚22´42.11″). This location is classified as River Bar (Figure 3.2) and Moderately Thick fill (Figure 3.3). Figure 3.31 demonstrates square root of Horizontal to Vertical spectral ratio (H/V) ranging between 2.23 and 5.65.

From Table 3.16, the maximum Horizontal to Vertical spectral ratio (H/V) is 4.78 where as predominant frequency is 1.22 Hz, at Sosan Ghat, Kamrangirchar (Lat. 23˚42´44.81"and Long. 90˚23´26.51″). The geology of this site is flood plain (Figure 3.2) and thick fill (Figure 3.3). Figure 3.32 shows Horizontal to Vertical spectral ratio (H/V) ranging between 4.07 and 5.71. The basic six H/V ratio in three segments along EW and NS direction, H/V ratio of three segments and their mean value are shown in Figure B3.69. The minimum Horizontal to Vertical spectral ratio (H/V) is 1.08 where as predominant frequency is 2.57 Hz at Royer Bazar (Lat. 23˚44´54″and Long. 90˚21´28″). The geology of this location is River Bar (Figure 3.2) and gently sloping Erosional terrace edge (Figure 3.3). Figure 3.33 shows Horizontal to Vertical spectral ratio (H/V) ranging between 0.87 and 1.28. The basic six H/V ratio in three segments along EW and NS direction, H/V ratio of three segments and their mean value are illustrated in Figure B3.66.

Out of 45 locations, the overall predominant frequency is 1.25 Hz with standard deviation 0.014. On the other hand, the overall H/V ratio is 2.72 with standard deviation 0.177. The predominant frequency of 45 locations has been classified into five types which are **Type**

I (0 – 0.49), **Type II** (0.50 – 0.99), **Type III** (1.0 – 1.99), **Type IV** (2.0 – 2.99) and **Type V** (> 3.00).

The classifications of predominant frequency at 45 locations are as follows:

Type I: SBH-31

Type II: SBH-02, SBH-03, SBH-04, SBH-05, SBH-07(B), SBH-10(B), SBH-14(A), SBH-18, SBH-20, SBH-22, SBH-24, SBH-25 and SBH-30.

Type III: SBH-01, SBH-06, SBH-07(A), SBH-08, SBH-09, SBH-10(A), SBH-12(A), SBH-12(B), SBH-13, SBH-14(C), SBH-15, SBH-16, SBH-17(B), SBH-19, SBH-26, SBH-27, SBH-28, SBH-32, SBH-33, SBH-35, SBH-36, SBH-37 and SBH-38.

Type IV: SBH-14(B), SBH-17(A), SBH-17(C), SBH-21, SBH-29 and SBH-34.

Type V: SBH-11 and SBH-23.

From this classification of predominant frequency, it can be said that most of the locations predominant frequency varies from 1.0 Hz to 1.99 Hz. These are classified as **Type III**. This classifications show the second most common predominant frequency ranging between 0.50 and 0.99. The number of locations predominant frequency ranging between 2.0 and 2.99 is six**.** Only SBH-31 is classified as **Type I** predominant frequency**.**

On the other hand, Horizontal to Vertical spectral ratio (H/V) has been classified into four types. **Type I** (0-0.99), **Type II** (1.0 – 1.99), **Type III** (2.0 – 2.99) and **Type IV** (>3.0).

The classifications of H/V ratio at 45 locations are as follows:

Type I: None

Type II: SBH-08, SBH-12(B), SBH-14(C), SBH-15, SBH-16, SBH-17(B), SBH-29 and SBH-39.

Type III: SBH-01, SBH-02, SBH-03, SBH-04, SBH-05, SBH-06, SBH-09, SBH-11, SBH-12(A), SBH-14(B), SBH-17(A), SBH-17(C), SBH-19, SBH-20, SBH-21, SBH-23, SBH-24, SBH-25, SBH-34, SBH-36 and SBH-38.

Type IV: SBH-07(A), SBH-07(B), SBH-10(A), SBH-10(B), SBH-13, SBH-14(A), SBH-18, SBH-22, SBH-26, SBH-27, SBH-28, SBH-30, SBH-31, SBH-32, SBH-33, SBH-37 and SBH-39.

From the above classification of H/V ratio, the common H/V ratio is **Type III** in 45 locations. The second most common H/V ratio is **Type IV.** The number of locations H/V ratio ranging between 1.0 and 1.99 is eight.

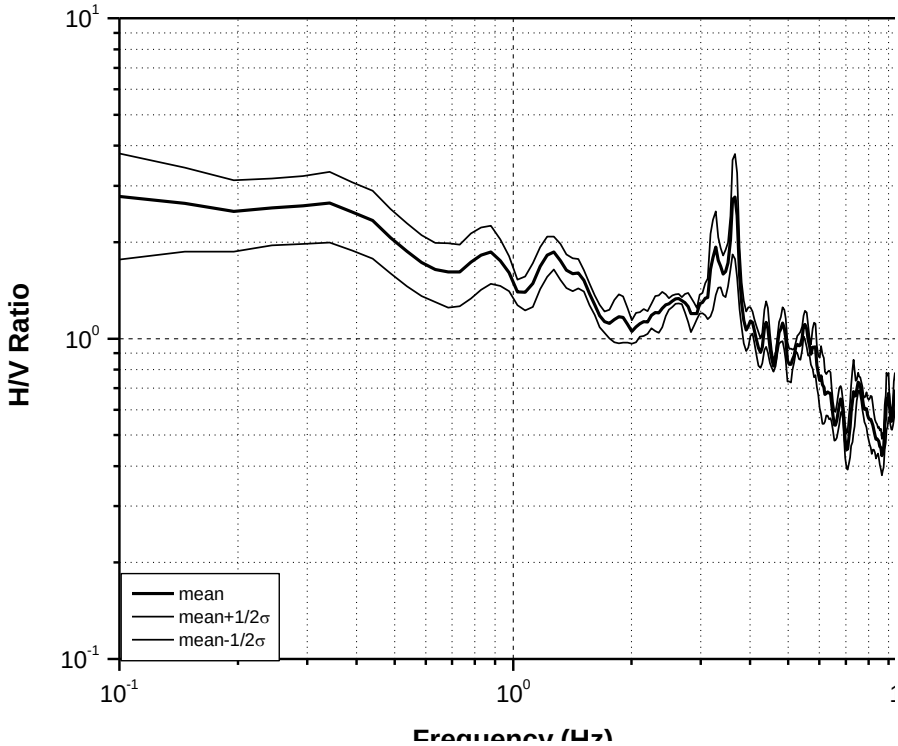

Figure 3.30: Predominant frequency and H/V ratio at Uttara Azampur.

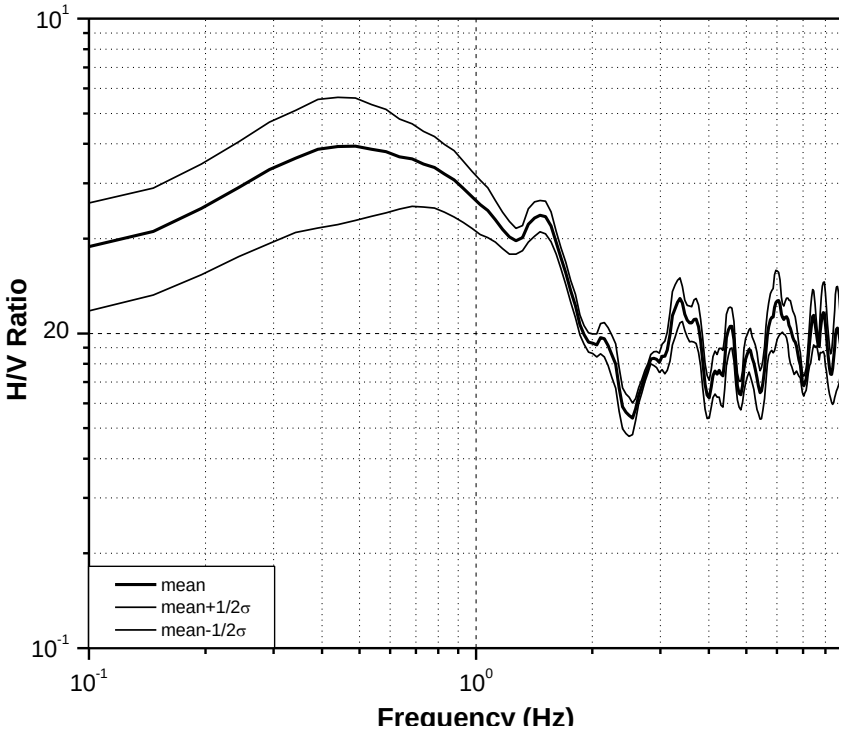

Figure 3.31: Predominant frequency and H/V ratio at Rab-10 Plot, Kamrangirchar.

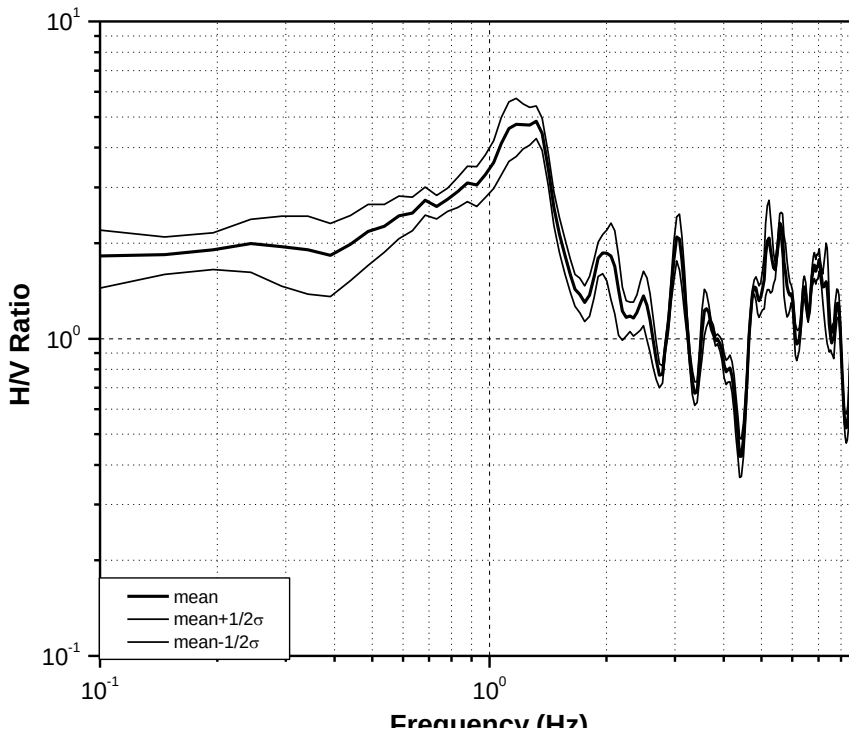

Figure 3.32: Predominant frequency and H/V ratio at Sosan Ghat, Kamrangirchar.

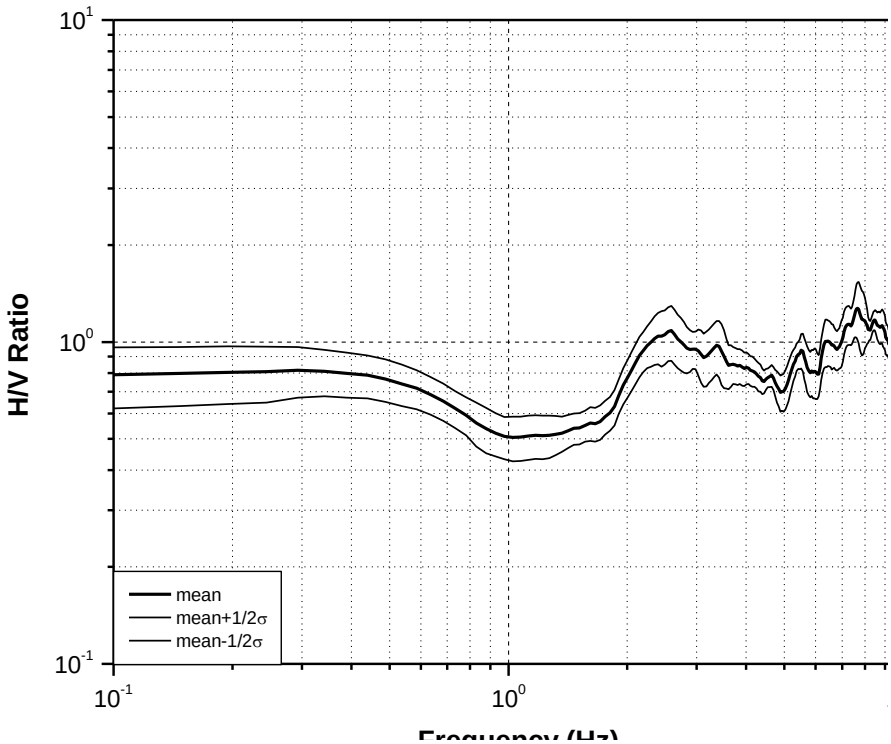

Figure 3.33: Predominant frequency and H/V ratio at RoyerBazar.

3.5.2 Microtremor Analysis Result within BUET Campus

The BUET campus is situated in latitude ranging from 23°43'16.58" N to 23°43'59.44" N and longitude from 90°23'13.31"E to 90°23'43.56" E. Microtremor observation at 132 selected points in soil and 45 locations in building have been carried out in BUET campus. The analysis results of these points are shown in this chapter and APPENDIX-C and APPENDIX-D.

3.5.2.1 Soil Sites

Table 3.17 shows predominant frequency and RM value of H/V ratio of 132 locations. Figure 3.34 demonstrates the observed microtremor locations at 132 selected locations. The details analysis results at 132 points are illustrated in APPENDIX-C from Figure C3.76 to Figure C3.207.

Out of 132 sites, the overall mean predominant frequency is 1.39 Hz where as standard deviation is 0.289. On the other hand, the overall peak mean H/V ratio is 2.09 where as standard deviation is 0.523.

Table 3.17 shows the predominant frequency and mean H/V ratio in 132 locations. Out of 132 microtremor observation locations, the maximum predominant frequency is around 9.62 Hz where as H/V ratio is 2.43 at MT82. The geology of this site is Upper Modhupur terrace (Figure 3.2) and Higher Pleistocene Terrace (Figure 3.3). Figure 3.35 (f) and C3.157 shows Horizontal to Vertical spectral ratio (H/V) ranging from 1.65 to 2.51. The basic six H/V ratio in three segments along EW and NS direction, square root of H/V ratio of three segments and their mean value are also shown in Figure C3.157. On the other hand, the minimum predominant frequency is around 0.25 Hz where as H/V ratio is 9.51 at MT72. This is the highest peak of H/V ratio in 132 selected locations in BUET campus. Figure 3.35(e) and Figure C3.147 demonstrates Horizontal to Vertical spectral ratio (H/V) ranging between 6.85 and 11.85. This lower predominant frequency and higher amplification ratio show that this site is highly susceptible due to any seismic hazard.

The predominant frequency of 132 locations has also been classified into five types. **Type I** (0 – 0.49), **Type II** (0.50 – 0.99), **Type III** (1.0 – 1.99), **Type IV** (2.0 – 2.99) and **Type V** (> 3.00).

The classifications of predominant frequency at 45 locations are as follows:

Type I: MT 02, MT 14, MT 17, MT 36, MT 62, MT 67, MT 72, MT 76, MT 77, MT 78, MT 80, MT 83, MT 84, MT 86, MT 108 and MT 120.

Type II: MT 03, MT 04, MT 05, MT 06, MT 11, MT 12, MT 15, MT 16, MT 18, MT 19, MT 22, MT 23, MT 24, MT 29, MT 30, MT 35, MT 41, MT 47, MT 48, MT 51, MT 52, MT 54, MT 56, MT 71, MT 79, MT 81, MT 85, MT 93, MT 99, MT 101, MT 103, MT 109 and MT 111.

Type III: MT 01, MT 07, MT 08, MT 09, MT 10, MT 13, MT 20, MT 21, MT 25, MT 26, MT 33, MT 34, MT 37, MT 38, MT 39, MT 40, MT 43, MT 44, MT 45, MT 46, MT 49, MT 50, MT 53, MT 58, MT 59, MT 60, MT 61, MT 63, MT 64, MT 65, MT 74, MT 87, MT 88, MT 90, MT 98, MT 102, MT 104, MT 106, MT 107, MT 110, MT 112, MT 113, MT 114, MT 115, MT 116, MT 121, MT 122, MT 128, MT 129, MT 130 and MT 132.

Type IV: MT 27, MT 28, MT 66, MT 89, MT 95, MT 105, MT 118, MT 119 and MT 123.

Type V: MT 31, MT 32, MT 42, MT 55, MT 57, MT 68, MT 69, MT 70, MT 73, MT 75, MT 82, MT 91, MT 94, MT 96, MT 97, MT 100, MT 117, MT 124, MT 125, MT 126 and MT 131.

From this classification of predominant frequency, it can be said that most of the locations predominant frequency ranging between 1.0 Hz and 1.99 Hz. These predominant frequencies are classified as **Type III**. The second most common type of predominant frequency is **Type II.** The number of locations predominant frequency classified as Type V is 21. In addition to this, there are sixteen Type I locations.

On the other hand, Horizontal to Vertical spectral ratio (H/V) has been classified into four types. **Type I** (0 - 0.99), **Type II** (1.0 - 1.99), **Type III** (2.0 - 2.99) and **Type IV** (>3.0).

The classifications of H/V ratio at 132 locations are as follows:

Type I: None

Type II: MT 01, MT 09, MT 10, MT 19, MT 20, MT 27, MT 28, MT 38, MT 47, MT 52, MT 58, MT 61, MT 66, MT 67, MT 68, MT 69, MT 70, MT 71, MT 73, MT 74, MT 75, MT 76, MT 77, MT 78, MT 80, MT 85, MT 86, MT 90, MT 91, MT 94, MT 97, MT 100, MT 104, MT 105, 108, MT 116, MT 117, MT 123, MT 124, MT 126, MT 127, MT 128 and MT 129.

Type III: MT 03, MT 04, MT 08, MT 11, MT 12, MT 13, MT 14, MT 15, MT 16, MT 17, MT 18, MT 21, MT 22, MT 23, MT 24, MT 25, MT 29, MT 30, MT 31, MT 32, MT 33, MT 34, MT 35, MT 37, MT 40, MT 41, MT 42, MT 43, MT 44, MT 45, MT 46, MT 48, MT 49, MT 50, MT 51, MT 53, MT 54, MT 55, MT 56, MT 57, MT 59, MT 63, MT 64, MT 65, MT 71, MT 79, MT 81, MT 82, MT 83, MT 87, MT 89, MT 92, MT 93, MT 95, MT 96, MT 98, MT 99, MT 102, MT 106, MT 107, MT 110, MT 111, MT 112, MT 113, MT 114, MT 115, MT 118, MT 119, MT 120, MT 121, MT 122, MT 125, MT 130, MT 131 and MT 132.

Type IV: MT 02, MT 05, MT 06, MT 07, MT 26, MT 36, MT 39, MT 60, MT 62, MT 72, MT 84, MT 88, MT 101, MT 103 and MT 109.

According to the above classification of H/V ratio, most of the selected locations are classified as **Type III.** There are seventy five Type III locations. **Type II** is the second most predominant H/V ratio. There is no H/V ratio ranging between 0 and 0.99. The number of locations H/V ratio greater than 3 is 15.

From Table 3.17, the minimum mean Horizontal to Vertical spectral ratio (H/V) is 1.24 where as predominant frequency is around 0.29 at MT 108. Figure 3.35(h) shows the Horizontal to Vertical spectral ratio (H/V) ranging between 0.93 and 1.56. The basic six H/V ratio in three segments along EW and NS direction, H/V ratio of three segments and their mean value are illustrated in Figure C3.183.

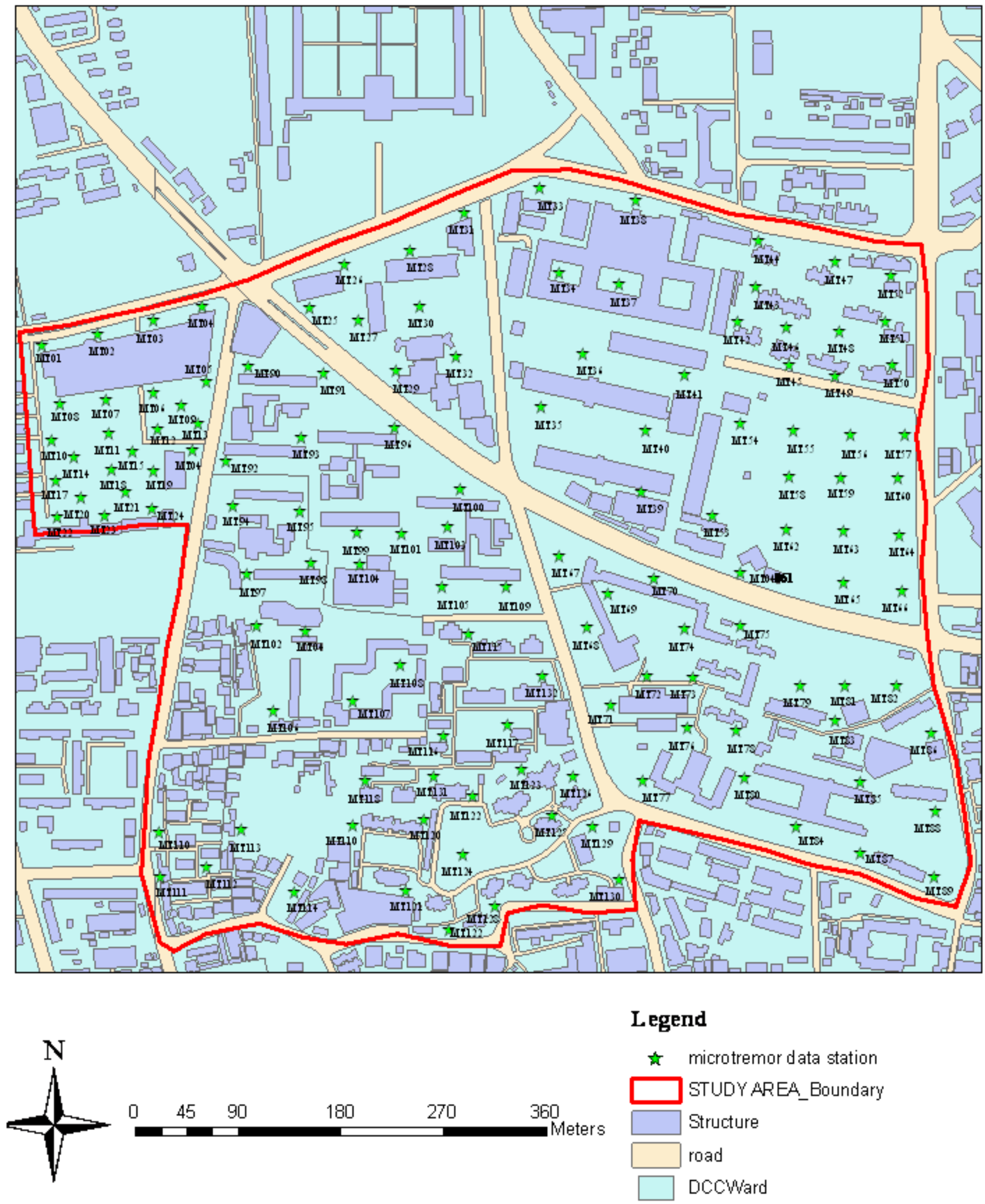

Figure 3.34: 132 Microtremor observation points in specific location of BUET campus.

Table 3.17: Microtremor Test Location, Predominant Frequency and H/V Ratio within at 132 selected locations in soil within BUET campus

Serial Number	ID	Predominant Frequency	H/V Ratio (RM)	Serial Number	ID	Predominant Frequency	H/V Ratio (RM)
1	MT-01	1.59	1.72	2	MT-02	0.35	3.37
3	MT-03	0.94	2.88	4	MT-04	0.70	2.29
5	MT-05	0.73	4.20	6	MT-06	0.90	3.27
7	MT-07	1.23	3.0	8	MT-08	1.21	2.94
9	MT-09	1.13	1.89	10	MT-10	1.14	1.48
11	MT-11	0.82	2.33	12	MT-12	0.94	2.38
13	MT-13	1.27	2.12	14	MT-14	0.45	2.88
15	MT-15	1.03	2.53	16	MT-16	1.45	2.00
17	MT-17	0.45	2.38	18	MT-18	0.97	2.79
19	MT-19	0.98	1.89	20	MT-20	1.03	1.97
21	MT-21	1.31	2.46	22	MT-22	0.70	2.48
23	MT-23	0.93	2.31	24	MT-24	0.92	2.53
25	MT-25	1.13	2.48	26	MT-26	1.34	3.13
27	MT-27	2.26	1.65	28	MT-28	2.44	1.87
29	MT-29	1.23	2.73	30	MT-30	1.31	2.67
31	MT-31	3.65	2.12	32	MT-32	3.98	2.03
33	MT-33	1.37	2.14	34	MT-34	1.21	2.06
35	MT-35	0.57	2.88	36	MT-36	0.48	3.67
37	MT-37	1.24	2.31	38	MT-38	1.23	1.89
39	MT-39	1.24	3.74	40	MT-40	1.27	2.38
41	MT-41	0.65	2.03	42	MT-42	3.81	2.31
43	MT-43	1.35	2.79	44	MT-44	1.31	2.33

Serial Number	ID	Predominant Frequency	H/V Ratio (RM)	Serial Number	ID	Predominant Frequency	H/V Ratio (RM)
45	MT-45	1.07	2.29	46	MT-46	1.27	2.31
47	MT-47	0.66	1.41	48	MT-48	0.77	2.73
49	MT-49	1.24	2.59	50	MT-50	1.27	2.03
51	MT-51	0.82	2.00	52	MT-52	0.84	1.85
53	MT-53	1.15	2.70	54	MT-54	0.85	2.19
55	MT-55	3.02	2.00	56	MT-56	0.50	2.48
57	MT-57	7.31	2.17	58	MT-58	1.65	1.60
59	MT-59	1.30	2.45	60	MT-60	1.29	3.23
61	MT-61	1.27	1.74	62	MT-62	0.40	6.20
63	MT-63	1.29	2.97	64	MT-64	1.34	2.21
65	MT-65	1.24	2.14	66	MT-66	2.75	1.68
67	MT-67	0.39	1.98	68	MT-68	5.80	1.58
69	MT-69	7.06	1.41	70	MT-70	4.89	1.65
71	MT-71	0.80	2.14	72	MT-72	0.25	9.51
73	MT-73	3.13	1.75	74	MT-74	1.37	1.85
75	MT-75	4.89	1.59	76	MT-76	0.38	1.27
77	MT-77	0.34	1.94	78	MT-78	0.34	1.48
79	MT-79	0.83	2.51	80	MT-80	0.34	1.58
81	MT-81	0.96	2.03	82	MT-82	9.62	2.43
83	MT-83	0.44	2.43	84	MT-84	0.42	4.38
85	MT-85	0.94	1.98	86	MT-86	0.39	1.29
87	MT-87	0.82	2.38	88	MT-88	0.90	3.37
89	MT-89	1.28	2.35	90	MT-90	0.91	1.77
91	MT-91	3.72	1.65	92	MT-92	0.87	2.67

Serial Number	ID	Predominant Frequency	H/V Ratio (RM)	Serial Number	ID	Predominant Frequency	H/V Ratio (RM)
93	MT-93	0.74	2.70	94	MT-94	3.10	1.31
95	MT-95	2.75	2.19	96	MT-96	3.38	2.12
97	MT-97	4.45	1.95	98	MT-98	1.27	2.48
99	MT-99	0.64	2.33	100	MT-100	7.5	1.51
101	MT-101	0.92	3.19	102	MT-102	1.27	2.35
103	MT-103	0.52	4.97	104	MT-104	2.64	1.61
105	MT-105	2.54	1.35	106	MT-106	1.33	2.85
107	MT-107	1.32	2.82	108	MT-108	0.29	1.24
109	MT-109	0.54	3.70	110	MT-110	1.36	2.82
111	MT-111	0.98	2.48	112	MT-112	1.21	2.51
113	MT-113	1.03	2.35	114	MT-114	1.27	2.14
115	MT-115	1.16	2.10	116	MT-116	1.39	1.95
117	MT-117	6.11	1.61	118	MT-118	1.33	2.59
119	MT-119	1.27	2.33	120	MT-120	0.39	2.08
121	MT-121	1.27	2.82	122	MT-122	1.27	2.35
123	MT-123	2.68	1.89	124	MT-124	4.00	1.42
125	MT-125	4.85	2.33	126	MT-126	5.95	1.77
127	MT-127	6.11	1.95	128	MT-128	2.52	1.47
129	MT-129	1.80	1.31	130	MT-130	1.26	2.35
131	MT-131	4.65	2.21	132	MT-132	1.18	2.46

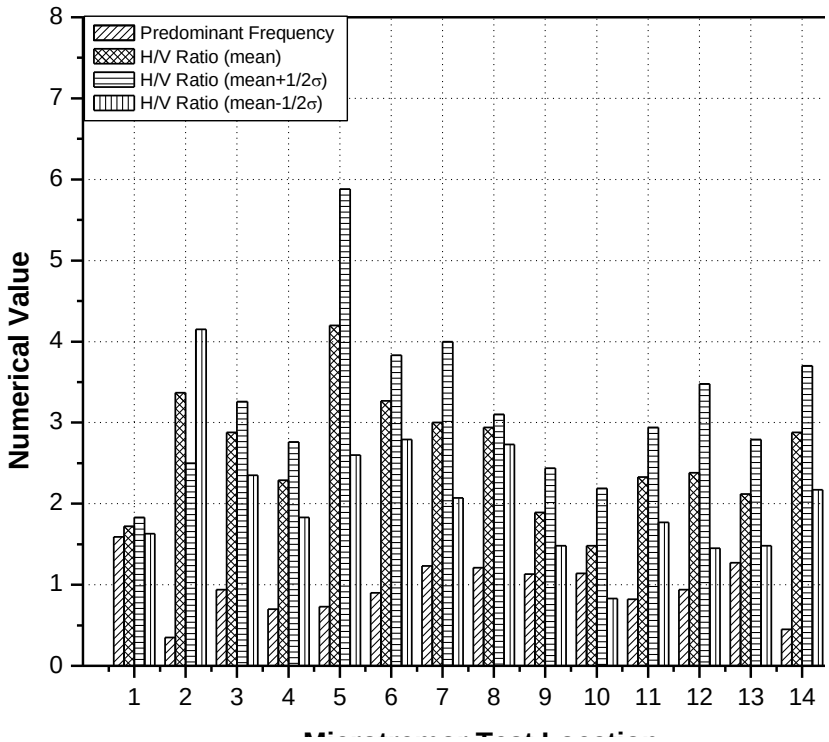

(a) Microtremor Test Location 1 to 15

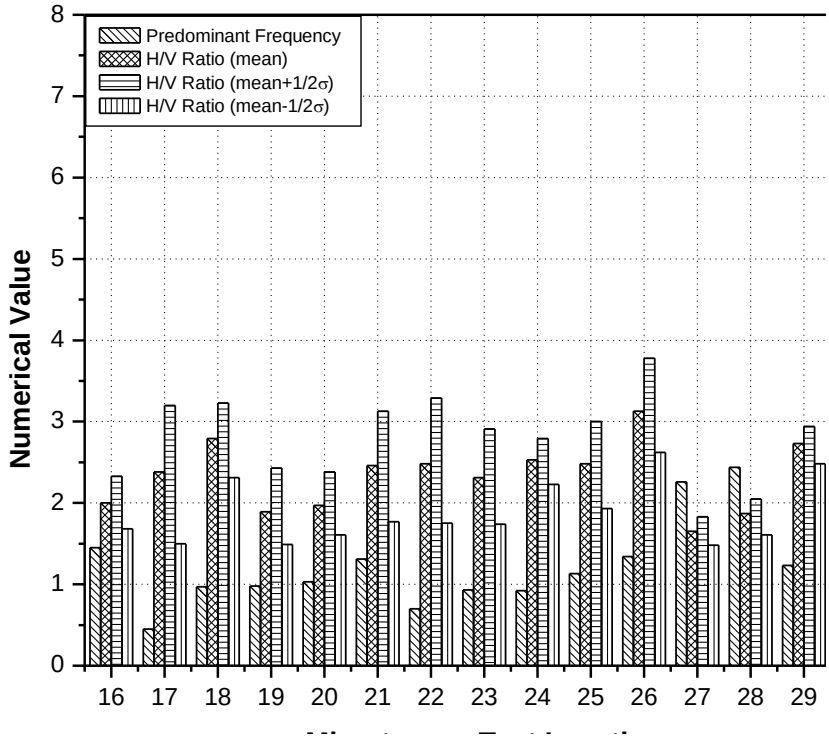

(b) Microtremor Test Location 16 to 30

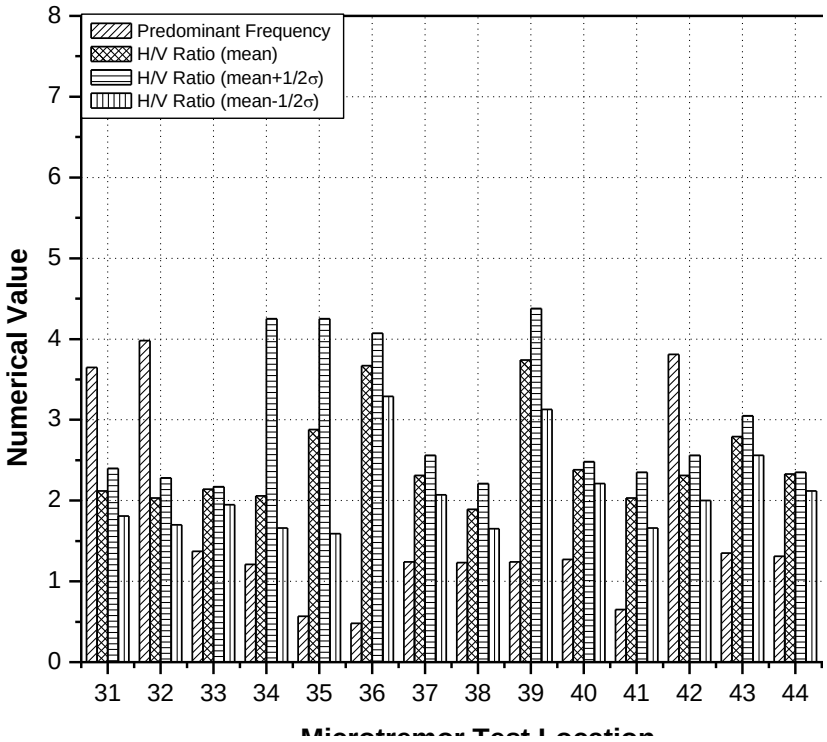

(c) Microtremor Test Location 31 to 45

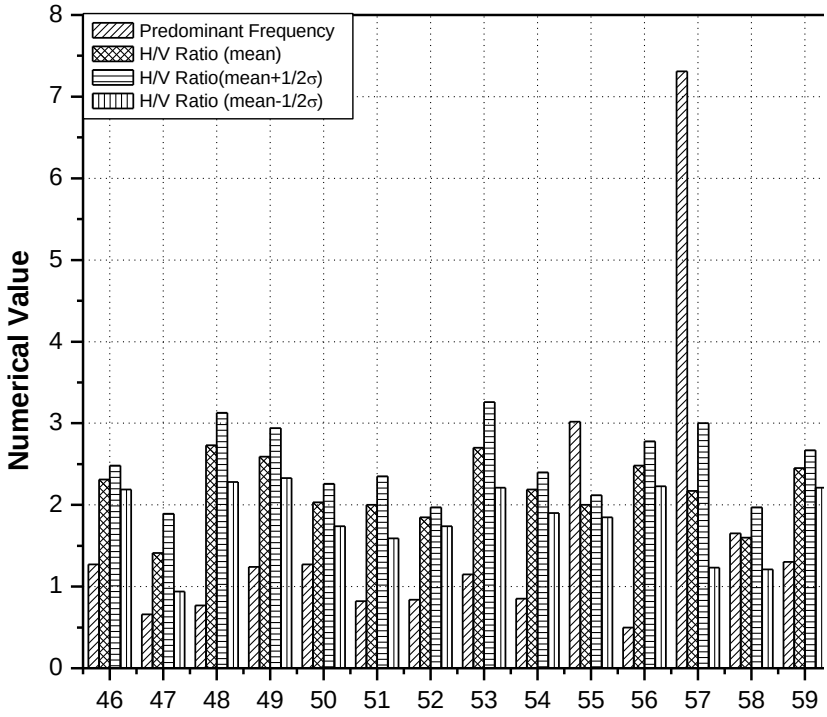

(d) Microtremor Test Location 46 to 60

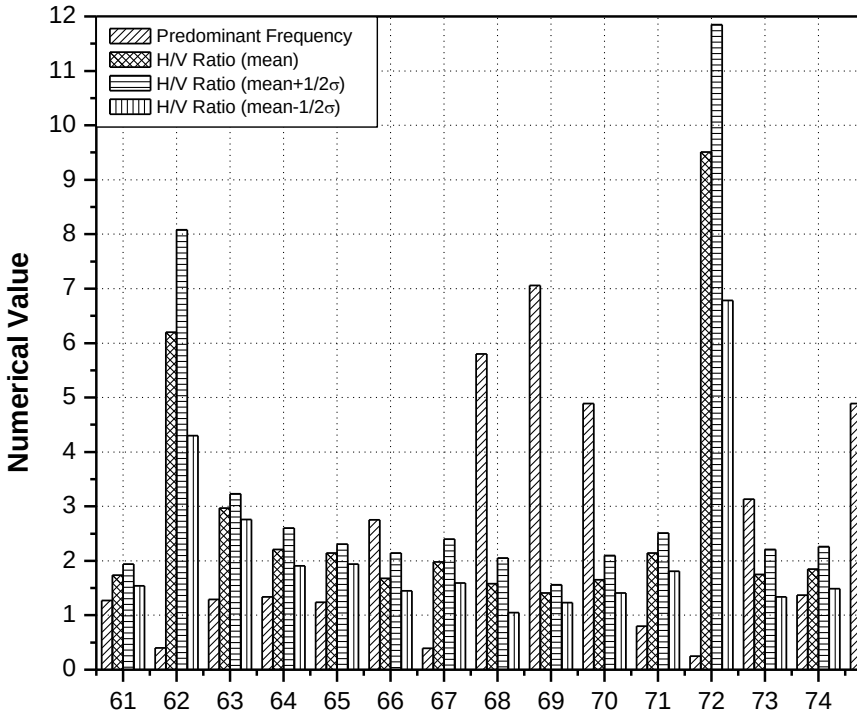

(e) Microtremor Test Location 61 to 75

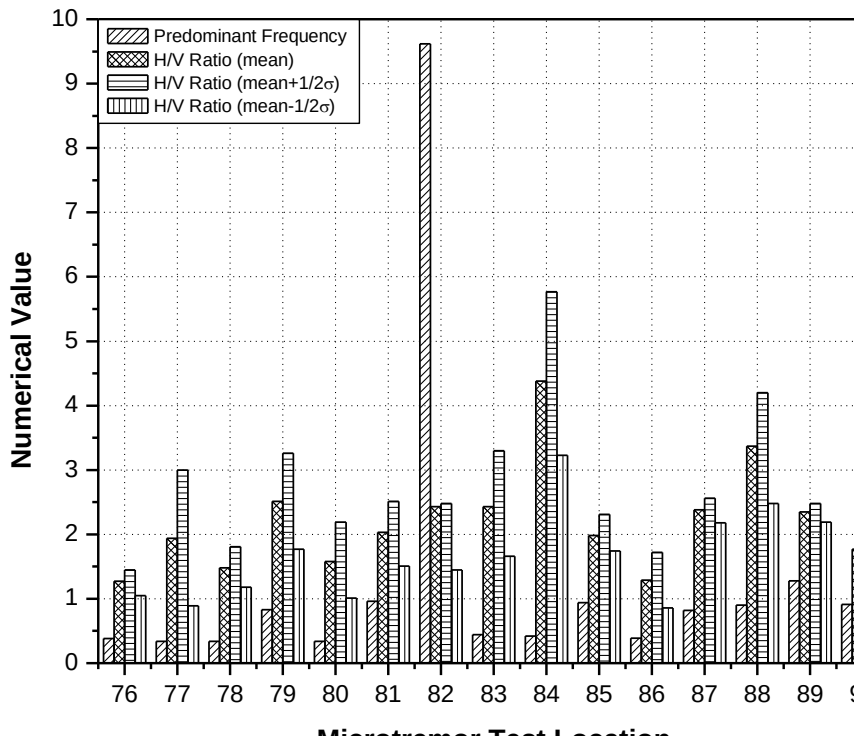

(f) Microtremor Test Location 76 to 90

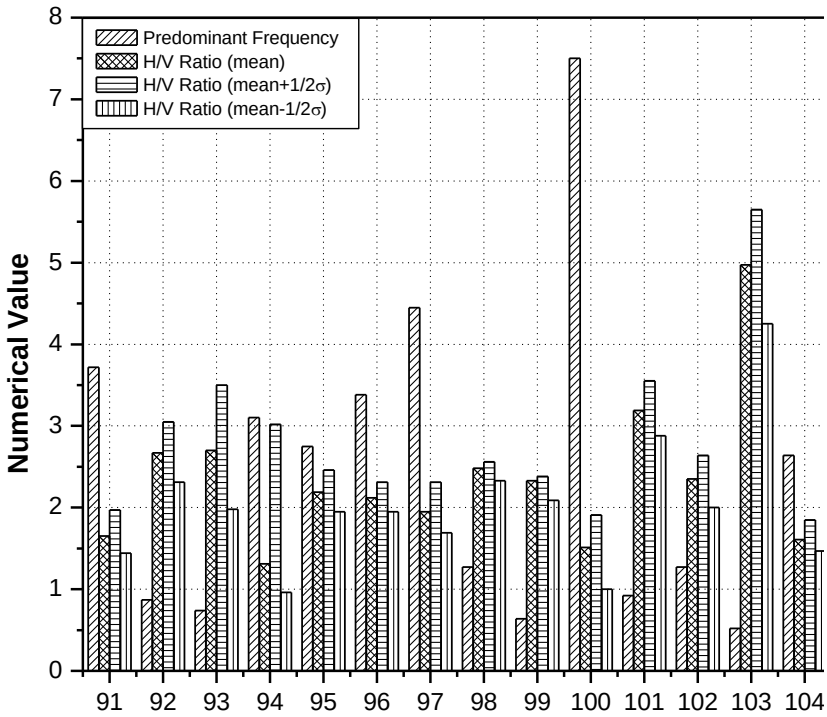

(g) Microtremor Test Location 91 to 105

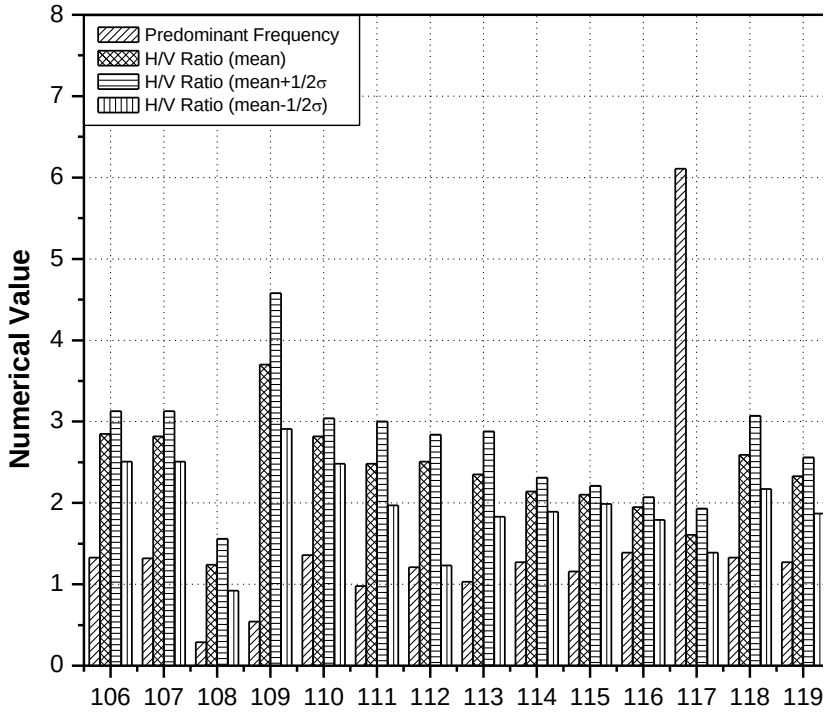

(h) Microtremor Test Location 106 to 120

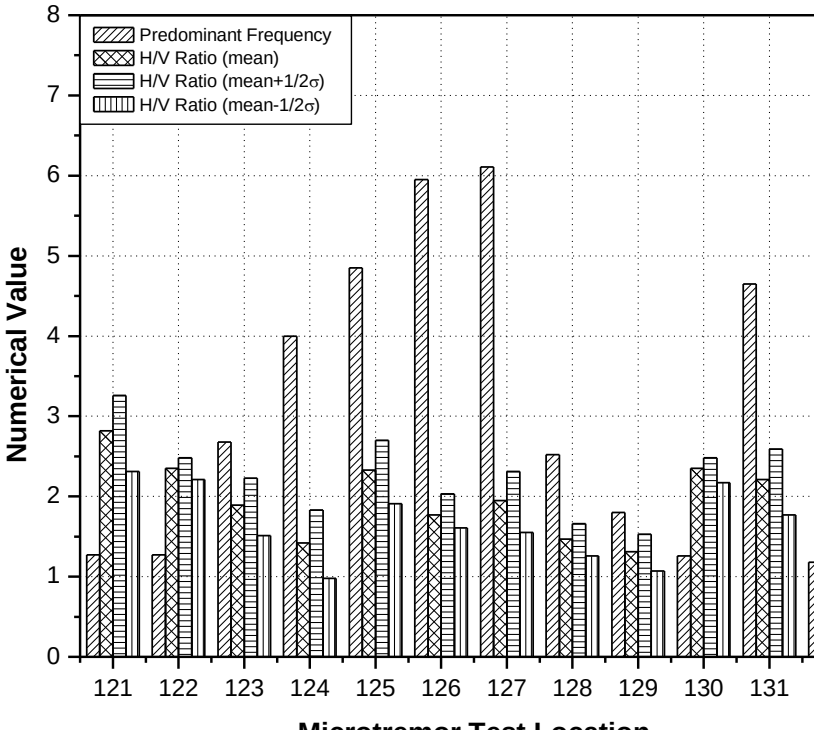

(i) Microtremor Test Location 121 to 132

Figure 3.35 [(a), (b), (c), (d), (e), (f),(g),(h) and (i)]: Predominant frequency and H/V ratio at 132 selected locations in soil within BUET campus.

3.5.2.2 Building Sites

Microtremor observations at 45 residential and academic buildings of BUET campus are shown in Figure 3.36 and google map in Figure 3.37. The Horizontal to Vertical spectra ratio at building does not provide reliable dynamic characteristics. In that case Fourier Spectrum provides better result of predominant frequency at building. Table 3.18 shows the mean predominant frequency of Fourier spectrum in EW and NS directions at 45 buildings. Fourier spectra of 45 buildings along EW, NS and UD directions are shown in APPENDIX-D from Figure D208 to D252. In some buildings, microtremor data is recorded at different floors or different locations in the same floor. Out of 45 microtremor observation in buildings, the maximum predominant frequency is 5.56 Hz along both EW and NS directions in MTB10 at Controller of Examination Building. This is a four-storied frame structure building with 324sqm floor area. There are no lift and shear wall in this building. The foundation of the building is individual footing. There are no structural

irregularities in building. But torsional irregularity, re-entrant corner and diaphragm discontinuity exist.

The minimum predominant frequency is 2.00 Hz along EW and NS directions at MTB02 at the Eleven Story Tower Building. This is an eleven-storied frame structure with 673sqm floor area. There are three lift cores and a shear wall in the building. The foundation of the building is pile-raft system. No structural irregularity exist in this building. But torsional irregularity, re-entrant corner and diaphragm discontinuity exist.

The predominant frequency of 45 building has also been classified into five types. **Type I** (0 – 0.49), **Type II** (0.50 – 0.99), **Type III** (1.0 – 1.99), **Type IV** (2.0 – 2.99) and **Type V** (> 3.00).

The classifications of predominant frequency along EW at 45 buildings are as follows:
Type I: None
Type II: None
Type III: None
Type IV: MT 01, MT 02, MT 03, MT 04 and MT 06.
Type V: MT 05, MT 07, MT 08, MT 09, MT 10, MT 11, MT 12, MT 13, MT 14, MT 15, MT 16, MT 17, MT 18, MT 19, MT 20, MT 21, MT 22, MT 23, MT 24, MT 25, MT 26, MT 27, MT 28, MT 29, MT 30, MT 31, MT 32, MT 33, MT 34, MT 35, MT 36, MT 37, MT 38, MT 39, MT 40, MT 41, MT 42, MT 43, MT 44 and MT 45.

In addition to this, classifications of predominant frequency along NS direction at 45 buildings are as follows:
Type I: None
Type II: None
Type III: None
Type IV: MT 02, MT 03, MT 04, MT 05, MT 06, MT 07, MT 13 and MT 45.
Type V: MT 01, MT 08, MT 09, MT 10, MT 11, MT 12, MT 14, MT 15, MT 16, MT 17, MT 18, MT 19, MT 20, MT 21, MT 22, MT 23, MT 24, MT 25, MT 26, MT 27, MT 28, MT 29, MT 30, MT 31, MT 32, MT 33, MT 34, MT 35, MT 36, MT 37, MT 38, MT 39, MT 40, MT 41, MT 42, MT 43 and MT 44.

Table 3.18: Predominant period and frequency of fourty five BUET buildings (after Russel et al., 2006)

Serial Number	Building Name/Number	No. of story	Predominant period (sec)		Predominant Frequency (Hz)	
			EW direction	NS direction	EW direction	NS direction
1	IFCDR Building	4	0.38	0.30	2.63	3.33
2	Eleven Story Tower Building	11	0.50	0.50	2.00	2.00
3	Civil Engineering Building	7	0.50	0.40	2.00	2.50
4	EME Building	6	0.40	0.39	2.50	2.56
5	Library Building	4	0.26	0.37	3.85	2.70
6	Architectural Building	5	0.37	0.36	2.70	2.78
7	URP Building	5	0.33	0.38	3.03	2.63
8	ARI Building	6	0.26	0.30	3.85	3.33
9	New Academic Building	13	0.27	0.30	3.70	3.33
10	Controller of Examination Building	4	0.18	0.18	5.56	5.56
11	Engg. University School Building	4	0.27	0.23	3.70	4.35
12	Titumir Hall	4	0.32	0.31	3.13	3.23
13	Sher-e-Bangla Hall	4	0.27	0.40	3.70	2.50
14	Dr. M.A. Rashid Hall	5	0.24	0.27	4.17	3.70
15	Ahsan-Ullah Hall	4	0.27	0.25	3.70	4.00
16	Shahid Smrity Hall (Middle Building)	4	0.27	0.21	3.70	4.76
17	Shahid Smrity Hall (North Building)	4	0.30	0.28	3.33	3.57
18	Register Building	2	0.20	0.20	5.00	5.00
19	# 1	4	0.25	0.25	4.00	4.00
20	# 2	4	0.25	0.26	4.00	3.85
21	# 3	4	0.28	0.22	3.57	4.55
22	# 4	5	0.33	0.29	3.03	3.45
23	# 5	4	0.22	0.26	4.55	3.85
24	# 6	4	0.23	0.27	4.35	3.70

Serial Number	Building Name/Number	No. of story	Predominant period (sec)		Predominant Frequency (Hz)	
			EW direction	NS direction	EW direction	NS direction
25	# 7	4	0.25	0.27	4.00	3.70
26	# 8	4	0.32	0.28	3.13	3.57
27	# 9	4	0.24	0.22	4.17	4.55
28	# 12	5	0.30	0.28	3.33	3.57
29	# 13	5	0.28	0.28	3.57	3.57
30	# 14	5	0.31	0.31	3.23	3.23
31	# 18	5	0.33	0.29	3.03	3.45
32	# 21	4	0.23	0.30	4.35	3.33
33	# 22	4	0.33	0.29	3.03	3.45
34	# 23	4	0.25	0.30	4.00	3.33
35	# 24	4	0.24	0.29	4.17	3.45
36	# 25	4	0.25	0.30	4.00	3.33
37	# 26	4	0.25	0.30	4.00	3.33
38	# 27	4	0.23	0.29	4.35	3.45
39	# 28	5	0.33	0.28	3.03	3.57
40	# 30	4	0.26	0.24	3.85	4.17
41	# 43	5	0.29	0.25	3.45	4.00
42	# 45	5	0.27	0.29	3.70	3.45
43	# 46	5	0.30	0.26	3.33	3.85
44	# 47	6	0.32	0.32	3.13	3.13
45	# 62	6	0.39	0.34	2.56	2.94

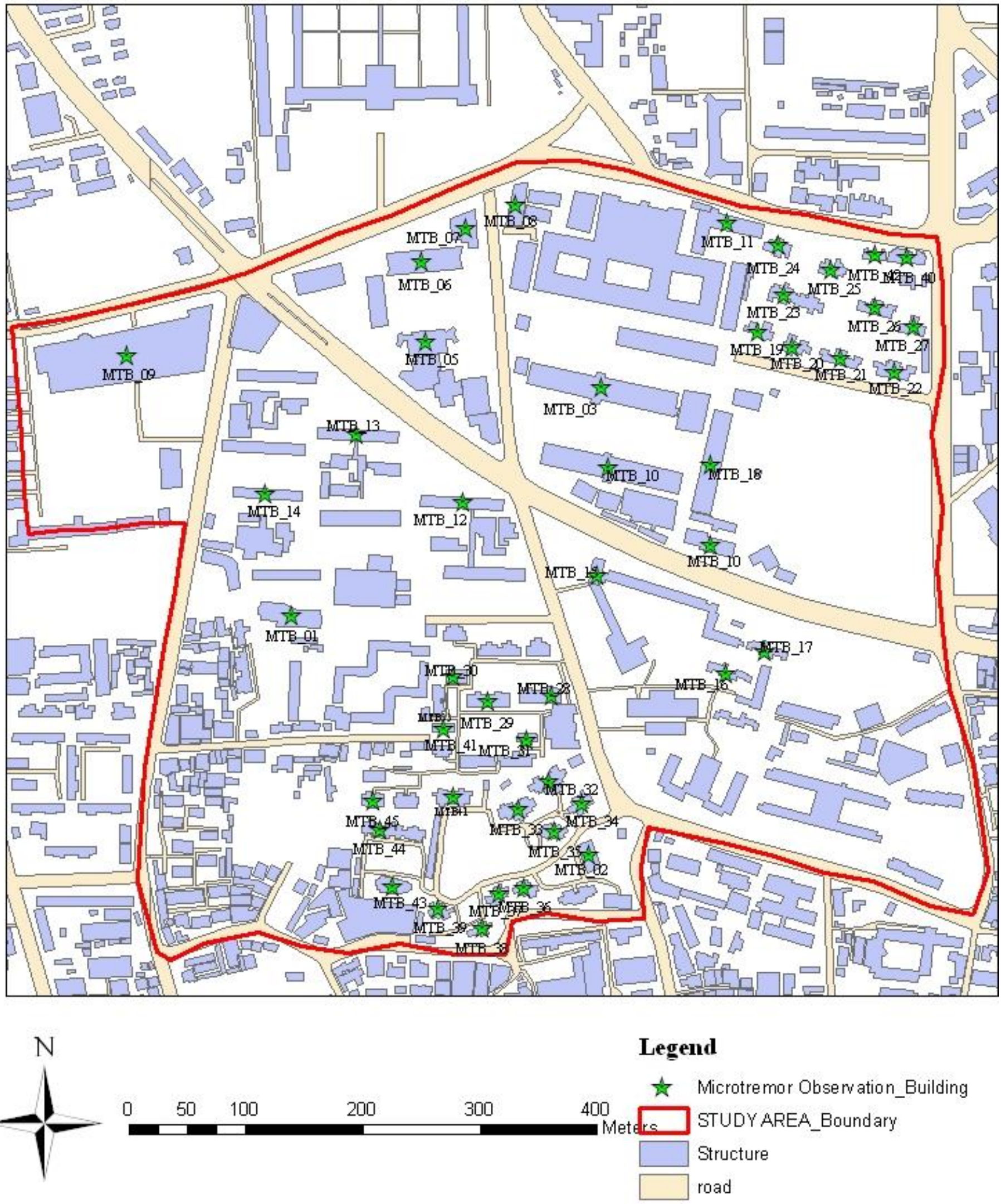

Figure 3.36: 45 microtremor observation points in various building of BUET campus.

Figure 3.37: Google Map of BUET Campus.

3.7 CONCLUDING REMARKS

Chapter three is the main body of this research which shows the data collection and analysis result of microtremor test locations. This chapter includes geological and geomorphological classification of the study points. The characteristics of soil of the investigated locations have been explained here. The shear wave velocity estimated by various empirical correlations has been illustrated. The comparison between the field shear wave velocity at fourteen locations and the correlated shear wave velocity has been presented in tabular form.

The stability of microtremor data at fourteen different locations has been demonstrated with various time instants within a day. Both Fourier spectra and horizontal to vertical (H/V) ratio data has been illustrated in these locations. From this research, it has been found that microtremor H/V ratio data is more stable than Fourier spectra in soil at the investigated points. Due to this inference, microtremor H/V technique has been applied at different locations of the study area.

The effects various factors on microtremor result have been demonstrated in this chapter. These factors are resultant of H/V ratio (RM, RMS, RS and Mean), five analysis windows and smoothing function. The suitability of RM over other resultants has been shown in three study areas. The variations of microtremor data due to analysis windows have been illustrated. The mean data does not show significant changes in microtremor analysis result. Finally, the rectangular window has been selected among these five windows. Five smoothing function have been applied on the microtremor H/V ratio data to show the effects of smoothing. From these comparision, it has been found that smoothing function has significant effect on the final microtremor results.

The microtremor observations have been carried out at 132 locations within BUET campus where soil condition is relatively stiff and outside BUET campus at 45 locations of Dhaka city which falls on reclaimed and non-reclaimed areas. The H/V ratio data and predominant frequency of these observed locations have been classified to assess the amplification of soil. Microtremor observations for 45 buildings within BUET campus are collected for comparison purpose from a previous study.

CHAPTER 2

LITERATURE REVIEW

2.1 GENERAL

Microtremor consists of different types of waves producing in soil from various sources. The common noise sources are vibrating machine, traffic, environment and human movement. Microtremor observation is carried out to record time history of noise data. Horizontal to Vertical (H/V) Fourier spectral ratio technique is applied to assess the vulnerability of soil and building. Figure 2.1 shows various sources of microtremor for site response analysis. Microtremor is composed of fundamental mode of Rayleigh wave (Sato et al., 1991; Tokimatsu and Miyadera, 1992). Higher frequency microtremor bears resemblance to Shear Wave characteristics (Nakamura, 1989; Wakamatsu and Yasui, 1995). On the other hand, microtremors can also be dominated by Love-wave (Tamura et al., 1993). Recently, Suzuki et al. (1995) has applied microtremor measurements to the estimation of earthquake ground motions based on a hypothesis that the amplitude ratio defined by Nakamura can be regarded identical with half of the amplification factor from bedrock to the ground surface. However, the real generation and nature of microtremors have not yet been established.

This chapter presents the past researches related to microtremor technique. The reliability of Horizontal to Vertical Spectral Ratio (H/V) has been discussed from different points of view. The relationship between microtremor analysis and seismic activity has also been included in this chapter. The characteristics of various types of microtremor waves have been illustrated using mathematical expressions. The theory and procedure of one dimensional (1D) response analysis using the programme SHAKE has been included. The empirical soil correlation of field SPT-N value and Shear Wave Velocity has also been shown. Finally, seismic damage assessment of building using resonance criteria and Nakamura's Vulnerability Index for damage estimation of soil has been included.

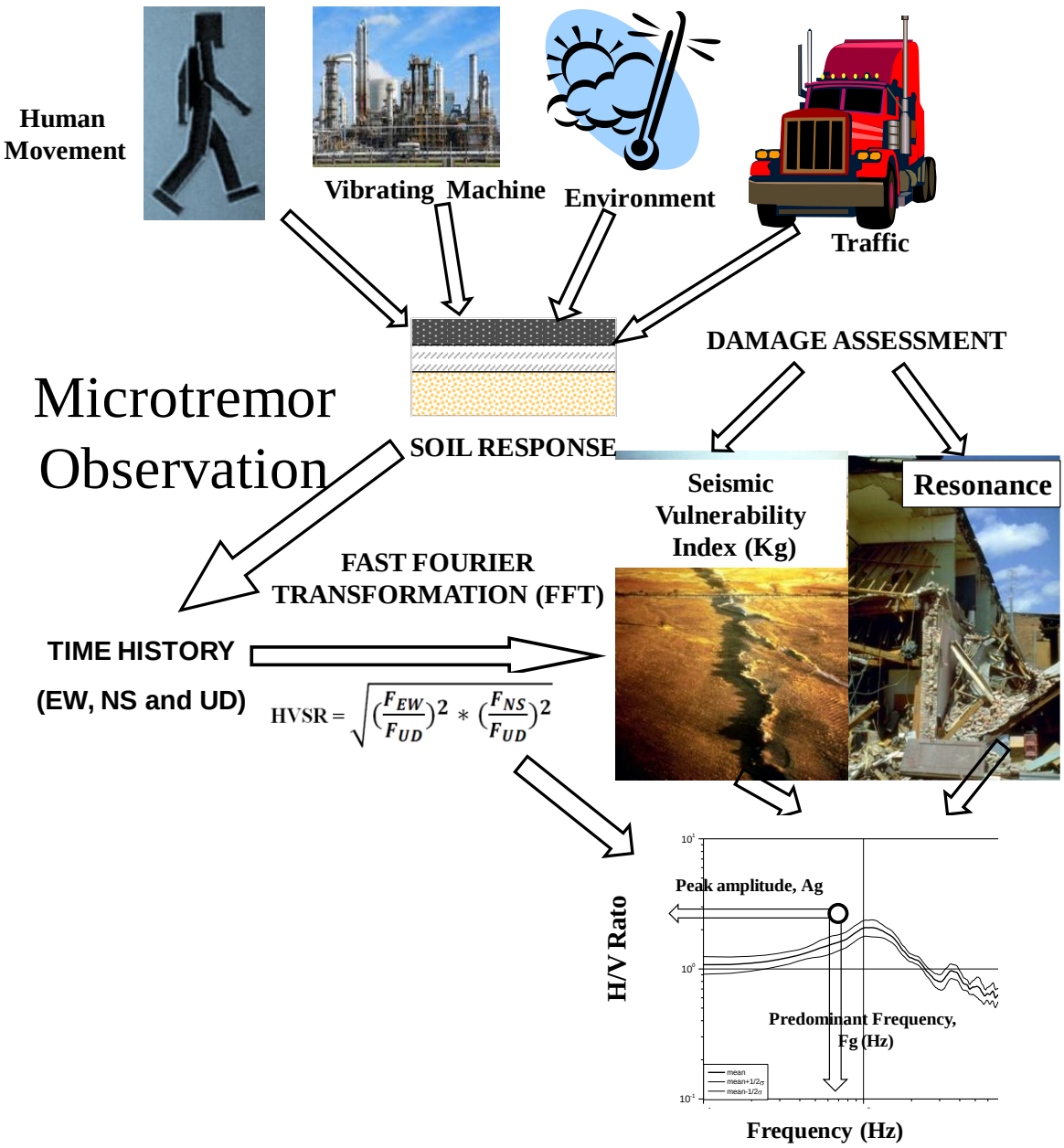

Figure 2.1: Microtremor observation and damage assessment.

2.2 PAST RESEARCHES ON MICROTREMOR

The infrequent occurrence of destructive earthquakes does not permit the compilation of enough data to support the estimation of the distribution of damages in the future. To overcome this lacking, different authors proposed the use of alternative sources of excitation, such as, distant earthquakes, small near earthquakes, explosions, aftershocks and microtremors. Wave propagation mechanism of microtremor and its relation with ground vibration characteristics have been studied from the beginning of microtremor studies (Aki, 1957; Kanai and Tanaka, 1961). Meanwhile, practical application of microtremor in the field of engineering has advanced tremendously. One of the powerful and simplest application of microtremor observation is in seismic micro-zoning.

The use of microtremors, an idea pioneered by Kanai et al. (1954) turns into one of the most appealing approaches in site effects studies, due to its relatively low economic cost and the possibility of recordings without strict spatial or time restrictions (Rodriguez and Midorikawa, 2002). In recent studies, ambient noise measurements have been widely applied (Seo (1994). The results obtained from the application of long period ambient noise measurements (Ohta et al., 1978; Yamanaka et al., 1993, 1994) allow the application microtremor for site effects. Short period ambient noise measurements have been applied to a wide range of seismic settings (Morales et al., 1991, 1993; Lermo and Chavez-García, 1993; Field and Jacob, 1993; Field et al., 1995; Seo, 1994). The H/V spectral ratio method (Nakamura 1989) has been discussed at great length and proven to be a suitable, quick and effective method (Konno and Ohmachi, 1998; Bard, 1999; Enomoto et al., 2002) for determining the predominant period of soil. This method has been applied to different Spanish cities exposed to a moderate seismic hazard (Vidal et al., 1996; Seo, 1994; Pujades et al., 2000; Alfaro et al., 2001; Navarro et al., 2001).

Dividing the research area into regions in line with material conditions is a very useful way of reducing the number of sites whose effect has to be considered. The first step is the geological and geotechnical identification of the materials, after which the obtained soil conditions have been extrapolated. Due to close relation between microtremors and the fundamental dynamic behavior of the surface soil layer Taga (1993), microtremor measurements can prove a useful tool for evaluating the properties of earthquake ground

motion and also for extrapolating the seismic motion observed at a given point to its surrounding area.

The concentration of human activity in urban areas implies an accumulation of risk elements, to which traditional seismic hazard studies do not devote enough attention. This is why specific studies based on very detailed research of close sources are essential, as are in situ measurements that take into account local effects. Priority has to be given to this sort of studies in order to prevent, mitigate and manage seismic risks. The superficial geology of an urban area has a remarkable influence on the distribution of the damages caused by an earthquake. It has been proved that soil movement during an earthquake can be amplified by local landform conditions (Aki, 1993 and Bard, 1999) and in some cases it amplifies the seismic shake in a range of periods that coincide with the period of vibration of the damaged structures (Seo, 1994), showing the relationship between the amplification caused by surface geology and the degree of destruction. Even though urban geomorphology is a term that appeared only recently, its use has spread significantly over the last few years.

The H/V spectral ratio technique of microtremors gained popularity in the early nineties, after the publication of several papers (Nakamura, 1989; Field and Jacob, 1993; Lermo and Chavez- Garcia, 1994) claiming the ability of this technique to estimate the site response of soft sedimentary deposits satisfactorily. The mathematical expression of Microtremor H/V Technique is discussed in section 2.3 of this Chapter. The method is rather attractive in developing countries characterized by a moderate seismicity, where only very limited resources are available for seismic hazard studies.

The single-instrument microtremor method has been widely applied across southwestern British Columbia, Canada. This area exhibits a high level of seismic hazard due to its close proximity to the deep earthquakes under the Strait of Georgia / Puget Sound. The moderate seismicity combined with the majority of the provincial population, building stock and infrastructure creates great concern for earthquake engineering. Microtremors are short period vibrations that result from coastal effects, atmospheric loading, wind interaction with structures and vegetation, and cultural sources. The single-instrument microtremor method initially proposed by Nogoshi and Igarashi (1971), and popularized by Nakamura (1989), produces an estimate of site geological conditions by providing the

peak period of amplification from the horizontal to vertical (H/V) spectral ratio (amplification occurs where the ratio amplitude is greater than one). Site response has been presented by H/V ratio for a site, shown as a function of frequency (Hz) and generated from Fourier amplitude spectra. In Canada, the single-instrument microtremor method has been used most extensively by studies across SW British Columbia (Molnar et al., 2007; Molnar et al., 2006a; Molnar et al., 2006b; Molnar and Cassidy, 2006; Onur et al., 2004; Ventura et al., 2004), along with a study of the seismic microzonation for Montreal, Quebec (Chouinard et al., 2004) and at seismic instrument sites across Ontario (Sneider et al., 2005). The ground's responses from microtremors at strong-motion instrument sites have been compared with all possible earthquakes recorded at these sites to validate whether or not microtremors can be used as a proxy for linear earthquake response.

An important question refers to the composition of the elastic waves which make up ambient seismic noise. In the original Nakamura's explanation, horizontal component of microtremors consists of multi-reflected S-waves whereas the vertical component is mainly dominated by P-waves which is not suffer amplification in a thin sedimentary layer because of its higher wavelength. Amplification of vertical motion is due, under this hypothesis, to the effects of Rayleigh waves. Considering that H/V ratio is 1 at bedrock, Nakamura (1989) concludes that spectral ratio at surface is a reliable estimation for transfer function of surface layers corrected of the effects of Rayleigh waves.

Current researches show that Nakamura´s explanation, based on body waves, does not really demonstrate that spectral ratio is the soil response for horizontal oscillations neither around predominant frequency (Bard, 1999). Better results have been obtained supposing that microtremors are composed by a high ratio of surface waves. This assumption is supported on the presence of dispersion in seismic noise which is a typical characteristic of Rayleigh waves and Love waves. That evidence has been obtained from multiple experiments using arrays of sensors (Flores et al., 2003; Enomoto et al., 2002). The general agreement between ellipticity curves of Rayleigh waves and microtremor spectral ratio is established (Nogoshi and Igarashi (1971); Lachet and Bard (1994); Konno and Ohmachi, 1998). Ellipticity curves represent the horizontal to vertical ratio for the motion of a particle due to a plane Rayleigh wave. In case of a soft layer over a stiff half space, exist enough impedance contrast (upper than 2.5 - 3), these theoretical functions show a

well defined peak which position is in fairly good accord with the fundamental resonant frequency of vertically incident S-waves f_0.

Although the real contribution of surface and body waves is still discussed (Nakamura, 2000; Konno and Ohmachi, 1998; Arai and Tokimatsu, 2004), all they recognize that Nakamura´s method provides a reliable estimation of the fundamental frequency for this kind of geological structure. Lachet and Bard (1994) show from simulations using surface sources that this agreement appears again for many layered profiles. Other interesting matter is the possibility that information about the level of amplification for the case of earthquake could be obtained from microtremor spectral ratio. In the case of high contrast of impedance between sedimentary layer and basement the ellipticity curve of fundamental Rayleigh mode suffer a divergence for a frequency near to f_0. So, the identification of amplification factors seems difficult for this approach.

Though, Konno and Ohmachi (1998) developed a smoothing function in order to deal with these infinite peaks and found reasonable correlations with the theoretical maximum amplification for vertically incident S-waves. On the other hand, Lachet and Bard (1994) found, taking simulations of body and surface waves into account, worse correlation and a high influence of Poisson's ratio for the upper layer on the peak amplitude. Several recent works have been executed to obtain more information than the fundamental frequency from the whole shape of the spectral ratio and not only from the region around f_0. In Konno and Ohmachi (1998) is already noticed that this function shows a trough for a frequency about 2 f_0 which can be used to obtain the resonant frequency. The possibility of a good characterization for the sedimentary structure is analyzed by Fäh et al. (2003) by using genetic algorithms in order to invert the soil profile from a fitting of the measured H/V. The fundamental Rayleigh mode is used in the forward calculation and the method fails for some particular structures in which higher modes of surface waves and body waves should be considered. Arai and Tokimatsu (2004) improve that method taking all modes for surface waves and the relative contribution of Rayleigh and Love waves as 40% and 60% respectively for the entire considered frequency band. It has been used the scheme developed by Arai and Tokimatsu (2000, 2004) in order to check the reliability of this technique for a known soil profile which characteristics have been obtained from downhole and from S-wave refraction surveys.

When recordings of microtremors are analyzed using Nakamura's method Nakamura (1989), the Horizontal to Vertical Spectral Ratio (HVSR) plots for certain soft sites have the characteristic appearance of a peak, with a height of more than five, followed by a trough with a height of less than one, at a higher frequency. According to Haskell (1953), in the course of changing from retrograde to prograde particle orbits as frequency increases, the particle motion theoretically becomes a horizontal line, and in changing from prograde to retrograde particle orbits at a higher frequency, the motion theoretically becomes a vertical line. These transitions would result in an infinite and a zero HVSR, respectively. It has therefore been suggested (Lachet and Bard, 1994; Lermo and Chavez-Garcia, 1994a, 1994b; Konno and Ohmachi, 1998) that the mechanism which governs Nakamura's method is the propagation of Rayleigh waves, contrary to the original view (Nakamura, 1989) that any Rayleigh wave contribution detracts from the method. Accepting this interpretation of the origin of the peak/trough structure of many HVSR plots, it becomes important to investigate the geotechnical circumstances under which prograde Rayleigh wave orbits (and therefore an HVSR peak and trough structure) may arise.

A Rayleigh wave travelling along the interface between a homogeneous half space and the empty space above it has a particle motion which is elliptical in a plane containing vertical and the propagation direction (Bullen and Bolt, 1985). In contrast to water waves, the particle motion is always retrograde, that is, if a Rayleigh wave is travelling from left to right the particle motion describes an anti clockwise ellipse. However, when the Rayleigh wave travels in a more flexible layer on top of the half space, there may be a range of frequencies for which the particle motion is prograde, that is, if a wave is travelling from left to right the particle motion describes a clockwise ellipse. In changing between prograde and retrograde the motion must at some frequency become a straight line (which is neither retrograde nor prograde). It sometimes happens (Haskell, 1953) that for one transition the straight line is vertical and for the other it is horizontal. If the motion is completely horizontal at some frequency, the HVSR will be infinite at that frequency, and if the motion is completely vertical at some other frequency, the HVSR will be zero at that frequency. It has been shown (Lachet and Bard, 1994) that the peak of a Nakamura's ratio plot corresponds to the resonant frequency of the layer. Further modeling (Lermo and Chavez-Garcia, 1994a, 1994b) showed the theoretical existence of a trough as well, but the significance of the trough has not been remarked upon.

Subsequently the peak/trough structure has been noted (Konno and Ohmachi, 1998), with the comment that the frequency ratio between trough and peak is approximately two, and that the frequency of the trough could be used as an additional control on the natural frequency of the layer. It has been also asserted (Konno and Ohmachi, 1998) that some layer/half space stratigraphies can result in a trough structure. Such a result has also been encountered in the investigations described here, but it is a relatively rare occurrence. The HVSR predicted by a simple one-layer model has a close correspondence to the actual frequencies at which the HVSR peak and trough occur. The very existence of sharp resonant peaks in some HVSR plots is suggestive of an abrupt change in shear wave velocity at some depth, and therefore a suitable tactic to start investigations must lie in exploring the properties of a simple homogeneous layer lying on top of a stiffer half space, even though such simple circumstances must seldom occur in nature. Accordingly, a uniform layer upon a half space, is the model adopted for this work. In addition, it is useful to adopt likely values for the layer and half space properties. A typical soft site has a superficial layer of saturated soil, which has a high P-wave velocity and a low S-wave velocity (Poisson ratio n approaching 0.5). By contrast rock is closer to being a poisson solid.

The Nakamura technique (Nakamura, 1989), first proposed by Nogoshi and Igarashi (1970, 1971), is today one of the most commonly applied methods for microzonation studies of large areas (Parolai et al., 2001). A large number of studies using this rapid, economical and therefore attractive technique have been published (Field and Jacob, 1993; Mucciarelli, 1998; Bard, 1999; Fah et al., 2001). More recent studies (Fah et al., 2003; Scherbaum et al., 2003; Arai and Tokimatsu, 2004; Parolai et al., 2005; Picozzi et al., 2005; Parrolai et al., 2006) proposed and tested the possibility of inverting the Horizontal to Vertical (H/V) spectral ratio of noise (alone or in a joint inversion scheme) for investigating the S-wave subsoil structure. All these studies require the assumption that the noise wave field is generally dominated by surface waves. Moreover, attempts to provide standards for the analysis of seismic noise have only recently been carried out (Bard, 1999; SESAME, 2004; Picozzi et al., 2005). To this regard, a point frequently debated by the seismological community is whether only the stationery part of the recorded signal should be considered in the analysis, or could transients (due to human activities) also be considered (excluding obviously very strong and clipped signals). Most

authors disregarded the non-stationery noise from the analysis (Horike et al., 2001), while others (Mucciarelli et al., 2003) showed that the H/V ratio of non-stationery noise might be more similar, especially in amplitude, to the H/V ratio of non-stationery noise might be more similar, especially in amplitude, to the H/V spectral ratio determined for small-size earthquakes. By applying an optimal filtering procedure to empirical data and using numerical simulations, Parolai and Galiana-Merino (2006) showed that transients might cause large variability in the H/V shape, depending on source type and distance from the receiver relative to the thickness of the sedimentary cover. However, they showed that when dealing with a sufficient number of real data, the H/V technique is not biased by including transients. Recently, Chatelian et al. (2007) suggested to avoid the use of transients in the H/V analysis. Nevertheless, they showed that H/V does not significantly change if the sensor is located just a few meters from the major sources of transients (in their case, cars on a highway). Furthermore, at only 2 m from the highway, the peak in the H/V spectral ratio is still visible, when it disappears when the sensor is placed directly on the highway. These results (except for those from the stations located directly on the highway) seem to be in agreement with the pioneering study of Taniguchi and Sawada (1979) who made systematic noise measurements close to a highway under constructions and observed that (1) the frequency peak in the transient spectra has been stable independent of the mass of the source (a truck), hinting to the fact that the frequency of the traffic-induced vibration is mainly determined by ground soil conditions, and (2) traffic-generated vibrations have been dominated by Rayleigh waves. A recent investigation of seismic noise wave field induced by several source types can be found in Kim and Lee (2007).

Additional evidence of the role played by transients has been reported by Mucciarelli (1998) who showed that when generating transients with a sledge hammer near the recording sensor, the H/V peak becomes more clear. This result, probably too often overlooked, stimulates many intriguing questions. Since the energy released by the blow of sledge hammer peaks at frequencies much higher (50-70 Hz) than the fundamental resonance frequency of the site (1 Hz), how can the transients modify the H/V? Similarly, human generated seismic noise mainly affects frequencies higher than 1-2 Hz, with cars generating signals with frequencies mainly between 10-20 Hz (Toniguchi and Sawada.

1979; McNamara and Buland, 2004). Therefore, the question arises if there is any important information carried by the transients that one could try to extract.

2.2.1 Earthquake and Microtremor Spectral Ratio

Worldwide, microtremor studies have shown that the peak amplitude of the microtremor H/V ratio tends to underestimate the peak amplitude of earthquake spectral ratios with respect to a reference (bedrock) site (Bard, 1999). The H/V spectral ratio determined from microtremors has shown a clear peak that is well correlated with the fundamental resonance frequency at "soft" soil sites (Bard, 2004; Horike et al., 2001; Lachet et al., 1996; Field and Jacob, 1995; Lachet and Bard, 1994; Lermo and Chavez-Garcia 1994a, 1994b). Numerical analysis suggests that microtremor site response can only be generated when the impedance contrast is greater than 3.5 (Malischewsky and Scherbaum, 2004), thus the good correlation at "soft" soil sites. Only a few studies claim rough agreement between the peak amplitude of the microtremor H/V ratio and earthquake site-to-reference spectral ratios (Molnar and Cassidy, 2006; Mucciarelli et al., 2003; Horike et al., 2001; Lermo and Chavez-Garcia, 1994a, 1994b). In general, the site response shown by the earthquake site-to-reference spectral ratio method is regarded as the best approximation for engineering use, whereas H/V spectral ratios from earthquakes and/or microtremors are regarded as providing the fundamental peak and lower bound estimate of amplification for a soil site.

Figure 2.2 demonstrates the remarkable similarity between the earthquake site-to-reference and H/V ratio response, with the microtremor H/V ratio response at three strong-motion earthquake recording sites in greater Victoria. Traditionally strong-motion instrument has been used for earthquake recordings, rather than recordings from weak-motion sensors, as these instruments are designed to record the largest ground motions, and are generally present at sites of geologic interest (i.e. not bedrock). There are six BC Hydro substations in greater Victoria with a permanent strong-motion instrument. Since 1996, up to seven weak motion (peak ground acceleration $\leq$ 5.5 % g) earthquakes, ranging in magnitude from M_L 3.6 to M_W 6.8, have been recorded at these sites.

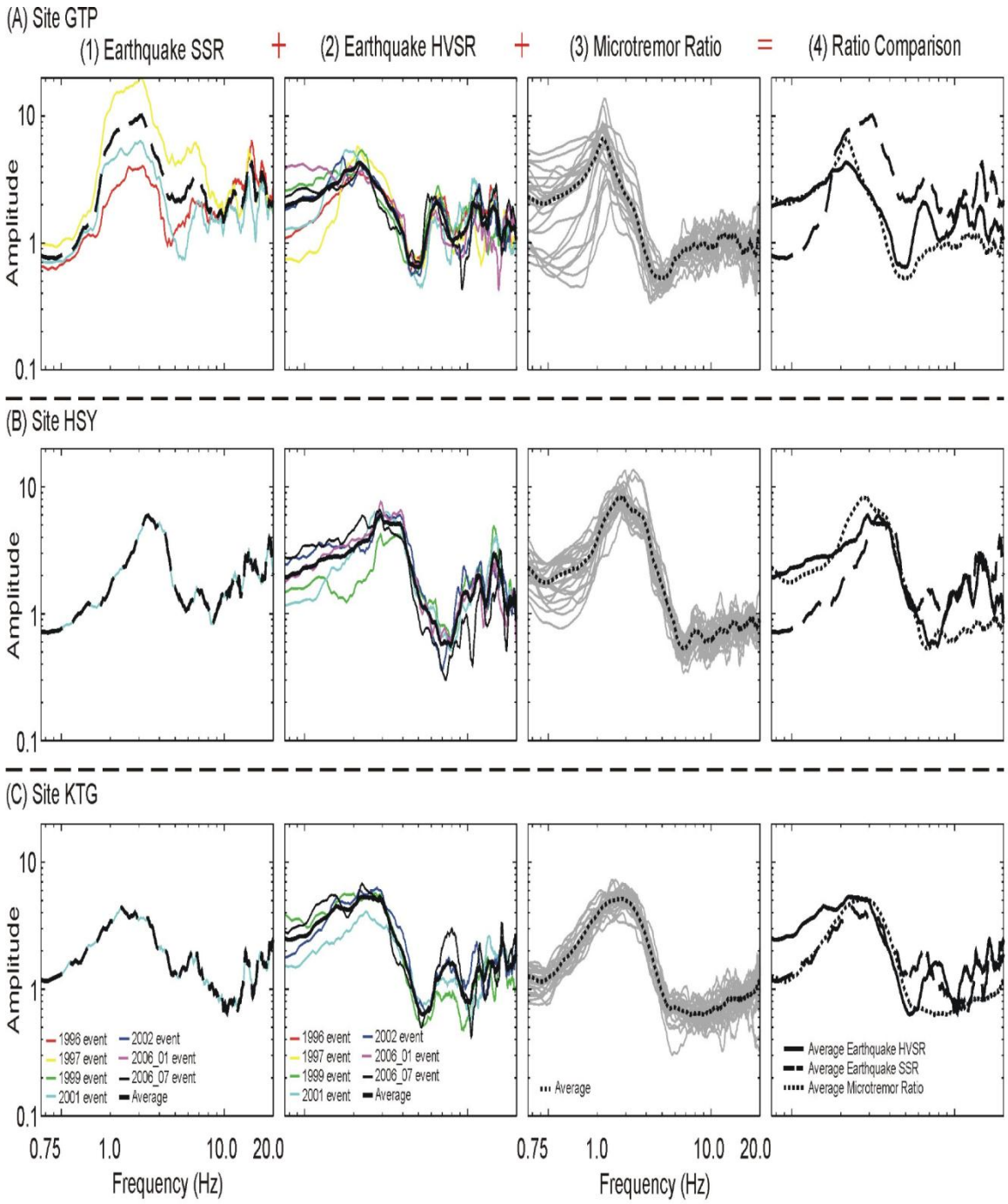

Figure 2.2: Comparision of (1) the average earthquake site-to-reference spectral ratios (SSR) with (2) the average earthquake H/V spectral ratios (HVSR) of up to seven earthquakes, and (3) the average microtremor H/V spectral ratio at three strong-motion instrument sites in greater Victoria. (After Molnar et al., 2007)

All six BC Hydro instrument sites show similar response regardless of excitation source (weak-motion earthquakes or microtremors) and spectral ratio method (Molnar and Cassidy, 2006b). This suggests that microtremor recordings are valid for estimation of linear earthquake response at sites in greater Victoria.

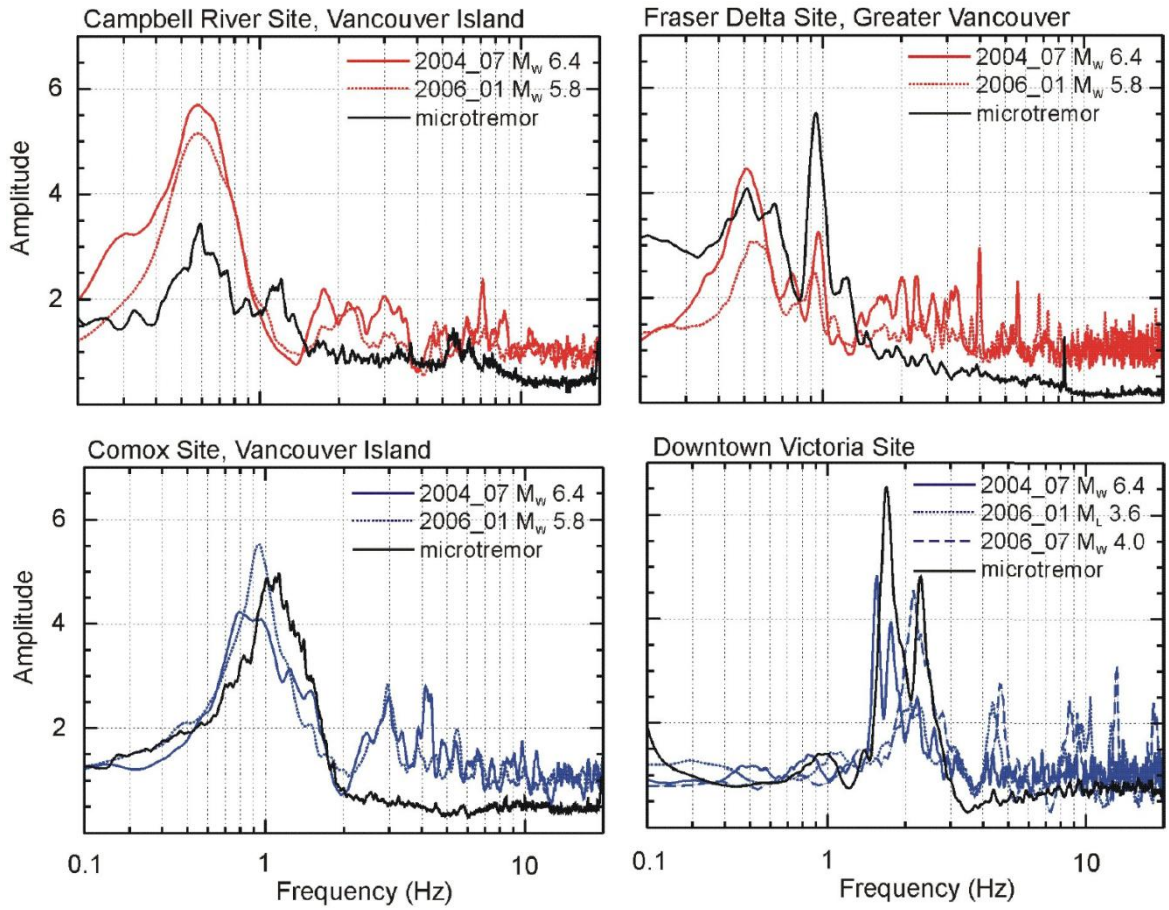

Figure 2.3: Comparision of the H/V spectral ratio from up to four weak-motion earthquakes and microtremors at four sites across SW British Columbia.(After Molnar et al, 2007)

Another source of strong-motion earthquake recordings comes from the Geological Survey of Canada. In 2002, they began to operate strong-motion instruments that continuously record and communicate in near real-time over the Internet (Rosenberger et al., 2007, Molnar et al., 2006b, Molnar et al., 2006c). These new instrumentation features have provided around 500 earthquake acceleration recordings across SW British Columbia (Cassidy et al., 2007) from only four earthquakes ranging in magnitude from M_W 4.0 to M_W 6.4. However, the recordings are all relatively low-level, varying in peak

ground accelerations between 0.6 and 3.9 % g. Figure 2.3 shows good similarity of the fundamental period of the H/V spectral ratio response from these earthquake recordings with the microtremor response at four strong-motion instrument sites across SW British Columbia (Molnar et al., 2006d).

Overall, for SW British Columbia excellent agreement has been observed in the fundamental period of a site 413 between earthquake and microtremor spectral ratio responses, and good agreement in the level of amplification, especially at sites in greater Victoria. The microtremor response at higher modes is always lower than that of the earthquake response. The microtremor underestimates earthquake response amplitude at frequencies greater than 2 to 3 Hz. Figures 2.2 and 2.3 demonstrate the validity of the single-instrument microtremor method as a proxy for earthquake site response across SW British Columbia.

2.2.2 Observed and Analytical Amplitude Ratio

A microtremor research has been carried out at thirteen locations in Japan (Ansary et al, 1996). Soil model has been developed for theoretical analysis using the existing boreholes and PS loggings. The transfer function of the shear wave (The surface motion versus the incidental motion at some depth) and the amplitude ratio for the fundamental mode of Rayleigh wave have been calculated at the sites using those soil models. For the calculation of transfer function of shear wave, a damping ratio of 2 % has been used, assuming input motion at the outcrop.

Figure 2.4 shows the transfer function of shear wave, amplitude ratios of Rayleigh wave and microtremor for six locations in Japan. During the comparision of theoretical curves, the amplitude ratio, AR (T), of microtremor used have been expressed by the following equation:

$$\text{AR (T)} = \frac{\sqrt{F_{NS}(T)F_{EW}(T)}}{F_{UD}(T)} \tag{2.1}$$

Where F_{NS}, $F_{EW}(T)$ and $F_{UD}(T)$ are average Fourier spectra of six time instants.

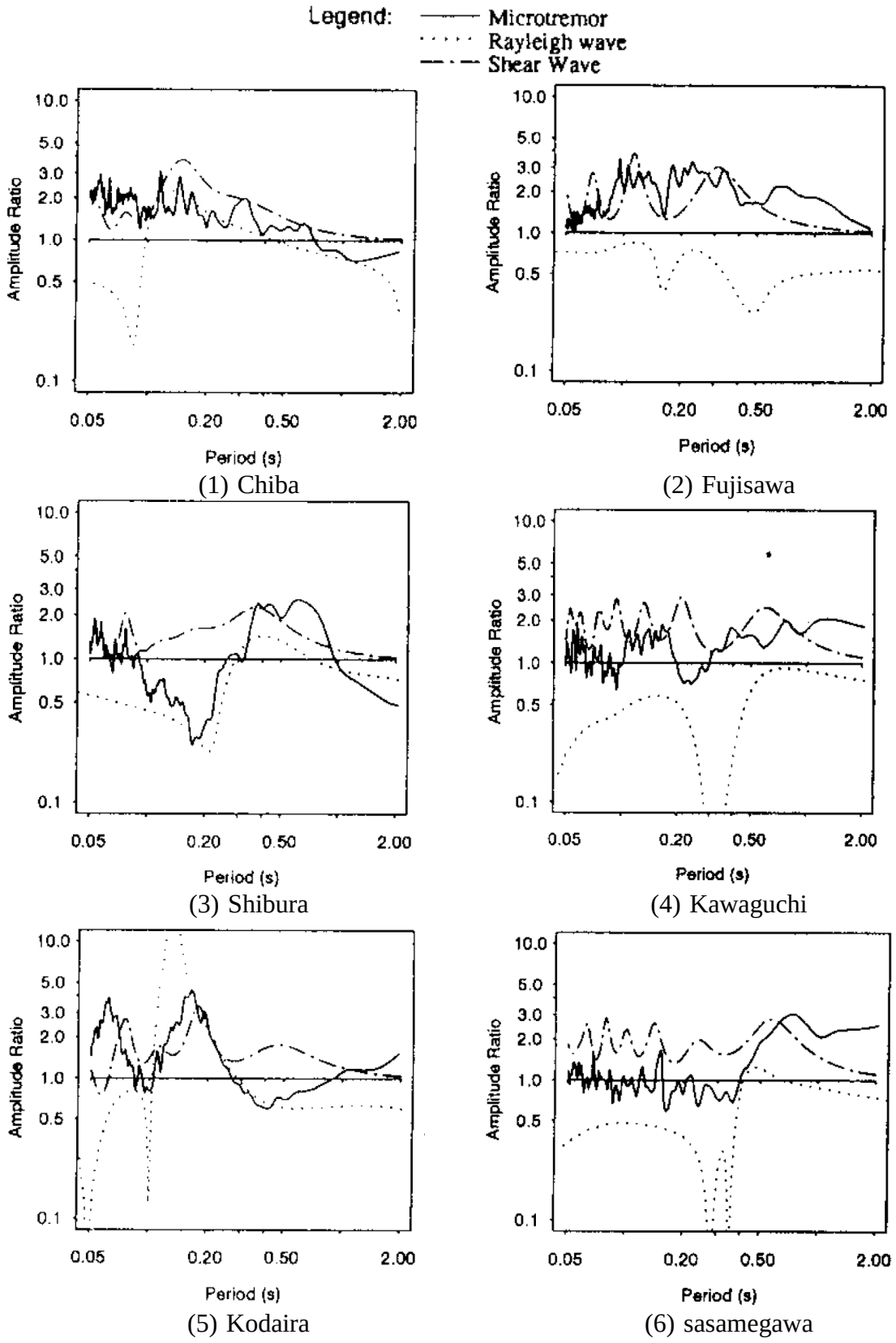

Figure 2.4: Amplitude ratios of microtremor and theoretical Rayleigh-wave plotted with transfer function of shear wave. (After Ansary et al., 1996)

The trend of three curves, i.e., two theoretical and one observed, somewhat resembles each other for these sites. Ansary et al. (1996) found that the period at which the Rayleigh wave amplitude ratio either suddenly drops or peaks, microtremor amplitude ratio closely resembles it. In a general sense, amplitude ratio for pure Rayleigh wave is always lower than the amplitude ratio of microtremor. The reason is that microtremor may contain some shear wave and Love wave contents as well as Rayleigh wave. Ansary et al. (1996) concluded that the characteristics of the microtremor's amplitude ratio are similar to that of Rayleigh wave and the period corresponding to the peak amplitude ratio corresponds to the peak periods of Rayleigh wave amplitude ratio and Shear wave transfer function.

2.3 MICROTREMOR H/V TECHNIQUE

Damages caused by the recent earthquakes are concluded as a direct result of local geological conditions affecting the ground motion. Best approach for understanding ground conditions is through direct observation of seismic ground motion, but such studies are restricted to areas with relatively high rates of seismicity. Because of these restrictions in other methods, such as high rates of seismicity and the availability of an adequate reference site, non-reference site methods have been applied to site response studies. Microtremor is a very convenient tool to estimate the effect of surface geology on seismic motion without needing other geological information. H/V technique fits very well to this description and it has received great attention from all over the world with its simplicity together with quick information about dynamic characteristics of ground and structures. Although several researchers claimed that theoretical background of this technique is not clear, there have been many successful experimental studies performed. Method is attractive since it gives the ease of data collection and it can be applied in areas of low or even no seismicity.

2.3.1 Method of Microtremor H/V Technique

Techniques for analyzing microtremors are generally divided into two main categories: non-reference site (H/V) and reference site (Hs/Hr) techniques. In Hs/Hr method, assumptions are that at nearby sites, source and path effects are believed to be identical

and reference site is free of any site effect. Therefore, motion recorded at the reference station is representative of the excitation arriving at the interface sediments under the soft soil site and spectral ratio, Hs/Hr, constitute a reliable estimate of site response. This technique, introduced first by Borcherdt (1970), is still widely used and is very popular for the analysis of weak or strong motion records. It has been applied to microtremor measurements by Kagami et al. (1986) with good results. In the traditional spectral ratio method, Hs/Hr, site and source effects are estimated from observations at a reference site. In practice, adequate reference site are not always available especially in flat areas. Therefore, methods have been developed that do not need reference sites (Bard, 2004).

A technique using horizontal to vertical spectral ratios (H/V) of the microtremors, which was first applied by Nogoshi and Igarashi (1970, 1971) and popularized by Nakamura (1989), has been widely used to estimate the site effects. Several recent applications of this technique have proved to be effective in estimating fundamental periods as well as relatively amplification factors. Several methods have been proposed for spectral calculation of ground motions including microtremors. Fourier spectrum is the most convenient one that is used widely. Some investigations showed that different methods give similar results (Dimitriu et al., 1998). However some researchers declare that a suitable spectral method gives more reliable results. Ghayamghamian and Kawakami (1997) introduced segmental cross-spectrum (SCS), as an effective tool for compensating unknown effects like source effects and noise in input and output measurements. They evaluated the performance of SCS in contrast with the conventional methods, i.e. Fourier or power spectra through the mathematical modeling and numerical simulations. Results of their studies indicated that SCS gives more reliable results for both amplification factor and predominant resonance frequency of the site than the conventional methods.

2.3.2 Theory of Microtremor H/V Technique

The typical geological structure of sedimentary basin has been shown in Figure 2.5. Definition of ground motions and their spectra at different places are defined in following lines. Here microtremor is divided into two parts considering it contains Rayleigh wave and other waves. Then, horizontal and vertical spectra on the surface ground of the sedimentary basin (H_f, V_f) can be written as follows.

$$H_f = A_h * H_b + H_s \quad V_f = A_v * V_b + V_s \tag{2.2}$$

$$T_h = \frac{H_f}{H_b} \quad T_v = \frac{V_f}{V_b} \tag{2.3}$$

Where $A_h$and A_v are amplification factor of horizontal and vertical motions of vertically incident body wave. H_b and V_b are spectra of horizontal and vertical motion in the basement under the basin (outcropped basin).

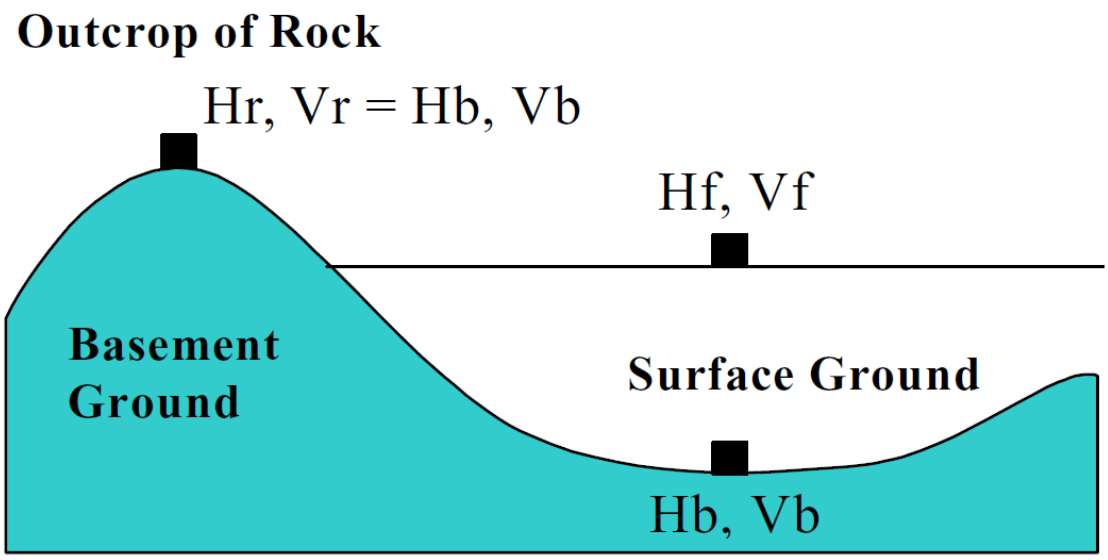

Figure 2.5: Typical geological structure of sedimentary basin

H_s and V_s are spectra of horizontal and vertical directions of Rayleigh waves. T_h and T_v are amplification factor of horizontal and vertical motion of surface sedimentary ground based on seismic motion on the exposed rock ground near the basin. In general, P wave velocity is more than three-four times of S wave velocity. In such sedimentary layer, vertical component cannot be amplified (A_v=1) around the frequency range where horizontal component receives large amplification. If there is no effect of Rayleigh waves, $V_f \approx V_b$. On the other hand, if V_f is larger thanV_b, it is considered as the effect of surface waves. Then estimating the effect of Rayleigh waves by V_f/V_b (= T_v), horizontal amplification can be written as,

$$T_h^* = \frac{T_h}{T_v} = \frac{\frac{H_f}{V_f}}{\frac{H_b}{V_b}} = \frac{QTS}{\frac{H_b}{V_b}} = \frac{\left[A_h + \frac{H_s}{H_b}\right]}{\left[A_v + \frac{V_s}{V_b}\right]} \tag{2.4}$$

$$\text{QTS} = \frac{H_f}{V_f} = \frac{A_h * H_b + H_s}{A_v * V_b + V_s} = \frac{H_b}{V_b} \cdot \frac{\left[A_h + \frac{H_s}{H_b}\right]}{\left[A_v + \frac{V_s}{V_b}\right]} \tag{2.5}$$

In equation (2.5), $\frac{H_b}{V_b} \approx 1$. $\frac{H_s}{H_b}$ and $\frac{V_s}{V_b}$ are related with the route of energy of Rayleigh waves. If there is no influence of Rayleigh wave, QTS = A_h/A_v. If amount of Rayleigh wave is high, then second term in above formulation gets dominant and QTS = H_s/V_s and the lowest peak frequency of H_s/V_s is nearly equal to the lowest proper frequency F_o of A_h(Figure 2.6).

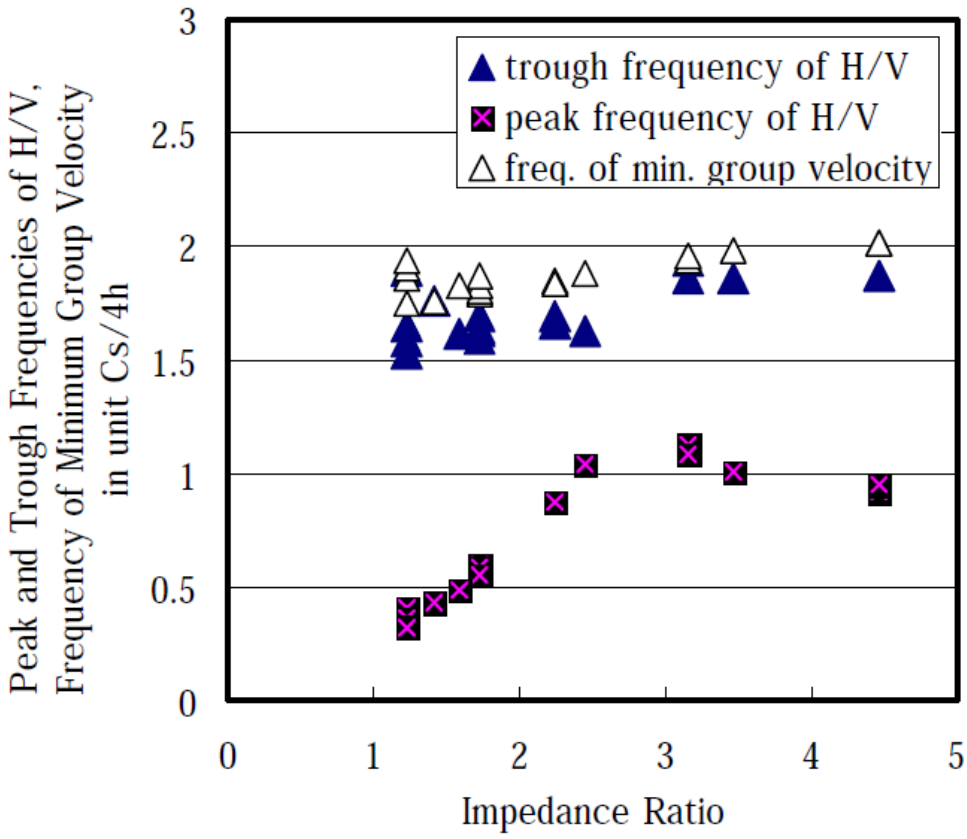

Figure 2.6: Relationship between charactersistics of Rayleigh Wave and Impedance Ratio. (After Nakamura, 2000)

In the range of, A_v= 1. QTS shows stable peak at frequency, F_0. Even when influence of Rayleigh wave is large, V_s becomes small (which results in a peak of H_s/V_s) around the first order proper frequency due to the multiple reflection of horizontal motions. And QTS = A_h, if microtremors of the basement V_b is relatively large comparing to the Rayleigh wave.

Figure 2.7 shows a schematic comparison of Horizontal (H_f), Vertical (V_f), H_f/H_b (spectral ratio of sediment site to the reference site) and H_f/V_f (H/V technique). As it can be followed QTS is smaller than the theoretical transfer function. Since H_f includes the effects of Rayleigh waves, H_f/H_b is bigger than the theoretical transfer function. If influence of Rayleigh wave becomes larger, QTS < 1 in the wide range of frequency and if influence is small, QTS locally expected to be smaller than one, in the narrow frequency range at frequency several times higher than F_o, because of the influence of vertical motion. Main waves consisting of microtremors are either body waves or Rayleigh waves, or depending on the location and other conditions can be mixture of both waves.

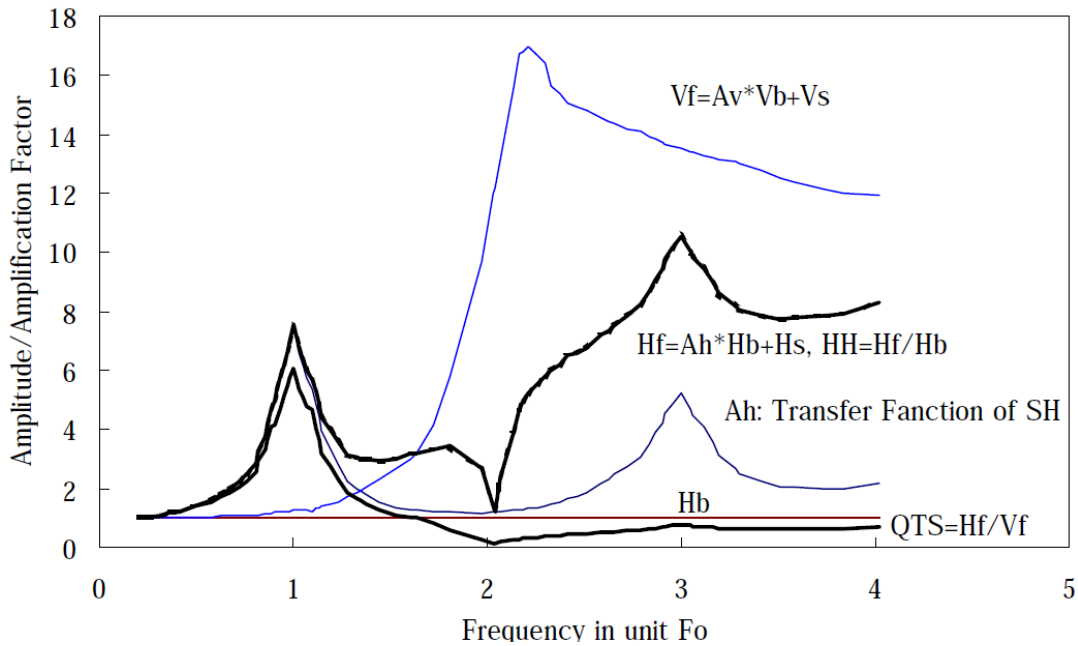

Figure 2.7: Schematic comparison of Horizontal (H_f), Vertical (V_f), H_f/H_b (spectral ratio of sediment site to the reference site). (After Nakamura, 2000)

2.4 WAVE PROPAGATION

Microtremor records various types of waves like seismic waves: body waves and surface waves. So, it is important to understand the characteristics of these waves for microtremor study. Different types of microtremor waves are shown in Figure 2.8.

Body waves, which can travel trough the interior of the earth, are two types: P-waves and S-waves (Figure 2.10). P-waves, also known as primary, compressional, or longitudinal waves, involved successive compression and refraction of the materials through which they pass. They are analogous to sound waves; the motion of an individual particle that a p-wave travels through is parallel to the direction of travel. Like sound wave, P-waves can travel through solids and fluids. S-waves, also known as secondary, shear, or transverse waves, because shearing deformations as they travel through a material. The motion of an individual particle is perpendicular to the direction of S-wave travel. The direction of particle movement can be used to divided s-wave into two components, SV (Vertical plane movement) and SH (Horizontal plane movement). The speed at which body waves travel varies with the stiffness of the materials they travel through. Since geologic materials are stiffest in compression, P-waves travel faster than other seismic waves and are therefore the first to arrive at a particular site. Fluids, which have no shearing stiffness, can not sustain S-waves.

Surface waves result from the interaction between body waves and the surface and surficial layers of the earth. They travel along the earth's surface with amplitudes that decrease roughly exponentially with depth. Because of the nature of the interactions required to produce them, surface waves are more prominent at distances farther from the source of the earthquake. At distances greater than about twice the thickness of the earth's crust, surface waves, rather than body waves, will produce peak ground motions. The most important surface waves, for engineering purposes, are Rayleigh waves and Love Waves. Rayleigh waves, produced by interaction of P- and SV- waves with the earth's surface, involve both vertical and horizontal particle motion. They are similar, in some respects, to the waves produced by a rock thrown into a pound. Love waves result from the interaction of SH-waves with a soft surficial layer and have no vertical component of particle motion. The mathematical expressions of these waves are discussed in this chapter.

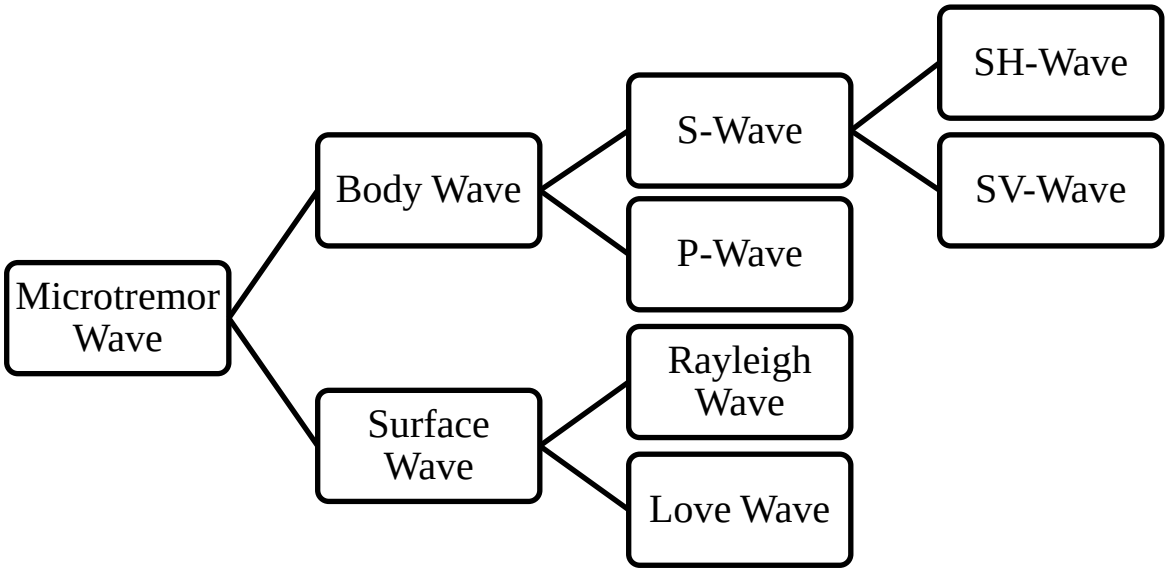

Figure 2.8: Different type of Microtremor Wave due to ambient noise of ground.

2.4.1 Equation of Motion for a Three-Dimensional Elastic Solid

Three-dimensional equations of motion for an elastic solid are obtained from equilibrium requirements, except that equilibrium must be ensured in three perpendicular directions. The variation in stress across an infinitesimal cube aligned with its sides parallel to the x-y-z axes has been shown in Figure 2.9. Assuming that the average stress on each face of the cube is represented by the stress shown at the centre of the face, the resultant forces acting in the x-, y-, and z-directions can be evaluated. In the x-direction, the unbalanced external forces must be balanced by an inertial force in that direction, so that

$$\rho\, dx\, dy\, dz \frac{\partial^2 u}{\partial t^2} = (\sigma_{xx} + \frac{\partial \sigma_{xx}}{\partial x} dx)\, dy\, dz - \sigma_{xx}\, dy\, dz$$

$$+ (\sigma_{xy} + \frac{\partial \sigma_{xy}}{\partial y} dx)\, dx\, dz - \sigma_{xy}\, dx\, dz \qquad (2.6)$$

$$+ (\sigma_{xz} + \frac{\partial \sigma_{xz}}{\partial z} dx)\, dx\, dy - \sigma_{xz}\, dx\, dy$$

Which simplifies to

$$\rho \frac{\partial^2 u}{\partial t^2} = \frac{\partial \sigma_{xx}}{\partial x} + \frac{\partial \sigma_{xy}}{\partial y} + \frac{\partial \sigma_{xz}}{\partial z} \qquad (2.7a)$$

Repeating this operation in the y- and z-directions gives

$$\rho \frac{\partial^2 v}{\partial t^2} = \frac{\partial \sigma_{yx}}{\partial x} + \frac{\partial \sigma_{yy}}{\partial y} + \frac{\partial \sigma_{yz}}{\partial z} \tag{2.7b}$$

$$\rho \frac{\partial^2 w}{\partial t^2} = \frac{\partial \sigma_{zx}}{\partial x} + \frac{\partial \sigma_{zy}}{\partial y} + \frac{\partial \sigma_{zz}}{\partial z} \tag{2.7c}$$

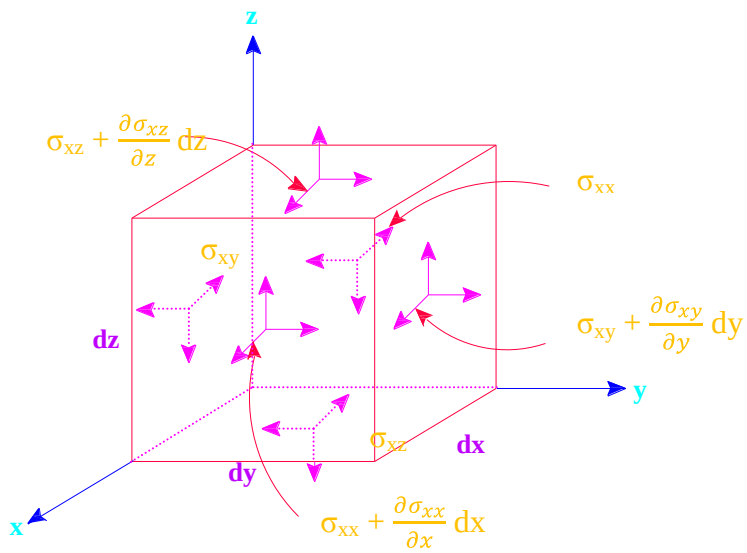

Figure 2.9: Stresses in x-direction on infinitesimal cube.

Equations (2.7) represent the three-dimensional equations of motion of an elastic solid. These equations have been derived solely on the basis of equilibrium consideration and thus apply to solids of any stress-strain behavior. To express these equations of motion in terms of displacements, it is again necessary to use a stress-strain relationship and a strain-displacement relationship. Using Hook's law, the first of the equations of motion [equation 2.7(a)] can be written as.

$$\rho \frac{\partial^2 u}{\partial t^2} = \frac{\partial}{\partial x}(\lambda\, \bar{\varepsilon} + 2\mu\, \varepsilon_{xx}) + \frac{\partial}{\partial y}(\mu\, \varepsilon_{xy}) + \frac{\partial}{\partial z}(\mu\, \varepsilon_{xz}) \tag{2.8}$$

Substituting the strain-displacement relationships

$$\varepsilon_{xx} = \frac{\partial u}{\partial x} \qquad \varepsilon_{xy} = \frac{\partial v}{\partial x} + \frac{\partial u}{\partial y} \qquad \varepsilon_{xz} = \frac{\partial w}{\partial x} + \frac{\partial u}{\partial z}$$

into equation (3) produces the desired equation of motion in terms of displacements:

$$\rho \frac{\partial^2 u}{\partial t^2} = (\lambda + \mu) \frac{\partial \bar{\varepsilon}}{\partial x} + \mu \nabla^2 u \tag{2.9a}$$

where the Laplacian operator ∇^2 represents

$$\nabla^2 = \frac{\partial^2}{\partial x^2} + \frac{\partial^2}{\partial y^2} + \frac{\partial^2}{\partial z^2}$$

Repeating this process in the y and z directions gives

$$\rho \frac{\partial^2 v}{\partial t^2} = (\lambda + \mu) \frac{\partial \bar{\varepsilon}}{\partial y} + \mu \nabla^2 v \tag{2.9b}$$

$$\rho \frac{\partial^2 w}{\partial t^2} = (\lambda + \mu) \frac{\partial \bar{\varepsilon}}{\partial z} + \mu \nabla^2 w \tag{2.9c}$$

2.4.2 Solution of the Three-Dimensional Equations of motion

Together, equation (2.9) represents the three-dimensional equations of motion for an isotropic, linear and elastic solid. It turns out that these equations can be manipulated to produce two wave equations. Consequently, only two types of waves can travel through such an unbounded solid. The characteristics of each type of wave have been revealed their respective wave equations.

The solution for the first type of wave can be obtained by differentiating each type of equations (2.9) with respect to x, y and z and adding the results together to give

$$\rho \left(\frac{\partial^2 \varepsilon_{xx}}{\partial t^2} + \frac{\partial^2 \varepsilon_{yy}}{\partial t^2} + \frac{\partial^2 \varepsilon_{zz}}{\partial t^2} \right) = (\lambda + \mu) \left(\frac{\partial^2 \bar{\varepsilon}}{\partial x^2} + \frac{\partial^2 \bar{\varepsilon}}{\partial y^2} + \frac{\partial^2 \bar{\varepsilon}}{\partial z^2} \right)$$

$$+ \mu \left(\frac{\partial^2 \varepsilon_{xx}}{\partial x^2} + \frac{\partial^2 \varepsilon_{yy}}{\partial y^2} + \frac{\partial^2 \varepsilon_{zz}}{\partial z^2} \right)$$

or

$$\rho \frac{\partial^2 \bar{\varepsilon}}{\partial t^2} = (\lambda + \mu) \nabla^2 \bar{\varepsilon} + \mu \nabla^2 \bar{\varepsilon} \tag{2.10}$$

Rearranging yields the wave equation

$$\frac{\partial^2 \bar{\varepsilon}}{\partial t^2} = \frac{(\lambda + 2\mu)}{\rho} \nabla^2 \bar{\varepsilon} \tag{2.11}$$

Recalling that $\bar{\varepsilon}$ is the volumetric strain (which describes deformations that involves no shearing rotation), this wave equation describes an irrotational, or dilatational, wave. It indicates that a dilatational wave will propagate through the body at a velocity

$$v_p = \sqrt{\frac{(\lambda + 2\mu)}{\rho}} \tag{2.12}$$

This type of wave is commonly known as a P-wave (or primary wave) and V_P is referred to as the P-wave velocity of the material. The general nature of P-wave motion has been illustrated in Figure 2.10(a). Note that particle displacements are parallel to the direction of wave propagation.

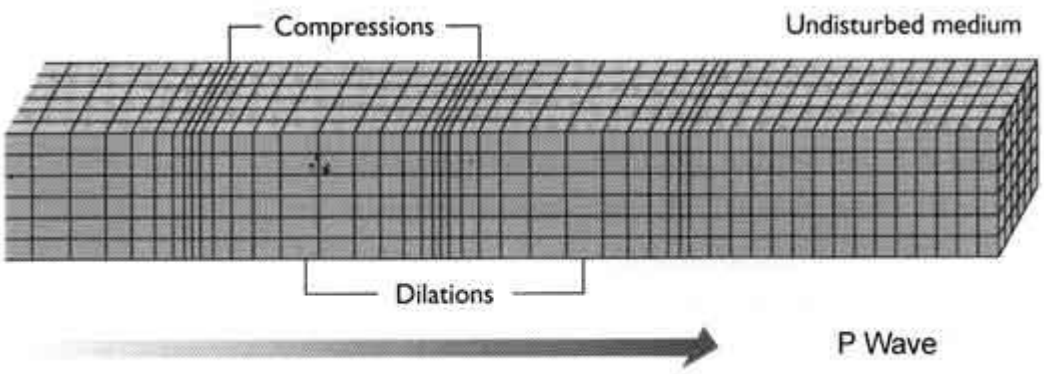

(a)

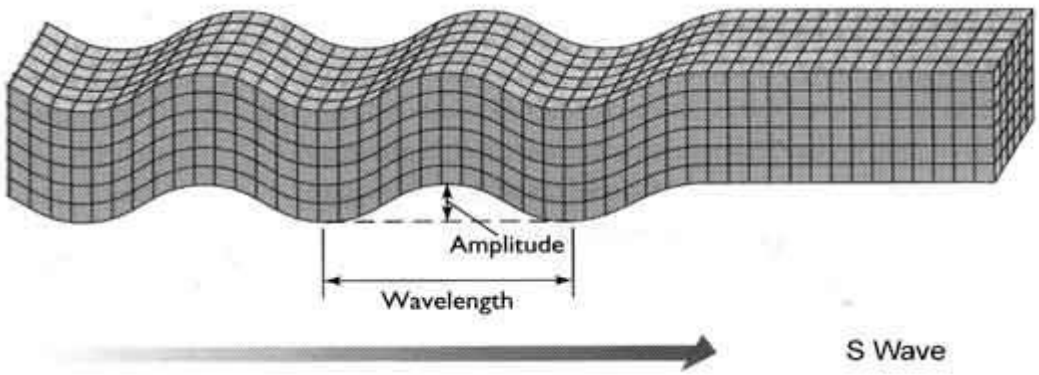

(b)

Figure 2.10: Deformation produced by body waves: (a) P-wave; (b) SV-wave.

v_p can be written in terms of shear modulus and Poisson's ratio as

$$v_p = \sqrt{\frac{G(2-2\upsilon)}{\rho(1-2\upsilon)}} \tag{2.13}$$

As υ approaches 0.5 (at which point the body becomes incompressible, i.e., infinitely stiff with respect to dilatational deformations), v_p approaches infinity.

To obtain the solution for the second type of wave, $\bar{\varepsilon}$ is eliminated by differentiating equation (2.9b) with respect to z and equation (2.9c) with respect to y, and subtracting one from the other:

$$\rho \frac{\partial}{\partial t^2}\left(\frac{\partial w}{\partial y} - \frac{\partial v}{\partial z}\right) = \mu \nabla^2 \left(\frac{\partial w}{\partial y} - \frac{\partial v}{\partial z}\right) \tag{2.14}$$

According to Hook's law, the generalized form of stress-strain can be written as follows:

$$\begin{aligned}
\sigma_{xx} &= C_{11}\varepsilon_{xx} + C_{12}\,\varepsilon_{yy} + C_{13}\,\varepsilon_{zz} + C_{14}\,\varepsilon_{xy} + C_{15}\,\sigma\varepsilon_{yz} + C_{16}\,\varepsilon_{zx} \\
\sigma_{yy} &= C_{21}\varepsilon_{xx} + C_{22}\,\varepsilon_{yy} + C_{23}\,\varepsilon_{zz} + C_{24}\,\varepsilon_{xy} + C_{25}\,\sigma\varepsilon_{yz} + C_{26}\,\varepsilon_{zx} \\
\sigma_{zz} &= C_{31}\varepsilon_{xx} + C_{32}\,\varepsilon_{yy} + C_{33}\,\varepsilon_{zz} + C_{34}\,\varepsilon_{xy} + C_{35}\,\sigma\varepsilon_{yz} + C_{36}\,\varepsilon_{zx} \\
\sigma_{xy} &= C_{41}\varepsilon_{xx} + C_{42}\,\varepsilon_{yy} + C_{43}\,\varepsilon_{zz} + C_{44}\,\varepsilon_{xy} + C_{45}\,\sigma\varepsilon_{yz} + C_{46}\,\varepsilon_{zx} \\
\sigma_{yz} &= C_{51}\varepsilon_{xx} + C_{52}\,\varepsilon_{yy} + C_{53}\,\varepsilon_{zz} + C_{54}\,\varepsilon_{xy} + C_{55}\,\sigma\varepsilon_{yz} + C_{56}\,\varepsilon_{zx} \\
\sigma_{zx} &= C_{61}\varepsilon_{xx} + C_{62}\,\varepsilon_{yy} + C_{63}\,\varepsilon_{zz} + C_{64}\,\varepsilon_{xy} + C_{65}\,\sigma\varepsilon_{yz} + C_{66}\,\varepsilon_{zx}
\end{aligned} \tag{2.15}$$

From the definition of rotation [equation (2.14) and equation (2.15)] can be written in the form of the wave equation

$$\frac{\partial^2 \Omega_x}{\partial t^2} = \frac{(\mu)}{\rho}\nabla^2\,\Omega_x \tag{2.16}$$

This describes an equivoluminal, or distortional wave, of rotation about the x-axis. Similar expressions can be obtained by the same process for rotation about the y-and z-axes. Equation (2.16) shows that a distortional wave will propagate through the solid at a velocity

$$v_s = \sqrt{\frac{\mu}{\rho}} = \sqrt{\frac{G}{\rho}} \tag{2.17}$$

This type of wave is commonly known as a S-wave (or shear wave) and v_s is referred to as the shear wave velocity of the material. Note that the particle motion is constrained to a plane perpendicular to the direction of wave propagation. Consequently, the torsional wave represented a form of an S-wave. The close relationship between S-wave velocity and shear modulus is used to advantage in many of the field and laboratory tests. The general nature of S-wave motion has been illustrated in Figure 2.10(b).

S-waves are often divided into two types, or resolved into two perpendicular components. SH-waves in which particle motion occurs only in a horizontal plane. SV-waves are S-waves whose particle motion lies in a vertical plane. A given S-wave with arbitrary particle motion can be represented as the vector sum of it's SH and SV components.

In summary, only two types of waves, known as body waves, can exist in an unbounded (infinite) elastic solid. P-waves involve no rotation of the material they pass through and travel at velocity, v_p. S-waves involve no volume change and travel at velocity, v_s. The velocity of P- and S-waves depends on the stiffnesses of the solid with respect to the types of deformation induced by each wave. Comparing the velocities [equations (2.13) and (2.17)]

$$\frac{v_p}{v_s} = \sqrt{\frac{2-2\upsilon}{1-2\upsilon}} \tag{2.18}$$

The P-wave velocity can be seen to exceed the S-wave velocity by an amount that depends on the compressibility (as reflected in Poisson's ratio) of the body. For a typical geologic materials, the ratio v_p/v_s = 1.87.

2.4.3 Waves in a Semi-infinite Body

The earth is obviously not an infinite body- it is a very large sphere with an outer surface on which stresses cannot exist. The earth is often idealized as a semi-infinite body with a planar free-surface (the effects' of the earth's curvature are neglected). The boundary conditions associated with the free surface allow additional solutions to the equations of motion to be obtained. This solutions describe waves whose motion is concentrated in a shallow zone near the free surface (i.e., surface waves). Surface waves are very important since they attenuate with distance more slowly than body waves.

Two types of surface waves are of primary importance in microtremor study (Figure 2.11). One, the Rayleigh wave, can be shown to exist in a homogeneous, elastic half-space. The other surface wave, the Love wave, requires a surficial layer of lower S-wave velocity than the underlying half-space. Other types of surface waves exist but are much less significant.

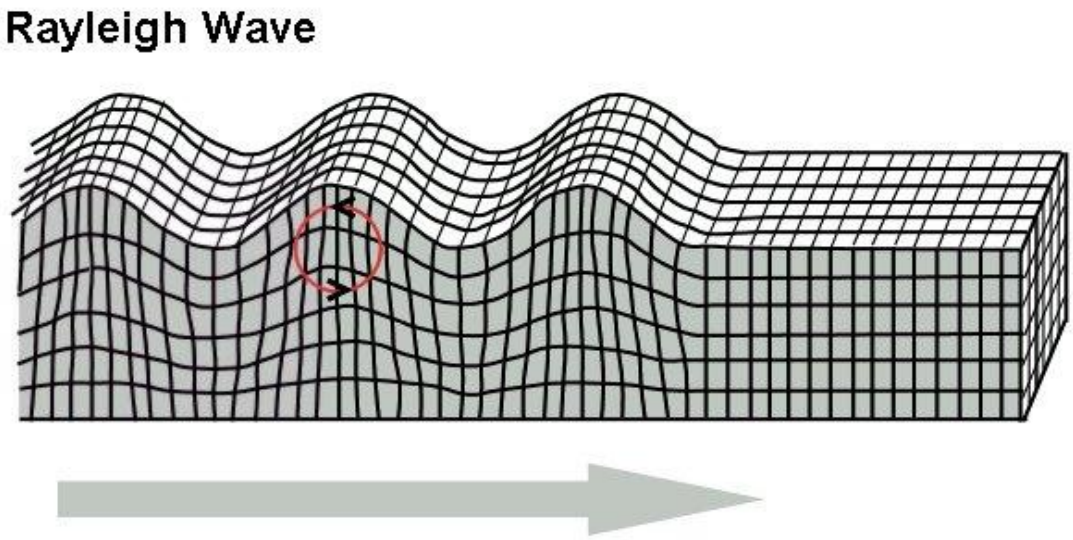

(a)

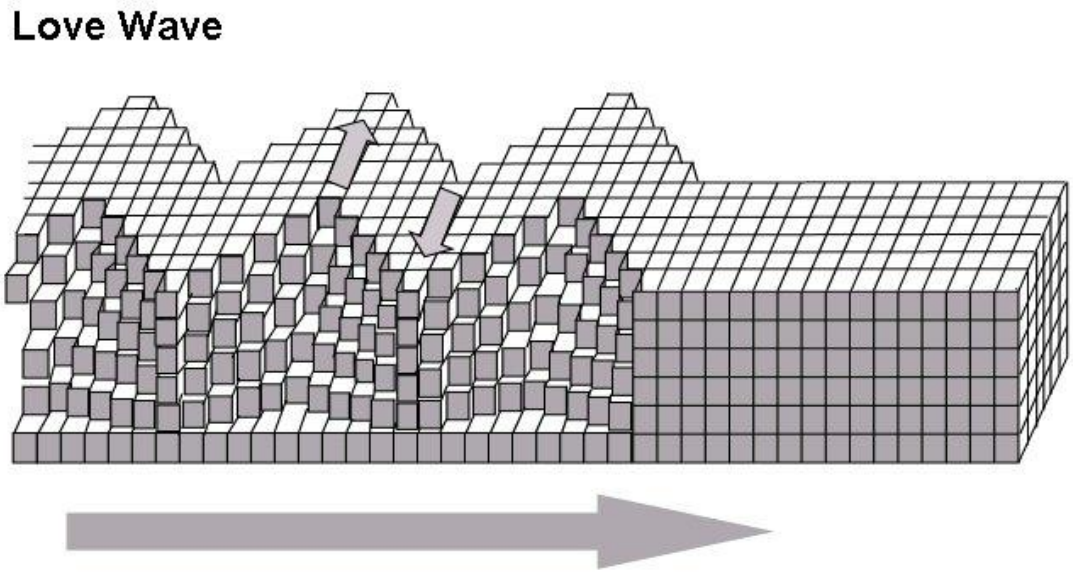

(b)

Figure 2.11: Deformation produced by Surface Waves: (a) Rayleigh Wave; (b) Love Wave.

2.4.3.1 Rayleigh Waves

Waves that exist near the surface of a homogeneous elastic half-space have been first investigated by Rayleigh (1885) and known to this date as Rayleigh waves. Figure 2.11a shows the Rayleigh wave propagation. To describe Rayleigh waves, consider a plane wave (Figure 2.12) that travels in the x-direction with zero particle displacement in the y-direction (v = 0). The z-direction is taken as positive downward, so all particle motion occurs in the x-z plane. Two potential functions, Φ and ψ, can be defined to describe the displacements in the x- and z-directions:

$$u = \frac{\partial \Phi}{\partial x} + \frac{\partial \psi}{\partial z} \tag{2.19a}$$

$$w = \frac{\partial \Phi}{\partial z} - \frac{\partial \psi}{\partial x} \tag{2.19b}$$

The volumetric strain, or dilatation, $\bar{\varepsilon}$, of the wave is given by $\bar{\varepsilon} = \varepsilon_{xx} + \varepsilon_{zz}$, or

$$\bar{\varepsilon} = \frac{\partial u}{\partial x} + \frac{\partial w}{\partial z} = \frac{\partial}{\partial x}\left(\frac{\partial \Phi}{\partial x} + \frac{\partial \psi}{\partial z}\right) + \frac{\partial}{\partial z}\left(\frac{\partial \Phi}{\partial z} + \frac{\partial \psi}{\partial x}\right) = \frac{\partial^2 \Phi}{\partial x^2} + \frac{\partial^2 \Phi}{\partial z^2} = \nabla^2 \Phi \tag{2.20}$$

The rotation in the x-z plane is given (equation 2.15) by

$$2\Omega_y = \frac{\partial u}{\partial z} - \frac{\partial w}{\partial z} = \frac{\partial}{\partial z}\left(\frac{\partial \Phi}{\partial x} + \frac{\partial \psi}{\partial z}\right) - \frac{\partial}{\partial z}\left(\frac{\partial \Phi}{\partial z} - \frac{\partial \psi}{\partial x}\right) = \frac{\partial^2 \Phi}{\partial z^2} + \frac{\partial^2 \psi}{\partial x^2} = \nabla^2 \psi \tag{2.21}$$

Use of the potential functions allows separation of the effects of dilatation and rotation [equations (2.20) and (2.21)] indicate that Φ and ψ are associated with dilatation and rotation, respectively. Therefore, Rayleigh waves can be thought of as combinations of P- and S-waves (SV waves for this case, since the x-z plane is vertical) that satisfy certain boundary conditions.

Substitution of the expressions for u and w into the equations of motion as written in equations (2.9a) and (2.9c).

$$\rho\frac{\partial}{\partial x}\left(\frac{\partial^2 \Phi}{\partial x^2}\right) + \rho\frac{\partial}{\partial x}\left(\frac{\partial^2 \Phi}{\partial x^2}\right) = (\lambda + 2\mu)\frac{\partial}{\partial x}(\nabla^2 \Phi) + \mu\frac{\partial}{\partial z}(\nabla^2 \psi) \tag{2.22a}$$

$$\rho\frac{\partial}{\partial z}\left(\frac{\partial^2\Phi}{\partial t^2}\right) - \rho\frac{\partial}{\partial x}\left(\frac{\partial^2\psi}{\partial t^2}\right) = (\lambda + 2\mu)\frac{\partial}{\partial z}(\nabla^2\Phi) - \mu\frac{\partial}{\partial x}(\nabla^2\psi) \qquad (2.22b)$$

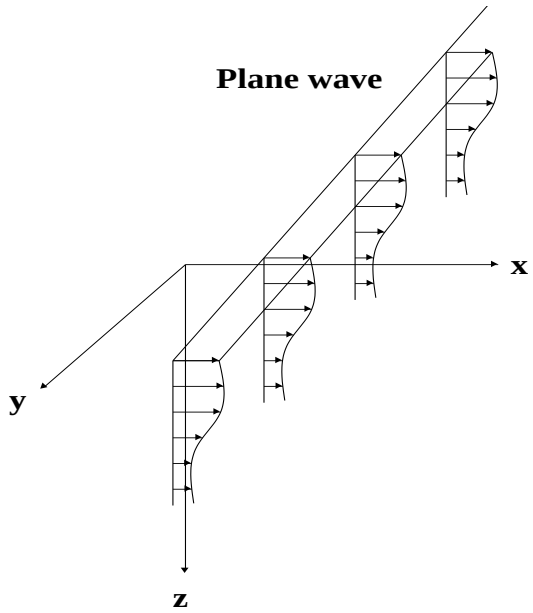

Figure 2.12: Motion induced by a typical plane wave that propagates in the x-direction. Wave motion does not vary in the y-direction.

Solving equations (2.22) simultaneously for $\frac{\partial^2\Phi}{\partial t^2}$ and $\frac{\partial^2\psi}{\partial t^2}$ shows

$$\frac{\partial^2\Phi}{\partial t^2} = \frac{\lambda + 2\mu}{\rho}\nabla^2\Phi = v_p^2\nabla^2\Phi$$

(2.23a)

$$\frac{\partial^2\psi}{\partial t^2} = \frac{\mu}{\rho}\nabla^2\psi = v_s^2\nabla^2\psi \qquad (2.23b)$$

If the wave is harmonic with frequency ω and wave number k_R, so that it propagates with Rayleigh wave velocity $v_R = \omega^2/k_R$, the potential function can be expressed as

$$\Phi = F(z)\, e^{i(\omega t - k_R x)} \qquad (2.24a)$$

$$\Psi = G(z)\, e^{i(\omega t - k_R x)} \qquad (2.24b)$$

Where F and G are functions that describe the manner in which the amplitude of the dilatational and rotational components of the Rayleigh wave vary with depth. Substituting these expressions for Φ and ψ into equations (2.23) gives

$$- \frac{\omega^2}{v_p^2} F(z) = - k_R^2 F(z) + \frac{d^2F(z)}{dz^2} \quad (2.25a)$$

$$- \frac{\omega^2}{v_s^2} G(z) = - k_R^2 G(z) + \frac{d^2G(z)}{dz^2} \quad (2.25b)$$

Which can be rearranged to give the second-order differential equations

$$\frac{d^2F}{dz^2} - (k_R^2 - \frac{\omega^2}{v_p^2}) F = 0 \quad (2.26a)$$

$$\frac{d^2G}{dz^2} - (k_R^2 - \frac{\omega^2}{v_s^2}) G = 0 \quad (2.26b)$$

The general solution to these equations can be written in the form

$$F(z) = A_1 e^{-qz} + B_1 e^{qz} \quad (2.27a)$$

$$G(z) = A_2 e^{-sz} + B_2 e^{sz} \quad (2.27b)$$

Where

$$q^2 = k_R^2 - \frac{\omega^2}{v_p^2}$$

$$s^2 = k_R^2 - \frac{\omega^2}{v_s^2}$$

The second term of equations (2.27) corresponds to a disturbance whose displacement amplitude approaches infinity with increasing depth. Since this type of behavior is not realistic, B1 and B2 must be zero, and the potential functions can finally be written as

$$\Phi = A_1 e^{-qz+i(\omega t - k_R x)} \quad (2.28a)$$

$$\Psi = A_2 e^{-sz+i(\omega t - k_R x)} \quad (2.28b)$$

Since neither shear nor normal stresses can exist at the free surface of the half-space, σ_{xz}= 0 and σ_{zz}= 0 when z = 0. Therefore,

$$\sigma_{zz} = \lambda \bar{\varepsilon} + 2\mu \varepsilon_{zz} = \lambda \bar{\varepsilon} + 2\mu \frac{dw}{dz} = 0 \quad (2.29a)$$

$$\sigma_{xz} = \mu\ \varepsilon_{xz} = \mu\ (\frac{dw}{dx} + \frac{du}{dz} = 0 \qquad (2.29b)$$

Using the potential function definitions of u and w (equations 2.19) and the solution for the potential functions (equations 2.28), the free surface boundary conditions can be rewritten as

$$\sigma_{zz}(z = 0) = A_1\,[(\lambda + 2\mu)\ q^2 - \lambda k_R^2\ ] - 2i\ A_2\ \mu K_R s = 0 \qquad (2.30a)$$

$$\sigma_{xz}(z = 0) = \frac{A_1}{A_2}\frac{(\lambda+2\mu)q^2 - \lambda\ k_R^2}{2i\mu k_R s} - 1 = 0 + A_2\,(s^2 + k_R^2\ ) = 0 \qquad (2.30b)$$

Which can be rearranged to yield

$$\frac{A_1}{A_2}\frac{(\lambda+2\mu)q^2 - \lambda\ k_R^2}{2i\mu k_R s} - 1 = 0 \qquad (2.31a)$$

$$\frac{A_1}{A_2}\frac{2iqK_R}{s^2 + K_R^2} + 1 = 0 \qquad (2.31b)$$

With these results, the velocities and displacement patterns of Rayleigh waves can be determined.

(a) Rayleigh Wave Velocity

Rayleigh waves are often mechanically generated and their velocities measured in the field to investigate the stiffness of surficial soil. Adding equations (2.31) and cross-multiplying gives

$$4q\mu s k_R^2 = (\ s^2 + K_R^2)\ [\ (\lambda + 2\mu)q^2 - \lambda\ k_R^2] \qquad (2.32)$$

Which, upon introducing the definitions of q and s and factoring out a $G^2 k_R^8$ term, yields

$$16\ (1 - \frac{\omega^2}{v_p^2 k_R^2})\ (1 - \frac{\omega^2}{v_s^2 k_R^2}) = (2 - \frac{\lambda+2\mu}{\mu}\ \frac{\omega^2}{v_p^2 k_R^2})^2 (2 - \frac{\omega^2}{v_s^2 k_R^2})^2 \qquad (2.33)$$

Defining K_{Rs}as the ratio of the Rayleigh wave velocity to the s-wave velocity

$$K_{Rs} = \frac{V_R}{V_s} = \frac{\omega}{V_s K_R}$$

then

$$\frac{V_R}{V_p} = \frac{\omega}{V_p K_R} = \frac{\omega}{V_S k_R \sqrt{(\lambda+2\mu)/\mu}} = \alpha\, K_{Rs}$$

Where $\alpha = \sqrt{\frac{\mu}{(\lambda+2\mu)}} = \sqrt{\frac{(1-2v)}{(2-2v)}}$. Then equation (2.33) can be rewritten as

$$16\,(1 - \alpha^2 k_{Rs}^2)\,(1 - k_{Rs}^2) = (2 - \frac{1}{\alpha^2} k_{Rs}^2)^2 (2 - k_{Rs}^2)^2 \qquad (2.34)$$

Which can be expanded and rearranged into the equation

$$K_{Rs}^6 - 8\,K_{Rs}^4 + (24-16\alpha^2)\,K_{Rs}^2 + 16\,(\alpha^2-1) = 0 \qquad (2.35)$$

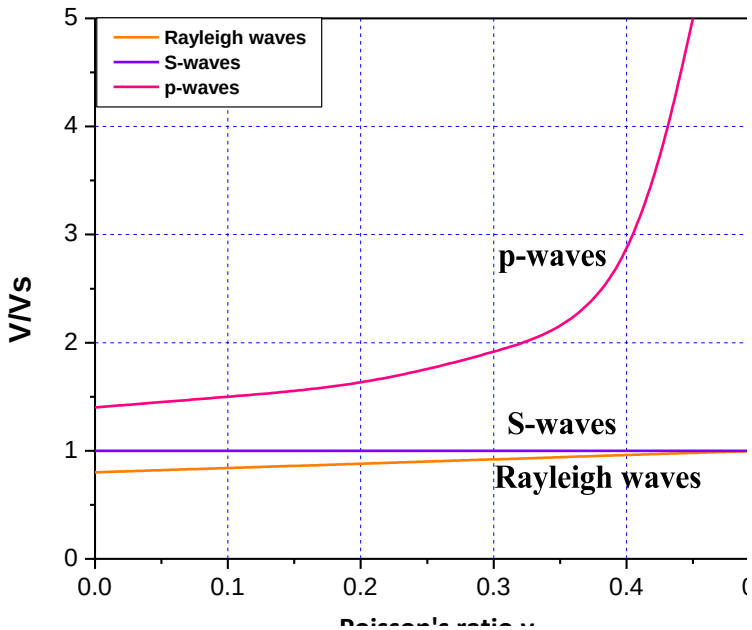

Figure 2.13: Variation of Rayleigh Wave and Body Wave propagation velocities with Poisson's ratio. (After Kramer, 1996)

This equation is cubic in K_{Rs}^2, and real solutions for K_{Rs} can be found for various values of Poisson's ratio. These allow evaluation of the ratios of the Rayleigh wave velocity to both S- and P-wave velocities as functions of v. The solution shown in Figure 2.13 that Rayleigh waves travel slightly slower than S-waves for all values of Poisson's ratio except 0.5.

(b) Rayleigh Wave Displacement Amplitude

Article 2.4.3.1(a) showed how the velocity of a Rayleigh wave compares with that of P- and S-waves. Some of the intermediate results of that section can be used to illustrate the nature of particle motion during the passage of Rayleigh waves. Substituting the solutions for the potential functions Φ and Ψ [equations 2.28] into the expressions for u and w (equations 14) into the expressions for u and w (equations 2.19) and carrying out the necessary partial differentiations yields

$$u = - A_1 ik\, e^{-qz+i(\omega t- k_R x)} - A_2 s\, e^{-sz+i(\omega t- k_R x)} \qquad (2.36a)$$

$$w = - A_1 i k_R\, e^{-qz+i(\omega t- k_R x)} + A_2 i k_R\, e^{-sz+i(\omega t- k_R x)} \qquad (2.36b)$$

From equation (2.31b),

$$A_2 = - \frac{2qiK_R}{s^2+K_R^2} A_1$$

Which, substituting into equations (2.36), gives

$$u = A_1 \left(-i\, k_R\, e^{-qz} + \frac{2iqsK_R}{s^2+K_R^2} e^{-sz}\right) e^{i(\omega t- k_R x)} \qquad (2.37a)$$

$$w = A_1 \left(\frac{2qK_R^2}{s^2+K_R^2} e^{-sz} - q e^{-qz}\right) e^{i(\omega t- k_R x)} \qquad (2.37b)$$

Where the terms in parentheses describe the variation of the amplitudes of u and w with depth. These horizontal and vertical displacement amplitudes are illustrated for several values of Poisson's ratio in Figure 2.14. Examination of equations (2.37) indicates that the horizontal and vertical displacements are out of phase by 90°. Hence the horizontal displacement will be zero when the vertical displacement reaches its maximum (or minimum), and vice versa. The motion of a particle near the surface of the half –space is in the form of a retrograde ellipse (as opposed to the prograde ellipse particle motion observed at the surface of water waves). The general nature of Rayleigh wave motion has been illustrated in Figure 2.11a.

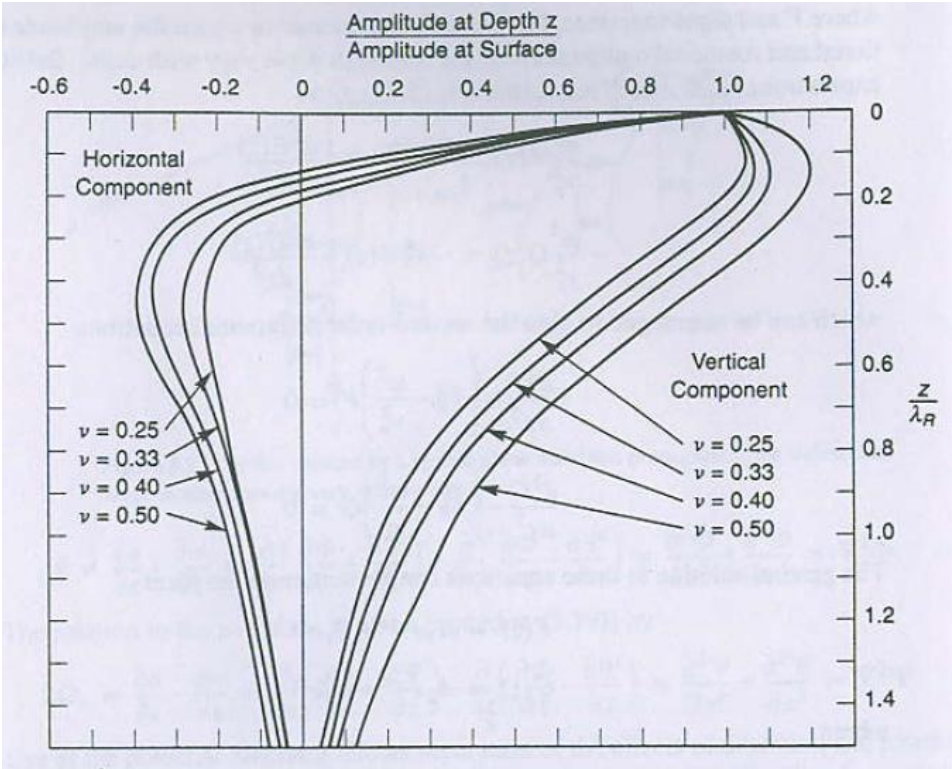

Figure 2.14: Horizontal and vertical motion of Rayleigh waves. A negative amplitude ratio indicates that the displacement is in the opposite direction of the surface displacement. (After Richart et al., 1970)

The Rayleigh waves produced by earthquakes were once thought to appear only at very large epicentral distances (several hundred km). It is now recognized, however, that they can be significant at much shorter distances (a few tens of kilometers). The ratio of minimum epicentral distance, R, to focal depth, h, at which Rayleigh waves first appear in a homogeneous medium, is given by

$$\frac{R}{h} = \frac{1}{\sqrt{\left(\frac{v_p}{v_R}\right)^2 - 1}} \tag{2.38}$$

Where v_p and v_R are the wave propagation velocities of P-waves and Rayleigh waves, respectively (Ewing et al., 1957).

2.4.3.2 Love Waves

In a homogeneous elastic half-space, only P-waves, S-waves, and Rayleigh waves can exist. If the half-space is overlain by a layer of material with lower body wave velocity, however, Love waves can develop (Love, 1927). Love waves essentially consist of SH-waves that are trapped by multiple reflections within the surficial layer. Consider the case of a homogeneous surficial layer of thickness H overlying a homogeneous half-space as shown in Figure 2.15. A love wave traveling in the + x-direction would involve particle displacements only in the y-direction (SH-wave motion), and could be described by the equation

$$v\,(x, z, t) = V\,(z)\, e^{i(K_L x - \omega t)} \tag{2.39}$$

Where v is the particle displacements in the y-direction, V (z) describes the variation of v with depth, and K_L is the wave number of the Love wave. The Love must satisfy the wave equations for S-waves in both the surficial layer and the half-space

$$\frac{\partial^2 v}{\partial t^2} = \begin{cases} \frac{G_1}{\rho_1}\left(\frac{\partial^2 v}{\partial x^2} + \frac{\partial^2 v}{\partial z^2}\right) & \text{for } 0 \le z \le H \quad (2.40a) \\ \frac{G_2}{\rho_2}\left(\frac{\partial^2 v}{\partial x^2} + \frac{\partial^2 v}{\partial z^2}\right) & \text{for } z \ge H \quad (2.40b) \end{cases}$$

The amplitude can be shown (Aki and Richards, 1980) to vary with depth according to

$$V\,(z) = \begin{cases} A_1 e^{-v_1 z} + B_1 e^{v_1 z} & \text{for } 0 \le z \le H \quad (2.45a) \\ A_2 e^{-v_2 z} + B_2 e^{v_2 z} & \text{for } z \ge H \quad (2.45b) \end{cases}$$

Where the A and B coefficients describe the amplitudes of downgoing and upgoing waves, respectively, and

$$V_1 = \sqrt{\frac{K_L^2 - \omega^2}{\frac{G_1}{\rho_1}}} \qquad V_2 = \sqrt{\frac{K_L^2 - \omega^2}{\frac{G_2}{\rho_2}}} \tag{2.46}$$

Since the half-space extends to infinite depth, B_2 must be zero (no energy can be supplied or reflected at infinite depth to produce an upgoing wave).

The requirement that all stresses vanish at the ground surface is satisfied if

$$\frac{\partial v}{\partial z} = \frac{\partial V(z)}{\partial z} e^{i(K_L x - \omega t)} = -A_1 v_1 e^{-v_1 z} + v_1 B_1 e^{v_1 z} = (A_1 - B_1)\, v_1 \left(e^{-v_1 z} + e^{v_1 z} = 0 \right.$$

In other words, if $A_1 = B_1$. The amplitude can now be rewritten in terms of the two remaining unknown amplitude as

$$V(z) = \begin{cases} A_1 (e^{-v_1 z} + e^{v_1 z}) & \text{for } 0 \le z \le H \quad (2.47a) \\ A_2 e^{-v_2 z} & \text{for } z \ge H \quad (2.47b) \end{cases}$$

At the z = H interface, continuity of stresses requires that

$$2iG_1\, v_1\, A_1 \sin i v_1 H = G_2 v_2\, A_2\, e^{-v_2 H} \qquad (2.48)$$

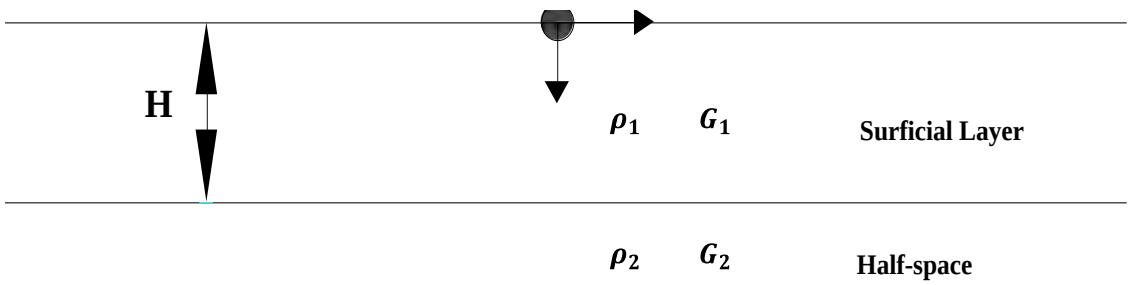

Figure 2.15: Schematic illustration of softer surficial layer ($G_1\rho_1 < G_2\rho_2$) overlying elastic half space, the simplest conditions for which Love waves can exist.

And compatibility of displacements require that

$$2A_1 \cos(i v_1 H) = A_2\, e^{-v_2 H} \qquad (2.49)$$

Using equations (2.48) and (2.49), A_2 can be expressed in terms of A_1 by

$$A_2 = \frac{2 \cos(i v_1 H)}{e^{-v_2 H}} A_1 \qquad (2.50)$$

Substituting equations (2.47) and (2.48) into (2.39) gives

V (x, z, t) =

$$\begin{cases} 2A_1\cos\left[\omega\left(\frac{1}{v_{s1}^2}-\frac{1}{v_L^2}\right)^{1/2}\right]e^{i(K_L x-\omega t)} & \text{for } 0 \le z \le H \quad (2.51a) \\ 2A_1\cos\left[\omega\left(\frac{1}{v_{s1}^2}-\frac{1}{v_L^2}\right)^{\frac{1}{2}}H\right]\exp\left[-\omega\left(\frac{1}{v_L^2}-\frac{1}{v_s^2}\right)^{\frac{1}{2}}(z-H)\right]e^{\cdots} & \text{for } z \ge H \quad (2.51b) \end{cases}$$

Where v_{S1} and v_{S2} are the shear wave velocities of materials 1 and 2, respectively and v_L is the velocity of the Love wave. Equation (2.51) shows, as illustrated in Figure 2.16, that the Love wave displacement amplitude varies sinusoidally with depth in the surficial layer and decays exponentially with depth in the underlying half-space. Because of this, Love waves are often described as SH-waves that are trapped in the surficial layer. The general nature of Love wav displacement has been shown in Figure 2.11(b).

The Love wave velocity is given by the solution of

$$\tan \omega H\left(\frac{1}{v_{s1}^2}-\frac{1}{v_L^2}\right)^{\frac{1}{2}} = \frac{G_2}{G_1}\sqrt{\frac{\frac{1}{v_L^2}-\frac{1}{v_{s2}^2}}{\frac{1}{v_{s1}^2}-\frac{1}{v_L^2}}} \qquad (2.52)$$

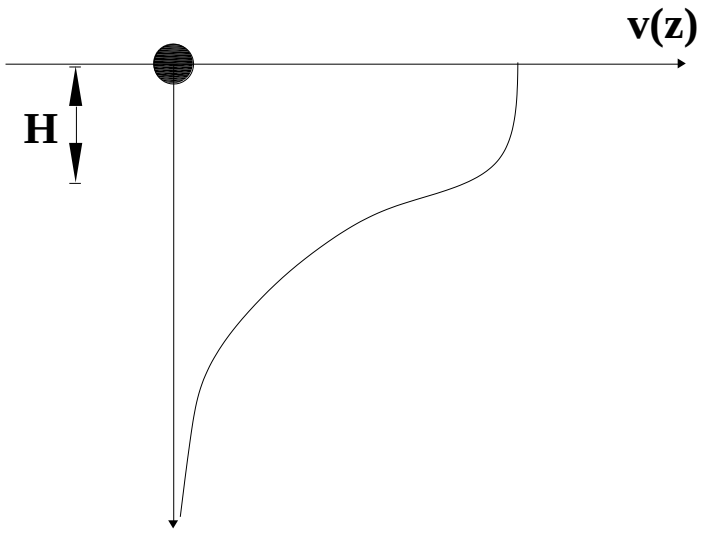

Figure 2.16: Variation of particle displacement amplitude with depth for Love waves.

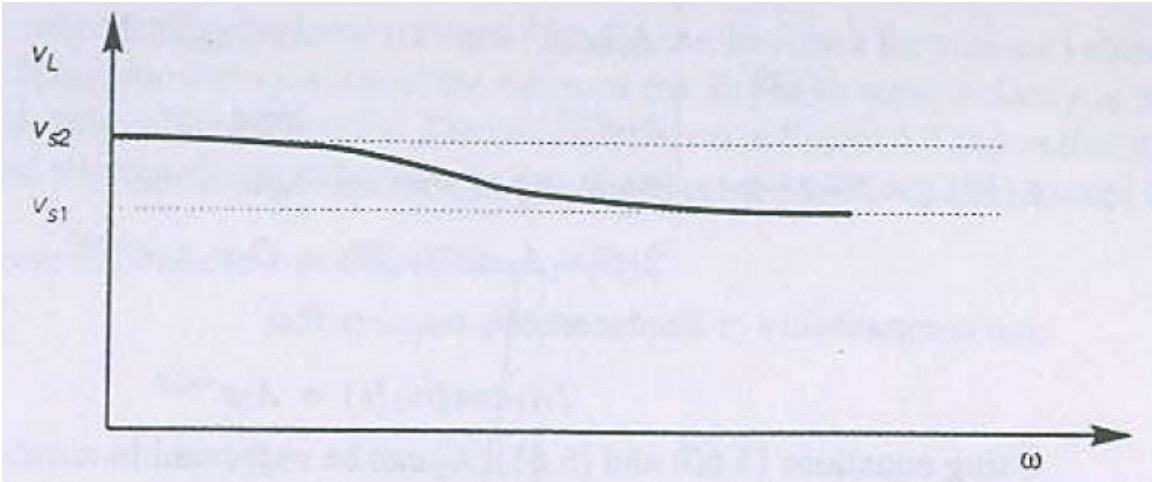

Figure 2.17: Variation of Love wave velocity with frequency.

Which indicates, as illustrated in Figure 2.17 that Love wave velocities range from the S-wave velocity of the half-space (at very low frequencies) to the S-wave velocity of the surficial layer (at very high frequencies)? This frequency dependence indicates that Love waves are dispersive.

2.4.3.3 Higher-Mode Surface Waves

Any surface wave must (1) satisfy the equation of motion, (2) produce zero stress at the ground surface, and (3) produce zero displacement at infinite depth. Nontrivial solutions do not exist for arbitrary combinations of frequency and wave number; rather, a set of discrete and unique wave numbers exist for a given frequency. Each wave number describes a different displacement pattern, or mode, of the surface wave. The preceding derivations have been limited to the fundamental modes of Rayleigh and love waves, which are the most important.

2.4.3.4 Dispersion of Surface Waves

For a homogeneous half-space, the Rayleigh wave velocity has been shown to be related to the body wave velocities by Poisson's ratio. Since the body wave velocities are constant with depth, the Rayleigh wave velocity in a homogeneous half-space is

independent of frequency. The velocity of the Love wave, on the other hand, varies with frequency between an upper and a lower limit.

Dispersion is a phenomenon in which waves of different frequency (and different wavelength) propagate at different velocities. Hence Love waves are clearly dispersive, and Rayleigh waves in a homogeneous half-space are nondispersive. Near the earth's surface however, soil and rock stiffness usually increase with depth. Since the depth to which a Rayleigh wave causes significant displacement increases with increasing wavelength, Rayleigh waves of long wavelength (low frequency) can propagate faster than Rayleigh waves of shorter wavelength (High frequency). Therefore, in the real world of heterogeneous materials, Rayleigh waves are also dispersive. The dispersion of Rayleigh waves can be used to evaluate subsurface stiffness profiles by field testing techniques.

Since velocities of both Rayleigh waves and Love waves decreases with increasing frequency, the low-frequency components of surface waves produced by earthquakes can be expected to arrive at a particular site before their high-frequency counterparts. This tendency to spread the seismic energy over time is an important effect of dispersion.

2.4.3.5 Phase and Group Velocities

The solutions for Rayleigh wave velocity,v_R, and Love wave velocity, v_L, have been based on the assumption of harmonic loading which produces an infinite wave train. These velocities describe the rate at which points of constant phase (e.g., peaks, troughs, or zero points) travel through the medium and are called phase velocities. A transient disturbance may produce a packet of waves with similar frequencies. This packet of waves travels at the group velocity, cg, given by

$$c_g = c + k\frac{dc}{dk} \tag{2.53}$$

Where c is the phase velocity (equal to $v_R$or v_L, depending on which type of wave is being considered) and k is the wave number (equal to ω/V_RR or ω/v_L). In a nondispersive material, dc/dk = o, so the group velocity is equal to the phase velocity. Since both v_R and v_L generally decrease with increasing frequency in geologic materials, dc/dk is less than zero and the group velocity is lower than the phase velocity. Consequently, a wave packet

would appear to consist of a series of individual peaks that appear at the back end of the packet, move through the packet to the front, and then disappear. The opposite behavior can be observed by (for $c < c_g$) dropping a rock into a calm pond of water and watching the resulting ripples carefully.

2.5 CORRELATION BETWEEN FIELD SPT-N AND SHEAR WAVE VELOCITY

There are several empirical relations correlating the SPT-N value and Shear Wave Velocity (Vs) as shown in Table 2.1. The overburden correction of SPT-N value is demonstrated in Figure 2.18. The Standard Penetration Test (SPT) has been widely used to investigate soil deposit for identifying subsurface soil profiles. The empirical relationships presented here can be used to convert SPT-N value into Shear Wave Velocity which is needed as one of the input parameters for the program SHAKE.

Recently under CDMP (2009) project, OYO Corporation of Japan has carried out PS logging test to estimate shear-wave velocity at seven locations in Dhaka, where six locations are situated in our study area. This is the first time shear-wave velocity for any locations are estimated using PS logging in Bangladesh. The Small scale microtremor measurement has been carried out at nine different locations of Dhaka city in order to determine shear wave velocity (Hossain, 2009). Eight researched locations lie in our study area. These fourteen Shear Wave Velocity data have been used to develop soil model in the study points.

Standard Penetration Test (SPT) has been executed at twenty seven different locations according to ASTM D 1586 (ASTM, 2000). In addition to, the remains SPT data has been collected from other sources. These SPT data has been used to estimate the SWV using different empirical SPT N-value and Shear wave velocity (Table 2.1). Figure 2.19 shows correlations of Shear Wave Velocity and SPT N-value for sand and clay for those locations (Ansary et al., 2010). These correlations have been used to convert SPT N-value to Shear Wave Velocity for. The SWV of other empirical methods have been calculated to compare SWV. These results of converted SWV have been shown in Chapter 3 and APPENDIX-A.

Table 2.1: Empirical correlation between SPT N-value and Shear Wave Velocity (After TC4, ISSMFE, 1993)

Researchers	**Equation**
Imai and Yoshimura (1970)	$Vs = 76\ N^{0.33}$
Ohba and Toriumi (1970)	$Vs = 84\ N^{0.31}$
Ohta and Goto (1978)	$Vs = 69\ N^{0.17}\ D^{0.2}\ F_1\ F_2$ Where F_1 = 1.0 (H); F_2 = 1.00 (clay) = 1.3 (P); = 1.09 (f. sand) = 1.07 (m. sand) = 1.14 (c. sand) = 1.15 (g. sand) = 1.45 (gravel)
Imai (1977)	$Vs = a\ N^{b}$ Where a = 102; b = 0.29 (H. clay) = 81; = 0.33 (H. sand) = 114 = 0.29 (P. clay) = 97 = 0.32 (P. sand)
Okamoto et al. (1989)	$Vs = 125\ N^{0.3}$ (P. clay)
Tamura and Yamazaki (2002)	$Vs = 105\ N^{0.187}\ D^{0.179}$

Here,

Vs = Shear Wave Velocity (m/s); N = Corrected SPT blow count

D = Depth (m); H = Holocene; P = Pleistocene

f = Fine; m = Medium; c = Coarse; g = Gravel

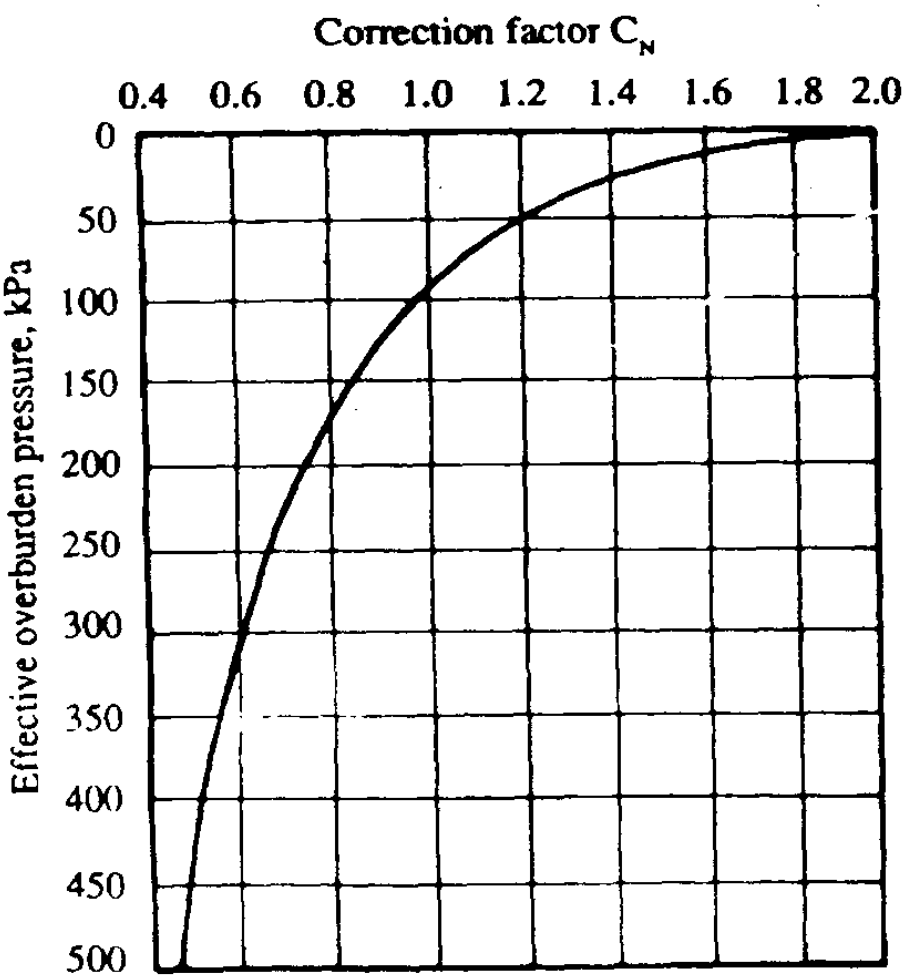

Figure 2.18: Recommended Curves for Correction Factor from Effective Overburden Pressure. (After Murthy, 1991)

2.6 1D RESPONSE ANALYSIS USING PROGRAMME SHAKE

Site response analysis aims at determining the response of a soil deposit to the motion of the bedrock immediately beneath it. The overburden stress plays a very important role in determining the characteristics of the ground surface motion thus emphasizing the need for ground response analysis. A number of techniques have been developed for ground response analysis. These techniques can be grouped as one-, two-, and three-dimensional analyses according to the dimensionality of the problems they can address. A one-dimensional method can be used if the soil structure is essentially horizontal.

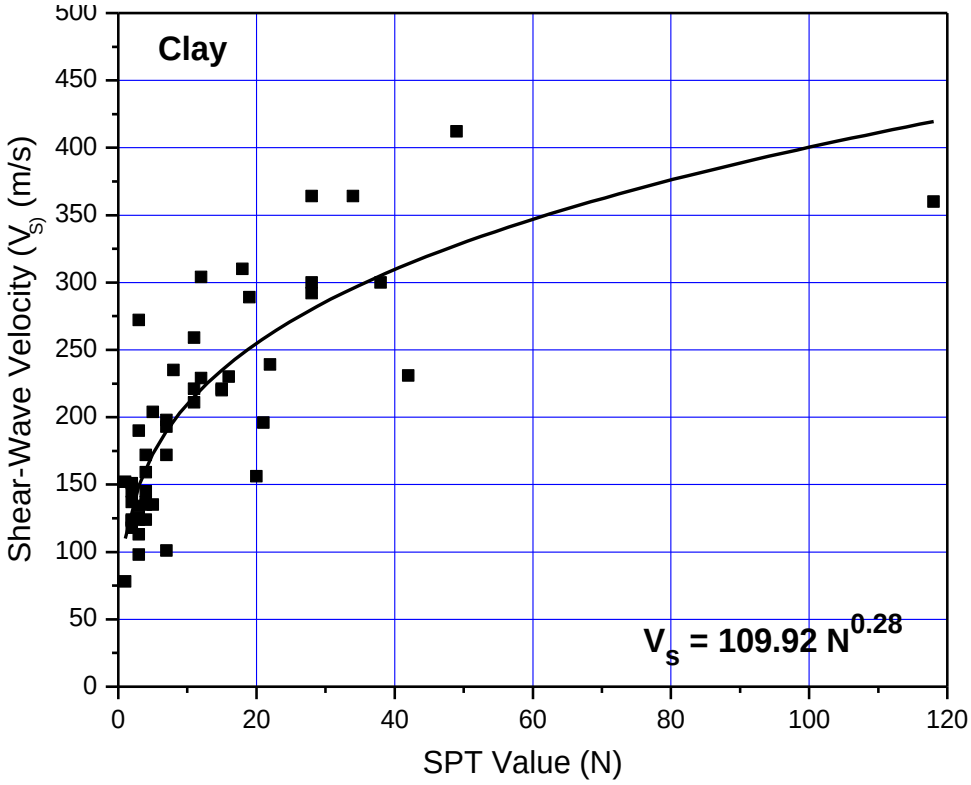

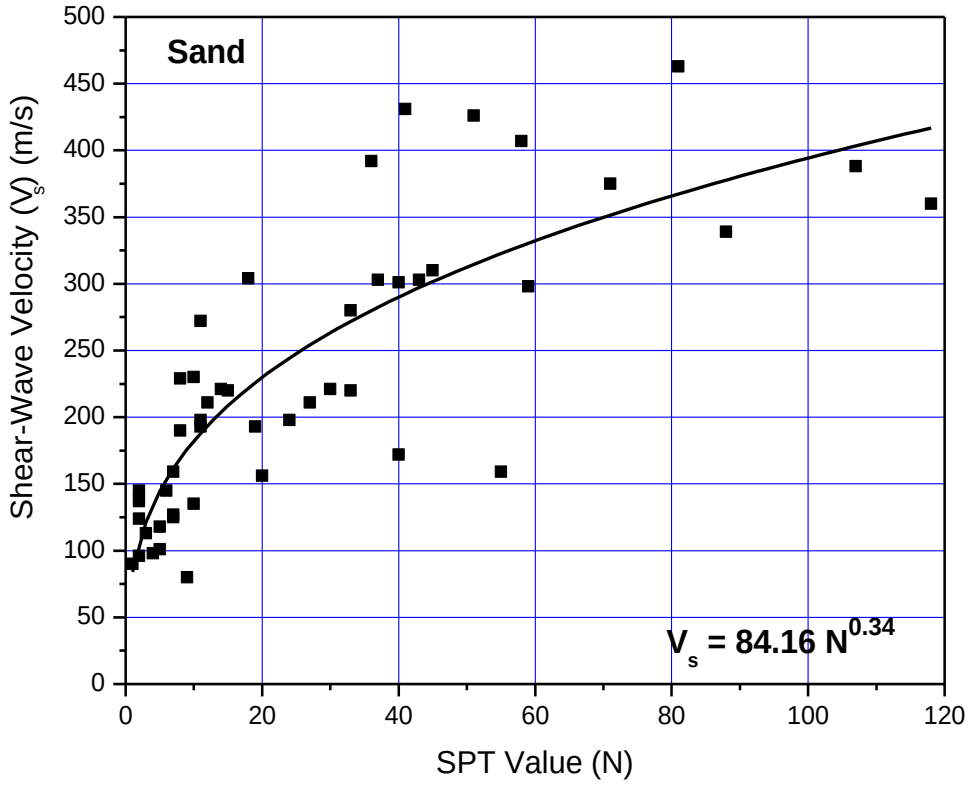

Figure 2.19: Proposed Shear Wave Velocity and SPT N-value correlations. (After Ansary et al., 2010)

2.6.1 Method for Amplification Analysis

One dimensional method of ground response analysis is widely used in earthquake geotechnical engineering. A number of different techniques are available for one-dimensional response analysis, which can be broadly categorized as linear analysis, equivalent linear analysis and nonlinear analysis. The most popular method used in professional practice is the "equivalent linear" approach which is incorporated in the computer program SHAKE. The program 'SHAKE' is capable of computing the responses for a known motion given anywhere in a system. It requires three input parameters such as bedrock motion, dynamic material properties and site specific soil properties. The accelerograms measured on a known soil deposit can be used to predict underlying rock motions using 'SHAKE', which, in turn, can be used to obtain the surface motion for other soil deposits as shown in Figure 2.20 (After Schnable et al., 1971). The rock motion is assumed not to vary within a region. The program incorporates non-linear soil behavior, the effect of the elasticity of the base rock and systems with variable damping.

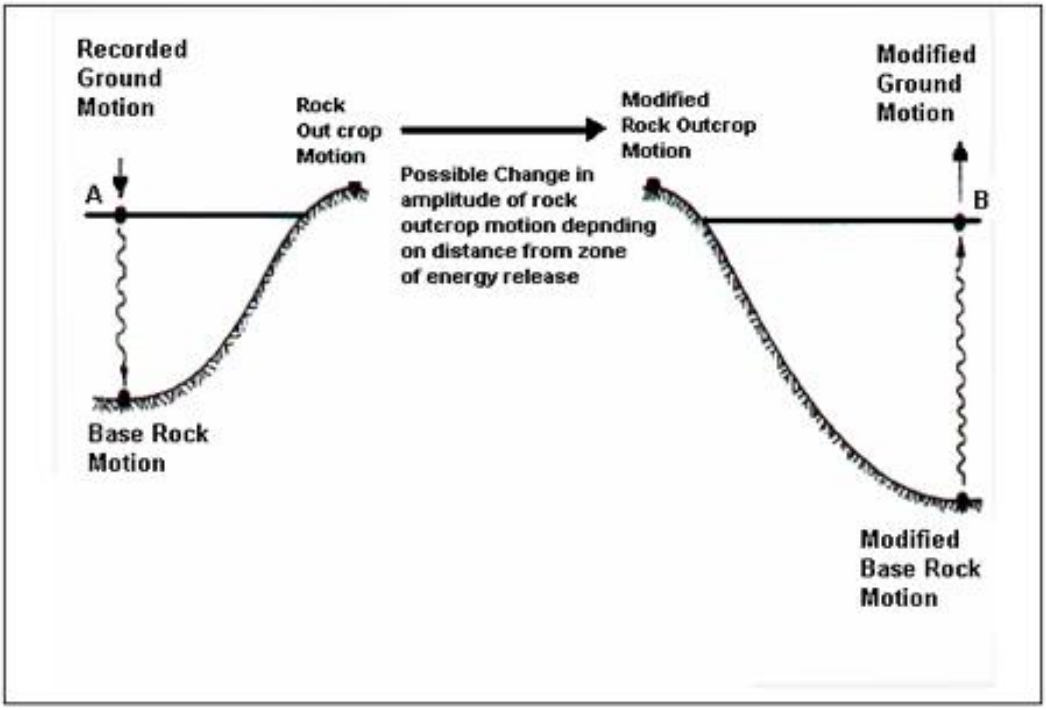

Figure 2.20: Schematic representation of procedure for computing effects of local soil conditions on ground motions. (Schanbel et al., 1971)

2.6.2 Theory to the Program

The theory (behind SHAKE) considers the responses associated with vertical propagation of shear waves through the linear visco-elastic system shown in Figure 2.21. The system consists of N horizontal layers which extend to infinity in the horizontal direction and has a half space as the bottom layer. Each layer is homogeneous and isotropic, and is characterized by the thickness, h, mass density, ρ, shear modulus, G, and damping factor, β.

2.6.3 Description of the Program SHAKE

Program SHAKE computes the responses in a system of homogeneous, visco-elastic layers of infinite horizontal extent subjected to vertically travelling shear waves. The system is shown in Figure 2.21**.** The program is based on the continuous solution to the wave- equation adapted for use with transient motions through the fast Fourier transform algorithm. The nonlinearity of the shear modulus and damping is accounted for by the use of equivalent linear soil properties using an iterative procedure to obtain values for modulus and damping compatible with the effective strains in each layer. The following assumptions are implied in the analysis:

- The soil system extends infinitely in the horizontal direction. Each layer in the system is completely defined by its value of shear modulus, critical damping ratio, density, and thickness. These values are independent of frequency.
- The responses in the system are caused by the upward propagation of shear waves from the underlying rock formation.
- The shear waves are given as acceleration values of equally spaced time intervals. Cyclic repetition of the acceleration time history is implied in the solution.
- The strain dependence of modulus and damping is accounted for by an equivalent linear procedure based on an average effective strain level computed for each layer.

The program is able to handle systems with variation in both moduli and damping, and takes into account the effect of the elastic base. The motion used as a basis for the

analysis, the object motion, can be given in any one layer in the system and new motions can be computed in any other layer. The set of operations can be performed by the program:

- Read the input motion, find the maximum acceleration, scale the values up or down, and compute the predominant period.
- Read data for the soil deposit and compute the fundamental period of the deposit.
- Compute the maximum stresses and strains in the middle of each sub-layer and obtain new values for modulus and damping compatible with a specified percentage of the maximum strain.
- Compute new motions at the top of any sub-layer inside the system or outcropping from the system.

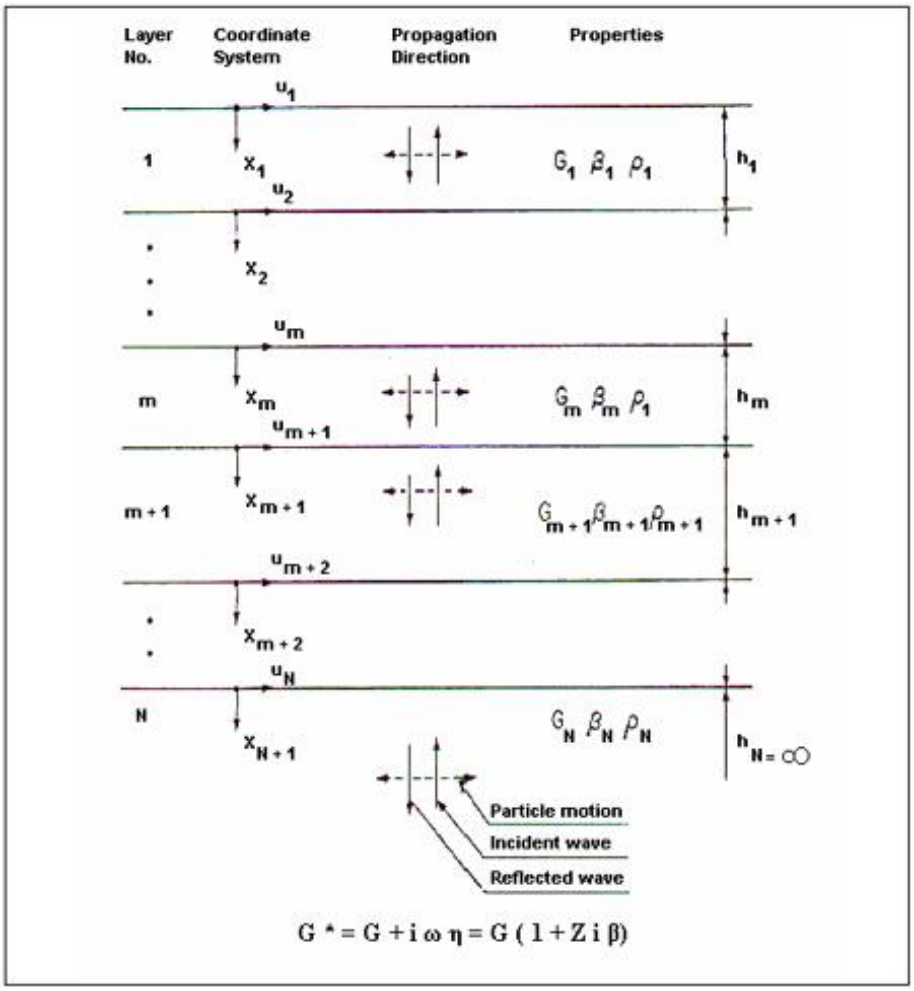

Figure 2.21: One dimensional wave propagation system. (After Schanbel et al., 1971)

2.7 DAMAGE ASSESSMENT

Soil conditions are often variable even inside of a relatively small area as a town. So it is necessary to find a low-cost method to obtain a detailed dynamic characterization of soil. Microtremor is the most convenient, reliable and low-cost technique to assess the damage of any site and building. Damage assessment of any building and site can be done in two ways. First one is Resonance Criteria, which is assessed from the analysis microtremor data in both building and site. Second one is Nakamura's Seismic Vulnerability Index, K_g. These two techniques have been discussed in this section.

2.7.1 Resonance Criteria for Building

If the predominant frequency of any building coincides with the predominant frequency of soil, resonance is said to occur. Ground motions that are not influenced by the presence of structures are referred to as free-field motions. When a structure founded on solid rock is subjected to an earthquake, the extremely high stiffness of the rock is considered to be fixed-base structures.

On the other hand, the same structure would respond differently if supported on a soft soil deposit. First, the inability of the foundation to conform to the deformations of the free-field motion would cause the motion of the base of the structure to deviate from the free field motion. Second, the dynamic response of the structure itself would induce deformation of the supporting soil. This process, in which the response of the soil influences the motion of the structure and the response of the structure influences the motion of the soil, is referred to as soil-structure interaction.

Soil-structure interaction has little effect on the dynamic response of many structures and foundation systems (Kramer, 1996). In other cases, however, its effects can be significant. Whether the neglect of its effect can be significant, whether the neglect of its effects is conservative or unconservative depends on the details of the problem at hand and must be evaluated on a case-by-case basis.

The resonance frequency of a structure can be calculated using the following equation:

$$f_n = \frac{1}{2\Pi}\sqrt{\frac{K}{m}} \tag{2.54}$$

Where,

f = Natural frequency, K = Stiffness of material and m = Mass of the body.

The natural frequency of a system depends on the stiffness and mass of the structure (Equation 2.54). The stiffer two Single degree of freedom (SDF) systems having the same mass will have the higher natural frequency. Similarly, the heavier (more mass) of two structures having the same stiffness will have the lower natural frequency and the longer natural period. To emphasize the fact that these are natural properties of the system when it is allowed to vibrate freely without any external excitation. Because the system is linear, these vibration properties are independent of initial displacement and velocity. So, almost all the structure has two natural frequencies (except rectangular structure). But, in real it is difficult to estimate the exact natural frequency of a structure. The natural frequency also depends on the two major irregularities. These are Structural irregularities in plan (Torsional irregularity, Re-entrant corner, Diaphragm discontinuity, out of plan vertical element offset and Nonparallel system) and Structural irregularities in height (Storey stiffness irregularity, Storey mass irregularity, Storey geometry irregularity, Discontinuity of structural element and discontinuity in capacity).

The existence of non-consolidated sedimentary deposits in the shallow part of a geological structure may be the cause of increase in the seismic hazard. The reason is the possibility of amplifications of seismic waves for certain frequency bands due to the velocity contrast between soft and stiff materials (Sánchez-Sesma and Luzón, 1995). An especially dangerous situation occurs when the resonant frequency coincides with the natural frequency of the buildings and additional effects of resonance appear on the edifies.

Recently, the H/V technique (Nakamura, 1989) is becoming more popular with its data collection facilities and application allowance in areas with low or even zero seismicity. Previous studies had suggested that the vertical component of ambient noise not only maintains the characteristics of source ground of sediments, but also is significantly

influenced by Rayleigh waves on the sediments. Therefore, they can be used to remove both the source and the Rayleigh wave effects from the horizontal components. This technique is effective in identifying the fundamental resonant frequency of a sedimentary layer while providing amplification factors that are more realistic than those obtained sediment to rock site ratios. Many researchers (Ohmachi et al., 1991; Lermo et al., 1992; Field and Jacob, 1993, 1995) have, in fact, shown how such H/V ratios of noise can be used to identify the fundamental resonant frequency and amplification factor of sediments.

Ohmachi et al. (1991) and Lermo and Chavez-Garcia (1994a, 1994b) applied the H/V ratio method to analyze microtremor measurements. Lermo and Chavez-Garcia (1993) used it to assess the empirical transfer function of the intense S-wave, part of an earthquake record, obtained from three cities in Mexico. Their results clearly indicated that the H/V ratio could provide a robust estimate of the frequency and amplitude of the first resonant mode, albeit not of the higher modes, In the meantime, Field and Jacob (1993) and Field et al. (1995) considered the response of sedimentary layers to ambient seismic noise and claimed that the H/V ratio method has been an effective and reliable tool to identify the fundamental resonant frequencies of a layered sedimentary basin. Further evidence has been given by Suzuki et al. (1995) who used both microtremor and strong-motion data in Hokkaido, Japan and ascertained that the peak frequency determined by the H/V ratio seemed to correspond with the predominant frequency estimated from the thickness of an alluvial layer. Based on numerical calculations, many other researchers (Lermo and Chavez-Garcia, 1993, 1994a, 1994b; Lachet and Bard, 1994; Dravinski et al., 1996) have shown that the H/V ratio method is obviously able to predict fundamental resonant frequency as well.

The damage of building due to resonance effect has been analyzed at the town of Bonefro (Mucciarelli et al., 2004). During the 2002 seismic sequence in Molise (Italy), the town of Bonefro suffered moderate damage (*I*MCS _ VII) except for two reinforced concrete (RC) buildings. These buildings are located on soft sediments, close to each other and very similar in design and construction. The main difference is the height: the most damaged one (European Macroseismic Scale damage 4) has four stories, whereas the less

damaged (EMS damage 2) has three stories. The *M* 5.4 shock on 31 October damaged both of them. The second shock on 1 November (*M* 5.3) increased the damage on the four-story building substantially, just while a 5-minute seismic recording has been taken. The data has been analyzed by four different techniques: short-time Fourier transform (STFT), wavelet transform (WT), horizontal-to vertical spectral ratio (HVSR) and horizontal-to-vertical moving window ratio (HVMWR). All the results agree upon the estimate of the main building frequency before the second shock and upon the shift of frequency due to damage.

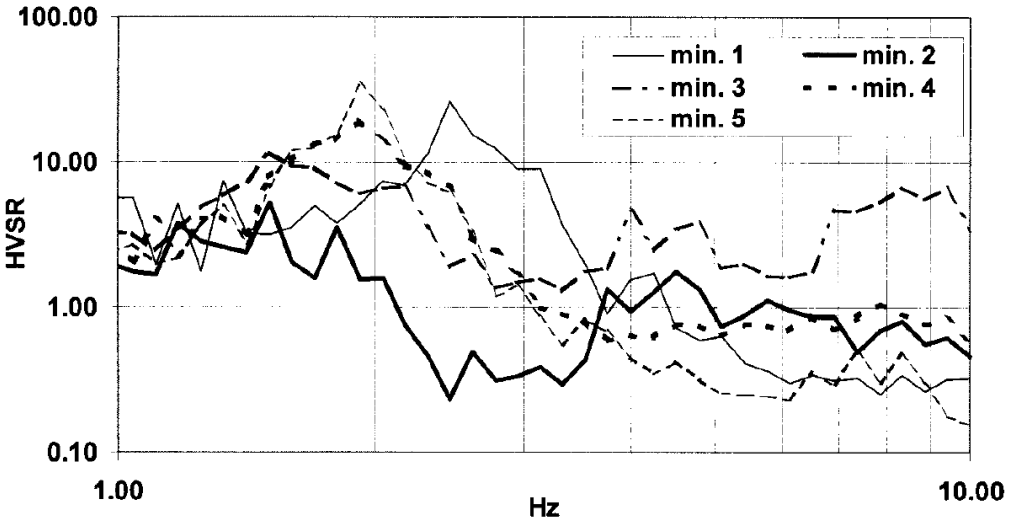

Figure 2.22: HVSR analysis for five different time windows of strong-motion recording atop the more damaged building. (After Mucciarelli et al., 2004)

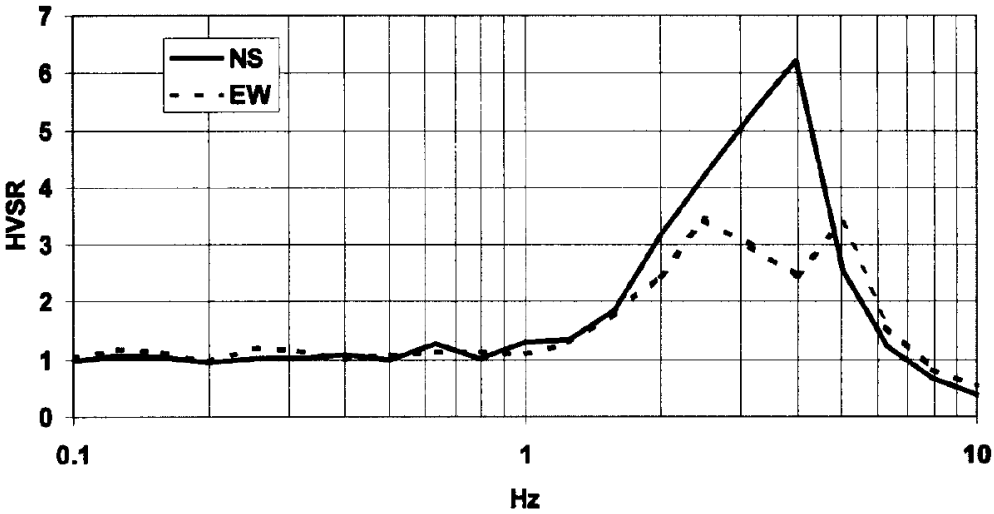

Figure 2.23: HVSR analysis for ambient noise recordings atop the less damaged building.(After Mucciarelli et al., 2004)

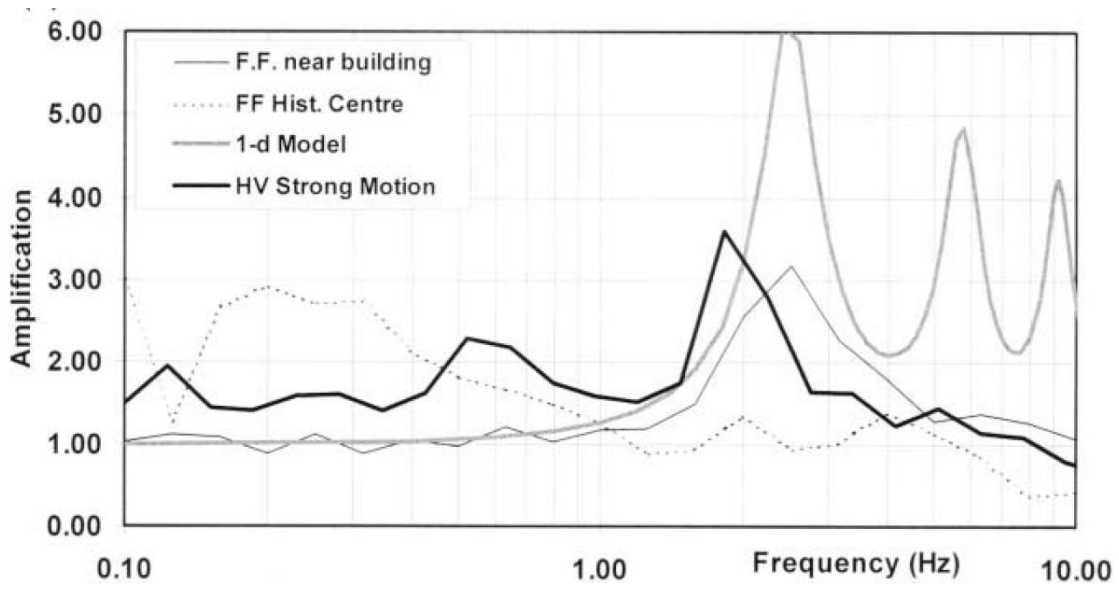

Figure 2.24: Soil amplification in Bonefro estimated with different techniques: free-field noise HVSR, 1D modeling and HVSR of seven accelerometric recordings of aftershocks.(After Mucciarelli et al., 2004)

All the fundamental frequencies (pre-, during, and post damage) lies between 1.5 and 2.5 Hz. Figure 2.22 represent HVSR analysis for five different time windows of strong-motion recording atop the more damaged building for the average of the north–south and east–west components. The first minute includes ambient noise before the quake, minutes 2 and 3 comprise the strong motion part, minute 4 is the coda of the earthquake, and minute 5 is again ambient noise. The fundamental frequency of the less damaged building has been estimated around 4 Hz (Figure 2.23). To justify soil–building resonance effect could have increased the damage, the soil fundamental frequency have been evaluated by three different techniques: noise HVSR, strong motion HVSR of seven aftershocks and 1D modeling based on a velocity profile derived from noise analysis of surface waves (NASW) measurements (Figure 2.24). The results are again in good agreement, showing that resonance frequencies of the soil and of the more damaged building are very close.

2.7.2 Seismic Vulnerability Index for soil

Kg values have been proposed by Nakamura (1996) for accurately estimating earthquake damage of surface ground and structures. Here in this study, only the formulation of K_g, have been given an example of application of outputs from QTS method. For calculating K_g, shear strain of the ground is considered.

Figure 2.25 simply shows the shear deformation of surface ground.

$$\gamma = A_g.\frac{d}{h} \tag{2.55}$$

Where, A_g is amplification factor of surface layer, h is thickness of surface layer and d is seismic displacement of the basement.

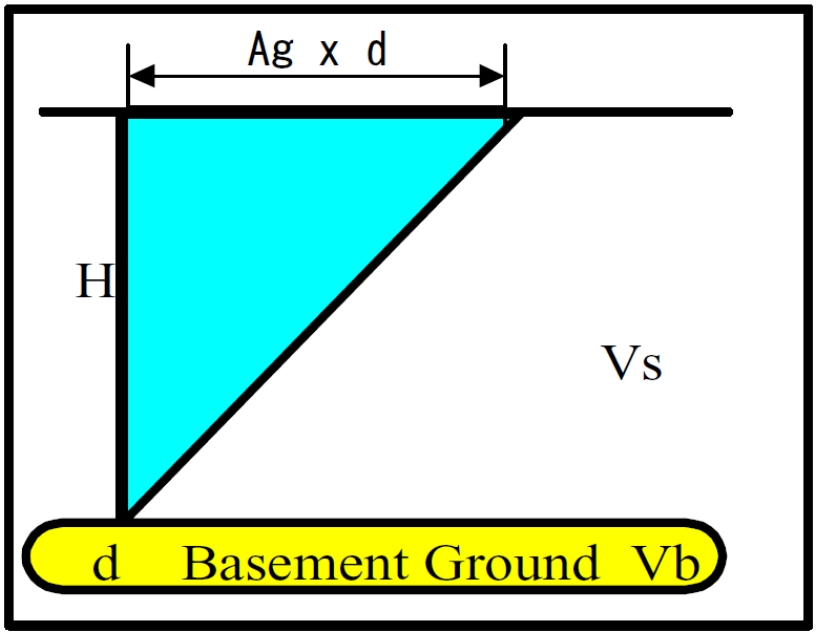

Figure 2.25: Surface ground deformation.

Putting the S wave velocities of the basement and surface layer (C_b and C_f) natural frequency Fg of the surface layer can be expressed as,

$$F_g = \frac{V_b}{4A_g.h} \tag{2.56}$$

Acceleration α in the basement can be written as

$$\gamma = \frac{A_g.\alpha_b}{(2\Pi\ F_g)^2} \cdot 4A_g.\frac{F_g}{C_b} \tag{2.57}$$

$$= \frac{A_g^2}{F_g}.\frac{\alpha_b}{\Pi^2 C_b}$$

$$= c.K_g\alpha$$

$\alpha_b = (2\Pi\ F_g)^2 d$ and shear strain γ is expressed as follows,

Where,

$$c = \frac{1}{\Pi^2.v_b}; \qquad K_g = \frac{A_g^2}{F_g} \tag{2.58}$$

C is expected to be almost constant for various sites. Effective shear strain defined by e % of equation (2.55) becomes to nearly equal to the product of K_g and α_b, under the assumptions of e = 60 % and C_b = 600 m/s. K_g is a value corresponding to the site and can be considered as a vulnerability index of the site, which might be useful to select weak points of ground.

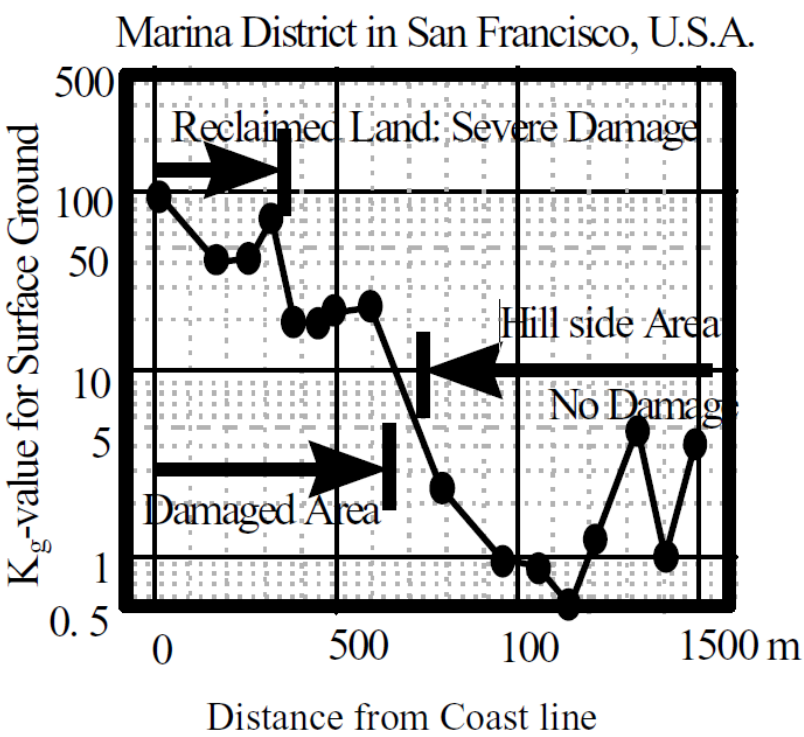

Figure 2.26: K_g values calculated for Loma Prieta Earthquake. (After Nakamura et al., 1990)

The damage assessment using Nakamura's (2000) Vulnerability Index (Kg) for Loma Prieta Earthquake has been shown in Figure 2.26. The result shows the similarity between actual damage and theoretical damage assessment using Kg value.

2.8 CONCLUDING REMARKS

In this chapter definition of microtremor, its sources and relevant literatures such as relationship between microtremor and earthquake, relationship between microtremor H/V ratio and theoretical transfer function of shear wave etc. have been reviewed.

Different types of wave propagation are important for microtremor analysis. Microtremor consists of various waves which may be body waves or surface waves. Body waves are classified as P-wave and S-wave whereas surface waves include Rayleigh wave and Love wave. Various microtremor waves which are related to seismic wave have been described in this chapter using mathematical expression. The high mode of surface wave and their dispersion are also included in this chapter. The phase and group velocities are also described.

Empirical correlation of field SPT N-value and shear wave velocity has been discussed. Different researchers suggested different forms of these correlations, which are discussed here. The theory of one dimensional soil response analysis for the programme SHAKE has been illustrated. The input and output parameters of the SHAKE programme has been explained.

Finally, the literature related to damage assessment using H/V technique has been described in this chapter. The resonance between site soil and building from various studies has been included. These are the practical application of H/V technique. The theory and methodology of the vulnerability of site soil according to Nakamura's (2000) Vulnerability Index (Kg) has been illustrated. The application of seismic Vulnerability in various places also included.

All the above discussions are relevant to the current study and has been referred in chapters three and four.

CHAPTER 4

COMPARISON OF MICROTREMOR DATA WITH THEORETICAL ANALYSIS

4.1 GENERAL

The reliability of microtremor observation to estimate predominant frequency and amplification of any particular site has been illustrated in Chapter 2. These parameters may be used to assess the response of site soil due to any seismic activities. Comparison of H/V ratio of microtremor observation with theoretical transfer function of site soil using the 1D site response program SHAKE is important. This chapter provides comparison of these two ratios for 42 locations of Dhaka city. In 14 locations shear-wave velocity are obtained directly using PS-logging and SSMM method and in other 28 locations correlations are used to obtain shear-wave velocity from SPT-N value. Resonance between site soil and building within BUET campus as well as Nakamura's seismic vulnerability index (Kg) for soils for 45 locations has also been estimated.

4.2 COMPARISON OF MICROTREMOR DATA WITH 1D RESPONSE ANALYSIS USING THE PROGRAMME SHAKE

From the existing borelogs, SSMM and PS-loggings, soil model at each site has been established for theoretical analysis. The transfer function of the shear wave (the surface motion versus the incidental motion at depth) has been calculated using the soil models. For the calculation of transfer function of shear-wave and a damping ratio of 2% has been used, assuming input motion at the outcrop.

Figure 4.1 and Figure 4.2 show the typical graphs for comparison of amplitude ratio between the transfer function of shear wave and microtremor H/V ratio. The comparision of amplitude ratio between transfer function and microtremor H/V ratio for fourty two sites in and around the Dhaka city have been illustrated in Appendix-E. Characteristics transfer function curve have been found from the 1D response analysis using the

programme SHAKE. On the other hand, microtremor H/V ratio curve has been found from the Horizontal to Vertical spectral ratio (H/V) of Fourier spectra.

From the comparison of microtremor and transfer function, four types of characteristics curves have been observed. These curves are classified as similar, dissimilar, right side shifted and left side shifted compared to the microtremor H/V ratio curve. Among 42 models thirty five transfer function have been shifted in the right side of microtremor and only one has been shifted in the left side. There are six sites where two curves have similar pattern. The rest two sites have been found where no similarity between microtremor H/V ratio and transfer function.

Figure E4.38 shows the comparison of amplitude ratio between microtremor and Transfer Function at Rajendapur. The amplitude ratio of Transfer function is similar to microtremor H/V ratio. However, peak of transfer function has been moved into right side slightly. The amplitude ratio of both curves is around 2.65. The predominant frequency of microtremor H/V ratio is 1.17 Hz whereas transfer function shows 2.5 Hz. Similar curves between transfer function and microtremor have been found in nine locations which are shown in Figure E4.1, E4.4, E4.5, E4.6, E4.11, E4.13, E4.17, E4.19 and Figure E4.24.

Figure E4.35 demonstrates that the peak amplitude ratio of transfer function has been moved toward right side of microtremor at Bashundhara River view Project. But, the peak value of transfer function is lower amplified than microtremor H/V ratio. The predominant frequency of microtremor H/V ratio is 1.05 Hz where as transfer function shows this value is 1.85 Hz. On the other hand, peak H/V ratio of microtremor is 3.51 wheras transfer function shows this value 3.03. The similar types of right shifted and lower amplified locations of transfer function have been found in Figure E4.2, E4.3, E4.7, E4.8, E4.10, E4.14, E4.15, E4.16, E4.17, E4.21, E4.23, E4.26, E4.29, E4.30, E4.31, E4.33, E4.34, E4.42 and Figure E4.35.

Figure E4.20 shows that amplitude ratio of transfer function is higher than microtremor H/V ratio at Pallabi. The predominant frequency of microtremor is 1.24 Hz whereas the predominant frequency of transfer function is 1.60 Hz. The amplitude ratio of microtremor is 2.64 wheras this value is 4 Hz in Transfer Function. The similar pattern of curves between microtremor and Transfer function have been observed in Figure E4.9, E4.13, E4.18, E4.20, E4.26 and Figure E4.41.

Figure E4.36 shows the left side shifted transfer function curve at Matuail, Demra. The peak value of H/V ratio of microtremor is similar to Transfer Function. The Predominant frequency of transfer function is around 1.7 Hz whereas this value is 2.73 Hz in microtremor. The peak value of amplitude ratio of transfer function is 2.48 where as microtremor shows 2.3.

The similar predominant frequency of microtremor and transfer function has been found in nine locations. Figure E4.12 represents the similar predominant frequency between microtremor and transfer function. The predominant frequency of microtremor and transfer function is around 3.65 Hz. The peak amplitude ratio of microtremor is 2.73 wheras this value is 1.90 in transfer function. The similar patterns of curve have been illustrated in Figure E4.22.

The similar predominant frequency but higher amplification has been found in Figure E4.27 at Adabor. The predominant frequency in both curves is 3.35 Hz. The peak amplitude ratio of microtremor is 2.26 Hz wheras this value is 2.9 in Transfer Function.

The dissimilarity between transfer function and microtremor H/v ratio has been found in Figure E4.29 at Aftab Nagar Housing project. The transfer function curve is right shifted. The predominant frequency and amplitude ratio of transfer function are 6 Hz and 2 where as these value are 0.95 Hz and 2.76 in microtremor. Figure E4.37 demonstrates that amplitude ratio of transfer function is right shifted at Jilmil Project. The predominant frequency and H/V ratio of microtremor are 1.0 Hz and 3.26. The predominant frequency and H/V ratio of transfer function have been found 8.0 Hz and 3.0.

From these result, it can be said that although amplitude values of the ratios are close, the predominant frequency for the two cases differs slightly. The reason of this difference is that microtremor consists of different types of waves, but the theoretical transfer function is based on shear-wave only. In Chapter 2 it has been described that Rayleigh wave has significant effect on microtremor result. If these waves are dispersed from the microtremor, microtremor results may be more close to the transfer function.

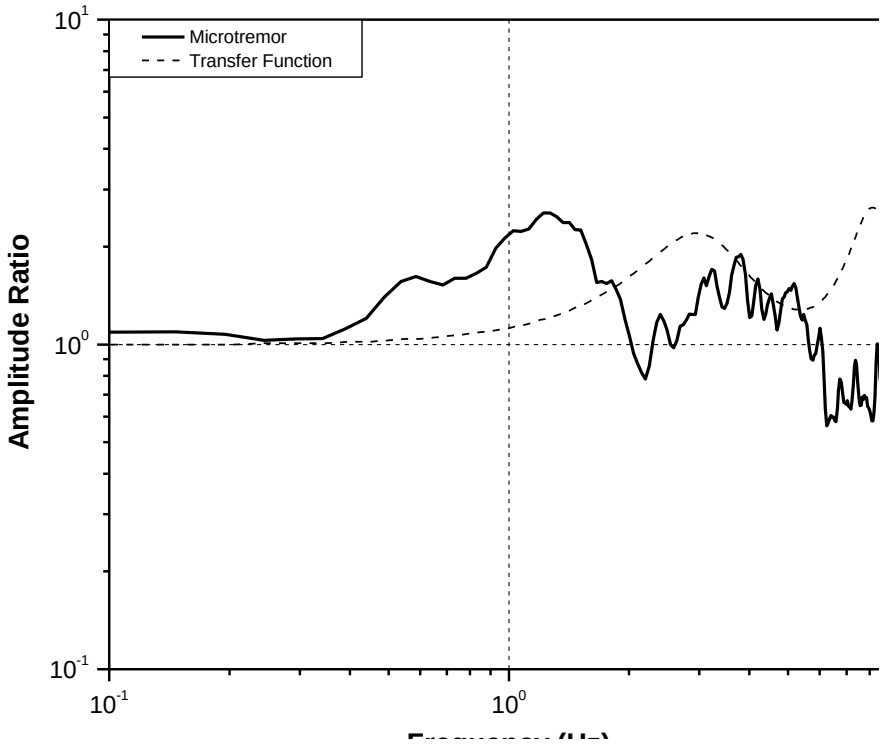

Figure 4.1: Amplitude ratios of microtremor and theoretical transfer function of shear wave at National University.

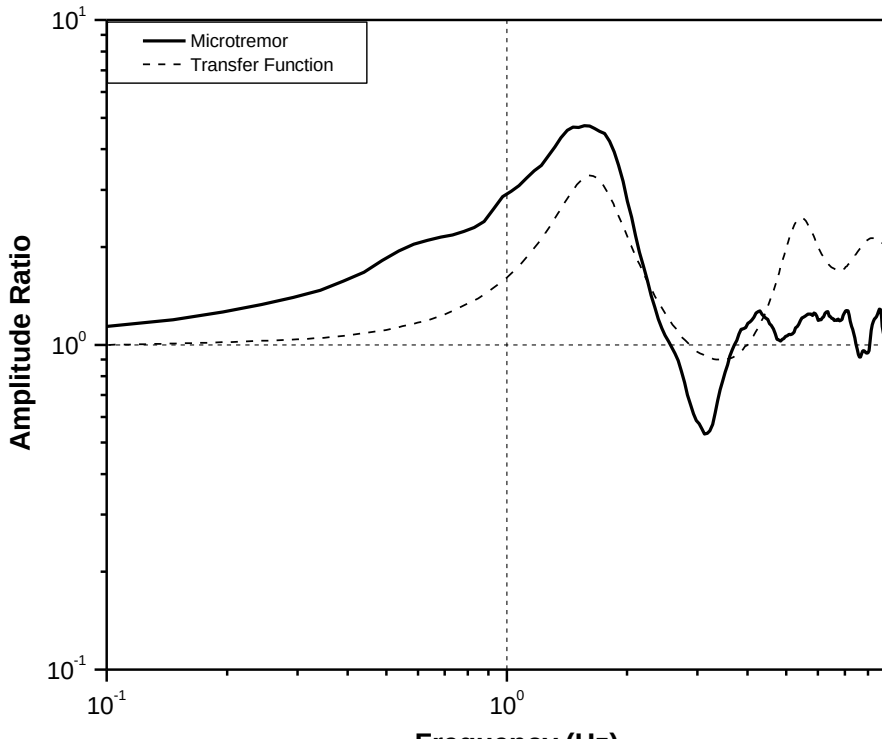

Figure 4.2: Amplitude ratios of microtremor and theoretical transfer function of shear wave at Block-D, Bashundhara.

4.3 VULNERABILITY ASSESSMENT

Earthquake vulnerability of the 45 buildings within BUET campus is carried out from predominant frequency obtained by the analysis of microtremor data. Microtremor observation has been carried out at 132 selected free-field locations within BUET campus which has been discussed in Chapter 3. The Horizontal to Vertical spectra ratio (H/V) of these locations have been compared with the predominant frequency of building along EW and NS direction, respectively. Fourier spectra of 45 buildings of BUET campus have been shown in APPENDIX-D from Figure D208 to D252. The mean square root of H/V ratio (RM) obtained from microtremor observations of nearby soils have been compared with Fourier spectra of microtremor observations at the top floor of the buildings. The occurrence of resonance between building and soil has been discussed in article 4.3.1. The damage assessment of consolidated soil using Nakamura's Seismic Vulnerability Index (Kg) has been included in article 4.3.2.

4.3.1 Resonance between Site Soil and Building

The resonance criteria of building and soil can be explained using the following simple relation:

$$\text{Resonance criteria, } \beta_R = \frac{f_B}{f_S} \tag{4.1}$$

Where, β_R = Coefficient for resonance occurrence, f_B = Predominant frequency of building and f_S = Predominant frequency of soil.

In equation (4.1), if β_R becomes close to 1 (1±0.20), resonance may occur. The resonance between buildings and soil has been analyzed using this resonance criterion, β_R, in both EW and NS directions. Table 4.1 presents the predominant frequency of the buildings and their adjacent soils and shows possibility of resonance to occur. Four buildings have been found as vulnerable due to resonance occurrence. These buildings are Eleven Story Tower Building, URP Building, Titumir Hall and Building # 1.

Table 4.1: Analysis of resonance criteria of 45 buildings at BUET campus

Serial No.	Building Name/ Number	Predominant Frequency of Building (Hz)		Predominant Frequency of site soil (Hz)	Remarks on resonance occurrence
		EW direction	NS direction	Resultant, RM	
1	IFCDR Building	2.63	3.33	0.96	No
2	Eleven Story Tower Building	2.00	2.00	1.80	Yes
3	Civil Engineering Building	2.00	2.50	0.75	No
4	EME Building	2.50	2.56	1.24	No
5	Library Building	3.85	2.70	2.17	No
6	Architectural Building	2.70	2.78	1.88	No
7	URP Building	3.03	2.63	3.05	Yes
8	ARI Building	3.85	3.33	2.26	No
9	New Academic Building	3.70	3.33	0.96	No
10	Controller of Examination Building	5.56	5.56	1.24	No
11	Engg. University School Building	3.70	4.35	1.37	No
12	Titumir Hall	3.13	3.23	3.52	Yes
13	Sher-e-Bangla Hall	3.70	2.50	1.65	No
14	Dr. M.A. Rashid Hall	4.17	3.70	1.87	No
15	Ahsan-Ullah Hall	3.70	4.00	5.92	No
16	Shahid Smrity Hall(Middle Building)	3.70	4.76	0.34	No
17	Shahid Smrity Hall(North Building)	3.33	3.57	3.13	No
18	Register Building	5.00	5.00	0.65	No
19	# 1	4.00	4.00	3.81	Yes
20	# 2	4.00	3.85	1.07	No
21	# 3	3.57	4.55	1.24	No
22	# 4	3.03	3.45	1.27	No

Serial No.	Building Name/ Number	Predominant Frequency of Building (Hz)		Predominant Frequency of site soil (Hz)	Remarks on resonance occurrence
		EW direction	NS direction	Resultant, RM	
23	# 5	4.55	3.85	1.31	No
24	# 6	4.35	3.70	1.31	No
25	# 7	4.00	3.70	0.66	No
26	# 8	3.13	3.57	0.77	No
27	# 9	4.17	4.55	0.82	No
28	# 12	3.33	3.57	1.18	No
29	# 13	3.57	3.57	1.18	No
30	# 14	3.23	3.23	1.16	No
31	# 18	3.03	3.45	6.11	No
32	# 21	4.35	3.33	2.68	No
33	# 22	3.03	3.45	1.27	No
34	# 23	4.00	3.33	5.95	No
35	# 24	4.17	3.45	4.85	No
36	# 25	4.00	3.33	1.80	No
37	# 26	4.00	3.33	2.52	No
38	# 27	4.35	3.45	1.27	No
39	# 28	3.03	3.57	6.11	No
40	# 30	3.85	4.17	0.84	No
41	# 43	3.45	4.00	1.39	No
42	# 45	3.70	3.45	0.66	No
43	# 46	3.33	3.85	1.36	No
44	# 47	3.13	3.13	0.88	No
45	# 62	2.56	2.94	1.39	No

4.3.2 Seismic Damage assessment of soil using Nakamura's Technique

Seismic vulnerability index (Kg) is an index indicating the level of vulnerability of a layer of soil to deform. Therefore, this index is useful for the detection of areas that are weak zone (unconsolidated sediment) at the time of occurrence of earthquakes. Some studies like Daryono (2009) and Nakamura (2000) showed a good correlation between seismic vulnerability index (Kg) and the distribution of earthquake disaster damage. This index is obtained from the peak value of HVSR squared, divided by the value of the predominant frequency. For this research area (Kg) values for 45 locations are shown in Table 4.2.

The seismic vulnerability index has been classified into four major types. These are Low (0-5), Moderate (6-10), High (11-20) and Very High (>20). Table 4.2 demonstrates the highest (Kg) value at Rab-10, Plot, Kamrangirchar. Most of the zones having higher Vulnerability Index (Kg) are situated in reclaimed areas.

Table 4.2: Damage assessment of site soil using Nakamura's empirical formula

SL. No	ID	Location	Predominant Frequency, F_g (Hz)	H/V Ratio, A_g	Vulnerability Index, $K_g = \frac{A_g^2}{F_g}$	Remarks
1	SBH-01	National University	1.24	2.59	5.41	Low to moderate
2	SBH-02	Board Bazaar, Gazipur	0.82	2.73	9.09	Moderate
3	SBH-03	Kaunia, Boro Bari, Moddopara	0.72	2.79	10.81	Moderate to high
4	SBH-04	Tongi, Ershadnagar	0.97	2.51	6.49	Moderate
5	SBH-05	Tongi BSCIC area	0.95	2.73	7.85	Moderate
6	SBH-06	Abdullahpur	1.32	2.33	4.11	Low
7	SBH-07(A)	Ijtema field (North and East side)	1.17	3.37	9.71	Moderate
8	SBH-07 (B)	Ijtema Field (South and West side)	0.86	3.26	12.35	High
9	SBH-08	Ashulia Toll Plaza	1.14	1.75	2.69	Low
10	SBH-9	Uttar Khan	1.09	2.09	4.01	Low
11	SBH-10(A)	Uttara Phase 3 (North side)	1.18	3.16	8.46	Moderate
12	SBH-10(B)	Uttara Phase 3 (South side)	0.97	4.43	20.48	Very high
13	SBH-11	Azampur School, Uttara	3.65	2.73	2.04	Low

SL. No	ID	Location	Predominant Frequency, F_g (Hz)	H/V Ratio, A_g	Vulnerability Index, $K_g = \frac{A_g^2}{F_g}$	Remarks
14	SBH-12 (A)	Mirpur DOHS (South side)	1.54	2.46	3.93	Low
15	SBH-12 (B)	Mirpur DOHS (North side)	1.21	3.44	9.78	Moderate
16	SBH-13	Ashiyan city, Askona, Dakkhin Khan	1.12	3.19	9.08	Moderate
17	SBH-14(A)	Purbachal-1, Randokpur Hazi bari, Rupganj	0.94	3.04	9.83	Moderate
18	SBH-14(B)	Purbachal-2, American City	2.00	2.69	3.62	Low
19	SBH-14(C)	Purbachal Picnic Park, Gazipur	1.34	2.23	3.71	Low
20	SBH-15	Adjacent to Mirpur Zoo	1.52	2.43	3.88	Low
21	SBH-16	Field Ground, Pallabi	1.24	2.64	5.62	Low to moderate
22	SBH-17 (A)	Block-B, Basundhara	2.09	3.12	4.66	Low
23	SBH-17 (B)	Block-D, Basundhara	1.57	4.71	14.13	High
24	SBH-17 (C)	Block-H, Basundhara	2.52	2.94	3.43	Low
25	SBH-18	Civil Aviation Quarter	0.64	3.70	21.39	Very high
26	SBH-19	Kuril Flyover	1.97	2.73	3.78	Low
27	SBH-20	Sarengbari, Mipur-2	0.59	2.84	13.67	High
28	SBH - 21	Purachal, Uttar Badda	2.11	2.59	3.18	Low
29	SBH-22	City Corporation, Gabtoli	0.82	3.67	16.42	High

SL. No	ID	Location	Predominant Frequency, F_g (Hz)	H/V Ratio, A_g	Vulnerability Index, $K_g = \frac{A_g^2}{F_g}$	Remarks
30	SBH-23	Adabor	3.35	2.26	1.52	Low
31	SBH-24	Agargoan Trade Fair area	0.86	2.12	5.23	Low to moderate
32	SBH-25	Aftab Nagar Housing Project	0.95	2.76	8.02	Moderate
33	SBH-26	Umme Had Nagar, Nadda	1.32	3.83	11.11	Moderate
34	SBH-27	South Banasree	1.39	3.86	10.72	Moderate to high
35	SBH-28	Basila Garden City	1.12	4.47	17.84	High
36	SBH-29	Royer Bazar Boddhobumi	2.57	1.08	0.45	Low
37	SBH-30	Kalunagar, Hazaribagh	0.88	2.48	6.99	Moderate
38	SBH-31	Rab-10, Plot, Kamrangirchar	0.48	3.91	31.85	Very High
39	SBH-32	Sosan Ghat, Kamrangirchar	1.22	4.78	18.72	High
40	SBH-33	Basundhara River view	1.05	3.51	11.73	High
41	SBH-34	Matuail, Demra	2.77	2.48	2.22	Low
42	SBH-35	Jilmil Project, Equria	1.00	3.26	10.63	Moderate to high
43	SBH-36	Rajendapur	1.17	2.59	5.73	Low
44	SBH-37	Bramangaon	1.08	3.55	11.67	High
45	SBH-38	Meradia, Uttar Banasree	1.26	2.84	6.40	Moderate

Figure 4.3 shows the classification of vulnerability site at 45 locations using Nakamura's Vulnerability Index (Kg). Figure 4.3 demonstrates four major and two in between vulnerability type. The number of low vulnerability type locations, which is 16, is the most common among 45 locations. The second most predominant number of vulnerability type is moderate type which varies between 6 and 10. The number of very high type vulnerable site is 4.

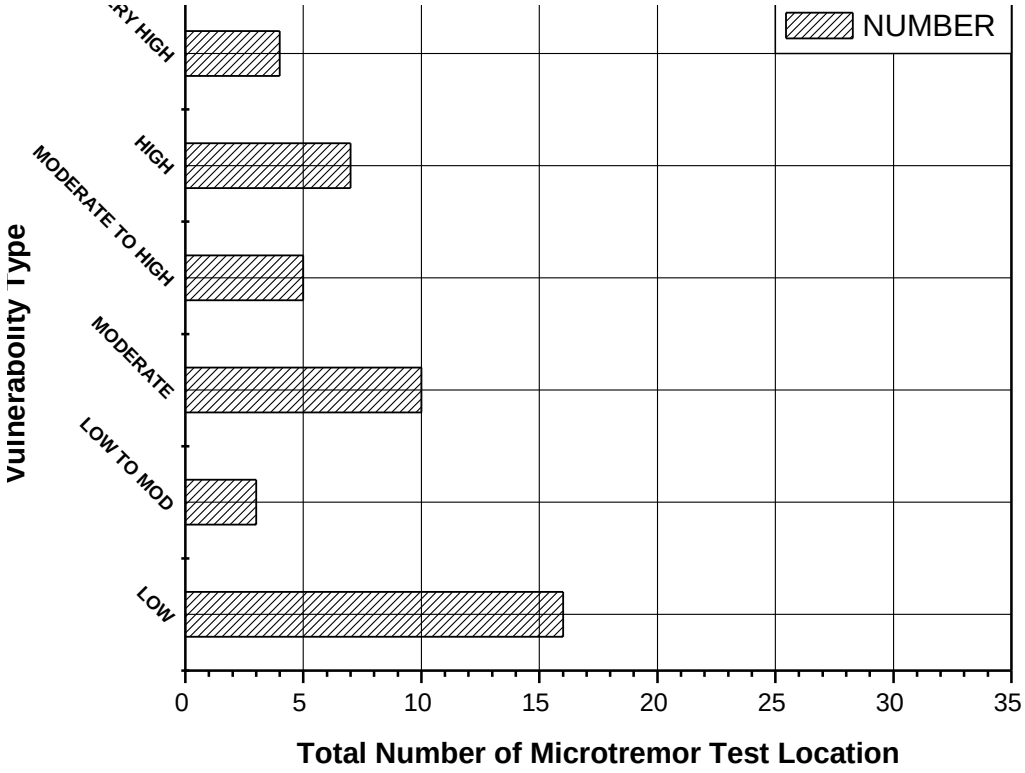

Figure 4.3: Damage assessment of 45 test locations using Nakamura's Vulnerability Index (Kg).

To further ensure this, research on the acceleration of seismic waves in the basement need to be estimated. Vulnerability Index together with the acceleration of seismic waves in the basement has been suggested by Nakamura (2000) to calculate the value of shear strain (γ) of surface soil layers. Damaging earthquakes will occur when the limits are exceeded due to the shear strain deformation surface layer of soil. Soil is plastic at $\gamma = 1000 \times 10^{-6}$, whereas at $\gamma > 10.000 \times 10^{-6}$, the ground will deform. Only predominant frequency is not effective to classify a site due to Nakamura's vulnerability index. Both predominant frequency and H/V ratio are required to estimate vulnerability type.

4.4 CONCLUDING REMARKS

This chapter shows the comparison of theoretical analysis with microtremor observation. One dimensional response analysis using the programme SHAKE has been executed at fourty two locations. The theoretical transfer function of the program SHAKE has been compared with the microtremor H/V ratio. From these result, it can be said that although amplitude values of the ratios are close, the predominant frequency for the two cases differs slightly. The reason of this difference is that microtremor consists of different types of waves, but the theoretical transfer function is based on shear-wave only.

The resonance between the site soil and building has been analyzed using the H/V ratio of soil and Fourier spectra of building in both EW and NS direction. It has been found that resonance may occur at four BUET buildings.

In addition to this, the seismic vulnerability of soil has been analyzed at the study points using the Nakamura's (2000) Vulnerability Index (Kg). The Vulnerability Index of fourty five locations in and around the Dhaka city has been classified into four types which are Low, medium, high and very high vulnerable. Most of the reclaimed sites fall within high medium to high vulnerability range.

.

CHAPTER 5

CONCLUSIONS AND RECOMMENDATIONS

5.1 GENERAL

The purpose of this research is to apply microtremor Horizontal to vertical spectral (H/V) ratio technique for site soil response analysis in and around the Dhaka city. For this purpose fourty five selected locations in and around Dhaka city as well as one hundred and thirty two points within BUET campus has been selected. The locations are selected on the basis of different geomorphic units.

After checking the stability of microtremor at different time instants microtremor observation has been carried out. The dynamic properties of soil, which are predominant frequency and amplification, have been estimated from microtremor analysis. The variation of microtremor H/V ratio due to various analysis windows have been carried out in this research.

The soil model using one dimensional response analysis using the programme SHAKE has been executed for the investigated sites. To carry out this research shear wave velocity data has been used as input for the programme SHAKE. Fourteen shear wave velocity data of the investigated site has been collected from the direct field test (PS logging and SSMM). The shear wave velocity of other investigated locations has been estimated using empirical correlation between SPT-N and shear-wave velocity. The comparision of amplitude ratio of microtremor and transfer function has been presented in this research. It should be mentioned that microtremor consists of different types of body and surface waves.

The resonance criteria between the site soil and buildings have been analyzed. Finally, vulnerability of site soil using Nakamura's (2000) technique has been carried out for this research.

5.2 CONCLUSIONS

From the overall result and analysis of the study following findings may be summarized.

(a) Stability of microtremor data on ground

In order to check the stability of microtremor data fourteen different locations of BUET campus have been selected to carry out microtremor observation from morning to midnight. The stability of microtremor H/V ratio for site amplification has been discussed in chapter 2. Fourier spectra depend on the source of vibration. This data does not show significant site amplification. That's why horizontal to vertical spectral ratio (H/V) of both East-West and North-South have been calculated. Microtremor H/V ratio do not show the source vibration effect. Whatever the source is, the amplification result is similar for different time instants. From this research, it can be concluded that Horizontal to Vertical spectral (H/V) ratio of microtremor is effective for site response analysis. This technique is reliable for site soil response compared to Fourier spectra.

(b) Resultant of EW and NS direction data

It is necessary to estimate the resultant H/V ratio because microtremor Horizontal to Vertical spectral (H/V) ratio data is found in East-West and North-South direction. Four resultant H/V ratio data are available to estimate the dynamic characteristics which are RM (Root multiplication), RMS (Root square mean), RS (Root square) and Mean. In this research the variations of four resultant H/V ratios have been carried out in three study locations (Bashundhara, Block-D; Board Bazar, Gazipur; Uttar Khan). From the observation it can be concluded that RM of H/V ratio data is close to other three resultants. Therefore, Root multiplication of East-West and North-South data have been used for the estimation of dynamic properties of soil.

(c) Various windows filtering technique

Five filtering windows are available for microtremor data analyses which are Rectangular, Welch, Hamming, Hanning and Blackman window. For this research, time

history microtremor data at Bramangaon has been selected to be analyzed using five filtering windows. From analysis of data in filtering windows it can be concluded that the peak H/V ratio is almost same in five windows. Rectangular window has been selected for microtremor data analysis in this research.

(d) Smoothing effect on the microtremor data

Smoothing has significant effect on the of microtremor data. In this research six average smoothing points (2, 3, 5, 10, 15 and 20) have been applied on microtremor H/V ratio at four study locations (Bramangaon, Tongi Ershad Nagar, Ashiyan city and Agargaon Trade fair). From this research it can be concluded that suitable smoothing function helps to estimate peak H/V ratio and predominant frequency easily. The peak of H/V ratio decreases if higher average smoothing points is applied.

(e) H/V Ratio data in and around Dhaka city

Microtremor measurement has been carried out in 45 locations**.** Out of 45 locations, the overall predominant frequency is 1.25 Hz with standard deviation 0.014. On the other hand, the overall H/V ratio is 2.72 with standard deviation 0.177. The maximum predominant frequency is 3.65 Hz, where H/V ratio is 2.73 at Azampur School, Uttara. The Horizontal to Vertical spectral ratio (H/V) lies between 1.81 and 3.74. On the other hand, the minimum predominant frequency is 0.48 Hz, where H/V ratio is 3.91, Rab-10, Plot, Kamrangirchar. The Horizontal to Vertical spectral ratio (H/V) lies between 2.23 and 5.65. The maximum Horizontal to Vertical spectral ratio (H/V) is 4.78 where as predominant frequency is 1.22 Hz, at Sosan Ghat, Kamrangirchar. The Horizontal to Vertical spectral ratio (H/V) lies between 4.07 and 5.71. The minimum Horizontal to Vertical spectral ratio (H/V) is 1.08 whereas predominant frequency is 2.57 Hz at Royer Bazar. From this classification of predominant frequency, it can be said that most of the locations predominant frequency varies from 1.0 Hz to 1.99 Hz. These are classified as **Type III**. From the classification of H/V ratio, the most common H/V ratio is **Type III** in 45 locations. The second most common H/V ratio is **Type IV.** The number of locations having H/V ratio ranging between 1.0 and 1.99 is eight. No location has been observed as **Type I**.

(f) Microtremor observation within BUET Campus

Microtremor observation at 132 selected points in soil has been carried out in BUET campus. Out of 132 locations, the overall predominant frequency is 1.39 Hz where as standard deviation is 0.289. On the other hand, the overall peak H/V ratio is 2.09 where as standard deviation is 0.523. The maximum predominant frequency is around 9.62 Hz where as H/V ratio is 2.43 at MT82. The Horizontal to Vertical spectral ratio (H/V) varies from 1.65 to 2.51. On the other hand, the minimum predominant frequency is around 0.25 Hz where as H/V ratio is 9.51 at MT72. This is the highest peak of H/V ratio in 132 selected locations within BUET campus. The Horizontal to Vertical spectral ratio (H/V) lies between 6.85 and 11.85. This lower predominant frequency and higher amplification ratio show that this location is highly susceptible due to any seismic hazard. The minimum Horizontal to Vertical spectral ratio (H/V) is 1.24 at MT 108. The Horizontal to Vertical spectral ratio (H/V) lies between 0.93 and 1.56.

From this classification of predominant frequency, it can be said that most of the locations predominant frequency ranging between 1.0 Hz and 1.99 Hz. These predominant frequencies are classified as **Type III**. The second most common type of predominant frequency is **Type II.** The number of locations predominant frequency classified as **Type V** is 21. There are sixteen **Type I** predominant frequency locations. From the classification of H/V ratio, most of the selected locations are classified as **Type III.** There are seventy five **Type III** locations. **Type II** is the second most predominant H/V ratio. There is no H/V ratio ranging between 0 and 0.99. The number of location H/V ratio greater than 3 is 15.

Microtremor observation on 45 buildings has been carried out within BUET campus. Fourier Spectrum provides better result of predominant frequency for buildings. Out of 45 microtremor observation in buildings, the maximum predominant frequency is 5.56 Hz along both EW and NS directions at Controller of Examination Building. This is a four-storied frame structure building with 324sqm floor area. There are no lift and shear wall in this building. The foundation of the building is individual footing. There are no structural irregularities in building. But torsional irregularity, re-entrant corner and diaphragm discontinuity exist.

The minimum predominant frequency is 2.00 Hz along EW and NS directions at Eleven Story Tower Building. This is an eleven-storied frame structure with 673sqm floor area. There are three lift cores and a shear wall in the building. The foundation of the building is pile-raft system. No structural irregularity exists in this building. But torsional irregularity, re-entrant corner and diaphragm discontinuity exist. From this classification of predominant frequency along EW direction, most of the locations predominant frequency is more than 3.0 Hz. These are classified as **Type V**. The second most common type of predominant frequency is **Type IV.** The number of building predominant frequency ranging between 2.0 Hz and 2.99 Hz is 5. There is no predominant frequency of **Type I**, **Type II** and **Type III**. **Type V** is the most common predominant frequency in 45 buildings of BUET campus along NS direction. **Type IV** is the second most predominant frequency. There are no buildings of predominant frequency ranging between 0 and 1.99**.**

(g) Comparison between microtremor H/V ratio and Transfer Function using the program SHAKE

The comparison of amplitude ratio between transfer function and microtremor H/V ratio for fourty two locations in and around the Dhaka city has been studied.

From the comparison between microtremor H/V ratio and transfer function using the programme SHAKE four types of characteristics curves have been observed. These curves are classified as similar, dissimilar, right side shifted and left side shifted compared to the microtremor H/V ratio curve. Among 42 models predominant frequency of thirty five transfer function have been shifted in the right side of microtremor and only one has been shifted in the left side. Similar pattern amplitude ratio curves have been found in six locations. The rest two locations have been found where no similarity between microtremor H/V ratio and transfer function.

The same amplitude ratio but higher frequencies of transfer function have been found in ten locations. The higher frequency but low amplified locations have been found in nineteen different locations. On the other hand, both higher frequency and higher amplified locations of transfer function have been found in six locations. The similar predominant frequency but lower amplified transfer function has been found in three

locations. But, the same predominant frequency but higher amplified location is Adabor. The dissimilar types of pattern curve have been found in three locations.

From these results, it can be said that although amplitude values of the ratios are close, the predominant frequency for the two cases differs slightly. The reason of this difference is that microtremor consists of different types of waves, but the theoretical transfer function is based on shear-wave only.

(h) Resonance between site soil and building

The resonance between the site soil and building has been analyzed using the H/V ratio of soil and Fourier spectra of building in both EW and NS direction. It has been found that resonance may occur at four BUET buildings. These buildings are Eleven Story Tower Building, URP Building, Titumir Hall and Building # 1. For most of the building predominant frequency is not close to the predominant frequency of soil. From the sub-soil characteristics within BUET campus, it can be concluded that stiff soil with higher SPT value exists in most of the investigated locations.

(i) Seismic Vulnerability Index (Kg) for soil

Seismic vulnerability index (Kg) is an index indicating the level of vulnerability of a layer of soil to deform. This index is useful for the detection of areas that are weak zone (unconsolidated sediment) at the time of occurrence of earthquakes. The details result of Vulnerability Index (Kg) of the investigated areas in 45 locations has been illustrated in section 4.3.2. The vulnerability index of fourty five locations in and around the Dhaka city has been classified into four types which are low (0-5), moderate (6-10), high (11-20) and very high (>20). From the analysis the highest (Kg) value has been found at Rab-10, Plot, and Kamrangirchar. So, it can be concluded that this location is more weak zone that other locations. The seismic vulnerability index (Kg) for 45 sites varies between 0.45 and 31.85. Sixteen sites have been classified as low vulnerable of soil layers. Five sites have been identified as having moderate to high vulnerable of soil layers to deform.

5.3 RECOMMENDATIONS

Although the study covers the objectives of study, more significant study would be needed to cover other aspects of the research. Specific recommendations are follows:

- Compare Microtremor data with Strong Motion Earthquake data.
- Compare microtremor data with Rayleigh wave.
- Details investigation of Resonance criteria between soil and building by resonance column test. Details investigation of soil structure interaction is required.
- Investigation of Microtremor H/V technique in Bangladesh using reference site where exposed rock is found.
- Liquefaction Potential Analysis using H/V Technique. In order to compare result Liquefaction based on Shear Wave Velocity and Standard Penetration Test (SPT) should be carried in the microtremor test location. Laboratory analysis such as Grain Size Analysis, Atterberg's Limit Test, Direct Shear Test, Cyclic Loading Test and Shaking Table test are required to compare the actual soil behavior with the microtremor estimated behavior.

CONTENTS

		Page
BOARD OF EXAMINEERS		i
DECLARATION		II
ACKNOWLEDGEMENT		III
ABSTRACT		IV
TABLE OF CONTENTS		VI
LIST OF TABLES		X
LIST OF FIGURES		XI
NOTATION		XVI
CHAPTER 1	**INTRODUCTION**	
	1.1 General	1
	1.2 Objective of the Research	3
	1.3 Study Area and Site Selection	4
	1.4 Outline of Methodology	7
	1.5 Geology and Geomorphology of the study area	11
	1.5.1 Geological subdivisions of Dhaka city	12
	1.5.2 Geomorphological subdivisions of Dhaka city	17
	1.5.3 Seismicity and Tectonics	21
	1.7 Overview of the Thesis	22
CHAPTER 2	**LITERATURE REVIEW**	
	2.1 General	24
	2.2 Past Researches on Microtremor	26

Page

2.2.1 Earthquake and Microtremor Spectral ratio 33

2.2.2 Observed and Analytical Amplitude Ratio 36

2.3 Microtremor H/V Technique 38

2.3.1 Method of Microtremor H/V Technique 38

2.3.2 Theory of Microtremor H/V Technique 39

2.4 Wave Propagation 43

2.4.1 Equation of Motion for a Three-Dimensional Elastic Solid 44

2.4.2 Solution of the Three-Dimensional Equations of motion 46

2.4.3 Waves in a Semi-infinite Body 49

2.4.3.1 Rayleigh Waves 51

2.4.3.2 Love Waves 58

2.4.3.3 Higher-Mode Surface Waves 61

2.4.3.4 Dispersion of Surface Waves 61

2.4.3.5 Phase and Group Velocities 62

2.5 Correlation between Field SPT-N and Shear Wave Velocity 63

2.6 1D Response Analysis using programme SHAKE 65

2.6.1 Method for Amplification Analysis 67

2.6.2 Theory to the Program 68

2.6.3 Description of the Program SHAKE 68

2.7 Damage Assessment 70

Page

2.7.1 Resonance Criteria for Building 70
2.7.2 Seismic Vulnerability Index for soil 75

2.8 Concluding Remarks 77

CHAPTER 3 DATA COLLECTION AND ANALYSIS

3.1 General 78
3.2 Location of Investigated Sites within the Study Area 79
3.2.1 Geological and Geomorphological classification 79
3.3.2 Sub-Soil Characteristics 87
3.3 Microtremor Data Collection 118
3.4 Microtremor Data Analysis 121
3.4.1 Stability of Microtremor Data 124
3.4.1.1 Stability of Amplitude of Fourier Spectrum 125
3.4.1.2 Stability of Horizontal to Vertical Spectral Ratio 127
3.4.2 Resultant of H/V Ratio Curve 137
3.4.3 Window Effect on microtremor data 139
3.4.4 Smoothing Effect on Microtremor Data 142
3.5 Analysis Result 145
3.5.1 Microtremor Analysis Result in and around Dhaka City 145
3.5.2 Microtremor Analysis Result within BUET Campus 152
3.5.2.1 Soil Sites 152
3.5.2.2 Building Sites 163
3.7 Concluding Remarks 169

Page

CHAPTER 4 COMPARISON OF MICROTREMOR DATA WITH THEORETICAL ANALYSIS

4.1 General 170
4.2 Comparison of Microtremor Data with 1D Response Analysis using the Programme SHAKE 170
4.3 Vulnerability Assessment 174
4.3.1 Resonance between Site Soil and Building 174
4.3.2 Seismic Damage assessment using Nakamura's Technique 176
4.4 Concluding Remarks 181

CHAPTER 5 CONCLUSIONS AND RECOMMENDATIONS

5.1 General 182
5.2 Conclusions 183
5.3 Recommendations 188

REFERENCES 189

APPENDIX-A SPT-N value and estimated Shear Wave Velocity 199

APPENDIX-B Microtremor H/V ratio at 45 locations in Dhaka City 219

APPENDIX-C Microtremor H/V ratio at 132 locations within BUET 232

APPENDIX-D Microtremor Fourier Spectrum of selected BUET buildings 266

APPENDIX-E Comparison of Microtremor with Transfer Function using the programme SHAKE 289

REFERENCES

Aki, K. (1957). Space and time spectra of stationery stochastic waves, with special reference to microtremors, Bull. Of earthquake research institute 35, PP. 415-456.

Aki, K. and Richards, P. G. (1980). Quantitative seismology: Theory and Methods, Volumes 1 and 2, W. H. Freeman, San Francisco, California.

Aki, K. (1993). Local site effects on weak and strong ground motion, Tectonophysics, 218, PP. 93-111.

Alfaro, A., Pujades, L., Goula, X., Susagna, T., Navarro, M., Sánchez, J. and Canas, J. A. (2001). Preliminary Map of Soil's Predominant Periods in Barcelona Using Microtremors, Pure appl. Geophys. 158, PP. 2499-2511.

Alam, M. K., Hasan, A.K.M. Shahidul, Khan, M. R. and Whitney, J. W. (1990). The Geological Map of Bangladesh, the Geological Survey of Bangladesh in Collaboration with United States Geological Survey.

Ansary, M. A., Yamazaki, F. and Katayama, T. (1996). Application of microtremor measurements to the estimation of site amplification characteristics, Bulletin of Earthquake Resistant Structure Research Center, IIS, University of Tokyo, No. 29, PP. 95-113.

Ansary, M. A., Rahman, S., Murad, E. M., Chowdhury, S. A. and Shuvra, D. P. (2010). Proposed Time History and Response Spectrum for Dhaka, Chittagong and Sylhet cities, Proceedings, 3rd International Earthquake Symposium, March 5-6, Dhaka, Bangladesh, PP. 349-356.

Arai, H. and Tokimatsu, K. (2000). Effects of Rayleigh and Love Waves on microtremors H/V spectra. Proc. 12th World Conf. on Earthquake Engineering, paper 2232, CD-ROM.

Arai, H. and Tokimatsu, K. (2004). S-wave velocity profiling by inversion of microtremor H/V spectrum. Bull. Seism. Soc. Am., 94, 1, PP. 53-63.

ASTM (2000). Annual Book of ASTM Standards, vol. 04.08: Soil and Rock (I). Standard No. D 1586-99, Standard Test Method for Penetration Test and Split-Barrel Sampling of Soils, West Conshohocken, PA, PP. 139-143.

Banglapedia (2006). National Encyclopedia of Bangladesh, Prepared by Asiatic Society of Bangladesh, CD edition.

Bard, P. Y. (1999). Microtremor measurements: A tool for site effect estimation?, Proceedings of the second international symposium on the effects of surface geology on seismic motion, Yokohama, Japan, December 1998, PP. 1251-1279.

Bard, P. Y. (2004). Effects of surface geology on ground motion: Recent results and remaining issues, Proceedings of the 10th European Conference on Earthquake Engineering, Vienna, Austria, August 28 – September 2, 1994, PP. 305-325.

Bilham, R., Gaur, V. K. and Molnar, P. (2001). Himalayan Seismic Hazard, SCIENCE, 293.

Borcherdt, R. D. (1970). Effects of local geology on ground motion near San Francisco Bay, Bulletin of seismological society of America, 60, PP. 29-61.

Bullen, K. E. and Bolt, B. A. (1985). An introduction to the theory of seismology. Cambridge University Press.

Cassidy, J. F., Rosenberger, A., Rogers, G.C., Little, T. E., Toth, J., Adams, J., Munro, P., Huffmann, S., Pierre, J. –R., Asmis, H. and Pernica, G. (2007). Strong motion seismograph networks in Canada, Proceedings of the Canadian Conference on Earthquake Engineering, June 24-27th 2007, Ottawa.

CDMP (2009). Ongoing Research Work, CDMP-UNDP Fault Map Delineation for Bangladesh, 2009.

Chatelain, J. C., Guillier, B., Cara, F., Duval, A. M., Atakan, K., Bard, P.Y. and The WP02 SESAME team (2007). Evaluation of the influence of experimental conditions on H/V results from ambient noise recordings. Bull. Earthquake Eng., doi: 10.1007/s10518-007-9040-7.

Chouinard, L., Rosset., P., de la Puente, A., Madriz, R., Mitchell, D. and Adams, J. (2004). Seismic hazard analysis for Montreal, Proceedings of the 13th World Conference of Earthquake Engineering, Vancouver, BC, Paper 7010.

Curry, J. R. and Moore, D. G. (1974). Sedimentary and Tectonic processes in Bengal Deep Sea Fan and Geosyncline, The geology of continental margins, Springer-Verlag, New York.

Daryono (2009). Eftek Tapek Lokal (Local site effect) di Graben Bantul Berdasarkan Pengakuran Mikrotremor. International Conference Earth Science and Technology. Yogjakarta.

Dimitriu, P. P., Papaioannou, Ch. and Theodulidis, N. P. (1998). EURO-SEISTEST strong motion array near Thessaloniki, Northern Greece: a case study of site effects. Bulletin of seismological society of America, No. 3, PP. 862-873.

Dravinski, M., Ding, G. and Wen, K. L. (1996). Analysis of spectral ratios for estimating ground motion in deep basins, Bull. Seism. Soc. Am., 86, PP. 843-847.

Enomoto, T., Kuriyama, K., Navarro, M. and Iwatate, T. (2002). Site-effects evaluation by H/V spectra comparing microtremor with strongmotion records observed at ground surface and basement using borehole, 12th European Conference on Earthquake Engineering, paper 596. Londres.

Ewing, M., Jardesky, W. and Press, F. (1957). Elastic Waves in Layered Media, McGraw-Hill, New York, PP. 380.

Fäh, D., Kind, F. and Giardini, D. (2001). A theoretical investigation of average H/V ratios. Geophys. J. Int., 145, PP. 535-549.

Fäh, D., Kind, F. and Giardini, D. (2003). Investigation of local S-wave velocity structures from average H/V ratios, and their use for the estimation of site effects. Journal of Seismology, 7, PP. 449-467.

Field, E. H. and Jacob, K. H. (1993). The Theoretical Response of Sedimentary Layers to Ambient Seismic Noise, Geophysical Research Letter, 20, PP. 2925-2928.

Field, E. H. and Jacob, K. H. (1995). A comparison and test of various site-response estimation techniques, including three that are not reference-site dependent, Bulletin of the Seismological Society of America, 85, PP. 1127-1143.

Field, E. H., Clement, A. C., Jacob, K. H., Aharonian, V., Hough, S. E., Friberg, P. A., Babaian, T. O., Karapetian, S. S., Hovanessian, S. M. and Abramian, H. A. (1995). Earthquake site response study in Giumri (Formerly Leninakan), Armenian using ambient noise observation. Bull. Seism. Soc. Am., 85, PP. 349-353.

Flores, H., Aguirre, E. and Aguirre, J. (2003). SPAC: An Alternative Method to Estimate Earthquake Site Effects in Mexico City. Geofís, Int. Vol. 42 (2), PP. 227-236.

Ghayamghamian, M. R. and Kawakami, H. (1997). Segmental cross-spectrum in microtremor spectral ratio analysis. 7th International Conference on Structural Safety and Reliability, Kyoto, November 1997, 24-28, PP. 1487-1494.

Geological Survey of Bangladesh, GSB (2008). Geomorphological Map of Dhaka city, Preapared by GSB under the project of Comprehensive Disaster Management Programme (CDMP).

Haskell, N. A. (1953). The Dispersion of Surface Waves on Multilayered Media. Bull. Seism. Soc. Am., 43(1), PP. 17-34.

Horike, M., Zhao, B. and Kawase, H. (2001). Comparison of site response characteristics inferred from microtremors and earthquake shear waves, Bulletin of the Seismological Society of America, 91, PP. 1526-1536.

Hossain, M. T. (2009). Estimation of Earthquake Induced Liquefaction Potential of Selected areas of Dhaka City Based on Shear Wave Velocity, Thesis paper of Master of Science in Civil Engineering, November, 2009.

Huang, H. C. and Tseng, Y. S. (2002). Characteristics of soil liquefaction using H/V of microtremors in Yuan-Lin area, Taiwan, TAO,Vol.13, No.3,325-338, September, 2002.

Kagami, H., Okada, S., Shiono, K., Oner, M., Dravinski, M. and Mal, A. K. (1986). Observation of 1 to 5 second microtremors and their application to earthquake engineering. Part III. A two-dimensional study of site effects in S. Fernando valley. Bulletin of seismological society of America, 76, PP. 1801-1812.

Kamal, A.S.M. Maksud and Midorikawa, S. (2003). GIS-based Landfill Mapping of Dhaka City area, Bangladesh, Using Remote sensing data, Proceedings on the second International Symposium on New Technologies for Urban Safety of Mega cities in Asia, University of Tokyo, Japan.

Kanai, K., Tanaka, T. and Osada, K. (1954). Measurements of Micro-tremors 1. Bulletin Earthquake Research Institute, Tokyo University, 32, PP. 199-210.

Kanai, K. and Tanaka, T. (1961). On microtremor VIII, Bull. Of earthquake research institute 39, PP. 97-114.

Khan, M. R. and Munimullah., compilers (1988). Stratigraphic lexicon of Bangldaesh: Geology Survey of Bangladesh record, Vol. 5, pt. 1, PP. 61.

Kim, D. S. and Lee, J. S. (2007). Propagation and attenuation characteristics of various ground vibrations. Soil Dynamics and Earthquake Engineering, 19, PP. 115-126.

Khan, F. H. (1991). Geology of Bangladesh, University Press Limited, PP. 1-207.

Konno, K. and Ohmachi, T. (1998). Ground motion characteristics estimated from spectral ratio between horizontal and vertical components of microtremor», Bull. Seism. Soc. Am., 88, N. 1, PP. 228-241.

Kramer, S.L. (1996). Geotechnical Earthquake Engineering, Prentice Hall, Inc., Pearson Education Pte. Ltd., Singapore, Chapter 5, PP.149-165.

Lachet, C. and Bard, P. Y. (1994). Numerical and theoretical investigations on the possibilities and limitations of Nakamura's technique, Journal of the Physics of the Earth, 42, PP. 377-397.

Lachet, C., Hatzfeld, D., Bard, P. Y., Theodulidis, C. P. and Savvaidis, A. (1996). Site effects and microzonation in the city of Thessaloniki (Greece): Comparison of different approaches, Bulletin of the Seismological Society of America, 86, PP. 1692-1703.

Lermo, L., Francisco, S. and Chavez-García, F. J. (1992). Site effect evaluation using microtremors: a review (abstract). EOS, 73, PP. 352.

Lermo, L. and Chavez-García, F. J. (1993). Site effect evaluation using spectral ratios with only one station, Bull. Seism. Soc. Am., 83, PP. 1574-1594.

Lermo, J. and Chavez-Garcia, F. J. (1994). Are Microtremors Useful in Site Response Evaluation? Bulletin of Seismological Society of America, 84, PP. 1350-1364.

Lermo, J. and Chavez-Garcia, F. J. (1994a). Are Microtremors Useful in Site Response Evaluation? Bulletin of Seismological Society of America, 84, PP. 1350-1364.

Lermo, J. and Chavez-Garcia, F. J. (1994b). Site effect evaluation at Mexico city: dominant period and relative amplification from strong motion and microtremor records, Soil dyn. Earthquake eng. 13, PP. 413-423., 84, PP. 1350-1364.

Love, A. E. H. (1927).The mathematical theory of elasticity, 4th ed., University Press, Cambridge.

Malischewsky, P. G. and Scherbaum, F. (2004). Love's formula and H/V-ratio (ellipticity) of Rayleigh waves, Wave Motion, 40, PP. 57-67.

Matin, M.A., Maroof Khan, M.A., Fariduddin, M., Boul. M.A., Taolad Hossain, M.M. and Kononov, A.I. (1983). The Techtonic Map of Bangladesh-Past and Present, Vol-2, PP. 29-36.

McNamara, D. E. and Buland, R. P. (2004). Ambient noise levels in the continental United States. Bull. Seism. Soc. Am., 94, PP. 1517-1527.

Molnar, S. and Cassidy, J. F. (2006). A comparison of site response techniques using weak-motion earthquake and microtremors, Earthquake Spectra, 22, PP. 169-188.

Molnar, S., Cassidy, J. F., Monahan, P. A., Onur, T., Ventura, C.E. and Rosenberger, A. (2006a). Application of microtremor measurements for earthquake site response studies in southwestern British Columbia, Proceedings 100th Anniversary Earthquake conference, EERI/SSA, San Francisco, April 18-22, 2006.

Molnar, S., Rosenberger, A., Cassidy, J. F. and Rogers, G. C. (2006b). Internet Accelerograph recordings of low-level earthquakes in southwestern British Columbia from 2002 to 2003, Geological Survey of Canada Open File 5266, PP. 2.

Molnar, S., Rosenberger, A., Cassidy, J. F. Rogers, G. C. and Ristau, J. (2006c). Digital accelerograph recordings of the July 15 and 19, 2004 earthquakes, west of Vancouver Island, Geological Survey of Canada Open File 5010, PP.76.

Molnar, S., Rosenberger, A., Dosso, S. and Cassidy, J. (2006d). Earthquake and microtremor site response at Internet Accelerograph sites in British Columbia, Canada, Proceedings 1st European Earthquake Engineering and Seismology Conference, Geneva, Switzerland, September 4-8, 2006.

Molnar, S., Cassidy, J. F. Monahan, P. A. and Dosso, S. E. (2007). Comparison of geophysical methods to determine shear-wave velocity, Proceedings of the Canadian Conference on Earthquake Engineering, June 24-27th 2007, Ottawa, ON, Paper 1173.

Morales, J., Vidal, F., Peña, J. A., Alguacil, G. and Ibáñez, J. (1991). Microtremor study in the sediment filled basin of Zafarraya, Granada (Southern Spain), Bull. Seism. Soc. Am., 81, PP. 687- 693.

Morales, J., Seo, K., Samano, T., Peña, J. A., Ibañez, J. and Vidal, F. (1993). Site response on seismic motion in the Granada basin (southern Spain) based on microtremor measurements, J. Phys. Earth, 41, PP. 221-238.

Morgan, J. P. and Mclntire, W. G. (1959). Quaternary geology of the Bengal Basin, East Pakistan and India: Geological Society of America Bulletin, V.70, PP. 319-342.

Mucciarelli, M. (1998). Reliability and applicability range of the Nakamura's technique. Journ. Earthq. Eng., 2, 4, PP. 625-638.

Mucciarelli, M., Gallipoli, M. R. and Arcieri, M. (2003). The stability of the horizontal to vertical spectral ratio of triggered noise and earthquake recordings, Bulletin of the Seismological Society of America, 93, PP. 1407-1412.

Mucciarelli, M., Masi, A., Gallipoli, M. R., Harabaglia, P., Vona, M., Ponzo, F. and Dolce, M. (2004). Analysis of RC Building Dynamic Response and Soil-Building Resonance Based on Data Recorded during a Damaging Earthquake, Bulletin of the Seismological Society of America, October, Vol. 94, No. 5, PP. 1943–1953.

Murthy, V.N.S. (1991). Soil Mechanics and Foundation Engineering. Volume 2, Revised and enlarged third edition, SAITECH, Bengalore, India.

Nakamura, Y. (1989). A Method for Dynamic Characteristics of Sub-surface Using Microtremors on the Ground Surface, Quick Report of Railway Technical Research Institute, 30, No. 1, PP. 25-33 (in Japanese).

Nakamura, Y. (1996). Real Time Information Systems for Seismic Hazards Mitigation UrEDAS, HERAS and PIC, Quarterly Report of RTRI, Vol. 37, No. 3, PP. 112-127.

Nakamura, Y. (2000). Clear identification of fundamental idea of Nakamura's Technique and its applications, Proc. Of the 12th World Conference on Earthquake Engineering, Auckland, New Zealand, PP. 2656-2664.

Nakamura, Y. and Takizawa, T. (1990) Evaluation of Liquefaction of Surface Ground using Microtremor (in Japanese), Proc. 45th Annual Meeting of JSCE, I-519, PP. 1068-1069.

Navarro, M., Enomoto, T., Sánchez, F. J., Matsuda, I., Iwatate, T., Posadas, A., Luzón, F., Vidal, F. and Seo, K. (2001). Surface Soil Effects Study Using Short-period Microtremor Observations in Almeria City, Southern Spain, Pure Appl. Geophys., 158, PP. 2481-2497.

Nogoshi, M. and Igarashi, T. (1970). On the propagation characteristics of microtremors. J. Seism. Soc. Japan, 23, PP. 264-280 (in Japanese with English abstract).

Nogoshi, M., and Igarashi, T. (1971). On the amplitude characteristics of microtremor (Part 2), Journal of the Seismological Society of Japan, 24, PP. 26-40.

Ohta, Y., Kagami, H., Goto, N. and Kudo, K. (1978). Observation of 1 to 5 second microtremors and their application to earthquake engineering. Part I. Comparison with long period accelerations at the Tokachi-Oki earthquake of 1968, Bull Seism. Soc. Am., 68, PP. 767-779.

Ohmachi, T., Nakamura, Y. and Toshinawa, T. (1991). Ground motion characteristics in the San Francisco Bay area detected by microtremor measurements, Proc. 2nd International Conference on Recent Advances in Geotech. Earth. Eng. & Soil Dyn. Saint Louis, Missouri, PP. 11-15 March: PP. 1643-1648.

Onur, T., Molnar, S., Cassidy, J. F., Ventura, C. E. and Hao, K. X. -S. (2004). Estimating site periods in Vancouver and Victoria, British Columbia using microtremor measurements and "SHAKE" analyses, Proceedings 57th Canadian Geotechnical Conference, Québec City, October 24-27, 2004.

Parolai, S., Bormann, P. and Milkereit, C. (2001). Assessment of the natural frequency of the sedimentary cover in the Cologne area (Germany) using noise measurements. Journal of Earthquake Engineering, 5, 4, PP. 541-56.

Parolai, S., Picozzi, M., Richwalski, S.M., and Milkereit, C. (2005). Joint inversion of phase velocity dispersion and H/V ratio curves from seismic noise recordings using

a genetic algorithm, considering higher modes. Geoph. Res. Lett., 32, doi: 10.1029/2004GL021115.

Parolai, S., Richwalski, S.M., Milkereit, C. and Fäh, D. (2006). S-wave velocity profiles for earthquake engineering purposes for the Cologne Area (Germany). Bull. Earthquake Eng., 4, PP. 65-94.

Parolai, S. and Galiana-Merino, J. J. (2006). Effect of transient seismic noise on estimates of H/V spectral ratios. Bull. Seism. Soc. Am., 96, PP. 228-236.

Picozzi, M., Parolai, S. and Richwalski, S. M. (2005) Joint inversion of H/V ratios and dispersion curves from seismic noise: Estimating the S-wave velocity of bedrock. Geoph. Res. Lett., 32, doi: 10.1029/2005GL022878.

Pujades, L., Canas, J. A., Mena, U., Espinoza, F., Alfaro, A. and Caselles, O. (2000). Seismic risk evaluation in Barcelona, Spain, Proc. Of the 12th World Conference on Earthquake Engineering, Auckland, New Zealand.

Richart, F. E., Hall, J. R. and Woods, R. D. 1970). Vibrations of Soils and Foundation, Prentice Hall, Englewood Cliffs, New Jersey, PP. 401.

Rayleigh, Lord (1885). On waves propagated along the plane surface of an elastic solid, Proceedings of the London Mathematical Society, Vol. 17, PP. 4-11.

Rodriguez, V. S. H. and Midorikawa, S. (2002). Applicability of the H/V Spectral Ratio of Microtremors in Assessing Site Effects on Seismic Motion, Earthquake Engineering and Structural Dynamics, 31, PP. 261-279.

Rosenberger, A., Rogers, G. C. and Cassidy, J. F. (2007). The new real-time reporting strong motion seismograph network in southwest BC: More strong motion instruments for less money, Proceedings of the Canadian Conference on Earthquake Engineering, June 24-27th 2007, Ottawa, ON.

Russel, S. Z. R., Yasin, M., Ansary, M. A., Saha, R., Kamruzzaman, M. and Noor, M. A. (2006). Evaluation of the Seismic Vulnerability of Bangladeshi Building using Non-Destructive Testing, an unpublished BNUS annual Report, Bangladesh Network Office for Urban Safety, International Centre for Urban Safety Engineering, Institute of Industrial Science, The University of Tokyo.

Sánchez-Sesma, F. J. and Luzón, F. (1995). Seismic Response of Three-Dimensional Alluvial Valleys for Incident P, S and Rayleigh Waves. Bulletin of the Seismological Society of America, Vol. 85, PP. 269-285.

Sato, T., Kawase, H., Matsui, M. and Kataoka, S. (1991). Array measurement of High frequency microtremors for underground structure estimation, Proc. 4th Int. conf. on seismic zonation II, PP. 409-416.

Scherbaum, F., Hinzen, K. G. and Ohrnberger, M. (2003). Determination of shallow shear-wave velocity profiles in Cologne, Germany area using ambient vibrations. Geophys. J. Int., 152, PP. 597-612.

Schnabel, P. B., Lysmer, J. and Seed, H.B. (1972). SHAKE: a computer program for earthquake response analysis of horizontally layered sites, Report no. EERC 72-12, Earthquake Engineering Research center, Univ. California, Berkeley, USA.

Seo, K. (1994). On the applicability of microtremors to engineering purpose, Preliminary report of the Joint ESG Research on Microtremors after the 1993 Kushiro-Oki (Hokkaido, Japan) earthquake. Proc. of 10th European Conf. on Earthq., 4, PP. 2643- 2648.

SESAME European project (2004). Guidelines for the implementation of the H/V spectral ratio technique on ambient vibrations measurements, processing and interpretation. DeliverableD23.12.http://sesame-fp5.obs.ujf grenoble.fr/SES_TechnicalDoc.htm.

Sesoren, Atila (1984). Geological Interpretation of Landsat Imagery of Bangladesh Ganges Delta, ITC Journal, PP. 229-232.

Sneider, A. J., Motazedian, D. and Atkinson, G. M. (2005). Seismic soil amplification studies for Ontario Polaris stations, 1st Polaris-Polo Research Workshop, Queen's University, Kingston, January 6th, 2005.

Suzuki, T., Adachi, Y. and Tanaka, M. (1995). Application of Microtremor measurements to the estimation of earthquake ground motions in the Kushiro city during the Kushiro-Oki earthquake of 15 January 1993, Earthquake Eng. Struc. Dyn. 24, PP. 595-613.

Taga, N. (1993). Measurement of microtremors in Earthquake Ground Motion and Ground Condition, edited by The Architectural Institute of Japan.

Tamura, T., Nagai. O., Kokubo, H. and Sumita, H. (1993). Characteristics of wave group of microtremors obtained by array measurement, J. struc. consr. Eng, AIJ 449, PP. 83-91 (in Japanese).

Taniguchi, E. and Sawada, K. (1979). Attenuation with distance of traffic-induced vibrations. Soils and Foundations, 19, 2, PP. 16-28.

TC4 (1993). Manual for Zonation on Seismic geotechnical hazards, published by ISSMFE.

Tokimatsu, K. and Miyadera, Y. (1992). Characteristics of Rayleigh waves in microtremors and their relation to the underground structures, J. struc. consr. Eng, AIJ 439, PP. 81-87 (in Japanese).

Ventura, C. E., Onur, T. and Hao, K. X-S. (2004). Site period estimations in the Fraser River delta using microtremor measurements–experimental and analytical studies, Proceedings of the 13th World Conference of Earthquake Engineering, Vancouver, BC, Paper 1075.

Vidal, F., Romacho, M. D., Feriche, M., Navarro, M. and Abeki, N. (1996). Seismic microzonation in Adra and Berja Towns, Almeria (Spain), Proc. of the 11th World Conference on Earthquake Engineering, Acapulco, Mexico, June 23-28, 1996.

Yamanaka, H., Dravinski, M. and Kagami, H. (1993). Continuous measurements of microtremors on sediments and basement in Los Angeles, California, Bull. Seism. Soc. Am., 83, PP. 1595-1609.

Yamanaka, H., Takemura, M., Ishida, H. and Niwa, M. (1994). Characteristics of long period microtremors and their applicability in exploration of deep sedimentary layers, Bull. Seism. Soc. Am., 884, PP. 1831-1841.

Wakamatsu, K. and Yasui, Y. (1995). Possibility of estimation for amplification characteristics of soil deposits based on ratio of horizontal to vertical spectra of microtremors, J. struct. consr. Eng, AIJ 471, PP. 61-70 (in Japanese).

LIST OF FIGURES

	Page
Figure 1.1: One hundred and thirty two microtremor observation in the free field locations of BUET campus.	5
Figure 1.2: Fourty five selected locations for microtremor observation in and around the Dhaka city. (Source: Google map)	6
Figure 1.3: Flow Chart for Microtremor Research in the Dhaka city.	9
Figure 1.4: Geology Map of Bangladesh. (Source: Geological Survey of Bangladesh, GSB)	14
Figure 1.5: Correlation of stratigraphic Sections from the Himalayan Foredeep across the Bengal Basin. (Source: Geological Survey of Bangladesh, GSB)	15
Figure 1.6: Classification of Bed Rock.	16
Figure 1.7: Geomorphological Map of Dhaka city. (Source: Geological Survey of Bangladesh, 2008)	20
Figure 1.8: Tectonic Map of Bangladesh. (Source: Banglapedia, 2006)	21
Figure 2.1: Microtremor observation and damage assessment.	25
Figure 2.2: Comparision of (1) the average earthquake site-to-reference spectral ratios (SSR) with (2) the average earthquake H/V spectral ratios (HVSR) of up to seven earthquakes, and (3) the average microtremor H/V spectral ratio at three strong-motion instrument sites in greater Victoria. (After Molnar et al., 2007)	34
Figure 2.3: Comparision of the H/V spectral ratio from up to four weak-motion earthquakes and microtremors at four sites across SW British Columbia.(After Molnar et al, 2007)	34
Figure 2.4: Amplitude ratios of microtremor and theoretical Rayleigh-wave plotted with transfer function of shear wave. (After Ansary et al., 1996)	37
Figure 2.5: Typical geological structure of sedimentary basin.	40
Figure 2.6: Schematic comparison of Horizontal (H_f), Vertical (V_f), H_f/H_b (spectral ratio of sediment site to the reference site). (After Nakamura, 2000)	41

Page

Figure 2.7: Relationship between charactersistics of Rayleigh Wave and Impedance Ratio. (After Nakamura, 2000) 42

Figure 2.8: Different type of Microtremor Wave due to ambient noise of ground. 44

Figure 2.9: Stresses in x-direction on infinitesimal cube. 45

Figure 2.10: Deformation produced by body waves: (a) P-wave; (b) SV-wave. 47

Figure 2.11: Deformation produced by Surface Waves: (a) Rayleigh Wave; (b) Love Wave. 50

Figure 2.12: Motion induced by a typical plane wave that propagates in the x-direction. Wave motion does not vary in the y-direction. 52

Figure 2.13: Variation of Rayleigh Wave and Body Wave propagation velocities with Poisson's ratio. (After Kramer, 1996) 55

Figure 2.14: Horizontal and vertical motion of Rayleigh waves. A negative amplitude ratio indicates that the displacement is in the opposite direction of the surface displacement. (After Richart et al., 1970) 57

Figure 2.15: Schematic illustration of softer surficial layer ($G_1\rho_1 < G_2\rho_2$) overlying elastic half space, the simplest conditions for which Love waves can exist. 57

Figure 2.16: Variation of particle displacement amplitude with depth for Love waves. 59

Figure 2.17: Variation of Love wave velocity with frequency. 61

Figure 2.18: Recommended Curves for Correction Factor from Effective Overburden Pressure. (After Murthy, 1991) 65

Figure 2.19: Proposed Shear Wave Velocity and SPT-N correlations. (After Ansary et al., 2010) 66

Figure 2.20: Schematic representation of procedure for computing effects of local soil conditions on ground motions. (Schanbel et al., 1971) 67

Figure 2.21: One dimensional wave propagation system. (After Schanbel et al., 1971) 69

Figure 2.22: HVSR analysis for five different time windows of strong-motion recording atop the more damaged building. (After Mucciarelli et al., 2004) 73

Page

Figure 2.23: HVSR analysis for ambient noise recordings atop the less damaged building. (After Mucciarelli et al., 2004) 73

Figure 2.24: Soil amplification in Bonefro estimated with different techniques: free-field noise HVSR, 1D modeling and HVSR of seven accelerometric recordings of aftershocks. (After Mucciarelli et al., 2004) 74

Figure 2.25: Surface ground deformation. 75

Figure 2.26: K_g values calculated for Loma Prieta Earthquake. (After Nakamura et al., 1990) 76

Figure 3.1: Microtremor observation at fourty five selected locations in and around Dhaka City. 80

Figure 3.2: Superimposed study points on Geomorphological Map of Dhaka City. (Source: Geological Survey of Bangladesh, GSB) 84

Figure 3.3: Superimposed study points on Geomorphological Map of Dhaka City. (Source: A. S. M. Maksud Kamal) 85

Figure 3.4: Microtremor Measurement Apparatus. 119

Figure 3.5 [(a), (b) and (c)]: Microtremor data recording in and around Dhaka city. 120

Figure 3.6: Time history field data recording at Uttara Phase-3 (North side). 121

Figure 3.7 [(a), (b), (c), (d), (e), (f), (g), (h) and (i)]: Fourier Transformation of three segments at Uttara Phase-3 (North side). 122

Figure 3.8 [(a) and (b)]: Predominant Frequency and H/V ratio at Uttara Phase-3 (North side). 124

Figure 3.9 [(a), (b) and (c)]: Stability of Fourier Spectrum at different times along EW, NS and UD directions at MT05, MT06 and MT07. 126

Figure 3.10 [(a), (b) and (c)]: Stability of Fourier Spectrum at different times along EW, NS and UD directions at MT08, MT09 and MT10. 128

Figure 3.11 [(a), (b) and (c)]: Stability of Fourier Spectrum at different times along EW, NS and UD directions at MT11, MT12 and MT13. 129

Figure 3.12 [(a), (b) and (c)]: Stability of Fourier Spectrum at different times along EW, NS and UD directions at MT15, MT16 and MT19. 130

Figure 3.13 [(a) and (b)]: Stability of Fourier Spectrum at different times along EW, NS and UD directions at MT22 and MT23. 130

Page

Figure 3.14 [(a), (b) and (c)]: Stability of H/V ratio data at different times along EW and NS direction at MT05, MT06 and MT07. 132
Figure 3.15 [(a), (b) and (c)]: Stability of H/V ratio data at different times along EW and NS direction at MT08, MT09 and MT10. 133
Figure 3.16 [(a), (b) and (c)]: Stability of H/V ratio data at different times along EW and NS direction at MT11, MT12 and MT13. 134
Figure 3.17 [(a), (b) and (c)]: Stability of H/V ratio data at different times along EW and NS direction at MT15, MT16 and MT19. 135
Figure 3.18 [(a) and (b)]: Stability of H/V ratio data at different times along EW and NS direction at MT22 and MT23. 136
Figure 3.19: Comparision of RM, RMS, RS and MEAN resultant H/V ratio of EW and NS direction at Bashundhara, Block-D. 138
Figure 3.20: Comparision of RM, RMS, RS and MEAN resultant H/V ratio of EW and NS direction at Board Bazar, Gazipur. 138
Figure 3.21: Comparision of RM, RMS, RS and MEAN resultant H/V ratio of EW and NS direction at Uttar Khan. 139
Figure 3.22: Five different windows effect on Microtremor data at segment 1 of Bramangaon. 141
Figure 3.23: Five different windows effect on Microtremor data at segment 2 of Bramangaon. 141
Figure 3.24: Five different windows effect on Microtremor data at segment 3 of Bramangaon. 142
Figure 3.25: Five different windows effect on mean microtremor data at Bramangaon. 142
Figure 3.26: Variation of predominant frequency and H/V ratio due to smoothing effect at Bramangaon. 143
Figure 3.27: Variation of predominant frequency and H/V ratio due to smoothing effect at Tongi, Ershadnagar. 144
Figure 3.28: Variation of predominant frequency and H/V ratio due to smoothing effect at Ashiyan city. 144
Figure 3.29: Variation of predominant frequency and H/V ratio due to smoothing effect at Agargaon Trade Fair. 145
Figure 3.30: Predominant frequency and H/V ratio at Uttara Azampur. 150

Page

Figure 3.31: Predominant frequency and H/V ratio at Rab-10 Plot, Kamrangirchar. 150

Figure 3.32: Predominant frequency and H/V ratio at Sosan Ghat, Kamrangirchar. 151

Figure 3.33: Predominant frequency and H/V ratio at RoyerBazar. 151

Figure 3.34: 132 Microtremor observation points in specific location of BUET campus. 155

Figure 3.35 [(a), (b), (c), (d), (e), (f),(g),(h) and (i)]: Predominant frequency and H/V ratio at 132 selected locations in soil within BUET campus. 159

Figure 3.36: 45 microtremor observation points in various building of BUET campus. 167

Figure 3.37: Google Map of BUET Campus. 168

Figure 4.1: Amplitude ratios of microtremor and theoretical transfer function of shear wave at National University. 173

Figure 4.2: Amplitude ratios of microtremor and theoretical transfer function of shear wave at Board Bazar Gazipur. 173

Figure 4.3: Damage assessment of 45 test locations using Nakamura's Vulnerability Index (Kg). 180

LIST OF TABLES

Page

Table 2.1: Empirical correlation between SPT-N value and Shear Wave Velocity. (After TC4, ISSMFE, 1993) 64

Table 3.1: Geological and Geomorphological classification of the study area. 81

Table 3.2: SPT-N and Shear Wave Velocity at Uttar Khan. 92

Table 3.3: SPT-N and Shear Wave Velocity at Azampur School, Uttara. 94

Table 3.4: SPT-N and Shear Wave Velocity at Mirpur DOHS (South side). 95

Table 3.5: SPT-N and Shear Wave Velocity at Field Ground, Pallabi. 99

Table 3.6: SPT-N and Shear Wave Velocity at Block-B, Bashundhara. 100

Table 3.7: SPT-N and Shear Wave Velocity at Block-D, Bashundhara. 101

Table 3.8: SPT-N and Shear Wave Velocity at Block-H, Bashundhara. 102

Table 3.9: SPT-N and Shear Wave Velocity at Adabor. 105

Table 3.10: SPT-N and Shear Wave Velocity at Agargoan Trade Fair area. 106

Table 3.11: SPT-N and Shear Wave Velocity at Aftab Nagar Housing Project. 107

Table 3.12: SPT-N and Shear Wave Velocity at Sosan Ghat, Kamrangirchar. 110

Table 3.13: SPT-N and Shear Wave Velocity at Matuail, Demra. 112

Table 3.14: SPT-N and Shear Wave Velocity at Meradia, Uttar Banasree. 115

Table 3.15: SPT-N and Shear Wave Velocity at BUET Play ground. 116

Table 3.16: Microtremor Test Location, Predominant Frequency and H/V ratio in and around the Dhaka city. 146

Table 3.17: Microtremor Test Location, Predominant Frequency and H/V Ratio within BUET campus. 158

Table 3.18: Predominant period and frequency of 45 BUET buildings. (After Russel et al., 2006) 168

Table 4.1: Analysis of resonance criteria of 45 buildings in BUET campus. 175

Table 4.2: Damage assessment of site soil using Nakamura's empirical formula. 177

The thesis titled "Applicability of H/V Microtremor Technique for Site Response Analysis in Dhaka City", Submitted by Md. Saidur Rahman, Roll No. 1009042209, Session April 2011 has been accepted as satisfactory in partial fulfillment of the requirement for the degree of Master of Science in Civil Engineering on 12th July 2011.

BOARD OF EXAMINEERS

(Dr. Mehedi Ahmed Ansary) Professor Department of Civil Engineering Bangladesh University of Engineering and Technology.	Chairman (Supervisor)
(Dr. Md. Zoynul Abedin) Professor and Head Department of Civil Engineering Bangladesh University of Engineering and Technology.	Member
(Dr. Abu Siddique) Professor Department of Civil Engineering Bangladesh University of Engineering and Technology.	Member
(Dr. Md. Mahmudur Rahman) Professor Department of Civil Engineering Ahsanullah University of Science and Technology.	Member (External)

DECLARATION

It is hereby declared that except for the contents where specific references have been made to the work of others, the studies contained in this thesis are the result of investigation executed by the author under the supervision of Dr. Mehedi Ahmed Ansary, Professor, Department of Civil Engineering, Bangladesh University of Engineering and Technology.

It is hereby declared that this thesis or any part of it has not been submitted elsewhere for the award of any degree or diploma.

_____

(Signature of the Author)

APPLICABILITY OF H/V MICROTREMOR TECHNIQUE FOR SITE RESPONSE ANALYSIS IN DHAKA CITY

A Thesis Submitted by

Md. Saidur Rahman
Student No. 1009042209

In partial fulfillment of requirement for the degree of

MASTER OF SCIENCE IN CIVIL ENGINEERING
(Geotechnical)

July, 2011

DEPARTMENT OF CIVIL ENGINEERING
BANGLADESH UNIVERSITY OF ENGINEERING AND TECHNOLOGY
Dhaka-1000, Bangladesh